THIRD EDITION

DYNAMICS OF MARINE ECOSYSTEMS

BIOLOGICAL–PHYSICAL INTERACTIONS IN THE OCEANS

K. H. MANN AND J. R. N. LAZIER

Blackwell Publishing

DYNAMICS OF MARINE ECOSYSTEMS

Dedicated to the memory of
GORDON A. RILEY
a good friend and colleague
who was thinking and writing about
these same topics 60 years ago

DYNAMICS OF MARINE ECOSYSTEMS

Biological–Physical Interactions in the Oceans

Third Edition

K.H. Mann & J.R.N. Lazier

Department of Fisheries and Oceans
Bedford Institute of Oceanography
Dartmouth, Nova Scotia
Canada

Blackwell
Publishing

BLACKWELL PUBLISHING
350 Main Street, Malden, MA 02148-5020, USA
9600 Garsington Road, Oxford OX4 2DQ, UK
550 Swanston Street, Carlton, Victoria 3053, Australia

First edition published 1991 by Blackwell Publishing Ltd
Second edition published 1996
Third edition published 2006

1 2006

Library of Congress Cataloging-in-Publication Data

Mann, K.H. (Kenneth Henry), 1923–
Dynamics of marine ecosystems : biological-physical interactions in the oceans / K.H. Mann & J.R.N. Lazier.—3rd ed.
p. cm.
Includes bibliographical references and index.
ISBN-13: 978-1-4051-1118-8 (pbk. : alk. paper)
ISBN-10: 1-4051-1118-6 (pbk. : alk. paper) 1. Marine ecology. 2. Biotic communities. I. Lazier, J.R.N. II. Title.

QH541.5.S3M25 2005
577.7—dc22

2005004139

A catalogue record for this title is available from the British Library.

Set in 10/12.5pt Book Antiqua
by Graphicraft Limited, Hong Kong
Printed and bound in India
by Replika Press Pvt., Ltd.

For further information on
Blackwell Publishing, visit our website:
www.blackwellpublishing.com

Contents

Preface to third edition

Since the appearance of the second edition of this book, in 1996, there have been major changes in our understanding of the relationships between physics and the biology of the oceans on the large scale. We now see clearly that decadal-scale changes in physical properties of ocean basins are linked to changes in the biological components of the ecosystems. At times these changes in both physical properties and biology are so striking that they are described as regime shifts. Major changes occur in patterns of atmospheric circulation and, with the inevitable lags, in the major fish stocks. It seems probable that such shifts have occurred many times in the past, but over the last one hundred years or so the patterns have been somewhat modified by human exploitation and possibly the 0.6 °C warming of the globe.

It has been noticed that that changes in one ocean basin occur concurrently with changes in the others, and in 1998 Klyashtorin put forward a hypothesis to explain the connections. He observed that for 20–30 consecutive years the atmospheric circulation over the North Atlantic Ocean and Asia was dominated by east–west zonal movement, then a change occurred and north–south meridional movement became more prominent, while east–west movements diminished in strength and frequency. This condition persisted for another 20–30 years, before shifting back to the zonal regime. The cycle has a periodicity of about 55 years. During the twentieth century there was one complete cycle, and we are apparently now in the later stages of a second cycle. It is probable that the dominant circulation pattern over the North Atlantic and Asia also occurs simultaneously in other regions of the northern and southern hemispheres, allowing the ocean basins to react similarly. Of the 10 or 11 major commercial fish stocks of the global ocean, some thrive and expand during zonal regimes, while others do so during meridional regimes. At this scale, there is a predictability to the changes that holds exciting possibilities of being able to anticipate trends in exploited populations and adjust harvesting regimes accordingly.

The physical–biological interactions reviewed in various chapters of this book provide plausible mechanisms by which the atmospheric changes might be

linked to the food webs and the fish-stock changes. We might say, following Steele (1998), that the area of study now ranges from carbon flux to regime shift.

Steele (1998) also stated that the basic assumption in biological oceanography is that physical forcing at a wide range of space and time scales determines most of the dynamics of marine populations. Evidence for this assumption has been the theme of the two previous editions of this book. However, recent developments have drawn attention to the part played by the properties of the organisms themselves, and of the biological communities, in modifying the outcomes of physical–biological interactions.

For example, it now appears that in large areas of the ocean the larger cells of the phytoplankton are limited in their reproduction by a shortage of iron. The phytoplankton biomass is dominated by very small cells capable of growth in low concentrations of iron but incapable of using nitrate. Their numbers are controlled by predators in the microplankton. The arrival of a pulse of iron in the form of iron-rich dust permits the larger iron-limited phytoplankton to bloom. The predators of this size group cannot multiply fast enough to prevent this happening. The physiological properties of the various organisms and the predator–prey relationships within the community play a major role in the dynamics of this situation. Development of models that adequately reflect biological community responses to physical forcing at time scales ranging from days to decades are badly needed as contributions to the prediction of global climate change.

The writing of this volume was carried out while the authors were holding positions of Research Scientists Emeritus in the Department of Fisheries and Oceans, Canada. We thank Neil A. Bellefontaine, Director of the Maritimes Region, Michael Sinclair, Director of Science, and Paul Keizer and John Loder, our respective Division Managers, for support in the appointments and generous allocation of the resources of the Bedford Institute of Oceanography. Many colleagues, including Allyn Clarke, Glen Harrison, Peter Jones, Bill Li, and Trevor Platt, offered valuable advice and assistance.

To Hannah Berry, Sarah Shannon, and Rosie Hayden in the Oxford office of Blackwell we extend our thanks for expert advice and encouragement throughout the process. We are grateful to Anna Fiander and the staff of the library in the Bedford Institute of Oceanography for friendly assistance with the literature, and for providing one of us with working space over an extended period. We also wish to thank Ms Linda Paysant, and Drs J.P. Ryan, J. Pineda, and R.G. Lough for providing digital versions of color plates. We thank our wives Isabel Mann and Catherine Lazier for their continuing support and encouragement.

K.H.M., J.R.N.L.

Preface to second edition

We have been surfing a wave of interest in biological-physical interactions in the ocean. In the course of updating this text we have found that there has been an explosion of publications in integrated oceanography, particularly at the two ends of the space–time scale.

At the scale of millimeters to meters there have been important advances in our understanding of the influence of turbulence on processes in plankton. There have been numerous experimental studies on the effects of turbulence on nutrient uptake by phytoplankton, and on the encounter rate between predator and prey. A new understanding has been reached of the physical processes that cause dissolved organic matter to aggregate on surfaces and form colloids, which in turn aggregate until there are organic particles of the size range suitable for food for plankton and benthos.

At the scale of hundreds of meters, there have been numerous field experiments on the relationship between the mixed layer and the deep ocean, designed to elucidate the mechanisms governing the seasonal rise and fall of phytoplankton and zooplankton biomass. When combined with the results of remote sensing on a much larger scale, it has been possible to describe and quantify the seasonal patterns of primary production for all parts of the world ocean. This development holds enormous potential for advancing our understanding of the role of the ocean biota in global climate change.

In the past five years we have come to a much deeper understanding of the importance of the major interannual patterns of atmospheric change, such as the Southern Oscillation and the Aleutian and Icelandic low pressure systems. Local shifts in biological production and the concomitant changes in fish stocks are now seen as part of global scale processes.

A view of the global ocean and the atmosphere as a coupled system is just coming into focus for the first time and the implications for biology are exciting. They are likely to lead to a new appreciation of the role of global processes, over which we have little or no control, in determining the magnitude and distribution of the fish and shellfish stocks that are an important part of the food resources of the

human population. This, in turn, should lead to a more conservative approach to the management of marine living resources.

We thank Neil Bellefontaine, Steve McPhee, Jim Elliott, Allyn Clarke, Mike Sinclair, Don Gordon, and Paul Keizer for their continued interest and support during the revision of this volume. We are especially grateful to Jane Humphreys, our editor in the Cambridge office of Blackwell Science, for her friendly advice and assistance throughout the process, and to our wives Isabel Mann and Catherine Lazier for their continuing support and encouragement.

K.H.M., J.R.N.L.

Preface to first edition

In an earlier book by the senior author entitled *Ecology of Coastal Waters: A Systems Approach*, marine ecosystems were described in terms of their characteristic primary production, whether by phytoplankton, seaweed, mangrove, marsh grass or seagrass. Estimates were presented of the annual mean values for primary production, and pathways of energy flow were traced through the food webs. One chapter was devoted to water movement and productivity. A reviewer commented that the book was too much about mean flows and not enough about variance.

Reflecting on this, it was clear that much of the variance in marine productivity is a function of water movement. Decomposition and liberation of nutrients tend to take place in deep water or on the sea floor and water movement is needed to bring those nutrients back up into the euphotic zone for use by the primary producers. Tides give water movement a diurnal and fortnightly periodicity, while seasonal changes in solar heating impose changes in the mixed layer on scales of months to a year. Long-term climatic cycles impose their own variations on water movement and hence on biological productivity. The theme for this book began to crystallize as an expansion of the earlier chapter on water movement and productivity considered at a range of temporal and spatial scales.

While the ideas were developing, remarkable changes were occurring in oceanography. More and more, biological oceanographers were teaming up with physical and chemical oceanographers to study marine ecosystems in their totality. Physical oceanographers were increasingly able to explain to their colleagues what was going on in gyres, at fronts, on banks or in estuaries, and the biologists were developing the instrumentation needed to obtain continuous records of biological variables to supplement the spot samples that had been characteristic of biological oceanography for decades. Satellite observations of ocean color were giving large-scale perspectives on ocean productivity undreamed of by earlier generations. The feeling emerged that marine ecology was coming of age. It was developing a new maturity based on the integration of disciplines, and in the process yielding important new understanding about ecosystem function.

We therefore decided to use the theme of physical processes and productivity as a starting point for an account of recent developments in marine ecology, in which physics, chemistry and biology are inter-related aspects of the dynamics of marine ecosystems.

Formal courses in oceanography tend to separate marine biology and marine physics. Our aim is to emphasize the links between the two subjects by presenting in each chapter the relevant physical processes along with the biology. Because the reader is expected to have a more complete background in biology than in physics the two subjects are written from slightly different viewpoints. The presentation of the physics is fairly elementary and emphasizes the important physical processes, while the presentation of the biology emphasizes the recent development of the field. To assist the physical presentation we have used some mathematical symbols and equations simply because they are part of the language of the subject and provide a useful shorthand for presenting ideas. It is for example much easier and more precise to write the symbol for the derivative of a variable than to write it out every time it is used. In a further attempt to present the physics in manageable portions some of the details required for a more advanced understanding have been separated into boxes which may be skipped on first reading. The references for both the physics and biology, though numerous, are by no means exhaustive and where good reviews exist we have drawn attention to them and left the reader to find the original sources.

In view of the current concern about the role of the oceans in climate change, we believe that there will be an increasing need to understand the integrated biological-physical functioning of marine ecosystems. We therefore hope that professional researchers in the various disciplines of oceanography will find this book of value in broadening their understanding of marine ecology, as an aid to defining those research programs that will be needed if we are to anticipate the consequences of global change.

In covering such a broad field we have relied heavily on the advice and assistance of many colleagues. For biological material Glen Harrison, Steve Kerr, Alan Longhurst, Eric Mills, Trevor Platt, and Mike Sinclair have been particularly helpful, while on the physics and chemistry side we have enjoyed the advice of Allyn Clarke, Fred Dobson, David Greenberg, Ross Hendry, Edward Horne, Peter Jones, Hal Sandstrom, John Loder, Neil Oakey, and Stuart Smith. We thank Mark Denny, Mike Keen, and Jim McCarthy for helpful comments on various parts of the manuscript, and we particularly thank our editor, Simon Rallison, for his most helpful advice and guidance at all stages of this project. We wish to thank Betty Sutherland and her library staff in the Bedford Institute of Oceanography for expert assistance with the literature and for suffering more or less continuous occupation of part of the library over an extended period. We also wish to thank Steve McPhee, Jim Elliott and Mike Sinclair of the Science Branch of the Department of Fisheries and Oceans for supporting us in our endeavors and our wives Isabel Mann and Catherine Lazier for their encouragement, enthusiasm and patience.

K.H.M., J.R.N.L.

1

Marine ecology comes of age

Marine ecology of the open ocean, as traditionally understood, is the study of marine organisms and their relationships with other organisms and with the surrounding environment. The subject parallels similar studies of organisms on land but, while terrestrial organisms are relatively easy to observe and manipulate, marine organisms are much more inaccessible. This inaccessibility has led to a slower growth of knowledge. The physical factors leading to fertile and infertile areas are very different on land than in the ocean. The nutrients required by land plants are generated nearby from the decaying remains of previous generations, but decaying matter in the ocean tends to sink and leave the sunlit euphotic layer where phytoplankton grow. The nutrients supplied by the decay are thus unavailable for phytoplankton growth unless some physical mechanisms bring the nutrients back up to the surface. This book is largely concerned with those mechanisms and the resulting biological phenomena. Compared with the extensive body of knowledge about physical–biological interactions in open water, much less is known about physical–biological interactions in intertidal communities. Hence the greater part of this book is about the ecology of open-ocean communities.

It is now possible to add an extra dimension to marine ecology. Instead of putting the organisms at the center of the picture and considering them in relationship to other organisms and the environment, it is possible to work with marine ecosystems in which physical, chemical, and biological components are equally important in defining total system properties. Those properties include production of living organisms such as fish, but flux of carbon dioxide as determined by both physical and biological processes may be more important in the context of climate change.

Interest in and research activity in marine ecology are intensifying. There are many reasons for this trend, of which four may be mentioned:

1 The physical processes underlying some of the large-scale biological phenomena are now better understood. For example, the North Pacific Ocean and the North Atlantic Ocean are seen to undergo oscillations in their near-surface physical

properties on a time scale of about five decades, and these oscillations have a profound effect on biological processes, including the production of fish. The changes in physical oceanography appear to be driven by changes in the atmospheric circulation. In tropical regions, an atmospheric cycle known as the Southern Oscillation is seen to drive major changes in the coastal upwelling system in the Humboldt Current, and to have links to changes in climate and biological production in many parts of the world.

2 There have been important advances in our ability to make continuous, fine-scale biological measurements by means of automated sensors feeding into computers. It is now possible to collect biological data with a coverage and resolution comparable with the best physical data and to make integrated biological–physical studies at a wide range of time scales. For example, on a global scale the satellite image in Plate 1 shows the distribution of chlorophyll in surface waters, and reveals a great deal about the incidence of upwelling and the exchange of gases with the atmosphere. On a scale of tens of meters, Plate 5 shows how timely deployment of an intensive array of instruments made it possible to investigate the functioning of a breaking internal wave and its relationship to plankton.

3 The need to understand marine ecological processes influencing the greenhouse effect and other aspects of world climate is becoming more urgent. The flux of carbon dioxide from the atmosphere into surface waters and on down into the deep ocean, as a result of biological processes, is believed to be an important part of the mechanism of climate change. In this connection, there is important new information on the limitation of phytoplankton production in some areas by low concentrations of iron in the water, and on the stimulation of primary production in otherwise unproductive areas by a variety of intermittent mechanisms.

4 Our enormous increase in understanding fundamental processes over second to decadal time scales and centimeter to megameter space scales is beginning to influence the management of the ocean's living resources. We are seeing that year-to-year and decade-to-decade changes in the atmosphere are reflected in property changes in the near-surface ocean. The way in which these changes affect the growth and survival of fish larvae and the distribution of fish are two topics that will receive a great deal of attention in the coming decades.

For all of these reasons, marine ecology has changed rapidly and may be said to have come of age. The dominant theme of this book is that physical processes create the conditions for many important biological processes; the biology cannot be understood in isolation. One good example is the jump in understanding why shelf-break fronts are so productive. This came about through a combination of a high-resolution numerical model and some clever field experiments. The model revealed details of the physical processes that would be impossible to observe with fixed instruments such as moored current meters. The field experiment tracked dye to reveal flow details that bring nutrient-rich water from deeper to shallower water within the front. In this volume, the connections between the physical and

biological processes are emphasized and brought into focus more sharply than before.

The nature of the relationships between physical and biological processes is subtle and complex. Not only do the physical processes create a structure, such as a shallow mixed layer, or a front, within which biological processes may proceed, but they also influence the rates of biological processes in many indirect ways. Discussion of this relationship has most often been in terms of energy flow. Biologists often model food-web relationships in terms of the flow of solar energy, captured in photosynthesis by the phytoplankton and passed from organism to organism by means of feeding transfers. The physical phenomena such as currents, turbulence, and stratification also rely on solar energy, transmitted to the water directly as heat or indirectly as momentum from the wind. These two fluxes of solar energy are in one sense quite distinct: organisms do not use the energy of water motion for their metabolic needs. In another sense, they are interrelated. Water movement alters the boundary layers around organisms, transports nutrients and waste products, assists migrations, and influences the rate of encounter between planktonic predators and their prey. Stratification causes the retention of planktonic organisms in the upper layer of the ocean, making light more available but limiting access to inorganic nutrients. Water temperature has a profound influence on the rates at which biological processes proceed, and differences in water motion, from place to place, largely determine the kinds of organisms colonizing those places. From a biological point of view, the physical energy is termed auxiliary energy, which literally means "helping energy."

However, it is important not to fall into the trap of assuming that there are strict and unvarying relationships between physical oceanography and the dynamics of biological communities. It is now becoming clear that interactions between organisms modify the responses of communities to physical conditions. For example, the size composition of a phytoplankton community may be determined by the types of zooplankton feeding upon it, and when nitrate-rich water is brought up into the mixed layer the response of a community of large phytoplankton cells will be very different from the response of a community of very small cells.

Length scales

In approaching the subject it is useful to have a feeling for the dimensions of the organisms and phenomena to be discussed (Fig. 1.01). Ocean basins are typically 10,000 km wide and confine the largest biological communities. The average depth of the ocean is 3800 m but the depths of the euphotic layer (~100 m) and the mixed layer (~100 m) are more often critical to open-ocean biological processes.

The Coriolis and gravitational forces give rise to the Rossby internal deformation scale or radius, a frequently encountered length scale in physical/biological oceanography (see Section 5.2.3). It arises in flows of stratified water when a balance between the two forces is established. This scale, which varies strongly

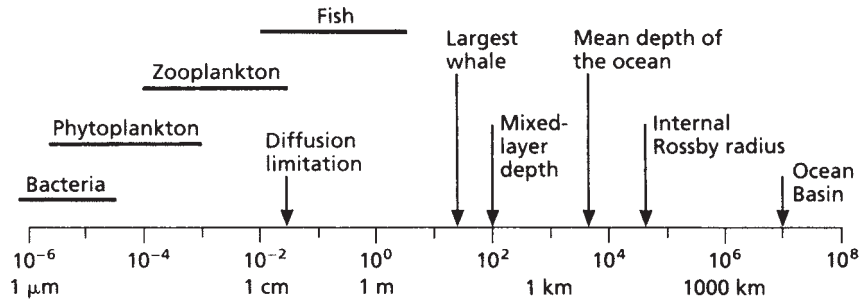

Fig. 1.01 The size scale from 1 μm to 100,000 km, showing some characteristic size ranges of organisms and physical length scales.

with latitude, is the typical width of ocean currents such as the Gulf Stream, the width of the coastal upwelling regions, or the radius of the eddies in the ocean.

The viscous or Kolmogoroff length is the scale where viscous drag begins to become important, that is, where viscosity starts to smooth out turbulent fluctuations in the water (see Section 2.2.6). The scale represents the size of the turbulent eddies where the viscous forces are roughly equal to the inertial forces of the turbulent eddies. The scale also indicates an important change in the methods of locomotion and feeding. Organisms larger than ~10 mm are not seriously affected by viscous drag, while for the smallest organisms swimming is akin to a human swimming in honey. Because of the change in the turbulent motions the smallest organisms must depend on molecular diffusion for the transfer of nutrients and waste products. For the larger animals nutrients and wastes are moved rapidly by turbulent diffusion, which is not affected by viscosity. These topics are developed in Chapter 2.

Time scales

As a first approximation, time scales change in direct proportion to length scales. On the global scale, the thermohaline circulation may take 1000 years to complete a circuit. On the ocean-basin scale, the major gyres may require several years to complete a circuit. Eddies and gyres spun off from the major currents have lifetimes of weeks to months, and as energy cascades through smaller and smaller scales of turbulence, the characteristic time for rotation decreases to seconds at the smallest scale.

While physical features determine the spatial scales of ecological processes, the organisms determine the time scales. While the life span of a large marine mammal may be close to 100 years, those of fish are more like 1–10 years, and zooplankton may complete a generation in a few days or weeks. Phytoplankton have doubling times on the order of days, and bacteria of hours. It follows that small organisms are likely to undergo more rapid fluctuations in numbers than

large ones. Since, in general, each type of organism tends to feed on organisms smaller than itself, the process of trophic transfer has the effect of smoothing out the rapid fluctuations. Conversely, predators may impose on their prey longer-term fluctuations that correspond with fluctuations in predator numbers.

Plan of the book

Part A begins by introducing turbulent motion and viscous boundary layers, which determine the unusual feeding and locomotion techniques of the very small organisms. These phytoplankton and zooplankton are the base of the food chain and account for about half of the total biomass of the ocean. Their survival depends on a variety of physical processes outlined in Chapters 3 and 4. In the open ocean survival depends on the annual creation and destruction of the seasonal pycnocline. In shallow coastal waters the effects of freshwater run-off and tidal mixing can be the dominant processes.

In Part B, Chapter 5 describes the consequences of winds near coasts and of the Coriolis force that lead to the Ekman drift in the surface layers and coastal upwelling. This process is responsible for some of the most productive regions in the ocean. The enhanced biological activity near various types of fronts is covered in Chapter 6 and is followed by a discussion of tides including explanations of tidally generated internal waves that transport nutrients onto the continental shelves.

Large-scale phenomena are treated in Part C, beginning with an explanation of the wind-driven circulation, the intense western boundary currents such as the Gulf Stream (Plate 2), and the warm- and cold-core rings that are generated by instabilities in the boundary currents. The unique biological properties of the rings and other circular circulation patterns such as gyres are then reviewed. The El Niño – Southern Oscillation story in Chapter 9 introduces the effect on biological productivity of changing circulation in the ocean. It is now clear that regular multi-decadal cycles in the atmosphere–ocean interactions of the major ocean basins cause predictable large-scale cycles in the abundance of fish. Chapter 10 reviews the greenhouse effect and the role of the oceans in this cycle, emphasizing the biological pump that is an important mechanism transferring carbon dioxide from the upper layers to the bottom of the ocean.

In the final chapter we discuss questions for the future. There is a sense in which the whole book is an exploration of these questions, so we give them here:

1 Is there a common mechanism to account for the occurrence of high biological productivity in a variety of physical environments?
2 To what extent are events in marine ecosystems determined by physical processes, and to what extent are the outcomes modified by interactions within the biological community?
3 How can we develop concepts and models that span the enormous range of scales in marine ecology, from the microscopic to the global and from seconds to geological ages?

4 How do we explain an apparent synchrony in the variations in the biomasses of fish stocks worldwide?

We shall see that a tentative answer to the first question was provided by Legendre (1981). He said, in effect, that vertical mixing followed by stratification of the water column leads to a phytoplankton bloom, and that this effect can be seen to happen in a variety of habitats and at a range of temporal and spatial scales. Our review supports this answer, but are there other mechanisms?

One is tempted to respond to the second question by saying that physical factors obviously determine the course of biological events, and the converse rarely happens. In fact, if we take a long-term view, we see that the greater part of the carbon dioxide released into the atmosphere during the life of the earth has been fixed by phytoplankton and deposited in marine sediments as carbonates or organic matter. Without these processes the carbon dioxide content of the atmosphere would be much higher, the earth would be much hotter, and the circulation of the oceans would be totally different. Even on the short time scale there are examples of phytoplankton altering the penetration of light and heat into the water column and hence the functioning of the ecosystem. Interactions between physics and biology are not entirely, or even mainly, in one direction. Moreover, while physical processes have predictable effects on individual organisms, their effects on whole biological communities are much less predictable. Community responses may be modified by the substitution of one species by another, or by predator–prey interactions.

The third question has been much discussed without any real resolution. It is a problem for ecologists generally, for we do not understand how to include bacterial processes on scales of millimeters and seconds in the same models that deal with animals that live for decades and may range over thousands of kilometers. Marine ecologists have the added difficulty that the biological events take place in a medium that exhibits physical processes on the same range of scales, thus compounding the difficulties.

The fourth question came into sharp focus at the end of the twentieth century. Multi-decadal changes in global patterns of atmospheric circulation correlate well with biomass changes in many of the major fish stocks. An enormous amount of work will be required to investigate, at a range of scales, the mechanisms responsible for the links between atmospheric changes and changes in marine ecosystems.

We have found it useful to keep these questions in mind as we review the developments of marine ecology as an integrated physical, chemical, and biological discipline.

Part A

Processes on a scale of less than 1 kilometer

2

Biology and boundary layers

2.1 Introduction

In this chapter we shall explore the intimate relationships between the small-scale processes in sea water and the lives of plants and animals. In order to do so, we shall have to shed many of the concepts that are ingrained in our way of thinking simply because we inhabit bodies of a particular size. To take one example, it seems natural for us to think that if we are in the sea and use our arms to push water backward, we shall move forward, coasting for many seconds or minutes before the viscosity of the water brings us to a halt. For a microorganism this is not true. Viscosity is all-important. A picoplankton cell of about 1 μm diameter swimming at about 30 μm s^{-1} and then stopping would come to a halt in about 0.6 μs, having traveled only about 10^{-4} μm (Purcell 1977). Alternatively, a small crustacean that extended a pair of stiff limbs at right angles to the body and attempted to "row" itself forward would rock forward and back, staying in exactly the same place. Hence, traditional ideas about the locomotion of small organisms have to be drastically modified. In order to do so we have to understand that motion through the water is a function of two key variables, momentum and viscosity, and that the relative proportions of these variables change according to the scale of events being studied.

Consider the situation of a planktonic larva that is approaching the sea bed and is about to choose a site for settlement and metamorphosis. Interesting laboratory studies have been made, showing, for example, how certain larvae respond to chemical cues. In the real world, most areas of the sea bottom are exposed to one or two daily cycles of tidal currents. As Simpson (1981) put it, "in stress terms, these tidal streams are equivalent to hurricane-force winds in the atmosphere blowing regularly twice per day." Careful analysis shows that the only place that larvae can find water quiet enough for them to swim about and explore the bottom is a thin layer about 100 μm thick immediately adjacent to the sea floor. In this thin layer they barely have room to maneuver, and it turns out that they

use their swimming powers only to descend, sample the sea floor, and rise again if it is unsuitable. An understanding of the situation requires familiarity with the fundamental properties of boundary layers that form around objects when the water is in motion relative to the object.

We turn now to a consideration of the small-scale boundary layers of the surfaces of phytoplankton or seaweeds. Viscosity causes the average speed of the flow to decrease from its value in the open water to zero at the boundary. The size of the turbulent eddies in the water also decreases to zero at the boundary. This change creates problems for organisms that require the transport of nutrients toward their surfaces and waste substances away from them. Turbulent eddies transport nutrients efficiently in the open water but are too weak to transport nutrients through the boundary layer. Unless some special action is taken, the organism's metabolism is restricted by the lack of turbulent transport, which is replaced by very slow transport due to molecular diffusion. This restriction is often known as diffusion limitation of metabolism. A different set of processes determine transport of nutrients through the cell membrane, but those are not under discussion here.

The thickness of a boundary layer is reduced in proportion to the speed of the water moving past it. For large plants such as seaweeds, thinning of the boundary layer is achieved by attaching themselves to a solid surface in a zone where tidal currents and wave action cause vigorous water movement. This technique has its dangers, for if the water movement is excessive, the drag on the plant may tear it from its attachment. Many seaweeds are capable of making changes in their shape during growth, to reflect the trade-off between the need to maximize turbulence close to the plant surface and the need to reduce drag.

The conventional understanding of a planktonic organism is that it moves passively with the water. However, the need to overcome diffusion limitation is just as real for a phytoplankton cell as it is for a seaweed. There are two main techniques available. One is to have a heavy cell wall that tends to cause the cell to sink through the water column. This technique is employed by diatoms and works best in mixed layers where the stirring tendency of the turbulent flow counteracts the sinking of the organisms. Without the turbulence the diatoms would all end up in deep water, where there is insufficient light for photosynthesis. Investigation of the efficacy of the technique requires an understanding of the physics governing the sinking rate of particles in a fluid, as well as the physics of small-scale boundary layers. Note that some diatoms can overcome the tendency to sink by incorporating positively buoyant substances.

The second technique adopted by phytoplankton is to perform locomotory movements. This solution has been adopted by the flagellates, but it is a far from simple process because of the problems associated with overcoming viscosity at small scales.

When we take all these physical aspects of life in the sea into consideration, we find that many of our existing concepts, based on experiments carried out in the laboratory in still water, are in need of drastic revision. Grappling with the physics of turbulent flow is hard labor for many biologists, but it is absolutely essential for understanding contemporary marine ecology.

2.2 Phytoplankton and boundary layers

Phytoplankton productivity in the world ocean is now a major concern, because of the role it is thought to play in modifying the carbon dioxide content of the atmosphere and hence the scenario for global climate change. One of the major themes running through this book is the need to understand how phytoplankton productivity is influenced by the physics of the ocean. This influence operates at many scales, from ocean basin circulation, through localized areas of upwelling, down to the smallest scales of turbulence that affect individual cells. Kinetic energy is imparted to the world ocean by sun, wind, and tides, and the energy of large-scale motions is transmitted progressively to smaller and smaller scales of motion until, at very small scales, the motion is resisted by the molecular viscosity of the water and is eventually dissipated as heat. In the sections that follow, we shall make a fairly long detour into the physics of turbulence, viscosity, molecular and turbulent diffusion, and the structure of boundary layers, before returning to the physiology of phytoplankton in Section 2.2.10.

2.2.1 Turbulent motion

To begin, consider the hypothetical record of velocity in the ocean shown in Fig. 2.01. The signal has a mean or average, $\bar{u}$, over the record, but at most times the velocity deviates from the mean by an amount u', called the fluctuating part of the flow. The sum of the two at any instant gives the total velocity.

The fluctuations in the motion indicate the presence of turbulence. When $u' = 0$, turbulence is absent and the flow is said to be smooth, or laminar. For turbulent flow, u' is a function of time and is made up of fluctuations of many periods randomly mixed together. The most rapid fluctuations may have a period of about a second and are the smallest turbulent motions with scales of a few millimeters. The longest fluctuation in the record may represent motions that are a few meters in size with periods of tens of minutes.

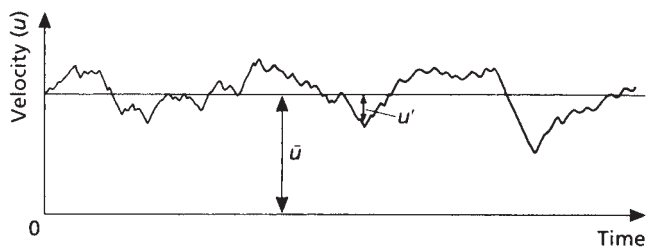

Fig. 2.01 A hypothetical record of water velocity in turbulent flow, illustrating the difference between the average value $\bar{u}$ and the fluctuating component u'.

Turbulent motions of these small scales are usually assumed to be three-dimensional and statistically similar in all directions; that is, the turbulence is said to be homogeneous or isotropic. This convention arose because many major advances in the theoretical understanding of turbulent motion associated with important practical problems became possible only by using this assumption, which allowed a great simplification to the equations governing turbulent motion. This idealized state is a fairly good assumption for scales between the viscous and buoyancy scales, calculated later, but for scales as large as or larger than the depth of water, the motions lose homogeneity and become two-dimensional eddies that are sometimes called geostrophic turbulence to denote the fact that the eddies are random, large, and adjusted to the influence of the rotation of the earth.

2.2.2 Sources of turbulent energy

The energy in the turbulent eddies is extracted from the larger-scale motions via many different instability mechanisms. The most common and widely known instability is the breaking of surface waves that occurs when the waves get too steep. The breaking converts the regular and predictable motion of the wave into random turbulent motion. Deeper down in the ocean, internal waves propagate on and through the vertical density gradients. These waves also can become unstable and break up into turbulence. In the upper layer of the ocean, the wind, besides generating waves, forces the water to move relative to the layers below. This relative movement, or shear, can also lead to unstable motions that break the flow up into turbulent motions. Finally, the large permanent currents, such as the Gulf Stream, develop meanders that create the large two-dimensional eddies of the geostrophic turbulence that eventually break up into smaller scales of motion.

2.2.3 Viscosity

The energy in turbulent motion is continually being transferred from large scales of motion to small scales. The little eddies that are 5 cm across get their energy from larger eddies, which in turn get their energy from still larger ones. This process, called the energy cascade, does not change the total amount of energy in the turbulence nor does it convert the kinetic energy of the turbulent motion to another form of energy.

With the decrease in the size of the turbulent eddies comes an increase in the velocity gradient across the eddies. When the eddies are small enough and the velocity shear is great enough, then molecular viscosity, the internal resistance of the water, acts to resist and smooth out the gradients in velocity. This smoothing of the flow by viscosity is the way the energy in the turbulence is finally converted to heat and dissipated. The stress generated by the viscous forces is discussed in Box 2.01.

Box 2.01 Calculating the stress due to viscosity

Viscous stresses for most oceanic phenomena are negligible, partly because the viscosity of water is so small – in fact one of the lowest found in naturally occurring liquids – and partly because only at the smallest scales are the velocity gradients large enough to make the viscous stresses significant when compared to the other forces present. A simple calculation shows the magnitude of the viscous forces in a specific situation. The molecular viscous stress τ that one layer such as A in Fig. 2.02 exerts upon layer B is

$$\tau = \rho v \, \mathrm{d}\bar{u}/\mathrm{d}z \tag{2.01}$$

where $\rho \approx 10^3$ kg m^{-3} is the density, $v \approx 10^{-6}$ m^2 s^{-1} is the coefficient of kinematic viscosity, and $\mathrm{d}\bar{u}/\mathrm{d}z$ is the gradient of the average velocity perpendicular to the flow. A typical change in mean velocity in the ocean of 1.0 m s^{-1} over 1000 m gives a velocity gradient of 10^{-3} s^{-1} and leads to a minute viscous stress of 10^{-6} N m^{-2}. Where velocity changes by 0.001 m s^{-1} over 0.01 m, as it may in small eddies, the viscous stress is a significant 10^{-4} N m^{-2}.

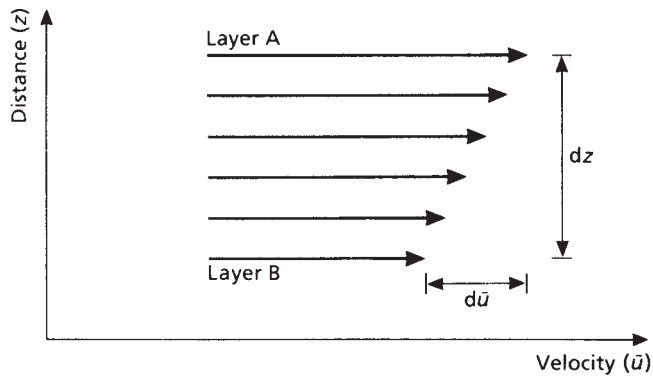

Fig. 2.02 The mean velocity $\bar{u}$, parallel to the x axis, increases by an amount $\mathrm{d}\bar{u}$ in the distance $\mathrm{d}z$, but viscosity creates a stress across the gradient that tends to retard the faster-moving water at level A, and speed up the slower-moving water at level B.

2.2.4 Comparing forces: the Reynolds number

The importance of the forces due to viscosity is often quantified by calculating the Reynolds number, which is the ratio of the inertial force to the viscous force acting on the body of interest, be it an animal or fluid element. The inertial force is the force that was necessary to accelerate the body to the velocity it now possesses, or to stop the body now traveling at a constant speed under its own

inertia. The ratio, a dimensionless number, works out to be the velocity u times a typical dimension d divided by the kinematic viscosity v,

$$Re = ud/v \tag{2.02}$$

Sometimes the ratio is applied to bodies of water. For example, if a mass of water, 1 km across, is moving with an average speed of 10 cm s^{-1}, $Re \approx 10^8$, indicating a region where the viscous forces are too small to suppress the small perturbations that grow into turbulent eddies. On the other hand, if the water mass is 1 cm across and moving at 1 cm s^{-1}, $Re \approx 10^2$, indicating a flow where viscous forces are getting to be important in suppressing small perturbations in the flow.

It is also common to see calculations of the Reynolds number of solid bodies in the water such as grains of sand and animals. A 0.1 m fish swimming at 1.0 m s^{-1}, for example, has a Reynolds number of 10^5. Obviously inertial forces dominate its life and viscosity can be ignored when considering the fish as a whole. A microscopic animal 50 μm long swimming at 10 μm s^{-1}, on the other hand, exhibits the minuscule Reynolds number of 5×10^{-4}. Inertial forces can be ignored in this animal's world, which is dominated by viscous forces. The Reynolds number is, then, a useful guide in assessing the relative strength of the inertial and viscous forces and for comparing similar situations.

The enormous range of Reynolds numbers associated with living organisms is illustrated in Table 2.01, compiled by Vogel (1996). The Reynolds number of an even wider range of organisms was calculated by Okubo (1987) using a characteristic dimension, d, and a typical swimming speed, u, for animals and bacteria, or sinking speed for phytoplankton. He performed this calculation for the whole range from bacteria to whales, then for good measure added the point for humans with a height of 2 m and a swimming speed of 1 m s^{-1}. The resulting plot (Fig. 2.03) shows that the Reynolds number increases systematically with the size of the organism according to the regression

$$Re = ud/v \approx 1.4 \times 10^6 \times d^{1.86} \tag{2.03}$$

Table 2.01 Approximations to the magnitude of the Reynolds number of various organisms. From Vogel (1996).

	Re
A large whale swimming at 10 m s^{-1}	300,000,000
A tuna swimming at the same speed	30,000,000
A duck flying at 20 m s^{-1}	300,000
A large dragonfly going 7 m s^{-1}	30,000
A copepod in a pulse of 20 cm s^{-1}	300
Flight of the smallest flying insects	30
An invertebrate larva, 0.3 mm long, moving at 1 mm s^{-1}	0.3
A sea urchin sperm advancing the species at 0.2 mm s^{-1}	0.03

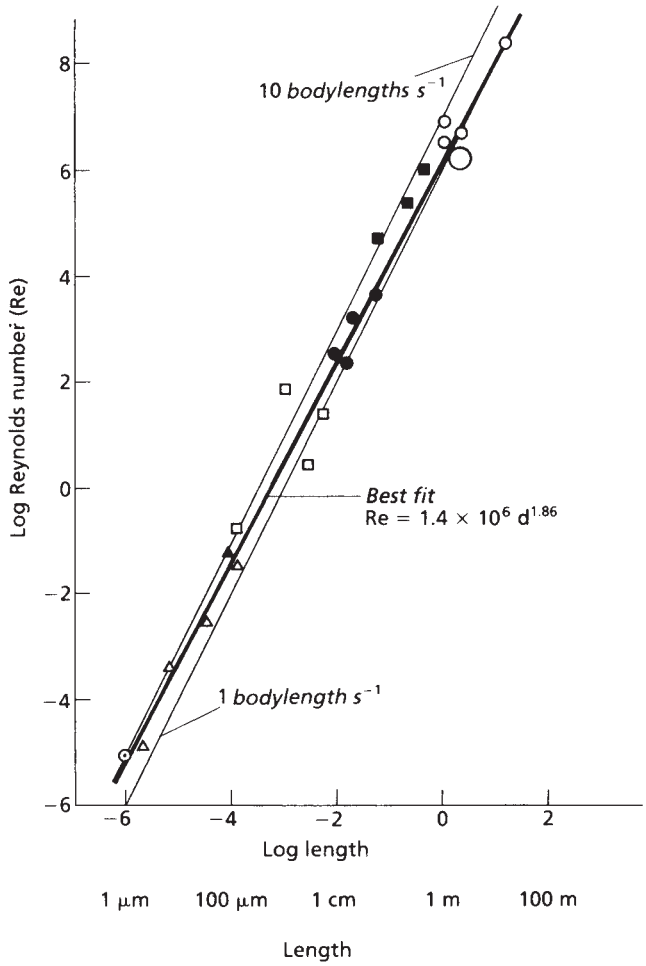

Fig. 2.03 Reynolds number (*Re*) versus organism size (*d*). ○, mammals; ■, fish; ●, amphipods; □, zooplankton; ▲, protozoa; △, phytoplankton; ⊙, bacteria; ○, human. The heavy line is the best fit to the data. Thin lines illustrate the relationships for swimming at 1 and 10 bodylengths per second. Adapted from Okubo (1987).

where d is measured in meters. Substituting $v = 10^{-6}\ \mathrm{m^2\ s^{-1}}$, we find the relationship between the characteristic length and swimming speed,

$$u(\mathrm{m\ s^{-1}}) = 1.4 \times d^{0.86} \tag{2.04}$$

These equations provide a useful quantification of the everyday observation that large animals swim faster than small ones. For additional clarification, we have added two lines to Fig. 2.03 to indicate what the relationship would look like if the organisms moved at 1 and 10 bodylengths per second. Okubo's best-fit line

lies at an angle between these two and suggests that small organisms can move about 10 bodylengths in a second but larger animals swim at close to 1 bodylength per second. Such statements must, however, be treated with caution as the values of swimming speed are quite scattered, especially for zooplankton, and the relationship may only be accurate to within a factor of 10. It is also worth remembering that many of the data, especially those for the smallest organisms, were obtained under a microscope in a laboratory and not in the natural environment.

2.2.5 Molecular diffusion

As indicated above, turbulent energy is passed from large to small eddies and the viscosity of the water limits the size of the smallest eddies to a few millimeters diameter (see below). Such turbulence is ineffective in transporting nutrients and wastes for organisms less than 1 mm in diameter (which make up more than half the total biomass of the oceans; Sheldon *et al*. 1972). Small organisms must rely on the flux due to molecular diffusion – that is, the slow mixing caused by the random motion of molecules. As is shown in Box 2.02, this process is very slow, requiring about 10 seconds to produce an effect over a distance of 100 μm.

BOX 2.02 FICK'S LAW AND THE DIFFUSION TIME SCALE

Molecular diffusion is the slow mixing caused by the random motion of molecules. The flux of some constituent through the water due to molecular diffusion is given by Fick's first law of diffusion. This law states that if the concentration of some constituent C changes by an amount dC over a short distance dz, the flow of C down the concentration gradient by molecular motion is

$$F = -D\, dC/dz \tag{2.05}$$

If C is in kg m^{-3}, F is the flux of C in kg m^{-2} s^{-1} and D is the coefficient of molecular diffusion, which for large chemical species such as chloride ion is about 1.5×10^{-9} m^2 s^{-1}.

The coefficient, D, contains information related to how fast the molecules of the diffusing substance move through the fluid. To use this information, the definition of D is converted into the formula

$$D = 10^{-9}\ \text{m}^2\ \text{s}^{-1} = L^2/t \tag{2.06}$$

where L and t are characteristic values of length and time. Turning the formula around yields $t = L^2/D = 10^9\, L^2$, giving an estimate of the time it takes molecular diffusion to go the distance L. If we use this relation, the time it would take molecular diffusion to cause an effect over 100 μm is about $(100 \times 10^{-6})^2 \times 10^9 \approx 10$ s.

2.2.6 Scales of turbulent structures

When dealing with small organisms living in turbulent water, it is sometimes important to estimate the distributions of velocity, temperature, and nutrients near the organisms. For example, we might want to know the sizes of the smallest turbulent eddies or the sizes of the smallest fluctuations in temperature, salinity, and nitrate.

The size of the smallest velocity fluctuation is determined by the strength of two competing forces. The force due to viscosity works to remove variations in velocity while the inertial force associated with the turbulent motions tends to create velocity fluctuations. The size of the eddies where these opposing forces are in balance is normally taken as the limiting size of the velocity fluctuations. If the viscous, or smoothing, force is represented by the kinematic viscosity v, while the twisting or shearing force in the turbulence is represented by the rate of turbulent-energy dissipation ε W kg^{-1}, the distance across the smallest eddies, known as the viscous or the Kolmogoroff length scale, L_v, is estimated from the following equation (Gill 1982),

$$L_v = (v^3/\varepsilon)^{1/4} \tag{2.07}$$

In much of the oceanographic literature, however, this length is written

$$L_v = 2\pi(v^3/\varepsilon)^{1/4} \tag{2.08}$$

where the factor of 2π has been added for mathematical convenience as it simplifies the manipulation of equations. As discussed by Lazier and Mann (1989), the factor of 2π also results in a more realistic value of the length scale. Measurements have shown that there is virtually no energy in the turbulent eddies at the scale defined by Eqn. 2.07.

The variable ε, representing the dissipation of turbulent energy, is estimated from measurements of the finest scales of the velocity gradient. By doing this, Oakey and Elliott (1980) calculate that ε in the top 50 m layer over the Scotian shelf off Nova Scotia varies from 10^{-6} W kg^{-1} when the wind is 15 m s^{-1} to 10^{-8} W kg^{-1} when the wind is less than 5 m s^{-1}. In these situations the smallest scales L_v, using Eqn. 2.08, would vary roughly from 6 to 20 mm. At greater depths or when the wind is light, the level of turbulent energy decreases to roughly 10^{-9} W kg^{-1}, corresponding to a smallest eddy size of 35 mm (Osborn 1978). The smallest fluctuations of variables such as temperature and salinity are smaller than they are for velocity, as is shown in Box 2.03.

At the other end of the size range are the largest turbulent eddies, which are important because they determine the vertical excursion of the small passive organisms being moved about by the turbulent flow. Near the surface these large eddies determine how much time the organism spends in the euphotic zone. The largest eddies occur when the inertial forces associated with the turbulence, which tend to stir the water, are about equal to the buoyancy forces, which tend to keep the

Box 2.03 The smallest scale of different variables

We saw in Section 2.2.6 that viscosity limits the size of the smallest turbulent eddies to about 6 mm in a highly energetic environment. Viscosity may be thought of as the molecular diffusion of momentum, with a value of ~10^{-6} m^2 s^{-1}, while the molecular diffusivity of heat is about 1.5×10^{-7} m^2 s^{-1} or about one-tenth the value for viscosity. The diffusivities of salt and nitrate are two orders of magnitude lower again, 1.5×10^{-9} m^2 s^{-1}. The effect of these lower diffusivities is to permit smaller fluctuations to persist longer, before being smoothed out by diffusion.

The length scale of the smallest fluctuation of any property of diffusion constant D is given by

$$L_d = 2\pi(\nu D^2/\varepsilon)^{1/4} \tag{2.09}$$

which is called the Batchelor scale. If ε varies from 10^{-6} to 10^{-9}, as suggested earlier, the smallest scale for temperature fluctuations is 2–13 mm and the smallest scale for salt or nitrate fluctuations is 0.2–1.0 mm.

water stratified. This size is estimated from the turbulent-energy dissipation rate ε and the buoyancy or Brunt–Väisälä frequency N (Section 3.2.3), which is proportional to the density stratification. The size of the largest turbulent eddies, sometimes called the buoyancy length scale, is estimated by Gargett (1984) to be

$$L_b = (\varepsilon/N^3)^{1/2} \tag{2.10}$$

In the mixed layer, if $\varepsilon \approx 10^{-7}$ W kg^{-1} and $N \approx 10^{-3}$ rad s^{-1}, then $L_b \approx 10$ m. In the deep ocean, where ε is small, or in stratified regions, where N is high, the buoyancy length scale works out to about one-tenth of the value found in the mixed layer.

2.2.7 Turbulent or eddy diffusion

Across distances greater than a few millimeters the eddies of the turbulence mix the water much more effectively than does molecular motion. The eddy-caused diffusion works the same way as molecular diffusion except that the random movement of the eddies is much larger than the molecular motion. Eddy diffusion is also different from molecular diffusion in that it is the same for all properties – that is, heat, salt, and nitrate will have the same eddy diffusion constant. A typical eddy diffusivity for horizontal diffusion in the ocean is ~500 m^2 s^{-1}, which is about 10^9 times the molecular diffusivity for heat. More details about turbulent diffusion are contained in Box 2.04.

Box 2.04 Eddy fluxes and time scales

Ideally the turbulent flux of a constituent, C, can be determined by measuring the turbulent velocity fluctuations along with the fluctuations in the concentration of C. Such measurements are, however, difficult to make and are done only in special situations. Usually it is assumed, by analogy with the molecular case, that the flux is dependent on the gradient of C and a diffusion constant, except in this case the diffusion constant is a diffusion due to eddies rather than a molecular diffusion. Thus, the flux F of the constituent C is written

$$F = K_e \, dC/dz \tag{2.11}$$

where K_e is the eddy diffusivity and dC/dz is the gradient in C. The value of K_e varies greatly throughout the ocean, depending partly on the level of turbulence and partly on the stratification. Also, because of stratification, eddy diffusion is not the same vertically as horizontally. One estimate quoted by Gargett (1984) gives, deep in the ocean, a horizontal eddy diffusivity $K_h \approx 500 \text{ m}^2 \text{ s}^{-1}$ and a vertical eddy diffusivity $K_v \approx 0.6 \times 10^{-4} \text{ m}^2 \text{ s}^{-1}$.

As with the molecular case (Eqn. 2.06), the eddy diffusivity contains information on the rate of diffusion. For the case of turbulent diffusion, the approximate length of time the diffusion takes over a distance L is calculated from L^2/K_e, and if L is 1 km, horizontal eddy diffusion will show an effect in $L^2/K_e = 10^6/500 \text{ s} \approx 0.5$ hours. In the deep stratified ocean, eddy diffusion will transport an effect vertically through 10 m in $100/(0.6 \times 10^{-4})$ s ≈ 20 days. In the mixed layer where the eddy diffusion rate is high in all directions, the time taken to mix properties is obviously less than the time taken in the deep ocean.

2.2.8 Boundary layers

It was mentioned in the introduction that solid boundaries, such as the surfaces of organisms, have associated with them a boundary layer in which water movement is reduced. Since all organisms in the sea have a need to exchange molecules of O_2, CO_2, NH_3, and so forth, with the surrounding medium, the boundary layer is liable to reduce that rate of exchange. A boundary layer is also associated with the water above the sea floor, which can affect the process of exchange of essential substances between the benthic community of organisms and the overlying water. This section examines the properties of boundary layers.

The fundamental property to be considered is the "no-slip condition." Water molecules in contact with a solid surface stick to that surface and are, therefore, stationary with respect to it. If we plot the average velocity near the boundary as in Fig. 2.04(a), we see that it increases as we move away from the boundary until we come to water moving with the "free-stream velocity" – i.e., the velocity that

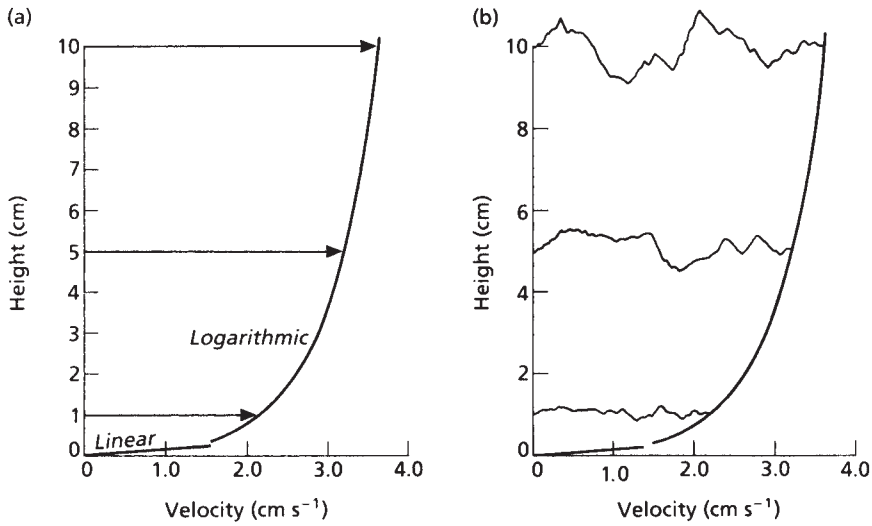

Fig. 2.04 (a) A vertical profile of mean water velocity through the boundary layer above a smooth surface showing the linear sublayer where viscous stresses dominate the stress between the water and the surface and the logarithmic layer where turbulent or Reynolds stresses dominate. (b) The same profile as in (a) including time-series measurements of velocity at three levels to illustrate the increase in the size of the turbulent fluctuations with height above the boundary.

it would have if the solid surface were not present. However, Fig. 2.04(a) is simplified, as if the water in a particular layer is moving at a constant velocity and always in the same direction. In real life, flows are turbulent and exhibit fluctuations perpendicular to the direction of the mean flow as illustrated in Fig. 2.04(b). The amplitude of these fluctuations decreases toward the boundary as there can be no flow into or out of the boundary.

The decrease in the magnitude of the mean flow is caused by the stress, τ, or drag exerted on the water by the solid boundary. The transmission of this stress across the layer of water is accomplished, in turbulent flow, by eddy diffusion. As the boundary is approached the flow decreases until a level is reached where viscosity smooths out almost all turbulence and the stress between the water and the solid is transmitted by viscous stresses.

It is therefore possible to recognize two distinct layers within the boundary layer, the part in which turbulent fluctuations transmit the stress (Reynolds stresses) and the viscous sublayer adjacent to the boundary. If the velocity profile in Fig. 2.04 is plotted on a semi-logarithmic scale, as in Fig. 2.05 (lower line), the different layers are easily distinguished. From 10 cm down to about 0.2 cm from the boundary the profile is represented by a straight line, commonly called a "log-linear" relationship. Adjacent to the boundary, in the viscous sublayer, the profile is no longer log-linear. In fact, in this thin, viscous sublayer the velocity decreases linearly, which appears as a curve on the logarithmic plot. The

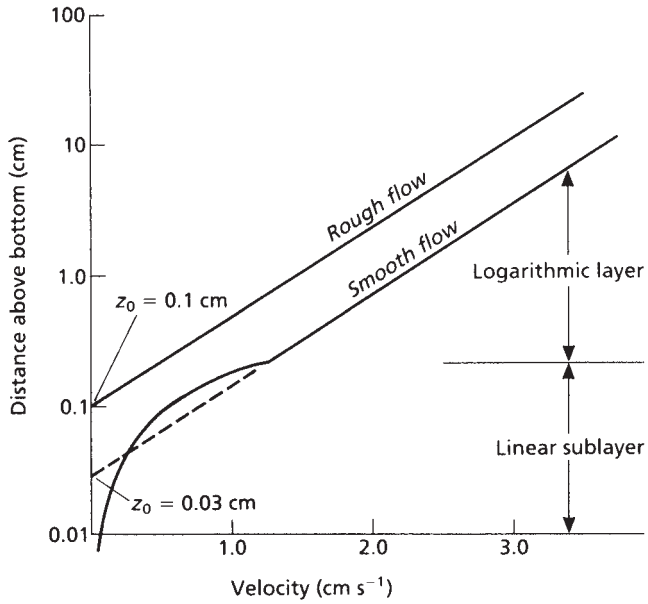

Fig. 2.05 Logarithmic profiles of mean velocity through a boundary layer for the cases of smooth ($z_0 = 0.03$ cm) and slightly rough ($z_0 = 0.1$ cm) flow. Both profiles have $u_* = 0.25$ cm s^{-1}. The linear sublayer where viscous forces are important is a prominent feature of only the smooth flow profile.

convention is to call the outer region the logarithmic layer, or "log-layer," and the region adjacent to the boundary the linear or viscous sublayer. The equations for these layers are presented in Box 2.05.

The thickness of the boundary layer surrounding an object moving through water increases with increasing distance from the leading edge. A familiar analogy is that of an aircraft wing. At the front of the wing the boundary layer is very thin but it increases in thickness with distance from the leading edge according to the expression (Prandtl 1969)

$$\delta = (xv/u)^{1/2} \tag{2.12}$$

where x is the distance from the leading edge, v is the viscosity of the medium, and u is the speed of the flow. When applied to an organism moving through water, two conclusions may be reached. The first is that the larger the organism, the thicker the boundary layer, since there are more places where the value of x is large. Second, the boundary layer becomes thinner as the velocity of the water relative to the organism increases. For sedentary organisms, rapidly moving water will cause a thinning of the boundary layer, and can be expected to assist exchange of substances. For motile organisms, rapid swimming can be expected to have the same effect.

BOX 2.05 EQUATIONS FOR THE BOUNDARY LAYERS

Two equations are required to describe these two layers (Chriss and Caldwell 1984). For the viscous boundary layer, as we have already seen (Eqn. 2.01, Box 2.01), the viscous stress between adjacent layers moving at different velocities is given by

$$\tau = \rho v \, \mathrm{d}u/\mathrm{d}z$$

Because τ and ρ are constant through the boundary layer, the ratio $(\tau/\rho)^{1/2}$ is also constant, and is conventionally replaced by u_*, which is called the "friction velocity." After integrating and introducing u_*, the velocity profile becomes

$$u(z) = u_*^2 z/v \tag{2.13}$$

From this equation, we see that in the viscous boundary layer the velocity, u, is a linear function of z, the distance from the boundary. Hence we have the straight line close to the boundary in Fig. 2.04.

For the log layer, the mean velocity is given by

$$u(z) = (u_*/k) \ln(z/z_0) \tag{2.14}$$

where k is the Von Karman constant, ~0.4. In this layer the velocity increases logarithmically with distance from the boundary.

In these examples we have assumed that the boundary is a smooth surface. In the real world few surfaces are perfectly smooth and the irregularities, or roughness elements, in the surface are liable to generate turbulent wakes in the sublayer. If these wakes are not smoothed out by viscosity, the whole sublayer becomes turbulent and the flow is called "rough." This development has two consequences. First, the boundary exerts more stress on the water because there is more friction. The velocity at any given distance from the boundary is, therefore, less than before, as indicated by the upper line in Fig. 2.05. Second, the relationship between velocity and distance from the boundary becomes logarithmic throughout the boundary layer and the linear sublayer controlled by viscosity disappears.

As indicated in Fig. 2.05, the height, z_0, where the mean velocity is predicted to go to zero, is greater in rough flow than in smooth flow. This height can be used as an estimate of the size of the roughness of the surface and is called the roughness length. In practice it is about one-tenth the height of the roughness elements. The logarithmic profile is reasonably accurate above the level of the roughness elements but among the roughness elements the flow is a complicated function of position and cannot be predicted by the equations.

The variable z_0, representing the size of the roughness elements, and the friction velocity u_* are sometimes used as the typical length and velocity scales, respectively, in the Reynolds number (Eqn. 2.02). In this case, it is called the roughness Reynolds number and is denoted by Re_*.

2.2.9 Drag

When a machine or an animal moves through water, two forces arise to oppose the motion. The first of these drag forces originates in the no-slip condition in association with viscosity. Because of the no-slip condition, the moving object is stuck to the immediately adjacent layer of fluid. Because of viscosity, this layer in turn pulls along some of the layers of fluid further out. The resultant shear in the water is maintained by a stress, or force per unit area (Eqn. 2.01), which must be supplied by the moving object if it is to maintain its motion. Because the magnitude of this drag force is directly dependent on the surface area of the object, it is often called skin friction instead of viscous drag. In cases of low-Reynolds-number flow, as encountered with small plants or animals falling or swimming slowly, this drag force is the only appreciable one encountered and is an important feature of the feeding strategies, as will be explored in Section 2.3.2.

The other drag force, called form or pressure drag, arises because the water, which has mass, must be pushed out of the way of the moving object, and then move back into place behind. Discussion of this force is thoroughly presented by Vogel (1996), who shows that it may be represented by the formula

$$F_D \approx \tfrac{1}{2} C_D \rho u^2 A \tag{2.15}$$

where ρ is the density of the water, u is the speed of the object, and A is some measure of the cross-sectional area of the object, such as the area projected onto the plane perpendicular to the direction of motion. The term C_D, the drag coefficient, is a complicated function of velocity that must be determined empirically for each object. C_D is so complicated because of the way water flows around the moving object, especially around the stern or back end. Objects that are designed to have as little drag as possible, like airplanes and fish, are shaped in a streamlined way so that the fluid moves in behind in a smooth and orderly way. If the object is not streamlined, the motion creates vortices and turbulent wakes at the back that lead to a reduction in pressure on the back side. Lower pressure at the back than at the front generates the pressure drag force in the direction opposite to the motion. The speed at which a particular object creates the turbulent wake or the place on the object where the wake will be produced cannot be deduced *a priori*, and the form or pressure drag can be determined only by experiment for each item. For some simple shapes, such as spheres and cylinders, values of C_D have been determined once and for all as functions of Reynolds number; these values are available in the reference literature. Plants, however, change shape as the speed of the flow changes and it is not yet possible to determine the form drag of such objects without direct measurements.

2.2.10 The problem for phytoplankton

Previous sections briefly referred to the problem of boundary layers around phytoplankton cells. The generally accepted story, first worked out quantitatively in a classic paper by Munk and Riley (1952), is that phytoplankton cells suspended motionless in the water tend to use up the nutrients in the water around them. Their nutrient uptake rate is then limited to the rate at which the nutrients can diffuse toward them. One way of overcoming this limitation is to generate movement relative to the water, so that the zone of nutrient-depleted water is periodically renewed. The cells may accomplish this goal either by sinking passively or by generating their own locomotion. As discussed earlier, there is inevitably a region around the organism in which the velocity of the water relative to the cell is less than the absolute rate of movement of the cell through the water. This region is created by the no-slip condition, which states that molecules in contact with the cell surface adhere to that surface and cannot slip past it. In the boundary layer around the cell, the water velocity relative to the cell changes from zero at the cell surface to the "free-stream velocity" beyond the boundary layer. A sinking or swimming phytoplankton cell drags its boundary layer with it, causing fluid in the depleted region to be sheared away. New fluid in which the nutrients have not been depleted takes its place. This replacement decreases the effective size of the depleted region and increases the rate of uptake by the cell. The magnitude of the increase depends on the velocity of the cell relative to the water.

2.2.11 Sinking of phytoplankton

Most phytoplankton cells are more dense than water. The density of sea water varies from about 1.021 to 1.028 g cm^{-3}, but the density of cytoplasm ranges from 1.03 to 1.10 g cm^{-3}. Diatoms have a cell wall of hydrated silicon dioxide with a density of about 2.6 g cm^{-3} and coccolithophorids have plates of calcite, aragonite, or valerite with a density of 2.70–2.95 g cm^{-3}. Some diatoms counteract negative buoyancy by generating positively buoyant substances, but plenty of evidence suggests that many phytoplankton cells are substantially more dense than water, which means that they will sink except where an upward movement of the water prevents it. The rate at which the cells fall can be estimated if the Reynolds number is ~1.0 and, if the cells are approximately spherical, by Stokes' law, defined by the equation

$$V = \frac{2}{9} g r^2 (\rho' - \rho) / \rho v \tag{2.16}$$

which shows that for a given excess density and viscosity, a sphere will increase its sinking speed in proportion to the square of the radius. Few phytoplankton

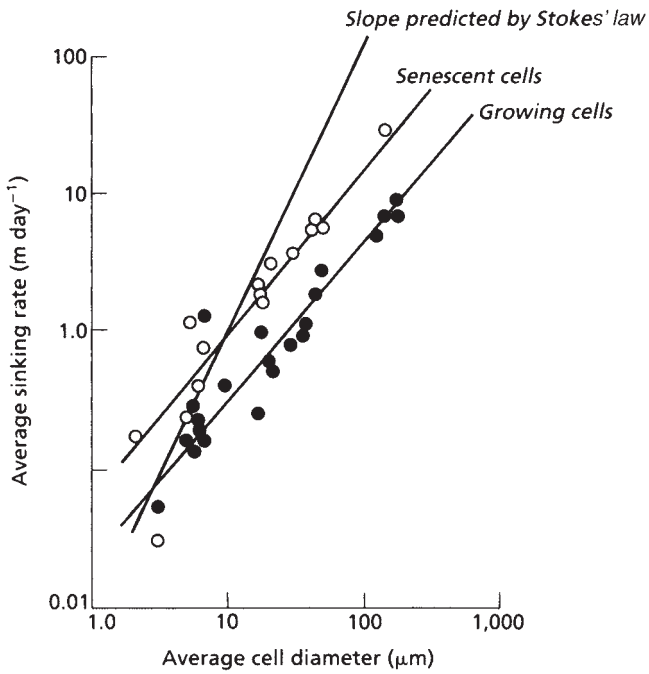

Fig. 2.06 Average sinking rate of phytoplankton cells grown in culture and measured in the laboratory, and line predicted by Stokes' law. After Smayda (1970).

cells are spherical; nevertheless for $Re \leq 0.5$, Stokes' law may be applied to non-spherical bodies without important errors (Hutchinson 1967). Roughly speaking, phytoplankton up to 500 μm in diameter fall within this category. Empirical evidence for increasing sinking speed with increasing size has been reviewed by Smayda (1970) (Fig. 2.06). Although the data fall within the 1–500 μm range, the slopes of the lines are considerably less than the value of 2 predicted by Stokes' law. In considering the reasons for this, shape can probably be ruled out. According to the theoretical analysis of Munk and Riley (1952), the effect of geometry is different in different size classes. In order of decreasing sinking rate, the pattern for 5 μm particles is plate > cylinder > sphere. For 50 μm particles it is cylinder ≈ plate > sphere, and for 500 μm particles it is cylinder > sphere > plate. Moreover, the sinking rates of different shapes tend to equalize with increasing size. The data in Fig. 2.06 have not been corrected for changes in density and viscosity with temperature. At the natural extremes this variance is not negligible: a change from 0 °C to 25 °C results in lowered density and viscosity so that the sinking rate of 20 μm particles approximately doubles. As the data displayed in Fig. 2.06 were not obtained over such an extreme temperature range it is still not clear why the relationship between sinking and size does not follow Stokes' law.

It is seen from Fig. 2.06 that senescent cells sink faster than actively growing cells. It has also been found that preserved cells sink faster than living cells, and that natural blooms of phytoplankton tend to sink in the water column as they

approach senescence. Factors that are thought to contribute to this effect include variation in the cell content of low density oils and fats, variation in the amount of light ions such as NH_4^+, and possible effects of excreted products on the viscosity of the fluid surrounding the cells. The effectiveness of sinking as a means of combating diffusion limitation is considered in Section 2.2.13.

2.2.12 Swimming by phytoplankton

Swimming is the alternative to sinking, as a means of reducing the diffusion limitation on nutrient uptake. The locomotion of small organisms is a very different proposition from what we are familiar with from our own attempts at swimming or from watching macroscopic organisms such as fish or insects (Purcell 1977). For small organisms that perform movements relatively slowly, the Reynolds number is low and viscous forces predominate. A picoplankton organism of about 1 μm radius moving at about 30 μm s^{-1} generates inertial forces that are so small that after the swimming effort ceases it will come to a stop in about 0.6×10^{-6} s, travelling only 10^{-4} μm. It is rather like a human swimming in a pool of molasses and forbidden to move any part of the body faster than 1 cm min^{-1}. One consequence of this situation is that jet propulsion just does not work: it relies on inertial forces. A scallop-like animal at this scale would just expel the liquid as it closed its shell and take it in again on opening, getting nowhere in the process. The mechanisms that work best under these conditions are the "flexible oar" (cilium) and the "corkscrew" (flagellum pointing forward) (Purcell 1977). Of the two, flagella are the most commonly used by phytoplankton.

2.2.13 The effectiveness of swimming or sinking

A stationary phytoplankton cell cannot take up nutrients faster than they are transported toward it by diffusion (Section 2.2.10). When nutrient concentrations are very high, the rate of diffusion (proportional to the concentration gradient) may be sufficient for the needs of most cells, and there are some types of phytoplankton that take up nutrients so slowly that diffusion is not a limitation on their metabolism under most conditions. However, in the low-nutrient conditions typical of tropical waters most of the time, and of temperate waters in summer time, most phytoplankters are nutrient-limited but can move relative to the water by sinking or swimming to increase their nutrient uptake (Pasciak and Gavis 1974). The critical question is: under conditions in which the cell's requirements for nutrients are limited by diffusion in the boundary layer, how effective is relative movement between the cell and the water in increasing the rate of nutrient uptake?

We see in the following discussions that the conclusions of various studies are quantitatively the same. For small organisms in the 1–10 μm range, viscosity dominates their world and diffusion is faster than water movement in supplying nutrients through their boundary layer. As far as we can tell, these small

organisms move to find better concentrations of nutrients in the environment, not to reduce their diffusion limitation.

On the other hand, flagellates larger than 10 μm, many of which are able to swim more than 10 times their own bodylength per second, may achieve a significant increase in nutrient uptake by swimming. The relative advantages of movement are greater still for cells of 50 μm or more, not only because they move faster but also because they have a smaller ratio of surface area to volume and have a stronger nutrient limitation in the first place.

Most diatoms are unable to swim, but create water movement past their surfaces by sinking. Large cells sink faster than small cells, and it is only the larger cells that sink fast enough to gain a significant advantage from it in terms of nutrient uptake. In no case can these cells abolish nutrient limitation by sinking, but the differences between cells are thought to be great enough to influence interspecific competition. The evidence for these findings is as follows.

Pasciak and Gavis (1974) considered the question of diffusion limitation in conjunction with conventional Michaelis–Menten nutrient dynamics. They concluded that when the concentration of nutrients in the environment is not many times greater than the half-saturation constant of the cell, and when the cell is small, diffusion can be a severe limitation on cell metabolism. Gavis (1976) then introduced motion relative to the water into the calculations. Taking published rates of sinking of phytoplankton cells, he concluded that an appreciable increase in nutrient uptake rate would occur only if the cells are relatively large (100 μm) and the concentration of nutrients is low. In the optimum case, sinking would alleviate only about 30% of diffusion limitation.

A similar result was obtained using published swimming rates. The effect was most marked with large (100 μm) cells swimming at about 3 bodylengths per second. There was an appreciable increase in nutrient uptake but it was still less than one-third what it would have been in the absence of diffusion limitation. Hence, the conclusion was that swimming and sinking are not very effective methods of alleviating diffusion limitation, but that they might make enough difference to affect the outcome of competition among species.

The theory of the process was advanced by Berg and Purcell (1977) and Purcell (1977), who considered the case of a spherical cell of radius r, propelled at a constant velocity u through water containing molecules "for which the cell is a perfect sink." They calculated the relationship between velocity and the fractional increase in the transport of nutrients to the cell. They showed that this increase was a complex function of ru/D where D is the diffusion constant of the molecules absorbed. Some years later Sommer (1988), building on the ideas of Goldman (1984a), took this formulation by Berg and Purcell (1977) and plotted the results for 19 species of marine flagellates for which the size and swimming velocity were known (Fig. 2.07). Swimming speeds ranged from about 2 to a maximum of 100 bodylengths per second, with the smaller cells having the higher relative velocities. Even so, the conclusion (Fig. 2.07) was that cells of 5 μm or less increased their nutrient flux by only 5–30% when swimming. On the other hand, flagellates of 50 μm diameter had the potential to double or even treble their nutrient uptake rate by swimming.

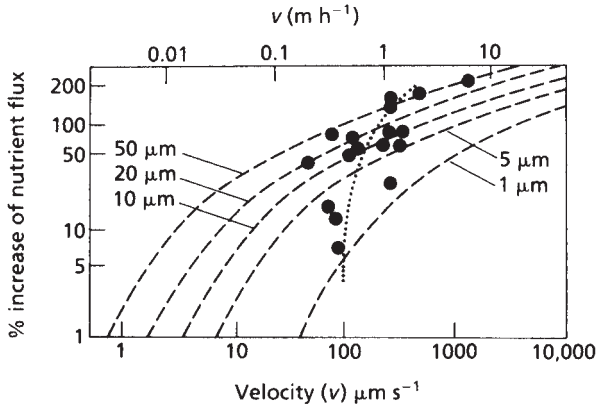

Fig. 2.07 Fractional increase of nutrient flux to the cell surface as a function of swimming velocity and cell diameter, calculated for spherical cells, after Berg and Purcell (1977). The circles represent observations and the finely dotted line is a regression through the observations. From Sommer (1988).

We may also apply this diagram to a consideration of sinking, treating it as a special case of locomotion. From Fig. 2.06 we see that a 50 μm diameter cell sinks at approximately 1 m d^{-1} or 12 μm s^{-1}. According to Fig. 2.07 this sink rate might increase the nutrient flux by 30–40%. On the other hand, a cell of 10 μm would sink at only about 3 μm s^{-1}, which would give it no increase in nutrient uptake rate.

The results of Berg and Purcell's (1977) determination of the increase in diffusive transport toward a spherical cell due to relative motion are shown in Fig. 2.08, along with earlier estimates by Munk and Riley (1952) and more recent ones by Karp-Boss *et al*. (1996). Each curve shows the increase in the diffusive flux for cells moving at 10 d s^{-1} as a function of cell size. Most of the variation between the curves is probably explained by the different techniques employed. Berg and Purcell (1977) performed a fluid mechanical experiment to estimate the flux while Munk and Riley (1952) used analytical analyses and Karp-Boss *et al*. (1996) used analytical and numerical analyses. In spite of the scatter they are in general agreement that cells less than 5–10 μm in diameter sinking or swimming at 10 d s^{-1} will have little or no effect on the rate of molecular diffusion in the neighborhood of the cell. For cells of larger diameter relative motion causes a significant increase in the diffusive flux. A 30–60 μm cell, for example, will increase the flux by about 100% if it moves through the water at 10 d s^{-1}.

2.2.14 The effect of turbulence

(a) Effect of turbulence on phytoplankton cells and population

In the foregoing discussion on diffusion limitation no mention was made of the effects of turbulent motion on the rate of nutrient uptake. Turbulence, we know,

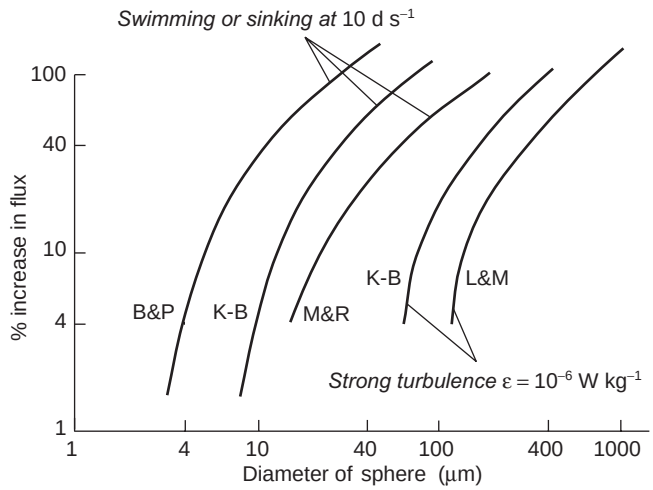

Fig. 2.08 Percentage increase in the diffusive flux toward a perfectly absorbing sphere of diameter *d* caused by the relative motion or the shear created by turbulence, adapted from Lazier and Mann (1989). The curves for relative motion are for sinking or swimming at 10 diameters per second (d s^{-1}), based on the work of Berg and Purcell (1977) (B&P), Karp-Boss *et al*. (1996) (K-B), and Munk and Riley (1952) (M&R). The data for the effect of turbulence for a dissipation rate of 10^{-6} W kg^{-1} were derived by Lazier and Mann (1989) (L&M) from the work of Purcell (1978), and by Karp-Boss *et al*. (1996) (K-B).

is a ubiquitous feature of the ocean but it is not immediately clear how the turbulent motion affects the flow around very small organisms or if that flow will alter the rate of molecular diffusion toward or away from a cell. Since the interaction between the small organisms and the turbulence cannot be observed directly in the ocean, we must rely on theoretical constructions and indirect observations.

The first discussion of the effect of turbulence on the molecular diffusion in the vicinity of small organisms is attributed to Munk and Riley (1952). They suggest that the turbulent-pressure fluctuations in the ocean create a small relative motion between the organisms and the water because the two are of slightly different densities. They conclude, however, that the effect of this relative motion on the diffusive flux near an organism would be negligible. The question was reexamined by Lazier and Mann (1989), who argued that turbulence is manifest across even the smallest distances by a linear shear whose magnitude depends on the strength of the turbulence. The shear is a property of the fluid and exists whether there are organisms present or not. The effect this shear has on the diffusion toward or away from a perfectly absorbing sphere was calculated using the experimental results of Purcell (1978). This was followed by Karp-Boss *et al*. (1996), who took advantage of analytical and numerical analyses published in the engineering literature to recalculate nutrient flux increases due to turbulent shear. The results

from these two analyses are given in Fig. 2.08, along with the curves describing the increase in flux due to relative motion. The curves show quite similar results for the effect of turbulent shear levels expected in the mixed layer of the ocean. Both curves suggest turbulence has no appreciable effect compared with that due to relative motion through the water. For stationary cells turbulence will be the only agent affecting the diffusive flux and will have an effect on cells greater than 100 μm in diameter.

Various authors have made practical investigations of the effect of turbulence on phytoplankton. Savidge (1981) created turbulence by placing an oscillating grid within a 25-liter culture. When the oscillation rate was increased by a factor of 10, nitrate uptake of the diatom *Phaeodactylum tricornutum* was enhanced by 21%, but phosphate uptake and carbon fixation decreased. Nevertheless, the growth rate increased 25–40%. For the flagellate *Brachiomonas submarina*, the higher level of turbulence resulted in a 60% increase in its growth rate. Increase in turbulence may have affected the levels of light experienced by the cells and may have contributed to the results.

The same type of apparatus was used by Howarth *et al*. (1993) to test the effect of turbulence on the nitrogen-fixing activity of heterocystic cyanobacteria. Although they used turbulence levels greater than those normally encountered in lakes or coastal waters (except perhaps in surf zones), no inhibition of nitrogen fixation was found. Howarth's group considered that, at the levels of turbulence used, anoxic microzones could not possibly have persisted on the surfaces of the cyanobacteria. In the past, anoxic microzones have been considered essential to nitrogen fixation by these organisms, and the inhibition of these zones by higher turbulence in coastal waters has been given as an explanation of the lower rates of N fixation as compared with lakes. This idea is no longer tenable.

In general it seems that turbulence stimulates the growth of many kinds of phytoplankton, but inhibits the growth of dinoflagellate populations. For example, Pasciak and Gavis (1975) subjected the diatom *Dytilium brightwellii* to shear by holding the cultures between two cylinders, one of which was rotated (a Couette device). At a shear rate of 5 s^{-1}, nutrient uptake was enhanced about 10%. Aguilera *et al*. (1994) studied the effect of turbulence, created by bubbling, on the freshwater microalga *Dunaliella viridis*. By measuring the pressure of the air in the inflowing and outflowing lines, they were able to calculate the energy supplied to the system. Over the energy range 0–2.0 W m^{-2} they found that the specific growth rate peaked at 0.63 W m^{-2} and the maximum rate of primary production occurred at 1.67 W m^{-2}. The authors concluded that the main effect of the turbulence was the breakdown of boundary layers around the cells. Interestingly, the carbon fixation rates (but not the growth rates) of cells in an unstirred medium were higher than those in low levels of turbulence (0.02–0.2 W m^{-2}). The addition of 0.2 W m^{-2} of mechanical energy permitted 0.21 W m^{-2} of primary production in the cultures. These numbers are of the same order of magnitude as those calculated for natural systems by Margalef (1978a) (see Chapter 11).

When they studied the effect of shear and turbulence on dinoflagellates, Thomas and Gibson (1990, 1992) also used a Couette device. They consistently found that

turbulence inhibited growth. For example, with *Gonyaulax polyedra*, which is responsible for "red tides" in coastal waters, the threshold for growth inhibition was about 3 s^{-1} and growth was inhibited completely above 8 s^{-1}, at which level the cells lost their flagella, so that active locomotion became impossible. Subsequent work showed that there was little or no disruption of photosynthesis during periods of turbulence, just inhibition of cell division accompanied by enlargement of individual cells. This suggested that in nature, when turbulence levels decline, cells may divide rapidly using the accumulated material (Thomas *et al*. 1995). This could explain the observations that dinoflagellate blooms seem to correspond with periods of calm water after high levels of turbulence.

Working with *Gymnodinium splendens*, which is an important food item for the first-feeding larvae of northern anchovies (see Section 5.5.2), Thomas and Gibson (1992) found that growth inhibition was present at the low level of 1 s^{-1}, but did not change much over the range 1–40 s^{-1}. Moreover, the cells remained quite healthy at all levels of turbulence and after 3–5 days appeared to acclimate and partially regain their normal growth rates. From these observations, the authors concluded that *G. splendens* is not particularly sensitive to turbulence, and the observed sensitivity of anchovy recruitment to turbulence (Sections 2.3.6 and 5.5.2) is not explained by the direct effect of the turbulence on the food organisms.

In a review of plankton production processes, Wyatt and Jenkinson (1993) pointed out that many phytoplankton species form strings or networks that straddle different turbulent structures and may increase the flow of water past their constituent cells. In other species, individual cells secrete strands or nets of mucilaginous polymers, changing the relationship of the cells to turbulence structures and strongly modifying sinking rates. Thus, the relationship of phytoplankton to the fine structure of the water column may be modified by the activities of the cells themselves.

In a later Section (2.2.17) we trace the mechanisms for the formation of aggregations of colloidal material with bacteria. Frequently, phytoplankton cells are also trapped in these aggregations, and the sinking of the aggregations may increase the flow of water past the phytoplankton cells.

In summary, these works suggest that when a species is subject to a tenfold increase in turbulent shear, it may increase the uptake of one nutrient while decreasing the uptake of another. This factor appears to have a dome-shaped relationship to turbulent shear that is different for each species, so that at high levels some species are damaged and have decreased metabolism, while others have enhanced nutrient uptake and growth. Thus, we see that the conclusions reached on theoretical grounds by Lazier and Mann (1989) are only partly borne out by experiment. Some of these differences may relate to the higher turbulence levels used in some of the experiments. Lazier and Mann (1989) considered the effects of the shear associated with turbulence levels commonly observed in the ocean – that is, turbulence dissipation rates between 10^{-6} and 10^{-9} W kg^{-1}, equivalent to shear levels between 0.56 and 0.018 s^{-1}, respectively. In most of the laboratory experiments, the shears are considerably higher – in some cases, by an order of magnitude.

(b) Effect of turbulence on mixed phytoplankton communities

Since diatoms have a dense silica cell wall and will sink in calm water, it is clear that turbulent upward motion is needed to keep them in the water column and is a prerequisite for the formation of dense populations of diatoms. This accords with observations. Diatoms predominate in the turbulent mixed layer of temperate waters in spring, in newly upwelled water in coastal upwelling systems, and in tidally mixed waters of estuaries. Cushing (1989) drew attention to the fact that many of the great fisheries are dependent on a food chain that begins with diatoms and proceeds by way of copepods to young fish. It might be thought that the abundance of diatoms and hence the productivity of the fisheries could be explained mainly by the diatoms' ability to increase their nutrient uptake by sinking. This is not so. Kiørboe (1993) showed that even in turbulent waters, smaller cells still have the potential to out-perform the larger diatoms. He suggested that the predominance of diatoms is explained by the fact that their size gives them a temporary refuge from predation. The smaller cells are preyed upon by small heterotrophs such as protozoa, which reproduce rapidly and maintain a constant predation pressure, while diatoms are preyed upon by copepods and similar mesozooplankton which require several weeks to build up their population density. During the build-up period the diatom populations can grow to bloom proportions while the small cells are still held to low population densities by their predators. An interesting observation of coexisting diatoms and dinoflagellates in an estuary (Lauria *et al*. 1999) showed that the stability within the water column during slack water periods permitted surface aggregation of dinoflagellates, while diatoms rely on increased turbulence during ebb and flood tides to bring them in to surface waters. These matters are discussed further in Chapters 3 and 4.

It seems that the effect of turbulence can been seen across the size spectrum of phytoplankton, and is not confined to the separation of diatoms from flagellates. Rodriguez *et al*. (2001) used an image-analysis system to count and size phytoplankton collected from a turbulent region of the northwest Mediterranean Sea. They plotted the size–frequency distribution and found that the regression of log abundance on log cell volume was always negative. They calculated for each sample the vertical velocity, using hydrodynamic measurements, and found that in the range of vertical velocity between –5 and +5 m d^{-1} the slope of the regression decreased with increasing vertical velocity (Fig. 2.09). In other words, the relative proportion of larger cells increased with increasing vertical velocity. The authors suggested that there is a direct effect of vertical velocity on the size spectrum, rather than an effect mediated by upwelled nutrients.

Flow cytometry is another technique that permits the rapid counting and sorting of phytoplankton cells. Li (2002) distinguished between picophytoplankton (<2 μm), small nanoplankton (2–10 μm) and large nanoplankton (10–20 μm), and related their abundance to the stratification index as an indicator of degree of turbulent mixing. Numbers of the small nanophytoplankton remained constant, but the numbers of the larger cells increased with decreasing stratification (= increasing turbulence), while the numbers of the smallest cells decreased. Cell diversity was

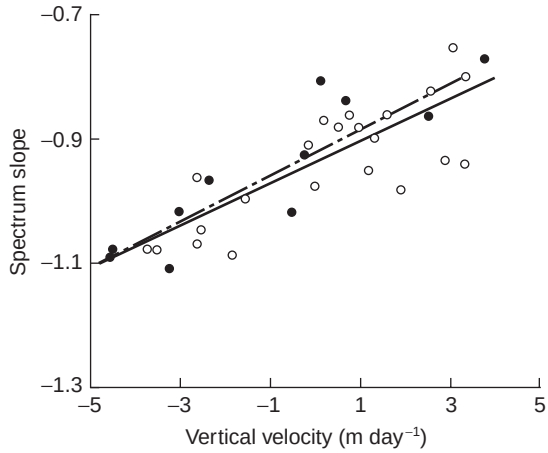

Fig. 2.09 Slope of the size–abundance spectrum (open circles), plotted against vertical velocity, in the range ±5 m d^{-1}. Continuous line is linear regression; filled circles are data from the deep chlorophyll maximum, and are fitted by the broken line. From Rodriguez *et al*. (2001). Reproduced by permission of Nature Publishing Group.

greatest at intermediate levels of stratification. If we consider turbulence as a disturbance, this result is in accord with the general ecological theory that community diversity is at a maximum at intermediate levels of disturbance.

(c) Effect of turbulence on mixed phytoplankton and zooplankton communities

There are indications that the effects of turbulence on whole plankton systems may be different from their effects on individual phytoplankton populations. Petersen *et al*. (1998) experimented with replicated 1 m^3 experimental ecosystems in which all elements of a coastal plankton except fish were represented, and which were subjected to differing levels of turbulent mixing. Mixing reduced the abundance of copepods (Fig. 2.10) and gelatinous zooplankton, caused modest increases in primary production, but had negligible effects on the productivity or respiration of the whole system. It seems possible that ecosystem-level processes in planktonic systems may be less sensitive to differences in small-scale turbulence than are community and population dynamics.

Working in a natural community on Georges Bank, Incze *et al*. (2001) found that larval stages of copepods were at the bottom of the surface mixed layer when the water was stratified. When turbulence dissipation rates increased as a result of wind stress the larval stages were found in the pycnocline at 20–25 m depth. After passage of the wind event the organisms returned to their previous distribution. These distribution changes could affect the whole trophic food web.

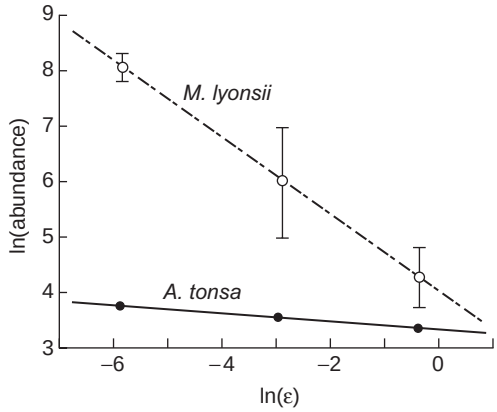

Fig. 2.10 Relationships between zooplankton abundance and the turbulent energy dissipation rate (ε) in three mixing treatments. Values for the gelatinous zooplankter *Moerisia lyonsii* are means ±SE. Error bars for *Acartia tonsa* abundance are smaller than the width of the symbols. From Petersen *et al*. (1998). Reproduced by permission of Inter-Research.

2.2.15 The paradox of cell growth in low-nutrient environments

Photosynthesis has been shown to occur in waters where the concentration of nitrogenous nutrients falls below the limit of detection (McCarthy and Goldman 1979). How can phytoplankton be physiologically active and grow enough to maintain their populations when nutrients appear at such a low level? It has been suggested that the phytoplankton can take up the nutrients from small local concentrations such as might be produced by the excretion of a single zooplankton organism, or the regenerated nutrients from the bacterial decomposition of a particle of organic matter. Lehman and Scavia (1982a, 1982b) produced experimental evidence and models in support of the claim that the freshwater alga *Chlamydomonas* could derive nutrients from the excretion of the zooplankter *Daphnia pulex*. In contrast, Jackson (1980), Williams and Muir (1981), and Currie (1984) argued that the natural concentrations of organisms and the probable rates of nutrient dispersal by turbulent diffusion rendered the transfer of nutrients from zooplankton to phytoplankton insignificant.

The case for transfer of nutrients from bacteria to phytoplankton rests on the observation that small particles of organic matter, which are often formed on the surfaces of bubbles (Riley 1970), tend to form aggregates that are widely distributed in the ocean (Silver *et al*. 1978, Silver and Alldredge 1981). These aggregates typically contain concentrations of bacteria, protozoa, and phytoplankton. Goldman (1984b) put forward an "aggregate spinning-wheel hypothesis" (Fig. 2.11) according to which phytoplankton, micrograzers, and bacteria live attached to the surfaces of the aggregates and are involved in the rapid recycling of nutrients.

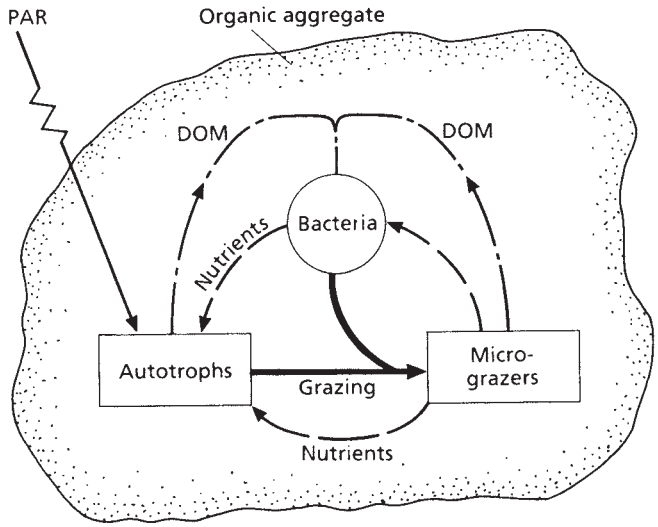

Fig. 2.11 Conceptual scheme of a microbial food chain within a discrete organic aggregate. DOM, dissolved organic matter; PAR, photosynthetically available radiation. From Goldman (1984b).

Evidence suggests the existence of both photosynthesis and respiration within aggregates (Alldredge and Cohen 1987) and the presence of elevated concentrations of phosphate ammonium and nitrate (Shanks and Trent 1979). We shall return to this topic in Section 2.2.17.

2.2.16 Uptake of nutrients by bacteria

(a) In the absence of turbulence

Jumars *et al*. (1993) reviewed uptake of nutrients by bacteria free-living in the plankton. Heterotrophic bacteria (i.e., those that do not perform photosynthesis) receive their energy supply from the uptake of organic nutrients from solution by a process known as osmotrophy. They may take the nutrients directly from the surrounding water or they may attach themselves to particles and secrete exoenzymes that convert the particulate material to soluble form. In the following discussion, we shall see that bacteria attached to particles appear to take up nutrients faster, and the processes that convert dissolved organic matter to particulate form are critical to the nutrition of marine bacteria in the water column.

Because the surface area of a sphere increases as the square of the radius, while volume increases as the cube of the radius, it was once thought that organisms that rely on diffusion for the transport of nutrients should maximize their surface-area-to-volume ratio by being as small as possible. Jumars *et al*. (1993) have shown that the optimum size for an osmotrophic bacterium changes with the external

concentration of nutrients. In a stagnant, homogeneous ocean, the rate of flux of a nutrient to a spherical cell, J_D (mol cell^{-1} T^{-1}), by diffusion alone is given by

$$J_D = -4\pi r_o D(C_\infty - C_o) \tag{2.17}$$

where r_o is the radius of the cell, C_∞ is the ambient concentration of the nutrient beyond the boundary layer, and C_o is the concentration at the cell surface. Therefore, a cell can increase the flux to itself by enhancing its active uptake system, thus lowering C_o, or by increasing the cell radius. The rate of use of the diffusing substance varies as T_o^a where a lies between 1 and 3. As a consequence of an uptake rate that changes linearly with cell radius and a use rate that changes nonlinearly, the optimum cell size depends on the ambient concentration of nutrients and is larger for cells in high-nutrient conditions than for those in low-nutrient conditions. This requirement explains the empirical observation that bacteria tend to be larger in high-nutrient conditions. In the context of optimal feeding strategies, we may extend the consideration of optimal conditions for a given organism to include risk of predation. As large size increases vulnerability to predators, the size of a bacterium which maximizes population growth may therefore be smaller than that dictated by nutrient considerations alone. The importance of leakage of metabolites from cells of different sizes appears not to have been investigated in this context.

(b) In the presence of turbulence

In a turbulent water column, the shear created by the turbulence can affect the diffusive flux toward an organism, but (as we saw in Section 2.2.14) this effect is negligible for organisms of diameter around 1 μm, which might be taken as typical for bacteria. On the other hand (as will be discussed in Section 2.3.5), turbulence increases the encounter rate between a predator and its prey, and in the context of optimal feeding strategy this effect may not be negligible, even for bacteria-size organisms.

Simulation models have been used to investigate whether bacteria could, by active locomotion, improve their chances of encounter with the cloud of leaked organic matter surrounding a phytoplankton cell. Jackson (1989) did not include the effects of turbulent shear, while Bowen *et al*. (1993) included them. The basic conclusion was the same in each case. Clusters of bacteria around exuding phytoplankton cells are unlikely to significantly change either the uptake of nutrients by the phytoplankton or the magnitude and fate of bacterial production.

(c) In the presence of turbulence and predators

To test whether the effect of turbulence on bacteria would be different if their natural predators were present, Peters *et al*. (1998) took natural sea water and filtered it (a) through 0.8 μm filters to remove everything except the bacteria and (b) through 150 μm filters to remove mesozooplankton but allow the phytoplankton and the

protozoan predators to pass. As predicted, turbulence had no effect on the abundance and activity of bacteria isolated from the remainder of the microbial community, but when this community was present turbulence caused an increase of bacterial numbers and activity. They postulated that the turbulence increased the prey encounter rate of the protozoa and permitted them to shift from preying on bacteria to preying on the larger but less abundant phytoplankton. Thus, predation pressure on bacterial populations was removed and their populations were able to grow.

The realization that predation interacts with turbulence to modify the structure of planktonic populations is one of the more significant advances in this field during the 1990s.

2.2.17 Bacteria and colloids

Molecules in true solution are usually less than 1 nm in diameter, and are distinguished from particulate matter by their ability to pass through very fine filters. Occupying the size range of 1 nm to a few micrometers are colloids, which have properties that are in some ways intermediate between dissolved and particulate fractions. In their relationship to bacteria, colloids may often be treated as particles.

The colloidal fraction represents a reservoir of organic matter in the ocean that has a far larger mass than either the phytoplankton or the bacteria, though it is not readily accessible to bacterial degradation by virtue of its particle size characteristics (1 nm to a few μm). A number of mechanisms in the ocean tend to cause these colloids to aggregate, however, after which they are more readily attacked by bacteria. The process has been reviewed by Kepkay (1994).

The basic mechanisms causing colloids to aggregate are:

1 Brownian motion, in which particles undergo random walk caused by the impact of solute molecules.
2 Shear, in which particles traveling at different speeds in shear flows collide.
3 Differential settling, in which particles sinking at different rates collide.
4 Diffusive capture, in which a particle is advected until it enters the diffusion-limited boundary layer of another particle. It is effectively captured and will eventually collide with that particle.
5 Surface coagulation, in which colloids are trapped on the surfaces of rising bubbles.
6 Filtration, either by organisms with special mechanisms for filtering very small particles or by sinking macroaggregates known as marine snow (see Section 2.2.15), which are often porous, so that water passes through them and colloidal particles are captured.
7 Bacterial motility. A few observations have been made of bacteria moving fast enough and far enough to capture colloidal particles, but it is not known how important this process is relative to those already mentioned.

The first of these mechanisms, Brownian movement, causes small colloidal particles to collide and create small aggregates. These aggregates again collide, until they form particles several μm in diameter, a process referred to as the Brownian pump.

The next three mechanisms lead to still larger aggregations in which the bacteria themselves are included. The resulting aggregate provides an excellent site for bacterial feeding and multiplication. Furthermore, it is large enough to undergo a significant rate of sinking, with consequent renewal of the supply of gases and nutrients at its boundary layer. With the capture of phytoplankton and the arrival of micrograzers, such an aggregation has all the components necessary to fit Goldman's "aggregate spinning-wheel hypothesis" (see Section 2.2.15).

Coagulation on the surface of bubbles has long been suspected as an important mechanism for converting dissolved organic matter to particulate form. Some quantification of this process has been achieved. Kepkay and co-workers have found that coagulation by bubbles leads to a marked increase in food available to bacteria and thereby to increased bacterial respiration. A storm at sea can lead to a 36-fold increase in respiration, lasting for two to four hours.

Alber and Valiela (1995) used bubbles to coagulate dissolved organic matter released from decaying seaweeds. This material was labeled with ^{15}N (by growing the algae in a solution of $^{15}NH_4Cl$), and it was shown that bay scallops *Argopecten irradians* ingested the particles formed in this way and incorporated the labeled N in their tissues. This process demonstrates that dissolved organic matter released by decaying algae can be a significant pathway for the transfer of energy and materials to filter-feeding macroinvertebrates.

Marine aggregates, often known as "marine snow," are frequently formed during algal blooms. The algae may aggregate with one another or they may be captured in colloidal aggregates. Either way, their rate of sinking is accelerated, since large particles sink faster than smaller ones. It is thought that aggregation and sinking is a major component of the loss of algae from surface waters. Modeling the sinking process requires a knowledge both of the aggregation process and of the changes that follow when aggregates break up due to turbulence.

Aggregation theory is well developed and has been checked against natural phenomena (Jackson 1990, 1995). The essential terms are the initial concentration of the cells, C_1, their radius, r, the shear rate, G, and a stickiness coefficient, α. By also introducing a specific growth rate, g, Jackson (1990) was able to include both the increase by growth and the loss by aggregation and sinking:

$$dC_1/dt = gC_1 - 20.8\alpha r^3 GC_1^2 \tag{2.18}$$

This is a two-state system, with aggregation a relatively unimportant term at low cell concentrations, but increasingly important as the cells become more abundant. Fig. 2.12 shows results from the North Sea from Riebesell (1991).

However, it appears that the aggregates break up in surface waters when the turbulence levels are high (Riebesell 1992). Ruiz and Izquierdo (1997) provided a model for this break-up, thus completing the dynamic equation for the dynamics of pelagic particles presented by McCave (1984).

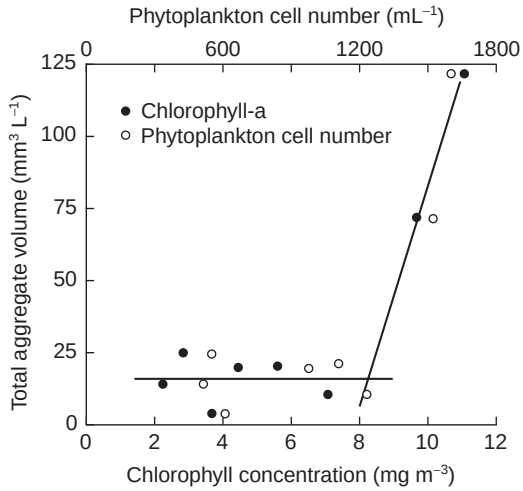

Fig. 2.12 Total volume of aggregated cells plotted against cell concentrations (cells mL^{-1}) and equivalent chlorophyll concentrations, in samples from the North Sea. Note the sharp increase in aggregation at higher concentrations of cells and chlorophyll. From Riebesell (1991). Reproduced by permission of Inter-Research.

2.2.18 Reductionist modeling of phytoplankton population dynamics

Various models have been put forward to provide insights into specific aspects of the ecology of phytoplankton, but Baird and Emsley (1999) suggested that it is now possible to work towards a model of phytoplankton population dynamics, based on several of the physical mechanisms discussed in this chapter. Their model contained formulations based on individual species characteristics, derived from measurements in laboratory experiments. They included such features as diffusion and convection of nutrients to phytoplankton cell surfaces, light capture by phytoplankton pigment assemblages, sinking rates of phytoplankton cells, and encounter rates of predators and prey. Nutrient uptake to a single phytoplankton cell, J, was represented by

$$J = \Psi D\, Sh\, (C_b - C_w) \tag{2.19}$$

where Ψ is the effect of cell shape on the rate of diffusion, D is the molecular diffusivity of the nutrient, Sh is the Sherwood number, C_b is the background nutrient concentration, and C_w is the concentration at the wall of the cell. The shape factor was derived from theoretical considerations, taking the cell shape as the nearest approximation to a sphere, oblate spheroid, prolate spheroid, general ellipsoid, or cylinder. The Sherwood number is a dimensionless relative measure of the additional flux of nutrients due to the motion of fluid surrounding the cell.

The basic equation for nutrient uptake was modified by consideration of such factors as internal cell quota of a species for a specified nutrient, and enzyme-mediated processes at the cell surface. Light capture was modeled as a function of incident light, wavelength, pigment concentrations, cell geometry, and the presence of other attenuating components in the water column. Phytoplankton growth was modeled by analogy to chemical kinetics, as a function of intracellular nutrient and energy reserves. It was therefore temperature-dependent. Each species was allocated an appropriate sinking rate (see Section 2.2.11) and grazing loss was calculated using the principles discussed in Section 2.3.5.

The dynamics of mixed-species populations were modeled by constructing a system in which the equations for the various species interacted. Simulations were run at environmental conditions similar to the oceanic mixed layer at Bermuda and a North Atlantic weather station *India* (59° N 19° W), and compared to earlier models and to field data sets. Many features were well represented by the model, but some were not. The authors suggested that it would be worth persevering to improve the model, because it is particularly suitable for being coupled to a multilayer, turbulent closure mixing model.

2.2.19 Conclusions

We have seen that a phytoplankton cell that remained neutrally buoyant in still water would soon deplete the nutrients in the water surrounding it and create a gradient. Under these conditions, the only mechanism that would tend to replace the nutrients would be molecular diffusion. This mechanism may be adequate for very small cells of the order of 1 μm, but it tends to be extremely limiting of the metabolism of phytoplankton of the scale 10–100 μm. It has been proposed that they overcome this difficulty by either sinking or swimming, rather than floating neutrally buoyant. A detailed study of the dynamics suggests that the observed rates of sinking go some way toward reducing diffusion limitation, perhaps enough to account for one species having a competitive edge over another, but even then the uptake rate of nutrients is likely to be no more than one-third of what the rate would be in the absence of diffusion limitation.

Swimming is found in all classes of organisms from bacteria-size upward. For bacteria and picoplankton it seems that the role of swimming is to move the organisms to regions of higher nutrient concentration. The relative importance of viscosity is so great for these organisms that their locomotion does not materially change their diffusion limitation. For cells of about 100 μm the effect of viscosity is less drastic, and it has been calculated that at observed rates of swimming they have the possibility of reducing diffusion limitation by about one-third.

There has been some study and much speculation about the possibility that the excretion of microbes and animals creates microzones of high nutrient concentration in the sea, and that phytoplankton are capable of taking advantage of them. Most calculations from field conditions suggest that the nutrient plumes generated by zooplankton are too few, and disperse too rapidly to be of great significance to phytoplankton.

An idea that is still largely untested holds that, especially in oligotrophic seas, amorphous organic aggregates function as miniature ecosystems. Phytoplankton cells live in close proximity to bacteria on the surfaces of the aggregates. The bacteria may be consumed by micrograzers such as ciliates and these organisms may be responsible for the excretion of the nutrients needed by the phytoplankton. These ideas are intriguing but await further investigation.

Consideration of the problems facing bacteria in their need to absorb organic molecules in solution shows that uptake from solution in the water column is subject to severe limitations but that the progressive formation of ever-larger aggregations of colloids may lead to the formation of particles to which bacteria become attached and feed by the production of exoenzymes that convert the particulate matter into soluble form for absorption.

Aggregations formed when phytoplankton collide, or when phytoplankton and bacteria are captured in colloidal aggregates, have the effect of holding all the microscopic elements of a planktonic food web in close proximity. It is possible that nutrient fluxes and trophic interactions are accelerated, but details are lacking.

2.3 Zooplankton

2.3.1 Life in a viscous environment

For particles of the size of phytoplankton, inertial forces are very small and by comparison viscous forces are strong and predominate. As a consequence, the relationship between a zooplankter and its food is quite different from anything in our own experience. Viscous flow is reversible, and a limb moving backward and forward creates a symmetrical pattern of flow. A copepod may scratch a bacterium from its surface, but if the motion is symmetrical the bacterium will return to the place of origin. A complex asymmetrical movement must be made if the bacterium is to be removed from the cuticle (Strickler 1984). On the other hand, viscous properties can be used to advantage when feeding. Algae captured by copepods and assembled between the setae of the mouthparts will remain there so long as the mouthparts make only symmetrical movements.

When it comes to swimming, zooplankton occupy an interesting transitional range of Reynolds number, between 0.1 and 500 (Fig. 2.03). At the scale of the setae on the feeding appendages, viscous forces are important and inertial forces are trivial. However, some copepods are capable of accelerating their mass to 35 cm s^{-1} and inertial forces can then be exploited (Strickler 1984).

2.3.2 Feeding in a viscous environment

The effect of boundary layers on the action of mouthparts, when viscous forces are predominant, is graphically illustrated by a scaled-up model (Strickler 1984). The medium is honey, the food particle to be captured is a grain of rice, and the

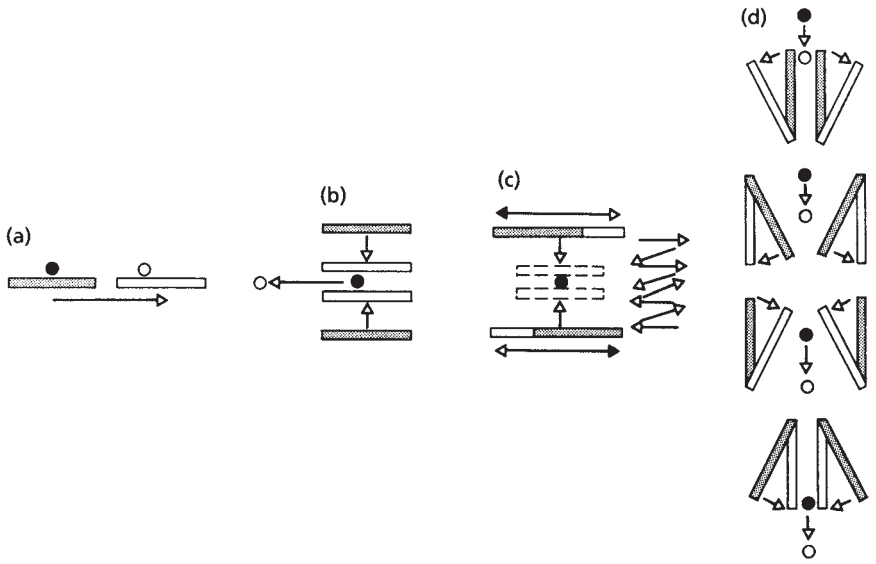

Fig. 2.13 Diagrams of experiments on low-Reynolds-number flow. Starting positions are shaded. For details see Section 2.3.2. Modified from Strickler (1984).

mouthparts are a pair of knife blades. Figure 2.13(a) shows that if a food particle is close to the surface of the mouthpart and that mouthpart is moved in a direction parallel to its flat surface, the particle will move with it, because the medium closest to the blade does not slip, and layers of medium progressively further from the blade are drawn along by viscous stress. Figure 2.13(b) shows that if the two mouthparts are brought together in the vicinity of the food particle (a clap) the particle escapes because its inertia is negligible compared with the viscous forces carrying it away in the fluid (in contrast to the situation in which we successfully capture a mosquito in air by clapping). Figure 2.13(c) shows that if the mouthparts move in opposite directions simultaneously they can exert equal and opposite viscous drag forces on the particle so that it remains approximately stationary and is captured. Finally, Fig. 2.13(d) shows a technique that has come to be known as "fling and clap." The two mouthparts are flung apart, drawing in a parcel of medium containing the food particle. The edges closest to the inflow then converge behind the particle, effectively trapping it.

Koehl and Strickler (1981) tethered specimens of *Eucalanus pileatus* in an optical glass cuvette holding 120 mL of water. They took high-speed cinematographic movies of the feeding process while India ink was released from a micropipette close to the animal. They found that second antennae, mandibular palps, first maxillae, and maxillipeds combined in action to produce a pulsing stream of water past the ventral side of the animal. When a food particle came within range, the appendages began to beat asymmetrically, simultaneously drawing the particle toward the midventral line and turning the animal toward the particle. At the critical moment, the second maxillae performed a fling-and-clap movement that

drew the alga and a small volume of water into the space between them, then closed in to retain the alga while forcing the surrounding water out through the spaces between the setae. There are several important points to note. First, forcing water continuously through a fine sieve is an energetically costly activity, and the copepods avoid much of this cost by scanning the water moving past them and forcing through the second maxillae only that small volume of water surrounding the food particle. Second, the flow of water around and between the setae of the second maxillae is very different on the small scale and low *Re* from what we expect from observing events on the larger scale, and it seems that algae are often directed into the mouth without actually making contact with the setae. When they do make contact with the setae, they stick, as mentioned earlier, and they are combed off by the endites of the first maxillae. The large-scale analogue of this operation is using a fork to comb crumbs off another fork when both are immersed in honey (Koehl 1984) – clearly not a trivial task.

The observations that the feeding appendages change the symmetry of their beat when an alga is in the proximity shows that there is a mechanism for sensing the algal presence before it makes any contact with the copepod, and that the animal is performing a "detect and capture" operation rather than behaving as a passive filter-feeder.

Using a technique of laser-illuminated video monitoring, Yen *et al*. (1991) investigated the paths taken by algal particles and used them to reconstruct the flow fields around the copepod *Euchaeta rimana* when it is feeding. They noted that the currents generated by the appendages served not only to enable the animal to detect and capture prey, but also to maintain the animal in position in the water column, by overcoming negative buoyancy. They found that the sheared laminar flow was most intense near the paired second antennae, but decreased rapidly as distance from the animal increased. They interpreted this condition as an adaptation to minimizing the information available to potential predators, as the currents and associated patterns of turbulence could be used by the copepod's predators to detect its presence.

The authors also compared energy dissipation generated by the animals with that caused by purely physical processes. Viscous energy dissipation rates within the feeding current were higher than those due to natural turbulence, although the rates lost this advantage when spatially averaged, except possibly in the case of very dense swarms of copepods. The spatially averaged vertical eddy diffusivity caused by feeding currents was several orders of magnitude less than that caused by turbulence.

2.3.3 Detection of food

The first evidence that free-swimming copepods attack *non-motile* inert particles located outside the influence of the feeding current was presented by Bundy *et al*. (1998). *Diaptomus sicilis* was observed, by laser-illuminated video monitoring, in the process of attacking and capturing 50-μm-diameter polystyrene beads that

were outside the influence of the copepod feeding current. The beads were often more than half a bodylength away and were attacked after the "bow wake" of the moving copepod displaced a bead away from the copepod. A finite-element numerical model was used to reveal that under these conditions fluid velocity fluctuations and streamline deformations arise in the region between the two objects. These changes could almost certainly be detected by mechanoreceptors on the first antennae. Since the particles were inert, the study also demonstrated that chemoreception does not necessarily play a part in prey detection.

If mechanoreceptors can detect deformation in streamlines and water velocities, the possibility is open that predators can detect feeding crustaceans by the changes they produce in the turbulent field in their wakes, as well as by their chemical traces. The forms of these wakes vary from one species to another. Yen and Strickler (1996) showed that *Euchaeta rimana* produces a relatively uniform, smooth velocity gradient, while Gries *et al*. (1999) found that the freshwater *Daphnia pulicaria* produces complex patterns depending on the swimming behavior. The wake volume is much greater than the volume of the organism itself, and it is likely that these wakes play an important role in detection of prey by the zooplankton predators, and in the transmission of chemical signals (such as mating pheromones) from one zooplankter to another.

2.3.4 Calculation of mesozooplankton feeding rates

A lack of agreement exists between measurements of mesozooplankton feeding rates in the laboratory and calculations made on the basis of budgets constructed for field situations. In general, the latter calculations suggest much higher figures. The evidence was reviewed by Cushing (1975). One of the few laboratory data sets to obtain high rates of feeding approaching those deduced from field observations was obtained by Corner *et al*. (1972). These workers carried out the experiments in glass columns that were rotated in the vertical plane and completed one revolution every two minutes. Although the strategy was intended to ensure that the phytoplankton cells remained in suspension throughout the experiment, the method also maintained a relatively high level of turbulence in the containers. Corner *et al*. found that the maximum daily rations of the zooplankton were equivalent to 47.5% of the body nitrogen.

Cushing (1968) developed a theory of grazing in which the herbivore is assumed to search a volume that is the product of the area swept by the sensors and the distance swum. As the animal stops to eat, the volume searched becomes reduced. Others have modified the concept by introducing irregular swimming tracks and varying speeds of swimming, and by introducing threshold densities of food below which the animals did not feed. Many of the assumptions underlying this work have been challenged by Rothschild (1988), whose basic thesis is that the rate of contact between a planktonic organism and its food is strongly affected by small-scale turbulence in the water. Building on the theoretical formulation of Gerritsen and Strickler (1977), he developed an example using data for

Table 2.02 Relative velocity and number of contacts among different kinds of organisms. Zero, low-turbulence (0.005 cm s^{-1}), and high-turbulence (0.02 cm s^{-1}) RMS velocity, *w*, is incorporated in the computation. From Rothschild (1988).

		Bacteria		*Phytoplankton*		*Nanoplankton*	
	Turbulence	*Relative velocity*	*Contacts per hour*	*Relative velocity*	*Contacts per hour*	*Relative velocity*	*Contacts per hour*
Pseudocalanus	Zero	720	22×10^6	720	2262	721	4.5×10^4
	Low	720	22×10^6	720	2262	721	4.5×10^4
	High	1187	37×10^6	1187	3729	1188	7.5×10^4
Nanoplankton	Zero	36	113	36	—	—	—
	Low	43	135	43	—	—	—
	High	961	3019	961	0.03	—	—
Phytoplankton	Zero	0.1	1	—	—	—	—
	Low	24	301	—	—	—	—
	High	960	12,064	—	—	—	—

Georges Bank during the month of May, from Backus and Bourne (1987). Using wind velocities of 10 knots and 20 knots, Rothschild made some assumptions about levels of turbulence in the mixed layer and calculated the root-mean-square (RMS) turbulent velocities. He then calculated the contact rates shown in Table 2.02, which show that turbulence has an important effect. The impact affects the smallest organisms most dramatically, because their rates of locomotion are small compared with the velocity of the turbulent water. The rates of contact of bacteria with phytoplankton are enhanced 3–4 orders of magnitude by high turbulence, and even the contacts of macrozooplankton with phytoplankton are almost doubled.

Several experiments have been designed to test the theoretical developments of Rothschild (1988) and Rothschild and Osborn (1988). In the sections which follow, most of the experimental results are for mesozooplankton and fish. However, calculations show that the effect of turbulence on feeding rates should be even stronger in microzooplankton, and should enhance contacts between bacteria and potential food particles.

Saiz and Alcaraz (1991) followed the development and growth of the copepod *Acartia grani* in replicated 10-liter containers, half of which were turbulent (vertical eddy diffusivity coefficients 1–5 $cm^2\ s^{-1}$) and the other half quiescent, with food present in excess. Growth was accelerated and development time shortened in the turbulent chambers throughout the naupliar stages. The effect was less marked in later development stages, however, and the total development time through to the adult was not significantly different in the two treatments. The authors acknowledged that the effect on naupliar growth could have been caused partly by differences in the composition of the planktonic food community under the different turbulence regimes.

In a study of behavior of another species of *Acartia* at three levels of turbulence, Saiz and Alcaraz (1992) found that the highest level of turbulence increased feeding activity by a factor of 2.7, but also increased a locomotory activity known as "jumping" by a factor of 1.7–1.9. It was not clear whether the increased metabolic activity of "jumping" burned off the additional energy acquired through increased feeding.

Food abundance can change the effect of turbulence on zooplankton. Saiz *et al*. (1992) determined feeding rate (food clearance rates and ingestion rates) and gross growth efficiency (from rate of egg production) at two levels of turbulence and in saturating and non-saturating food conditions. For all three species studied, turbulence significantly enhanced feeding rates in non-saturating food conditions, but not in saturating conditions. With one species, *Acartia clausi*, feeding declined at higher levels of turbulence, even at low food concentrations. Saiz *et al*. suggested that, while moderate levels of turbulence enhance encounter probability, strong turbulence could have a detrimental effect on the feeding currents used to ingest the prey.

Working with another species, *Acartia tonsa*, Saiz and Kiørboe (1995) found that it exhibits two different feeding modes, each of which is affected differently by turbulence. When feeding on small phytoplankton cells it sets up a feeding current and acts as a suspension feeder. When feeding on motile prey it acts as an ambush feeder, i.e., it hangs in the water without moving the feeding appendages and detects its ciliate prey from the hydromechanical disturbance created by the swimming of the ciliate. It then jumps towards the prey, attempting to catch it. Turbulence had a minimal effect on the rate of filter-feeding, but considerably enhanced the rates of successful ambush feeding, up to four times the rates found in the absence of turbulence. Very high levels of turbulence depressed rates for both suspension feeding and ambush predation.

Using these and other similar observations, Caparroy and Carlotti (1996) simulated the physiological processes of ingestion, assimilation, and gut clearance for *Acartia tonsa*. They showed that by switching from suspension feeding on diatoms in calm conditions to ambush predation on ciliates in turbulent conditions, the copepod is able to maintain a good growth efficiency over long periods.

Osborn (1996) suggested that the original assumption in the Rothschild and Osborn (1988) model, that copepods normally feed by sweeping prey from a volume of water that moves past them, may be incorrect. It seems possible that they set up feeding currents which trap the prey, even though they are well beyond the range of visual or chemical detection, causing the particles to move towards the copepod by turbulent diffusion. The difference would be that in the swept-volume model there should be a volume of algae-depleted water behind the animal, while in the turbulent-diffusion model the algae-depleted volume would be mostly in front of the animal. This suggestion has been taken seriously by several investigators (e.g. Strickler *et al*. 1997). They pointed out that observations on tethered animals cannot be expected to yield realistic results because the copepods cannot move with the turbulence and encounter abnormally large changes in flow conditions around their bodies. Therefore, detailed

observations of the feeding of free-swimming animals is called for – a daunting task.

Yamazaki *et al*. (1991) investigated plankton contact rates in a turbulent flow simulated directly from the Navier–Stokes equations, using a Reynolds number of 38. In all cases, a significant increase in contact rates occurred when turbulence was present, compared with the "no turbulence" scenarios.

In general, the theoretically derived ideas of Rothschild and Osborn – that turbulence strongly affects contact rates between zooplankton and their prey – are supported by experimental evidence. However, there are qualifications. The effect is more marked at low food concentrations than at food saturation, and a dome-shaped relationship probably exists, with feeding rate declining when turbulence is too strong

A further complication is introduced by observations on the distribution of marine snow in natural water columns (MacIntyre *et al*. 1995). Marine snow (aggregated particles over 0.5 mm diameter) off central California appears to be more abundant at density discontinuities in the water column. Various mechanisms, including patterns of turbulence, have been suggested to account for this accumulation. The net result is that marine-snow aggregations are more vulnerable to grazers than are individual small particles, both because very small particles are aggregated in the marine snow and because the marine snow is aggregated at certain depths in the water column.

2.3.5 Turbulence and food contact rates in larval fish

The influence of wind- and tide-induced turbulence on the encounter rates between larval fish and their zooplankton prey was quantified in simulation models by MacKenzie and Leggett (1991). They found that failure to consider the influence of small-scale turbulence when prey density was less than 35 L^{-1} could result in as much as an 11-fold underestimate of contact rates, under conditions prevailing at tidal fronts in summer. As a result, they suggested that turbulence may be a factor stimulating food-chain productivity at such fronts.

We should not, however, assume that increase in turbulence will enhance larval fish ingestion over the whole range of small-scale turbulence in nature. MacKenzie *et al*. (1994) modeled the probability of ingestion as the product of the probability that the prey is encountered and the probability of successful pursuit. The latter measure was quantified by calculating the probability, for different levels of turbulence, that the prey will remain within the larva's encounter sphere long enough for it to approach and orient toward the prey, and then adopt an effective strike position. This interval is called the pursuit time. The encounter probability was calculated in the usual way from Rothschild and Osborn (1988). They concluded that the relationship of feeding rate to turbulence is dome-shaped. At low levels of turbulence, a rise in turbulence increases the feeding rate; at high levels of turbulence, a rise in turbulence decreases the feeding rate by disrupting the pursuit after initial encounter.

Sundby and Fossum (1990) sought empirical evidence for the effect of turbulence on the feeding rate of cod *Gadus morhua* larvae. They collected data on the number of prey per cod larval gut, the concentration of prey (*Calanus finmarchicus* nauplii), the wind speed, and static stability of the water column, expressed as

$$F = W^3/N \tag{2.20}$$

where N is the average Brunt–Väisälä frequency between 5 and 25 m depth, and W is the average wind speed during 8 hours previous to the sampling.

Sundby and Fossum found that as the wind speed increased from 2 m s^{-1} to 6 m s^{-1}, the contact rate increased by a factor of 2.8. This result was in reasonable agreement with the theory of Rothschild and Osborn (1988). Substituting reasonable values for the predator speed, prey speed, and RMS turbulent velocity in their equation gave an increase in contact rate of 2.2 times for the same change in wind speed. They found that when wind speeds were in excess of 4 m s^{-1}, turbulent velocity made a greater contribution to contact rate than larval swimming speed. Sundby and Fossum concluded that wind speed is an important factor in year-class survival and subsequent recruitment.

In further studies (Sundby *et al*. 1994), the feeding rate of cod larvae off northern Norway was found to increase by a factor of 7 as the wind speed increased from 2 to 10 m s^{-1}. Under these conditions, any negative effect of wind speed on feeding rate must occur at levels higher than 10 m s^{-1}. These results do not necessarily contradict the results of modeling studies reported earlier. It is likely that the density gradient factors influencing the Brunt–Väisälä frequency at the study site were not the same as those in the model. Hence, the relationship between wind speed and turbulence would be different.

Sundby (1995) extended his studies to a consideration of the feeding of cod larvae from first hatching to 65 days of age. During this time the larvae grew and increased their swimming speed, but also changed to larger prey items, present at lower concentrations. The increase in contact rates was calculated for wind speeds of 2.5, 5.0, and 7.5 m s^{-1}. For the largest larvae, their swimming speed is much greater than the turbulent velocity and the effect of turbulence on contact rate is minimal. The turbulence-induced contact rate is at its maximum for the slowly moving first-feeding larvae, reaching a value of nearly 8 times the still-water rate for a wind speed of 15 m s^{-1} and low prey concentration. Even for 2-month-old larvae, the contact rate is enhanced 2.5 times at high wind speeds and average prey concentration

The feeding rate of haddock *Melanogrammus aeglefinus* larvae on Georges Bank showed an interaction between larval size, abundance of prey, and turbulent dissipation rate (Lough and Mountain 1996). Feeding rate was estimated from gut contents, and turbulence dissipation rate was modeled using information on wind speed and tidal currents. As Fig. 2.14 shows, 5–6 mm larvae had highest feeding rates at low turbulence and high prey densities. The 7–8 mm and 8–9 mm larvae also had a maximum feeding response at high prey densities and low turbulence,

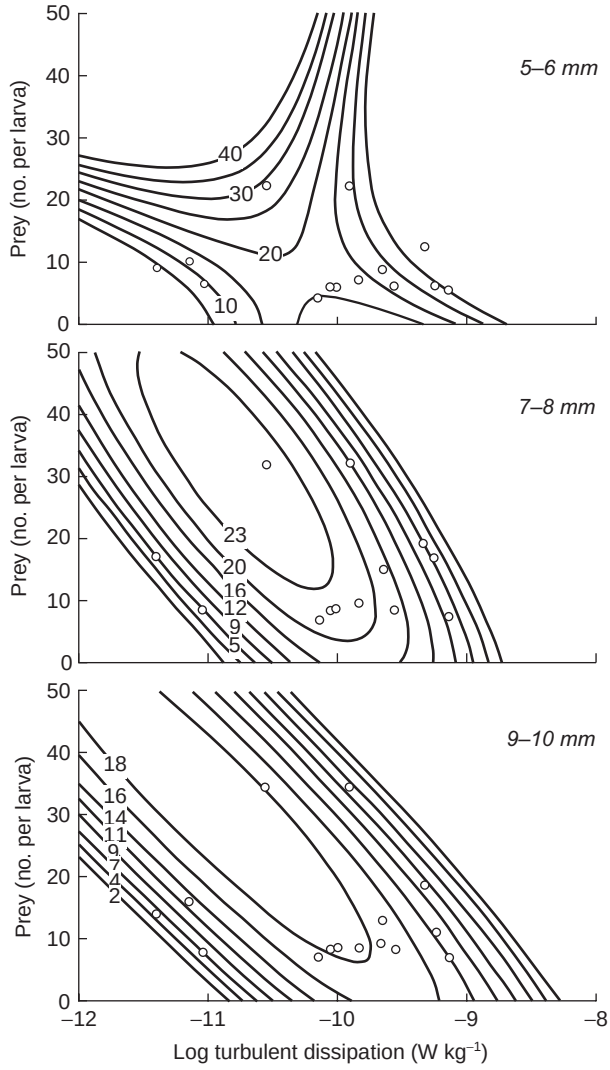

Fig. 2.14 Response surface estimation of feeding ratio (mean number of prey per larva) for three size classes of haddock larvae, at average prey densities and minimum turbulence levels observed in the upper 50 m of the water column. Actual data points are shown as small circles. From Lough and Mountain (1996).

but as turbulence increased the larvae were able to maintain a high feeding rate at low prey densities. Dower *et al*. (1997) provided a useful review of turbulence and the feeding of fish.

Landry *et al*. (1995) exposed fathead minnow *Pimephales promelas* larvae to four turbulent velocities at a single food concentration (30 brine shrimps *Artemia* sp. L^{-1}) and again to four levels of turbulence at three different prey concentrations.

In the first experiment they found a dome-shaped relationship, with enhancement of feeding rate at low levels of turbulence and reduction at high levels. In the second experiment they obtained the same dome-shaped relationship with the highest concentration of prey (500 L^{-1}), but with 50 prey L^{-1} and 15 prey L^{-1} they obtained a depression of feeding rate at all levels of turbulence, compared with the no-turbulence condition.

For fish in coastal upwelling systems (see Chapter 5), Cury and Roy (1989) and Ware and Thomson (1991) have found that survival of newly hatched fish and subsequent recruitment is optimal at average wind speeds of 5–8 m s^{-1} and that a dome-shaped relationship exists between the range of wind speeds encountered in nature and year-class success. The results of Landry *et al*. (1995) provide a possible mechanism for this phenomenon.

In a modeling study, Davis *et al*. (1991) added another component to the relationship of planktonic predators to their prey – namely, microscale (<10 m) patchiness. They found that the growth rate of predators is strongly dependent on the existence of patches in which prey density is well above the large-scale average. Physical turbulence, at levels corresponding to winds of 5 m s^{-1}, tends to homogenize prey patches and reduce the growth rate of predators. Winds of 10 m s^{-1}, on the other hand, lead to more frequent encounters between predators and prey, and have the effect of restoring predator growth rates to low-turbulence values.

Herring *Clupea harengus* larvae are particularly abundant in a region of strong tidally generated turbulence off southwest Nova Scotia. Muelbert *et al*. (1994) investigated whether the turbulence assisted prey capture by the larvae. They carried out a dimensional analysis, using the modifications by Rothschild and Osborn (1988) of the Gerritson and Strickler (1977) model of interactions between a moving predator and its prey in a water column. They derived two nondimensional numbers from the existing models and proposed a third that incorporates the minimum encounter rate required for larval maintenance.

Muelbert *et al*. showed that when RMS turbulence velocities are the same order of magnitude as the prey velocities, they have a small influence on encounter rates; when they are an order of magnitude larger than predator velocities, they dominate the encounter process. In tidally well-mixed regions, herring larvae could apparently survive on an order of magnitude lower food concentration than in stratified water where the turbulence is lower. At the food concentrations occurring in the study area in winter, it appears that turbulent, tidally well-mixed areas provide ideal feeding conditions for the herring larvae and that fish in stratified water have a much lower probability of survival. These results appear to support the ideas of Iles and Sinclair (1982) that the spawning of herring occurs predominantly in tidally mixed areas, and that the larvae tend to be retained within these areas during critical stages of development (see Section 7.3.2).

In a similar way, Lynch *et al*. (2001) asked "Can Georges Bank larval cod survive on a calanoid diet?" They developed a simple conceptual model for larval fish feeding on stage-structured calanoid prey populations, during March and April, using all available information about distributions of organisms and the

influence of turbulence on the food transfer process. The model showed that *Calanus* populations alone are insufficient to support the smallest cod larvae (4–6 mm) but provide good growth for larger larvae (10–12 mm). *Pseudocalanus* populations alone potentially provide good growth for all sizes, but do not have the same distribution as the cod larvae. The two genera taken together are able to supply good growth conditions for larvae of 6 mm and over, but the smallest larvae require a supplementary diet beyond these two genera.

2.3.6 Emerging generalities on turbulence and the plankton

There are now enough studies of the effects of turbulence on plankton for some general trends to be observed. Peters and Marrasé (2000) analyzed 38 published papers, of which 26, with 452 data points, contained enough information to calculate rate parameters, under both still-water and turbulent conditions.

They first considered whether the experimental turbulence intensities were realistic for ocean conditions. They found that the intensities in experimental conditions were 2–3 orders of magnitude higher than the values generally reported for oceanic conditions. However, they also noted that recent measurements in the upper few meters of the ocean under high-wind conditions and in coastal waters suggest turbulence intensities 1–2 orders of magnitude greater than the highest values previously reported. They therefore concluded that the turbulence levels in the laboratory experiments may more closely approximate the levels in the high-energy regions rather than the ocean in general.

For phytoplankton, on average, turbulence appears to have a negative effect on growth rates, but the results are heavily influenced by studies with dinoflagellates. Other types of phytoplankton often experience positive effects. For heterotrophs, ingestion rates and/or encounter rates are favored at all but the highest levels of turbulence. The results were different for different size classes. Organisms under 20 μm showed only minor positive effects at intermediate levels of turbulence. Those in the 20–200 μm range (all protozoa and all in one study) showed markedly higher ingestion rates in turbulence, while larger organisms demonstrated positive effects of turbulence on ingestion, but a decrease with increasing turbulence.

Encounter rates between predators and prey usually increased with turbulence, but did not always result in higher ingestion rates. The most common pattern was for low turbulence to have insignificant effects on ingestion rate, intermediate levels to show increased ingestion, and high levels to have insignificant or negative effects on ingestion, probably by interfering with prey capture.

Peters and Marrasé (2000) found that almost all the significant effects of turbulence (defined as producing at least a 50% increase in growth rate over still water) were on organisms smaller than the Kolmogorov length (Eqn. 2.08). Yamazaki *et al*. (2002), in their recent review of the subject, suggest this result is expected from the theoretical analysis of Rothschild and Osborn (1988) and those that followed afterward. Two organisms very close together move together. Their

motion is highly correlated. As they separate they experience a shear between them created by the turbulence. With increasing distance the shear increases and eventually, at about the Kolmogorov length, the correlation between the organisms' motion begins to decrease. As the separation increases the relative motions between the organisms becomes more uncorrelated and eventually random. When the organisms are close together the shear flow moves them past each other – like walking on the sidewalk you encounter more people than if you were all standing still. This increased encounter rate is the key to the effect of turbulence on feeding. As the distance between the organisms increases the relative motion between them becomes more and more random and the turbulence has less and less effect on encounter rates.

Reviewing the effect of small-scale turbulence on processes in the plankton, we see that it influences trophic transfers at all levels from dissolved nutrients to fish. Turbulent shear causes aggregation of colloidal particles into particles that bacteria can digest. It also affects the uptake of nutrients by phytoplankton, enhancing it for some organisms and inhibiting others, depending on the level of turbulence. It seems probable that a dome-shaped relationship exists between turbulence and feeding rates for both zooplankton and fish. At low levels of turbulence feeding is enhanced by increasing rates of contact with food particles; at higher levels the process of food handling may be disrupted, leading to a reduced feeding rate. The optimum turbulence rate differs for various species, and there is a complex interaction of levels of turbulence with food density and with the patchiness of its distribution.

2.4 Benthic plants

2.4.1 The problem

The concept applied to phytoplankton of the uptake of nutrients being limited by the boundary layer around the organism applies also to attached benthic plants. If a plant is surrounded by completely still water it will soon produce a zone around itself in which the nutrients are depleted and metabolism is limited by the rate at which nutrients are able to diffuse along the concentration gradient (Box 2.02). The problem is alleviated if there is a movement of water relative to the plant, for the zone of nutrient depletion is partially replaced by less depleted water. We saw that phytoplankton achieve a movement relative to the water by passively sinking or by actively swimming. They may also preferentially occupy zones of locally high nutrient concentration. For benthic plants, the key to their productivity is the movement of water over them while they are held in one place by their attachment to the substrate.

Benthic plants are limited to areas where the sea floor is within the zone in which there is sufficient light to support photosynthesis, and it is usual to find a fringe of marine macrophytes associated with the various types of coastline. Seaweeds (i.e., attached algae) predominate in eroding areas where there is a rocky bottom for

attachment of the holdfast, while flowering plants such as seagrasses, marsh grasses, and mangroves predominate in sedimenting areas where their roots can take hold and obtain nutrients. In the section that follows we shall explore the question of how dependent benthic plants are on the movement of water around them.

2.4.2 Water movement, nutrient uptake, and productivity

Hurd (2000) has given a good summary of the water flow encountered by benthic marine algae. Giant kelps that colonize water of about 10 m depth and have buoyant fronds near the surface encounter orbital water movement as a result of surface wave motion. Closer to shore, where the water depth is less than half the crest-to-crest distance of the waves, the algae experience a back-and-forth oscillation of the water, parallel with the bottom, as the waves pass overhead. This movement is accentuated in the shallow intertidal zone, where waves break and water rushes up the shore, to recede again after each wave.

Within these broad zones of water movement, algae are able to experience flow microhabitats, according to their growth habit. Very small forms or encrusting species may be so close to the substrate that they are in the boundary layer of slowly moving water, either the viscous sublayer or the turbulent zone described in Section 2.2.8. Because the boundary layer builds up as water moves across a surface, as described by Eqn. 2.13, algae further from the leading edge of a structure such as a rock will experience a thicker boundary layer than those living near the edge. Again, algae growing close to one another may be compressed into one large clump at high water velocities, so that water currents are directed around, rather than through the clump, and current speed within the clump is markedly reduced. Full quantification of these processes has not yet been achieved, but there are interesting studies of components of the problem.

Gerard and Mann (1979) found a trade-off between blade morphology, drag, and productivity in *Laminaria*. In high-energy sites the algae have narrower, thicker blades and solid stipes, which are an adaptation to withstanding drag (see Section 2.4.3). At more sheltered sites the algae have hollow stipes that help lift the blades closer to the water surface and thinner, more frilly blades that increase turbulent exchange at their surface. Despite having less water movement over the blades, algae at the sheltered sites showed better growth and productivity.

A different result was obtained by Sjøtun *et al*. (1998), in a mixed-age stand of *Laminaria hypoborea*. The annual growth of 4-year-old algae was positively correlated with wave exposure. For 2- to 3-year-old specimens the growth was correlated with population density, but not with wave exposure.

More elaborate, instrumented studies were carried out by Koehl and Alberte (1988), working on the Pacific coast of North America with *Nereocystis*. This kelp also has narrow, flat blades in exposed situations and wider, undulate blades in more sheltered localities. They used electronic current meters to produce continuous records from the vicinity of the plants, and water velocity profiles in the seaweed's boundary layer by placing a blade in a tank through which particles

moved while being illuminated by strobe flashes. They demonstrated that the effect of current on photosynthetic rate was through the change in the velocity gradient at the blade surface. They also found that there were conditions of low flow in nature that led to gradients corresponding to a definite limitation on photosynthetic rate.

From measurements made in a flow tank Koehl and Alberte determined that frilly wide blades "flapped" with a greater amplitude than narrow blades in response to the current, but caused greater drag on the plant. Narrow flat blades, on the other hand, collapsed into more streamlined bundles in a strong current, but in this position they were subjected to more self-shading. They showed that photosynthetic rate decreased in slow flow, but that blade flapping enhanced it. Hence, the frilly blade morphology, which caused increased flapping, enhanced photosynthesis. There was a trade-off between the photosynthetic advantages of wide, frilly blade morphology and the risk of the plant's breaking due to increased drag.

Anderson and Charters (1982) placed the bushy alga *Gelidium nudifrons* in a water tunnel in the laboratory and observed turbulence by a dye-stream technique. They found that local turbulence was damped at low velocities, but the alga created its own microturbulence at higher velocities. How this difference relates to the realities of life on a rocky shore remains unclear.

Macrocystis integrifolia is another species with distinct blade types according to the degree of wave exposure. At sheltered sites the blades are wide and have undulations along the margins, while at exposed sites the blades are narrow, without marginal undulations. Hurd *et al*. (1996) set out to test the hypothesis that the sheltered morphology causes enhanced uptake of nutrients at a given rate of water movement. They measured nitrate and ammonium uptake in the laboratory at a range of seawater velocities, and found that for any given current velocity the uptake per unit area by the sheltered forms was on average slightly *lower* than by the exposed forms, although the difference was not significant. Visualization of the boundary layers under laboratory conditions (Hurd *et al*. 1997) showed no obvious functional differences between the two morphologies. For both of them, the boundary layers switched from laminar to turbulent at free-stream water velocities of 2 cm s^{-1}, and at Reynolds numbers between 10^2 and 10^4, which are lower than predicted by boundary-layer theory. This work leads one to question the way in which the undulate morphology is an adaptation to life in low-velocity environments.

A comparative study in which flow fields were visualized around nine different kinds of seaweeds (Hurd and Stevens 1997) showed that the transition from laminar to turbulent flow in the boundary layer was at the same free-stream velocity (1.5 cm s^{-1}) for four different species having single blades of similar size and shape to *M. integrifolia*. For four multiple-bladed seaweeds the transition occurred at 2.5–3 cm s^{-1} and for a small, much-branched seaweed it occurred at 5 cm s^{-1}. The authors observed that flow features such as separation, recirculating eddies, and vortices were generated by various structures, leading to the conclusion that in nature most seaweeds experience turbulent conditions most of the

time, either because the free flow is above the critical velocity, or because they experience the turbulence created by neighboring seaweeds.

In her recent review article, Hurd (2000) pointed out that most laboratory experiments involve holding an algal blade in a uniform relationship to a constant laminar flow, whereas in nature the blades are subject to cross-flows, to velocities varying on a scale of seconds, and to turbulence generated by neighboring algae. She suggested that the idea, first proposed by Wheeler (1980), that kelps in nature are often nutrient-limited may have been over-emphasized. The phenomenon may be restricted to a few species in exceptionally sheltered environments.

It could still be possible that the morphological adaptations associated with wave-sheltered sites have the effect of increasing productivity, as demonstrated by Gerard and Mann (1979), but more studies are needed to confirm the generality of this finding.

2.4.3 Water movement and drag

Seaweeds often respond phenotypically to ambient levels of water movement, tending to be undulant or frilly in sheltered sites, but streamlined in exposed sites. It is at present unclear what is the function of the frilly form, but it is quite clear that it increases drag, thus increasing the risk of the seaweeds being torn from their attachments and cast up on a beach to die.

An obvious adaptation to minimizing drag in an oscillating current is the ability of a plant to bend in the direction of the flow at a given time, minimizing the area presented to the current. However, as Koehl (1986) pointed out, flexibility may have disadvantages as well. A stiff plant may be able to hold its blades above those of its more flexible neighbors, out-competing them for light. On the other hand, a flexible plant, by its lashing about, may shake off epiphytes, or herbivorous animals. Some seaweeds, as they bend in the wave-induced currents, sweep the area of sea floor surrounding each plant, keeping it free from competitors. What degree of flexibility is optimal for this? Koehl's (1986) review gives a great deal of information about the biomechanics of seaweed structures, and interested readers may care to go more deeply into this subject.

Since 1994 there has been considerable progress in analyzing the forces exerted on sessile algae of the intertidal and subtidal zones. Gaylord (1999) made detailed measurements of the velocities and accelerations induced by breaking waves on a rocky shore. Waves of 1.0–1.5 m in height can produce water velocities of over 6 m s^{-1} and accelerations up to 150 m s^{-2}. Gaylord *et al*. (1994) measured drag and acceleration forces on three intertidal algae of contrasting shape. They confirmed that the drag coefficients decrease with increasing water velocity, as is typical for flexible organisms, but when stretched to their limit in the direction of the flow, their tissues exert a surprisingly high inertial drag on the stipe and holdfast. They hypothesized that these accelerational forces combined with the drag limit the size of the seaweeds.

There have been several studies of the drag on giant kelps and understory species (Utter and Denny 1996, Gaylord and Denny 1997, Denny *et al*. 1997, 1998). By having flexible stipes which allow the fronds to "go with the flow," there is a temporary decrease in the drag. However, if the flow stretches the kelp to its limit, the fronds are pulled up with a jerk and very high inertial forces are exerted on the stipe and holdfast. The forces involved have been both predicted and measured in the field. Denny *et al*. (1998) calculated a dimensionless index, the "jerk number," for predicting when inertial forces will be important. They discuss the possibility that kelps can be tuned, either by evolution or by physiological response, to avoid potentially damaging loads.

An interesting and unusual seaweed is the sea palm *Postelsia palmaeformis*, which lives intertidally and is sufficiently stiff to stand more or less upright when not bent over by wave action. Holbrook *et al*. (1991) investigated the physical properties that make this possible. The elastic modulus, E, is low enough to permit bending down to the substratum without breaking, and is not very different from that found in other large marine algae. The stipe is wide in relation to its height, however, and this property confers a flexural stiffness. When subject to extreme drag, the stipe is extended 20–25% before breaking. Holbrook *et al*. contrasted this behavior with terrestrial trees. Wood is much stiffer but has a much lower breaking extension. Trees often break in strong winds, while *Postelsia* withstands forces from breaking waves that are about 850 times greater than those on a tree hit by wind moving at the same velocity and acceleration.

Drag on animals

In contrast to the results for macroalgae discussed earlier, it has proved difficult to determine the mechanisms that limit the size of benthic marine animals in wave-swept areas (Denny 1999). Explanations relating the hydrodynamic acceleration forces to the strength of the organism do not work. As Koehl (1999) pointed out, life-history adaptations can offset the results of mechanical failure. For example, staghorn corals frequently break under mechanical stress, but the broken pieces remain and grow. This mechanism is part of the reproductive strategy of these organisms.

Meantime, we note that hydromechanical stress may impair the efficiency of organisms in unsuspected ways. Mead and Denny (1995) showed that turbulence-induced shear stress reduces fertilization success in sea urchins, probably by interfering with contact between eggs and sperm. They speculated that few of the sea urchins on exposed rocky shores would be contributing to the next generation.

2.4.4 Water movement and community structure in kelp beds

Several interesting studies have focused on the way in which kelp beds influence water movement, and through it the structure of the biological community (see

Eckman and Duggins 1991 and references therein). Earlier work by G.A. Jackson showed that beds of giant kelp *Macrocystis* on the California coast attenuate internal waves passing through them, and reduce longshore currents to about one-third of their value outside the bed. When the water column contains invertebrate larvae that are competent to settle, slowing the current has the effect of concentrating newly settled larvae within the bed.

Eckman, Duggins, and their colleagues made similar studies in beds of smaller kelps, *Agarum* and *Laminaria*, off the coast of Washington State. As expected, they found reduced currents within the beds; they also found a greater rate of deposition of particles, which they attributed to the increase in retention time of the water containing the particles. The light intensity was lower within the beds than outside them, a condition that was associated with reduced cover of microalgae on the substratum. When they investigated the influence of these factors on settlement of planktonic larvae, the results varied widely from one species to another, depending on the duration of planktonic larval life and individual responses to sedimentation and light. Similarly, when the growth rates of invertebrates living outside and inside the kelp beds were compared, barnacles, mussels, and serpulid worms often showed enhanced growth rates within kelp beds, while bryozoans and sponges showed no significant differences.

2.5 Benthic animals

2.5.1 Filter-feeding in the benthic boundary layer

It has long been known that the growth and productivity of benthic organisms is a function of the current speed. Wildish and Kristmanson (1979) produced evidence that benthic communities in areas affected by tidal currents formed a spectrum. In waters with very low tidal currents, deposit-ingesting animals such as polychaete worms, nematodes, and certain kinds of bivalves predominated; in areas with more water movement, suspension-feeding bivalves and holothurians were much more abundant. Finally, in areas where the mean tidal currents, measured 1–2 m above the bottom, exceeded 30 cm s^{-1}, they showed that the communities were stressed and the fauna impoverished. Conditions at the two extremes can be understood without much difficulty. In very quiet waters nutritious organic matter accumulates on the bottom, where it is most easily utilized by animals that ingest sediment directly. At the other extreme, high currents erode the sediments, leaving little organic matter and making suspension feeding difficult because there is so much inorganic matter in suspension. For the intermediate stages, the authors found a gradient in abundance of suspension-feeding organisms that they thought could be explained by interactions between the filter feeders and the tidal currents. They suggested that the suspension-feeding organisms depleted the concentration of food particles near the sediment–water interface, and moderate tidal currents generated enough turbulence in the bottom boundary layer to increase the supply of food to the suspension-feeders by turbulent diffusion. In later work,

the same authors (Wildish and Kristmanson 1984) confirmed in a laboratory flume tank that blue mussels *Mytilus* and horse mussels *Modiolus* were able to cause a reduction in the living organic matter in suspension at a height of 1 cm above the bottom, compared with 30 cm above the bottom.

A more detailed study of the dynamics of a benthic community in relation to turbulent diffusion in the water column was made by Frechette and Bourget (1985a, 1985b) and Frechette *et al*. (1989). For their study area, they chose a dense intertidal bed of the mussel *Mytilus edulis* in the St Lawrence estuary, Canada. They demonstrated depletion of the particulate organic matter above the mussels and showed that the effect was inversely proportional to current speed. They also showed that animals situated 1.0 m above the bottom had better growth rates than those found on the bottom, presumably because more food was available. The relationship between current speed, vertical profile of density of suspended organic matter, and consumption rate of the mussels was demonstrated in a simulation model.

Formation of a food-depleted layer near the bottom is a function of the species of filter-feeder and the location. Mussels feeding on bacterioplankton in cold, deep methane/sulfide seeps in the Gulf of Mexico, where water movement is of the order of 2 cm s^{-1}, were found to generate sufficient turbulence by their own pumping that there was no near-bottom depletion of the food supply (Pile and Young 1999).

A study of the feeding behavior of barnacles (Trager *et al*. 1990) has shown how intricate are their adaptations to life in a variable flow. In currents greater than 3.1 cm s^{-1}, they extended their cirri and passively filtered the water. At lower current speeds, the barnacles actively swept the water with their cirri. In an oscillating current, they reversed the direction of their cirri just before the current changed direction. They also swept actively while the current was accelerating and changed to passive filtering when it exceeded 3.1 cm s^{-1}.

Sanford *et al*. (1994) observed the effect of water flow, food concentration, and water temperature on the feeding of acorn barnacles *Semibalanus balanoides* both in tanks and around the shores of Narragansett Bay, Rhode Island, USA. They found that the percentage of barnacles feeding increased with flow speed and food concentration, but was depressed at temperatures over 15 °C.

In the shallow Odense Fjord, Denmark, the polychaete worm *Nereis diversicolor* lives in burrows in the sediment and achieves population densities of 1000–2000 worms m^{-2}. It feeds by pumping water through the burrows, and laboratory experiments showed that, in still water, it is capable of depleting the water column of phytoplankton to a maximum of 26 cm above the bottom (Vedel 1998). In the field, the natural water movement reduced the maximum height of the depleted zone to only 4–8 cm. It was observed that the worms could filter up to 14 times the volume of the water column in a day, but were prevented from having a major impact on the phytoplankton biomass by the presence of the depleted boundary layer.

Thus, the evidence from community structure, single-species populations, and physiological experiments on individual animals supports the view that food

consumption of benthic filter-feeders is a function of current speed in the benthic boundary layer, as well as of the more traditional variables, such as food concentration and temperature, that have been investigated in the past.

In the case of the mussels discussed above, the animals normally live attached to solid substrates in areas where water movement is sufficiently vigorous to prevent the accumulation of sediment. There are also many kinds of benthic animals that live in areas where the intensity of turbulence is sufficiently low to permit the accumulation of sediment. Some of these animals feed exclusively by ingesting the sediment, but many ingest food from the suspension of particles that is found just above the sediment. In the next section we look at the vertical distribution of these particles and its effect on the feeding strategies of animals.

2.5.2 Suspension-feeding benthos

If we envisage a current just above the bottom carrying relatively heavy mineral particles and lighter organic particles, we might guess that the heavy particles would be concentrated close to the bottom and the lighter particles higher up. Muschenheim (1987a) made a theoretical analysis which supported this idea. He then studied the feeding of a polychaete worm, *Spio setosa*, which builds a sand tube that allows it to feed 4–6 cm above the sediment (Muschenheim 1987b). Worms taken from the field were found to have gut contents that were enriched in organic–mineral aggregates, relative to the sediment surface. In a flume-tank study, half of the worm tubes were cut down close to bed level so that the worms were forced to feed at a height of 0–2 cm, while the remainder were left at 4 cm length so that the worms fed at 4–6 cm. Those feeding at the lower level were found to collect particles with a significantly lower organic content. Measurement of the settling velocity of surficial sediment collected from the field site showed that it had a Rouse number consistent with it being carried in suspension several centimeters above the sediment surface.

These results, therefore, support the view that in a boundary layer above a sediment surface, the differential settling velocities of particles of different densities have a natural sorting effect, such that the maximum flux of organically rich particles occurs at a higher level above the sediment than the maximum flux of inorganic particles. This observation explains why a number of different organisms, especially polychaete worms, build tubes that protrude above the sediment surface.

Riisgård *et al*. (1996) placed the worm *Nereis diversicolor* in glass tubes at intervals above the bottom and found that worms 10 cm above the bottom showed better growth than those on the bottom. They attributed this difference to the depletion of food mentioned in Section 2.5.1, but did not investigate the sorting of particles by density, as reported by Muschenheim (1978b).

Abelson *et al*. (1993) generalized the foregoing results. Using a physical model, supported by field experiments, they grouped benthic organisms according to the ratio of height to width in the plane normal to the flow. Organisms with a high

slenderness ratio (SR) caused divergent flow around the base, while the upper regions experienced a good exposure to fine suspended particles. Organisms with a low slenderness ratio caused the flow lines near the substratum to lift over the top of them and expose them mainly to bed-load particles. Abelson *et al*. offered the generalization that high-SR species are suspension feeders, while low-SR species are coarse-particle or bed-load feeders. For example, a species of crab that inhabits tips of coral branches filter-feeds on fine suspended particles, while another species that lives on low, massive corals feeds on coarse particles.

2.5.3 The boundary layer and larval settlement

In this section we consider the problems encountered by small planktonic larvae as they descend from the water column into the benthic boundary layer prior to settling on the bottom to begin their adult life. Tidal currents above the bottom often greatly exceed the swimming speeds of the larvae, but they decrease in a logarithmic manner as the bottom is approached. A viscous layer exists close to the bottom in which turbulence is minimal. Can the larvae enter this layer and then swim strongly enough to be able to select a site for settlement, or are they forced to locate a settlement site by some more haphazard approach?

Butman (1986) studied the question at a site where the tidal currents 0.5 m from the bottom reached 5–10 cm s^{-1} on each ebb and flow. A vertical profile of the boundary layer was constructed by deploying current meters at 30, 50, 100, and 200 cm above the sea floor, and using the data to calculate u_* and Re_* (Box 2.05). Calculations were made for smooth-turbulent and rough-turbulent velocity profiles; these measurements were compared with the size and swimming speed of polychaete larvae (Figs. 2.15 and 2.16). In smooth-turbulent flows, larvae of 300 μm would not have room to maneuver by swimming if they found themselves below the horizontal line, and would not be able to swim against the current if they were in the region to the right of the vertical line. When rough-turbulent profiles were calculated, it was concluded that eddies would reach so close to the sea floor that there would be no region in which the larvae could effectively move by swimming.

Hence, it seemed that during about 40% of the tidal cycle it is physically possible for the larvae to swim around near the bed, exploring sites available for settlement. They would be confined to a region within 100 μm of the bed. However, the real world includes the additional complication that wind-driven and density-driven currents are superimposed on the tidal cycle. The author concluded that the larvae probably do not search for preferred habitats by active horizontal swimming near the bed. It seems more likely that they swim vertically in smooth-turbulent flows, going down to test the substrate and up to be advected to another site downstream. This process has been called the "balloonist technique."

From this study we see how consideration of the physics of the boundary layer creates a totally new perspective on the settlement of planktonic larvae. Results from classical studies conducted in the laboratory are in need of reinterpretation.

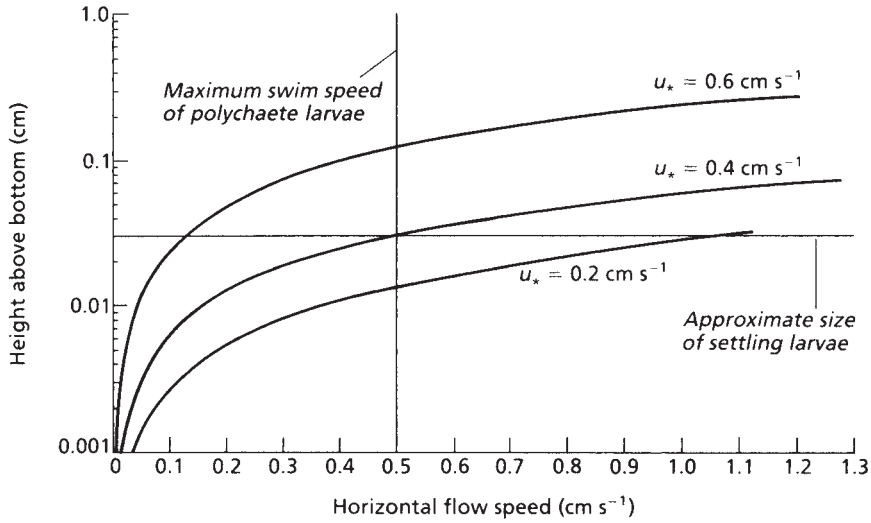

Fig. 2.15 Smooth-turbulent velocity profiles in the viscous sublayer, calculated for a range of near-bottom flow speeds measured at a site in Buzzards Bay, Massachusetts, USA. Light lines indicate size and swimming speed of settling worm larvae. From Butman (1986).

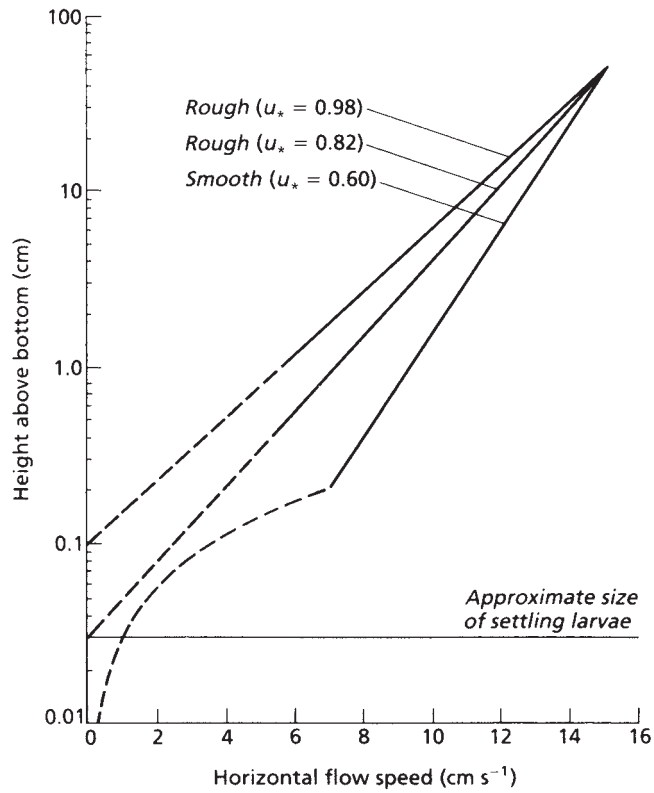

Fig. 2.16 Two rough-turbulent velocity profiles and a smooth-turbulent profile from a site in Buzzards Bay, Massachusetts, USA. From Butman (1986).

Interactions between chemical cues and hydrodynamic effects on larval settlement have been investigated for a reef-building polychaete worm, *Phragmatopoma lapidosa californica* (Pawlik *et al*. 1991, Pawlik and Butman 1993). In still water, larvae of this worm settle preferentially on sand derived from adult worm tubes, or on sand treated with free fatty acids extracted from the cemented sand matrix of the tubes. When the experiments were repeated in flowing water, it was found that larvae settled most readily at 15–25 cm s^{-1}. At slower flows, they left the bottom and swam in the water column. At the highest rate of flow, the larvae were eroded from the bed and carried passively as bed load. Preference for intermediate flow rates probably reflects the requirement of the settled worms for a current strong enough to bring a supply of sand for their tubes, as well as organic matter for food.

Pawlik and Butman (1993) also reviewed other examples of interactions between larval settlement behavior and the near-bed flow regime. Barnacle larvae actively explore a substrate on which they have settled, but exploration occurs only along the line of flow at the surface. The larvae of the worm *Capitella* swim up and down as they are carried by the flow, either accepting or rejecting sediments as they are encountered. The larvae of the bivalve *Cerastoderma edule* become concentrated in the viscous sublayer in relatively fast, turbulent flows, suggesting that fast flow increases their opportunities for habitat selection.

2.5.4 The boundary layer and coral reefs

Primary production on coral reefs results from two main processes: photosynthesis by the zooxanthellae embedded in the tissues of the coral, and photosynthesis of algae attached to the surface. Patterson *et al*. (1991) studied the effect of changing flow rate on heads of the coral *Monastrea annularis*, using a recirculating flow respirometry system deployed from an underwater habitat. Not surprisingly, both primary production and respiration of the coral increased with increasing flow. By plotting the average Sherwood number against the Reynolds number, Patterson *et al*. obtained the relationship $Sh = 0.01\ Re^{1.30}$ for dark respiration, and $Sh = 0.71\ Re^{0.63}$ for maximal photosynthetic rate. According to White (1988), an exponent less than 0.5 indicates transport through a laminar boundary layer, while values greater than 0.6 indicate increasing importance of turbulent transport. A value of 1.30 indicates a performance better than predicted by available theory, and may relate to the role played by cilia in assisting transport.

Measurements on the productivity of algae attached to the reef surface, under different flow regimes in a chamber, were made by Carpenter *et al*. (1991). They found that both primary production and nitrogenase activity increased over unidirectional flow speeds of 0–10 cm s^{-1}. Introduction of oscillatory flow (as would be experienced as a result of wave action in the water column above) led to even more marked increases in photosynthesis and nitrogenase activity.

Subsequently, Carpenter and Williams (1993) investigated flow profiles on the surface of a reef in the US Virgin Islands. They found that where the algal turf

was short (usually as a result of grazing) the boundary layer was dominated by turbulent eddies, but in significant areas (such as depressions) the algal turf was longer and the boundary layer dominated by viscous forces, leading to diffusion limitation on metabolism.

2.5.5 Processes at the sediment–water interface

Benthic sediments are sites of processes important to the functioning of marine ecosystems. Dead organic matter accumulates at those sites, where it becomes subject to microbial decomposition. This degradation requires a supply of oxygen and leads to a release of nutrients to the overlying water. The diffusive sublayer of the benthic boundary layer presents a barrier to the downward flux of oxygen and the upward flux of nutrients.

Jørgensen and Revsbech (1985) used oxygen microelectrodes to investigate the properties of the viscous sublayer. They found that when oxygen was being taken up by the sediments, a layer of water with rapidly decreasing oxygen concentration, which they interpreted as being the viscous sublayer, was found close to the sediment surface. It varied in thickness from 0.2 mm to more than 1 mm, depending on the velocity of the flow and the roughness of the sediment surface. This finding is in accordance with the theory presented in Section 2.2.8. Using the calculation shown in Box 2.02 and a molecular diffusion coefficient, D, for oxygen of 2.0×10^{-9} m^2 s^{-1}, they found that the mean time for diffusion of oxygen across the boundary layer was 1.2–9 minutes. For sediments with high oxygen demand, this result constituted a serious resistance to oxygen flux.

A near-shore sediment covered with a mat of the filamentous, colorless sulfur bacterium *Beggiatoa* was found by Jørgensen and Revsbech (1985) to have such a steep gradient of oxygen through the viscous sublayer that almost zero oxygen was present at the surface, even though the overlying water in the turbulent layer was near saturation. As water movement over this surface increased, the diffusive sublayer became thinner, the oxygen gradient became steeper, and the rate of diffusion of oxygen increased. The group noted that the small polychaete worm *Pygospio elegans* builds sediment tubes that extend a few millimeters above the sediment surface, penetrating the viscous sublayer and enabling the worm to draw water from the well-aerated turbulent layer above. They also suggested that suspension-feeding ciliates such as *Vorticella* and *Carchesium* (which live on decomposing detritus) have a stalk several millimeters long so as to enable them to reach the oxygen-rich water above the viscous sublayer. Conversely, bacteria requiring anaerobic or near-anaerobic conditions can live on the surface of a piece of detritus or a sediment with a high oxygen demand. Even though the water in the turbulent layer above is rich in oxygen, the bacteria will experience near-zero oxygen at the surface–water interface. This means that complete nutrient-biogeochemical cycling can occur on marine snow, even supporting methanogenesis (a strictly anaerobic process) within the open water column (van der Maarel *et al*. 1999). Further experiments (Gundersen and Jørgensen 1990, Dade 1993) have shown that in still

waters boundary layers present strong barriers to the flux of oxygen and nutrients above bottom sediments, but that water movements resulting from tidal and wind actions increase the fluxes by factors of 2.5 to 3.0.

Working in the Northeast Water Polynya on the northeastern shelf of Greenland, Ritzrau (1996) showed how microbial activity in the turbulent boundary layer adjacent to the sea floor was up to 7.5 times higher than in the adjacent water column. He attributed this to enhancement of nutrient flux from bottom sediments as a result of the fluid shear.

In a low-energy estuarine site in the middle of lower Chesapeake Bay, USA, where the sediment particles form a relatively smooth, flat surface, Wright *et al*. (1997b) found that epifaunal organisms increased the relief amplitude of the sediment–water interface by more than 8 cm, thus increasing the hydraulic roughness. The system was adapted to prevailing conditions, so that sediment resuspension by tidal or wave-induced currents seldom occurred. The biological activity in the bed was mediated by the mixing of the sediment by the benthic animals (bioturbation) and by the turbulence generated by the interaction between biological roughness and the prevailing levels of water movement.

Similar conclusions were reached on Dry Tortugas Bank, Florida (Wright *et al*. 1997a). There were two somewhat opposing biological effects. Shrimp burrows and worm mounds generated significant roughness on an otherwise smooth surface. However, on areas of smooth sediment an algal crust bound the sediments, making them more resistant to resuspension. When the bound layer was scraped away, wave-induced ripples appeared in the sediment, and these generated more roughness than the biological features. It was concluded that physically induced roughness is biologically suppressed, and only partially replaced by biological roughness caused by the macrofauna.

The general conclusion of these studies is that simple one-dimensional models of flux over smooth surfaces greatly underestimate natural fluxes at sediment–water interfaces.

2.6 Summary: life in boundary layers

In this chapter we have explored the influence of the small-scale properties of sea water on the life of plants and animals. Two phenomena crop up most frequently: the existence of a boundary layer around all organisms and the importance of the viscosity of the water at scales of millimeters. We saw that large-scale turbulence generated by ocean currents, tides, and waves cascades down through various scales of turbulence until its energy is dissipated by viscosity in small-scale eddies. This mixing transports essential substances such as carbon dioxide, plant nutrients, and food particles into the general vicinity of the organisms, but the last stage of the journey into the organisms is inhibited by the boundary layer. Water molecules stick to the surface of organisms, creating a zone of zero water movement. Beyond this zone, viscosity creates a zone of reduced water movement known as the viscous boundary layer, into which turbulent eddies cannot

penetrate, so that the passage of essential substances is limited by the very slow rates of molecular diffusion. The thickness of this boundary layer decreases with the speed of the water moving beyond it.

For large plants, such as seaweeds, thinning of the boundary layer is achieved by attaching themselves to a solid surface in a zone where tidal currents and wave action cause vigorous water movement. It has been shown that if the drag on them is excessive the plants are in danger of being broken free and cast up on the shore to die. Many of them are capable of elegant changes in shape during growth, reflecting the trade-off between the need to maximize turbulence close to the plant surface and the need to reduce drag.

For medium- to large-size phytoplankton, thinning of the boundary layer is achieved either by passive sinking or by active swimming. The ability to sink in the water column varies from species to species according to the amount of skeletal material present, and a careful analysis shows that the limitations caused by the boundary layer can be alleviated by up to one-third by either passive sinking or active swimming. Differences in these properties may account for differing growth rates among species, and account in part for the succession of dominant species observed to occur with the progression of the seasons. It is now known that the activities of predators interact with physical factors in determining the occurrence of intermittent blooms of phytoplankton.

Very small phytoplankton and bacteria live in a world where viscous forces predominate and any swimming mechanism that relies on the inertial properties of water is simply unworkable. These organisms must make complex asymmetrical flagellar movements to travel through water. When they do so, they do not reduce their boundary layers significantly. The main advantage of moving about appears to be the increased possibility of encountering a higher concentration of nutrients.

Physical processes ranging from Brownian movement to turbulent strain cause colloidal particles to collide with one another, forming ever-larger aggregates. Bacteria can attach to the surfaces of these aggregates and digest them by secreting exoenzymes. This process can be a much more efficient method of bacterial feeding than absorption of dissolved organic substances from low concentrations in the water column. It seems likely that phytoplankton that become enmeshed in aggregates are favorably placed to take up nutrients released by bacterial decomposition of organic matter.

On the sea floor, a boundary layer of reduced water movement extends for tens of centimeters above the bottom. Animals living on the sea floor benefit from the turbulence created by tidal currents, which have the effect of increasing downward transport of food material through this boundary layer. In areas of low turbulent energy soft sediments containing both organic and inorganic matter accumulate on the sea floor. When this sediment is transported laterally by tidal or wind-generated currents, a natural sorting mechanism ensures that the denser inorganic materials are in a higher concentration close to the bottom, while the lighter organic materials are concentrated a few centimeters above the bottom. Many animals such as tube worms are adapted to take their food from

the upper of these two layers. Microscopic larvae are unable to hold their position above the bottom during the ebb and flow of tidal currents, unless they are in the viscous layer very close to the bottom. This layer is often too thin for them to move about and they are forced to select their sites for settlement by making vertical excursions in and out of the viscous layer. Finally, we see that boundary layers are important in the functioning of coral reefs, and have a key role in sediment–water exchanges.

The classic view of benthic community structure is that sediment type controls community structure. The evidence for this view is the large number of correlations that have been demonstrated between sediment type and presence or absence of various organisms. In the light of more recent knowledge about the way in which the hydrodynamics of the benthic boundary layer influences both the structure of the sediment and the life processes of the flora and fauna, it seems more likely that the correlations result from the strong influence of hydrodynamics on the composition of both the sediment and the community (Jørgensen and Boudreau 2001).

3

Vertical structure of the open ocean: biology of the mixed layer

3.1 Introduction

One of the problems confronting phytoplankton in the ocean is that they need light and nutrients for growth and reproduction, but the source of light comes from above, while the source of nutrients is at depth. The sun's energy that reaches the surface waters is absorbed as it passes downward, decreasing exponentially with depth. In a finite layer, the euphotic zone, there is enough light for photosynthesis and growth to take place. In a water column with no turbulence, the euphotic zone would become depleted of nutrients as a result of uptake by the phytoplankton.

The reserve of nutrients in deeper water is constantly replenished by the decomposition of organisms from the euphotic zone that sink and decay. In the situation of zero turbulence that we have envisaged, there would be a very low level of nutrients in surface waters, a high level at depth, and the only mechanism for transfer from one to the other would be molecular diffusion, which, as we have seen, is extremely slow. In the real world, the ocean is filled with turbulent motion, generated by wind stress at the surface, internal waves, and so on. Phytoplankton depend absolutely on this turbulence to bring nutrients into the euphotic zone where they can be utilized in photosynthesis. This chapter is, therefore, concerned with some of the physical processes that affect the vertical distributions of light, heat, and nutrients, so as to better understand the dynamics of phytoplankton production.

On average, the situation in the open ocean is less complex than in coastal waters, where the influence of freshwater run-off from the land, of tidal currents, and of coastal topography lead to a high degree of complexity. This chapter deals with the open ocean, while coastal waters are deferred until Chapter 4.

3.2 Vertical structure and phytoplankton production: tropical waters

Figure 3.01 shows a vertical profile of temperature, chlorophyll, primary production, and nitrate from the eastern tropical Atlantic. It may be taken as representative of large areas of tropical ocean, and has been referred to as "typical tropical structure," or TTS (Herbland and Voituriez 1979). The water column is clearly divided into a warmer, lighter, upper mixed layer, and a cooler, heavier, lower layer, separated from the upper layer by a region of rapid change of temperature and density, known as the thermocline or pycnocline. The mixed layer has a very low level of nitrate, the lower layer has a higher level, and the zone of rapid change is referred to as the nutricline. The difference in nutrient concentration between upper and lower layers was noted in the introduction, but it is not immediately obvious why there is a sharp gradient in properties such as nitrate and a maximum concentration of chlorophyll and primary production at a depth of 20–30 m.

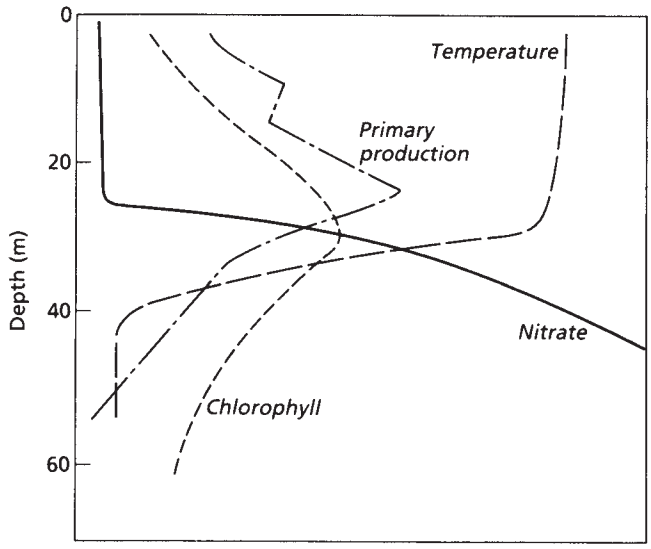

Fig. 3.01 Schematic diagram showing typical vertical structure of the water column in tropical latitudes ("typical tropical structure," TTS). Note that the thermocline and the nutricline are at the same depth. The peak of primary production is more shallow than the peak of chlorophyll (= phytoplankton biomass).

Several explanations have been offered for the subsurface chlorophyll and production maxima. Some, especially the early theories, depend on biological factors such as the sinking of diatoms or the alteration of the sinking rate according to light or nutrient levels. The grazing impact of the zooplankton has also been suggested as a significant process. Recently, the decrease with depth in the vertical mixing rate of the ocean has likewise been demonstrated to cause a subsurface chlorophyll maximum in certain circumstances. Before treating these ideas in detail, we first explore the physics of mixed layers and thermoclines, beginning with the way heat is gained and lost through the surface of the ocean.

3.2.1 Heat gain and loss

The heat that warms the upper ocean comes, of course, from the sun, and the amount that arrives each day at the outer surface of the atmosphere varies in predictable ways with latitude and season (Budyko 1974). The amount that reaches and penetrates the sea surface, however, depends on unpredictable variables such as the amount of cloud cover. Measurements of the radiation reaching the sea can be made directly but they are difficult and expensive. Usually estimates are made by using empirical relationships derived from ships' observations of cloud cover. Examples of these calculations are given in the climate atlas of Isemer and Hasse (1987).

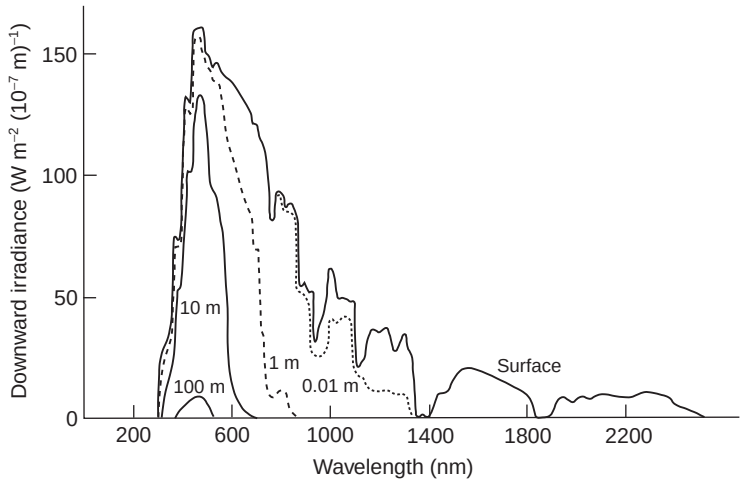

Fig. 3.02 Spectrum of short-wave radiation reaching the sea surface and four depths. Note the progressive elimination of longer wavelengths as depth increases. From Jerlov (1976).

The sun's radiation that reaches the sea surface, often called the short-wave radiation, contains energy over a wide range of wavelengths from the ultraviolet light at 300 nm to the far infrared at 2400 nm. Visible radiation lies between 360 nm (violet) and 750 nm (red). The amount of energy at each wavelength is as shown in Fig. 3.02, with minimal amounts at the shortest and longest wavelengths and with a maximum at a wavelength of about 500 nm.

The short-wave radiation is absorbed as it passes through water and the intensity at each wavelength decreases exponentially with depth, but the rate of decrease is different for each wavelength (Fig. 3.02). The intensity of the light of wavelength λ, at depth z, can be calculated from the intensity of the light at the sea surface, I_o, as

$$I = I_o \exp(-\alpha_\lambda z) \tag{3.01}$$

where the absorption coefficient α_λ is a function of wavelength, increasing from 0.004 m^{-1} for blue light to 1000 m^{-1} in the infrared at a wavelength of 1000 nm. Thus blue light is absorbed much less rapidly than infrared, and at any particular depth the intensity of blue light is a larger fraction of its surface value than is the longer wavelength light.

Figure 3.03 shows curves of attenuation with depth for infrared, red, and blue light, calculated using Eqn. 3.01. For purposes of comparison, the intensity of all wavelengths at the surface is taken to be 100% and the water is assumed to be the clearest water of the open ocean. The variation with depth of the total amount of short-wave radiation is also shown in the figure. This curve represents the cumulative effect of the different wavelengths being absorbed exponentially

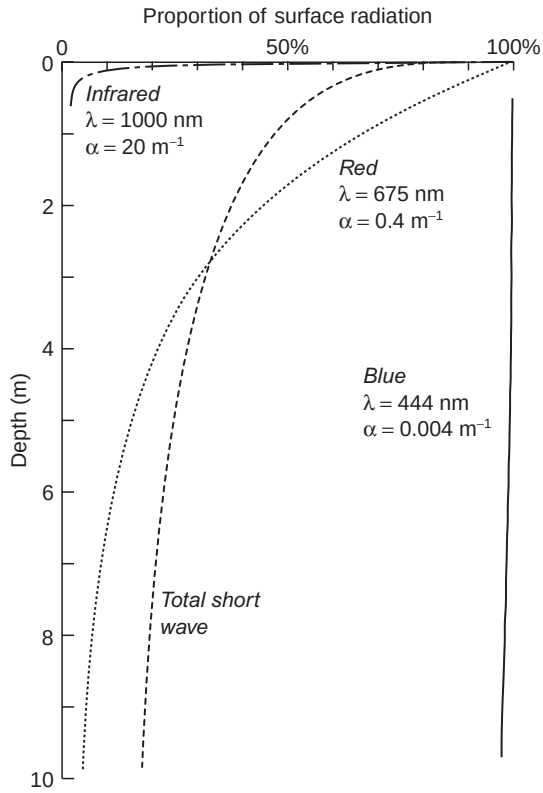

Fig. 3.03 Vertical profiles in sea water of light intensity relative to the surface for three wavelengths and for the total incoming short-wave radiation.

with depth at different rates. It is thus made up of many exponential curves although not itself an exponential function.

In locations where the water is not clear open ocean water α_λ values are higher and the absorption of radiation more rapid with depth than shown in Fig. 3.03. Chlorophyll-*a*, a phytoplankton pigment, is usually the main light-absorbing constituent making ocean water less clear. Because the color of chlorophyll-*a* is known it is possible, from a color image of the ocean surface, to estimate the chlorophyll concentration. By making such estimates at different wavelengths concentrations are obtained over different depth intervals because the light penetration varies with wavelength. This ability makes it possible to estimate the light absorption profile similar to the "total" curve in Fig. 3.03 (Bissett *et al*. 2001). Since this curve defines where the incoming radiation is absorbed it can be used to calculate the temperature increase in the water from a known quantity of radiation.

Satellite color images of the ocean surface have been obtained since 1978, first with the Coastal Zone Color Scanner (CZCS) and since 1997 with the Sea-viewing Wide Field-of-view Sensor (SeaWiFS). The program's website, seawifs.gsfc.nasa.gov/SEAWIFS.html, provides a number of images showing variations in chlorophyll-*a* over the months and years. These images make possible the detailed

mapping of chlorophyll-*a* concentrations and light absorption profiles throughout the oceans. These in turn lead to a more detailed understanding of the biological and physical processes in the upper layer. It is also anticipated that the data collected to date will form the base from which to detect future shifts in biological and physical processes due to climate change.

Although the absorption of radiation and the resultant gain of heat occurs through the top few meters of the ocean, the loss of heat is almost entirely from the top centimeter. Losses occur mainly through evaporation, infrared (long-wave) radiation, and conduction. Like the estimates of short-wave radiation, estimates of heat losses are calculated from empirical formulae derived from the common meteorological observations obtained from ships at sea. These formulae and their applications are discussed in Isemer and Hasse (1987).

3.2.2 Temperature increases and mixed layers

Absorption of short-wave radiation causes the temperature of the water to increase by an amount directly proportional to the amount of energy absorbed. Thus, the temperature rise after a given length of time will be very similar to the curve in Fig. 3.03 representing the total absorption of short-wave radiation. The greatest increase will be in the surface layers where the absorption is greatest and it will decrease rapidly with depth. Observations of temperature with depth in the ocean, however, do not normally resemble this absorption curve because the upper layer of the ocean is usually stirred up by wind waves or by convection that is generated by the loss of heat at the surface. This stirred layer where the temperature remains constant with depth is, of course, called the mixed layer. Sometimes it is called the surface mixed layer to distinguish it from homogeneous layers in the interior or at the bottom. A method for estimating the increase in temperature in the mixed layer is outlined in Box 3.01.

3.2.3 The pycnocline barrier

At the base of the mixed layer a density gradient or pycnocline separates the lighter water of the mixed layer from the denser water below (Fig. 3.04). If a particle of density ρ_2 from below the pycnocline gets displaced above the pycnocline, as shown in the diagram, it will be surrounded by water of density ρ_1. The denser particle will be heavier than the surrounding water and will fall back toward the interface. Similarly, a particle of water from the upper layer displaced below the interface will be lighter than the surrounding water and will move up to the interface. The buoyancy force per unit volume that pushes the displaced particles back to the interface is

$$(\rho_2 - \rho_1)g \tag{3.02}$$

where the constant g is the gravitational acceleration (≈ 10 m s^{-2}). The restoring force increases as the density difference $(\rho_2 - \rho_1)$ increases and is the same as the

Box 3.01 Calculating the temperature increase in the mixed layer

The temperature increase that results from the absorption of short-wave radiation can be estimated with the equation

$$\Delta T = \Delta Q / mc \tag{3.03}$$

where ΔT is the temperature increase, ΔQ is the energy absorbed in kJ, m is the mass of the water, and c, the specific heat (i.e., the amount of heat required to raise the temperature of 1 kg of water 1 °C), ≈ 4.2 kJ kg^{-1} °C^{-1}. Over short periods of time, the amount of energy absorbed is estimated from the empirical formulae mentioned above; for periods of a month or more, however, the data may be extracted from climate atlases.

To give an example, Isemer and Hasse (1987) indicate that over the course of an average July day in the North Atlantic Ocean, at 40° N 40° W, roughly 22,500 kJ m^{-2} of energy are absorbed by the ocean. The heat loss, from evaporation and other processes, over the same period is about 10,400 kJ m^{-2}. If the mixed layer is 5 m deep, Fig. 3.03 indicates about 76% or 17,100 kJ m^{-2} of the incoming energy is absorbed in the 5 m mixed layer and the remainder is absorbed below 5 m depth. Since 10,400 kJ m^{-2} is lost from the surface of the water, the net energy gain or ΔQ in the mixed layer over the day is 6700 kJ m^{-2}. To get the temperature increase this ΔQ must be divided by the mass, which for the 5 m mixed layer is 5000 kg, and the specific heat (4.2 kJ kg^{-1} °C^{-1}). This calculation works out to about 0.3 °C.

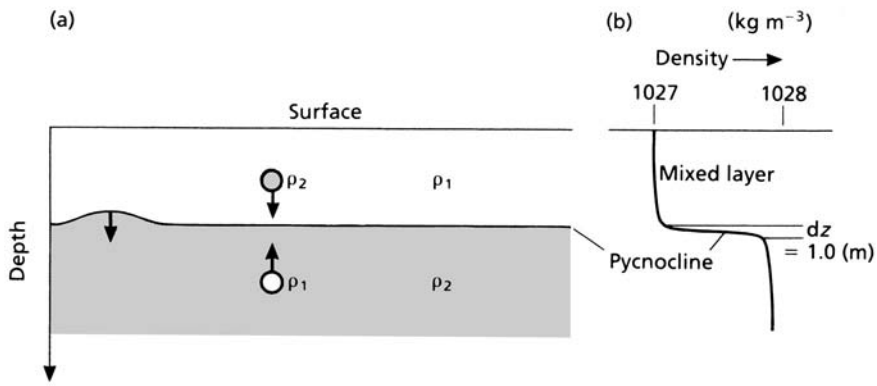

Fig. 3.04 (a) A cross-section through two layers of homogeneous water having unequal density separated by a thin pycnocline. Displacements above or below the pycnocline give rise to the buoyancy forces indicated by the arrows. (b) A vertical profile of the density through the two layers.

force required to displace the particle initially. Since displacing particles from one side of the pycnocline to the other is equivalent to stirring, it follows that it takes more energy to stir water across a pycnocline with a large density difference than one with a small density difference. The fact that energy must be supplied by the turbulent motions for vertical mixing to occur in the pycnocline presents a barrier to vertical transport.

The effectiveness of the barrier increases with increasing density difference ($\rho_2 - \rho_1$). The reduced vertical transport means that the layers on either side of the pycnocline are somewhat isolated from one another. This separation, as we discuss in the next section, has important biological consequences: the phytoplankton grow mostly in the upper layer but the supply of nutrients from the lower layer into the upper layer is, to some degree, blocked by the pycnocline.

A variable defining the strength of the density gradients in the ocean is often required. It could be specified by the density gradient $\mathrm{d}\rho/\mathrm{d}z$ but it is more usual to use the Brunt–Väisälä or buoyancy frequency

$$N = (g/\rho \ \mathrm{d}\rho/\mathrm{d}z)^{1/2} \tag{3.04}$$

where g is again the acceleration due to gravity ($\approx 10\ \mathrm{m\ s^{-2}}$), ρ is the density ($\approx 1000\ \mathrm{kg\ m^{-3}}$), and z is the depth. Physically, N is the frequency of the oscillation that results when the pycnocline is displaced, then left to return to its rest position. For example, in Fig. 3.04(a) the pycnocline has been pushed above its position of rest. Buoyancy forces then act to push it back, but because of inertia the interface overshoots the rest point and moves below the original position. Buoyancy forces then act in the opposite direction and push the interface back up. This process continues and results in an oscillation of the pycnocline, which spreads out as a moving wave. The process is just the same as when waves are made at the surface of the water. The buoyancy frequency is the most popular variable representing the strength of the vertical density gradient because physicists use it as a reference in studies of other types of waves in the ocean. It is calculated by the method shown in Box 3.02.

BOX 3.02 ESTIMATING THE BRUNT–VÄISÄLÄ FREQUENCY

The value of the Brunt–Väisälä frequency is easily found using a profile of the vertical density gradient, such as that shown in Fig. 3.04(b). Here the density difference across the pycnocline is $1\ \mathrm{kg\ m^{-3}}$ and the thickness of the pycnocline is about 1 m. These values give $N = [10(\mathrm{g}) \times 1.0(\Delta\rho)/1000.0(\rho) \times 1.0(\Delta z)]^{1/2} \approx 0.1\ \mathrm{rad\ s^{-1}}$. The radian frequency is 2π times the cycle frequency f – that is, $N = 2\pi f$ or $2\pi/\tau$ where τ is the period of the waves; thus $\tau = 2\pi/N \approx 2\pi/0.1 \approx 1$ min. This is an atypically high gradient and a fast wave for the open ocean. The minimum period in the upper ocean is about 10 minutes, while in the deep ocean or in a well-mixed surface layer the period may be as high as 2–4 hours.

3.2.4 Phytoplankton production in tropical and subtropical oceans

As we saw at the start of Section 3.2, large areas of the world ocean are permanently stratified, with a high concentration of nutrients below the pycnocline, a low concentration above, and the pycnocline acting as a barrier to turbulent diffusion of nutrients from one area to the other. This situation does not completely inhibit photosynthesis, because the organisms that graze upon the phytoplankton excrete nutrient substances such as ammonium, so that phytoplankton growth and reproduction can be maintained at a certain level with these recycled nutrients. The situation is potentially unstable, however, because any removal of organisms and their contained nutrients will lead to a running-down of the production based on recycling. For example, the sinking of dead organisms and excretion by zooplankton that migrate down through the thermocline both deplete the nutrients in the mixed layer. If the food web in the mixed layer of a particular locality consists of phytoplankton, zooplankton, and small forage fish that feed upon the zooplankton, and a shoal of tuna comes through the area, consumes large quantities of forage fish, and moves away, the amount of nutrients available for recycling is diminished. On the other hand, if some physical event occurs that permits the vertical transport of a significant quantity of nutrients from below the thermocline, the nutrient pool in the mixed layer is increased. It is clear that in the long term the persistence of a phytoplankton community in the mixed layer depends on the losses from the pool of recycling nutrients being balanced by vertical transport from below. There might, of course, be horizontal advection from one part of the mixed layer to another, but it remains true for the mixed layer as a whole that primary production ultimately depends on the vertical transport of nutrients.

Dugdale and Goering (1967), working with nitrogen metabolism, noted that recycled nitrogen is usually in the form of ammonium, while nitrogen transported from below is usually in the form of nitrate. They introduced the term "regenerated" production for the recycled material based on ammonium and "new" production for that based on nitrate. More recently, the ratio of new production to total production, the *f* ratio (Eppley and Peterson 1979), has come to be widely discussed in the context of the global carbon budget (see Section 10.3.1).

In tropical waters vertical distributions of nitrate, chlorophyll, and primary production are more or less the same in all seasons of the year, resembling Fig. 3.01. This constancy suggests that the processes maintaining the low nitrate levels in the surface mixed layer and the maxima of chlorophyll and primary production near the pycnocline must be in balance. This steady-state condition is quite unlike the situation found in temperate waters, where the vertical structure changes from season to season.

All through the 1980s and well into the 1990s, studies were carried out with an underlying assumption that the subsurface chlorophyll maximum and peak of primary production in tropical waters were a response to the slow turbulent

diffusion of nitrate upwards through the thermocline. This assumption has been thrown into doubt by the finding that up to 60% of the phytoplankton biomass in many open-ocean situations is composed of cyanobacteria which cannot use nitrate (McCarthy 2002). Their productivity is not dependent directly on the upward mixing of nitrate from deep water. Instead these organisms are using ammonium excreted by other organisms. The details are as follows.

The discovery of **Prochlorococcus**

The development of flow cytometry to count, size, and recognize pigment characteristics of very small planktonic organisms, the picoplankton, led to the recognition that certain cyanobacteria, which are photosynthetic, are extremely abundant and play a major role in many planktonic ecosystems. During the 1980s *Synechococcus* was found to be abundant in the upper ocean, some estimating that it could account for more than half the primary production in oceanic ecosystems. Subsequently *Prochlorococcus* (Chisholm *et al*. 1988, 1992), a cyanobacterium ranging in length from 0.5 to 0.8 μm, was found to be an order of magnitude more abundant than *Synechococcus*. It has an unusual pigment composition, divinyl chlorophylls *a*(a_2) and *b*(b_2), and lacks phycobilin accessory pigments. It is probably the most abundant phytoplankton group in tropical and subtropical waters (Fig. 3.05).

McCarthy (2002) has reviewed the evidence that indicates that *Prochlorococcus* is unable to use nitrate. If true, a major component of the oceanic phytoplankton (60% of the biomass in the North Pacific gyre, for example) is not directly related to the supply of nitrate from deep water. It is incapable of new production. Instead it is unusually efficient at harvesting light at low intensities near the base of the mixed layer, and utilizes recycled nitrogen in the form of ammonium excreted by other organisms. These properties account, at least in part, for the subsurface chlorophyll maximum.

The new findings do not eliminate the need to understand how the overall nitrogen balance of tropical mixed layers is maintained. The tropical structure is very similar in appearance to the late-summer structure observed in the temperate zones, and the following tentative explanation of the tropical profiles is extrapolated from the more complete body of knowledge that exists for the temperate areas, described more fully in Section 3.3.4. In this section "phytoplankton" refers to phytoplankton using nitrate.

To begin with the simplest case, consider the idealized vertical profile of density in Fig. 3.06(a). Here a homogeneous mixed layer lies over a thin pycnocline and a homogeneous deep layer. The level of vertical mixing, as symbolized by the column of circles, is vigorous enough to keep the upper layer homogeneous and the pycnocline thin. The light intensity, Fig. 3.06(b), allows the phytoplankton growth to a depth somewhat below the pycnocline. Any nitrate diffusing up through the pycnocline is quickly spread by the turbulence throughout the mixed layer and is consumed by the phytoplankton, which is also distributed evenly through the layer. If the nitrate level is low in the mixed layer, the phytoplankton production will be low and limited by the vertical flux of nitrate. Below the pycnocline,

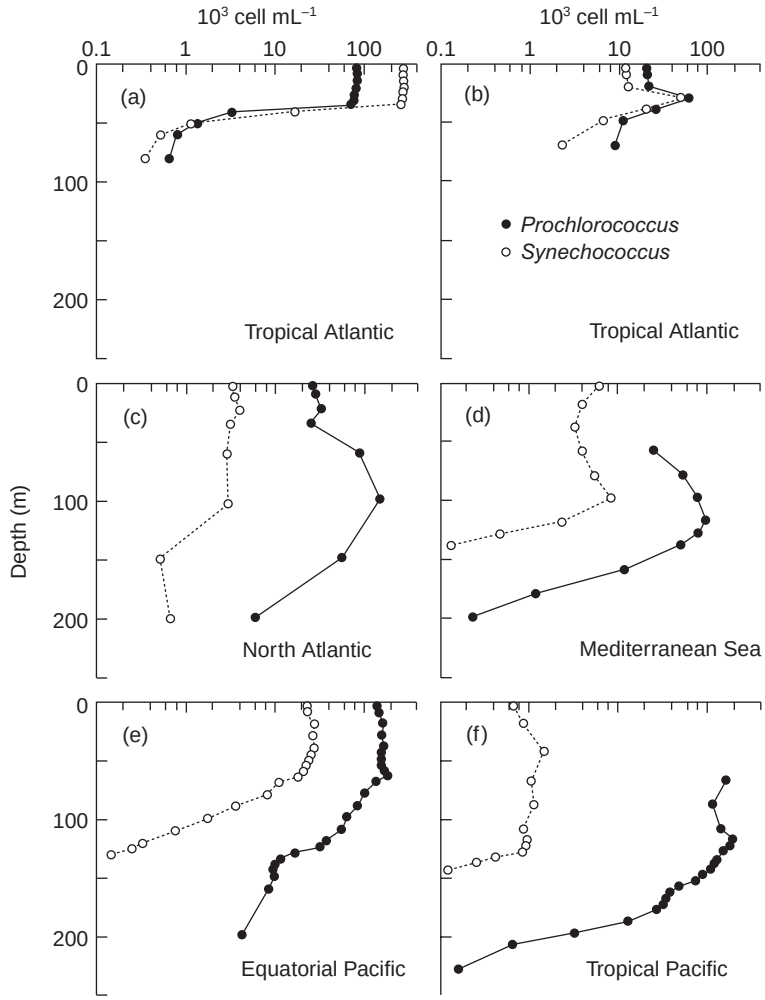

Fig. 3.05 Typical vertical distributions of *Prochlorococcus* and *Synechococcus*: (a) and (b), surface layer maximum; (c) and (d), deep maximum; (e) and (f), uniform distribution in the euphotic zone. After Partensky *et al*. (1999), with permission from the American Society for Microbiology.

the phytoplankton are mixed into the lightless deep layer by the turbulence, and lost. This arrangement, then, is not capable of exhibiting chlorophyll maxima.

In the more realistic situation illustrated in Fig. 3.06(c), it is possible to create the maxima because the intensity of vertical mixing decreases with depth gradually, rather than suddenly as in the simpler model. Nitrate diffusing up is not quickly spread through the mixed layer but moves slowly up through the pycnocline. At the depth where the light intensity is high enough, the photosynthesis begins. The nitrate flux is sufficient to support photosynthesis through a few meters of the water column but there is not enough nitrate to keep phytoplankton growing

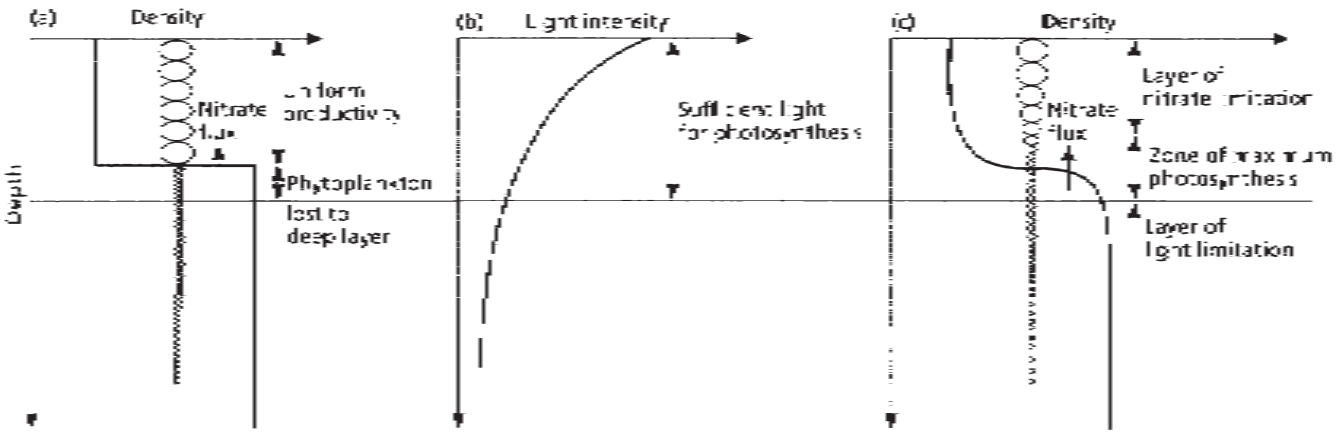

Fig. 3.06 (a) A vertical density profile through a thin pycnocline separating two homogeneous layers. The rate of vertical mixing, symbolized by the circles, changes abruptly through the pycnocline, and is high above and low below the pycnocline. (b) A vertical profile of the average light intensity with an indication of the depth where phytoplankton growth is light-limited. (c) A vertical density profile similar to (a) except that the density increases and the vertical mixing decreases gradually through the pycnocline.

through the whole upper layer. The vertically diffusing nitrate is consumed in a layer of production bounded on the bottom by low light and on the top by low nitrate.

This explanation of the subsurface chlorophyll and productivity maxima in the tropics must be viewed skeptically. It is not, as we show in Section 3.3.4, the only possible mechanism, and it is neither quantitative nor rigorous. Although it has been extrapolated from work carried out in temperate oceans and may not apply in the tropics, it is a promising starting point from which improvements can be devised. The most important factor in the argument, the vertical variation in the turbulent diffusion coefficient, K_v, is very difficult to measure directly and has only recently been done in a few special locations. The main thrust of investigations of vertical profiles in the tropics has been to determine: (i) how much of the primary production is new production and how much is based on recycled nutrients; (ii) the rate of nitrate consumption in the euphotic zone; and (iii) the vertical flux of nitrate through the pycnocline.

Several studies have calculated the vertical eddy diffusivity in stratified tropical and subtropical waters, using either the rate of nitrate uptake by the phytoplankton or physical measurements, such as heat flux through the thermocline, radiochemical tracers, or microscale velocity shear (King and Devol 1979, Eppley *et al*. 1979, Lewis *et al*. 1986). The results converge on low values of vertical eddy diffusivity, of the order of $0.01–0.05 \times 10^{-4}$ m^2 s^{-1}. Using the equation

$$F = K_v \, dN/dz \tag{3.05}$$

where F is the flux of the property N, and K_v is the vertical eddy diffusivity, they were able to calculate vertical fluxes of nitrate that averaged 0.1–0.2 mmol N m^{-2} d^{-1}, which is stoichometrically equivalent to a carbon fixation rate around 0.1 mmol C m^{-2} d^{-1}. This very low figure indicates that in the absence of special upwelling situations, the new production in oceanic waters is extremely low and is limited by the stable vertical structure with its pycnocline barrier and low level of vertical transport of nitrate and other nutrients. However, special upwelling situations are numerous. Storms cause short-term vertical mixing events (Dandonneau 1988), and there are large areas of equatorial upwelling, and large areas where cyclonic gyres cause the pycnocline to rise in a dome towards the surface (see next section).

3.2.5 Equatorial upwelling and domes

In many parts of the tropical oceans, the concepts of a stable mixed layer and a low coefficient of vertical eddy diffusivity in the thermocline do not apply. The first of these areas is at the equator, where extensive upwelling occurs. The detailed physics of the process is best presented in connection with major ocean currents, but a general description is needed here.

At the equator, westward-blowing trade winds give rise to a westward flow along the equator in the mixed layer (Gill 1982; Leetmaa *et al*. 1981). In the Pacific

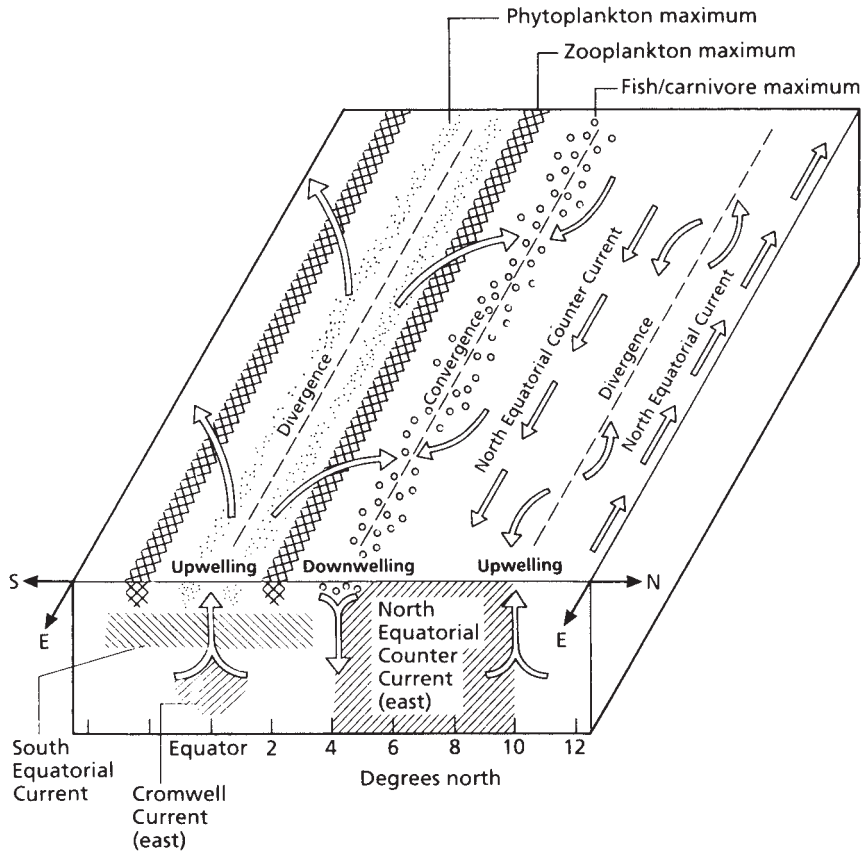

Fig. 3.07 Schematic diagram of equatorial upwelling system. Based on information in Vinogradov (1981). Water upwelling at the equator diverges north and south. Water traveling north eventually converges with water from the North Equatorial countercurrent and sinks. For explanation of the biological zones, see text.

(Fig. 3.07), this westward current is the south equatorial current found roughly between 5° S and 5° N. A short distance away from the equator the Coriolis force (Section 4.2) causes the current north of the equator to be deflected north (i.e., to the right in the Northern Hemisphere), while the current south of the equator is deflected south (i.e., to the left in the Southern Hemisphere). A divergence or spreading of the water is thus set up in the surface layers at the equator. The lost water is replaced by water that upwells from beneath the equator.

Because of the continuous flow of surface water from east to west along the equator, the mixed layer is deeper in the west than in the east. At 155° W it is 80 m or more while at 100° W it is only 10–20 m thick. The water upwelled along the equator comes from the nutrient-rich waters below the shallow pycnocline in the east, but further west, where the mixed layer is deep, the upwelled water comes partly from the nutrient-depleted water in the mixed layer. As Sorokin *et al*. (1975)

have pointed out, this difference leads to greater biological productivity in the east. The trade winds blow from the northeast and generate the westward-flowing north equatorial current between 10° and 20° N. In the band between this current and the south equatorial current, from 5° to 10° N, is the north equatorial counter-current, so called because it is counter to the prevailing winds. Right at the equator at the top of the thermocline is another counter- or eastward-flowing current. This current is the Cromwell in the Pacific and the Lomonosov in the Atlantic. They are about 100 m thick and 200 km wide, and have top speeds of $\approx 1\ ms^{-1}$.

Equatorial upwelling leads to a biological community with a striking pattern that runs parallel with the lines of latitude (Vinogradov 1981). Consider the fate of a parcel of water upwelling at the equator. It is rich in nutrients but not in phytoplankton. As time passes it moves away from the equator and the phytoplankton population grows rapidly. A zone of maximum biomass is found between latitudes 0.5° and 1.0° from the equator. After a further period of time the water has moved further from the equator and a population of grazing zooplankton has developed. Still later, and further from the equator, a population of carnivorous zooplankton reaches its maximum. Finally, by the time the parcel of water is close to the boundary with the north and south equatorial counter-currents, a mature community including macroplankton and young fishes has developed. While these biological events are in progress, the water mass also travels westward with the surface drift. Vinogradov (1981) estimated that water containing a fully developed community has been displaced 250–450 km away from the equator and 1800–2500 km west since being upwelled. Predatory fish such as tuna congregate near the convergence of the two currents to feed on the products of the equatorial upwelling system. A line of high phytoplankton biomass along the equator can easily be seen in satellite images (Plate 1).

A seasonal study of the equatorial upwelling system has been carried out at 5° W (Vinogradov 1981). Between February and May, a warm season occurs that is characterized by a slackening of the southeast trades. The surface layers reach their highest seasonal temperature and upwelling is at a minimum. This event coincides with the period of minimum phytoplankton productivity, the equatorial area showing little difference from the surrounding oligotrophic ocean. In June–July the southeast trades strengthen to force 4–5 and upwelling becomes very vigorous. After a bloom of phytoplankton the process of development of a large biomass of zooplankton follows, reaching its peak between September and November. As a result, the production in these systems may show as much seasonal variability as in temperate latitudes.

As the equatorial counter-currents approach the coast on the eastern boundaries of the major oceans, part of the water turns to the left and part to the right, eventually joining the north and south equatorial currents, respectively. In doing so, they create cyclonic gyres that have ascending water masses in their centers. A well-studied example is the Costa Rica dome, so named for the tendency of the mixed layer to be thin and the thermal structure below it to be dome-like (Wyrtki 1964). The ascending velocity within the dome is estimated at $10^{-6}\ ms^{-1}$, with the

upwelling water originating between 75 and 200 m. Physically, chemically, and biologically the waters in the domes are similar to the water in the equatorial divergence (Blackburn 1981), with a rich development of phytoplankton downstream of the upwelled water. At the eastern end of the Atlantic equatorial countercurrent is found the Guinea dome. Unlike the Costa Rica dome, it is probably seasonal. A similar feature, again seasonal, exists in the Indian Ocean south of Java (Wyrtki 1962).

Chavez and Smith (1995) give a useful review of the biology of open-ocean upwelling areas. The most recent estimates of average primary production for the equatorial Pacific Ocean are 325 g C m^{-2} y^{-1}, four times higher than older estimates. They suggest that the difference is partly due to better measurements, but a systematic increase cannot be ruled out. The production of the total equatorial Pacific is given as 3.65 Pg C yr^{-1}, of which less than 1 Pg is new production. For a perspective on how this contributes to global primary production, see Section 3.5.

3.2.6 Magnitude of equatorial phytoplankton production

The eastern half of the equatorial region of the Pacific is particularly productive. As the satellite picture (Plate 1) shows, there is a triangular region that clearly has higher chlorophyll biomass than the central gyres. Chavez and Barber (1987) made an estimate of its contribution to global phytoplankton productivity. They recognized a "cold tongue" area of equatorial upwelling extending from 90° to 180° W, extending 10° in meridional width, with a total area of 1.3×10^{10} km^3. They found that the mean primary productivity was 0.54 g C m^{-2} d^{-1}, or 197 g C m^{-2} y^{-1}. For the total area Chavez and Barber estimated annual production at 1.9×10^{15} g C y^{-1}. Using the model of Eppley and Peterson (1979), they estimated that 0.85×10^{15} g C y^{-1} is new production. As will be seen in Chapter 5, the Peru upwelling system, which has been widely regarded as a major contributor to global fish production, has a total primary production that is an order of magnitude less than the eastern Pacific equatorial upwelling system. The rate of production per unit area in the coastal upwelling system is much higher, but the area is only a minute fraction of that of the equatorial upwelling system. Taken together, the two contribute about 10% of the global primary production as estimated by Shushkina (1985) or 18% of that estimated by Platt and Subba Rao (1975). The old idea that Pacific waters are mostly nutrient-deficient and unproductive is no longer tenable.

3.2.7 The paradox of high nutrients and low productivity: the iron and the silicate limitation hypotheses

Throughout this chapter it has been taken as axiomatic that if nutrients are present in the mixed layer and the phytoplankton is not light-limited, nutrients will

be taken up until the concentrations reach a very low level. This assumption does not hold for some areas of the ocean where significant amounts of nutrients persist for long periods, while phytoplankton biomass and productivity remain at moderate levels. These conditions exist in parts of the eastern equatorial Pacific, in the Southern Ocean, in parts of the subarctic Pacific and possibly over a large part of the South Pacific.

Two explanations have been suggested for this paradox (Cullen 1991). The grazing hypothesis says that environmental stability permits the evolution of a balanced food web in which phytoplankton biomass is held at a low level by the grazers. The phytoplankton is never allowed to become sufficiently abundant to use all the available nutrients. The second hypothesis suggests that the standing crop of phytoplankton is constrained by the availability of iron. If more iron became available, the standing crop of phytoplankton would increase and deplete the major nutrients, despite any grazing pressure.

Martin and Fitzwater (1988) showed that iron deficiency limited the growth of larger phytoplankton (mainly diatoms) in the northeast Pacific. Martin (1990), invoking the iron-limitation hypothesis, proposed that a cause of the onset of glacial periods in the earth's history could have been the deposition of iron-rich dust into the Southern Ocean. Such deposition would have caused massive phytoplankton blooms, which removed large amounts of carbon dioxide from the atmosphere, transferring them to the deep ocean when the blooms sank. This would be expected to cause global cooling and possibly trigger ice ages (Kumar *et al*. 1995). Morel *et al*. (1991) explained what they believed to be the sequence of events in the phytoplankton after iron enrichment. Their explanation was based on the results of others, and they called it "the ecumenical hypothesis." It has gained wide support. They proposed that the normal phytoplankton cells in regions of high nitrate and low chlorophyll (HNLC) are mostly small, fast-growing cells incapable of using nitrate but using ammonium as their nitrogen source. These cells are in balance with microplanktonic grazers. When iron is introduced into the community, the small numbers of iron-limited larger phytoplankton that are present are able to multiply rapidly. The larger zooplankton that would graze them require several weeks to multiply, so the larger phytoplankton reproduce unchecked, giving rise to a bloom. The resulting community uses nitrate nitrogen as its main source for growth. At the end of the bloom, the sinking of senescent cells and of zooplankton fecal pellets would lead to a downward export of carbon and nitrogen.

This hypothesis invited large-scale field experiments. There have been five, known as Ironex I, Ironex II, SOIREE, SOFeX, and SEEDS. The first two were conducted in the equatorial Pacific, the third in the Southern Ocean, the fourth south of New Zealand and the fifth in the western subarctic Pacific. In the 1993 Ironex I experiment, conducted just south of the Galapagos islands (Martin *et al*. 1994), iron and a highly sensitive tracer were pumped into the propeller wash of a research vessel as it steamed back and forth across an 8×8 km area over 24 hours, raising the iron concentration from about 0.05 nM to about 4 nM. In the first three days the phytoplankton biomass doubled, the chlorophyll increased threefold and

plant production increased fourfold. This response was of short duration, and was small compared with changes observed in shipboard incubation experiments. Macronutrients were not significantly depleted, and a relatively small decrease was observed in the concentration of carbon dioxide.

In Ironex II, in May–June 1995 (Falkowski 1995), a very different result was obtained. A similar total amount of iron was added, but in several batches over a period of 17 days, to give a final concentration between 1 and 2 nM. The chlorophyll concentration rose 30- to 40-fold, nitrate was drawn down from 15 to 4 μM, and carbon dioxide in the water decreased by about 50 ppm. The bloom consisted mainly of diatoms, and mesozooplankton abundance increased markedly. It was believed that there was a very significant export of organic carbon to the depths of the ocean. These findings, coupled with the findings that a large part of the phytoplankton biomass is made up of *Prochlorococcus*, which responds to iron enrichment but not to nitrate upwelling, supports the view that much of the variability in productivity in tropical regions is the result of intermittent aeolian transport of iron.

The SOIREE (for Southern Ocean Iron Release Experiment) used techniques similar to those employed in Ironex II. Boyd *et al*. (2000) distributed 8663 kg of an iron compound over a patch of ocean 8 km in diameter, some 2000 km south-southwest of Hobart, Tasmania (Chisholm 2000). The experiment was a dramatic success. Phytoplankton chlorophyll tripled and remained at that level for a month, and there was a shift from small cells to diatoms. After four weeks the patch of elevated chlorophyll had formed a ribbon 150 km long and 4 km wide. Surprisingly, there was no evidence of enhanced export to the deep ocean, perhaps because diatoms get lighter when released from iron starvation, and settle more slowly.

Even though SOIREE provided no evidence for increased downward export, Watson *et al*. (2000) suggested that the data from SOIREE could be used to support the Martin (1990) hypothesis. They used a model of the ocean–atmosphere carbon cycle (see Section 3.5.4), using parameters from SOIREE, and found that when the model was forced with atmospheric iron fluxes taken from ice-core data, the simulated atmospheric carbon dioxide followed the carbon dioxide levels in the ice-core data. Lancelot *et al*. (2000), using a different model, also found support for the Martin (1990) hypothesis. Ridgwell and Watson (2002) elaborated a possible feedback mechanism in which an initial trend towards global cooling (possibly due to changing insolation) would lead to a less vigorous hydrological cycle, which in turn would favor the production and transport of dust. The dust would cause an increase in CO_2 uptake from the atmosphere by the phytoplankton and hence provide a positive feedback to global cooling. By the year 2000 there were already serious proposals (reported in Chisholm 2000) to attempt to modify the earth's atmosphere by means of large-scale ocean fertilization, and attention was being drawn to the possibilities for unforeseen harm to the ocean ecosystem.

In a preliminary report on SOFeX (Dalton 2002), it was explained that in an area south of New Zealand iron fertilization resulted for the first time in transport of carbon below 100 meters depth. However, the efficiency of the process

was much lower than had been previously calculated, and there were undesirable side effects, including production of large amounts of methyl bromide, which is harmful to the ozone layer.

SEEDS stands for Subarctic Pacific Iron Experiment for Ecosystem Dynamics. Tsuda *et al*. (2003) enriched an area in the western subarctic Pacific and demonstrated a large increase in phytoplankton standing stock and a decrease in nutrients. The dominant phytoplankton species shifted from a pennate to a centric diatom, which doubled 2.6 times per day.

It is now clear that the North Pacific is one of the major high-nitrate, low-chlorophyll areas of the world. The ecology of the plankton at ocean station *P* in the northeast Pacific was reviewed and reinterpreted by Harrison *et al*. (1999). As in other areas showing iron limitation, the phytoplankton is dominated by small cells (< 5 μm) that are not nitrogen limited and whose abundance is controlled by micrograzers. Bursts of production by larger cells may be triggered by deposition of iron-rich dust blown from Asia.

Meantime, Behrenfeld and Kolber (1999) used a more indirect method to suggest that much of the South Pacific gyre is iron-limited. They made frequent measurements of the fluorescence response of the phytoplankton (mostly *Prochlorococcus and Synechococcus*) on a 7000-kilometer transect of the South Pacific Ocean and an even longer transect in the Atlantic Ocean. They discovered diel patterns of fluorescence that were different in the two oceans, and showed experimentally that the features characteristic of the South Pacific phytoplankton were manifestations of iron limitation. Those special features were rapidly lost after *in situ* iron enrichment. They strongly suggested that primary productivity is iron-limited not only throughout the equatorial Pacific but also over much of the vast South Pacific gyre.

Platt *et al*. (2003a) were able to throw new light on proposals to fertilize the oceans with iron. They defined a new dimensionless number, *S*, to be the ratio of nitrogen supply to nitrogen demand of new primary production in the pelagic ecosystem. They developed a new model of nitrogen input and consumption for the mixed layer and calculated *S* for various oceanic regimes. As expected, HNLC conditions were characterized by $S < 1$. The effect of iron enrichment was simulated using the known response of bio-optical terms in the model. In each case, the magnitude of *S* was reduced, but not always below unity. The results were used to assess the possible long-term effects of iron enrichment. We shall return to this topic in Section 10.4.

Attention has also been drawn to the possibility that silicate, rather than nitrogen or iron, is the nutrient limiting primary production in some parts of the ocean. Dugdale *et al*. (1995) described a "silicate pump" that acts in diatom-dominated communities to enhance the loss of silicate from the euphotic zone to deep water (Fig. 3.08). Zooplankters are the key to the pump. While they take both nitrogen and silicate from diatoms when they ingest them, much of the nitrogen is excreted as ammonium or urea in the mixed layer, while the silicon is exported to deep water with the sinking fecal pellets. Dugdale *et al*. (1995) showed that the upwelling waters to the west of Peru at 15° S, already described as high-nitrate,

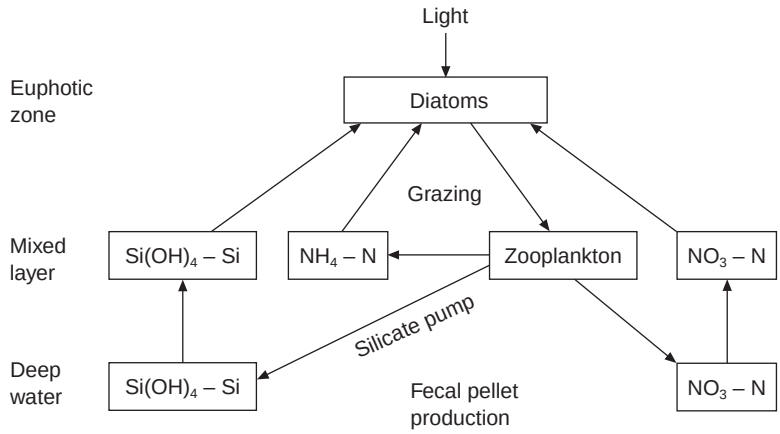

Fig. 3.08 Idealized flow diagram showing the flow of nitrogen and silicon (silicate pump) in a diatom-dominated grazing system. From Dugdale *et al*. (1995), with permission.

low-chlorophyll (HNLC) are also low in silicate and should be described as high-nitrate, low-silicate, low-chlorophyll (HNLSLC). The authors put forward a coupled silicon–nitrogen new production model and offered it as a firmly based alternative to the iron hypothesis, for the control of production in HNLC regions. It was subsequently discovered that the silicate pump does not act efficiently in all upwelling systems (Brezinski *et al*. 1997). We shall return to this topic in Chapter 5.

Trull *et al*. (2001) in discussing the possibility for iron fertilization of the southern ocean, pointed out that while the SOIREE site has high silicate year-round, most of the Southern Ocean north of 59° S is depleted in silicate by mid-summer. As a consequence, the response of these waters to iron fertilization is unlikely to be production of diatoms, but more likely to be the production of non-siliceous organisms. These might not cause export of carbon to the deep ocean.

3.3 Vertical structure and phytoplankton production: temperate and polar waters

We discussed the mixed layer of the open tropical ocean as if it were relatively constant and unchanging, except in special upwelling areas. This assumption is a reasonable first approximation. In temperate and polar waters seasonal change is very evident, however, and it is now being realized that diurnal changes are also important.

As we move poleward from the stable tropical and subtropical waters, we find that in the winter season downward mixing by convection of cooled surface water and wind-driven turbulence combine to cause a progressive deepening of the mixed layer. Turbulence penetrates deeper and deeper into the zone of high nutrient

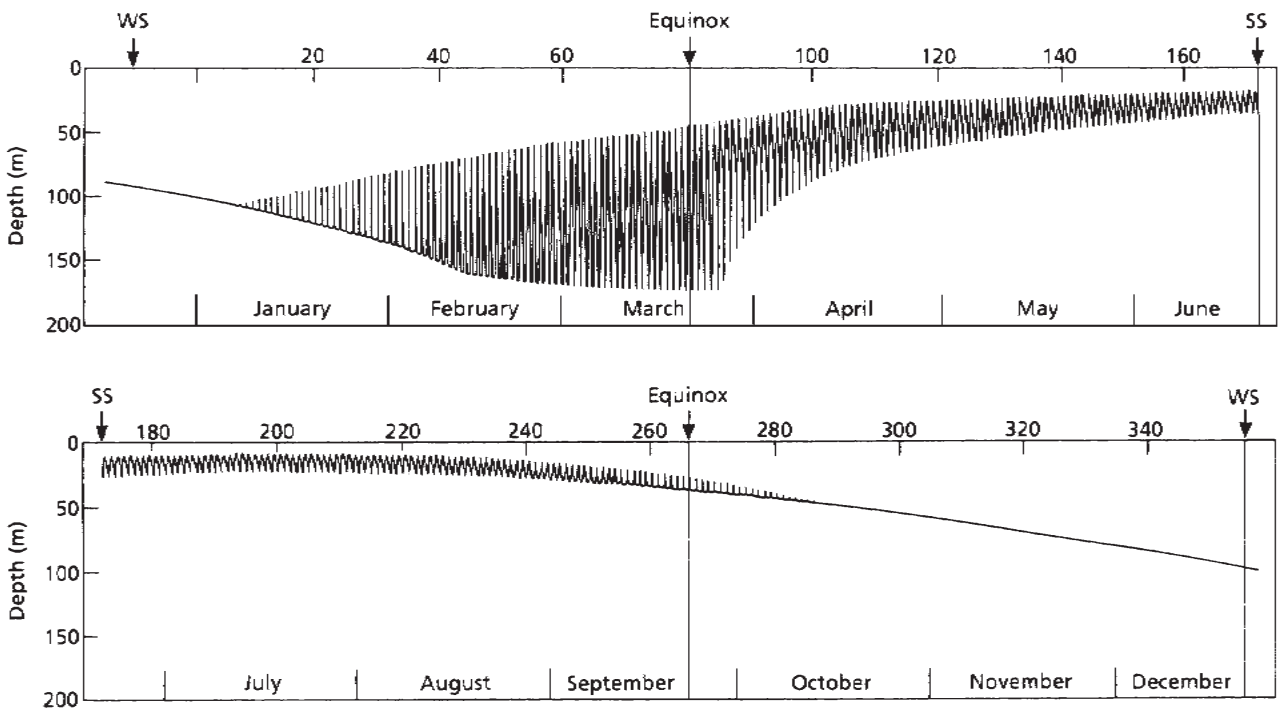

Fig. 3.09 Model simulation of the diurnal variation of the mixed layer depth over the year at latitude 41° N. Note the diurnal movement of the thermocline from January to October. WS, winter solstice; SS, summer solstice. From Woods and Barkmann (1986).

concentration and brings nutrients up into the euphotic zone. On the other hand, phytoplankton cells are carried deeper and deeper by the turbulent mixing, and spend a large proportion of their time below the euphotic zone, where photosynthesis is exceeded by respiration. At the end of winter, when surface warming begins, the reverse process occurs. The mixed layer becomes shallower and phytoplankton cells trapped above the pycnocline spend more and more of their time in the euphotic zone. The net result is a great burst of phytoplankton activity that we call the spring bloom (see Section 3.3.2). Reference to the model calculation in Fig. 3.09 shows that at latitude 41° N deepening of the mixed layer continues until late March, but rapidly shallows during the early part of April. The figure also shows that from January onward, a diurnal oscillation occurs in the depth of the mixed layer. In the next section we consider the physics of these processes.

3.3.1 Diurnal and seasonal changes in mixed layer depth

The discussion in Section 3.2.2, concerning changes of temperature and depth of the mixed layer, assumed the inputs of heat and mixing energy to be constant in time. These factors, however, vary over the day and the year, giving rise to diurnal and seasonal changes in the temperature and depth of mixed layers.

To illustrate diurnal changes, the variation of net heat gain through the ocean surface at 40° N 40° W, mid-Atlantic site, through the course of an average day in both July and December is shown in Fig. 3.10. In July the sea loses heat at the

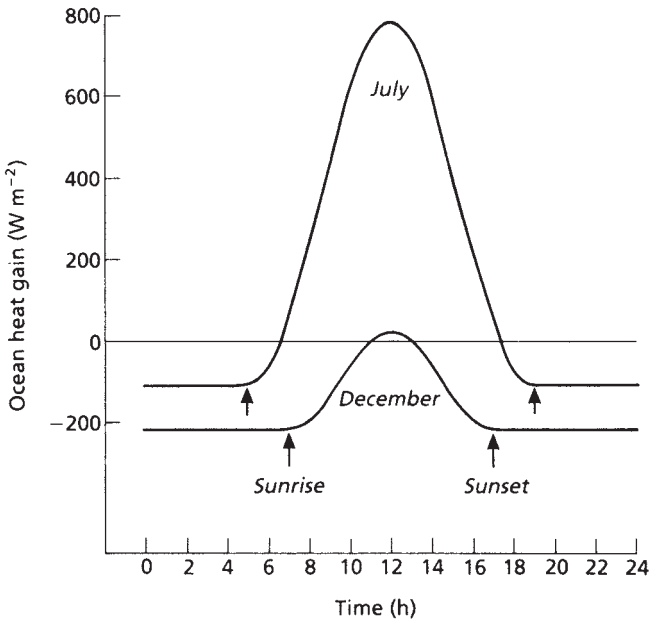

Fig. 3.10 Diurnal changes in the net heat gain during an average day in July and December at 40° N, 40° W.

rate of ~120 W m^{-2}, mostly by evaporation and long-wave radiation. The losses continue at much the same level throughout the day because the controlling factors, such as wind speed, air–sea temperature difference, and cloud amount, tend to remain fairly constant.

Heat gain, on the other hand, depends mostly on the altitude of the sun, which varies greatly throughout the day. Heat input varies from zero during the night to almost 900 W m^{-2} at noon. Under these circumstances a mixed layer of constant depth becomes warmer during the day and cooler at night but, because there is a net gain of energy over the day, there will be a net increase in temperature over the day. If the wind decreases, the mixed layer becomes thinner and the temperature increase in the layer will be greater. This change occurs because most of the radiant energy is absorbed in the top few meters, as indicated in Figs. 3.02 and 3.03, and because weaker winds allow the heat to be concentrated in a thinner layer. If the wind increases, the mixed layer becomes deeper and the heat input is spread throughout a greater depth, leading to a smaller temperature rise over the day.

In December the sun is above the horizon each day for only 10 hours at 40° N 40° W and delivers a total of only 4300 kJ m^{-2} over the day, while the heat losses total 19,000 kJ m^{-2}. Under these circumstances not enough heat is gained during the day to form a warm surface layer for even part of the day.

The annual variations of the heat budget components at the site of ocean weather ship *Echo*, 35° N 48° W, are illustrated in Fig. 3.11. Included are the heat input from short-wave radiation, and the losses from radiation, evaporation, and conduction. These data, extracted from the atlas of Isemer and Hasse (1987), show that short-wave radiation is the only source of heat and that the latent heat of evaporation is responsible for most of the heat loss in all months. The sum of all the factors indicates that the sea is gaining heat through the sea surface at this location only from April to August, and over the year more heat is lost than is gained, which indicates that heat must be advected into this region to keep the mean temperature the same from year to year.

The curve of total gains and losses suggests that all the heat gained through the surface in the summer would likely be lost by the following January or February. By that time no seasonal thermocline would remain in the upper layers of the ocean.

The model prediction of the depth of the mixed layer shown in Fig. 3.09 incorporates both the diurnal and seasonal variations in the heat gains and losses from 41° N 27° W (north of the Azores). In mid-December at the winter solstice the model indicates there is no diurnal thermocline, but that the depth of the seasonal thermocline is approaching 100 m. In early January a diurnal thermocline begins to be formed. Its minimum depth decreases from about 100 m in January to 10 m in July. The maximum depth of the diurnal thermocline, which is the depth of the seasonal thermocline, continues to increase from December through late March. It then quite suddenly decreases when the heat gained during the day is neither lost at night nor mixed down to great depths by the wind.

Through the spring and early summer the upper mixed layer becomes more stable. The depth of the seasonal thermocline decreases, as does the difference

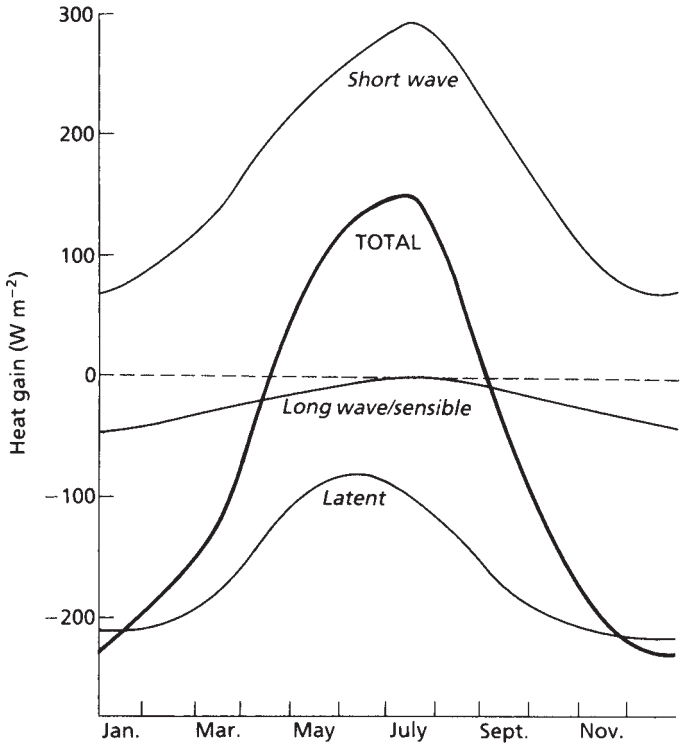

Fig. 3.11 Seasonal changes in net short-wave radiation, net long-wave radiation/sensible heat exchange, and latent heat exchange, and the total at 35° N 48° W.

between the minimum and maximum depths of the diurnal thermocline. From late summer through early winter the amount of heat lost to the atmosphere from the sea steadily increases, as does the mixing energy from the wind. The diurnal thermocline tends to disappear as the seasonal one moves to greater depths.

3.3.2 The mechanism of the spring bloom

Early biological oceanographers on both sides of the North Atlantic became aware that, in temperate coastal waters and in the open ocean, there was a marked increase in abundance of phytoplankton in spring time. This growth was christened the spring bloom. In this section we follow the development of our understanding of this process. We now know that no distinct bloom occurs in large areas of the temperate Pacific Ocean, but rather a gradual increase in phytoplankton abundance from mid-winter to mid-summer (see Section 3.3.8).

Working in the waters off England and Scotland, Atkins (1928) suggested that the spring bloom was triggered by the spring increase in solar radiation. Marshall and Orr (1928), on the other hand, found that enough light was present

for vigorous phytoplankton growth at the latitude of the British Isles even in winter. In the course of an investigation into the productivity of the Bay of Fundy, Gran and Braarud (1935) suggested that stabilization of the water column by thermal stratification could have the effect of greatly stimulating primary production. The idea was that in winter time in temperate latitudes the phytoplankton cells are being circulated to the full depth of the mixed layer; hence they spend a large proportion of their time in regions lacking enough light for growth. With the onset of surface warming and the formation of a much shallower mixed layer, phytoplankton cells are held for longer periods in the euphotic zone (i.e., the zone in which there is sufficient light for growth and cell division). Mills (1989) traced the evolution of this line of thinking through earlier publications by Gran (e.g., Gran 1931).

We shall see in later chapters that this mechanism – by which turbulent mixing of the entire water column brings nutrients to the surface waters, after which stratification sets in and the phytoplankton are held in the euphotic zone so that they can multiply rapidly – is the key to understanding phytoplankton productivity in a variety of situations including estuaries, upwelling areas, and tidal fronts. The idea was further developed by G. A. Riley and used to explain the spring bloom on Georges Bank (Riley 1942). It was also incorporated into a major model of the phytoplankton dynamics of the North Atlantic (Riley *et al*. 1949). However, the classic quantitative exposition of the theory that we present here in detail is by Sverdrup (1953) and is entitled "On conditions for the vernal blooming of phytoplankton."

Consider the situation (Fig. 3.12) of a water column in which the mixed layer extends to depth d, the turbulence is sufficiently strong to distribute the phytoplankton cells uniformly through it, nutrients are not limiting, and the extinction coefficient of light (α in Eqn. 3.01) is a constant. Because photosynthesis is proportional to light intensity, and assuming that the light intensity at the surface is not high enough to inhibit photosynthesis, the expected distribution of the daily rate of phytoplankton production will be as shown, with a maximum at the surface, decreasing logarithmically to a low level at depth. The rate of respiration, on the other hand, being more or less independent of light, will be constant throughout the mixed layer. At some depth D_c the daily rate of photosynthesis is just balanced by the daily rate of respiration. This level is the compensation depth. Experiments have shown that for commonly occurring diatoms the light energy flux I_c at the compensation depth is ~1.5–1.7 W m^{-2} (converting between watts (W) and μmol s^{-1} is described in Box 3.03).

This information, together with the daily irradiance at the surface and the extinction coefficient, permits calculation of the compensation depth, D_c. Taking the daily mean surface irradiance of I_o as 200 W m^{-2} and the extinction coefficient α as 0.4 m^{-1} we have, from Eqn. 3.01, $I_c/I_o = 1.5/200 = \exp(-0.4D_c)$. Taking the natural logarithm of each side gives $-4.9 = -0.4D_c$ from which $D_c \approx 12$ m.

Now consider a phytoplankton cell circulating in a random manner throughout the mixed layer. When it is near the surface, the rate of photosynthetic production will greatly exceed respiration. When it is near the bottom of the mixed

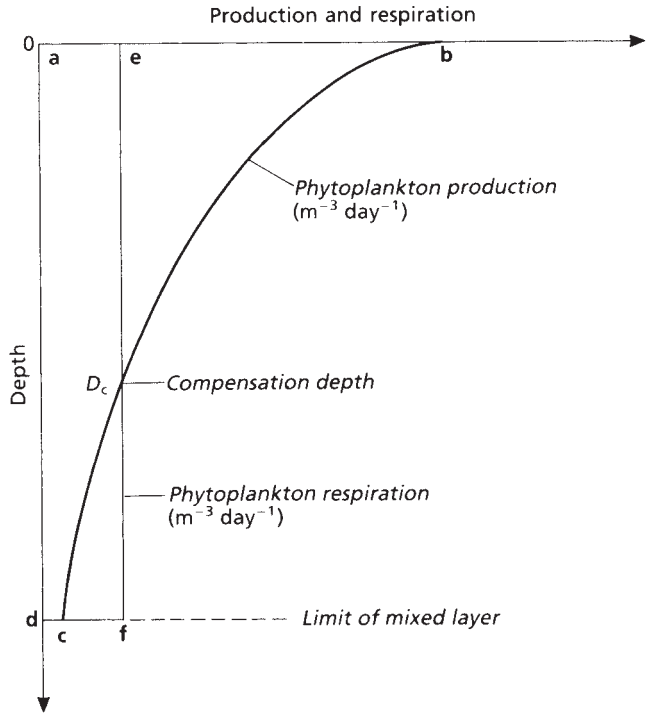

Fig. 3.12 Diagram illustrating theoretical distribution of phytoplankton production and phytoplankton respiration. After Sverdrup (1953).

Box 3.03 Converting light energy flux units: watts to μmoles s^{-1}

Physicists use watts to measure the flux of radiant energy because it is a convenient unit when estimating the quantity of heat or light in the radiation. Marine biologists prefer to use μmoles s^{-1}. This term better suits analyses of photosynthesis because it, like photosynthesis, varies with both the number and frequency of the incident photons.

The energy of a photon of light is $h\nu$, where h is Plank's constant (6.63×10^{-34} J s) and ν is the frequency of the radiation. The frequency and wavelength of the light are related by $c = \nu\lambda$, where c is the speed of light (3×10^8 ms^{-1}), ν the frequency and λ the wavelength.

As an example let us say that the peak of the short-wave radiation at 10 m depth in Fig. 3.01 is at a wavelength of 480 nm. Each photon of light will have a frequency of c/λ, i.e., $3 \times 10^8 / 480 \times 10^{-9} = 6.25 \times 10^{14}$ s^{-1}. Each of these photons will have an energy of $6.63 \times 10^{-34} \times 6.25 \times 10^{14} = 4.14 \times 10^{-19}$ J.

A mole of photons contains 6.022×10^{23} photons (Avogadro's number). Thus the energy in a mole of photons is $4.14 \times 10^{-19} \times 6.022 \times 10^{23} = 24.9 \times 10^4$ J and in a μmole is 0.249 J, which is equivalent to stating that 1 J = 4 μmole (at 480 nm). Since a watt is a J s^{-1} we can conclude that 1 W = 4 μmole s^{-1} (at 480 nm).

layer, the reverse will be true. The condition for net positive population growth is that the integrated production, represented by the area *abcd*, be greater than the integrated respiration, represented by the area *aefd*. As the depth of the mixed layer increases, respiration increases proportionately but production increases by a small amount, or not at all. There is, therefore, a critical depth of the mixed layer at which integrated production just equals respiration. At shallower mixed-layer depths the phytoplankton population has an excess of production, and therefore grows. At greater depths of the mixed layer it fails to grow. Note that the effect of grazers has not been considered up to this point.

Sverdrup (1953) showed that the critical depth of the mixed layer D_{cr} can be calculated by algebraically equating the areas representing production and respiration. Assuming that daily photosynthetic production at any depth is proportional to the mean daily light energy at that depth, we may regard the line *bc* in Fig. 3.12 as the distribution with depth of the mean daily light energy or the mean daily photosynthetic production. The length of the line *df* or *ae* is equal to the light intensity at the compensation depth, D_c, and is proportional to the rate of respiration at all depths in the mixed layer. From the discussion above, the intensity of radiation I_c or the length of *df* or *ae* at the compensation depth D_c can be expressed following Eqn. 3.01 as

$$I_c = I_o \exp(-\alpha D_c) \tag{3.06}$$

When the depth of the mixed layer is equal to the critical depth D_{cr}, the area *aefd* representing the total respiration is given by $I_c D_{cr}$. The area *abcd* representing the total photosynthesis is given by

$$I_o \int_{D_{cr}}^{0} \exp(\alpha z)\, dz = I_o[1 - \exp(\alpha D_{cr})]/\alpha \tag{3.07}$$

Equating the two areas gives

$$I_c D_{cr} = I_o[1 - \exp(\alpha D_{cr})]/\alpha \tag{3.08}$$

which can be solved graphically for D_{cr}.

Sverdrup then proceeded to calculate the values of D_{cr} for ocean weather ship *M* in the Norwegian Sea in the spring of 1949 (Fig. 3.13). When plotted with data for the actual depth of the mixed layer and the numbers of phytoplankton and zooplankton, it became clear that the critical depth increased from about 30 m at the beginning of March to nearly 300 m at the end of May, and that the major increase of populations of both phytoplankton and zooplankton occurred when the depth of the mixed layer was much less than the critical depth.

Detailed examination of Fig. 3.13 reveals the following: (i) through March the amounts of phytoplankton and zooplankton were very small, and during this period the depth of the mixed layer was much greater than the critical depth; (ii) the mixed-layer thickness changed from more than 300 m on April 2 to 50 m on April 7, which probably indicated advection of a different water mass containing abundant

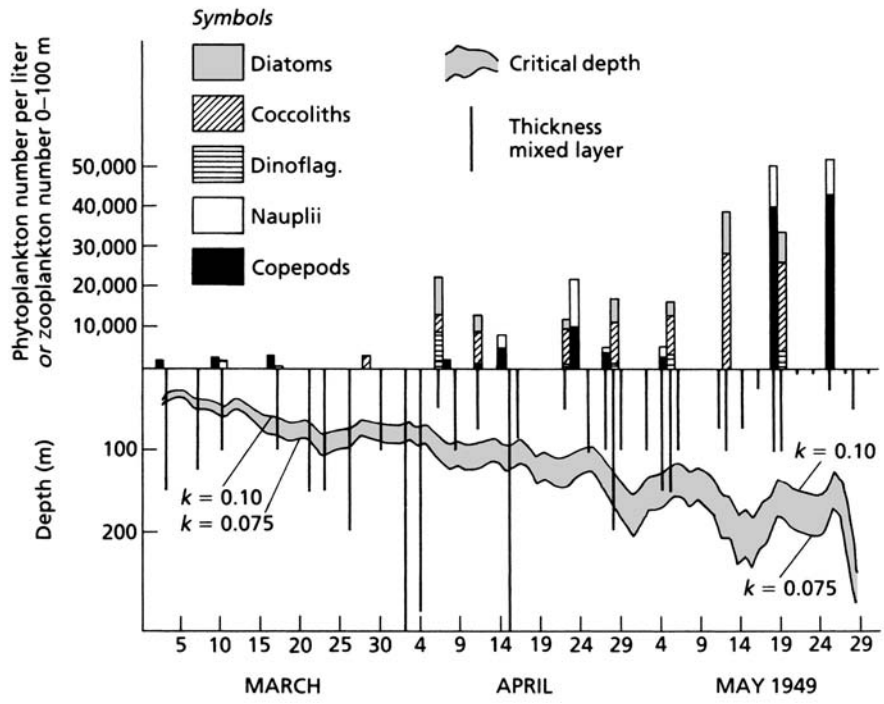

Fig. 3.13 Data from ocean weather ship *M* in the Norwegian Sea on plankton, mixed layer thickness, and critical depth. $k = 0.10$ and $k = 0.075$ represent the range of values of extinction coefficient (α in text). Note that the mixed layer is always deeper than the critical depth until early April, when a large increase in phytoplankton biomass occurs. From Sverdrup (1953).

phytoplankton, rather than stabilization by warming; (iii) the development of zooplankton populations in April undoubtedly reduced the size of the phytoplankton populations; and (iv) during May, when the depth of the mixed layer was much less than the critical depth, phytoplankton populations reached high densities in spite of the presence of sizable zooplankton populations. The overall picture was in accordance with the theory that the spring bloom is strongly dependent on the stability of the water column. We may note that this model takes no account of diurnal variation in the thickness of the mixed layer.

Sverdrup's (1953) paper was, then, a quantitative exposition and a field check of the phenomenon first described by Gran in 1931. In later chapters we shall find that enhancement of primary production by stabilization of the water column after a period of strong mixing is a phenomenon that occurs in many situations, in estuaries and in coastal upwelling areas, for example. Most oceanographers refer to it as the Sverdrup mechanism, but it would be more accurate to call it the Gran effect.

It is important to remember that Sverdrup's model applies to temperate latitudes where, after the winter deepening of the mixed layer, surface waters contain a

good supply of nutrients, and where spring warming leads to a shallowing of the mixed layer. We may now proceed to follow the fate of the phytoplankton as the year progresses. During the period of stratification the pycnocline presents a barrier to the vertical diffusion of nutrients and the phytoplankton progressively depletes those nutrients present in the mixed layer. At the same time, zooplankton are consuming phytoplankton and excreting nutrients. A common result of these processes is a rapid depletion of the dissolved inorganic nitrogen content of the mixed layer and a fall in phytoplankton biomass, marking the end of the spring bloom.

During the summer period conditions may be similar to those described in Section 3.2.5 for tropical oceans – i.e., there may be stable stratification and very limited diffusion of new nutrients into the mixed layer. Phytoplankton production is then confined to that which can be sustained by recycled nitrogen and the small amount of diffusion, and it is common to find that the larger phytoplankton community changes from one dominated by diatoms to one dominated by flagellates. This change occurs partly because the flagellates have a better surface : volume ratio and are able to perform locomotion out of microenvironments with low nutrient concentrations (see Section 2.3.4 and Margalef 1978a), and partly because silicate becomes limiting to diatoms. As the days shorten and surface waters begin to cool, however, convective and wind-driven processes once more begin to cause a deepening of the mixed layer, so that new nutrients are entrained from below the thermocline, and an autumn bloom may occur before the depth of the mixed layer once again exceeds the critical depth. Deep winter mixing leads to increasing concentrations of nitrate in surface waters, and these levels reach a maximum in March. Spring warming and a shallowing of the thermocline lead to a spring bloom in late April and early May, as shown by the peak in chlorophyll concentration. Nitrate concentration declines rapidly during the spring bloom. During summer, primary production is moderately high and the chlorophyll low, because zooplankton remove the phytoplankton biomass almost as fast as it is produced. Most of the primary production is made possible by the regeneration of ammonium through excretion of the consumers.

The timing of spring and autumn blooms is dependent in part on latitude. At high latitudes, where the spring warming comes late and autumn cooling begins early, it is common to find just one bloom in mid-summer. This bloom is often more pronounced than in temperate waters and two factors undoubtedly contribute (Cushing 1975). The first is the longer daylight characteristic of high latitudes in summer, which permits the phytoplankton populations to grow for up to 24 hours per day. The second is the low temperature, which slows the metabolism of the grazers and allows the phytoplankton populations to grow in spite of them.

During the early 1990s there was a reevaluation of the usefulness of the Sverdrup (1953) formulation (summarized in Platt *et al*. 1994). Several reports had been made of the initiation of blooms in the absence of stratification (e.g., Eilertsen 1993). A typical scenario involves clear water with good light penetration and a low level of turbulence. A rapid increase in phytoplankton biomass precedes the shallowing of the mixed layer. Huisman *et al*. (1999) offered an

explanation for the formation of blooms in the absence of stratification. They called it the critical-turbulence model and proposed that when turbulence is below a critical level, phytoplankton growth rates can exceed the vertical mixing rates, and a bloom develops irrespective of the depth of the upper water layer. They supported their ideas with numerical simulations.

A global-scale test of Sverdrup's theory

Obata *et al*. (1996) checked, on a global scale, whether the critical-depth theory of Sverdrup (1953) is adequate to explain the formation and destruction of phytoplankton blooms. Data on shallowing of the mixed layer were taken from published climatological data, and critical depth was calculated according to Sverdrup's formula, using published data for clear-sky insolation, cloud cover, and optical water types. The incidence of phytoplankton blooms was inferred from remotely sensed chlorophyll data.

The authors found that the critical-depth theory explained the occurrence of spring blooms in middle and high latitudes of the North Atlantic and in the western North Pacific, but in the eastern North Pacific and the Southern Ocean there was no spring bloom, even though the mixed layer was shallower than the critical depth. These anomalies are discussed in Sections 3.2.7 and 3.3.8.

The feedback that can occur between the biological events and the physics of the mixed layer has also spurred discussion in relation to the Sverdrup model. Stramska and Dickey (1993) summarized earlier examples of a heating effect on the mixed layer due to absorption of light in the phytoplankton cells. They also contributed new data from the North Atlantic and a model showing that the increase in phytoplankton abundance induced an increase in sea surface temperature of about 0.2 °C. This increase, in turn, led to stronger near-surface thermal stratification and shallower mixed layers. It was a factor in the formation of a bloom that preceded the formation of the seasonal thermocline. This topic is discussed further in Section 11.3.

3.3.3 Large-scale turbulence and phytoplankton performance

In Chapter 2 we discussed the relationship between phytoplankton and small-scale turbulence. In this section we turn our attention to turbulence on the scale of meters or tens of meters that is characteristic of the mixed layer. The exponential decay of light intensity with depth means that as a phytoplankton cell is carried passively from near-surface to depth and back again it is exposed to a changing light environment. There has been a controversy over the question of whether phytoplankton cells in a fluctuating light regime are more productive than they would be if exposed to light of a constant average value. Marra (1978) produced experimental evidence that seemed to show a strong effect, but Falkowski and Wirick (1981) and Gallegos and Platt (1982) concluded that the effect was negligible.

Resolution of the controversy was provided by Lewis *et al*. (1984a), who pointed out that the metabolic machinery of a phytoplankton cell is complex and there is no reason to suppose that all of its component parts would adapt to changes in light level at the same rate. They proposed a model in which properties that adapted rapidly to the changing light levels would show marked differences between cells taken from the top and from the bottom of the mixed layer, while properties that adapted slowly would show minimal differences between surface and depth. They suggested that this variation would explain the difference in the results of earlier investigations.

To test this model Lewis *et al*. (1984b) made a series of measurements of the turbulent energy dissipation rate (as a measure of vertical motion through the light gradient) in the mixed layer of a coastal inlet on different days, and simultaneously measured two photoadaptation properties of the phytoplankton on those same days. As an example of a relatively slowly adapting parameter they chose P_M^B, the maximum potential photosynthetic rate normalized to chlorophyll-*a*. The difference between surface samples and those from the base of the mixed layer was labeled ΔP_M^B. There was a marked decrease in ΔP_M^B with increase in turbulent energy dissipation rate. For their example of a property with a rapid photoadaptive response they chose *in vivo* fluorescence per unit chlorophyll. Its value was less at the surface than at depth on all days except one, which was the day of highest turbulence.

The results were in accordance with the model. At slow rates of turbulent mixing, and hence of light fluctuation, there was a marked difference in values between samples from the top and the bottom of the mixed layer for the slowly adapting parameter, as well as for the fast-adapting parameter. As the rate of light fluctuation increased, the differences between top and bottom in the slowly adapting parameter decreased while those in the fast-adapting parameter persisted.

Lewis *et al*. (1984b) then calculated the time scale of the turbulent mixing. We saw in Box 2.04 that the approximate time for vertical diffusion to occur over the distance L can be estimated using the vertical eddy diffusivity K_v from $\tau = L^2 K_v^{-1}$. Following Osborn (1980), the authors substituted $\varepsilon/4N^2$ for K_v (where ε is the energy dissipation and N is the Brunt–Väisälä frequency), so that they were able to calculate the time scale of turbulent mixing from the energy dissipation:

$$\tau = 4N^2L^2\varepsilon^{-1} \tag{3.09}$$

They found that on the various days of observation the mixing time scale ranged from about 1 to more than 10 hours. Since it had previously been shown that the time scale for adaptation of the *in vivo* chlorophyll fluorescence is about 1 hour, while the time scale for photoadaptation of P_M^B is 6–10 hours, the results were in good agreement. Hence they concluded that the time scale of turbulence has strong effects on some of the parameters of photosynthetic performance, but is less strong for others. Between 1996 and 2003 several complex mechanistic models of photoacclimation in phytoplankton were developed. For details see Flynn (2003a) and references therein.

3.3.4 The oligotrophic phase in temperate waters

We have seen that, after the termination of the bloom in temperate oceans, the water is stratified and the vertical diffusion of new nitrogen through the pycnocline is restricted. Production in the mixed layer is then largely confined to that which can be supported by nitrogen regenerated by the grazers. During this phase the profiles of nutrients, chlorophyll, and production resemble those of an oligotrophic tropical system, and the similarity extends to the presence of a subsurface chlorophyll maximum. In the course of the debate about what mechanism causes the formation of a subsurface chlorophyll maximum in temperate waters, much light has been thrown on the mechanisms that sustain production at the permanent chlorophyll maximum in tropical waters. However, in reviewing the history of the ideas we must remember that the investigators were not aware of the major role played by cyanobacteria such as *Prochlorococcus*, which do not use nitrate but use ammonium very efficiently at low light levels (see Section 3.2.4). The observations apply mainly to diatoms and flagellates in the plankton.

It was realized early that if phytoplankton forming the spring bloom sink, they carry the chlorophyll maximum to greater depths. The sinking rate may vary with the physiological condition of the cells. It was later suggested that since the cycle of phytoplankton growth and decay is faster near the surface, nutrient depletion and population decay will occur there earlier, while populations in deeper water are still actively growing. Hence the chlorophyll maximum will occur at successively greater depths. Furthermore, since turbulent mixing declines in and below the thermocline, there will be limited mixing between deeper and less-deep populations. These mechanisms were the basis of models by Riley *et al*. (1949), Steele and Yentsch (1960), and Bienfang *et al*. (1983).

Jamart *et al*. (1977) produced a complex model that included all conceivably important factors. They had terms representing the seasonal change in light intensity, the phytoplankton sinking rate, the rate of grazing by zooplankton, the phytoplankton respiration, and the decrease with depth in the turbulent diffusion coefficient (K_v). They succeeded in reproducing the main features of the developing chlorophyll maximum through the spring and summer of the temperate zone. In a subsequent paper (Jamart *et al*. 1979) they showed by means of sensitivity analysis that changes in sinking rate were not important in their model. The decrease in turbulent diffusion with depth was the main factor inducing a progressive deepening of the chlorophyll maximum.

The simple explanation for the subsurface chlorophyll and productivity maxima in tropical waters, presented in Section 3.2.4, is based primarily on this model by Jamart *et al*. (1977). We assumed that the decrease in the turbulent diffusion with depth combined with the decreasing light intensity are the two most important factors that the authors incorporated. The profile in Fig. 3.06(c) that is intended to represent the tropical situation is similar to that found in late summer in the Jamart *et al*. (1977) model.

Summarizing to this point, two processes have been proposed to explain the existence of the subsurface chlorophyll maximum in temperate waters. The first is mainly biological and depends on the sinking rates of phytoplankton. Increase of biomass is assumed to begin near the surface and to sink subsequently, where it is observed as a subsurface maximum. We should note that diatoms in the spring bloom sink, but the picoplankton that replace them in summer have a negligible sinking rate. However, fecal pellets containing picoplankton may sink.

The second process is physical in nature and depends on the gradual decrease in turbulent mixing through the pycnocline coupled with the decrease in light intensity with depth. As the light decreases, the time for phytoplankton to grow, deplete nutrients, and decay increases. This increase, together with the smaller vertical mixing, allows the maximum in production to occur at different times at different depths. Grazing is not a critical factor. It seems likely that both the biological and physical processes are important, but which dominates will depend on the circumstances.

3.3.5 The results of Lagrangian modeling

A new type of model of phytoplankton growth was introduced by Woods and Onken (1982). They pointed out that all previous models had studied a cloud of individual plankters relative to a continuous property of sea water – for example, chlorophyll concentration. They called this the Eulerian-continuum method. This procedure suffers from the disadvantage that processes such as cell growth are assumed to proceed at the average rate. The authors suggested that it was important to understand the interactions of the physiology of each phytoplankton cell with the diurnal changes in mixed-layer depth, light intensity, and nutrient concentration. For this purpose they proposed to follow an ensemble of individual phytoplankters. At each time step of the model, the growth or decay of each cell was determined from the light and nutrient environments it was in. This incremental change was then added to or subtracted from the existing cell. They called this process of following the cells through their individual lives the Lagrangian-ensemble method.

The authors drew particular attention to the diurnal changes in the depth of the mixed layer. As we saw in Section 3.3.1, increased cooling at night causes a progressive deepening of the mixed layer. This process continues until about one hour after sunrise, when solar heating begins to exceed the rate of surface cooling and the mixed layer gets progressively shallower, continuing until noon. This diurnal cycle changes with the seasons (Fig. 3.09). The net result is that the water column can be divided into four zones that vary in thickness with the seasons. They are: (i) the mixed layer; (ii) the diurnal thermocline; (iii) the seasonal thermocline; and (iv) the interior of the ocean.

In a version of the Lagrangian-ensemble model (Wolf and Woods 1988), which simulates a water column in the open ocean at 41° N 27° W, the seasonal variation in the mixed-layer depth was as shown in Fig. 3.09. In the model, it was

assumed that the time scale of turbulence in the mixed layer was 30 minutes. Since the model ran with time steps of 1 hour, it was assumed that at the end of each period a particle in the mixed layer had equal probability of lying at any depth between the surface and the base of the mixed layer. Particles lying near the bottom were left isolated below the diurnal thermocline and were subject to only their normal sinking of 2 m d^{-1}. Most of them were re-entrained into the mixed layer when the thermocline descended the next night, but at times when the diurnal mixed layer was becoming shallower, a proportion were not re-entrained and entered the seasonal thermocline, where they remained until the following spring. The model simulated well the course of events in nature.

Wolf and Woods (1988) pointed out that phytoplankton cells in the model arrived at a particular depth and time with differing histories of exposure to light and to nutrients and hence differing degrees of adaptation to the prevailing conditions. This "adaptation diversity" makes the model performance significantly different from that of Eulerian models. The broad conclusions were that the chlorophyll maximum formed as a consequence of the surface exhaustion of nutrients, with growth limited to cells in and below the nutricline. Cell division was nutrient-limited in the upper reaches of the nutricline and light-limited below. In these respects the model is similar to the one by Jamart *et al*. (1977) discussed in the previous section. The chlorophyll maximum moves down through the water column because of the change in the turbulent mixing rates between the mixed layer and the pycnocline. Also, as in the Jamart *et al*. (1979) model, the chlorophyll maximum in the model descends through the seasons without the invocation of a change in phytoplankton sinking rate. We must remember that these models predict chlorophyll distribution, not biomass. The ratio of chlorophyll to carbon varies by a factor of five. It would be useful to re-examine these questions using mechanistic photoacclimation models, of the kind described in Flynn (2003a).

In the standard model with no upwelling the nutricline moved deeper and deeper below the bottom of the mixed layer throughout the summer period. With moderate upwelling, at a speed less than the sinking rate of the phytoplankton, production increased but the nutricline and chlorophyll maximum stayed well below the mixed layer. Upwelling rates greater than the sinking speed caused the nutricline and chlorophyll maximum to move upward until they entered the mixed layer and produced an explosive burst of phytoplankton growth. The authors proposed that episodic upwelling events are responsible for the transient patches of high surface chlorophyll ("hot spots") seen in satellite images of ocean color (see Section 3.2.6).

Considering this and the previous sections, it appears that the nutricline is formed as a result of progressive depletion of nutrients in the mixed layer during the oligotrophic phase in temperate waters, and that the subsurface chlorophyll maximum forms in and around the nutricline, with a magnitude of production that depends on the intensity of upwelling. While experimental evidence shows that reduction in light intensity and/or increase in nutrient concentrations brings about a reduction in phytoplankton sinking rate, this mechanism appears not to be essential to the formation of a subsurface chlorophyll maximum. It is enough

that the growth and decay of phytoplankton occur more slowly in the pycnocline than in the mixed layer.

McGillicuddy (1995) compared the Lagrangian model of Wolf and Woods (1988) with a Eulerian model of Lande and Lewis (1989) at two levels of mixing. For relatively weak mixing, the population growth rates predicted by the two models differed by less than 5%, but in vigorously mixed conditions Lagrangian effects caused a 20% reduction in population growth rate. The key to the variation lies in the differing parameters used for photoadaptation in the two types of models. If similar formulations were used, the two models would be reconciled. The literature appears to show that the values used by Lande and Lewis are more appropriate.

Lagrangian-ensemble (LE) simulation models of the population dynamics of diatoms in the water column of the Azores and off Greenland (Woods and Barkmann 1993) were used to assess the usefulness of the Sverdrup (1953) model for predicting the onset of the spring bloom. The authors pointed out that the Sverdrup model assumes a homogeneously distributed population of identically adapted phytoplankton circulating in a mixed layer which does not vary diurnally, whereas the LE model calculates the distribution of the cells in the water column at each instant, allowing for the effect of diurnal changes in mixed-layer depth, and allowing photoadaptation to take place according to the position of each cell in the water column (see Section 3.3.3). One result is that the modeled distribution of light does not vary exponentially with depth, but is influenced by the distribution of phytoplankton in the water column.

In the Sverdrup model, the critical depth descends steadily from winter solstice to summer solstice, but in the LE model the critical depth, calculated for the photo-adapted population of diatoms in the diurnally varying mixed layer, descends rapidly in January and February. The compensation depth in the LE model also differs markedly from the Sverdrup model because of the different assumptions. In the LE model the compensation depth tracks the mixed-layer depth within 1 m as it rises from 100 to 40 m, during the one month after the vernal equinox.

Woods and Barkmann (1993) concluded that the relationship between the critical depth and the mixed-layer depth in the Sverdrup model is not a good predictor of the onset of the spring bloom. They proposed that the best predictor is the intersection of the noon turbocline (region of sharp change in turbulence) depth with the compensation depth calculated from the vertical distribution of daily net production. The principle is the same in both models. When the mixed-layer depth is less than a certain critical depth, a bloom may occur. However, Woods and Barkmann obtained better predictions when they took into account the diurnal variability of the mixed-layer depth and the photoadaptation of the individual phytoplankton cells according to their positions in the water column.

3.3.6 The poleward migration of the spring bloom

The use of undulating towed sensors, often referred to as "batfish," has made possible higher horizontal resolution of vertical profiles along transects than was

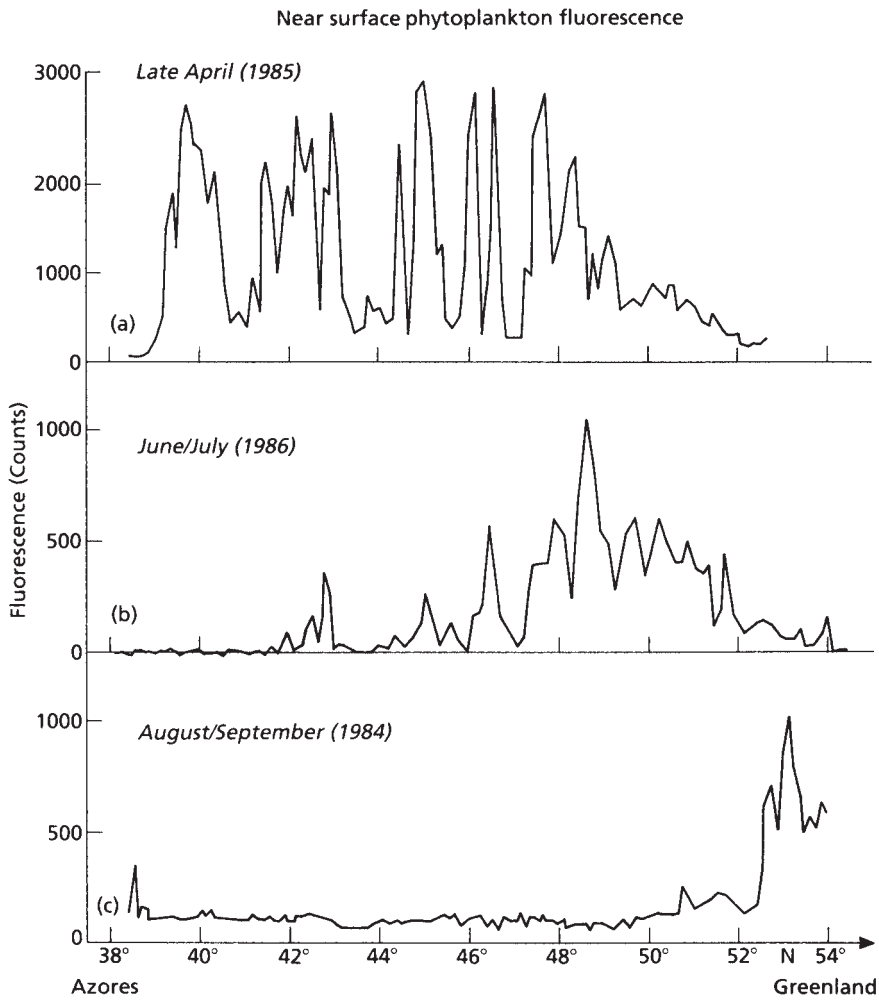

Fig. 3.14 Near-surface chlorophyll fluorescence at three times of the year on a transect lying between the Azores and Greenland, showing poleward migration of chlorophyll maximum. From Wolf and Woods (1988).

possible with traditional "bottle stations." Strass and Woods (1988) reported on a series of such transects running 2000 km north–south in the mid-Atlantic from the Azores (38° N) past ocean weather ship *C* (52.5° N 35.5° W) into the cyclonic subarctic gyre at 54° N. The batfish cycled between 10 and 200 m every 1.4 km. Representative transects were obtained in late April 1985, June–July 1986, and August–September 1984. The records of near-surface chlorophyll fluorescence (Fig. 3.14) showed patchy bloom conditions to about 49° N in late April, a bloom centered on 49° N in June–July, with oligotrophic conditions well established south of 42° N, and oligotrophic conditions over the whole transected area except for bloom conditions north of the polar front at 52° N in August–September.

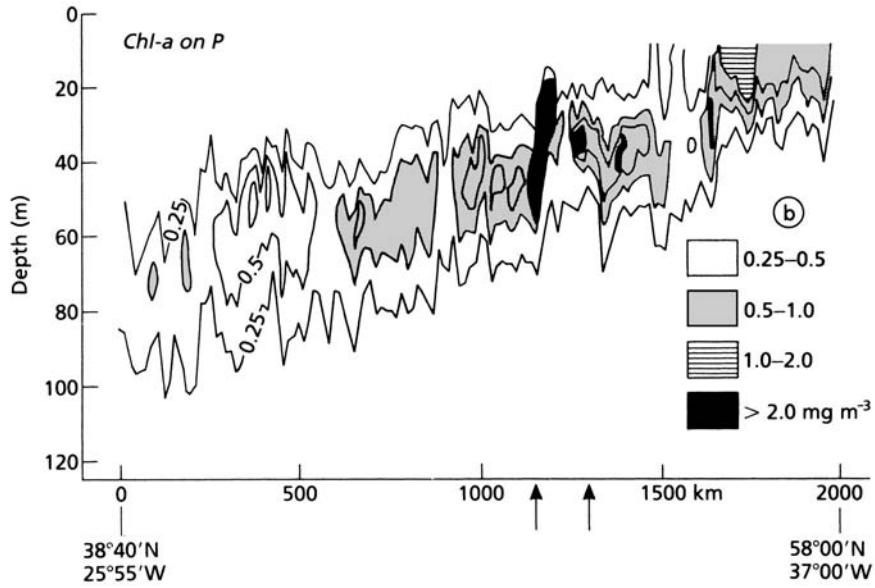

Fig. 3.15 Vertical distribution of chlorophyll on a transect between the Azores and Greenland in late summer. Note that the zone of maximum chlorophyll gets progressively more shallow as one moves north. From Wolf and Woods (1988).

Examination of the vertical structure showed that the horizontal migration of the near-surface chlorophyll maximum did not keep pace with the northward movement of the region of mixed-layer shallowing, but followed the slow propagation of the 12 °C isotherm outcrop. This trend suggests that, in addition to the need for stable stratification before a bloom can occur, there may be a temperature limitation on bloom processes.

Strass and Woods (1988) also found that during summer the deep chlorophyll maximum descended through the seasonal thermocline at approximately 10 m month^{-1}. They interpreted these data as indicating that phytoplankton were using new nutrients from greater and greater depths. Since events occurred at progressively later dates as one moved north, the August–September transect showed the chlorophyll maximum sloping upward from south to north (Fig. 3.15).

The sites where the highest concentrations of chlorophyll were found – between 1150 and 1300 km, for example – were sites where the isopycnals were displaced upward and closely spaced, indicating frontal upwelling probably associated with a cyclonic gyre or eddy. In the next section we shall review the evidence for the occurrence of events inducing localized upwelling.

3.3.7 Transient upwelling events

In addition to the biological enrichment that occurs in open waters as a result of upwelling at divergences at relatively fixed locations, satellite observations show

that there are transient pulses of increased surface chlorophyll that indicate mesoscale (10^3–10^5 m) upwelling events widely distributed in otherwise oligotrophic waters (Gower *et al*. 1980). Two main mechanisms have been proposed to explain them: internal waves, and fronts. Fasham and Pugh (1976) proposed that patches of high chlorophyll they encountered were best explained by the presence of internal waves, and Holligan *et al*. (1985) showed that at a station with a water depth of 4000 m there was upwelling of nutrient-rich water into the surface layer caused by large soliton-like internal waves that had been generated more than a day earlier at the shelf edge (see Section 6.4).

Woods (1988) has pointed to mesoscale patches of high chlorophyll concentrations with horizontal dimensions of about 10 km, which are a frequent component of satellite images, and has proposed that they are caused primarily by the jets associated with mesoscale fronts. Shelf-edge processes are considered in more detail in Chapter 6, and open-ocean fronts in Chapter 8.

3.3.8 Seasonal events in the plankton of the North Pacific

Most of the early work on seasonal events in the plankton was performed in the North Atlantic, so that we now have a fairly detailed understanding of the processes leading to a peak of phytoplankton production in the spring of the year and almost no production in the winter. The North Pacific produces a different seasonal pattern of events because phytoplankton production, accompanied by zooplankton, continues throughout the winter.

This continuous production is possible because the surface mixed layer in the North Pacific does not deepen in winter as much as in the Atlantic (120 m versus 400–600 m). The reasons for this variation have been examined by Warren (1983), who points out the greater density difference between the upper mixed layer and the deep water in the Pacific, which limits the depth of wintertime deepening. The cause of the greater density contrast lies in the salinity of the surface layer, which is low relative to the deep water. For example, in the Atlantic the salinities of the surface and deep layers are about 34.9 and 34.9–35.0 respectively; in the Pacific they are 32.8 and 34.6, so that even if the surface waters in the Pacific were cooled to freezing they would not be dense enough to sink as deeply as those of the Atlantic. Warren suggests two fundamental reasons for the lower salinity. First, the evaporation rate in the Pacific is lower. Second, the surface circulation in the Pacific is, compared with the Atlantic, relatively closed to the input of high-salinity water from the subtropics (see also Sections 8.2.5 and 8.6).

Because of the continued biological production throughout the winter, the zooplankton population is ready and able to prevent a build-up of phytoplankton biomass when the phytoplankton production increases in spring with the shallowing of the mixed layer. This idea was first proposed by Evans and Parslow (1985) and has been confirmed by detailed studies (Boyd *et al*. 1995a, 1995b). Boyd and co-workers carried out the first biological rate process measurements in the winter season. At ocean station *P* they found a phytoplankton standing stock of about 20 mg C m^{-3}, dominated by pico- and nanophytoplankton, which was

growing at about 50% of its maximum capacity. Mesozooplankton biomass in the mixed layer was only 1–4% of its summer value, but a strong component of microzooplankton was judged able to prevent the formation of a spring bloom. Because many mesozooplankton prey on microzooplankton, the low winter biomass of the former was considered to be an important factor in maintaining a high microzooplankton biomass and eliminating the spring bloom. A more recent analysis of production at ocean station *P*, by Harrison *et al*. (1999), takes into account the fact that the northeast Pacific is a region of iron limitation (see Section 3.2.7). Events are interpretable as an iron–light co-limitation, as in the model of Flynn and Hipkin (1999).

3.3.9 The Antarctic divergence

The waters of the Southern Ocean exhibit a phenomenon not found in temperate or polar waters elsewhere – a region of strong upwelling known as the "Antarctic divergence," caused by two wind systems circling Antarctica.

As shown in Fig. 3.16, there is a zone of easterly winds close to Antarctica, giving rise to a current known as the "east wind drift." The Coriolis force causes this water to flow towards the coast and leads to downwelling. This region is biologically productive. Five to ten degrees of latitude north of Antarctica one enters the "west wind drift," or "Antarctic circumpolar current." Again the Coriolis force causes flows to the left of the wind, towards the equator. Along the line separating the two winds there is upwelling, the Antarctic divergence. A major flow of this upwelled water extends northward as far as the "Antarctic

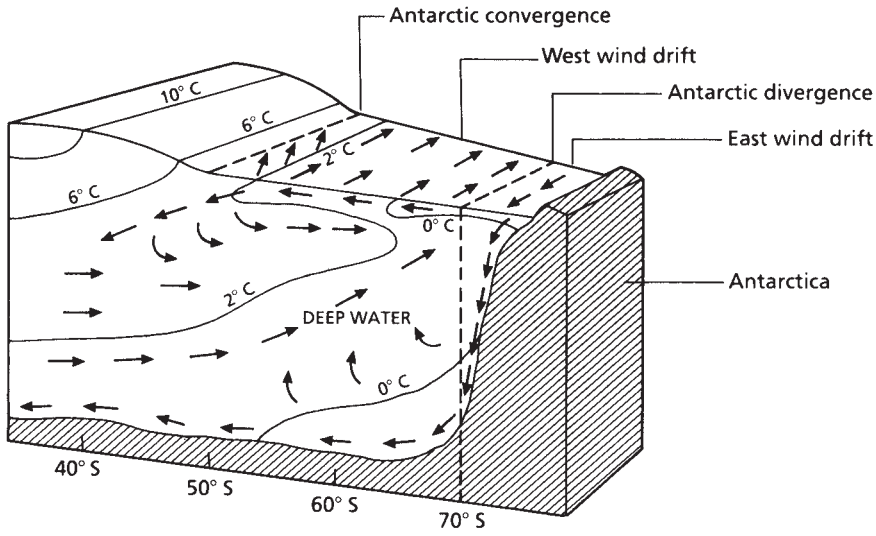

Fig. 3.16 Diagram of the Southern Ocean to show the Antarctic divergence and the Antarctic convergence. Antarctica is on the right, and north is to the left.

convergence" or "polar front" at about 50° S. It is rich in nitrate but not particularly productive, and it is now believed that phytoplankton new production is iron-limited over most of the area and that the diatoms are silicate-limited in the northern half (Holm-Hansen 1985) (see Section 3.2.7).

3.3.10 The Arctic polar front

Sakshaug and Slagstad (1992) summarized a large body of information about primary production in the Barents Sea, which is divided into a northern and a southern part by the polar front. North of the polar front, the melting of ice in spring induces stability in the upper 20 m of the water column, initiating a spring bloom. Nutrients rapidly become depleted and the strong pycnocline prevents the upwelling of nutrients by wind mixing. The short-lived bloom moves steadily north with the melting ice.

South of the polar front, the events associated with a classic spring bloom occur. After the bloom, periodic vertical mixing of nutrient-rich water driven by wind events stimulates further bursts of diatom production. Total annual productivity is, therefore, about 115 g C m^{-2} north of the polar front and about 165 g C m^{-2} south of it.

3.4 Neither tropical nor temperate: the distinctive subtropical pattern

Longhurst (1995) has drawn attention to the fact that extensive subtropical areas, comprising almost half the area of the world ocean, have a seasonal pattern of pelagic production that conforms with neither the classic pattern of temperate/polar waters (Section 3.3) nor the typical tropical pattern of stability with little seasonal variability (Section 3.2). The dynamic principles invoked by Gran and Braarud (1935) and Sverdrup (1953) are applicable, but the relatively light winter winds ensure that the mixed layer is deepened for only a short period. Since the sun is high in the sky, and phytoplankton biomass is low, phytoplankton is never light-limited. The effect of the brief period of mixed-layer deepening is to recharge the upper layers with nutrients, so that the rate of primary production increases through the winter and peaks in late spring before nutrients again become limiting. Phytoplankton biomass does not reflect the peak in primary production, probably because it is removed by zooplankton grazing. Instead, a broad peak occurs in mid-winter.

3.5 An integrated world view of primary production

The technique of measuring surface ocean chlorophyll from satellite radiometer data has stimulated new attempts to estimate global primary production (Platt

and Sathyendranath 1988, Longhurst *et al*. 1995) and new syntheses of planktonic food web processes (Banse and English 1994, Longhurst 1995, 1998)

3.5.1 Definition of characteristic subdivisions of the world ocean

As Longhurst has said, the starting point for a rational inquiry about functions within pelagic ecosystems must be the identification of the marine equivalents of forests, tundra, and grasslands. He recognized four primary ecological divisions which he called domains in 1995, but biomes in 1998. We shall follow the 1998 usage. The first, characterized by the processes described in Section 3.3 for a spring bloom in open temperate waters, he called the *westerlies biome*. The second, in which the same basic mechanism of bloom formation occurs but is constrained by the presence of ice and by the low-salinity water that results from ice melting, is called the *polar biome*. The third major grouping (corresponding approximately with our Section 3.2.5 on tropical and subtropical oceans) Longhurst called the *trades biome*. Stratification is a permanent feature, with the depth of the mixed layer being influenced by changing trade winds, and algal blooms being produced by Ekman transport, eddy upwelling, and other processes. Finally, in the *coastal boundary zone biome*, algal blooms are produced by classical seasonal changes in insolation and wind, as well as coastal upwelling, shelf-break and tidal fronts, river discharges, and other forces. These mechanisms are discussed later, in Chapters 5, 6, and 7. To these he added a miscellaneous category, *exceptional regions*, comprising boundary layers and high-nitrate, low-chlorophyll areas.

For purposes of the global descriptions and calculations, each of the four biomes was further categorized into biogeochemical provinces based on the seasonal patterns of primary production and chlorophyll accumulation. A total of 56 provinces were identified and, with the use of existing data sets, the mean seasonal cycle of events in the plankton was described for each of them. On the basis of the pattern of primary production, eight distinct groups of seasonal cycles emerged (Fig. 3.17). A clear distinction must be made between primary production, which is most clearly related to physical events, and the pattern of chlorophyll accumulation, which is also influenced by factors such as grazing and sinking rates. The satellites see only the chlorophyll accumulation at the surface.

The list of biomes and their seasonal cycles is as follows:

Polar biome

Model 1 – Primary production has a midsummer peak mediated by polar irradiance. Phytoplankton biomass peaks in the summer and again in the autumn. Two explanations are possible for the autumn peak: reduced grazing as the zooplankton sink to overwintering depths, or reduced phytoplankton sinking rates.

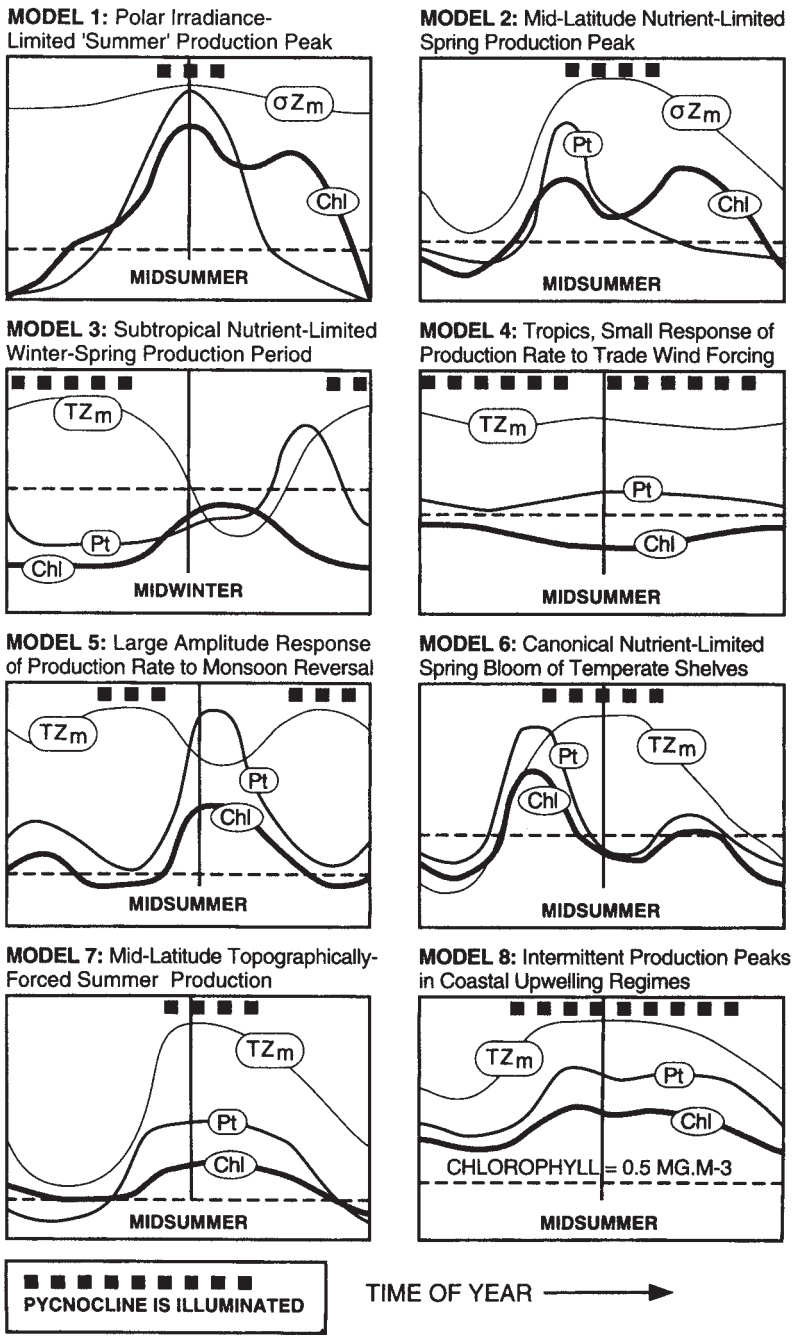

Fig. 3.17 Diagrams of the seasonal cycles in rate of primary production (Pt), pigment concentration (Chl), and mixed-layer depth using temperature (TZ_m) or density (σZ_m) criteria. The horizontal dotted line indicates the position of Chlorophyll = 0.5 mg m^{-3}, as a reference point for the values of chlorophyll in each model. For explanation of models 1–8, see text. From Longhurst (1995).

Westerlies biome

Model 2 – A spring production peak is limited by nutrients, which is characteristic of four poleward provinces within the domain. In the North Atlantic drift region, the pattern of chlorophyll accumulation follows the classical pattern, with a spring peak and a subsidiary peak in the autumn, except that the North Pacific subarctic gyre experiences no peak in spring and chlorophyll reaches its maximum abundance there in the autumn. (For discussion of this pattern, see Section 3.3.8.)

Model 3 – Winter–spring production occurs with nutrient limitation. This pattern is characteristic of a large part of the subtropical open ocean at mid-latitudes. Productivity is not light-limited and increases during winter with the deepening of the mixed layer. Nutrient limitation occurs in early summer and a subsurface chlorophyll maximum forms. Total chlorophyll peaks in winter (see Section 3.4).

Trades biome

Model 4 – A small-amplitude response occurs with trade-wind seasonality. This temporal pattern is associated with the structure described in Section 3.2 as typical tropical structure (TTS).

Coastal boundary zone biome

Model 5 – A large-amplitude response occurs with monsoon reversal. Strong winds cause coastal upwelling, which controls the pattern of primary production. Chlorophyll accumulation follows primary production. This model has been most intensively studied in the Arabian Sea and western Indian Ocean.

Model 6 – This pattern includes the classical nutrient-limited spring and autumn blooms of the mid-latitude continental shelves. Problems of cloud cover and suspended sediment make it impossible to observe these blooms by satellite, so shipboard data were used.

Model 7 – Similar to model 6, production in model 7 is continued into the summer because locally strong winds interact with the topography to force the upwelling of nutrients. This pattern is characteristic of three provinces (Alaskan shelf, New Zealand, and Falkland), all of which are special cases.

Model 8 – Intermittent production occurs in coastal upwelling systems (see Chapter 5).

In addition, six provinces are recognized in which the annual cycle of production is forced by the seasonal pattern of river discharge. The pattern is highly variable and cannot be generalized. The principles are discussed in Chapter 4.

3.5.2 Estimating global primary production

Longhurst *et al*. (1995) used the measurements of near-surface chlorophyll from the radiometer carried aboard the *Nimbus 7* satellite from 1979 to 1986 as a basis for calculating global primary production in the sea. To convert these chlorophyll measurements to estimates of primary production, they used an approach developed by Platt and Sathyendranath (1988). Surface chlorophyll values were combined with local data previously obtained from ships to evaluate: (i) the depth of the chlorophyll maximum; (ii) the standard deviation around the peak value; and (iii) the ratio of the chlorophyll peak height at its maximum to total peak biomass. These figures were used to construct a chlorophyll profile for each grid point at each time step. Surface radiation was computed from the relevant sun angle and information on cloud cover climatology. Finally, appropriate values of the initial slope of the photosynthesis–light curve and the assimilation number, which represented polar, mid-latitude, and low-latitude conditions, were taken from earlier experimental work. All of these factors were combined in a local algorithm to generate an estimate of the rate of primary production for each chlorophyll profile.

The local parameters of the chlorophyll profiles were obtained by analyzing more than 26,000 profiles from about 60 different sources. These profiles were partitioned among the 57 biogeochemical provinces, and, by inserting estimated values where none was available, the authors succeeded in making estimates for four quarters of a year, centered on the fifteenth days of January, April, July, and October. This calculation led to weighted monthly mean production values for each province, which were then integrated over the year for the whole ocean to give the global water-column primary production.

The grand total was a global net primary production of 50.17 Pg C y^{-1}. A major cause of uncertainty is the error caused by suspended sediment in coastal waters. If it is assumed that turbid waters contain only 25% of the chlorophyll indicated by the color scanner, the global estimate drops to 44.70 Pg C y^{-1}.

Previously published estimates based on extrapolation from shipboard estimates of production using the radiocarbon technique are in the range 20–31 Pg C y^{-1}, but Martin *et al*. (1987), by extrapolation from a small number of ^{14}C incubations made under ultra-clean conditions, had estimated 51 Pg C y^{-1}. It is interesting to note that the estimate by Longhurst *et al*. (1995) discussed here is independent of all previous ^{14}C estimates, yet is of similar magnitude.

The search continues for the best way to use satellite-sensed chlorophyll data in the estimation of ocean productivity. Behrenfeld and Falkowski (1997) proposed that daily depth-integrated phytoplankton carbon fixation could be estimated from a smaller data set that does not include vertical profiles of chlorophyll. They put forward a vertically generalized production model (VGPM) which is a single equation relating water-column primary production to five variables: (i) surface chlorophyll as determined by satellite, (ii) depth of the euphotic zone, (iii) photoperiod, (iv) maximum carbon fixation rate in the water column, and

(v) daily photosynthetically active light input. They found that adding details of the vertical profile of chlorophyll did not improve model performance. Using this model, they estimated a global carbon fixation rate of 43.5 Pg C yr^{-1}, close to the estimates of Longhurst *et al*. (1995).

Behrenfeld *et al*. (2002) proposed a more elaborate approach using VGPM but introducing variability in the carbon-fixing capacity of the Calvin cycle reaction as a function of nutrient and light conditions. They called it the PhotAcc model. When applied to global net primary production it yielded an estimate of 41 Pg C y^{-1}.

Meanwhile, Bouman *et al*. (2000) continued to test and refine the spectral model for working with satellite-sensed chlorophyll data as pioneered by Platt and Sathyendranath (1988). They made measurements of phytoplankton biomass, absorption coefficients, and photosynthetic performance at many stations in the subtropical Atlantic, and used them to derive standard sets of bio-optical parameters for application to the spectral model of primary production. For the eastern half of the basin, the performance of the model was improved by making corrections for non-photosynthetic pigments, but they found that without them the errors in computations of integrated water-column primary production were no more than 10%.

3.5.3 Use of satellite data to distinguish new from regenerated production

A distinction may be made (see Section 3.2.5) between primary production based on newly upwelled nitrate, called new production, and that based on the regeneration of ammonium excreted by heterotrophs in the mixed layer, called regenerated production. The ratio of new production to total production is the *f*-ratio. Oceanic new production is a potential avenue for the removal of carbon dioxide to the deep ocean, and is therefore an important factor in consideration of global warming (see Chapter 10). Watts *et al*. (1999) developed a method for using satellite data to calculate new production on ocean-basin scales, using real-time satellite data on ocean color and sea-surface temperature. The protocol was applied to the northwest Indian Ocean, but could be applied elsewhere.

Ship-based measurements during a monsoon period and an inter-monsoon period led to the division of the area into six provinces, based on bathymetry, sea-surface temperature, and chlorophyll measurements. Parameters defining the vertical structure in the biomass profile, and the photosynthesis–light curve, were established for each province, and were incorporated in the model of Platt and Sathyendranath (1988) (see Section 3.5.2). Incident light was calculated from first principles and corrected for real-time cloud cover. Satellite-derived surface chlorophyll data and sea-surface temperatures were fed into the model, which computed the instantaneous photosynthetic rate at depth z. These rates were integrated to give daily water-column primary production.

It had been established on earlier cruises in the northwest Indian Ocean that there is an empirical relationship between the integrated *f*-ratio and integrated primary production. Watts *et al*. (1999) were therefore able to calculate the *f*-ratio and hence new production, for each pixel of the satellite data. In this way they arrived at an estimate of the total new production of the area as about 0.5 Pg C yr^{-1}, which is approximately 30% of the total primary production of the area.

3.5.4 Modeling marine ecosystems on a global scale

We began this chapter by drawing attention to the extent to which the dynamics of marine production is influenced by the physical processes that affect the vertical distribution of light, heat and nutrients. It is now becoming possible to model the interactions of various classes of phytoplankton with one another, with their supplies of nutrients and with their predators, with sufficient generality that the model can be applied to a wide range of conditions, globally. For example, Moore *et al*. (2002a) have modeled for the mixed layer the interactions of diatoms, small phytoplankton, and diazotrophs (nitrogen fixers), with their zooplankton predators and with the input of five different nutrients from the lower boundary of the mixed layer. They included two classes of detritus: large particles, which sink from the mixed layer; and small particles, which are retained in the mixed layer and undergo mineralization. The model was given the appropriate inputs of light and nutrients for nine different locations worldwide, and was found to be in good agreement with field observations from these locations.

Moore *et al*. (2002b) used the model to study iron cycling and nutrient-limitation patterns in surface waters of the world ocean. They found that the model reproduced the observed high-nitrate, low-chlorophyll conditions in the Southern Ocean, northeast Pacific and equatorial Pacific. They found that primary production, community structure, and the sinking carbon flux were sensitive to large variations in the atmospheric iron source, thus supporting the iron hypothesis of Martin (1990). Moore *et al*. (2002b) suggested that the convention of equating nitrate inputs to the surface layer with carbon exports needs to be modified to include multiple limiting nutrients.

3.5.5 Use of newer satellite data

Joint and Groom (2000) give a useful critical review of the history of remote sensing of phytoplankton pigment concentration. From the Coastal Zone Color Scanner (CZCS, 1978–1986), through the Japanese Ocean Color and Temperature Sensor (OCTS, 1996–1997), the Sea-viewing Wide Field-of-view Sensor (SeaWiFS, 1997), to the Moderate Resolution Imaging Spectroradiometer (MODIS, 1999–), there has been a progressive increase in number of wavebands and signal-to-noise ratio. Joint and Groom (2000) went on to use SeaWiFS data to calculate primary

production during 1998 and 1999 for an area including the Celtic Sea and the western English Channel, using several different algorithms. They showed how continuous satellite data can capture short-lived phytoplankton blooms that are unlikely to be captured by ship-based operations, They suggested that the short-lived blooms account for strong inter-annual variability and higher annual estimates resulting from satellite techniques, when compared with those based solely on shipboard measurements.

3.6 Secondary production and the mixed layer

3.6.1 Oligotrophic waters

So far in this chapter we have paid scant attention to the role of the zooplankton. The truth is that, lacking readily available automated equipment to obtain continuous records of the abundance of zooplankton, we have far less information about interactions between zooplankton and physical processes than we have about phytoplankton. The relationship between vertical physical structure and zooplankton production is complicated by the ability of some mesozooplankters to make extensive vertical migrations. However, in oligotrophic waters microzooplankton predominate and they are mostly unable to migrate.

There have been many laboratory studies of the feeding rate of zooplankton, but turbulence of the water has seldom been a factor that was controlled. Recently, evidence has been brought forward suggesting that small-scale turbulence has a powerful effect on the rate of contact between a zooplankter and its food. If this is found to be true, classical studies of feeding rates will have to be re-evaluated.

Longhurst (1981) has provided a review of the vertical distribution of zooplankton. As before, it is most convenient to start with the relatively stable oligotrophic tropical systems. A very distinct pattern of vertical distribution is found in stable water columns with very shallow mixed layers, such as those found in low latitudes in the eastern parts of oceans, or in mid-latitudes toward the end of summer. The abundance of zooplankton is much greater in the mixed layer than below it, and within the mixed layer the greatest abundance is found just above the thermocline. Near the bottom of the thermocline there is typically a sharp decrease in the abundance of zooplankton, in a region that the specialists refer to as the planktocline.

Debate has arisen about whether the maximum of the zooplankton *biomass* occurs at the maximum of phytoplankton *biomass* or at the maximum of phytoplankton *productivity*. Ortner *et al*. (1980, 1981) favored the former, while Longhurst (1976, Longhurst and Herman 1981, Longhurst and Harrison 1989) favored the latter. It now seems possible that macrozooplankton feed at, or close to, the phytoplankton production maximum, while at other times and places microzooplankton predominate and feed at the biomass maximum (King *et al*. 1987; Le Fèvre and Frontier 1988).

3.6.2 Zooplankton and seasonal changes in vertical structure

Longhurst and Williams (1979) showed that at the ocean weather ship *India*, located south of Iceland (59° N 19° W), the situation at the end of winter (late March) was that most of the zooplankton biomass lay at depths greater than 350 m. By day, 85% of the biomass was found at that location, and at night, when many species made upward migrations, 56% of the biomass was still below 350 m. During April, when the spring bloom was initiated, there was a major upward shift of the zooplankton biomass, brought about chiefly by the upward shift of the *Calanus finmarchicus* population, so that by May *Calanus finmarchicus* had 94.5% of its population in the upper 100 m. At the same time, *Calanus* began rapid reproduction so that between late March and early May the proportion of copepodites I–IV changed from 1% to 65% of the individuals present. Longhurst and Williams (1979) pointed out that any realistic model of the development of a phytoplankton bloom in temperate waters must allow for changes in grazing pressure due to two factors, the upward translocation of biomass and the growth of the zooplankton population *in situ*. Before the extent of the grazing pressure can be calculated it is necessary to know the feeding rate of the individual zooplankters. This problem was discussed in Section 2.3.

In the life history of the American lobster *Homarus americanus*, early larval stages are planktonic and at stage IV the larvae settle to the bottom. Boudreau *et al*. (1992) showed experimentally that the presence of a thermocline tends to inhibit larval settlement. They proposed this as a mechanism for ensuring that larvae produced offshore of Nova Scotia in summer settle close to shore and provide recruitment to inshore stocks. The larvae remain in the mixed layer until they drift close to shore where the water column is mixed to the bottom by tidal or wind action. They then settle out and continue development as juveniles.

If, during the shoreward migration, the larvae are driven into deep water by the turbulent mixing associated with strong winds, this would be expected to adversely affect recruitment to the lobster stocks. Boudreau *et al*. (1991) found such a negative correlation between the incidence of strong winds and recruitment to the lobster stocks of the Gulf of St Lawrence.

3.7 Summary: the basic mechanisms of primary production

In this chapter we have focused attention on vertical processes on a scale of meters and tens of meters, generated by wind stress at the sea surface, convective circulation resulting from surface cooling, and turbulence at the pycnocline generated by internal waves and other forces.

We have seen that phytoplankton cells are at times carried from the surface to great depth on a time scale of 1–10 hours, and are thus exposed to a fluctuating light regime. It appears that some biochemical processes in the cells acclimate rapidly

to the changing light, while others change too slowly for there to be any noticeable response. In any case, the metabolic response of cells exposed to fluctuating light is not very different from the response of those exposed to the same amount of light delivered at a constant rate.

More than half of the world ocean is in tropical or subtropical latitudes, and a typical tropical profile of the water column shows a warm, stable, mixed layer separated from the cooler underlying water by a sharp pycnocline. Nutrient concentrations are very low above the pycnocline but relatively high below it. The peak of phytoplankton biomass, the chlorophyll maximum, is found at the nutricline. It appears that nutrients are slowly transported through the pycnocline and are rapidly taken up by the phytoplankton cells in the chlorophyll maximum. Light intensity is relatively low at the chlorophyll maximum and increases exponentially as one moves toward the surface. As a result, the greatest rate of primary production is usually found a few meters above the chlorophyll maximum.

A useful distinction can be made between the primary production that results from the utilization of upwelled nitrate, called new production, and that resulting from the utilization of ammonium excreted by heterotrophs in the mixed layer, called regenerated production. The ratio of new production to total production is called the *f*-ratio. In steady-state conditions the nitrogen removed from the mixed layer by sinking, or by predators that leave the area, must be balanced by the vertical transport of new nitrogen.

Interpretation of physical and chemical data has to be revised in the light of the discovery that photosynthetic bacteria, mainly the cyanobacterium *Prochlorococcus*, can constitute more than 50% of the biomass of phytoplankton in the major subtropical gyres. *Prochlorococcus* almost certainly cannot use upwelled nitrate, but flourishes in the deep chlorophyll maximum because it is unusually efficient at harvesting light at low intensities, and utilizes ammonium excreted by heterotrophs. The chief exception to the "typical tropical structure" (TTS) of the open tropical ocean is found in the equatorial upwelling zone, where major ocean currents cause upwelling and divergence of large volumes of nutrient-rich water from below the thermocline. Associated with this circulation pattern are several major cyclonic gyres that cause a dome-like structure in the isopycnals and an enhanced rate of vertical transport of nutrients. Other deviations from the TTS occur irregularly but not uncommonly and are associated with the passage of storms and with seasonal and longer-term climatic changes in tropical latitudes.

In temperate and subarctic latitudes of the North Atlantic, there is typically a burst of primary production known as the spring bloom. The mechanism underlying this condition is shallowing of the mixed layer after a period of vertical transport of nutrients. It was first recognized and described by Gran (1931), and was put on a quantitative physical basis by Sverdrup (1953). It has been shown that a wave of high chlorophyll biomass migrates poleward in the Atlantic in spring, approximately coincident with the 12 °C surface isotherm. Investigation of the vertical structure of the ocean while this migration is in progress shows that shallowing of the mixed layer to less than a critical depth is a precondition for

the spring bloom. We shall find that the alternation of a period of strong vertical transport of nutrients with a period of stratification is a recipe for high primary production in a wide variety of marine habitats.

In the temperate North Pacific, a spring bloom does not occur (see Section 3.3.8). The presence of a strong pycnocline at about 100 m depth keeps the phytoplankton in a well-lighted zone through the winter. Primary production is dominated by small cells (<5 μm) whose numbers are controlled by microzooplankton, while larger cells are iron-limited.

4

Vertical structure in coastal waters: freshwater run-off and tidal mixing

4.1 Introduction

Coastal waters (which we take as extending from the edge of the continental shelf to the high water mark) are subjected to the same seasonal cycles of warming and cooling as the open ocean, and in temperate climates the mixed layer may alternate between being shallow and deep in the same way as in open water. However, the process is greatly complicated by factors peculiar to the coastal zone. The first of these is the shallowness, which leads to a situation in which a relatively shallow mixed layer may extend to the bottom. Since dead biological material, detritus, tends to accumulate and decompose on the bottom, the nutrients released by it may be carried to the surface waters and rapidly used in photosynthesis. The second important factor is the presence of tidal currents that create turbulence in the water. If the depth is not too great in relation to the strength of a tidal current, tidally induced mixing may extend all the way to the surface. The third peculiar feature is the barrier to advection posed by the coastline itself. For example, if surface water is driven by wind action away from the coast, the only way for it to be replaced is by upwelling from below. Since there is a good chance that the upwelled water has been enriched in nutrients, an upwelling area is likely to be a site of enhanced biological production. When stratification first sets in, some phytoplankton is trapped in a well-lighted mixed layer and production is enhanced. In an area where stratification has been present for a relatively long time, the nutrients in the mixed layer may become depleted and their renewal from below is inhibited by the pycnocline, so that primary production tends to be depressed. Hence, stratification may act in a positive or a negative way on primary production, but its effects are always important.

In the open ocean, stratification is almost always induced by temperature differences between the layers. In coastal waters a very important additional factor must be considered – namely, the flow of fresh water from the land. Having salinity close to zero, it is much lighter than sea water and by lying on top of the sea water creates a stratification that can be independent of temperature differences between the layers. Furthermore this surface layer, being less dense, rides higher at the sea surface, creating a slope along which water flows. Since these flows depend on the buoyancy, they are known as buoyancy-driven currents. One way of trying to understand the complex relationships existing between physical and biological processes in coastal waters is to view freshwater run-off as a mechanism tending toward greater stratification while wind-driven and tidal currents are mechanisms tending to cause turbulence in the water column and to break down stratification. In the open ocean, horizontal gradients are small and vertical processes control the distributions of heat, salt, nutrients, and other factors. In estuaries and on continental shelves, however, horizontal movement of water and large horizontal gradients tend to determine the property distributions. The Coriolis force and geostrophic balance are important features of horizontal flows, so we begin by reviewing them.

4.2 The Coriolis effect and the geostrophic balance

4.2.1 The Coriolis effect

The Coriolis effect, as mentioned in the last chapter, is an apparent deflection to the right in the northern hemisphere and to the left in the southern hemisphere of objects traveling over the surface of the earth. The deflection is caused by the rotation of the earth, as illustrated in Fig. 4.01. Consider first the person at O in Fig. 4.01(a) who throws a ball at the sun as it rises in the east (E). (Let us ignore the friction of the air and the gravity that would bring the ball down to earth.) After an hour (Fig. 4.01b), the sun has risen above the horizon along a path slanting up to the right in the northern hemisphere and up to the left in the southern hemisphere. Is the ball that was thrown toward E still heading toward E or is it heading toward the sun?

Because there is no friction between the earth and the ball, the ball moves in a straight line relative to the sun and stars while the earth rotates underneath. The ball continues to head straight toward the sun while the horizon moves with the earth as shown in Fig. 4.01(b). Each point on the eastern horizon moves down and to the left of the ball, and the point E on earth is in a different direction relative to the fixed stars than when the ball was thrown.

The rate of the deflection may be calculated as follows. The point E, like all other points on the earth, moves around the axis of the earth once a day in a circle that lies perpendicular to the axis. The motion along this circle in degrees or radians per second is indicated in Fig. 4.01(b) by the arrow labeled Ω. This motion may be split into two components, one parallel and one perpendicular to the horizon. The parallel component is $\Omega \sin \Phi$, where Φ is the latitude of the observer's position, while the component perpendicular to the horizon is $\Omega \cos \Phi$. The component along the horizon is the one of interest to us because it is the cause of the apparent deflection of the ball. The ball moves in a straight line, while the horizon rotates toward the left at an angular rate of $\Omega \sin \Phi$.

Earthlings, however, find it much more convenient to ignore the fact that the earth rotates and assume that it remains motionless while the sun and stars move across the sky. The fact that objects, like the ball, are deflected from their original course is accounted for by a force that was invented by mathematicians to represent the effects that are due to the rotation of the earth. This imaginary force, the Coriolis force, results in the situation illustrated in Fig. 4.01(c). Here the earth remains motionless while the Coriolis force pushes the ball to the right, following the rising sun, at the angular speed of $\Omega \sin \Phi$. The derivation of the Coriolis force from the angular rate of the deflection is given in Box 4.01.

The "thought" experiment suggested in Fig. 4.01 is, of course, impossible to perform because gravity brings the ball back to earth before the sun has moved an appreciable amount, but the deflection is a very important factor in the flight of artillery shells that are separated from the earth for significant periods of time. Another common way of demonstrating the earth's rotation is with Foucault's

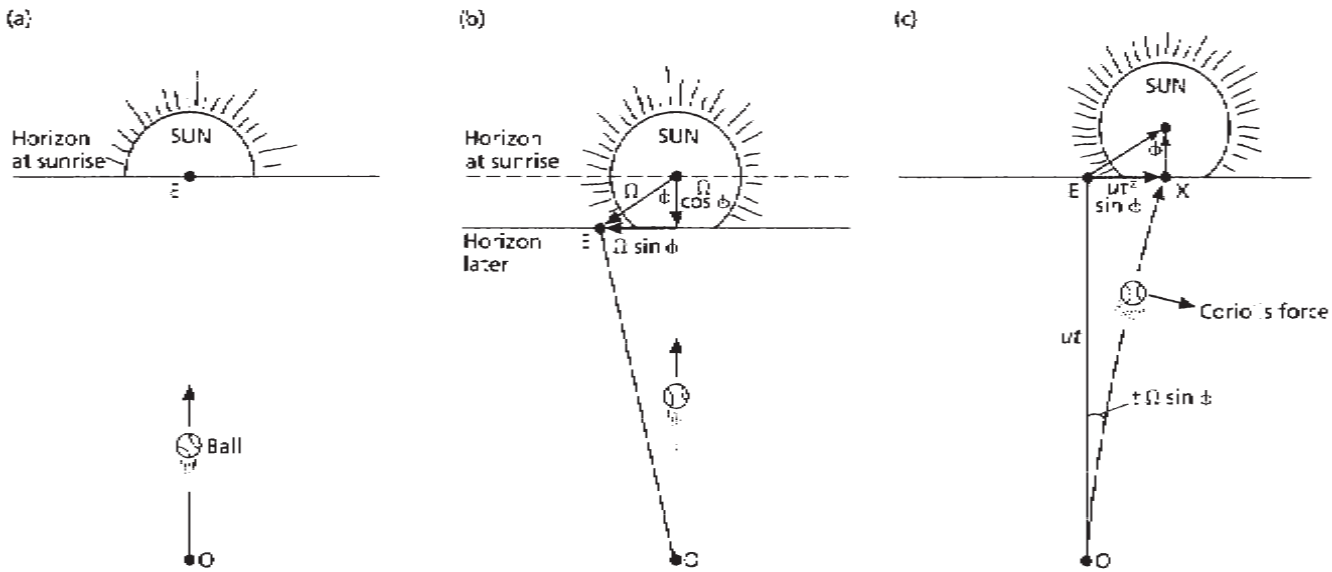

Fig. 4.01 (a) The person at O has just thrown a ball toward the sun rising in the east (E). (b) An hour later the earth has rotated on its axis and moved the horizon to the left and down relative to the sun and stars. The ball continues toward the sun because it is not connected to the earth. (c) If the horizon is assumed to remain motionless, the rising of the sun appears to be due to the sun's own motion rather than the rotation of the earth, and the fact that the ball turns toward the sun is due to the "fictitious" Coriolis force that pulls the ball to the right in the northern hemisphere but to the left in the southern hemisphere.

Box 4.01 The Coriolis parameter

The angular rate of the deflection cannot be used directly in the equations of motion that require that the effect be described in terms of a force or acceleration per unit mass. The acceleration that must exist to account for the observed deflection can be derived following Pond and Pickard (1983) with help from Fig. 4.01(c). Assume the ball is originally thrown from O toward E but is deflected to the right to land at X. The distance from O to E is the speed of the ball, u, times the time of flight, t. The angle EOX is the angular rate of the deflection, $\Omega \sin \Phi$, times the time of flight, t. The deflection from E to X is then the product of the angle $t\,\Omega \sin \Phi$, and the distance ut:

$$\mathrm{EX} = d = ut^2\,\Omega \sin \Phi \tag{4.01}$$

The acceleration that exists to produce this displacement starting from rest can now be calculated from the formula relating displacement, d, and acceleration, a, which is usually discussed in elementary physics courses, namely, $d = \frac{1}{2}at^2$. Substituting $d = ut^2\,\Omega \sin \Phi$ in this equation gives the acceleration or force per unit mass as $2u\,\Omega \sin \Phi$. This equation is usually written fu where $f = 2\,\Omega \sin \Phi$ and is called the Coriolis parameter.

The expression $2\,\Omega \sin \Phi$ shows that the Coriolis effect is a maximum at the north pole where $\Phi = 90°$, and zero at the equator where $\Phi = 0$. In the southern hemisphere, Φ, the latitude, is negative and the Coriolis force is in the opposite direction; objects moving over the earth's surface are deflected to the left. The direction of the earth's rotation is not different in the two hemispheres but the direction of gravity does change and what looks like rotation to the right in the north is rotation to the left in the south.

pendulum (Fig. 4.02). When carefully set up, as is often done in science centers, there is no friction between the long swinging pendulum and the rotating earth. Since there is no force to twist the plane of the pendulum's swing to follow the rotation of the earth, it stays fixed relative to the sun and stars as the earth rotates underneath. In the north the plane of the pendulum rotates clockwise relative to the earth at the rate $\Omega \sin \Phi$, which is the same as the component of the sun's motion parallel to the horizon noted above.

The time for a complete revolution of the pendulum relative to the earth is called the pendulum day and is $24/\sin \Phi$ hours long. At the pole the pendulum day is 24 hours, at 45° it is 34 hours, and at the equator it is infinitely long, when $\sin \Phi = 0$. As with the thrown balls, it is hard to see, at first glance, how the pendulum day must be longer than the day. One must, of course, be careful to separate the two components of the rotation that are each less than the total rate of rotation and remember that the period of each component is the inverse. The periods of the components are not components themselves and do not add up to

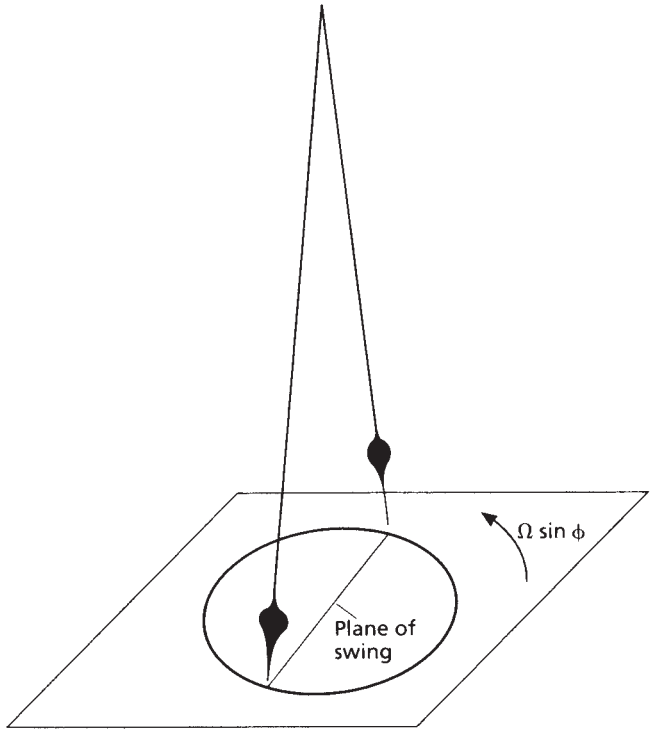

Fig. 4.02 The plane of the pendulum swing stays fixed relative to the stars, but appears to rotate to the right as the room rotates to the left with the earth at $\Omega \sin \Phi$ rad h^{-1}.

the period of the whole. This situation is a good illustration of the fundamental difference between vectors (rotation) and scalars (period).

4.2.2 The geostrophic balance

The Coriolis force is an important factor in ocean currents because friction in the water is so small that water can move, like the ball in Fig. 4.01(a), over the earth's surface and remain isolated from the spinning earth. The Coriolis force is not the force that makes the water move but is the apparent force that deflects the flow when the water is moving relative to the earth. Suppose, for instance, that all the surface water in a region in the northern hemisphere starts to move south because there is a pressure gradient from north to south. The Coriolis force deflects the flow around to the right of its southward path. Over the course of about one pendulum day the direction of flow comes around to the right by 90° and is toward the west. At this point the water is moving west while the north to south pressure gradient that started the water on its flow is still in the same direction and the Coriolis force is toward the north or 90° to the right of the flow direction. The

Box 4.02 Equations of the geostrophic balance

Mathematically, geostrophic motion is expressed by two equations that define the balance of forces for the east–west (x axis) and north–south (y axis) directions. In the x direction the equation is

$$fv = \frac{1}{\rho}\frac{\mathrm{d}P}{\mathrm{d}x} \tag{4.02}$$

where the Coriolis force (fv) along the x axis is balanced by the x component of the pressure gradient on the right side of the equation. The equivalent equation for the y direction is

$$fu = -\frac{1}{\rho}\frac{\mathrm{d}P}{\mathrm{d}y} \tag{4.03}$$

Here the y component of the pressure gradient is balanced by the Coriolis force arising from the flow in the x direction.

These equations express only a balance of forces. There are no sources or sinks of energy included in them. Because the flow is perpendicular to the forces, the forces do no work and the motion goes steadily on forever. This scenario may seem a little unrealistic as friction must eventually convert the motion to heat, but that is a very slow process, leaving the geostrophic approximation as very accurate, especially in the deep sea where friction is small.

Coriolis force and the force of the pressure gradient are now in opposite directions and balance one another. This condition is the geostrophic balance.

The geostrophic balance is an everyday occurrence in the atmosphere and is evident in the daily weather charts that display the distribution of isobars. The flow of air around the low- and high-pressure systems is parallel to the isobars – not across them – because the air is close to being in geostrophic balance. The mathematical expressions defining the geostrophic balance are discussed in Box 4.02.

4.3 Estuaries

"An estuary," according to the definition of Pritchard (1967), "is a semi-enclosed coastal body of water which has a free connection with the open sea and within which sea water is measurably diluted with fresh water derived from land drainage." The term fjord is used for the steep-sided estuaries found along mountainous coasts such as in Alaska, British Columbia, Norway, Chile, etc. Estuaries are economically important features of the ocean because of their high biological productivity, their proximity to large cities with their wastes, and their increasing use as sites for aquaculture. In the following we examine the processes

that contribute to the typical circulation pattern and describe the different types of estuaries.

4.3.1 Estuarine circulation

From the definition it is evident that an estuary is a bay, part of a bay, or a narrow inlet in which freshwater flow from the land has reduced the salinity of the ocean water. The flow of fresh water causes a characteristic circulation pattern to be set up in the estuary in which fresher, and therefore lighter, water flows out of the estuary in the surface layer and a deeper flow brings water from the open sea into the estuary (Fig. 4.03). This "estuarine circulation" is observed to be the dominant circulation pattern in estuaries where run-off is moderate and where mixing by tidal currents is weak.

The main force that drives the estuarine circulation is a horizontal pressure gradient created by the density difference between the newly added fresh water and the resident salt water. The force lies in the surface layer and is directed down the estuary, away from the source of fresh water. The resulting flow, being dependent on the buoyancy of the fresh water, is usually referred to as a buoyancy-driven flow.

The origin of the pressure gradient is illustrated in Fig. 4.04, in which a layer of fresh water of density ρ_1 overlies water of higher density, ρ_2. We assume there is no horizontal pressure gradient at the bottom of the low-density layer or at any deeper level. Thus, the pressure at A at the bottom of the upper layer is the same

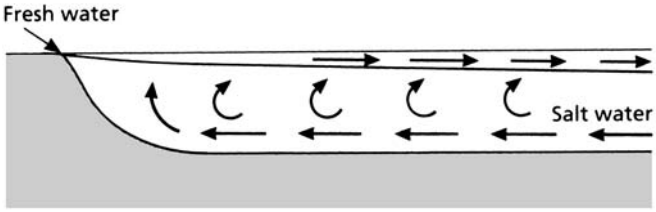

Fig. 4.03 Fresh water entering at the head of the estuary on the left creates a near-surface flow of light water out of the estuary and a compensating deep flow of saltier water up toward the head of the estuary. The upper layer gets thicker as it moves away from the source of fresh water because salt water is entrained from below.

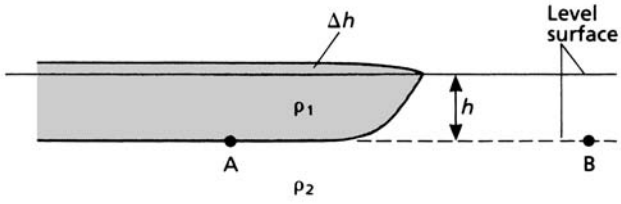

Fig. 4.04 A pool of light water, ρ_1, lies on top of and beside water of greater density, ρ_2. If the pressures at A and B are the same, the height of the sea surface above A must be higher than above B.

as the pressure at B, which is on the same level as A but beyond the freshwater layer. If the pressures are to be the same, the weight of the water above the two points must be the same and the column of the lighter water above A must, therefore, be higher than the column of denser water above point B. The difference in the height of the water surface in the two regions, Δh, can be calculated by equating the pressure at A with the pressure at B. Pressure is calculated by multiplying the density of the water times the height times the gravitational acceleration – i.e., $P = \rho g h$. Above A, the density is ρ_1 and the height is $h + \Delta h$, so the pressure is $\rho_1 g(h + \Delta h)$, and above B the density is ρ_2 but the height is only h, giving a pressure of $\rho_2 g h$. After equating these expressions, a little manipulation leads to the formula

$$\Delta h = h(\rho_2 - \rho_1)/\rho_1 \tag{4.04}$$

As an example let the freshwater layer with a density $\rho_1 = 1000$ kg m^{-3} have a thickness $h = 2$ m over the deeper layer of density $\rho_2 = 1025$ kg m^{-3}. Equation 4.04 states that the water above point A, in Fig. 4.04, is about 5 cm higher than above point B.

Since the pressures at A and B are the same there is no force to move the water horizontally between the two points. At all points above A, however, the pressure is greater than at the corresponding level above B. This higher pressure pushes the water in the upper layer to the right in the figure over the top of the denser water.

As the lighter water flows over the heavier layer toward the open sea, turbulence in the water causes the two layers to mix together, which reduces the differences existing between the two layers. The upper layer becomes thicker, increases in density, and slows down. The importance of this process to the circulation in the estuary is explained in Box 4.03.

Box 4.03 The balance of forces in an estuary

The driving force of the circulation is the difference in the pressure that is created down the estuary by the fresh water in the surface layer. This force (per unit mass) is expressed mathematically as

$$\frac{1}{\rho}\frac{\mathrm{d}P}{\mathrm{d}x} \tag{4.05}$$

The balancing force is generated by the mixing between the upper and lower layers. When fast-moving upper water is exchanged with slow-moving lower water, a force is generated that slows down the upper layer and speeds up the lower layer. A mathematical expression for the force starts with the equation

$$K_e \frac{\mathrm{d}\bar{u}}{\mathrm{d}z} \tag{4.06}$$

which is the diffusion equation for the vertical flux of momentum and is analogous to Eqn. 2.11. K_e is the eddy diffusivity and $d\bar{u}/dz$ is the vertical gradient in the mean velocity. The formula calculates the vertical flux of momentum through a horizontal layer of thickness dz. As long as the same amount of momentum is leaving the layer as is entering it, no force is being exerted on the layer. A force arises when the layer is gaining or losing momentum, which happens when the vertical flux is not constant with depth. This situation occurs when either the eddy diffusivity or the velocity gradient varies with depth. Usually K_e is considered constant and the convergence or divergence of momentum is attributed to variations in the vertical current shear. Since the shear is just the velocity gradient, the gradient of the shear is the gradient of the gradient of the velocity, which is commonly called the second derivative of the velocity. Thus if K_e is constant the force is

$$K_e \frac{d^2\bar{u}}{dz^2} \tag{4.07}$$

and the balance between the pressure gradient down the estuary, and the drag of the underlying water is expressed by

$$\frac{1}{\rho}\frac{dP}{dx} = K_e \frac{d^2\bar{u}}{dz^2} \tag{4.08}$$

The equation does not include the Coriolis force because we assume that the estuary is too narrow for this force to be important. The flow is considered to be two-dimensional or the same along any section cut lengthwise along the estuary. One problem with the equation is that it is not possible to go to an estuary and directly measure the magnitude of either the pressure gradient or the drag force. It is also well known that the eddy diffusivity is not a constant but a function of time and of position. The equation is, however, very useful because it can be used, in association with the other required equations, to construct a mathematical model of the estuarine flow (Rattray and Hansen 1962, Dyer 1973, Nunes Vas 1994). Then the flow and the property distributions predicted by the model can be compared with the observed distributions. By adjusting the model to produce distributions that are similar to those observed it is possible to determine which are the most important factors controlling the circulation.

One feature of estuarine circulation that is observed in the models is the deep flow of saline water into the estuary. This flow is a direct consequence of the turbulent exchange between the upper fresh layer and the layer immediately below. As the water in the upper layer proceeds out of the estuary it becomes slower and thicker because of the vertical diffusion of momentum. At the same time diffusion causes the fresher upper water to be exchanged with the deeper saltier water and the surface layer becomes saltier as it progresses out of the estuary. Salt then is transported out of the estuary by the outward flow in the upper layer. In time this movement would cause the water in the estuary to become completely fresh, which does not happen because the deep flow develops and brings salt into the estuary.

4.3.2 Sources of turbulence: the Richardson number

The turbulent motions that mix the fresh upper layer of an estuary with the saltier layer below may be generated by a number of different processes. Breaking waves at the surface and rough flow over the bottom and sides of the estuary could generate significant amounts of turbulence, but the largest contributions are provided by the turbulence generated by the breaking of waves on the interface between the two layers. These internal waves are generated on the density interface by wind waves at the surface, pressure fluctuations in the atmosphere, flow over irregularities in the bottom bathymetry, and other factors.

The likelihood that these internal waves will become unstable and break up into turbulence is usually estimated with the Richardson number. This number is a ratio of two opposing forces – one that tends to keep the density interface level and one that tends to increase the size of the waves. The first is generated by the density change across the interface, which creates a buoyancy-restoring force (Section 3.2.3) that tends to limit the amplitude of the waves. The energy to increase the size of the waves is generated from the difference in velocity between the two layers. The strength of the buoyancy force is usually represented by the square of the Brunt–Väisälä frequency (Eqn. 3.04) while the energy available in the shear flow is represented by the square of the velocity gradient. The Richardson number is the ratio of these two values:

$$Ri = \frac{g}{\rho}\frac{\mathrm{d}\rho}{\mathrm{d}z} \Big/ \left(\frac{\mathrm{d}u}{\mathrm{d}z}\right)^2 \tag{4.09}$$

If this number is high the buoyancy forces associated with the density stratification are strong, and waves on the interface do not grow and break but tend to be damped out. In fact, if the ratio is greater than 0.25, waves of all wavelengths are stable (Turner 1973). If the density difference decreases or the shear increases such that $Ri < 0.25$, waves will grow in amplitude by taking energy out of the velocity shear and eventually become unstable. This Kelvin–Helmholtz instability causes the waves to roll up and disintegrate into a patch of turbulence.

4.3.3 Different types of estuaries

The estuarine circulation outlined above is found in many estuaries, but there are a number of processes that can alter the basic pattern. In some estuaries the depth slopes gently from where the river reaches sea level and the river flow is strong enough to drag the seawater layer further out than it would be if there was no freshwater flow. In these cases the upper and lower layers appear as in Fig. 4.05. Because of the wedge-like shape of the lower layer, these layers are called salt-wedge estuaries. The position where the lower layer meets the bottom changes with the strength of the flow in the upper layer, and in the case of the Mississippi this point can vary by more than 200 km throughout the year.

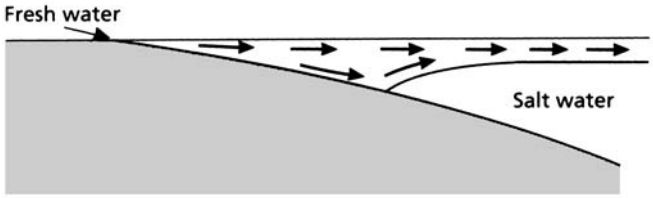

Fig. 4.05 The salt-wedge estuary. At the mouths of shallow rivers, high run-off may cause the salty water to be pushed outward in a wedge shape.

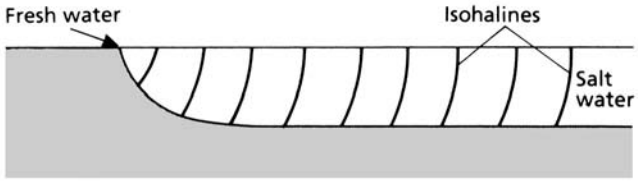

Fig. 4.06 The tidally mixed estuary. Highly turbulent estuaries tend to be well mixed vertically. Isohalines, or lines of equal salinity, are nearly vertical, with highest values near the sea and lowest values near the river.

Changing salinity at the boundary of the salt wedge leads to flocculation and sinking of fine particles carried in suspension. These particles get carried landward in the deeper waters and concentrate at the tip of the salt wedge, thus producing a zone of high turbidity, the "turbidity maximum," which also tends to move up and down the estuary according to the strength of the freshwater flow. In this way, sinking particles are distributed over a wide area and lead to the formation of intertidal mud flats so characteristic of estuaries.

In a second class of estuary, the partially mixed estuary, friction between the bottom and the tidal currents produces enough turbulence to weaken the vertical stratification. The estuary shown in Fig. 4.06, for example, shows this weaker stratification compared to that shown in Fig. 4.03. The reasons for the partial mixing, according to Pritchard (1989) could be due to decreasing river flow or depth or increasing tidal currents or width.

Estuaries in the first two classes have water depths tending to increase toward the mouths of the estuaries as suggested in Figs. 4.03, 4.05 and 4.06. Some fjords have similar depth profiles but many have shallow sills near the mouths and deep basins in the interior such as in Fig. 4.07. The waters in the deep basin are isolated from the waters of the continental shelf and are flushed only at irregular intervals when there is an influx over the sill of water dense enough to replace them. Above the sill depth, fjords usually exhibit the classic estuarine circulation.

The changes in density leading to renewal of the water behind the sill depth are depicted in Fig. 4.07. The longitudinal section of the estuary in Fig. 4.07(a) shows the bathymetry of a fjord with a sill at B separating the waters of the continental shelf from the deep basin at A. The densities of the water at the points

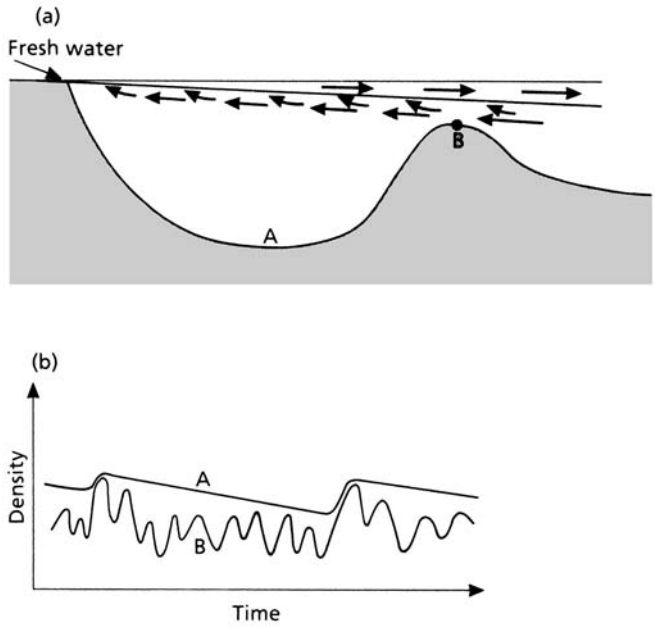

Fig. 4.07 (a) Longitudinal section of a fjord showing the sill at B and the deep interior basin at A. The estuarine circulation is confined to the waters above the sill. (b) The density in the deep basin at A decreases slowly with time because of vertical diffusion. The deep water is replaced and increases in density when the water coming over the sill at B is denser than the water in the deep basin.

A and B are plotted against time in Fig. 4.07(b). In the deep basin the density decreases slowly due to vertical turbulent diffusion, which is the only mechanism tending to exchange water between the light upper layer and the denser deep water. The density of the water coming into the fjord over the sill at B, on the other hand, fluctuates in time following changes in tidal currents, run-off, and wind stress. When these factors cause the density at B to be greater than the density at A, the inflowing water sinks down and replaces the water in the deep basin.

4.4 The effect of freshwater run-off on biological production in estuaries

4.4.1 Primary production examples

(a) Chesapeake Bay, USA

Chesapeake Bay is a partially mixed estuary with several significant tributaries and a complex bottom topography. In a review of the influence of physical processes on the biology of the Chesapeake Bay estuary, Brandt *et al*. (1986) demonstrated very clearly how the spring run-off at the head of the bay leads to a very strong

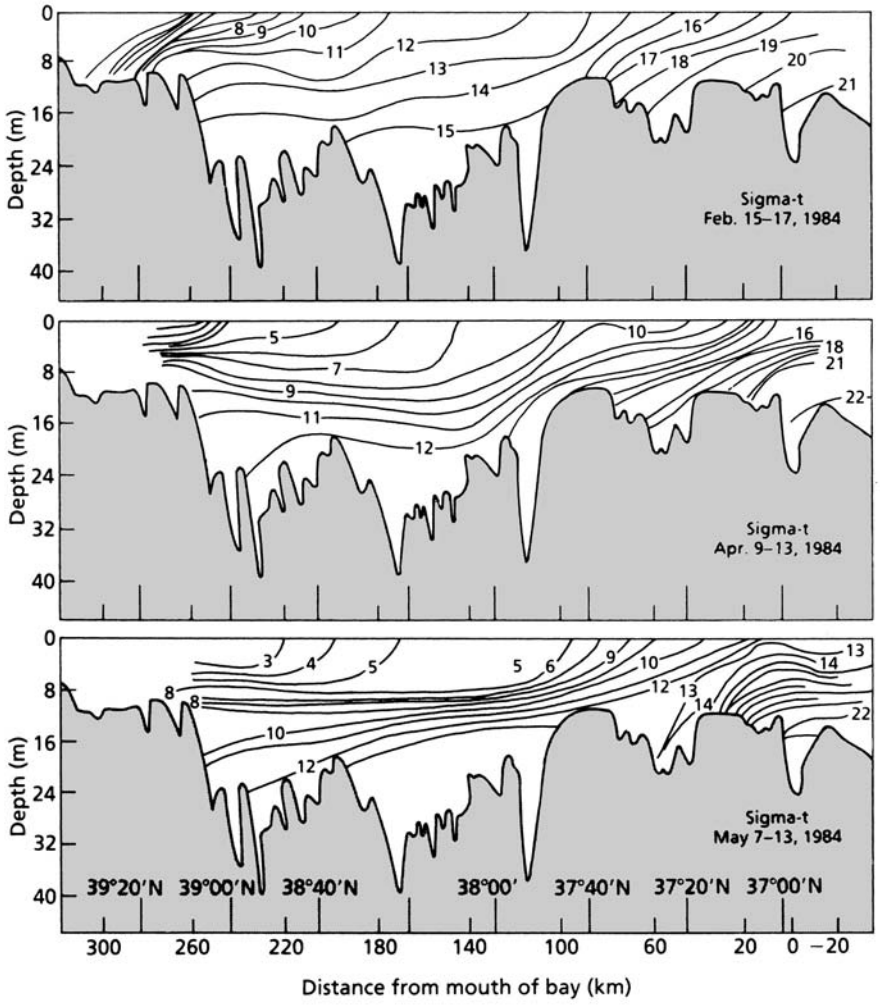

Fig. 4.08 Evolution of the pycnocline stratification in Chesapeake Bay in the spring of 1984. In February it is mainly between 200 and 300 km from the mouth. In May it extends almost the whole length of the bay. Shaded area is the bottom of the bay. After Brandt *et al.* (1986).

pycnocline with seaward-flowing surface waters and landward-flowing deeper waters. The combined effect of salinity and temperature is integrated into the plots of sigma-*t* in Fig. 4.08. (Sigma-*t*, or σ_t, is the density of the water minus 1000 kg m^{-3}.) The plots show clearly the movement of the pycnocline from a region near the head of the bay in February to a layer at 8–12 m depth extending about 160 km along the bay in May. In an open-ocean situation this flow would pose a formidable barrier to the vertical movement of nutrients, but the strong tidal currents in combination with net mean flows in opposite directions in the two layers result in strong internal wave activity, as revealed by acoustic records of

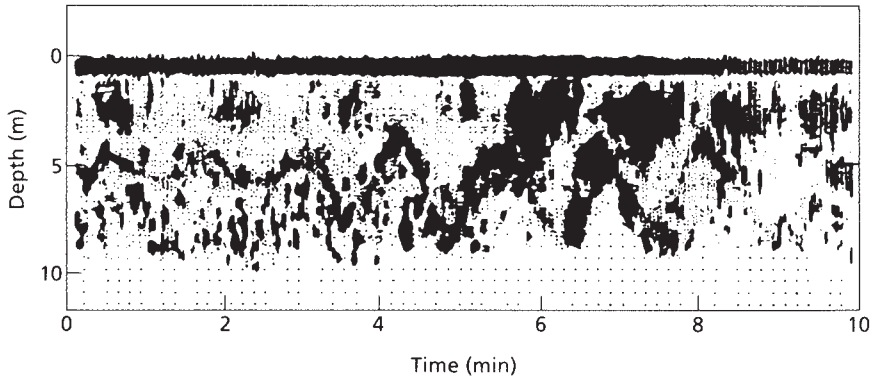

Fig. 4.09 Time series of acoustic backscatter intensity versus depth near Chesapeake Bay Bridge, May 31, 1984. Note evidence of vertical movement by internal waves. From Brandt *et al*. (1986).

the plankton (Fig. 4.09). The turbulence created when these internal waves break cause nutrients to be mixed into the surface waters. The landward-flowing counter-current is instrumental in causing both phytoplankton and zooplankton to move in a cyclical manner within the estuary. For example, Brandt *et al*. (1986) have documented the movement of high concentrations of the dinoflagellate *Prorocentrum* from near the mouth of the Chesapeake Bay to the shallow waters 250 km landward, traveling with the bottom waters. At the head of the bay they were mixed up into surface waters and caused a "red tide."

Webb and D'Elia (1980), working in the York River Estuary, a tributary of the Chesapeake Bay system, found that on neap tides the estuary was stratified and at this time the water below the pycnocline became oxygen-depleted while the nitrogen and phosphorus content rose. A few days after the peak of the spring tides the estuary became fully mixed by tidal currents, replenishing the oxygen at depth and upwelling large quantities of nitrogen and phosphorus. There was an inverse linear relationship between nitrogen and oxygen in the water, showing that benthic organisms were adding nitrogen in proportion to the rate that they were consuming oxygen. The relationship of oxygen to phosphorus was not linear, reflecting the fact that phosphorus binds to sediment particles but is released at low oxygen concentrations. The study showed very clearly how the balance between the stabilizing effect of freshwater run-off and the mixing effect of tidal currents can be so delicate that it shifts between neap and spring tides. This situation, alternating between upwelling of nutrients and stratification, provides the conditions for very high primary production. Once again, the parallel with the Gran effect is very striking.

Further work on the plankton of the York River estuary was carried out by Eldridge and Sieracki (1993). They concentrated on cyanobacteria and the protozoans that graze on them. The abundance of cyanobacteria in the estuary peaked during neap tides, when stratification set in, and decreased during spring tides

when tidal currents were strong enough to cause vertical mixing. Using appropriate growth rates and feeding rates, they simulated the interaction between the cyanobacteria and their grazers, showing that during the neap tide cycle the growth of the cyanobacterial populations saturated the grazers, but that during the spring tide cycles the protozoan grazers contributed significantly to reduction in numbers of cyanobacteria.

(b) Southampton Water, UK

This is a partially mixed estuary with a very unusual tidal regime, having four high tides and four low tides each day. Lauria *et al*. (1999) looked at the relationship of diatoms and dinoflagellates to varying levels of turbulence in the water column. They found that the diatoms relied on the periods of high kinetic energy from the tidal currents to prevent them sinking out of the water column, while the dinoflagellates used the period of stability during slack-water periods to aggregate near the surface. In this way, phytoplankton with very different requirements could coexist in the same body of water.

4.4.2 Primary production in shallow estuaries

Shallow estuaries cannot be defined by reference to average depth. The phenomena described below depend on the relationship of depth to the tidal range and to the seasonal fluctuations in freshwater flow. While the dynamics of stratified and partially mixed estuaries conform to recognizable patterns, the dynamics of shallow estuaries where tidal mixing is a major factor tend to be extremely variable and difficult to understand. In locations with very wet seasons, a strong freshwater input may wash almost all of the salt water out of the estuary. For example, in the estuary of the Great Ouse in eastern England, periods of very high freshwater flow, characteristic of winter, have the effect of flushing most of the phytoplankton out of the estuary, so that primary production is at a minimum (Rendell *et al*. 1997). In spring and summer periods of low flow the Great Ouse becomes a stratified, salt-wedge estuary with significant primary production.

In the Gernika estuary of northern Spain, episodes of high freshwater input displaced the normal estuarine planktonic community from the upper half of the basin. Primary and secondary productivity of the estuary appeared to be limited by frequent river run-off disturbances (De Madariaga *et al*. 1992).

Even in estuaries that are tidally mixed for most of the year, a strong freshwater input may cause temporary stratification. Cloern (1991) modeled bloom dynamics in South San Francisco bay. Maximum freshwater run-off occurs in the spring, and a bloom is initiated when the buoyancy of the surface layer inhibits tidal mixing and permits stratification. The greater the volume of freshwater, the greater the intensity of the bloom. When day-to-day events in the bloom cycle were analyzed, it was found that the increase in phytoplankton biomass always occurred in the neap tidal cycle and decreased during a spring tide cycle. A clear

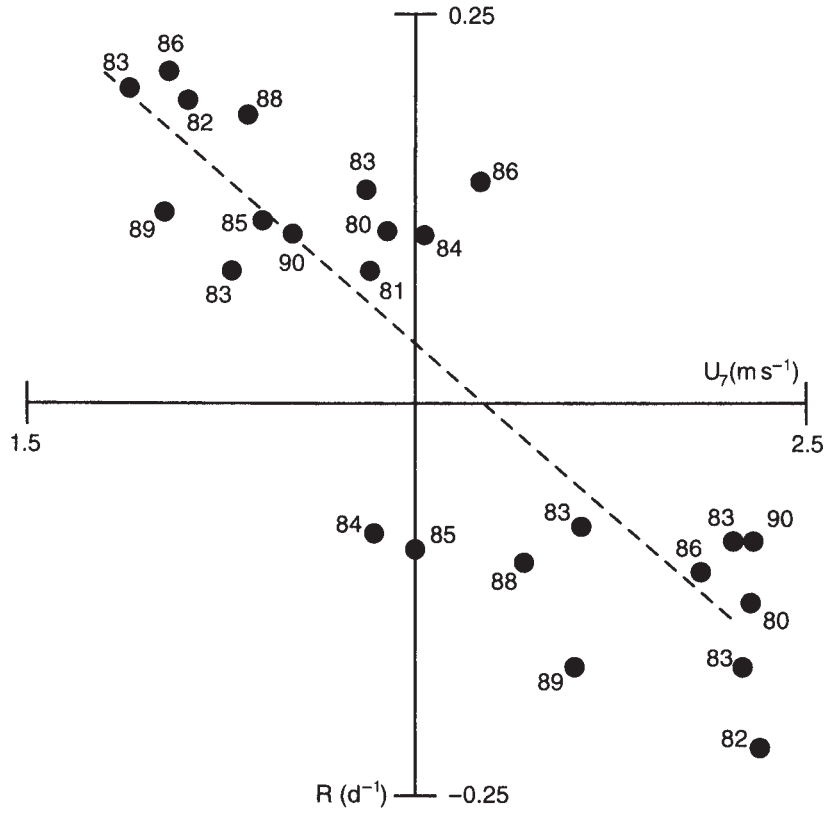

Fig. 4.10 The daily rate of increase or decrease of phytoplankton biomass (vertical axis) in San Francisco Bay plotted against daily maximum current speed (horizontal axis) averaged over the week preceding each sampling date. $r = -0.87$. From Cloern (1991).

correlation existed between strength of tidal currents and rate of growth of phytoplankton biomass. (Fig. 4.10).

Koseff *et al*. (1993) extended Cloern's (1991) model, in an attempt to more generally represent bloom formation in shallow, turbid estuaries. They showed that in the conditions of South San Francisco Bay, stratification itself is not sufficient to allow a bloom to develop. There must also be an absence of strong-wind mixing in the mixed layer. When stratification breaks down, consumption of phytoplankton by the benthic filter feeders is a factor in terminating the bloom. Conversely, isolation of the mixed layer from contact with benthic filter feeders during stratification contributes to, but does not control, the formation of a bloom.

Some of the subtleties of interactions between primary production, grazing, and turbidity in shallow estuaries were explored in a numerical model by Lucas *et al*. (1999). For example, under conditions of high turbidity and slow benthic grazing, the highest rates of phytoplankton population growth were found in the shallowest water, but with low turbidity and rapid benthic grazing the highest

growth rates occurred in the deepest areas. In the first case, turbidity caused light to be limiting and the phytoplankton experienced the greatest depth-averaged irradiance in shallow water. In the second case, light was abundant, benthic grazing was the limiting factor, and its influence on the water column was least where the water is deep. The model showed that these relationships with depth apply as one moves spatially from deep to shallow water, but also apply to the effect of rising and falling tides at a fixed station. The net result is that shallow estuaries tend to become an ever-changing mosaic of phytoplankton biomass.

Lucas *et al*. (1998) asked whether the Sverdrup critical-depth model (see Section 3.3.2) explains bloom dynamics in estuaries. In other words, is the shallowing of the mixed layer to a depth less than the critical depth for the phytoplankton an adequate predictor of a bloom? The result of their modeling was to show how complex are the interactions of the "competing" processes of average net growth of phytoplankton, sinking, and turbulent mixing of the water column. In energetic shallow systems, where net growth of phytoplankton is strongly influenced by turbidity of the water, and where tidally driven turbulent mixing varies in semi-diurnal and lunar cycles, the phytoplankton often leaks from the surface layer. The Sverdrup critical-depth model needs to be refined before it can be a predictor of the occurrence of phytoplankton blooms in these environments.

4.4.3 Freshwater run-off and secondary production in estuaries

A variety of animals have adapted to the characteristic circulation of stratified and partially mixed estuaries, with a seaward flow of low-salinity water and a compensatory landward flow of bottom water. By making vertical migrations at the appropriate times they can travel upstream for part of the time and downstream for another part, maintaining themselves in the estuary year-round or entering and leaving the estuary on a seasonal basis. Organisms thought to use this mechanism include barnacle larvae (Bousfield 1955), copepods (Grindley 1964), bivalve larvae (Wood and Hargis 1971), and blue crabs *Callinectes sapidus* (Provenzano *et al*. 1983). Graham (1972) suggested that larval herring *Clupea harengus* traveled up the Sheepscot estuary of Maine by staying near the bottom. On reaching the head of the estuary they rose to the surface waters and traveled to the mouth of the estuary before descending again into the landward net flow. In Cape Fear River estuary, North Carolina, Atlantic croaker *Micropogonias undulatus* stayed near the bottom and became concentrated near the head of the estuary, while white spot *Leiostomus xanthurus* and flounders *Paralichthys dentatus* made nocturnal excursions into surface waters during flood tides. This behavior carried them into salt-marsh creeks (Weinstein *et al*. 1980; Lawler *et al*. 1988).

In the estuary of the St Lawrence, the two dominant pelagic species capelin *Mallotus villosus* and herring were adapted differently to the estuarine circulation (Fortier and Leggett 1982, 1983). Capelin spawned in the upper estuary, stayed in the upper 20 m of the water column, and were carried to the more productive

zones of the lower estuary. Herring spawned in the lower estuary and larvae <10 mm long stayed at 40–60 m depth and were carried upstream. Herring larvae >10 mm long made diurnal vertical migrations and tended to remain in the same part of the estuary. Their vertical migrations followed the vertical migrations of the early stages of copepods, thus maximizing food availability.

Rowe and Epifanio (1994) quantified the transport of weakfish *Cynoscion regalis* in Delaware Bay, USA. They developed vertical profiles of physical flow and larval abundance at all states of the tide, and for each 1 m depth interval they calculated instantaneous larval flux (F_{zt}). For each depth and each flood or ebb tide they obtained the time-averaged water velocity U_z, time-averaged larval abundance D_z, and time-averaged larval flux F_z They then divided time-averaged larval flux by time-averaged larval abundance to give a term (U_z^*) that they called larval velocity. If larvae are well mixed in the water column, U_z^* is identical to the time-averaged water velocity; if the larvae migrate between levels during the time series, however, U_z^* differs from U_z. They found that in one year the estuary had the conventional circulation, but in another year net flow was landward at all depths, probably because of a lack of freshwater run-off. U_z^* for post-yolk-sac larvae was always more positive than time-averaged water velocity. For early-stage post-yolk-sac larvae it was about 5 cm s^{-1} greater, but for late-stage larvae it was about 5 cm s^{-1} greater near the bottom, increasing to 25 cm s^{-1} near the surface. In 1989, when the surface and deep waters were moving in opposite directions, the net landward flux of larvae was still positive, but 1–2 orders of magnitude lower than in the previous year.

Summarizing this section, we see that the secondary producers in an estuary are often adapted to the two-layered estuarine circulation that is found wherever the influence of freshwater run-off predominates over the influence of tidal mixing. A common form of adaptation is for the behavior of young stages to be related to the circulation pattern in a way that optimizes their opportunities for feeding and survival. The details are complex and not fully understood. One lesson is clear: a major change in the circulation pattern of an estuary brought about by damming the freshwater flow, a tidal dam, or other engineering projects, or even by changes in patterns of precipitation, may well have far-reaching effects on the primary and secondary productivity of the system. Examples will be given in Section 4.7. We may note in passing that organisms are capable of adapting their life histories to circulation patterns on many scales, even up to the scale of the Gulf Stream, where eels and squid, for example, ride with the current and return by another route.

4.5 The biological effects of tidal mixing

4.5.1 Physics of tidal fronts

The idea that the turbulence generated by high tidal currents keeps the water over some shallow regions mixed all year while the quieter regions in the deeper waters

become stratified in summer was first advanced more than 70 years ago. Bigelow (1927) suggested the process to explain the fact that the water over Georges Bank in the Gulf of Maine remained mixed all year while the water over the deeper regions became stratified in summer. Subsequently, Dietrich (1950) (quoted by Le Fèvre 1986) suggested that the summertime front across the western end of the English Channel exists because of an increase in the turbulent mixing in the shallower regions of the Channel. (Fronts are regions of strong gradients of temperature and other properties in the sea; the various types of fronts are discussed in Chapter 6.) Later Simpson and Hunter (1974) constructed an energy argument that has proved very successful in predicting the locations of these tidally mixed fronts. Before we try to understand the processes that may increase the biological activity at these fronts, however, we first take a look in some detail at the theory that predicts the locations of such fronts.

Simpson and Hunter (1974) postulated that a front would be found where the intensity of turbulent mixing was just enough to continuously overcome the barrier to mixing presented by the stratification. They estimated the amount of energy required to mix a stratified column by calculating the difference in the potential energy of the water column before and after mixing. Following this technique, Loder and Greenberg (1986) estimated the tidal velocities u and v with a numerical model for the whole Gulf of Maine, then plotted contours of estimated values of $\log_{10}(h/D_t)$, where h is the height (= depth) of the water column and D_t is the depth-integrated rate of dissipation of energy from tidal currents. They argued that the transition between mixed and stratified water should occur at $\log_{10}(h/D_t) = 1.9$. Values less than this number indicate well-mixed conditions and values greater than 1.9 will be stratified.

Pingree *et al*. (1978a) approached tidal fronts from the point of view of the turbulent energy dissipation rate due to tidal flow. They calculated an index $E = \log_{10}\varepsilon$ and showed (Fig. 4.11) that in areas where $E > -1.0$ the waters were tidally mixed throughout the year, and where $E < -2.0$ the waters were stratified in summer. This technique is the inverse of the Loder and Greenberg (1986) method, which explains why lower values define stratified conditions rather than higher values as in the Loder and Greenberg calculations.

Between the stratified and the well-mixed regions Pingree *et al.* (1978a) defined a transition zone in which the degree of tidal mixing varies according to the stage of the lunar tidal cycle (Chapter 7). They showed lines at $E = -1.5$ that they predicted would be the average positions of the fronts between stratified and tidally mixed waters. These predictions were, in general, confirmed by field observations. Extensive areas of tidal mixing occur in the southern North Sea, the English Channel, and the southern Irish Sea. The Celtic Sea is a stratified region. Pingree *et al*. (1976) studied the development of the spring bloom in this region and found that the thermocline established first in the region of weakest tidal currents, then gradually spread to areas of stronger tidal currents. The spring bloom of phytoplankton coincided with thermocline formation. The tendency of tidally generated turbulence to oppose stratification caused by surface heating is very clear.

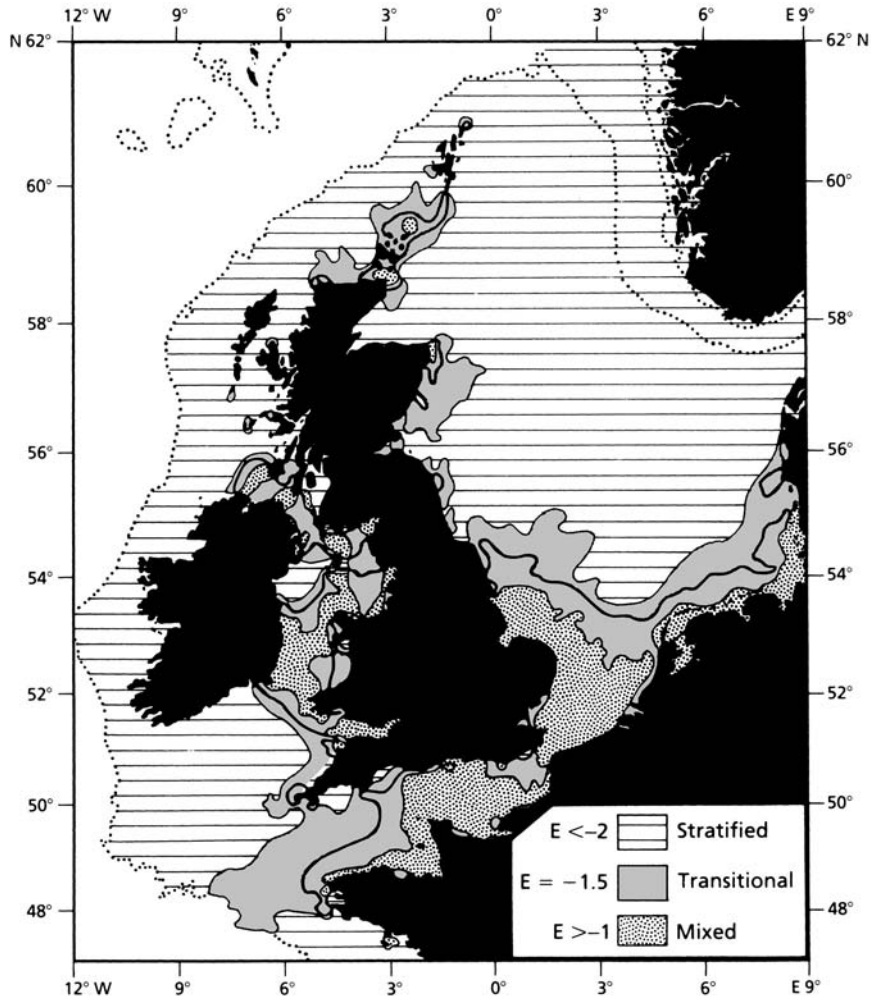

Fig. 4.11 Waters around the British Isles. Distribution of $E = \log_{10}\varepsilon$, where ε is the tidal energy dissipation per unit mass (erg g^{-1} s^{-1}). The continuous line $E = -1.5$ represents the predicted positions of frontal boundaries. Shading on either side indicates the transition zone between well-mixed and well-stratified waters. Note that the waters represented by light horizontal lines are stratified only in summer, but the waters indicated by stippling are tidally mixed all year. Reproduced with permission from Pingree *et al*. (1978b), Pergamon Press.

The theory of Simpson and Hunter (1974) has been refined by Simpson and Bowers (1981) and Loder and Greenberg (1986) to include the effects of wind mixing and of variable levels of mixing efficiency. Bowers and Simpson (1987) compared the various theoretical approaches with the observed positions of tidal fronts on the European shelf seas and concluded that in shallow water the models

incorporating wind mixing effects are most accurate. In deeper water the wind effects decline in importance and no theory is significantly superior to the others at predicting the front positions.

4.5.2 Tidal mixing and phytoplankton production

In light of the postulated dependence of the spring bloom on thermocline formation, what is the pattern of phytoplankton production in tidally mixed areas where no summer stratification occurs? The lack of stratification would be expected to decrease phytoplankton productivity. On the other hand, dead organic matter is continually decomposing on and in the sediments, providing a source of nutrients that can be mixed back into the water column to stimulate phytoplankton production. Georges Bank, in the Gulf of Maine, is one such tidally mixed area that has been intensively studied (Bumpus 1976; Backus and Bourne 1987). Chlorophyll-*a* concentrations are homogeneously distributed in the water column (O'Reilly *et al*. 1981) and the depth of the euphotic layer in summer averages about 50% of the depth of the water column. Under these conditions primary production continues throughout the year, with no clearly marked seasonal peak. O'Reilly and Busch (1984) reported fluctuating production levels with some indication of a peak in October. On the other hand, Riley (1941) and others had found a phytoplankton biomass peak in April. This finding is explained by the low level of zooplankton grazing at this time of year. As the season progresses, phytoplankton production remains at a high level, but most of the biomass is removed on a daily basis by the grazers.

Sissenwine *et al*. (1984) estimated that total primary production (^{14}C uptake) on Georges Bank was 450 g C m^{-2} y^{-1} on the shallow part (<60 m) and 320 g C m^{-2} y^{-1} on the deeper part. This level is higher than many other tidally mixed coastal areas in temperate waters. The explanation offered is that a clockwise gyre (see Chapter 6) retains water on the bank, nutrient-rich water from the slopes is advected onto the bank, and the continuous mixing of the waters makes nutrients regenerated from the sediments available to the phytoplankton.

Data for both biomass and productivity in various parts of the North Sea were reviewed by Fransz and Gieskes (1984). Their biomass data confirm the earlier results, that offshore sites within the tidally mixed area have well-marked spring and autumn peaks while coastal sites have relatively high biomass throughout the spring and summer. Their field data (Fig. 4.12) show that coastal waters have summer productivity almost twice as high as the offshore areas but a rapid falling off in autumn. This difference appears to be attributable to a larger flux of nutrients from the sediments and rivers into the tidally mixed water column (Mommaerts *et al*. 1984) but a poorer penetration of light in the autumn on account of the sediment load. The estimated annual productivity (^{14}C uptake) for the North Sea is considerably lower than for Georges Bank, 250 g C m^{-2} y^{-1} offshore and 200 g C m^{-2} y^{-1} in coastal waters.

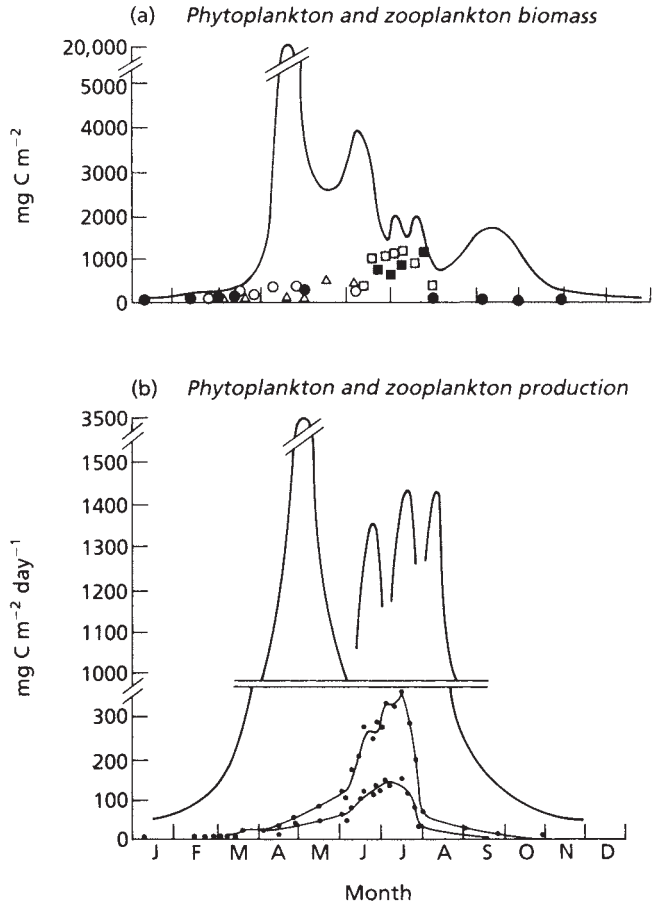

Fig. 4.12 Biomass and productivity in coastal waters of the southern North Sea. (a) Biomass of phytoplankton (line) and zooplankton (points). (b) Estimated production of phytoplankton (heavy lines) and zooplankton (fine lines). The estimates for zooplankton are of two types: "potential production" and "lowest estimate." For details see Fransz and Gieskes (1984).

In Naragansett Bay (Rhode Island, USA) the waters are tidally mixed at all times of the year (Kremer and Nixon 1978), and this results in a marked winter–early-spring bloom of phytoplankton followed by a series of summer blooms. Regeneration of nutrients from the benthos accounts for about half the needs of the phytoplankton, the remainder coming from allochthonous inputs and from regeneration within the water column.

It should be noted that the productivity of tidally mixed areas is also a function of the depth of the water column. Gowen *et al*. (1995) determined the productivity of stratified and tidally mixed waters in the Irish Sea. Production in the summer stratified waters, estimated at 101 g C m^{-2} y^{-1}, was close to the productivity of similar areas of the North Sea. However, the productivity of tidally

mixed waters, in places where the depth of the water column was 92–130 m, was less than half the figures for the shallower tidally mixed areas in the North Sea. It seems probable that in the Irish Sea the phytoplankton was light-limited for much of the year, because of the depth to which the phytoplankton cells were being mixed. In tidally mixed waters close to the coast of Ireland, with depths of only 18 m, primary production was much closer to that of the North Sea.

The conclusion from this section is that tidally induced mixing in relatively shallow coastal waters prevents stratification of the water column, but the potentially adverse effects on phytoplankton productivity are more than compensated for by the increased nutrient flux to the water column from the sediments. As a result, annual primary productivity in tidally mixed areas tends to be above the average for coastal waters. If the phytoplankton is being transported by turbulence throughout the water column and is exposed to abundant nutrients, the onset of the bloom in spring depends mainly on the seasonal increase in light, and not at all on the onset of stratification. The net result is that the annual production cycle appears to start earlier in tidally mixed areas.

4.5.3 Consequences of tidal mixing for zooplankton

We saw in Section 3.6.2 that in the open ocean initiation of the spring growth in the zooplankton population is often triggered by the upward migration of a large biomass of adult and late-stage copepods that have spent the winter at depths greater than 350 m. Reproduction begins as soon as this population reaches surface waters, and grazing pressure on the phytoplankton develops relatively early in the season. In part this process is made possible by the rapid warming of the surface waters after stratification. In tidally mixed waters, warming is delayed by the lack of stratification, and there is no population from deep water that can ascend to the euphotic zone and begin to feed on the phytoplankton. The net result is that tidally mixed waters tend to have a relatively slow growth of the zooplankton population, which often does not peak until early or mid-summer. It appears that much of the biomass of the spring bloom escapes grazing by the copepods and sinks to the bottom. For example, Fransz and Gieskes (1984) determined biomass and productivity of both phytoplankton and copepods in the coastal region of the North Sea adjacent to Belgium (Fig. 4.12) and concluded that only in June and July was there a match between the productivity of the phytoplankton and the food consumption of the copepods. It should be noted that Gieskes was concerned only with zooplankton larger than 50 μm and that others have noted high abundances of microzooplankton such as ciliates, especially in the late summer and autumn in many inshore locations.

Williams *et al*. (1994) studied 31 years of records, taken with the Longhurst–Hardy plankton recorder, on the European shelf seas. They found that copepods dominated the zooplankton, forming around 80% of the biomass. The shallower, tidally mixed waters were dominated by smaller copepods which, together with the microplankton, formed a complex food web that is rather inefficient in

providing food to young fish. By contrast, the waters that are thermally stratified in summer are dominated by two relatively large copepods, *Calanus finmarchicus* and *Calanus helgolandicus*, which are part of the food web: diatoms – copepods – larval fish. We saw in Section 2.2.14 that the turbulence that accompanies coastal upwelling episodes and convective mixing appears to favor this type of food web but it appears that long-term turbulence, associated with tidal mixing, does not.

4.6 River and estuarine plumes on the continental shelves

4.6.1 Physical mechanisms

In this section we are concerned with the effect of water from either a river or an estuary pouring out onto a continental shelf, or into a semi-enclosed sea. In some situations where river flow heavily predominates over any tidal effects, the surface outflow onto the continental shelf is mainly of fresh water from the river itself, and is called a river plume. In other situations there is strong penetration of salt water into the river valley to form an estuary, and the outflow onto the continental shelf is of river water mixed with considerable quantities of salt water. This flow constitutes an estuarine plume. Examples of river plumes that have been studied in an integrated biological/physical way include the Mississippi at each of its three passes in its delta, the Amazon River, the Fraser River, and the Connecticut River. Estuarine plumes are much more common, those of the Chesapeake, the St Lawrence, and the Hudson River being some of the more intensively studied in North America.

When the light upper water from an estuary or a river flows out into the open ocean, it leaves behind a narrow region where the flow is predominantly two-dimensional and enters a less confined world where the Coriolis force can change the direction of the flow. In the illustration in Fig. 4.13 the water moves down an estuary in the northern hemisphere at a velocity u. Because this motion is relative to the earth there is a Coriolis effect directing water to the right of the flow. The water, however, is not able to change direction because of the side boundaries of the estuary but the water does move to the right causing a slight tilt to the sea surface and a pressure gradient in the direction opposite to the Coriolis force. The flow is, therefore, in geostrophic balance and the slope of the sea surface can be estimated in the way shown in Box 4.04.

When the water flows out of the estuary this surface slope is missing, and cannot provide the pressure force to balance the Coriolis force. Being unopposed, the Coriolis force causes the flow to turn to the right but it comes under the influence of the shoreline again and sets up a situation similar to the one found within the estuary. As the Coriolis force pushes the water to the right, the blocking of the coast causes an opposing pressure gradient in the form of a slight slope in the sea level to be generated against the coast, and the plume of fresher water continues on its way as a coastal current in geostrophic balance parallel to the coast. A laboratory model of this process is described by McClimans (1986).

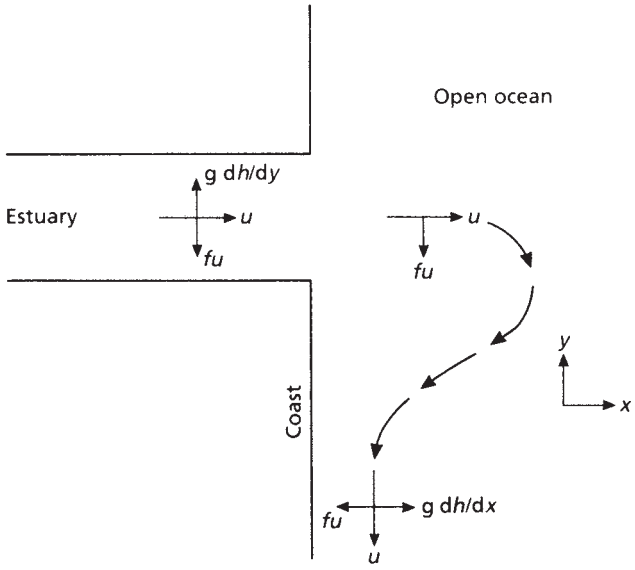

Fig. 4.13 Water moving down the estuary at velocity u is in geostrophic balance. The Coriolis force balances the pressure gradient. In the open ocean the flow is not in geostrophic balance and in the northern hemisphere the Coriolis force causes the flow to turn to the right and flow along the coast.

Box 4.04 The surface slope across an estuary

We first assume a coordinate system in which the x axis points down the estuary. Since there is no flow parallel to the y axis $v = 0$ and the balance of forces in the water is given completely by Eqn. 4.03:

$$fu = -\frac{1}{\rho}\frac{\mathrm{d}P}{\mathrm{d}y}$$

The pressure gradient can be written in terms of the sea surface slope by using the equation that relates pressure and water depth, i.e., the hydrostatic relation

$$P = \rho g h \tag{4.10}$$

where P is the pressure, ρ the density, g the acceleration due to gravity (10 m s^{-2}), and h is the height of the water column. Taking the first derivative of this and inserting $\mathrm{d}P = \rho g \mathrm{d}h$ in Eqn. 4.03 we get

$$fu = -g\frac{\mathrm{d}h}{\mathrm{d}y} \tag{4.11}$$

which states that the sea surface slope in the y direction ($\mathrm{d}h/\mathrm{d}y$) is equal to fu/g. In a narrow channel where the flow may be considered constant over the whole width, the difference in the height of the sea surface from one side to the other will be $\mathrm{d}h = fuW/g$, where W is the width of the channel. If u is 0.5 m s^{-1}, $f \approx 10^{-4}$ s^{-1}, and $W = 200$ m, then the change in height across the estuary is approximately 1 mm.

The Coriolis turning of the water coming out of rivers and estuaries is a common phenomenon and is often observed from aircraft and in satellite photographs. The fresher water in the current is usually distinguishable from the resident water of the ocean because it has more suspended material in it. A northward flowing coastal current driven by the run-off of rivers in British Columbia is described by LeBlond *et al*. (1986).

When the water leaving a river or estuary flows into a region where there is already a current, the movement of the freshwater plume is not as simple as in the case described above. The position of the plume in these cases will be the result of the relative strengths of the background flow in the ocean and the new flow entering from the river or estuary. A strong coastal flow will overwhelm a weak outflow and the plume may turn in an unexpected direction. In most cases the flows are tide-dependent and the plume changes position over the tidal cycle. For example, the Connecticut River has a well-developed river plume at its mouth (Bowman and Iverson 1978). Under light wind conditions a layer of fresh water only about 2 m deep spreads out over the coastal waters for a distance of about 10 km from the river mouth. The tendency for the plume to be turned to the right by the Coriolis force is obscured by the local tidal currents, which deflect the plume alternately to the right and to the left. The seaward flank of the plume is marked by a sharp front (see Chapter 6).

Siegel *et al*. (1999) studied the plume of the Oder River, which flows northward into the Baltic Sea at the boundary between Germany and Poland. Using satellite data, numerical modeling, and shipborne measurements, they showed that when the prevailing westerly winds are blowing the plume of the Oder turns to the right and flows along the Polish coast, sometimes for as much as 300 km, at a velocity of about 30 cm s^{-1}. Low-velocity winds from the east block the westward flow of the Oder plume and cause the formation of a stable plume off the mouth of the river. Strong easterly winds, which often occur at the time of maximum run-off in the spring, turn the plume so that it runs northwest along the German coast to the Arkona Sea off the southern tip of Sweden.

Estuarine plumes are normally of much larger volume than river plumes because the freshwater run-off has entrained considerable quantities of seawater within the estuary. For example, the Chesapeake Bay estuary discharges large volumes of water at a salinity of about 16 parts per thousand and the plume is deflected south by the Coriolis force to form a strong coastal current. In many parts of the world estuaries occur sufficiently close together around the main ocean basins that their plumes may overlap and reinforce one another to form a continuous counter-clockwise coastal current in the northern hemisphere or a clockwise current in the southern. In a workshop reported by Skreslet (1986) accounts were given of such currents in Scotland, Norway, Iceland, Greenland, eastern Canada, and the eastern United States, and Drinkwater (1986) suggested that they were part of a nearly continuous flow around the perimeter of the North Atlantic. A modeling study has predicted the existence of a similar counter-clockwise flow around the perimeter of the North Sea (Müller-Navara and Mittelstaedt 1985).

Others have pointed out that the plumes are sometimes deflected by wind stress. For example, the Hudson River plume, off New York, took up a position

approximately at right angles to the coast after three days of southwest winds (Bowman and Iverson 1978). The same plume also weakened under conditions of low river flow, to the point where it was temporarily obliterated by local tidal currents. More investigations are needed before the strength and variability of buoyancy-driven coastal currents can be assessed.

Johnson *et al*. (2001) showed how the Chesapeake plume was influenced by wind direction. A 3–5-day period of winds from the north or northwest (downwelling-favorable) held the plume close to the coast as a jet with a speed of about 0.5 m s^{-1}. Variation in wind strength produced wave-like variations in jet width. Upwelling-favorable winds from the south caused water from the jet to be dispersed on the shelf in a thin near-surface layer. The dispersion and recruitment of crab larvae were facilitated by these changes (Roman and Boicourt 1999). During downwelling-favorable wind episodes in spring, crab larvae were transported south along the coast at speeds that at times exceeded 168 km d^{-1}. During June and August upwelling-favorable winds from the south stopped the southward movement and dispersed the larvae across the shelf. At least 27% of the larvae spent part of the day in bottom water, which has a residual drift towards the bay.

In a modeling exercise, confirmed by remote-sensing data, short-term variation in precipitation in the watershed of Chesapeake Bay, with the consequent change in freshwater run-off, had a strong influence on the Chesapeake plume (Breaker *et al*. 1999). During hurricane Fran of 1996, the high discharge caused a marked lowering of salinity close to the mouth of the bay and generated a halocline, which was at 10 m depth close to shore, decreasing to 5 m at 60–75 km offshore. The model used, which was a quasi-operational ocean forecast model, provided good simulation of the direction of the plume under changing wind conditions, but failed to reproduce the full extent of lowered salinity close to shore.

4.6.2 Biological effects of river and estuarine plumes

The biological effects of freshwater discharge may be considered under three headings: (i) direct effects of the materials carried by the river on biological production in the plume; (ii) entrainment and consequent upwelling of nutrient-rich water, which is likely to enhance primary and secondary production; and (iii) enhancement of the stability of the water column, which may be expected to enhance productivity at the time of a spring bloom, but which may inhibit vertical mixing and hence reduce primary productivity at other times of the year. Commonly, all three effects are observed in the same plume.

(a) Mississippi River plume in the Gulf of Mexico

The nutrients carried into coastal waters by river plumes have a marked effect on productivity in a region surrounding the river mouth. The time of peak run-off of the river is normally a time of diatom bloom, and commonly the diatoms are deposited on the sea floor around the river mouth. As early as 1937, Riley (1937) found an area of enhanced chlorophyll and phosphorus extending about

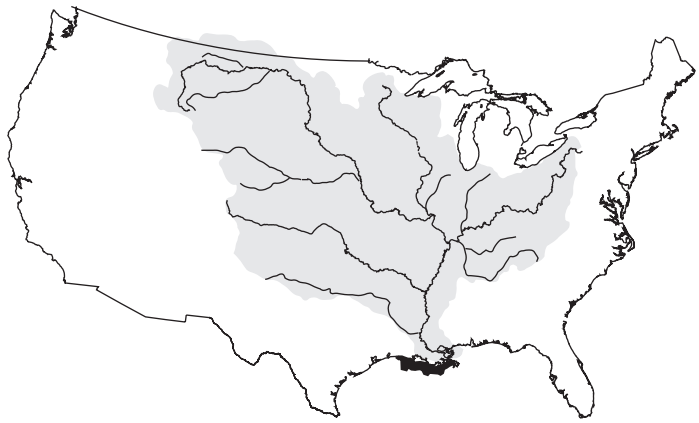

Fig. 4.14 The contiguous United States of America, showing the drainage basin (shaded) of the Mississippi River and its tributaries. Shading in the Gulf of Mexico shows the general area of oxygen depletion. After Rabalais *et al*. (1996).

50 km south and east of the Mississippi delta, and about 125 km westward in the coastal current. Since then, the effect has become much more pronounced. All evidence points to the river-borne nutrients being the main cause of eutrophication on the shelf.

The Mississippi is the seventh largest of world rivers and drains 41% of the contiguous United States (Fig. 4.14). Between 1949 and 1999 the nitrate and phosphate concentration in the river water doubled (summarized in Lohrenz *et al*. 1999), mostly as a result of agriculture in the drainage basin. Annual and interannual changes in river-borne nutrient inputs have been correlated with primary production in adjacent shelf waters. Enhanced primary production and sinking of organic matter have been correlated with the nutrient concentrations in surface waters and with the patterns of accumulation of biologically bound silica in sediments. Lohrenz *et al*. (1999) confirmed the connection of phytoplankton production with nutrient loading of the river by showing that the highest values of productivity (>10 g C m^{-2} d^{-1}) were at places where the surface nutrient concentrations exhibited large deviations from conservative mixing relationships, indicating that depletion of nutrient was related to phytoplankton uptake.

The consequence of increased phytoplankton production and sinking of phytoplankton biomass has been a great increase in bacterial activity and formation of zones of low oxygen (hypoxia) or zero oxygen (anoxia) in the lower 20 m of the water column, especially in summer (Rabalais *et al*. 1996). These conditions became more widespread and more severe through the 1990s. In some places hypoxia now begins in February and lasts until October, with anoxia from mid-May to mid-September.

Malakoff (1998), in a paper entitled "Death by suffocation in the Gulf of Mexico," drew attention to the magnitude of the problem and the consequences

for consumer organisms. In 1989 the area having less than 2 mg oxygen per liter covered about 9000 km^2, but in 1993 the volume of the spring river run-off was about twice the normal amount and the area of hypoxic water almost doubled its size. In subsequent years of normal river run-off, the low-oxygen zone shrank very little, and in 1998 was about 16,000 km^2. Mobile organisms such as fish and shrimp leave the hypoxic areas, but sedentary animals are killed in large numbers. Many fear that the loss of benthic invertebrates and the reduction in area of habitat for fish and shrimp will cause a major reduction in the fisheries, currently worth more than $3 billion to Louisiana alone. The remedy is believed to be a reduction in the use of agricultural fertilizers and construction of nitrogen-trapping vegetation buffers along the edges of farm fields. Since the river drains more than half the nation's farmland (Fig. 4.14), remedial action requires no less than a major change in national farming practices.

(b) The plume of the Po River in the Adriatic Sea

Similar problems exist at the mouth of the Po River, just south of Venice in the Adriatic Sea. Revelante and Gilmartin (1976) reported high nutrient uptake by phytoplankton in that area. Justic *et al*. (1993) showed that in the decade of the 1970s the average concentration of inorganic nitrogen in the river doubled, phosphate tripled, but silicate increased by less than 50 percent. There is a clear correlation between seasonal peaks in the flow of the river and peaks in primary production in the coastal waters. Associated with the river plume is a large area where oxygen falls below 20% saturation in the bottom waters, in the months of August and September when water-column stratification is most intense (Fig. 4.15).

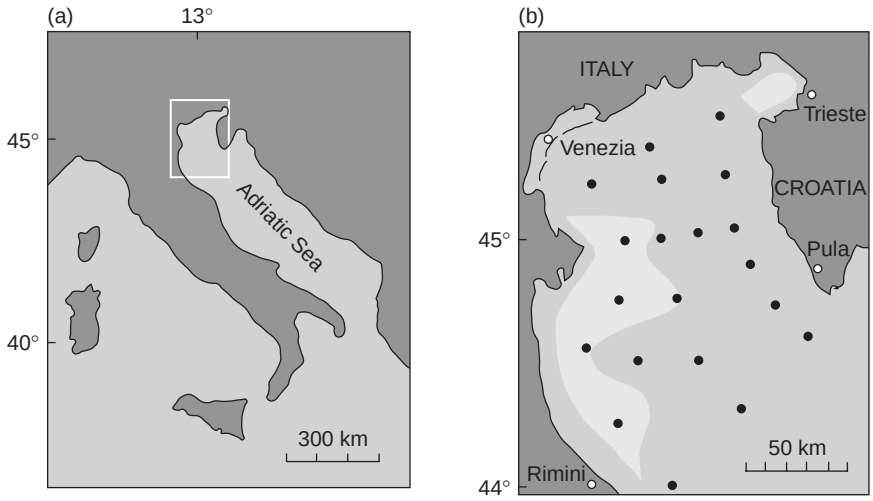

Fig. 4.15 (a) The Adriatic Sea. (b) Unshaded areas show where the bottom oxygen saturation during August and September was expected to fall below 20% (~1.1 mL O_2 L^{-1}). Dots show sampling stations. From Justic *et al*. (1993).

(c) The Amazon plume

The Amazon is the world's largest river in terms of water discharge (about 5800 billion metric tons a year) and nutrient flux (over one billion metric tons of sediment per year). Three main zones can be recognized within the plume. Closest to shore the water has a high sediment load. As the water moves out onto the shelf the sediment gradually flocculates and sinks. Primary production in this turbid, nutrient-rich water was found to average 2.18 g C m^{-2} d^{-1} (Smith and Demaster 1996, Demaster and Pope 1996) and is thought to be light-limited. Just seaward of this zone occurs a region of high algal biomass composed primarily of diatoms, in which the productivity averaged 2.61 g C m^{-2} d^{-1}, but occasionally exceeded 8 g C m^{-2} d^{-1}. In this zone, sinking of the sediment improved the penetration of light and productivity was probably nutrient limited. Out towards the edge of the shelf the water is clear, of high salinity and low nutrient content. Primary productivity averaged 0.81 g C m^{-2} d^{-1}. There have been many debates about whether the central zone of high productivity gets its nutrients from the river runoff, or more indirectly by entrainment or regeneration. Nutrient concentrations, phytoplankton biomass, and productivity were highest in the low-salinity water of the upper 10 m of the water column. All three variables were higher when the river flow was high, and vice versa. All this points to the importance of the river water as a source of nutrients.

An outflowing plume of fresh water entrains several times its own volume of salt water, and as this moves offshore there is a compensatory shoreward flow of bottom water. The onshore flow of subsurface water on the Amazon shelf was estimated at 5–10 times the river freshwater discharge, and this water receives a very large input of nutrients regenerated from sinking biological material. It was estimated that the algal blooms on the Amazon shelf receive 83% of their nitrogen, 69% of their phosphorus, and 59% of their silicon by regeneration and upward mixing, with the remainder coming from river water.

(d) The plume of the Hudson estuary

The foregoing examples are of distinct river plumes. In estuarine plumes the story is rather different because the nutrient load carried by the river is frequently utilized within the estuary itself. On the other hand, many major estuaries around the world are the sites of dense human settlement, so that the estuaries receive a heavy load of nutrients from land drainage or sewage. Frequently the estuary does not have the capacity to assimilate this material and the estuarine plume is strongly enriched with nutrients. The plume of the Hudson estuary, off New York, in the state it was in the early 1980s, is a good example (Malone 1982, 1984). The sewage input into the estuary itself was 1.6×10^5 kg N d^{-1}, which led to a nitrogen concentration in the water of about 60 μmol L^{-1}. Phytoplankton production within the estuary was severely light-limited on account of the high turbidity, so only a small proportion of the nutrients were utilized within the estuary. Most poured out into the estuarine plume, where the amount of chlorophyll in the water

column was 40–60 mg m^{-3} for most of the year, and may have had a monthly mean close to 200 mg m^{-3} during the spring bloom period. In the spring, grazing mortality was low and most of the production sank to the bottom. Later in the year the zooplankton biomass increased and in summer it was thought to consume about 30% of the phytoplankton productivity. Malone (1982) demonstrated that the area of high phytoplankton productivity associated with the sewage enrichment was concentrated within 20 km of the mouth of the estuary. Beyond that, chlorophyll-*a* concentration decreased as salinity increased. A budget for nitrogen supply and utilization indicated that the area required for the phytoplankton to assimilate all of the dissolved organic nitrogen from the sewage run-off varied from 670 km^2 during summer, when phytoplankton is most active, to 1350 km^2 during winter. In effect, all of the nutrients derived from sewage and land run-off were utilized within that region of the New York bight close to the estuary, known as the Apex.

(e) The plume of Chesapeake Bay

Surprisingly, in spite of all the studies on Chesapeake Bay, it was not until the work of Austin (2002) that a good estimate was obtained for the exchange of Chesapeake Bay with the ocean. There is a strong rotational circulation within the bay and, under the influence of the Coriolis force, water tends to enter the bay at depth on the northern side of the bay mouth and leave nearer the surface through the southern portion. Weiss *et al*. (1997) had shown from aircraft surveys that during spring blooms the chlorophyll content of the water was high on the western side of the bay, in the outward-flowing water, and low on the eastern side. Attempts to budget the flow with current meters at the mouth have led to highly variable, conflicting estimates of the average exchange rate. Austin (2002) made a salt-balance model of the whole Chesapeake Bay, using 16 years of survey data. He concluded that the mean exchange rate is about 8000 $m^3 s^{-1}$, corresponding to an exchange time scale of 90 days. According to the surveys, the mean nitrogen content of the water near the mouth of the bay is 0.32 mg L^{-1}. Hence the nitrogen export from the estuary is estimated as 2.56 kg s^{-1}, which can tentatively be extrapolated to about 80,000 t y^{-1} or 5.7 Gmol y^{-1}. Since the estimate for nitrogen export from all estuaries to the whole North Atlantic is 250 Gmol y^{-1}, (Howarth 1996), the Chesapeake appears to be contributing more than 2% of the total.

(f) The Fraser River plume

Yin *et al*. (1997a) reported on the interaction of river run-off and wind mixing in the plume of the Fraser River, near Vancouver, Canada, in summer time. On day 1 of their observations the water column was well stratified and nitrate was depleted in the top 7–13 m in the estuarine plume. A strong wind on day 2 mixed the water column, causing an increase in nitrate content and causing a phytoplankton bloom. Between day 3 and day 9, there was a rapid increase in Fraser River discharge,

causing the entrainment of nitrogen in the estuarine plume and formation of a subsurface maximum of chlorophyll-*a*. A minor influence of tidal mixing could also be detected in the nutrient profiles. It was clear that summer primary production in the estuarine plume was driven by a supply of nutrients from the nitracline, through vertical mixing induced by the interaction of winds, river discharge, and tidal cycles.

On another occasion Yin *et al*. (1997b) studied the Fraser River plume at a time of light winds and declining tidal influence. A rapid increase of river discharge over four days, followed by a decrease over three days, led to the entrainment of nitrogen into the euphotic zone. The enriched water was carried seaward in the estuarine plume and caused a burst of primary production. This was a clear demonstration of estuarine-plume entrainment in action. The authors were able to calculate that the amount of nitrate entrained was 5–10 times higher than the amount contributed by the river water. This result is in marked contrast to the situation with the highly polluted Mississippi and Po rivers discussed in the previous section.

4.6.3 Biological effects of estuarine entrainment

In places where estuaries discharge onto the continental shelf it has repeatedly been shown that deeper waters are drawn toward the mouth of the estuary from a considerable distance. Norcross and Stanley (1967) found that bottom drifters released 70 km seaward of the mouth of Chesapeake Bay (Fig. 4.16) were consistently drawn toward the mouth of the bay, and Pape and Garvine (1982) found a similar circulation off Delaware Bay. It is, therefore, reasonable to assume that nutrients regenerated into this bottom water are carried toward the coast and are eventually entrained into the estuarine plume, increasing biological productivity. Direct evidence of the magnitude of this effect is lacking mainly because of the difficulty of defining the boundaries of a plume that changes its direction under the influence of wind and tides (Section 4.6.1).

When Norcross (1991) sampled larval Atlantic croakers at various depths from surface to bottom in two transects off the mouth of Chesapeake Bay and one transect inside the mouth, she found that in vertically mixed water columns the fish were found throughout the water column, but in stratified water they were found in the inward-flowing lower layer. She concluded that the fish actively selected the lower layer, after which they were passively transported towards the head of the estuary.

4.6.4 The effects of fresh water on the stability of the water column

We have mentioned that addition of fresh water to salt water causes earlier stratification and greater resistance to breakdown of thermal stratification by tidal

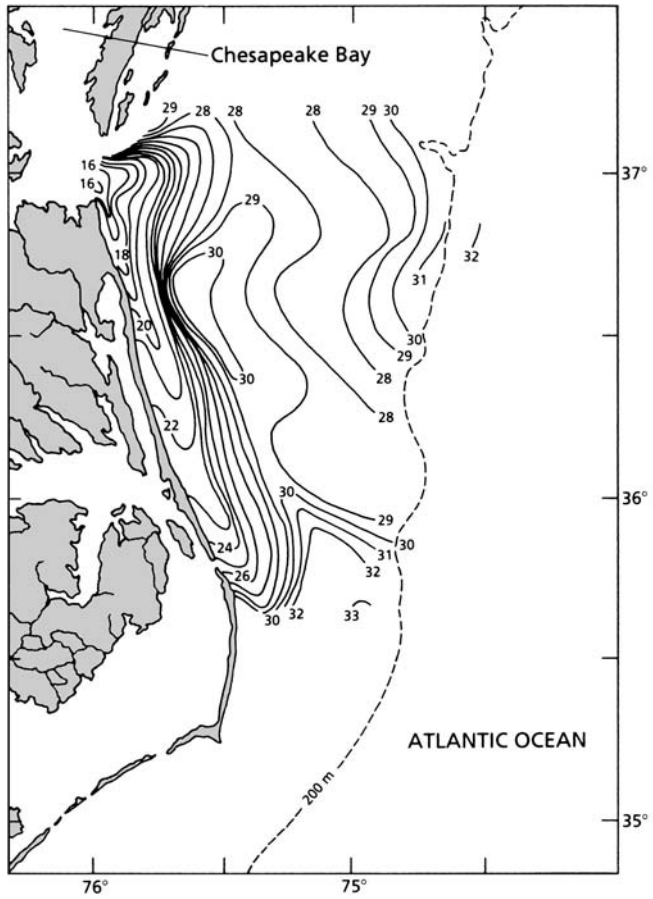

Fig. 4.16 The Chesapeake Bay plume, as revealed by salinity contours. The mouth of the bay is near the upper left corner, and the plume is directed south, close to shore. After Garvine (1986).

or wind-induced mixing. This process leads naturally to the idea that in temperate latitudes the spring bloom may start earlier close to the coast, where freshwater influence is most strong.

Thordardottir (1986) explained interannual variations in the timing of the onset of the spring bloom of phytoplankton off the coast of Iceland by interactions between freshwater run-off and the wind regime. When the primary production was averaged for the years 1958–1982 there were several distinct seasonal patterns. At the station furthest from shore there was little primary production in March and April, a single major bloom in May, and relatively low production for the rest of the season. Close to shore, production began in March and remained at a relatively constant level through the summer. At intermediate distance from shore there was a pattern with more or less equal blooms in spring and autumn.

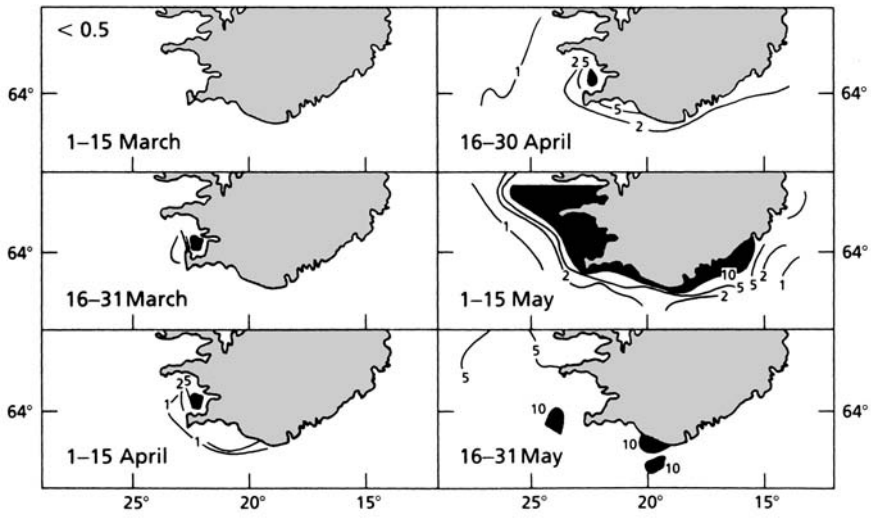

Fig. 4.17 Seasonal progression of the spring bloom off the southwest of Iceland. Contours show primary production (mg C m^{-3} h^{-1}) at a depth of 10 m. Pooled data 1958–1980. Areas of production greater than 10 mg C m^{-3} h^{-1} are shaded in black. After Thordardottir (1986).

The temperature and salinity profiles at various stations showed that the stratification associated with the beginning of bloom conditions was attributable to reduced salinity caused by freshwater run-off, rather than to surface warming. Breakdown of stratification was associated with strong winds. Hence the explanation of the pattern of primary production in time and space shown in Fig. 4.17 is that the blooms normally began in Faxafloi, a bay on the southwest corner of Iceland, which receives surface run-off and is sheltered from winds on three sides. Blooms then began close to shore along the south coast, where stratification was facilitated by freshwater run-off, but it was delayed somewhat by wind mixing. Blooms began last in the open ocean, where there was negligible influence of freshwater run-off, and stratification depended on surface warming. The interaction of many freshwater plumes and the Coriolis force results in a clockwise current around the whole of Iceland, characterized by phytoplankton blooms that are earlier than in the open ocean. A similar phenomenon was documented for the Norwegian coast by Peinert (1986).

We now see that there are two mechanisms that lead to geographic migration of the spring bloom in temperate latitudes. The movement of the spring bloom from south to north in the northern hemisphere has been shown (Section 3.3.6) to be associated with surface warming as indicated by the outcrop of the 12 °C isotherm. It now appears that the presence of river and estuarine plumes in coastal waters leads to a migration of the spring bloom from the coast out to deeper water as the season progresses.

4.6.5 Effects of river and estuarine plumes on secondary production

Sutcliffe (1973) studied the St Lawrence River, for which excellent data on run-off were available over a long period. He showed that there was an excellent correlation between the discharge of the St Lawrence River in April and the landing of lobsters *Homarus americanus* in the Gulf of St Lawrence nine years later. Since lobsters take about nine years to grow to marketable size, he concluded that in a year of high river run-off there was good survival of lobster larvae, and that this probably was reflected in good catches of that year-class nine years later. From this relationship it was concluded that the upwelling of nutrients associated with entrainment in the estuarine plume is a major factor influencing biological production in any given year. The correlation held good for the following 15 years (Drinkwater 1987), probably one of the best correlations of its kind anywhere.

Run-off and entrainment may not be the only physical mechanism influencing lobster productivity. As we saw in Section 4.6.4, freshwater run-off can lead to earlier stratification of the water column and to greater resistance to vertical mixing. As a result, the surface layer is likely to become warmer in summer, which may easily affect the productivity of the plankton and the survival of lobster larvae. In the Gulf of St Lawrence it seems that entrainment may be the key factor influencing plankton productivity in one area, while stabilization of the water column is more important in another (Bugden *et al*. 1982, Sinclair *et al*. 1986).

In Iceland, there is also a commercial interest in the effect of freshwater run-off, because the main spawning grounds of the rich Icelandic fish stocks are off the south and southwest coasts, in those areas most affected by fresh water. The early stages of copepods are an important component of the diet of first feeding larvae of cod *Gadus morhua* and it has been found that the years in which zooplankton densities were highest were the years in which phytoplankton production started early under favorable conditions provided by freshwater-induced stratification (Thordardottir 1986).

We saw in Section 4.6.2 how primary production in the plume of the Fraser River is influenced by interactions of winds, river discharge, and tidal cycles. A plume front (see Section 6.6), containing an aggregation of zooplankton, forms along the line where the freshwater plume meets the waters of the Strait of Georgia. Copepods, amphipods, and euphausiids were significantly more abundant in the estuarine plume than in either the riverine plume or the surrounding waters of the Strait of Georgia (St John *et al*. 1992a). Herring and salmonids were more abundant in the freshwater and estuarine plumes than in the surrounding water. The highest catches of juvenile salmonids were found at the front between the estuarine plume and the waters of the Strait of Georgia. St John *et al*. (1992b) suggested that juvenile salmonids migrating out of the Fraser River congregate at the plume fronts to feed on the aggregations of zooplankton and young fish occurring there.

Years of lower-than-average river discharge in the Fraser River appear to be associated with above-average production of chinook salmon *Oncorhynchus*

tshawytscha, coho salmon *O. kisutch*, chum salmon *O. keta*, and Pacific herring *Clupea pallasii*; the converse is also true (Beamish *et al*. 1994). It is suggested that when discharge is low, the water column has less stability and is more readily mixed by strong winds, thereby enhancing upwelling of nutrients into surface waters.

Another interesting situation of commercial importance is the Zambezi River, which discharges into the waters of the east coast of Africa in the southern hemisphere and has an estuarine plume that turns northward along the coast. The region of this plume is marked by high concentrations of organic matter in the sediments and by very productive fisheries for the shrimp *Penaeus indicus*. Da Silva (1986) has demonstrated that there is a very high correlation between the catch rate for the shrimps (taken as an index of abundance) and the run-off of the Zambezi from August to March.

The study was further developed by Gammelsrod (1992), using a time series 1974–1988. He confirmed that catch rate was positively related to river run-off and found that it was also negatively related to effort. In fact, effort contributed more to the total interannual variation than run-off. During the years 1980–1988, when variations in effort were small, the correlation between biomass catch rate and river run-off was 0.983, confirming the importance of the run-off. The author tentatively suggested that the key process is the flooding of the tidal plains near the outlet of the Zambezi River with brackish water, which stimulates the recruitment process. A large river outflow leads to lower salinity and flooding of a larger area, both of which are favorable for recruitment.

In summary, three physical mechanisms are interacting to influence secondary production in estuaries and plumes. First, the presence of fresh water in an estuary or coastal area often leads to earlier stratification and, therefore, an earlier spring bloom of phytoplankton. This bloom can be beneficial to organisms feeding in the plankton at that time – for example, cod larvae off Iceland. Second, buoyancy-driven currents can cause upwelling and entrainment of nutrient-rich water, which further enhances primary and secondary production. Finally, strong winds deepen the mixed layer and bring up nutrients that stimulate plankton production. This mechanism is an important determinant of primary and secondary production during the period of summer stratification. If strong buoyancy is present in the mixed layer at that time, it can reduce the effect of wind-mixing. Freshwater run-off can enhance plankton production at one time of year and depress it at another time, or it can enhance production in one part of an estuary and depress it in another. The interactions are complex and the organisms often show matching adaptations. One thing is clear: freshwater run-off has a strong influence on estuarine production, and modification of the magnitude or pattern of run-off can have marked effects on biological production.

4.7 Effects of anthropogenic modifications to river run-off

The ecological effects of anthropogenic changes in freshwater outflow to coastal waters were reviewed by Drinkwater (1988). In many parts of the world major

rivers have been dammed to provide hydroelectric power generation. Since the economic ideal is to have a year-round constant supply of electricity, the tendency is to store water at times of high flow and release it during times of low flow. This pattern has the effect of modifying the seasonal pattern of river run-off to which the organisms have become adapted over long periods of time, often leading to major disruption of biological events in coastal waters. In warm, dry climates storage of water in reservoirs is associated with considerable loss by evaporation, so that the total annual run-off is considerably diminished. A number of case histories of modification by mankind are given below.

4.7.1 The seas of southeast Europe

The effect of water development projects on the biology of the Black, Azov, Caspian, and Aral Seas was reviewed by Rozengurt and Haydock (1991). A well-documented example is that of the Dniester and Dnieper Rivers discharging into the Black Sea (Tolmazin 1985). Major hydroelectric projects were begun in the 1950s and more or less completed by the early 1970s. Figure 4.18 shows the seasonal pattern of the run-off of the Dnieper before and after the construction of dams. The loss of a major spring peak, and its replacement by a series of much smaller peaks, is very evident. Accompanying this process was a major loss of water quality, since much of the water from the reservoirs was used in agriculture, in industry, and by municipalities, returning to the system loaded with various contaminants.

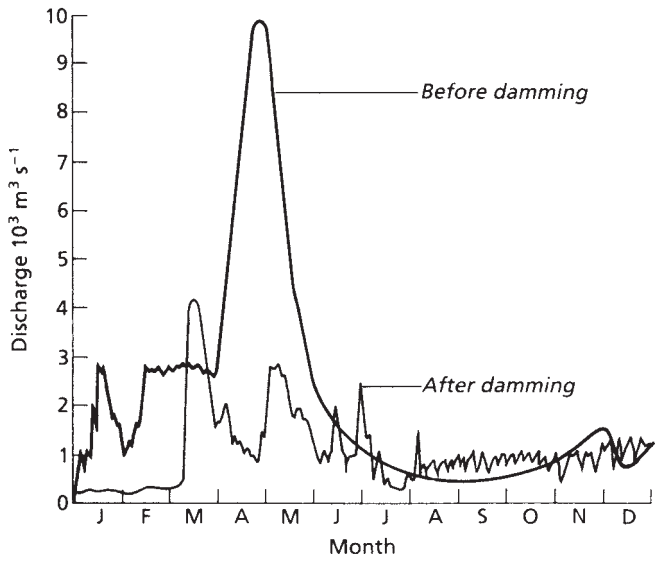

Fig. 4.18 Run-off of the Dnieper River before and after the construction of a series of hydroelectric dams. Note the major reduction in the spring peak of run-off. After Tolmazin (1985).

The lowering of the amplitude of the peak discharge of the Dnieper River resulted in the low-lying marshes in the Dnieper estuary not being covered during the period of peak fish migration. The average salinity in the Dnieper estuary increased, with an upstream extension of the near-bottom high-salinity layer. These environmental disruptions led to the disappearance of many species of zooplankton and fish from the estuary. Commercial landings of fish from the estuary decreased by a factor of five, and in the Dniester River they dropped to close to zero.

Nutrients from agricultural run-off and sewage led to greatly increased phytoplankton production both in the estuaries and in their plumes. The phytoplankton biomass was largely ungrazed and sank to the bottom. With the increased stratification caused by increased summer freshwater discharge, oxygen concentrations in the lower layers were reduced to zero and mass mortalities of invertebrates and fish resulted. Oxygen depletion had occurred near the estuarine plumes even before the construction of hydroelectric dams, but the anoxic events became more frequent and widespread, resulting in a sharp decrease in the catches of turbot *Scophthalmus maximus*, flounder *Platichthys flesus*, and various crabs.

A lesson to be learned from this case is that adverse biological effects are not necessarily caused by factors that decrease biological production. The total primary productivity in the estuaries and their plumes increased, but the changed distribution of salinity and oxygen killed the invertebrates and fish that had adapted over long periods to the more natural conditions. The primary production was consumed mainly by bacteria, and the commercial fish landings were severely reduced.

Economic losses in the Black–Azov Sea basins amounted to an estimated $0.8 billion per annum in fin-fisheries, $1.5 billion in mollusks, and $1.5 billion in seaweed harvests (Rozengurt and Haydock 1991). Similar losses have been incurred in the Caspian Sea basin, and the Aral Sea system is now a total disaster as a result of diversion of the inflowing waters to irrigation schemes. The Aral Sea's level has dropped 17 m, and the volume of water by 75%. The commercial catch of fish fell from 48,000 tons in 1957 to zero. By the year 2000, 42,000 km^2 of the original seabed had been exposed. Summer temperatures are higher and evaporation has caused salinity to rise to about 31 parts per thousand. Once-flourishing fishing villages are now far from the water's edge and have been abandoned. The diversity of mammals and birds in the area has been approximately halved. For an update on the state of the Aral Sea area, see enrin.grida.no/aral/aralsea/english/arsea/arsea.htm.

4.7.2 San Francisco Bay

Another example quoted by Rozengurt *et al*. (1985) and Drinkwater and Frank (1994) is the extensive modification of the Sacramento–San Joaquin river system, which flows into northern San Francisco Bay. The unmodified discharge of these rivers was about 34 km^3 per year. Of this amount, about 40% is now removed for

local consumption, and 24% diverted to central and southern California, leaving only 36% entering the estuary (Nichols *et al*. 1986). Correlated with these changes has been a marked reduction in primary production in northern San Francisco Bay, which is accentuated during summers of abnormally low flow. Two mechanisms for this drop in production have been suggested. Cloern *et al*. (1983) pointed out that stratified and partially mixed estuaries normally have a zone of high turbidity around the region of maximum penetration of the deep saline water. They suggested that reduced freshwater flow allowed the zone of high turbidity to penetrate further upstream than before so that primary production was reduced on account of lower light penetration. Nichols (1985) pointed out that during years of particularly low freshwater flow benthic filter-feeding animals associated with the more saline water penetrated further upstream into the estuary (without increasing their total biomass or productivity) and may have reduced the phytoplankton biomass by their grazing. Whatever the mechanism, reduced river flow into northern San Francisco Bay is correlated with reduced primary production, which is, in turn, correlated with reduced total secondary production.

The adult population of striped bass *Roccus saxatilis* has decreased by 75% since the mid-1960s and the chinook salmon population by 70% between the early 1950s and 1985 (Stevens *et al*. 1985, Kjelson *et al*. 1982). In the summer of 1977, when freshwater run-off was exceptionally low, the phytoplankton biomass dropped to 20% of normal levels, zooplankton and shrimp abundance decreased, and the striped bass population declined severely. The possible mechanisms involved include: (i) a decline in primary production as a direct result of reduced entrainment by the freshwater plume; (ii) degradation of fish spawning areas caused by the upstream migration of the turbidity maximum; and (iii) accumulation of higher concentrations of pollutants, resulting from reduced dilution by the freshwater run-off. The correlation of reduced run-off with reduced fish production is confirmed by examination of the historical records, which show, for the years before diversion (1915–1944), a strong correlation between mean annual run-off and commercial catches of salmon, striped bass, and shad *Alosa sapidissima*. Rozengurt *et al*. (1985) suggested that to ensure successful commercial landings of salmon, striped bass, and shad, the run-off should be restored to about twice the 1985 levels.

Since 1985 a great deal of attention has been paid to problems of contaminants in San Francisco Bay. According to Kimmerer (2002) several flow-based management actions were also put in place in the mid-1990s, but their effectiveness has not yet been evaluated.

4.7.3 Nile River

The High Aswan Dam in Egypt was fully operational by 1965. Before this, the Nile River discharged about 40 $km^3\ y^{-1}$ into the Mediterranean Sea, with the peak flow in September–October. By 1968, the river discharge had dropped to 10% of the previous value, with 50% of the flow occurring in January and February. This decrease led to increased salinity in the coastal region, a deeper mixed layer, and

a sharp decrease in both suspended sediments and nutrients. Before these changes, the river plume had been characterized by strong blooms of diatoms and copepods, and an extensive fishery had operated based on the sardines *Sardina pilchardus sardina* that migrated into the area to exploit the plankton. In addition, a strong shrimp fishery was based on stocks that were adapted to the pattern of river run-off.

After the dam was closed, the catch of sardines declined by 90% and the catch of shrimp declined by 75%. The stocks remained low for about 15 years. Starting in 1983, the fishery began a dramatic recovery, and the catches of finfish in the late 1990s were more than double the levels seen just prior to the dam closure (Fig. 4.19). Nixon (2003) has argued that nutrients derived from sewage and agricultural run-off are replacing the nutrients once provided naturally from the river

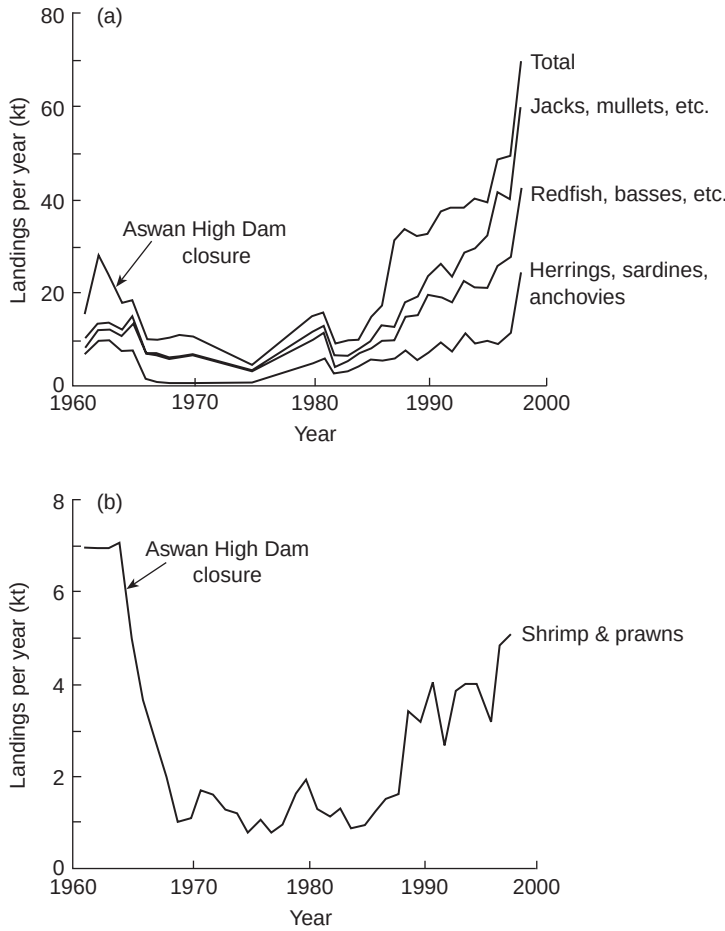

Fig. 4.19 Landings of finfish, shrimp, and prawns from the Egyptian Mediterranean coastal waters, 1960–1999: (a) finfish; (b) shrimp and prawns. From Nixon (2003), based on FAO online fisheries statistics.

basin. Chemical analyses show that while the concentrations of nitrogen and phosphorus have increased dramatically, the concentration of silicon has not. The waters off the delta are now relatively clear and the primary production is mainly by phytoplankton other than diatoms. So the food web supporting the fishery must now be very different from that which existed prior to the dam closure.

A different point of view has been expressed by Halim *et al*. (1995), who sought to explain the fluctuations in landing by the changes in fishing effort over the years. Nixon (2003) admits that these changes in effort undoubtedly influence the total landings, but argues that landings that are at more than twice the level of the pre-dam years must reflect a change in biological productivity supported by nutrients from anthropogenic sources.

4.7.4 James Bay

James Bay is in northern Quebec, Canada, and opens into the much larger Hudson Bay. As part of the first phase of a major hydroelectric development, the Eastmain River was diverted northward into the La Grande River system, causing the lower section of the Eastmain to become a salt-wedge estuary (Lepage and Ingram 1986). The biota of the affected section changed from predominantly freshwater species to mainly estuarine species.

In the La Grande River, which received the diverted Eastmain River, the mean flow increased 50–100% over pre-impoundment levels, with up to a 700% increase in flow during winter. The natural spring peak in run-off was eliminated, and summer flow became about the same as before dam construction. The flooding of forestland behind the dam caused a release of mercury compounds, so that fish became loaded with mercury to several times the pre-dam levels. Routine fish consumption by native peoples has resulted in excessive body loading of mercury. This result of flooding the land behind a dam is by no means unique to this dam, but is particularly critical in an area where the native peoples rely on fishing for their daily food intake.

As these examples show, the physical regime around the mouth of a river has a profound effect on the biology of the organisms, and often on the productivity of populations in the coastal waters. While damming rivers may seem like an attractive, relatively clean option for the generation of electricity, in that it does not involve the burning of fossil fuel or the production of toxic wastes, it is clear that other environmental consequences must be taken into account. Power dams are obstacles to the migrations of fish, water stored in artificial reservoirs or used in irrigation may be lost to the atmosphere if the climate is arid, and land inundated behind dams may release toxic substances into the water.

On the positive side, these experiments have revealed much about the connection between freshwater run-off and the productivity of estuaries and coastal waters. This information may be useful in making predictions about the fluctuations of fish and shellfish stocks resulting from natural variation in run-off. The work on fluctuations in lobster stocks discussed in Section 4.6.5, and on changes in cod

stocks to be dealt with in Chapter 9, are examples of how this information may be put to use.

4.7.5 Experimental approaches

There are at least two cases of an attempt to demonstrate the effect of a dam by opening the dam and releasing most of the contents of the reservoir, thus creating pre-dam conditions in the estuary below. The experiments were of short duration relative to the length of life of major components of the fauna, and it is perhaps not surprising that changes to the fauna were not pronounced.

In a branch of Sandsfjorden, Norway, the reservoir above a hydroelectric power plant was nearly emptied, at a rate of 230 $m^3 s^{-1}$, over a period of 51 hours (Kaartvedt and Svendsen 1990). Hydrographic and biological measurements were made prior to, during, and after the discharge. The freshwater run-off generated a two-layered estuarine circulation, which was most prominent along the mid-axis of the fjord. Ten kilometers downstream of the reservoir the surface current reached a velocity of 1 m s^{-1} and there was a compensatory current at 10 m depth, which reached a velocity of 0.6 m s^{-1}. Phytoplankton was partly flushed out of the upper layers, but abundance increased at depth in the outer fjord. There was a net import of zooplankton at the mouth of the fjord, but this could not be detected as a significant increase in biomass in the fjord as a whole.

Upstream of the Kromme Estuary, South Africa, is a large reservoir, which diverts 98% of the freshwater input (Wooldridge and Callahan 2000). As a consequence, the estuary is little more than an arm of the sea, lacking the diversity of habitat and biota originally present. An experimental release of the full reservoir of fresh water was predicted to create freshwater conditions throughout the upper half of the estuary, but the investigators must have underestimated the buoyancy of the fresh water relative to the mixing effect of the sudden discharge from the reservoir. The fresh water ran in a distinct low-salinity layer over the salt water for about two weeks, after which things returned to pre-release conditions. The investigators could find no significant changes in the zooplankton community either during or after the release. They concluded that nothing short of an increased continuous flow of fresh water would restore the earlier habitat and species diversity of the estuary.

4.8 Summary: river runoff and tidal mixing in coastal waters

There are many types of estuaries, but the feature they have in common is that they all have an input of fresh water. In low-energy conditions the fresh water forms a distinct layer on top of the salt water. This stratification is often broken down by internal waves at the interface between the two layers, or by the turbulence generated by the passage of tidal currents over a rough bottom. The strength of this turbulence depends on the tidal range and the depth of the estuary. Hence

the amount of freshwater run-off, the rise and fall of the tides, and the average depth of water in the basin determine the main features of each estuary. In a typical stratified estuary, the buoyancy-driven flow of fresh water towards the sea entrains salt water and carries it seawards near the surface. To compensate for this, there is a landward flow of salt water near the bottom and a mixing upwards near the head of the estuary.

In temperate latitudes there is typically a high volume of freshwater run-off in spring time, as winter snows melt. The strong freshwater run-off stimulates upwelling of nutrient-rich water in estuaries, leading to phytoplankton blooms. Many organisms have adapted their life histories to this seasonal rhythm. Construction of major dams for hydroelectric generation or irrigation often has the effect of damping out the spring peak in run-off, and disrupts the production processes supporting fish stocks. In subtropical and tropical climates it is common to find that there are distinct wet seasons and dry seasons, with corresponding changes in river and estuarine discharges.

Out on the continental shelves in temperate climates there are areas where solar heating causes temperature stratification in summer. In other areas the turbulent mixing caused by tidal currents can prevent stratification. It is possible to predict the positions of these mixed areas from the depth of the water and the strength of the tidal currents. The fronts at the boundaries of stratified and mixed areas are regions of particularly high biological productivity.

The physical diversity of continental shelves is further increased by the presence of plumes of low-salinity water which are formed by the discharge of rivers or estuaries onto the shelves. The position of a plume varies with the direction of the wind, but on average it is directed to the right (northern hemisphere) or left (southern hemisphere) by the Coriolis force. The interfaces between the plumes and the adjoining shelf water constitute fronts at which there is often accumulation of plankton and aggregations of fish. In the North Atlantic basin the cumulative effects of all the river and estuarine discharges is to create a flow of low-salinity water lying close to the coast and moving round the basin in a counter-clockwise direction.

In temperate zones the presence of low-salinity water in an area of the shelf tends to enhance stability of the water column, so that spring blooms occur earlier, but the ability of strong winds to break down summer stratification and bring up nutrients is decreased Hence there are both positive and negative effects on biological production.

Part B

Processes on a scale of 1–1000 kilometers

5

Vertical structure in coastal waters: coastal upwelling regions

5.1 Introduction

A theme running through the two preceding chapters on vertical structure is that the key to high biological productivity is the upwelling of "new" nutrients from deep waters into the euphotic zone and the retention of phytoplankton in well-lighted waters by stratification of the water column. We have seen that optimum conditions for phytoplankton production can be produced by patterns of alternating convective mixing and thermal stratification, by periods of strong tidal mixing alternating with stratification caused by freshwater run-off, or by some combination of these factors. Wind-induced mixing modifies these patterns by breaking down the stratification, but commonly the stratification is reestablished soon after the wind abates.

In this chapter we consider the special places where wind-induced upwelling is the dominant mechanism for bringing new nutrients to the surface. These upwelling areas have been well studied, partly because they are associated with economically important fish stocks. Cushing (1971), in a review entitled "Upwelling and the production of fish," estimated the total production of fish and squid in upwelling areas in the late 1960s. He calculated that over 26 million tons, mainly sardines *Sardinops* and *Sardina*, were produced in the Benguela Current system off the southwest coast of Africa and the Canary Current system off northwest Africa, over 12 million tons in the Peruvian anchoveta *Engraulis ringens* fishery, over 5 million tons of anchovy *Engraulis mordax* and hake *Merluccius productus* in the California Current system, and so on. It is impossible that all of this production could be harvested, but for comparison we may note that this weight of fish is equivalent to more than half of the world's annual commercial fish landings. If reckoned in monetary value, the percentage would be much lower because these species have traditionally been used primarily for the production of fishmeal. What is the explanation of this enormous biological production? The subject was extensively reviewed by Boje and Tomczak (1978), Richards (1981), and Barber and Smith (1981).

Wind blowing across the surface of the sea causes water to begin to move in the same direction. The Coriolis force, resulting from the earth's motion, causes the current to deviate to the right in the northern hemisphere, and to the left in the southern hemisphere. After some time, the net movement of surface water is at right angles to the direction of the wind, a condition known as Ekman transport. When Ekman transport is away from the coast, surface waters moving away from the shore are replaced by deeper water that upwells close to shore. This water is normally nutrient-rich and primary production is stimulated.

As we shall discuss in more detail in Chapter 8, the major ocean basins each have a western boundary current that tends to be fast and deep, and an eastern boundary current that is broad, shallow, and less well defined. Winds of the appropriate strength and direction to cause upwelling are more prevalent on the eastern sides of ocean basins. Nutrient-rich water below the pycnocline is closer to the surface in these areas, and is therefore more readily upwelled, giving a boost to phytoplankton production. Wind-driven upwelling does occur on the western sides of ocean basins, but tends to be of short duration and, because the pycnocline

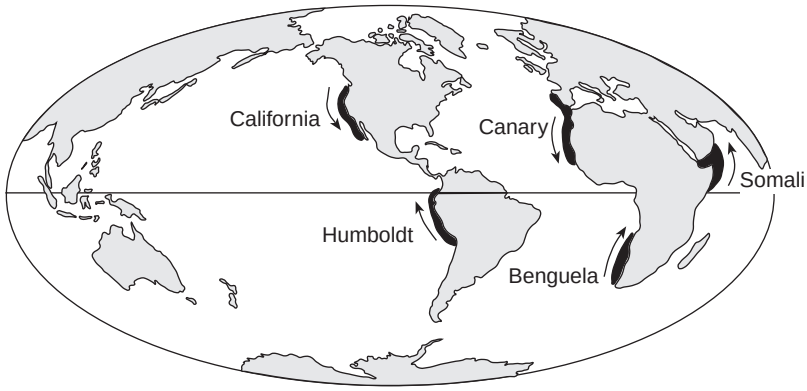

Fig. 5.01 Boundary currents associated with coastal upwelling. Arrows indicate prevailing winds.

tends to be deeper, often brings up water from above the pycnocline that is not nutrient-rich. Such upwelling is biologically less important.

Worldwide, there are five major coastal currents associated with upwelling areas (Fig. 5.01): the California Current (off Oregon and California), the Humboldt Current (off Chile and Peru), the Canary Current (off northwest Africa), the Benguela Current (off southern Africa), and finally a rather anomalous example, the Somali Current in the western Indian Ocean. Here the southwest monsoon sets up Ekman transport away from the coast of Somalia and the Arab states: this is the only major upwelling area occurring on the western side of an ocean basin. The first four of these upwelling areas are plainly visible on our satellite image (see Plate 1).

As we explore the processes occurring in these upwelling areas we shall find that there is great variability. For example, off Peru the upwelling continues more or less year-round but there are years when biological production almost ceases. Off Oregon and Portugal there are large seasonal changes in the strength of upwelling, clearly related to seasonal differences in wind strength and direction. Even within the six-month season of upwelling off Oregon, there are four or five periods of strong upwelling separated by periods of little or no upwelling. Each of these events gives rise to a burst of productivity equivalent to a spring bloom (Barber and Smith 1981). On still shorter time scales, the diurnal build-up of an onshore sea breeze and the semi-diurnal patterns of tidal current give rise to corresponding fluctuations in biological productivity.

5.2 The physics of coastal upwelling

5.2.1 The Ekman spiral

When the wind blows over the surface of the water it clearly generates waves, but it also drags the water along. This is how wind-driven currents begin. But

because the transfer of momentum from the air to the water occurs under the influence of the Coriolis force, the direction of the water movement is not the same as that of the wind. This difference was first pointed out in a theoretical analysis by V. W. Ekman in 1905 and now most phenomena connected with the process have his name attached – such as Ekman spiral, Ekman layer, Ekman drift, and Ekman pumping. Our main concern in this chapter is with the Ekman drift, which creates the coastal upwelling zones. We start with the Ekman spiral, which is the name given to the arrangement of the currents generated in the upper layer of the ocean by the wind.

We begin with an elementary physical explanation based on the simple situation outlined in Fig. 5.02. This figure shows the adjustment of the water at the surface to the drag of the wind. Each stage of the adjustment is illustrated on the left with a diagram of the horizontal forces on the water. A separate diagram of the resulting current is on the right. In stage I the wind is blowing parallel to the positive x axis and begins to drag the water along in the direction of the positive x axis with speed V. (Note that the force and velocity scales are not the same.) The friction in the water creates another force, the water drag, opposing this current, and the rotation of the earth generates the Coriolis force directed 90° to the right (left) of the current in the northern (southern) hemisphere. These three forces are clearly not balanced, in stage I, as there is no force opposing the Coriolis force and the drag of the wind along the positive x axis is greater than the drag of the water along the negative x axis.

In the second step the wind and its drag remain in the same direction along the positive x axis but the Coriolis force begins to cause the direction of the surface current to rotate around to the right (left) of the wind. The Coriolis force, always perpendicular to the current, also rotates with the current as does the water drag, which is always directly opposed to the current.

In stage III the forces have come into equilibrium. The component of the Coriolis force along the negative y axis is balanced by the component of the water drag along the positive y axis. The drag of the wind along the positive x axis is balanced by the sum of the components of the Coriolis force and the water drag along the negative x axis. The balance is attained when the surface water is moving at 45° to the right (left) of the wind. This angle is a consequence of assuming that the Coriolis and the drag forces are the only forces acting on the water and that they are equal in magnitude.

The water just beneath the surface is not dragged directly by the wind but by the surface water, which lies directly above and which is moving at 45° to the right (left) of the wind. An adjustment of the forces in this second layer, like the adjustment in the top layer, causes the flow to be slightly to the right (left) of the surface water – that is, at an angle greater than 45° to the right (left) of the wind. This process continues down through the water column until all the momentum that is transferred from the wind to the water is converted to motion in the water. The speed of the water in each layer gets progressively less with depth and turns more to the right (left) in the form of a spiral – the Ekman spiral. A horizontal projection of the currents at 11 equally

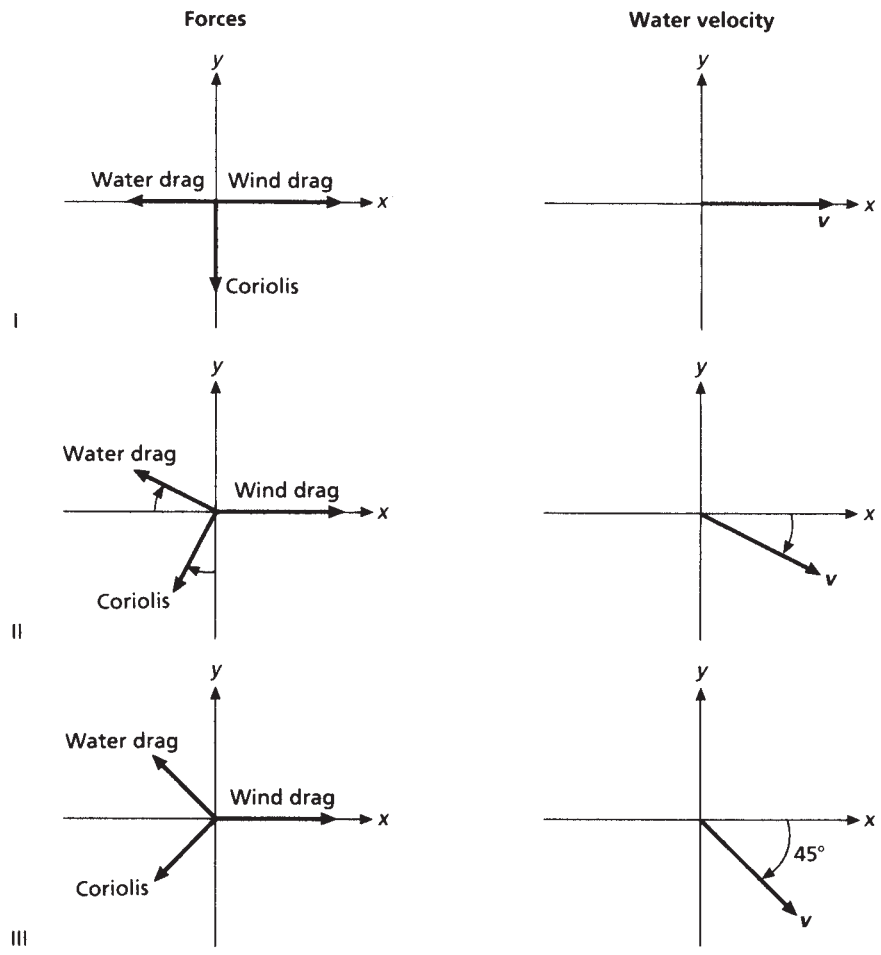

Fig. 5.02 The beginning of a wind-driven surface current in three stages showing the forces on the left and the water velocity on the right. In stage I the wind drag creates a flow of water that gives rise to the water drag and the Coriolis force. In stage II the Coriolis force causes the current in the water to rotate around to the right in the northern hemisphere. The force due to the water drag and the Coriolis force rotate with the current in the water. In the final stage the current has rotated the amount required to have the force due to the wind drag balanced by the combined effects of the Coriolis force and the drag of the water.

spaced levels between the surface and the bottom of the Ekman layer is shown in Fig. 5.03.

The form of the velocity spiral requires that the friction in the water, K_v, be constant throughout the depth of the Ekman layer. This requirement is a poor assumption in most regions of the upper ocean because of the vertical stratification that strongly affects K_v. It is also difficult to extract from velocity

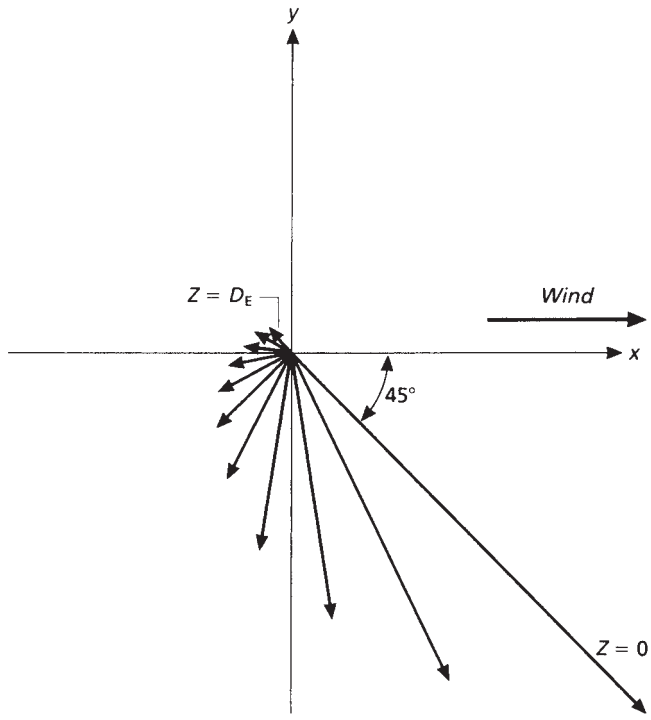

Fig. 5.03 A horizontal projection of the currents at 11 equally spaced levels from the surface to the bottom of the Ekman layer (D_E). The currents are generated by a wind blowing parallel to the positive x axis. For explanation, see text.

observations the part that is due only to the wind. For these reasons the spiral is a difficult phenomenon to observe in the ocean. However, Stacey *et al*. (1986), Richman *et al*. (1987), and Price *et al*. (1987) have been able, through the analyses of long current meter records obtained in the upper layer of the ocean, to demonstrate a spiraling of the flow with increasing depth which is in close agreement with the theory. In an analysis of drogued drifter tracks, Krauss (1993) found that K_v increases through the upper 25 m of the water column, which leads to an Ekman spiral with a deflection less than the original theory.

According to Pond and Pickard (1983) the depth of the Ekman layer is related to the speed of the wind and the latitude by the equation

$$D_E \approx 4.3\ W/(\sin \varphi)^{1/2} \tag{5.01}$$

where W is the wind speed in m s^{-1} and φ is the latitude. Thus for a given wind speed the depth of the Ekman layer increases from the pole to the equator where it is infinitely deep. One example in Pond and Pickard (1983) gives an Ekman depth of 100 m at 10° latitude for a 10 m s^{-1} wind. The same wind conditions give a depth of 50 m at 45° latitude.

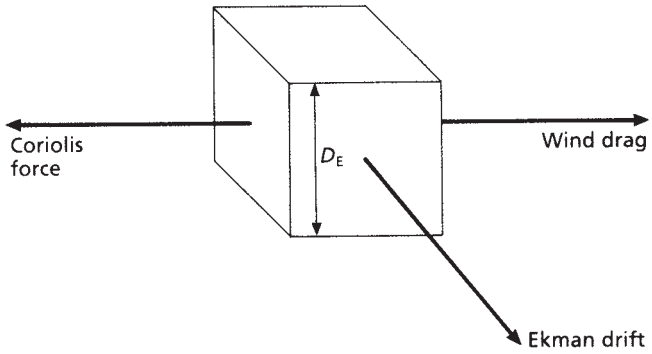

Fig. 5.04 A cube of water in the Ekman layer treated as a layer without frictional coupling to the remainder of the ocean lying below. The force due to the wind drag is assumed to act on the whole cube rather than just at the surface and is balanced by the Coriolis force that is generated by the Ekman drift moving perpendicular to both forces.

5.2.2 Ekman drift and coastal upwelling

One important consequence of the velocity spiral is that the net movement of the wind-driven flow, after averaging over the Ekman layer, is 90° to the right (left) of the wind. This result, which is one of the foundations of the wind-driven circulation in the oceans and of coastal upwelling, is derived mathematically by Pond and Pickard (1983). The result may also be derived, in a less rigorous manner, from the simple schematic diagram given in Fig. 5.04.

Here we assume that at the bottom of the Ekman layer the frictional forces that transfer the momentum of the wind down into the water become very small. This condition follows because the change in the velocity gradient becomes vanishingly small at this depth. All the wind energy transferred to the water is confined to the Ekman layer. Consequently the whole layer can be treated as a slab that absorbs all the momentum transferred from the wind and that moves without friction over the ocean. This simplification of averaging over the layer of frictional influence (the Ekman layer) allows us to ignore the details of the velocity distribution. We need only consider the force due to the drag of the wind and the Coriolis force, as illustrated in Fig. 5.04.

The wind drag shown in the figure as acting on the whole of the Ekman layer tries to pull the water in the direction of the wind. The Coriolis force, which is the only other force involved, must balance the wind drag and therefore must be equal in magnitude to the wind drag and in the direction opposite to the wind. The flow of water that gives rise to the Coriolis force must be 90° to the right (left) of both the Coriolis force and the wind. This flow is the Ekman drift. The reduction of the Ekman spiral to its net effect of a current perpendicular to the wind allows us to easily calculate the transport of water due to the wind.

The Ekman transport, commonly labeled M_E, is derived by Pond and Pickard (1983) and given by

$$M_E = -\tau/f \tag{5.02}$$

where τ is the wind stress at the surface of the water and f is the Coriolis parameter. A typical wind stress of 0.1 N m^{-2} and Coriolis parameter at a latitude of 45° of ~10^{-4} s^{-1} gives an M_E of 1000 kg m^{-1} s^{-1} – that is, one metric ton of water per second flowing, in the Ekman layer, at 90° to the right (left) of the wind for every meter along a line parallel to the wind.

The relationships between the wind, Ekman drift, and coastal upwelling are illustrated in the perspective drawing in Fig. 5.05, which suggests waters off California with an equatorward wind parallel to the coast. The Ekman drift, to the right (left) of the wind, is directed offshore and decreases to zero at the coast. The water that replaces the offshore drift cannot be supplied by horizontal flow because of the coastal boundary. Instead it is upwelled from the deeper layers. The illustration also indicates the commonly observed front in the near surface layers that separates the cooler upwelled water next to the coast from the warmer offshore water.

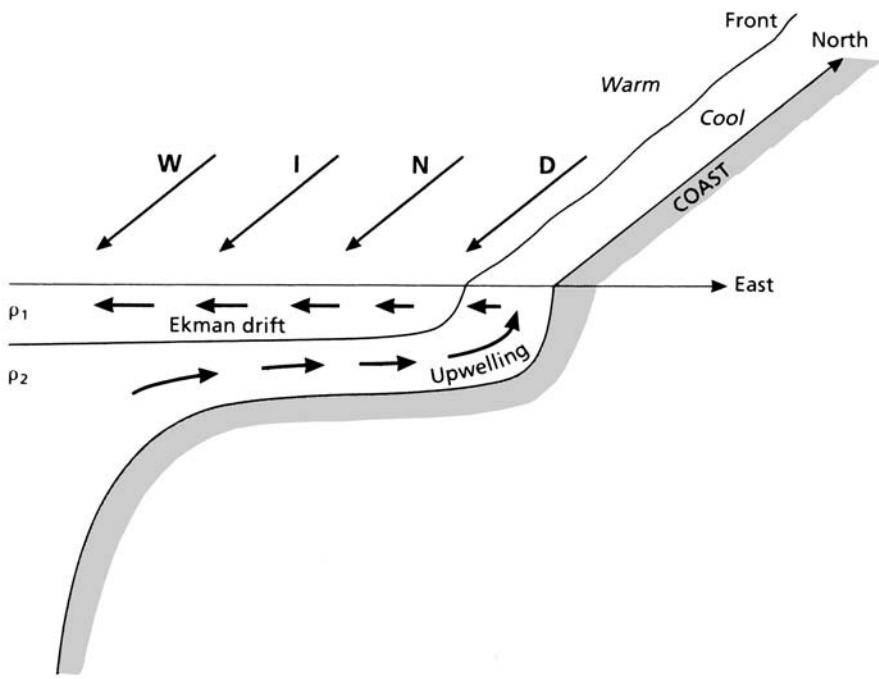

Fig. 5.05 A perspective drawing through an upwelling region illustrating the offshore Ekman drift in the upper layer being replaced near the coast by upward-moving water from the lower layer. The upwelling water, usually cool, is separated from the offshore warm water by a surface front parallel to the coast. The wind blows from north to south.

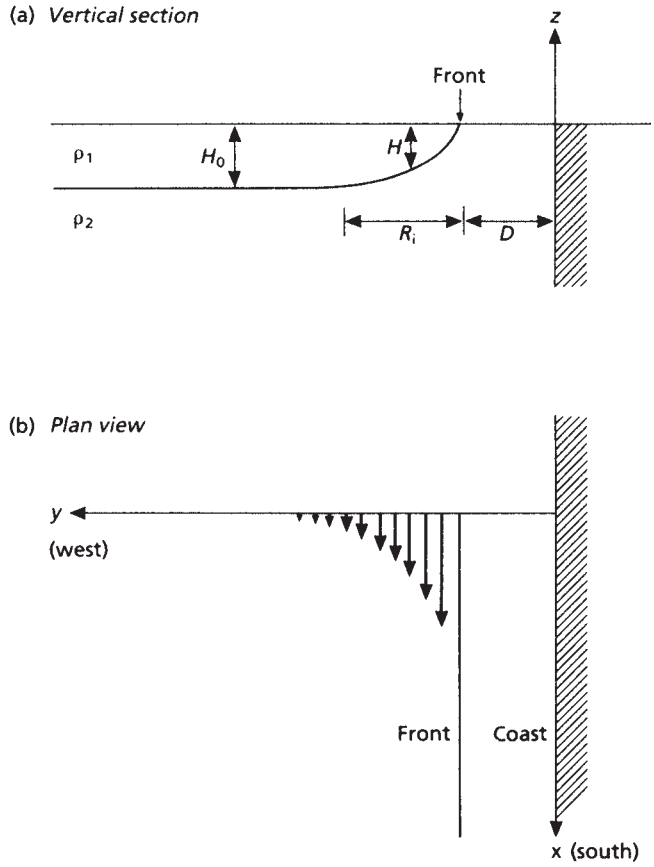

Fig. 5.06 (a) A section across an upwelling region in which the upper layer of density ρ_1 and depth H overlies a deep layer of density ρ_2. The interface between the layers rises from the undisturbed depth H_0 to the sea surface in the distance R_i. At the sea surface the interface lies a distance D from the shore. (b) A plan view of the currents parallel to the coast that are generated by the distribution of density in (a).

The upwelling creates a current parallel to the coast in the same direction as the wind. It is generated by the horizontal density gradient that arises because the upwelling water close to shore is denser than the water offshore. This gradient, shown in Fig. 5.06(a) by the rising interface between the two layers of different density, results in a horizontal pressure gradient directed toward the land, which in turn creates a geostrophic current parallel to the shore shown in Fig. 5.06(b). The horizontal pressure tries to push the water back to the shore but the Coriolis force turns the flow into a current parallel to the coast and toward the equator.

In the deeper levels the pressure gradient developed by the upwelling tends to be toward the offshore direction rather than toward the shore, and a poleward current develops. Such equatorward and poleward density-driven flows are

predicted by mathematical models (Gill 1982) and are commonly observed in the upwelling areas of the world, as will be illustrated in later sections. The widths of the upwelling zones and the associated poleward and equatorward currents are related to a natural horizontal length scale of the stratified ocean. This Rossby deformation scale is so important in oceanography that we make a slight detour to examine it in detail.

5.2.3 The width of coastal upwelling and the Rossby deformation scale

The vertical section through a coastal upwelling area in Fig. 5.06(a) indicates two horizontal lengths of interest. The first is D, the distance of the front from shore, while R_i is the width of the region where the interface between the upper and lower layer rises up to the sea surface. The distance D is discussed by Csanady (1981), who demonstrates mathematically that after the interface reaches the sea surface the front starts to move offshore. In his example of an upper layer 20 m thick, the interface reaches the sea surface with a 7 ms^{-1} wind blowing parallel to the coast for ~28 hours. If the wind is greater than 7 ms^{-1} over the 28 hours, the interface first moves to the surface, then moves offshore in proportion to the increase above 7 ms^{-1}.

The width of the region where the interface rises to the sea surface, shown as the length R_i in Fig. 5.06(a), is approximately equal to

$$(g'H)^{1/2}/f \tag{5.03}$$

where g' is the reduced gravity (see Box 5.01) and H is the depth of the upper layer. R_i is called the Rossby internal deformation scale after C. G. Rossby, who first discussed it. Because it is one of the fundamental length scales in oceanography we demonstrate mathematically how it arises in Box 5.01.

Box 5.01 Derivation of the internal Rossby deformation scale

In Eqn. 5.03 f is the Coriolis parameter, H is the depth of the upper layer, and g' is called the reduced gravity and is equal to the gravitational acceleration (g) times the fractional increase in density between the layers. Thus,

$$g' = \frac{\Delta\rho}{\rho} g \tag{5.04}$$

The reduced gravity is, therefore, the gravitational acceleration acting on a parcel of water that has been displaced vertically from its equilibrium position. If no vertical

change occurs in density there is no buoyancy force as given by Eqn. 3.03 and particles in the water "feel" no gravitational restoring force when they are moved vertically.

The pressure gradient that drives the current in Fig. 5.06(b) is derived from the horizontal gradient in density where the upper layer rises up to the surface. The shape of the interface between the layers is set by the internal adjustment of the layers and depends on two laws. The first is expressed by the balance of forces in the geostrophic balance. The second is the conservation of angular momentum, which says that if a fat object that is rotating becomes thinner (without losing mass) it will rotate faster. Everyday examples of this rule can be found in the twirling skater who changes her rate of spin by moving legs and arms closer and further away from the center of mass. The water draining in a sink speeding up as it approaches the central drain is another example of this conservation rule.

In oceanography conservation of angular momentum is discussed in terms of vorticity, which is a mathematically convenient term equal to twice the rate of rotation. Physically the two are identical except for the factor 2. In relation to the situation shown in Figs. 5.06(a) and (b) the conservation of vorticity is given roughly by

$$\frac{f+\zeta}{H} = \frac{f}{H_0} = 0 \tag{5.05}$$

Here again f is the Coriolis parameter representing the vorticity ($2 \times$ rotation) of the earth at the latitude φ, which is constant for this discussion. H is the depth of the upper layer with H_0 representing the thickness of the upper layer in the region where there is no current and ζ is the vorticity of the water relative to the earth:

$$\zeta = \frac{\mathrm{d}v}{\mathrm{d}x} - \frac{\mathrm{d}u}{\mathrm{d}y} \tag{5.06}$$

Since the v component of velocity is zero in Fig. 5.06(b), we can replace ζ by $-\mathrm{d}u/\mathrm{d}y$, in Eqn. 5.05, and the conservation of vorticity is now expressed by

$$f - \frac{\mathrm{d}u}{\mathrm{d}y} = \frac{H}{H_0} f \tag{5.07}$$

which states that the thickness of the upper layer (H) gets thinner as the horizontal velocity gradient ($\mathrm{d}u/\mathrm{d}y$) increases. If there is no horizontal velocity gradient, the depth of the upper layer is always equal to H_0.

The equation (Eqn. 4.12) for the other law, the geostrophic balance, is

$$fu = -g' \frac{\mathrm{d}H}{\mathrm{d}y} \tag{5.08}$$

where g' is the reduced gravity. Now we assume that the thickness of the upper layer decreases exponentially across the current – that is, let

$$H = H_0(1 - e^{-y/L}) \tag{5.09}$$

and we wish to determine L, the horizontal scale of the deformation of the upper layer, in terms of the other variables. This is easily done by substituting the value for H given in Eqn. 5.09 into Eqn. 5.08, which gives

$$fu = \frac{g'H_0}{L} e^{-y/L} \tag{5.10}$$

From this an expression for du/dy may be derived, which when equated to the value for du/dy derived from Eqn. 5.07, leads to the value of

$$L = \frac{(g'H_0)^{1/2}}{f} \tag{5.11}$$

L is then the natural horizontal scale of currents in the ocean and coastal upwelling regions when a geostrophic balance and the conservation of vorticity are the dominant physical laws. The scale is usually represented by the symbol R_i and called the Rossby internal deformation scale. Toward the equator as f goes to zero the Rossby deformation scale becomes very large, which as we shall see in Chapter 9 is an important feature of equatorial dynamics and El Niño. At the mid-latitudes $f \approx 10^{-4}$. If $g' \approx 0.02$ a 100 m upper layer will be deformed over ~20 km. In other words, the current will be about 20 km wide. The length L is also often called the internal Rossby radius. In this context it refers more to the natural horizontal scale of baroclinic eddies – i.e., those eddies with a vertical velocity gradient.

5.2.4 Variations in upwelling

The coastal upwelling described so far is a process that is assumed to be constant along a straight coast on the western side of a continent under the influence of a constant equatorward wind parallel to the shore. There are, however, many factors that can produce variations in this picture. Changes in the strength of the wind component parallel to the shore, the vertical structure of the water, variations in the bottom bathymetry, and instabilities in the currents can all create variations in the upwelling process.

When upwelling is present variations in the position of the upwelling front are easily observed in infrared images such as the one shown in Plate 3. Here the cool upwelled water is seen near the coast while the warmer lies offshore and the region between is dominated by eddies and plumes which mix the two. Narimousa and Maxworthy (1985, 1987) studied upwelling in a rotating tank in the laboratory and observed similar irregularities. The authors believed the eddies were created by waves that became unstable through complex interactions

in the flow. Petrie *et al*. (1987) attributed plumes moving offshore of an upwelling band next to Nova Scotia to baroclinic instability, which is a common instability of vertically sheared flows in stratified fluids.

Changes in the bathymetry can change the strength of the upwelling. A submarine ridge extending out from the coast, for example, produces conditions more favorable to upwelling than exist in the neighboring regions. Upwelling usually begins first at such ridges and remains stronger at the ridge even when it has developed in the other locations. Numerical models by Peffley and O'Brien (1976) and rotating tank models by Narimousa and Maxworthy (1985, 1987) show that a rise in the bottom is effective in creating preferred conditions for upwelling. Separation of the upwelling front to create an offshore plume is a possibility considered by Barth *et al*. (2000), who studied the flow of the upwelling jet downstream of a rise in the bottom at Cape Blanco, Oregon. The upwelling jet turned offshore south of the bathymetric rise then turned back shoreward when it encountered deeper water. On its return shoreward it encountered the top of the northward-flowing counter-current. An upper portion of the counter-current joined the jet and turned it offshore again. The jet was now strengthened but separated from the shelf as a "free unstable jet". Such a process may explain many of the long plumes of cool, high-chlorophyll water visible in many of the images of upwelling regions.

The wind that drives the upwelling is generated by the temperature difference between the warmer lighter air over the land and the cooler denser air over the sea. The wind results from the shoreward pressure gradient arising from this change in air density. In temperate latitudes the temperature contrast varies greatly with the seasons and the upwelling varies from being strong in the spring and summer to weak or nonexistent in the winter. In more tropical latitudes the temperature contrast and the upwelling tend to be constant throughout the year.

Global warming may also be affecting the rate of upwelling. This was first suggested by Bakun (1990), who noted that the alongshore wind stress off California, Portugal, Morocco, and Peru increased between 1950 and 1985. Schwing and Mendelssohn (1997) studied this phenomenon in more detail off California. Using observations of wind stress, sea level and sea surface temperatures and salinities between 1946 and 1990, they used a technique to separate the seasonal changes from the longer-term changes. They discovered that between April and July wind stress and upwelling steadily increased over the observing period along with a decrease in sea surface temperature. However over the longer term they found an upward trend in sea surface temperature about 10 times the decrease due to the increase in spring/summer upwelling. They concluded that the sea-surface temperature increase is not related to the upwelling process but to factors operating on a larger scale such as global warming.

Another factor that can affect the biological production in upwelling regions is the depth of the mixed layer. Off Peru, for example, when the upwelling brings nutrient-rich water up into the euphotic zone and stimulates phytoplankton production, the mixed layer is about 20 m deep. In times of El Niño the mixed layer is ~100 m deep because of the tilting of the pycnocline across the Pacific

(see Section 9.2.1), and the upwelled water comes from above the pycnocline, where the nutrients have already become depleted. In this case the upwelling can be just as strong as when the mixed layer is shallow but the effects on the biology are drastically different as there is no nutrient-rich water rising up to the euphotic zone.

5.3 The Canary Current system

Of the various upwelling systems that have been intensively studied, that off northwest Africa is perhaps the most straightforward to understand, as a basis for comparison with other systems (see Huyer 1976 and Hempel 1982).

The Canary Current upwelling system extends for almost 3700 km from the northern tip of the Iberian Peninsula at 43° N to south of Dakar around 10° N. The Azores high-pressure atmospheric system moves north and south with the seasons and the regions of upwelling move with it, so that the northern one-third of the system experiences upwelling favorable winds only during summer, while the southern one-third has upwelling mainly during winter.

5.3.1 Upwelling and primary production

During the 1974 JOINT I cruise, at a time of weak wind, a gentle equatorward flow averaging about 10 cm s^{-1} extended almost 100 km offshore and to a depth of about 200 m. From 200 to 400 m on the continental slope there was a poleward counter-current with a velocity up to 5 cm s^{-1} (Fig. 5.07a). At a time of strong wind an equatorward coastal jet developed with current speeds greater than 30 cm s^{-1} while the poleward counter-current had slightly increased velocities. During the strong winds a two-layered circulation developed over the shelf. There was offshore transport at rates greater than 15 cm s^{-1} in the upper half of the water column and onshore transport at speeds up to 20 cm s^{-1} in the lower half (Fig. 5.07b).

When isopycnals next to a western coast slope upward we infer that upwelling is in progress. Figure 5.07(c) shows that σ_t contours sloped gently upward toward the coast during the time of weak winds, but turned sharply upward during the strong winds. Barton *et al*. (1977) contoured the surface temperatures from February 26 to April 9, showing that there were five upwelling events during the JOINT I cruise. The cold water first appeared close to shore, but moved out across the shelf as the upwelling event persisted (Fig. 5.08). The distribution of nutrients (Codispoti and Friederich 1978) shows that the nitrate-rich waters followed the same pattern, being brought to the surface first in the inshore area, then carrying the maximum concentrations out to the mid-shelf area (Fig. 5.09).

It would be nice to be able to continue the story by reporting that upwellings of nitrate-rich waters were quickly followed by bursts of primary production. Huntsman and Barber (1977) reported on primary production during the JOINT I cruise, and the averages for the entire cruise show a consistent pattern with

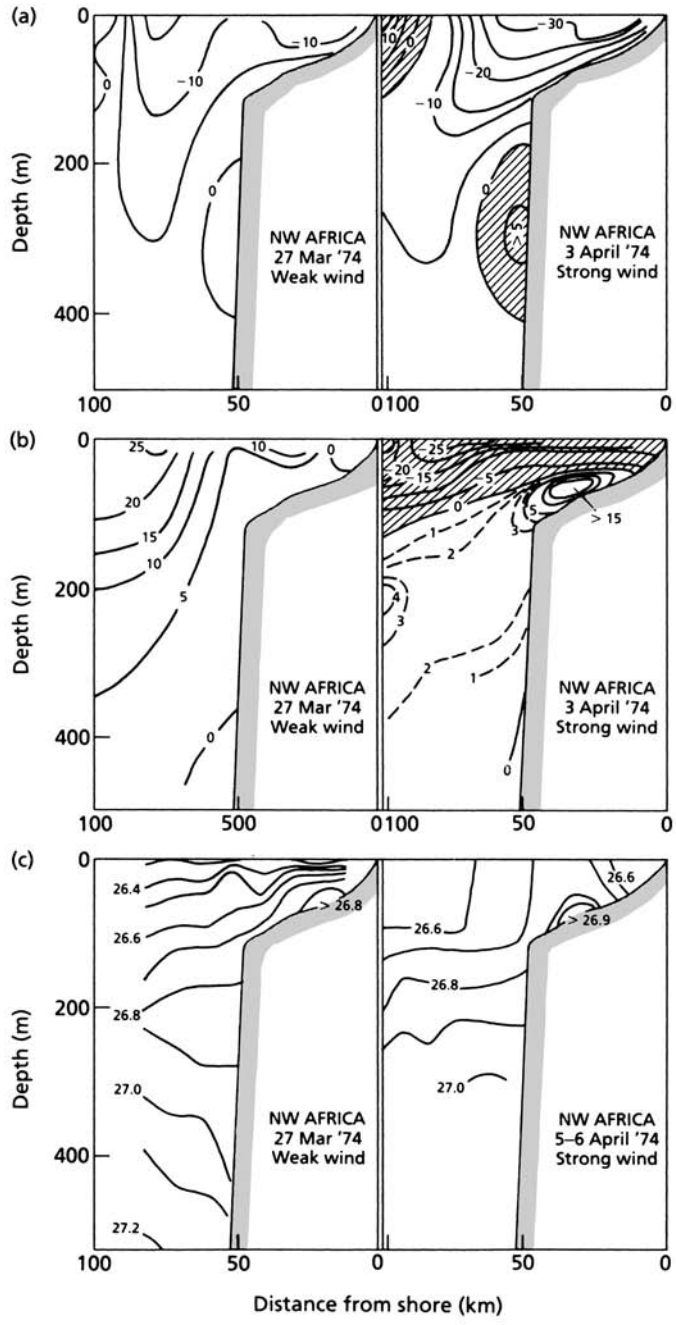

Fig. 5.07 Results of the 1974 JOINT I cruise off northwest Africa, after Huyer (1976). The line with stippled shading represents the sea bottom. (a) Sections showing the distribution of alongshore flow at times of weak wind and strong wind. Contour intervals are 5 cm s^{-1}. Positive values (hatched) are poleward and negative values equatorward. (b) Sections showing the distribution of onshore and offshore components of the flow during a weak wind and a strong wind. Offshore components (hatched) are negative. (c) Sections showing distribution of σ_t during weak winds and strong winds.

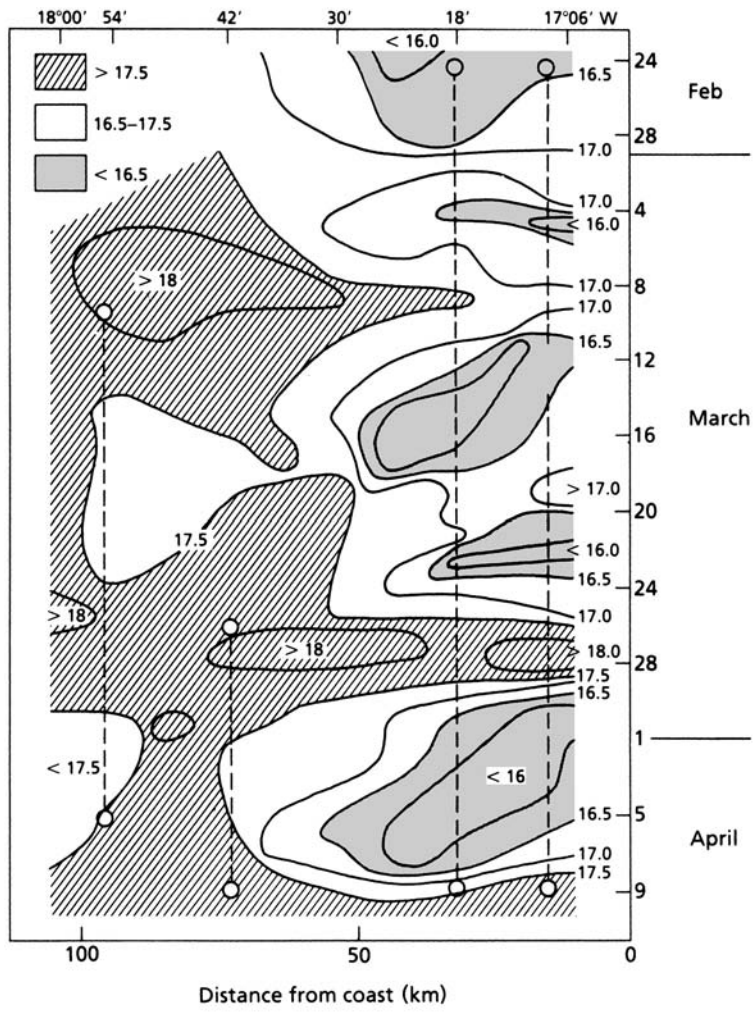

Fig. 5.08 Contours of surface temperatures from February 26 to April 9, 1974, during the JOINT I cruise off northwest Africa. Note that pulses of cold water (shaded) correspond with periods of strong alongshore winds. From Barton *et al.* (1977).

highest levels of nutrients in the 10 km zone closest to shore, and with the rate of primary production increasing steadily as they moved offshore, then leveling off to 2–3 g C m^{-2} d^{-1} across the entire shelf. Pulses of high productivity during early April and early May coincided with periods of high and steady wind stress and one might have thought that the wind stress generated upwelling of nutrient-rich water, which in turn led to increased primary production. This explanation is too simplistic. For one thing, there is a time delay between the onset of the wind and the arrival of nutrient-rich water out on the shelf. Second, there has to be a quantity of nutrient-limited phytoplankton cells ready to respond to the availability of nutrients.

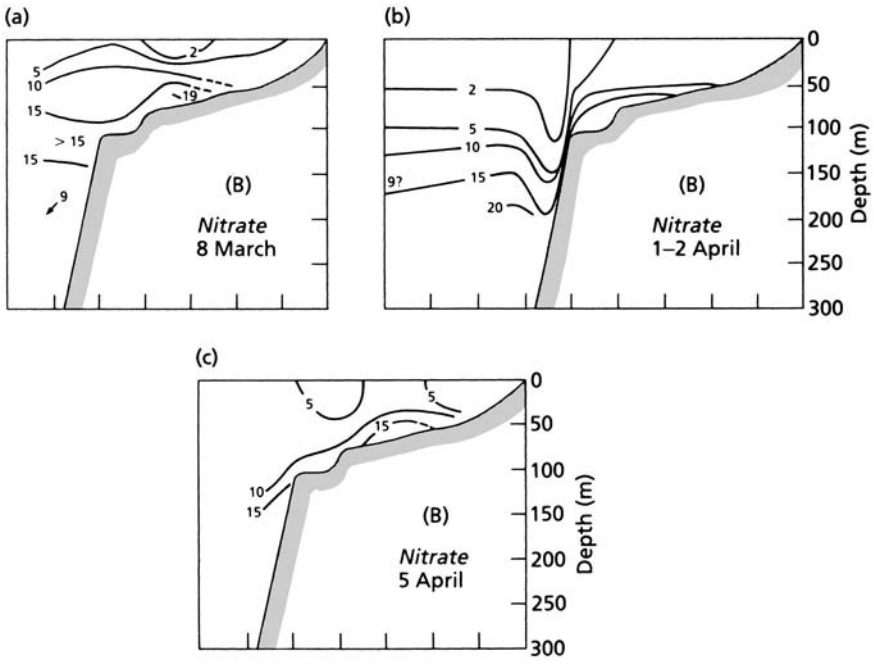

Fig. 5.09 Patterns of nitrate distribution (μmol L^{-1}): (a) during weak winds, (b) soon after the onset of strong winds, and (c) after persistent strong winds. Ocean floor shaded. Reprinted with permission from Codispoti and Friederich (1978), Pergamon Press.

Huntsman and Barber (1977) put forward the hypothesis that the observed high productivity results from the alternation of upwelling events and relatively calm periods. The upwelling brings nutrients into the surface waters, but during the calm periods stratification develops and the phytoplankton grows and multiplies while held in the shallow mixed layer. In other words, there is a miniature "spring bloom" during each calm period.

To test this hypothesis they made numerous measurements of the assimilation number, which is the amount of carbon fixed per unit time, per unit of chlorophyll-*a*. It is well known that when phytoplankton is growing and dividing rapidly under the stimulation of nutrient enrichment, the assimilation number is high. They found that the assimilation numbers were high during periods of calm and lower during periods of upwelling, thus supporting their hypothesis. Jones and Halpern (1981) published further data supporting this point of view.

5.3.2 Upwelling and zooplankton

Up to this point we have been able to follow physical and biological processes on the "event" scale, or mesoscale. Upwelling and primary production follow the onset of a strong wind within a few days. The next step in the food chain, the

growth of zooplankton populations, is decoupled from these events because typical zooplankton organisms, such as copepods, require weeks rather than days to complete a life cycle. Trumble *et al*. (1981) have reviewed the available data from JOINT I on seasonal changes in zooplankton biomass. Adult copepods from deep water are upwelled in spring and begin to reproduce. Their offspring thrive on the abundant phytoplankton but tend to be carried offshore during the periods of strong upwelling. The intensity of upwelling falls off in autumn so the zooplankton are able to stay over the shelf and the populations reach their peak density. The annual mean value has been estimated at about 60 g m^{-2} (wet weight), with low values at about 40 and high values at about 120 g m^{-2}. It must be remembered that we are talking about a dynamic situation in which the abundance of phytoplankton is a function of the grazing pressure as well as other environmental variables, and the abundance of the zooplankton is determined partly by the grazing pressure of the fish stocks. The consensus seems to be that, since phytoplankton populations are able to respond rather rapidly to the favorable conditions provided by upwelling areas while the zooplankton respond only slowly, the phytoplankton production normally exceeds the consumption by the zooplankton. In other words, the zooplankton are seldom food-limited. This may be contrasted with situations in which phytoplankton nutrients are scarce and the phytoplankton may have poor nutritive value for the zooplankton (Jones *et al*. 2002).

5.3.3 Upwelling and fish

The yearly cycle for fish species in the Cap Blanc region has also been summarized by Trumble *et al*. (1981). Seventy-five percent of the fish catch comprised only four types. Most abundant were clupeids (*Sardina pilchardu*s, the sardine, and *Sardinella aurita*). Next most abundant were jack mackerel *Trachurus* spp. and *Carynx rhonchus*. Redfish (Sparidae) and other species followed. *S. pilchardus* tends to dominate in the cooler water in the northern part of the upwelling, while *S. aurita* occupies the warmer, more southern waters. Their ranges tend to be adjusted with the changing seasons, with northward migrations taking place as summer approaches. In a study of the fish eggs and larvae present in the Cap Blanc region in spring, Palomera and Rubies (1982) found 65 different taxa, but 94% of all larvae examined were the sardine *S. pilchardus*. This heavy dominance of clupeids is characteristic of upwelling systems worldwide.

There is lack of agreement in the literature on what food is taken by the sardines and related clupeids, yet resolution of this question is needed for any calculation of a biological budget for an upwelling ecosystem. Truly phytophagous fish have a gizzard and a very long, coiled gut. Because larval sardines and anchovies do not have either feature, Cushing (1971) suggested that they feed mainly on zooplankton and take phytoplankton inadvertently. He conceded that first-feeding larvae might depend completely on algae. Muck *et al*. (1989) found that larval anchoveta in the Peruvian system have smaller mouths and longer guts than

sardines, and appear to consume a larger proportion of phytoplankton. He suggested that this characteristic might confer a competitive advantage on sardines when phytoplankton is scarce.

Mathisen *et al*. (1978) assumed that sardines fed mostly on small zooplankton while horse mackerel *Trachurus saurus* fed on larger zooplankton. Taking the biomasses of fish estimated acoustically during JOINT I, and some reasonable estimates of daily food requirements, these authors demonstrated that the estimated supply of food in the zooplankton was always in excess of the requirements of the fish stocks.

We have now followed the process through from the wind stress to the upwelling of nutrients, to the bursts of phytoplankton production during the periods of slack winds, to the build-up of zooplankton populations and their consumption by fish. The end result, from the point of view of human welfare, is the landing of large quantities of fish. Ansa-Emmin (1982) summarized the fish landings for the northwest Africa upwelling area. The reported catches of all species in 1974 totaled 2.68 million tons. Almost 1 million tons were Clupeidae, 0.67 million tons being sardines. Over 0.5 million tons were Carangidae, the horse mackerels, and 0.2 million tons were squid. The other major catches were true mackerel *Scomber* spp., hakes *Merluccius* spp., and sparids. The catch was taken by a dozen industrialized countries, the USSR alone taking 287,000 tons of sardines and 55,000 tons of sardinellas, 360,000 tons of horse mackerel, and nearly 200,000 tons of mackerel. Clearly, upwelling areas of the ocean can be very productive indeed.

A review of fish landings in Portugal, at the northern end of the Canary Current system, for the period 1959–99, showed that catches of *Sardina pilchardus* reached a peak of 160,000 tons in 1964, dropped steeply in 1970, remained fairly constant at about 90,000 tons for 20 years, but declined by 16% during the 1990s (Hill and Coelho 2001). Changes in fishing effort had some influence on the pattern, but as we shall see in Chapter 9, there was a regime shift (a major change in atmospheric and oceanic processes) in the North Atlantic around 1970–71, which may partly account for the drop in landings in 1970. The second most abundant species in the Portuguese catches has been Atlantic horse mackerel. At the southern end of the Canary Current system, off Western Sahara and Mauritania, Binet *et al*. (1998) reported that there were two periods of high abundance and southward spreading of *Sardina pilchardus* stocks. An industrial fishery (i.e., mainly for fish meal), conducted by the USSR and its associated Eastern Bloc countries peaked at over 600,000 tons in 1976–7, dropped to 200,000 tons in the early 1980s and rose again to 600,000 tons in 1989–90. Subsequently the Eastern Bloc fishing effort was severely reduced and the catch dropped. Possible correlations with long-term climate shifts will be discussed in Chapter 9.

The middle of the Canary Current system is off the coast of Morocco. In the southern part of Morocco the landings also peaked in 1976–7, dropped and then peaked again in 1989–90, clearly reflecting the same phenomenon as off Western Sahara and Mauritania. When the total Moroccan catch is considered, there was a peak of landings in 1976–7 at about 950,000 tons, a drop to about half that level in the early 1980s, then a recovery to over 1 million tons in 1989–90 (Kifani 1998).

5.3.4 Regeneration of nutrients

No account of an ecosystem would be complete without reference to the process that closes the loop, nutrient recycling. While upwelling of "new" nutrients is the distinctive feature of coastal upwelling systems, we should not lose sight of the fact that a proportion of the primary production that takes place makes use of nitrogen, usually in the form of ammonium, regenerated by benthic invertebrates, bacteria, zooplankton, and fish. Ammonium is the preferred form of dissolved nitrogen for uptake by phytoplankton.

There are two main possibilities for phytoplankton in the surface waters over the shelf. They may be consumed by zooplankton or they may sink to greater depths, even to the bottom. If they are consumed by zooplankton their nitrogen may appear as fecal pellets (which sink) or as excreted ammonia. If the phytoplankters sink to the bottom they may release ammonium during decomposition, or they may be consumed by benthic animals, which in turn excrete ammonium. One way or another, a high proportion of the phytoplankton nitrogen ends up being released in the shoreward-moving lower layer of the water column. As a result, there is an accumulation of ammonium close to shore, which is exactly what was found during the chemical investigations of JOINT I. Measurements of concentrations do not permit estimations of flux rates but Rowe *et al*. (1977) measured the flux of nutrients out of bottom sediments off Cap Blanc during JOINT I. The average total flux of nitrogen was 410 μmol N m^{-2} h^{-1}, which at the time of measurement would account for 30–40% of the nitrogen required in the water column for photosynthesis. When we remember that there would be additional regeneration of nitrogen in the water column, it is clear that upwelling of new nitrogen is by no means the only method of stimulating primary production in the area, and regenerated nitrogen may account for more than half of the primary production. The two-layered cross-shelf flow acts as a kind of nutrient trap in much the same way as the two-layered estuarine flow discussed in Chapter 4. When primary production is stimulated by upwelling, much of the nitrogen taken up by the phytoplankton ends up being regenerated in the shoreward-flowing deeper layer and returns to the coastal waters to further stimulate primary production. Barber and Smith (1981) (quoting Whitledge, unpublished data) estimated that on the shelf off Cap Blanc the regenerated nitrogen comprises 72% of the total nitrogen, with 33% coming from zooplankton excretion, 24% from benthos and sediments, and 15% from pelagic fish. Techniques now exist to model phytoplankton production in terms of ammonium and nitrate, and to take into account possible limitations on production by phosphorus, silicon, and iron (Flynn 2003b).

5.3.5 Upwelling off the coast of Portugal

Cunha (2002) reported an intensive study of physical oceanography, coastal bathymetry, and plankton off the coast of Portugal. This is the most northern part

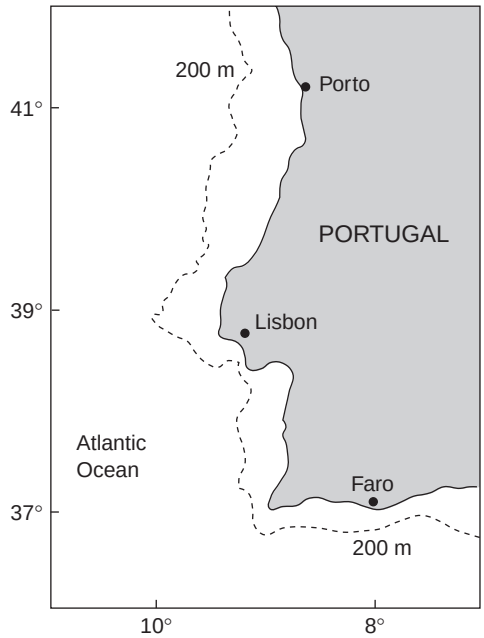

Fig. 5.10 The coast of Portugal, showing the 200 m depth contour.

of the Canary Current system, so upwelling occurs most strongly between June and October. There are marked differences between the shelf systems north and south of Lisbon (Fig. 5.10). In the north, the shelf is wider and there are more rivers and more rainfall. In the south, the shelf is narrower and there is less freshwater input, but there are more headlands and other coastal irregularities.

The fish landings are very different in the two regions. When expressed per 100 km of shoreline, the landings of pelagics at the time of the study were three times higher on the northern coast than on the southern coast. On the other hand, the landings of groundfish on the southern coast were almost twice as high as on the northern coast. Cunha (2002) was able to explain these differences on the basis of the functioning of the upwelling system. Off the northern coast, the phytoplankton blooms earlier because the buoyancy of the freshwater layer causes early stratification. Upwelling winds are more persistent, so more nutrient-rich water upwells, giving higher primary production and higher zooplankton biomass than in the south. As the upwelled water moves offshore over the broad shelf, there is a classic progression from nutrient-rich, plankton-poor water close to the coast, through a zone of high phytoplankton biomass to a zone of high zooplankton biomass over the outer shelf. The two-layered circulation described in Section 5.3.4 functions efficiently and the rich planktonic production supports strong populations of pelagic fish.

In the southern half of the system, the smaller input of fresh water means that there is less density stratification and the spring bloom of phytoplankton must

await surface warming. The time taken for upwelled water to traverse the narrow shelf is less, so there is less time for the food web linking nutrients to zooplankton to develop. Zooplankton populations are smaller and much of the ungrazed phytoplankton sinks to the bottom and supports a benthic food web. This leads to a higher proportion of benthic fish in the catch. This benthic food web is also supported by an organic load from the northern coast, which travels south in the geostrophic flow and settles to the bottom in the southern half of the system.

The more varied topography of the southern coast, together with more influence from subtropical waters, leads to a marked spatial diversity in the distribution of chlorophyll, and a greater species diversity in the plankton.

A numerical model of the northern Canary Current system demonstrated the generality of many of the features just described for the coast of Portugal. Batteen *et al*. (2000) used an eddy-resolving, limited-area eastern-boundary-current model, and described four numerical experiments of increasing complexity. In experiment 1 the coastline was represented as straight and the model demonstrated that wind forcing was the key generative mechanism for the boundary current, the upwelling, and many meanders, eddies, and filaments. In experiment 2 the model was run with an idealized irregular coastline with two headlands and a bay (representing the Gulf of Cadiz). In experiment 3 the coastline was a realistic representation of the coastline of Portugal and Morocco, with two prominent capes on the Portuguese coast and the Gulf of Cadiz south of Portugal. These two experiments showed that capes are areas for (i) enhanced upwelling, (ii) generation of extensive filaments, (iii) maximum current velocities, and (iv) enhanced growth of cyclonic meanders and eddies. An embayment like the Gulf of Cadiz is a primary region for development of an anticyclonic meander and eddies. Batteen (1997) had obtained similar results for the California Current system.

The fourth numerical experiment described by Batteen *et al*. set up a complex flow regime in which the realistic coastline was combined with realistic thermohaline gradients and the Mediterranean outflow. The model reproduced well the qualitative characteristics of the northern Canary Current system.

Santos *et al*. (2001) showed how strong upwelling can be advantageous for sardines and mackerel at one time of year, but disadvantageous at another. In an average year, the upwelling off Portugal is at a minimum in March and reaches its maximum in September. The sardines and mackerel spawn in winter, at a time when there is less Ekman transport to carry the larvae offshore, away from the food-rich coastal waters. On the other hand, they take advantage of the strong summer upwelling, which produces an abundance of food, at a time when they are large enough to swim against the offshore transport. In exceptional years, when there was strong upwelling in winter, there was a negative effect on recruitment of sardines and mackerel, presumably because large numbers of larvae were transported offshore.

Subsequently, Santos and Peliz (2003; Santos *et al*. 2004) showed that predictions based on Ekman transport are not adequate on all occasions. Shipboard observations during a strong winter upwelling revealed that the lens of low salinity water resulting from the run-off of rivers in the northern half of Portugal caused strong

winter stratification and an early phytoplankton bloom. As a result, there was an abundance of food for the fish larvae, even though they were being transported offshore by a strong winter upwelling. Furthermore, the subsurface Iberian Polar Current generated mesoscale features that helped to retain the larvae on the shelf.

During the 1990s there was a tendency for strong northerly wind in winter off the Portuguese coast, and the general trend was declining sardine recruitment. As we shall see in Section 9.8, this decline was part of a general trend for Atlantic sardine catches, associated with a preponderance of "latitudinal" forms of atmospheric circulation.

5.4 Comparison with the Humboldt Current system

The current responsible for upwelling off Chile and Peru has in the past been referred to as the Peru Current or the Peru–Chile Current. In fact there is a complex set of flows between the coast and 1000 km offshore (Alheit and Bernal 1993). Furthest offshore is a sluggish, wide flow towards the equator, the Chile–Peru Oceanic Current. Next towards the coast is the Peruvian Oceanic Counter-current. Closer again to the coast is the equatorward-flowing Humboldt Current, which is now regarded as the prime driving force for coastal upwelling. The area of upwelling migrates north and south with the seasons, but overall extends from about 38° S in central Chile, through northern Chile and the whole of Peru to parts of Ecuador just north of the equator. The early work was on the upwelling system off Peru, but more recently details of the Chilean upwelling system have been added. Off central Peru, upwelling is year-round but reaches a maximum in winter. Off northern Chile upwelling peaks during spring, while off central Chile it peaks during late spring and summer.

The Peruvian upwelling system at 15° S was studied intensively in 1976–7 in multidisciplinary cruises known as JOINT II (Fig. 5.11). There are three important differences between the upwelling site off Peru and that off northwest Africa. The first is that the shelf off Peru is narrower (20 km versus 50 km) and drops off more steeply (200 m at the shelf break versus 110 m). The second is that the deep water off Peru has higher nutrient concentrations (upwelled water contains 20–25 μmol L^{-1} of nitrate compared with 5–10 μmol L^{-1} off northwest Africa). Finally, the wind stress is less, and is more constant, averaging 0.79 ± 0.4 dynes cm^{-2} compared with 1.55 ± 1.0 off northwest Africa. The net result is that when the Ekman transport is active, offshore transport occurs mainly in the top 20 m, and shoreward transport is in an intermediate layer over the shelf, at depths of about 30–80 m, instead of in the whole of the water column down to the bottom, as it is off northwest Africa. Off Peru, the water close to the bottom is relatively still, and there is marked accumulation of organic matter to give chemically reducing sediment.

Two further differences are consequences of those listed above. One is that since the wind stress is less, the wind-induced mixing does not penetrate so deeply. During periods of strong upwelling, phytoplankton is still retained within the euphotic zone, which means that primary production is maintained at a relatively

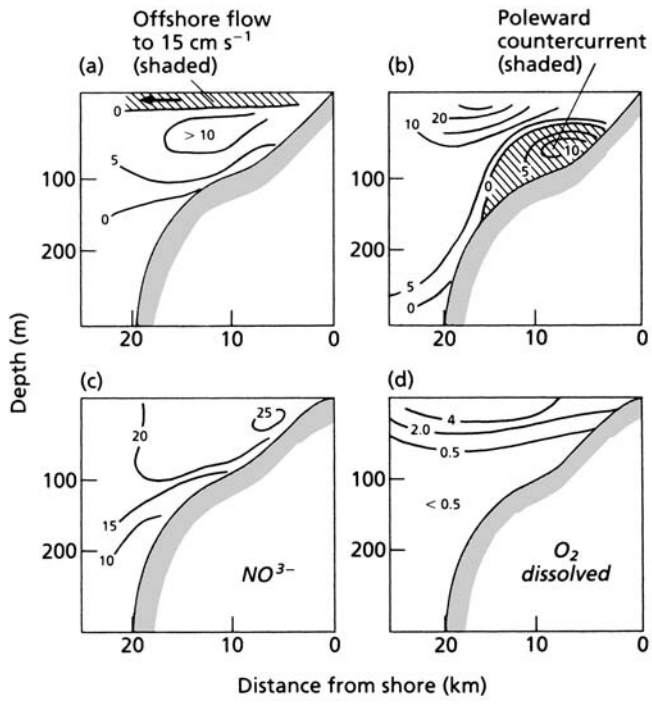

Fig. 5.11 Conditions off Peru, April–May 1977. From Brink *et al*. (1980) and Codispoti *et al*. (1982). (a) Onshore–offshore currents; (b) alongshore currents; (c) nitrate concentration; and (d) dissolved oxygen concentration.

constant level, whether the wind stress is high or low. Second, the poleward countercurrent, flowing beneath the equatorward coastal jet, is situated at intermediate depth over the continental shelf off Peru, whereas off northwest Africa it is located on the shelf slope (Fig. 5.07a). Figure 5.11 summarizes the features of the Peruvian upwelling system discussed above.

A detailed analysis of the primary production cycle in a segment of the Peruvian upwelling system at 15° S was published by MacIsaac *et al*. (1985). Because the upwelling is relatively constant it is possible to trace a distinct plume of cold water moving out from the coast and to recognize a number of zones along the axis of the plume. Zone I is the area of intense upwelling within about 7 km of the coast, where nutrients are abundant but phytoplankton biomass is relatively low. The phytoplankton cells are growing and taking up nutrients at rates considerably less than those of which they are inherently capable. In zone II the water column is stabilized by solar warming and the phytoplankton cells are found to increase their rates of nutrient uptake, photosynthesis, and synthesis of macromolecules, a process known as "shift-up." Zone III is characterized by the rapid depletion of nutrients by the "shifted-up" phytoplankton, so that there is a rapid accumulation of biomass and all processes occur at maximal rates. In zone IV nutrient depletion occurs, so that the cells experience nutrient limitation. In this

environment "shift-down" of physiological rates occurs. Using drogues to track water masses, MacIsaac *et al*. (1985) estimated that phytoplankton cells moved from zone I to zone IV in 8–10 days, during which time they traveled 30–60 km away from the coast. The chlorophyll maximum occurred about 18 km offshore.

5.4.1 Interannual variability in the Peruvian upwelling system

As Fig. 5.11 shows, the source of upwelled water off Peru in April–May 1977 was at a depth of 30–60 m. The water was at a temperature of 15.5–16.5 °C, and contained 20–25 μg nitrate. This state of affairs was only part of a larger structure extending across the whole of the South Pacific (see Chapter 9). Trade winds blowing across the Pacific Ocean from east to west drive the south equatorial current and cause the mixed layer to be only 10–20 m deep in the eastern Pacific but up to 80 m deep in the western Pacific. In other words, the thermocline is tilted upward at its eastern end. Then the winds blowing from south to north along the coast of Peru cause cool, nutrient-rich water to upwell from below the thermocline. This state of affairs is normal.

It is now known that in anomalous years the trade winds weaken or reverse, and the thermocline off the coast of Peru sinks to a depth of about 100 m (see Section 9.2.1). Ekman transport along this coast continues, but the water that is upwelled is now much warmer and not rich in nutrients. As a result, there is a sharp reduction in the biomass and productivity of the phytoplankton. The phenomenon, originally recognized from the warm-water anomaly that typically begins about Christmas time, was referred to as El Niño, which means the Christ-child. More recently it has come to be referred to as an El Niño – Southern Oscillation (ENSO) event. The physics of the Southern Oscillation will be dealt with in Chapter 9, but we should note that the Peruvian upwelling system seems to be uniquely vulnerable to such drastic changes, so that its interannual variability in productivity is very great. Sea-surface temperature anomalies were noted in 1965, 1969, 1972, and 1976 (Barber *et al*. 1985) but in 1982–3 an ENSO event occurred with a severity that is considered very rare, occurring with a periodicity of 100 years or more (Rasmusson and Wallace 1983). Barber *et al*. (1985) showed that at the height of the 1982–3 anomaly, in May 1983, the upwelling waters were at 29 °C instead of the usual 16–18 °C, and mean primary productivity was only 10 mg C m^{-3} d^{-1}. Two months later conditions had returned to normal and mean primary productivity was 219 mg C m^{-3} d^{-1}.

5.4.2 Total primary production in the Peruvian upwelling system

Many attempts have been made to calculate the total primary productivity of the Peruvian upwelling system, and to compare this figure with the total fish

production. Chavez and Barber (1987) gave the references to earlier calculations, which differed widely among themselves. One of the main reasons for the great discrepancies was the lack of agreement about the area of ocean influenced by the upwelling. For example, Cushing (1969) used 479,000 km^2 in his calculation while Ryther (1969) used 60,000 km^2. Chavez and Barber (1987) argued that the offshore dimension of coastal upwelling is limited by the Rossby deformation scale (Section 5.2.3). From Eqn. 5.11 we see that the formula for this scale is $(g' H_0)^{1/2}/f$. Thus the radius is a function of the Coriolis force f (which varies with latitude), the depth H_0, and the vertical density gradient. Taking these factors into account Chavez and Barber (1987) calculated that the width of the Peruvian upwelling system varied from 270 km at 4° S to 60 km at 18° S. Calculating the width at degree intervals they arrived at an area of 182,000 km^2, intermediate between the two values quoted above. The mean of the large number of determinations of primary production in 1983–4, after the recovery from the El Niño event, was 2.28 g C m^{-2} d^{-1} or 834 g C m^{-2} y^{-1}. This value converted into a total production of 1.52×10^{14} g C y^{-1}. With increased availability of satellite pictures of chlorophyll distribution, it should be possible to refine the estimate of the average area affected by upwelling, and to determine its variability. For example, Carr (2002) defined the area of an upwelling system as the area over which surface chlorophyll concentrations, as estimated by remote sensing, exceeded 1 mg m^{-3} on average (see Section 5.9).

5.4.3 Secondary production in the Humboldt Current system

Cushing (1971) described the fish and birds of the Peruvian upwelling as follows:

> Anchoveta . . . live in the upper part of the thermocline and presumably migrate towards the surface at night. On the bottom live flatfish in rather shallow water, and near the bottom in deeper water live hake and rosefish. The hake probably migrate upwards at night and feed on euphausiids. Between the anchoveta and the hake live the horse mackerel, possibly in the lower parts of the thermocline and below. At the surface live guano birds which are surprisingly abundant. In the Peru current there are 30 million birds, mainly pelicans, boobies and cormorants; during El Niño, the numbers are sharply reduced, because some migrate southwards out of the area when the fish are no longer accessible and some die of starvation. In 1958 during El Niño, the bird populations were sharply reduced but by 1962 the numbers of birds had fully recovered. So they must eat very large numbers of anchoveta.

It is clear that the same types of fish are found in the Humboldt Current system as in the Canary Current system. The sardines and anchovies usually spawn in the areas of most intense upwelling, close to shore, and Cushing speculated that both the juveniles and the adults make use of the two counter-currents (onshore and poleward) to maintain themselves within the upwelling system. As with the

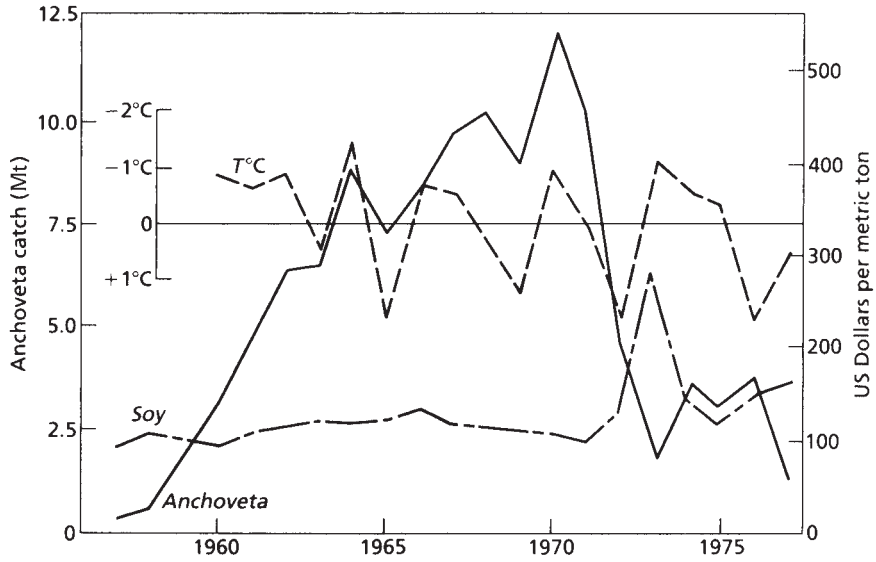

Fig. 5.12 Heavy line, anchoveta catch by Peru; *T* °C, temperature anomaly of the eastern Pacific; Soy, the cost of soya meal ($ ton^{-1}). After Barber *et al*. (1985).

northwest African system, there is lack of agreement about whether the anchovies and sardines predominantly consume phytoplankton. It seems that larvae consume mainly microzooplankton, while adults feed mainly on larger phytoplankton.

Barber *et al*. (1985) showed (Fig. 5.12) that the years of temperature anomalies (El Niño years) were associated with reduced landings of anchoveta *Engraulis ringens*. There are several possible explanations: the adults could have starved for lack of phytoplankton food, the fish could have migrated away from the areas where they are usually caught, or the larvae could have failed to survive through lack of both phytoplankton and zooplankton. There is some evidence for each of these hypotheses. Barber *et al*. (1985) report that anchoveta seek out the upwelling areas by exhibiting a preference for water of 16–18 °C. As an El Niño builds, the cool water is found only in certain more persistent centers of upwelling and the anchoveta concentrate there. There were reports of anchoveta having moved to cooler, deeper water at about 100 m, but such water has very little phytoplankton and it seems likely that the fish would not survive there long. Since anchovy stocks are known to have been present off central Peru for more than 2000 years, migration south to find cooler waters may well have been one of the strategies for survival (Valdivia 1978).

The question of larval survival is a complex one. The anchovies spread their spawning over 7–8 months of the year, presumably as an adaptation to the occurrence of unfavorable conditions at particular times and places. However, there are two peak periods: the austral winter–spring spawning (July–September) and the summer spawning (February–March) (Valdivia 1978). Walsh *et al*. (1980), investigating the survival of larvae off the northern coast of Peru during winter,

found that survival was higher when dinoflagellates in relatively high concentrations were available to the first-feeding larvae. Strong wind events had the effect of dispersing the dinoflagellate concentrations and adversely affected survival. We shall return to this topic in Section 5.5 on the California Current.

At the onset of the 1976 El Niño there was a bloom of the dinoflagellate *Gymnodinium splendens* along 1000 km of the coast from March until the end of May. It was attributable to the stabilization of the water column as the warm water invaded the area. While it provided an excellent feeding environment for the early larvae, it apparently was not a suitable food for the adult fish, which had smaller fat content, a reduced weight at a given length, and reduced length at sexual maturity. The 1977 recruitment of fish spawned in 1976 was extremely poor and the stock along the Peruvian coast fell to the lowest levels ever observed (Barber *et al*. 1985).

5.4.4 Exploitation of the Humboldt Current fish stock

As Fig. 5.12 shows, the ENSO events of 1965 and 1969 led to minor decreases in the landings of anchoveta, but the 1972 event was associated with a drastic decline from which the stock took 20 years to recover. The history of the anchoveta fishery in Peru was reviewed by Glantz (1985). For a century, beginning in the 1840s, the major industrial activity along the Peruvian coast had been the mining of the bird-droppings, guano, from the rocky islands. Large populations of fish-eating birds are characteristic of upwelling populations worldwide, and prominent white accumulations of droppings at their roosting sites are an inevitable concomitant. As Cushing (1971) remarked, it is no accident that upwelling areas commonly have a Cabo Blanco, Cap Blanc, or Cape Blanc. The guano of Peru was mined and exported for fertilizer to many parts of the world. Beginning in the 1950s, a lucrative industry to harvest the anchoveta and convert them to fishmeal was developed in Peru. The landings increased rapidly to a peak of about 12 million tons in 1970, then dropped to 2–3 million tons for a few years. After 1977 the catch hovered around 1 million tons but in 1985 there began a recovery which has persisted into the twenty-first century (Fig. 5.13). Alheit and Bernal (1993) suggested that there may have been massive migrations from the southern part of the Humboldt system. In fisheries circles a debate has centered around the question of whether these fluctuations have been part of a natural cycle of events that has occurred many times in the past, or whether they are primarily the result of gross overfishing.

In discussing the issue, Barber *et al*. (1985) pointed out that during the period of low anchoveta abundance there were increases in the abundance of sardine *Sardinops sagax*, jack mackerel *Trachurus picturatus*, and mackerel, suggesting a possible natural shift in species dominance. This change of species composition persisted into the 1990s (Alheit and Bernal 1993) (Fig. 5.14). However, the sediment records do not support the view that there has been dominance by sardine and mackerel for significant periods in the past. In 1975 conditions for anchoveta

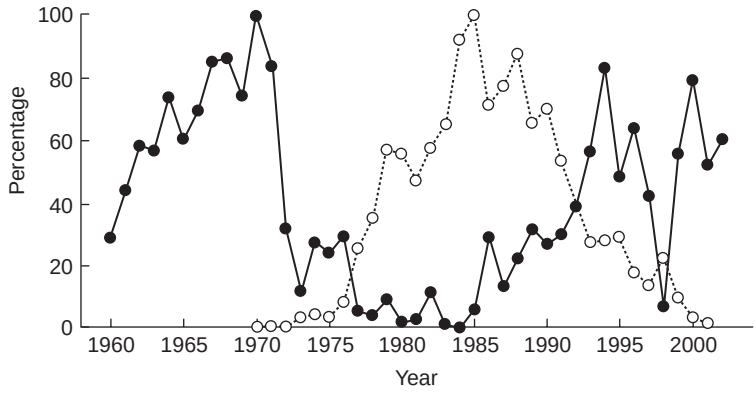

Fig. 5.13 Catches of anchovy and sardine stocks in the Humboldt Current ecosystem expressed as percentages. The highest catch per stock is taken as 100%. Filled circles, northern and central Peruvian anchovy (highest catch 10.9 Mt in 1970). Open circles, combined catches of anchovy from northern, central, and southern Peru, and from northern Chile (highest catch 5.5 Mt in 1985). From Alheit and Niquen (2004). Reproduced by permission of Kenneth Sherman.

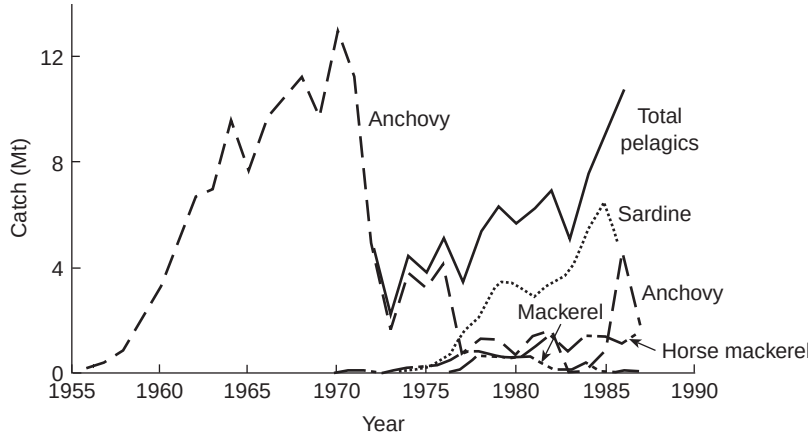

Fig. 5.14 Catches of pelagic fish in the Humboldt Current ecosystem. From Alheit and Bernal (1993). Reproduced by permission of Kenneth Sherman.

reproduction were excellent, the index of recruitment was one of the highest ever recorded, and by early 1976 the anchoveta stocks were estimated at 8.3 million tons. However, 1976 was the year of the *Gymnodinium* bloom mentioned earlier, and it was followed by an ENSO event. Then, from 1977 onwards there was an anomaly in the global pressure system (a regime change: see Chapter 9) that resulted in a weakening of the southeastern Pacific trade-wind system and a decrease in the thermocline tilt, which in turn meant poorer nutrient conditions in the Peruvian upwelling system. According to this view, anchoveta went into the 1982–3

ENSO event at a low population level because of the 1976 event followed by six years of unfavorable environmental conditions and overfishing. At the same time, sardine stocks in the Humboldt system increased steadily so that a record catch of over 6 million tons was possible in 1985.

Muck and Sanchez (1987) reviewed historical data on stock size, stomach contents, and energetics of mackerel and horse mackerel, and concluded that their consumption of anchoveta could at times equal or exceed the commercial fish catch. They therefore concluded that years of high abundance of mackerel and horse mackerel could explain, at least in part, years of low abundance of anchoveta.

A new perspective on the history of the Humboldt Current ecosystem was provided by Alheit and Niquen (2004). Their ideas are in harmony with newer discoveries about the importance of inter-decadal atmosphere–ocean changes, and the associated regime shifts, to be reviewed in Chapter 9. They pointed out that in the subtropical and southern Pacific Oceans, the regime shifts are associated with the approach or retreat of warm subtropical oceanic waters along the coast of Peru and Chile, giving long periods of warm or cool anomalies in coastal waters. The periods 1950–70 and 1985–2004 had mainly negative temperature anomalies and were characterized by dominance of anchovy (Fig. 5.13). The intervening period, 1970–85, had mainly positive anomalies and was characterized by the dominance of sardines.

The warm periods had an effect similar to an El Niño, drastically changing trophic relationships in the entire Humboldt Current ecosystem and exposing the Peruvian anchovy to several kinds of adverse conditions. Warm water moving shoreward drove the anchovies into the cooler waters close to the coast. This decreased their area of distribution and spawning and in turn increased egg and larval cannibalism and the catchability of the stock. Sardines, inhabiting the warmer waters, fed on anchovy eggs at the edges of the cool water mass. The presence of warm subtropical water reduced upwelling of cold nutrient water and decreased the production of phytoplankton and zooplankton on which the anchovy feed. The warm conditions also favored horse mackerel and mackerel, which are the main predators of adult anchovy.

The authors pointed out that anchovy can recover from an ENSO event in 1–2 years (Fig. 5.13). They made a partial recovery after the 1972–3 El Niño, and a full recovery after the 1997–8 event, but the decadal-scale period of warm anomalies, which began in 1968, held the anchovy populations at low levels from 1977 to 1985. Alheit and Niquen (2004) therefore concluded that the well-known crash of the anchovy fishery in the 1970s was caused primarily by the decadal-scale regime shift rather than by the 1972–3 ENSO events.

5.5 The California Current system

As we see from Fig. 5.01 there is a northern-hemisphere analogue of the Peruvian upwelling system. It is driven by prevailing northerly winds, and upwelling occurs along the Pacific coast of the United States from the Canadian border south to

Baja California and beyond. This upwelling is the California Current system. Detailed studies of upwelling events have been made, particularly off Oregon, and a comparison of northwest Africa and Oregon was made by Huyer (1976). In several respects the situation off Oregon resembles that off Peru. The poleward undercurrent appears over the shelf as well as the slope, and the shoreward flow is strongest at mid-depths over the shelf. Upwelling events are less strong and of shorter duration off Oregon than they are off northwest Africa.

Bakun (1973) examined records of wind strength over the ocean off northwest United States over a period of 20 years. He calculated the wind stress from the formula

$$\tau = \rho_a C_d v^2 \tag{5.12}$$

where ρ_a is the density of the air, taken as 0.00122 g cm^{-1}, and the drag coefficient C_d was taken as constant at 0.0026. He then computed the Ekman transport, M_E, from wind stress, τ, and the Coriolis parameter, f, according to Eqn. 5.02, i.e.,

$$M_E = \tau / f$$

Finally, he integrated the data to give the Bakun upwelling index, a 20-year average of monthly mean Ekman transport for different parts of the coast, expressed as cubic meters per second per 100 m of coastline. The range is from 300 m^3 s^{-1} (offshore direction) to –212 m^{-3} s^{-1} (onshore). Some of the results are displayed in Fig. 5.15. It can be seen that the index indicates year-round upwelling off southern California, with stronger upwelling in summer, but off Oregon and Washington in the north there is strong downwelling in winter, and upwelling is confined to the period April–September.

Figure 5.16 shows that in summer there is a negative temperature anomaly, indicative of upwelling of cold water, all the way along the coast from Oregon in the north to Baja California in the south, with the exception of a warm anomaly off San Diego. The upwelling is obviously most intense between Cape Mendocino and Monterey. Although the temperature anomaly in Fig. 5.16 shows an apparently uniform area of cold water, this area is an artifact of the method of calculation. The situation at any one time, as seen by satellite, is extremely complex, with coastal upwelling systems tending to be centered on topographical features such as capes and canyons, and with plumes of upwelled water extending far out into the California Current. As in other coastal upwelling systems, the strength of upwelling is strongly dependent on wind speed and direction, and changes from day to day. Fig. 5.17 shows the distribution of temperature and nitrate off Point Sur, California, on June 9, 1980, as inferred from satellite imagery supplemented by shipboard observations (Traganza *et al*. 1983). This situation is typical of an early phase of an upwelling event at this site. If the event persists for many days, interaction with the California Current may give rise to a cyclonic structure about 100 km in diameter, with high biological production along the associated fronts, or it may extend into a plume up to 250 km long (Traganza *et al*.

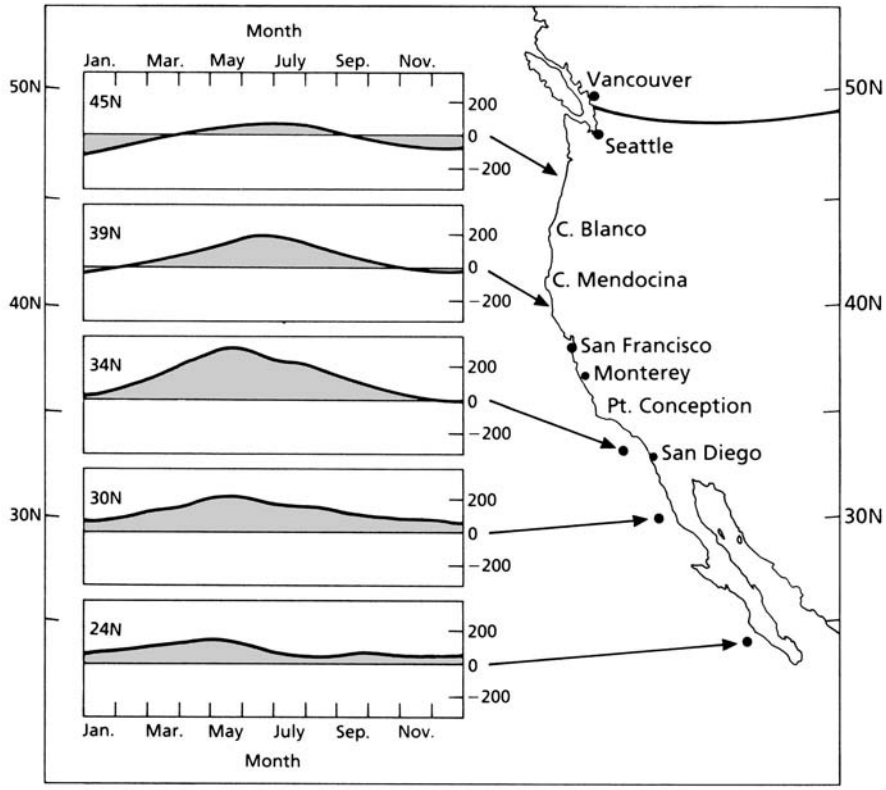

Fig. 5.15 Each plot on the left-hand side of the diagram is the upwelling index for each month of the year, averaged for the 20 years between 1948 and 1967. Each is for a different latitude, as indicated on the map on the right. Note that the strongest upwelling occurs at 34° N. In the southern half of the range the index is positive all year round, but at latitudes 39–45° N the index is negative in winter. Modified from Bakun (1973).

1981, 1987). In summer time, patterns of this kind may be found in various stages of development or decline all the way from Oregon to Baja California. As winter approaches, the upwelling is progressively restricted to the southern portion of the region and in spring the region of upwelling spreads north again.

There seems to be no good synthesis of the biological productivity of this dynamic system. In the Southern California Bight, where upwelling is not particularly strong, Smith and Eppley (1982) found that the 16-year average for primary production was 0.402 g C m^{-2} d^{-1}, about 150 g C m^{-2} y^{-1}. Using the temperature anomaly at the Scripps pier as an index of upwelling, they found that the highest daily rates were associated with the maximum amount of upwelling, and vice versa. In the California Current itself Hayward and Venrick (1982) found wide variation in the biomass and productivity of phytoplankton. Carbon fixation rates varied over an order of magnitude, from about 20 to nearly 200 mg C m^{-2} h^{-1}. These rates might

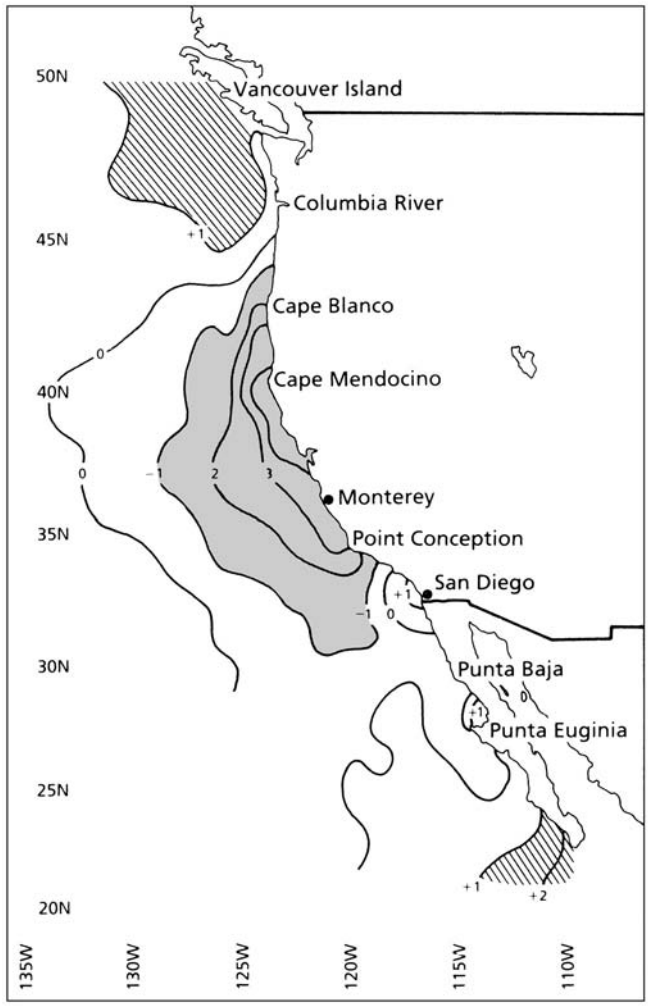

Fig. 5.16 Average coastal temperature anomaly (°C) in summer, calculated as the difference between each location and a smoothed reference temperature for offshore conditions at the same latitude. Positive anomalies hatched, negative anomalies shaded. From Bakun and Parrish (1982).

be roughly converted to a range of 0.2–2.0 g C m^{-2} d^{-1}. These differences reflect the heterogeneous nature of the California Current, with its admixture of advected and upwelled water. In trying to calculate the carbon flow from primary production to the pelagic fish stocks, Lasker (1988) used a value of 0.5 g C m^{-2} d^{-1} for the Southern California Bight and adjacent California Current, but commented: "It also seems likely that to the north, off central and northern California, the highly energetic 'jets and squirts' which move large quantities of cold, nutrient-enriched water offshore and become entrained in the southward moving California current . . . add more primary production to the habitat of the sardine than has been included in the gross overall average."

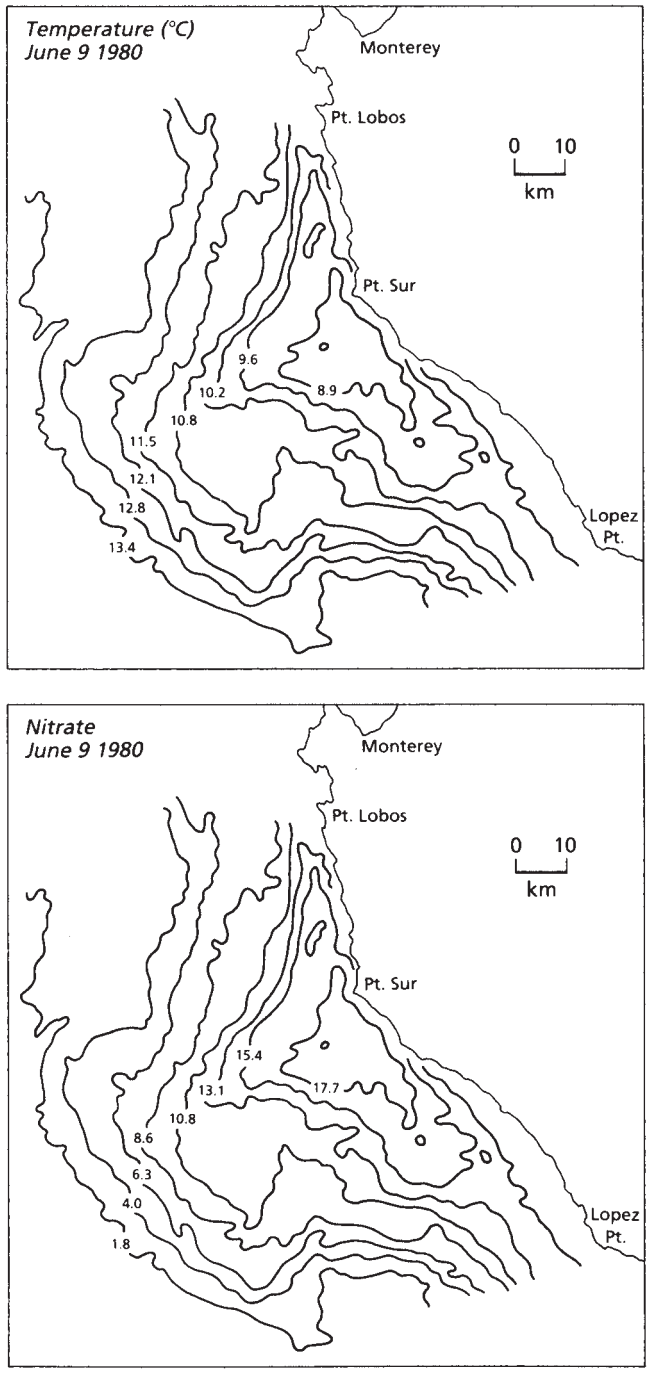

Fig. 5.17 Temperature and nitrate distributions off Point Sur, California, from satellite and shipboard operations. Note the difference between actual field data and the averaged long-term trends in the previous figure. From Traganza *et al*. (1983).

It is now possible to simulate both physical and biological events in the coastal transition zone, that zone characterized by the presence of highly productive jets, squirts, or filaments of highly productive upwelled water. Moisan and Hofmann (1996) modeled the fate of Lagrangian drifters placed in newly upwelled water and allowed to travel with a filament. Coupled physical and biological models were used, the biological parameters being determined from shipborne observations. The models reproduced well the formation of a subsurface chlorophyll maximum and the changing structure of the food web as the drifters moved offshore.

Digiacomo (2000) and Digiacomo and Holt (2001) used the latest satellite technology to study the mesoscale and sub-mesoscale eddies in the Southern California Bight. All the eddies were less than 50 km in diameter, and 70% were less than 10 km. They were observed to lie between the equatorward-flowing California Current and the shore, and appeared to be caused by topography (especially islands), wind, and current instabilities. Most of them were cyclonic eddies, with the potential to cause upwelling of nutrient-rich water in their cores. There was also evidence of lateral entrainment of highly productive coastal waters. Associated with the eddies were patches of high chlorophyll density, up to 15 km wide and 60 km long. The authors discussed the potential for influencing nutrient flux, plankton productivity, larval transport and recruitment, and dispersal of pollutants. This smaller-scale pattern was observed to interact with the large-scale variations in time and space of the California Current.

Details of small-scale features inshore of the California Current have been shown to have profound effects on the population dynamics of benthic invertebrates (Botsford 2001). When cold, upwelled water streams south past a headland, a cyclonic gyre containing warm water often develops on the south side of the headland, producing a signature in satellite images known as the upwelling shadow (Graham and Largier 1997). When the upwelling-favorable winds relax, poleward coastal currents driven by river run-off often become dominant features of the coastal oceanography. Wing *et al*. (1995) showed that crab larvae settled mainly during relaxation events on the open coast, but more continuously and in greater numbers on the south side of a headland. Settlement on the open coast appeared to coincide with the arrival of a front formed by warm water moving north along the coast during a relaxation event.

There was evidence that headlands also modified the settlement patterns of the larvae of rockfish and of sea urchins. Wing *et al*. (1998) pointed out that the areas in the lee of headlands are examples of retention features that profoundly influence the success or failure of cohorts of planktonic larvae and hence the productivity of the adult populations.

5.5.1 Fish production in the California Current system

As in other eastern boundary-current systems, the most abundant fishes in the California Current system are sardines, anchovies, hake, jack mackerel, and mackerel. Sardines *Sardinops sagax* were heavily exploited from 1916 to 1967

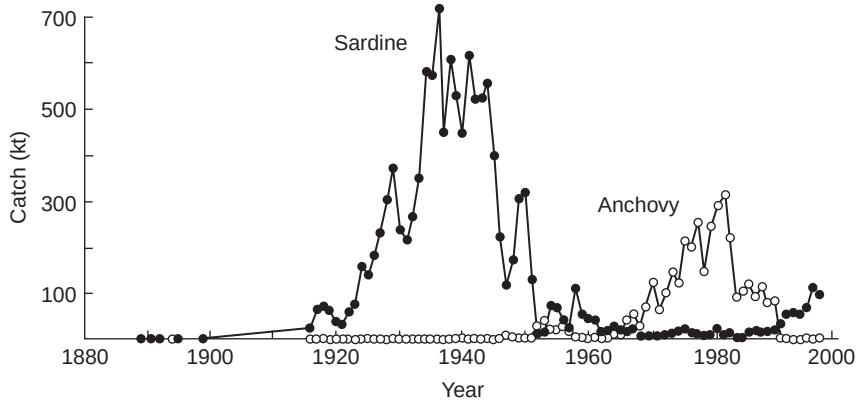

Fig. 5.18 Catches of sardines and anchovies in the California Current. From Schwartzlose *et al*. (1999)

(Fig. 5.18). The peak landings were in 1936–7 and exceeded 700,000 tons. The catch fell drastically in the 1950s and 1960s and in 1967 the California state legislature imposed a moratorium on the sardine fishery. The next most abundant species is the northern anchovy *Engraulis mordax*, closely related to *E. ringens* of the Peruvian upwelling. Its numbers began to increase as the biomass of sardines declined, and some postulated that the two were in competition so that the decline of sardine stocks released resources for the anchovies. However, Soutar and Isaacs (1969) studied the 1850-year record of fish scales in the anaerobic sediments off California and concluded that northern anchovy scales were present in large numbers throughout the series, while sardine scales appeared intermittently for periods of 20–150 years, with absences that averaged 80 years in duration. They concluded that the two species were not in competition.

The sardines of the California current system are divisible into four stocks. Of these, the largest by far before overfishing was the one that spawned in the Southern California Bight and migrated to the upwelling areas off northern California to exploit the dense zooplankton stocks that are associated with the coastal upwelling. The anchovies also have several subpopulations. The stock off Oregon spawns at about 44–46° N, mainly in July at the time of the northern upwelling. The central subpopulation spawns principally in the Southern California Bight. Eggs and larvae can be found throughout the year, but the peak abundance is in the spring, while the minimum is in the autumn. The fish remain in the Southern California Bight throughout their lives and in recent years this has been the largest stock. There is a southern stock off Baja California, for which peak larval abundance is from January to March.

It thus appears that the largest stocks of both sardine and anchovy spawn in the Southern California Bight. Upwelling is relatively weak and phytoplankton production is lower than in the California Current proper. Bakun and Parrish (1982) have suggested that strong offshore flow associated with Ekman transport is likely

to carry eggs and larvae too far offshore, to positions from which they may never return, and that the choice of the Southern California Bight for spawning area reflects a need to avoid areas of strong upwelling. They also suggested that areas of strong Ekman transport are areas where there are strong winds that may destroy the fine-scale strata of food organisms needed by first-feeding larvae. This idea, attributable to Lasker (1975), will be examined in more detail in Section 5.5.2.

Schwartzlose *et al*. (1999) showed that the exploitation of sardines in the California Current reached its peak with landings of 700,000 tons in 1936, but was down to extremely low levels by 1952. From 1916 to 1952 the catches of anchovy were negligible (Fig. 5.18). From 1952 to 1966 there were small catches of both sardines and anchovies, and in 1967 the sardine fishery was closed. After 1967 there was an expansion of anchovy populations, resulting in a catch of 310,000 tons in 1981, but in 1990 there was a switch to dominance of sardines once again, with a catch of 110,000 tons in 1997. The various hypotheses to explain the alternation of species have been discussed, but in the light of the findings of Alheit and Niquen (2004) for the Humboldt Current system, we may expect to find some influence of decadal-scale climate changes. These will be discussed in Chapter 9.

5.5.2 The survival of first-feeding larvae

Anchovy eggs are most abundant in the Southern California Bight during February, March, and April (Smith and Lasker 1978). After the absorption of the yolk sac, they must obtain sufficient food to meet their metabolic requirements within 2–3 days or they will die. Hunter (1972) studied the feeding behavior of the larvae and found that the food capture success rate of 3-day-old first-feeding larvae is very low but increases exponentially with age. As a consequence, 3-day-olds require a very high density of food organisms in their immediate environment to survive. He estimated that it was at a minimum of about 1790 dinoflagellates per liter.

Lasker (1975) made a field investigation of the feeding conditions for anchovy larvae in the Southern California Bight. Eggs were taken from anchovies held in the laboratory and were incubated under controlled conditions. They were then taken to sea so that a ready supply of first-feeding larvae was available for shipboard experiment. In March and April 1974 he found at several stations that there was a marked chlorophyll maximum at a depth of 30–35 m, and that the most abundant organism was the naked dinoflagellate *Gymnodinium splendens*, with a diameter of 40–50 μm, occurring at densities of 30–40 particles mL^{-1}. Larvae placed in waters from near the surface took very little food, but larvae placed in water from the chlorophyll maximum fed extensively. The experiments were repeated at stations where other kinds of phytoplankton dominated. It was concluded that spiny or chain-forming diatoms such as *Thalassiosira* or *Chaetoceros* did not stimulate the larvae to feed, nor did any phytoplankton of diameter much less than 40 μm. Finally, the larvae were stimulated to feed only when the phytoplankton

was at a population density of at least 20–30 cells mL^{-1}. The latter fact was confirmed in a very striking manner. Toward the end of the study a strong wind caused a deepening of the mixed layer and obliterated the chlorophyll maximum containing the *Gymnodinium*. After that it was impossible to stimulate the anchovy larvae to feed with water taken from any depth in the water column.

Lasker (1978) then investigated the horizontal and vertical extent of areas in the Southern California Bight suitable for anchovy feeding. Between September and December 1974 suitable food was abundant within 5 km of the shore in a chlorophyll maximum layer. During January 1975, gyral circulation redistributed the water so that adequate concentrations of dinoflagellates could be found at some depth all throughout the bight. In February 1975 northerly winds strengthened and strong upwelling began. The dinoflagellate populations were gradually replaced by small diatoms on which the anchovy larvae would not feed. These conditions persisted through the early spring and summer months.

On the basis of Lasker's (1975, 1978) results we may conclude that physical factors have a strong influence on year-class success of northern anchovy. The first-feeding larvae rely on high concentrations of phytoplankton such as naked dinoflagellates of a size class close to 40 μm. These high concentrations occur mainly at the chlorophyll maximum that forms near the thermocline under relatively calm conditions in the Southern California Bight. The onset of strong winds at a critical time may mix the water column to such a depth that the chlorophyll maximum is dispersed, or the winds may set up strong Ekman transport so that the water in the Southern California Bight is replaced by upwelled water containing mostly small diatoms in relatively low concentrations. Either of these situations renders the environment unsuitable for successful feeding, growth, and survival of small anchovy larvae. To put it another way, while the presence of upwelling and the consequent high biological productivity creates optimum conditions for the growth of juvenile and adult sardines, it is the absence of strong upwelling in late winter and early spring in the Southern California Bight that provides the optimum conditions for survival of first-feeding larvae. The timing of strong winds and the onset of upwelling in this region may well be a major determinant of year-class strength.

To summarize our understanding of factors influencing anchovy and sardine production in the California Current, we see that strong wind stress and associated upwelling, which are the most characteristic features of eastern boundary currents, appear in themselves to be detrimental to the success of the larvae. For good survival the larvae require a well-developed horizontal layer of high phytoplankton density, in which dinoflagellates are the dominant form. We have seen in Chapter 2 that diatoms, with their high sinking rate, tend to dominate in highly turbulent or newly upwelled water, while dinoflagellates, which are active swimmers, tend to replace diatoms in more stable water columns with lower nutrient concentrations. Hence, the optimum conditions for success of first-feeding anchovy larvae tend to occur in waters that have been free of strong upwelling and strong wind mixing for a considerable period. Strong wind mixing and upwelling at the wrong time can cause heavy mortality. Once past the

critical early stages of development, the juveniles migrate toward the areas of intense upwelling and exploit the high biological productivity found there.

Cury and Roy (1989) attempted to quantify the turbulence conditions optimal for recruitment for the Peruvian anchoveta *Engraulis ringens*, the Pacific sardine *Sardinops sagax caerulea*, and West African sardines and sardinellas. They found that recruitment increased with upwelling intensity until the year-round average wind speed reached 5–6 m s^{-1}, and decreased for higher values. Thus, up to this value, the advantages of the increased productivity caused by upwelling-favorable winds more than compensated for the disadvantages of having the food layer dispersed by turbulence; above an average of 6 m s^{-1}, the added turbulence outweighed the advantages of the upwelling. The conditions favorable for high recruitment were called an optimal environmental window.

Serra *et al*. (1998) performed a similar exercise for Chilean and Peruvian sardine recruitment data from 1974 to 1990. They used generalized additive models to analyze the relationship of recruitment to sea surface temperature, wind mixing, and upwelling indices. They found no relationship with temperature, but a dome-shaped relationship with upwelling or mixing. Switches between a sardine- and an anchovy-dominated system were also important contributors to recruitment variability.

A similar conclusion was reached by Ware and Thomson (1991). Noting a five-fold decline in the total landings of sardine, anchovy, and hake in the northeast Pacific between 1916 and 1942, and a parallel decrease in the average intensity of wind favoring upwelling, they calculated the average wind speed *during the peak spawning period* at various localities and found the optimum for recruitment to be 7–8 m s^{-1}. This finding is in fair agreement with Cury and Roy's (1989) figure of 5–6 m s^{-1} *averaged over the year*. A more detailed study (Jai Shin *et al*. 1998) showed that for 10 of 12 upwelling systems around the world the optimum environmental window for spawning of sardines and sardinellas is very narrow, with wind speeds between 5.3 and 6.1 m s^{-1}, but for anchovy there is apparently very little correspondence between the timing of reproduction and wind-speed values.

It is interesting to compare this conclusion with that reached in Section 5.3.1, where we saw that in the Canary Current upwelling provides the supply of nutrients to the euphotic zone but the relatively calm periods between upwelling events permit the development of high phytoplankton biomass – in effect a little "spring bloom." This mechanism almost certainly operates in all upwelling systems. At any given location there are periods of stronger winds which drive the upwelling of nutrients, and periods of relative calm when phytoplankton and zooplankton become abundant. The latter are the times that provide favorable conditions for first-feeding larvae. If the periods of calm are relatively short (a few days), records of average wind speeds would not necessarily reflect them.

A second factor to be considered in relation to larval survival is the risk that strong offshore transport will carry the larvae away from the favorable coastal environment. The two mechanisms occur on very different time scales and have quite different characteristics. The destruction of a chlorophyll maximum layer can occur within a few days and is in effect irreversible within the period

of development of a cohort of larvae. On the other hand, offshore transport in a system as complex as the California Current can take weeks to transport the larvae far enough from shore that their chance of completing their life history is placed in jeopardy. Furthermore, the offshore transport may be part of a gyral circulation that eventually begins to carry the larvae back toward shore, or the larvae may be able to migrate down into a shoreward-moving counter-current. In our present stage of understanding, there is no way to integrate these two mortality factors, beyond pointing out that both sardine and anchovy appear to avoid the regions of strongest upwelling in their choice of spawning location. By spawning downstream of those regions they appear to minimize the hazards while placing their larvae in a location from which, with a short migration, they can benefit from the high productivity associated with coastal upwelling.

5.6 The Benguela upwelling system

The last of the four major upwelling areas located in eastern boundary currents is the Benguela system, to the west of southern Africa (Fig. 5.01). The physics, chemistry, and biology of this system have been thoroughly reviewed (Payne *et al*. 1987, 1992). The latter reference, a symposium volume entitled *Benguela Trophic Functioning*, contains 26 papers in a section headed "Physical influences on ecological processes."

There is a northward-moving current, the Benguela Current, occupying a zone about 200 km wide off the west coast of southern Africa from Cape Town north to about latitude 15° S. It is the eastern part of the South Atlantic gyre and the driving force is the wind associated with the South Atlantic anticyclone. Since the system is in the southern hemisphere, a wind from the south blowing parallel with the coast gives rise to offshore Ekman transport. The temperature anomaly produced by the associated upwelling delineates the area occupied by the system, which is seen to be larger in winter than in summer (Fig. 5.19). The differences in shape of the sea surface temperature (SST) patterns in the two seasons are largely attributable to the fact that the upwellings centered on Lüderitz and on Cape Columbine (near Cape Town) reach their maxima in summer, while the very major upwelling at Cape Frio reaches its maximum in winter.

However, as we saw in connection with the California Current, the mean temperature anomaly obscures the complexity of the system. A satellite picture taken at any instant shows a complex pattern of whirls and jets, many of them determined primarily by the bottom topography. In some places the cold upwelled water is carried far out into the Atlantic, while at other places the upwelled water is confined to a relatively narrow band close to the coast. The picture is further complicated by variations in wind strength on a scale of a few days.

In the Benguela system it has been confirmed that optimal biological production occurs during an alternation of an upwelling phase, when the supply of nutrients in surface waters is replenished, followed by a quiescent phase during which stratification sets in and phytoplankton biomass increases. A lag of 1–4 days occurs

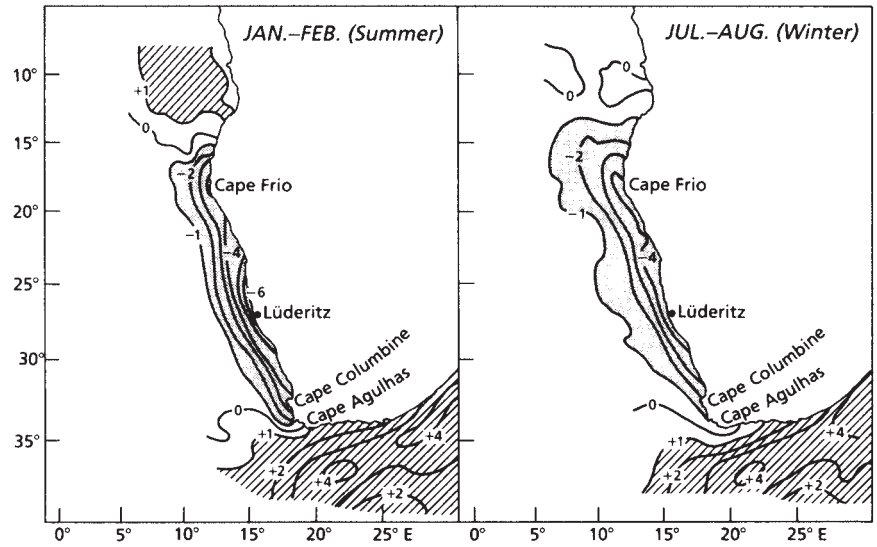

Fig. 5.19 Average sea-surface temperature anomalies in the Benguela current system, in summer and winter. From Parrish *et al*. (1983).

between the nutrient input and the blooming of the phytoplankton, and the bloom normally lasts 4–10 days. If the period of upwelling is too short, the phytoplankton will not have time to respond to the nutrients; if the interval between successive upwelling events is too long, the mesozooplankton will not have a continuous supply of food to permit optimum growth and reproduction. On biological grounds it would seem that a pulsing of upwelling with a duration of less than 5 days would be too short and one of more than 15 days would be too long. Ten days might be the optimum.

Nelson (1992) and Jury and Brundrit (1992) concerned themselves with the causes of variability in wind strength and upwelling intensity. Along the west coast of southern Africa an upwelling event is marked by north-directed upwelling-favorable wind, low sea levels, northward shelf currents, and declining coastal sea surface temperatures. Pulses of upwelling (as indicated by sea-level change) propagate southeastward along the west coast and continue eastward along the south coast, beyond Port Elizabeth, at speeds of 5–8 m s^{-1}. These wave-like features are generated by winds that alternately increase and decrease upwelling. Because the winds are associated with atmospheric high- and low-pressure systems moving eastward past southern Africa, the regions of enhanced upwelling also move around the Cape in concert with the wind systems.

The structure and speed of the upwelling features are similar to coastally trapped waves (Gill 1982). These are internal Kelvin waves which look like the waves pictured in Fig. 7.06, except that the horizontal scales are 30–60 km rather than the 1000 km or so of the waves associated with the tide in the figure. Because of the similarity, coastally trapped waves propagating south along the

west coast of southern Africa can enhance or diminish the upwelling events. For example, at the crests of the waves the deep, nutrient-rich water is raised nearer than normal to the surface, which leads to more productive upwelling. At the wave troughs the opposite occurs as the nutrient-rich water is pushed deeper than normal. The net result of this complex system of interactions is that upwelling events with a duration close to the optimal 10-day period of the coastally trapped waves occur with some regularity in the Benguela upwelling system.

Waldron and Probyn (1992) used an innovative method to estimate the total new primary production of the Benguela system. They established a set of correlations between surface water temperature and nitrate nitrogen in the euphotic zone. Using satellite images of sea surface temperature, they estimated the total nitrate upwelled in the course of one "upwelling event." They observed 19 upwelling events during 1987. After converting the nitrate to carbon equivalents in photosynthesis, Waldron and Probyn estimated the annual new production of the whole Benguela system to be 4.7×10^{13} g C y^{-1}. This value is 0.6–1.4% of various estimates of global total new production in the ocean. As the area of the Benguela system is about 0.02% of that of the world's oceans, it makes the Benguela system 30–65 times more productive per unit area than the average for the world's oceans.

5.6.1 Fish production in the Benguela system

As in other upwelling systems worldwide, sardines/pilchards *Sardinops* and anchovies *Engraulis* are the most abundant fishes. The stocks may be roughly divided into those breeding in the Cape area and those breeding further north off Namibia. The history of the fisheries in each area has been reviewed by Schwartzlose *et al*. (1999) (Fig. 5.20). There are interesting parallels with the fishery of the California Current. Beginning in the 1950s, there was an intensive fishery for *Sardinops ocellata* in both north and south locations. Total landings peaked at over 1.4 Mt in 1968, with by far the largest catches coming from Namibia. Catches fell sharply in 1970 and have not recovered. Fishing for anchovy began in 1963 and peaked in 1987 with landings of about 1 Mt in 1987, with the major landings occurring in South Africa. By 1996 catches were again at a low level, and in 1996 and 1997 catches of sardine exceed those of anchovy.

For the southern stocks, the main spawning ground for both anchovy and pilchards is the inshore water off the southern tip of Africa, centered on Cape Agulhas and extending to Cape Town in the west and Cape Infanta to the east. The area is not particularly productive of plankton, but during the breeding season has a layer of warm Indian Ocean water at the surface that confers stability in an otherwise turbulent area. Starting at the western end of this spawning area is a frontal jet, the "Good Hope Jet," which runs northward along the shelf edge for more than 250 km (Fig. 5.21). Shelton and Hutchings (1982) showed that anchovy eggs and young larvae are carried in the jet, and appear as recruits in the upwelling system north of Cape Town. Note that this arrangement, where the

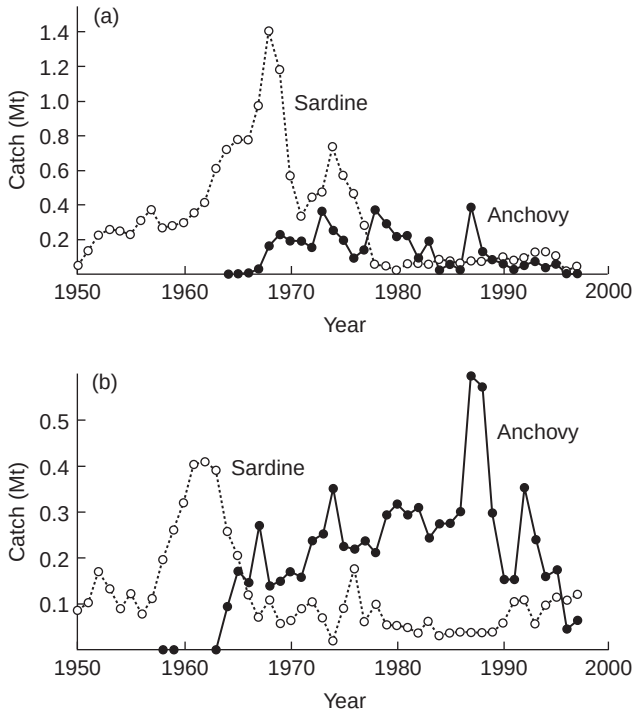

Fig. 5.20 Catches of sardines and anchovies off (a) Namibia and (b) South Africa 1950–96. From Schwartzlose *et al*. (1999).

anchovy spawning ground is "upstream" of the highly productive upwelling area, is the reverse of that found in southern California where the spawning area is downstream of the intensive upwelling.

There is evidence that the relative distribution of the spawning of sardines and anchovy has changed since 1994. Before that date, both species spawned in the same general area off the tip of southern Africa, between Cape Town and Cape Infanta. Since 1994 it has been found that anchovy spawn primarily east of Cape Point, while sardine spawn west of the Cape (van der Lingen *et al.* 2001). The year 1994 was the first in which the acoustically estimated spawning biomass of sardine was higher than that of anchovy, but there is no accepted explanation for the change in spawning habits.

Interesting new insights into the adaptations of a fish population can be obtained by simulating the evolutionary process according to chosen rules, while holding the fish population in a realistically simulated physical environment. Mullon *et al*. (2002) coupled a three-dimensional realistic hydrodynamic model of the Benguela upwelling system with an individual-based model of the anchovy population, in which an evolutionary-based reproductive strategy for adult fish and a passive transport for early life stages were implemented. The rules of the evolutionary model were varied, and it was found that the best fit for the

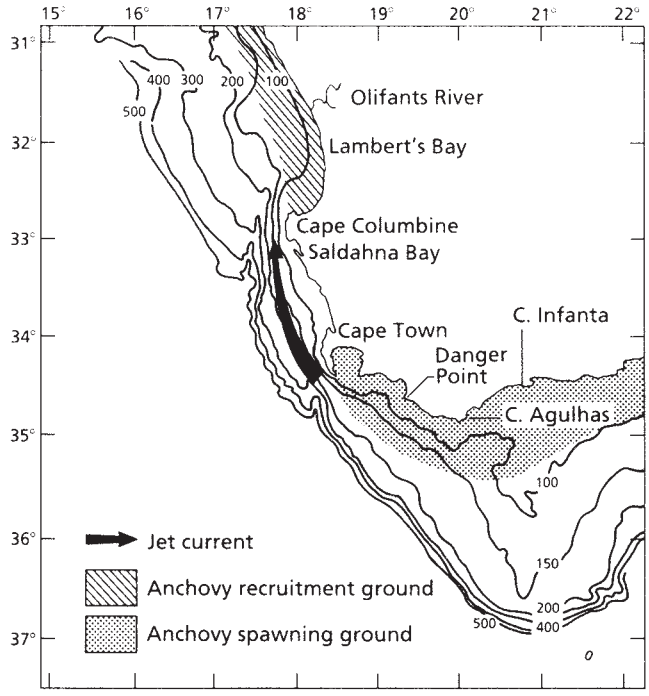

Fig. 5.21 Spawning and recruitment grounds of the South African anchovy, and the jet current that connects them. From Shelton and Hutchings (1982).

observed recruitment pattern was obtained when the fish were selected to avoid being advected offshore, to stay in waters between 16 and 19 °C, and to reach the nursery area between ages 30 days and 60 days. The spawning pattern that emerged from these constraints was a small area on the central Agulhas Bank. Since spawning is known to occur over a much wider area, it was postulated that the spawning population consists of several subpopulations, each with slightly different genetic programming.

5.7 The Somali upwelling system and the Arabian Sea

The Arabian Sea has a boundary current, the Somali Current, which is the analogue of the Gulf Stream in the Atlantic (McCreary *et al*. 1996). For part of the year it flows poleward and generates coastal upwelling. It is the only major upwelling system on a western boundary of an ocean. The upwelled water and the resulting chlorophyll bloom merges with another upwelling system offshore, to create one of the most productive regions of the world's oceans (Nair *et al*. 1989).

The Arabian Sea is characterized by strong seasonal oscillations of physical and biological properties. The warm Southwest Monsoon blows from June to September, and the cooler Northeast Monsoon from December to February. The

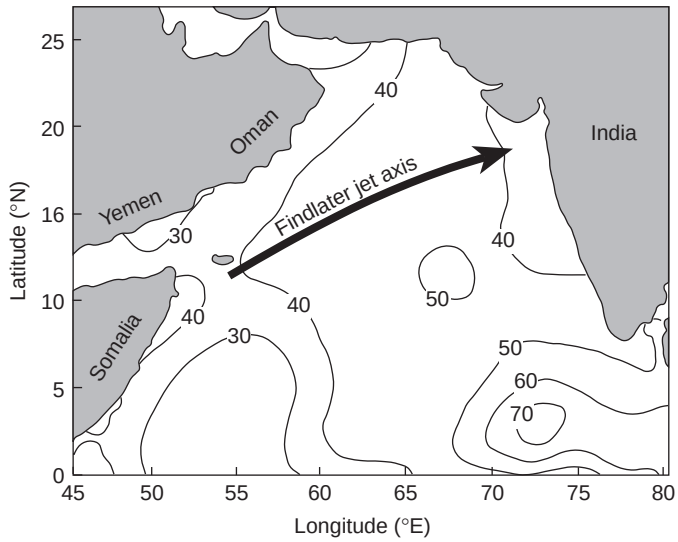

Fig. 5.22 Map of Arabian Gulf showing axis of the Findlater jet in July. Contours are mixed-layer depth in November. Modified, after Brock *et al*. (1993). Reproduced by permission of Inter-Research.

Somali Current, along the coasts of Somalia and Oman (Fig. 5.22) flows north and east during the Southwest Monsoon and gives rise to coastal upwelling. Major upwelling centers are found off the coast of Somalia at about 4° N and at 7–10° N. From the temperatures of the upwelled water it is inferred that some of it must have come from 100–200 m depth (Swallow 1984). Off Oman, the boundary current is relatively weak but the area of upwelling is broader. These upwelled waters have a high nitrate content and stimulate blooms of phytoplankton.

The water upwelled at the coast and carried offshore by Ekman transport merges with water brought to the surface by open-ocean upwelling (see Brock and McClain 1992). During the Southwest Monsoon a narrow, low-level, atmospheric jet, the Findlater jet, blows diagonally across the Arabian Sea, parallel with the coasts of Somalia and Oman (Fig. 5.22). The jet creates an Ekman transport (Section 5.2.2) in the ocean to the right of the wind. The transport is maximum at the center of the jet and decreases with distance toward the left and right. To the left of the jet center less water is moving toward the center than is leaving the center. This creates a divergence in the upper layer. Since sea level cannot drop, the divergence is balanced by water upwelling from below. This is called Ekman suction and is discussed further in Section 8.2.1. To the right of the jet center more water is arriving from the center than is leaving. This creates a convergence of water in the upper layer. The water responds by downwelling, i.e., Ekman pumping (Section 8.2.1). The coastal upwelling and the open-ocean upwelling complement one another and cause a really massive upwelling. It covers an area about 400 km wide and 1000 km long, with a volume estimated at 8 million $m^3\,s^{-1}$, and with an average upward velocity of $1–2 \times 10^{-3}$ cm s^{-1}

(Swallow 1984). The associated nutrients stimulate primary production averaging about 1.5 g C m^{-2} d^{-1} throughout the time of the Southwest Monsoon.

Many authors have described the open-ocean upwelling associated with the Findlater Jet, but it should be noted that McCreary *et al*. (1996) constructed a coupled physical–biological model which reproduced many of the bloom characteristics seen in remotely sensed data, but in their solution open-ocean upwelling was not significant. Instead, most of the observed phenomena during the Southwest Monsoon were explained by coastal upwelling.

During the inter-monsoon periods the waters become oligotrophic, with phytoplankton dominated by picoplankton (<2 μm) with a primary production of about 0.7 g C m^{-2} d^{-1}. When the Northeast Monsoon begins, it causes a complete reversal of the surface currents in the Arabian Sea basin, including the Somali Current. This is the greatest seasonal variation of surface-water components in any ocean basin. The cooler air causes surface-water cooling and deep mixing, which again brings nutrients to the surface and stimulates primary production of about 1.35 g C m^{-2} d^{-1} (Wiggert *et al*. 2000).

At times of phytoplankton blooms the composition of the phytoplankton changes, with a larger component of diatoms. The diatoms are grazed by mesozooplankton, and these are known to be taken by myctophid fish, but the details of the upper trophic levels are not well known. Much of the phytoplankton sinks below the mixed layer and decomposes, giving rise to large volumes of low-oxygen water (<0.2 ml O_2 L^{-1}) between 200 and 1000 m depth throughout the Arabian Sea.

5.8 Some smaller-scale upwelling systems

5.8.1 Summer upwelling off Nova Scotia

Upwelling is thought to occur sporadically on the western margins of the major oceans, but few examples have been well documented. A study of summer upwelling off Nova Scotia, Canada, suggests that it is a major mechanism for transporting nutrients onto the shelf from deep water (Petrie *et al*. 1987). First reports of coastal upwelling in this area go back to Hachey (1935). He found that strong winds from the southwest were correlated ($r^2 = -0.7$) with lower-than-normal sea surface temperatures (SSTs) such that a wind of about 0.9 m s^{-1} would produce a drop in SST of 1 °C. The observations of Petrie *et al*. (1987) are derived from infrared satellite images. Thirteen of them were available for the period June 24 to August 6, 1984. On July 7 most of the water over the Scotian shelf was around 16 °C except that there was a narrow band of cold water close to the coast. A week later there was a substantial area of water of 7–8 °C extending about 20 km from the coast on average with plumes extending up to 60 km from the coast. By July 21 the average width of the cold-water zone was 20–30 km and plumes extended up to 85 km offshore. Four days later plumes extended up to 175 km from the coast. Between July 25 and August 21 the zone of cooler water disappeared.

The authors examined records of alongshore wind stress and found that the mean for the period June 27 to July 27 was 0.03 Pa. They numerically solved the equations of motion for a two-dimensional, two-layer model of the shelf that included time-varying wind stress, representative bathymetry, bottom and interfacial friction, and the effects of varying layer depths. The model predicted that surface waters would move offshore and the thermocline would reach the surface after 8.1 days. The infrared images were spaced about 7 days apart, but the upwelling first appeared on the image of July 7, 10 days after the start of the winds. This observation was taken as good agreement with the model.

The pycnocline was found to upwell at a rate of 20 m in 10 days, over a coastal strip about 10 km wide and 500 km long. This finding gives a vertical transport of about 1×10^5 m^3 s^{-1}. At a mean nitrogen concentration of 10 μmol N L^{-1} the authors calculated that the upwelling of nutrients amounted to 10 μmol N s^{-1} for every strip of shelf normal to the coast and 1 cm wide (or 1 mmol N s^{-1} for every strip 1 m wide). This value is approximately equal to previously calculated nutrient requirements of the phytoplankton. It was therefore concluded that coastal upwelling is an important mechanism supporting primary production on the Scotian shelf.

The satellite images also showed that nearly stationary wave-like features with scales of 50–75 km appeared to grow rapidly in the upwelled temperature front. Results of modeling exercises suggested that these were caused by baroclinic instability. The properties of fronts will be discussed in detail in Chapter 6.

5.8.2 Summer upwelling off the west coast of Spain

The northwest corner of Spain, near Cape Finisterre, is near the northern limit of the upwelling associated with the Canary Current system (Wooster *et al*. 1976). Blanton *et al*. (1984) calculated the Bakun upwelling index off Cape Finisterre and showed that, in most years, winds from the north predominate, causing strong offshore Ekman transport. The authors argued that offshore Ekman transport lowers the sea level at the mouths of the coastal inlets (rias), setting up a seaward pressure gradient that forces the water above the pycnocline out of the rias. Oceanic water is upwelled onto the continental shelf then enters the rias close to the bottom. Tenore *et al*. (1982) documented the enormous biological productivity of these Spanish rias, especially in the form of cultured mussels. Around 1980, two thousand 20×20 m rafts in Ria de Arosa produced annually over 100,000 tons total weight of mussels *Mytilus edulis*. The upwelling and subsequent translocation of nutrient-rich water into the rias is believed to be the secret of this high level of productivity. Blanton *et al*. (1987) used atmospheric pressure maps to calculate the upwelling indices for a point off the western coast of Spain for the period April–September in each of the years 1973–83. They found that the condition index of the mussels (measured as dry weight as a percentage of wet weight of the flesh) was well correlated with the upwelling index ($r^2 = 0.66$, Fig. 5.23). In the best year, 1977, the meat had 15.8% dry weight, while in the worst year, 1983, it had only

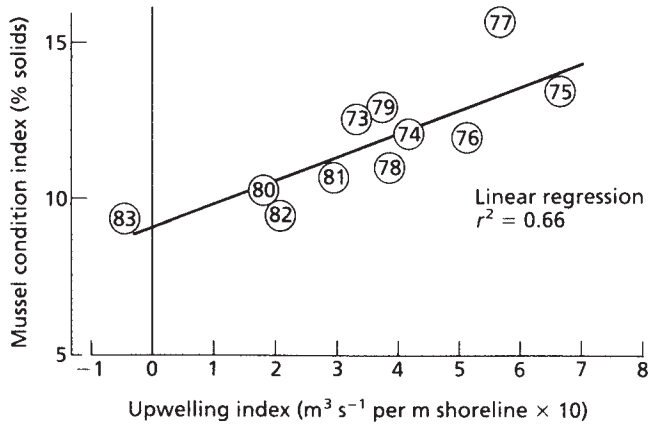

Fig. 5.23 Correlation between mussel condition index (% dry weight in meat) and upwelling index. Numbers indicate years. From Blanton *et al*. (1987).

9.5% dry weight. The authors suggested that if a prediction could be made in the early spring about the most probable intensity of upwelling in the ensuing summer, the mussel culture could be managed more economically. They pointed out that the winds off Spain are influenced by the relative positions of the high-pressure atmospheric cell off the Azores (the "Azores high") and the low-pressure cell off Greenland (the "Labrador" or "Icelandic low"). Long-range forecasts of synoptic-scale weather patterns could be used to provide the appropriate forecasts of pressure gradients and hence of wind strengths, Ekman transports, and the estimated carrying capacity of the rias for the ensuing season.

It seems highly probable that the productivity patterns of a wide range of coastal habitats are affected by the incidence of wind-induced coastal upwelling. We have evidence that it can occur on the western sides of ocean basins as well as in eastern boundary currents. The extent of the phenomenon appears to be a fruitful line of enquiry, which will be pursued in Chapter 9.

5.9 Comparison of system function in the various upwelling systems

Trophic-flow models of production in the four large eastern boundary-current ecosystems were constructed by Jarre-Teichmann and Christensen (1998). The models focused on the five dominant fish species: anchovy, sardine, horse mackerel, mackerel, and hake. They found that the systems were all rather inefficient in terms of energy transfer up the food web. Total catch was correlated with primary production and with the trophic levels of the fish. Properties related to the fishing regime, such as fishing mortality and the fraction of available primary production required to sustain fishery catches, are highly variable among systems and regimes.

In a different approach, Carr (2002) calculated the potential primary production of the four eastern boundary-current upwelling systems, during the years 1997–9, using remote-sensing data. She defined the active area of each upwelling system as the area over which chlorophyll exceeded 1 mg m^{-3}. She calculated primary production by the method of Howard and Yoder (1997), which uses the surface chlorophyll concentration, P_{max}, as a function of temperature, and the mean irradiance of the mixed layer calculated from the surface chlorophyll concentration. Primary production decreased with latitude within each upwelling system, while the extent of the active area was related to the magnitude of offshore transport. The ranking of total primary production (in Gt C yr^{-1}) was Benguela 0.37, Canary 0.33, Humboldt 0.20, and California 0.04. The results may have been atypical because 1997–8 was an El Nino year, which would depress the productivity of the Humboldt and California systems. Taking 1997 alone, the ranking was Humboldt 0.3, Benguela 0.22, Canary 0.09, and California 0.03, which is what one would expect from the ranking of fish landings (see next paragraph). Even so, the primary production does not lead one to expect that the landings from the Humboldt would be three to ten times greater than from the Benguela, as Cury *et al*. (1998) had pointed out. If the calculations are correct, there must be large differences in the efficiencies with which primary production is passed through the food web to support fish production. These differences in efficiency had been noted by Jarre-Teichmann and Christensen (1998).

Cury *et al*. (1998) used maximum yields from 10 upwelling areas around the world as rough indices of their productivity and noted that the productivity of the Peruvian upwelling system is three to ten times greater than the productivity of any of the others. The size of the continental shelf does not by itself explain the difference. Two other environmental variables were examined: the upwelling intensity and the wind mixing. The former was defined as the offshore component of the wind-induced Ekman transport ($m^3\ s^{-1}\ m^{-1}$), while the latter was calculated as the cube of the wind speed ($m^3\ s^{-3}$). Average upwelling indices varied from 0.31 $m^3\ s^{-1}\ m^{-1}$ for South Africa to 1.29 $m^3\ s^{-1}\ m^{-1}$ for Namibia. Wind-mixing indices varied from 103 $m^3\ s^{-3}$ for Ivory Coast–Ghana to 770 $m^3\ s^{-3}$ for South Africa. Using generalized additive models, it was shown that optimum environmental conditions appear to be a combination of high upwelling index with moderate wind mixing. The Peruvian upwelling system is the only one that has these characteristics, with an upwelling index of about 1.2 $m^3\ s^{-1}\ m^{-1}$ and wind mixing about 250 $m^3\ s^{-3}$. The high upwelling index indicates a good supply of upwelled nutrients, while the moderate wind mixing can be compared with the optimum environmental window for recruitment discussed in Section 5.5.2.

5.10 Summary: coastal upwelling and the production of fish

Reviewing this chapter, we see that major anticyclonic gyres in the atmosphere associated with similar gyres in the four major ocean basins – North and South Atlantic, North and South Pacific – give rise to equatorward winds parallel with

the coast along the eastern margins of those basins. The combination of wind stress and the Coriolis effect determine that Ekman transport will take place – i.e., surface waters will move away from the coast. Deeper waters upwell along the coast to take their place, but the intensity of vertical transport is not uniform. It appears to be influenced by topographic features such as headlands and canyons, so that satellite images show complex patterns of intense upwelling, which in the course of time give rise to complex plumes, jets, squirts, and gyres that penetrate varying distances from the coast into the main stream of the boundary current.

This complexity is further compounded by temporal variation in wind strength. Off Peru the process may be continuous more or less year-round but off Oregon, for example, it is confined to the summer season. This seasonality is in part explained by the tendency for the major anticyclones to move poleward in summer and equatorward in winter. Superimposed on this seasonality is "event"-scale variability in which wind stress and the associated upwelling event tend to build and decline over a period of 5–10 days.

Rather surprisingly, it seems that the event-scale variability tends to enhance biological productivity rather than the reverse. There is evidence from several locations that growth of phytoplankton populations (and also feeding by early larval stages of fish) occurs most rapidly when wind stress is low and the water column is well stratified. There seems to be a parallel with the "Gran effect" discussed in Section 3.3.2. In temperate waters it is the alternation between winter mixing and spring stratification that provides conditions required for the spring bloom. In upwelling areas the period of maximum wind stress provides for the upwelling of nutrients and the periods in between provide well-stratified conditions in which the phytoplankton is held in or near the euphotic zone, permitting high photosynthetic rate, rapid uptake of nutrients, cell division, and population growth.

We also saw in Chapter 3 that during well-stratified periods the phytoplankton have a tendency to accumulate in a chlorophyll maximum just above the pycnocline. It seems that these aggregations of phytoplankton cells are necessary for some kinds of zooplankton and for herbivorous fish to feed at their optimal rate. Hence, the times of low wind stress in upwelling areas are the times when strong chlorophyll maxima are formed and when the first-feeding larvae of sardine and anchovy encounter sufficient food for them to make the difficult transition from passive, yolk-absorbing creatures to active herbivores. The timing of their life histories is adapted to the average timing of the upwelling events. Any major disruption of the timetable leads to poor larval survival and hence a poor year-class of fish.

The fish stocks of upwelling areas worldwide are dominated by clupeids such as sardines, pilchards, and anchovies, with mackerel and hakes also being abundant. The clupeids, for the most part, tend to avoid the areas of strong Ekman transport at spawning time. Those in higher latitudes tend to spawn upstream of the major upwelling areas, while those in lower latitudes tend to spawn in sheltered bights with relatively little upwelling, located downstream of the major

upwelling areas. Historically, the lower-latitude stocks have had the higher biomasses. The lower-latitude stocks in the Humboldt Current system have had the largest biomass of all, and these appear to be able to spawn right in the plumes of the major upwelling areas. It has been suggested that it is possible because in the Peru upwelling system, relative to the others, the Ekman transport is less intense and less variable, and extends further from shore. Another analysis suggests that the critical factors for maximum fish production in the Humboldt system are a large volume of water upwelled, but moderate wind mixing.

Historically there have been large fluctuations in fish stocks as indexed by landings. Over-fishing is certainly a factor, but recent work points more and more to long-term changes in climate and ocean circulation as major factors in the fluctuation in stock size. Detailed considerations of large-scale, multi-decadal changes are the subject of Chapter 9.

6

Fronts in coastal waters

6.1 Introduction

It is obvious from the preceding two chapters that continental shelves are mosaics of water masses with different properties. The estuaries and estuarine plumes often have lowered salinities as a result of freshwater run-off, while adjacent waters may be fully saline. Some areas are strongly mixed by tidal currents while the adjacent water mass is stratified. At the boundaries between them there are normally sharp horizontal changes in temperature and other properties.

The waters over the continental shelves are usually less saline than the open ocean, but more prone to be cold in winter and warm in summer. The shelf-break front marks the point of transition. Almost all fronts are regions of enhanced plankton production, which leads to higher fish production. Mooers *et al*. (1978) showed that the shelf-break front off eastern North America moves considerable distances under the influence of winds and the meanders of the Gulf Stream. A long-term plot of the positions occupied by the shelf-break front delineates an envelope within which are found most of the highly productive fisheries of the region. An aerial survey of the distribution of fishing vessels on the east coast of Canada showed the highest concentrations in the vicinity of the shelf-break front (Fournier 1978).

In the coastal upwelling situation that we described in the last chapter, upwelled water moves away from the coast by Ekman transport and eventually arrives at a region where the surface water will be pushed back no further, so the upwelled water sinks under it (see Fig. 6.10, later in chapter). This frontal region is highly productive and one to which large numbers of tuna are attracted.

There is no agreement about the classification of fronts, but a partial listing of those occurring in coastal waters would be: tidal fronts (also known as shelf-sea fronts), shelf-break fronts, upwelling fronts, plume fronts, estuarine fronts, and fronts associated with geomorphic features such as headlands, islands, and canyons. In this chapter we investigate the distinctive physical and biological properties of each.

6.2 The physics of fronts

6.2.1 Introduction

As noted above, variables such as temperature, salinity, and density in the ocean do not change gradually with horizontal distance. Instead, we find large regions where horizontal gradients are small, bounded by narrow regions or fronts where horizontal gradients are large. Most of the fronts we are familiar with are identified by horizontal gradients in density. However the most numerous type of front is probably the compensating front found in the surface mixed layers of the open ocean. In these fronts there is no horizontal density gradient but there are horizontal gradients of temperature and salinity whose effects on density cancel or compensate each other.

The most biologically active fronts are the shelf-break fronts at the edges of many continental shelves, the tidal fronts discussed in Section 4.5.1, and the upwelling fronts discussed in Section 5.2.2. The latter tend to be on the eastern sides of the major oceans while the shelf-break fronts tend to be on the western sides. The largest fronts are found in the open ocean associated with the western boundary currents such as the Gulf Stream and the Kuroshio Current. The front associated with the Gulf Stream front is obvious in Plate 2 by the tongue of warm water flowing north with the cooler water on the left. There are many other fronts

visible in this as in other similar images now available from all parts of the world ocean.

The ubiquity of fronts in the ocean is further illustrated by two recent studies. Using temperature data derived from satellite-borne radiometers between 1985 and 1996, Mavor and Bisagni (2001) were able to map fronts over a large region of the western North Atlantic. They found fronts of all sizes and permanence throughout the region and were able to illustrate seasonal variability in some. In a study of open-ocean fronts Rudnick and Martin (2002) used 15 years of closely spaced profiles of temperature and salinity from towed instruments to map the presence of fronts in the Pacific, Atlantic, and Indian Oceans.

In the following we look more closely at tidal and shelf-break fronts in coastal waters and baroclinic fronts and compensating fronts in the open ocean. Over the past 10 years understanding of the mechanisms within these fronts has dramatically increased, especially for the fronts in coastal waters. Many of the advances have been made using computer simulations which have grown in sophistication in step with the increasing power of computers. We skip upwelling fronts, which were examined in Section 5.2.2.

6.2.2 Fronts in coastal waters

(a) Shelf-break fronts

From a biological point of view shelf-break fronts are probably the most important. Along the eastern seaboard of North America they can be found at the edge of the continental shelves from Davis Strait to Cape Hatteras, in close association with some of the worlds most productive fisheries.

It has been clear for many years that these fronts contain higher biological productivity. Fournier *et al*. (1977), for example, working on the Scotian Shelf south of Nova Scotia, observed maxima in biological variables such as chlorophyll, primary productivity, zooplankton, etc. in the region of the shelf-break front. The authors suggested that the higher productivity is due to upward mixing of nutrient-rich deeper water into the euphotic zone over the shelf. They further suggested that the deep water over the shelf is renewed from the offshore, and offered three mechanisms to accomplish this: estuarine circulation, wind, and Gulf Stream meanders. In the estuarine circulation it is assumed that freshwater run-off tends to move offshore, entraining more water as it goes. The deep flow onto the shelf is in reaction to this offshore upper-layer flow. Large-scale wind events and Gulf Stream meanders were expected to force similar flows. Marra *et al*. (1990) studied the shelf-break front in the Mid-Atlantic Bight and concluded that the higher productivity in the upper layer of the front was due to large-scale deformations of the front. As the front, which slopes seaward, is pushed shoreward, deep water lying over the shelf rises up the front. The higher concentration of nutrients in this water rising into the euphotic zone leads to higher productivity.

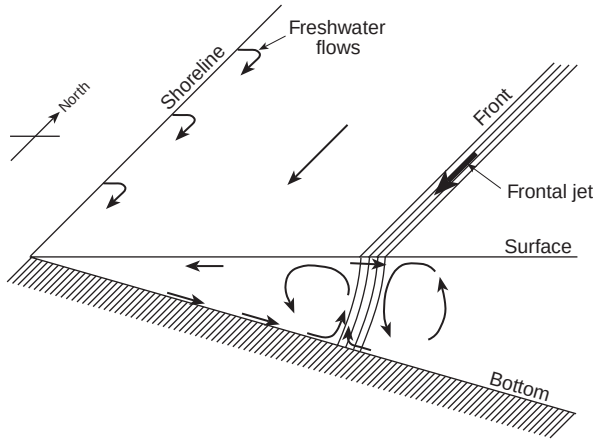

Fig. 6.01 Flows associated with a shelf-break front according to the numerical model by Chapman and Lentz (1994).

In the 1990s high-resolution numerical models were used to study the circulation in these fronts. One of the most satisfactory to explain the higher productivity in shelf-break fronts is by Chapman and Lentz (1994). Their model begins with a flow of fresh water into the ocean that is evenly distributed along the coast. Coriolis force turns the fresh water to the right (in the northern hemisphere) to flow parallel to the coast. A density front parallel to the coast is thereby created between the fresher water from the land and salt water of the ocean. As the front develops with time it moves offshore until there is an internal balance that maintains the front at a reasonably constant position. A summary of the flows of water when the front reaches a steady state are illustrated in Fig. 6.01.

The coast is on the left, running south to north. Arrows along the coast indicate the evenly distributed freshwater flow from rivers into the ocean. The offshore front is marked by isopycnals sloping from the surface to the bottom. At the surface of the front there is a high-velocity southward jet which diminishes with depth and reverses direction near the bottom. The water in the region between the front and the shore generally moves south as indicated, but important secondary flows are created. These are shown in the vertical plane between the surface and the bottom. At the bottom the generally southerly flow diminishes due to friction. This creates an Ekman transport toward the east within a thin boundary layer. This flow is similar to the surface Ekman layer discussed in Section 5.2.2. To compensate for the offshore flow there is return flow toward the west as indicated by the arrow near the surface.

Water nearer the shore tends to be lower in density than the water offshore. Thus the water in the eastward flow in the bottom boundary layer tends to be progressively less dense than the water above the boundary layer. This leads to the vertical circulation indicated on the shoreward side of the front whereby water from the bottom rises up toward the surface on the shoreward side of the front.

As mentioned, the southward flow in the frontal jet reverses direction to produce a northward flow in the deeper water of the jet. At the bottom of this northerly current there is another bottom Ekman layer in which the flow is toward the west, opposing the flow in the Ekman layer on the shoreward side of the front. These opposing flows are important both in keeping the horizontal position of the front stable and also in supplying the deep high-nutrient water from the offshore side to the interior of the front. As shown by the arrows in Fig. 6.01, water in the onshore boundary-layer flow moves westward then up into the interior of the front. The model also indicates the counterclockwise flow indicated on the offshore side of the front.

What makes this model most attractive is that the westward flow in the boundary layer under the front and its subsequent upward flow into the front have been confirmed by observation. This was done by Houghton (1997) in a superb experiment in which dye was injected into the water within the boundary layer on the offshore side of the front. The dye was then followed as it moved under the front then upward into the front in spite of the fact that the front itself moved 12–15 km toward the shore during the period of observation. This was the first time such a flow had been detected. Previous current measurements having been fixed in space rather than moving with the front could not capture the details of the flow within the front. Later experiments described by Houghton and Visbeck (1998) refined the technique and improved the estimates of the speed of the dye movement and the heat exchange between the dye-marked water and the surroundings. These authors strongly suggest that these flows are responsible for the increased biological activity in the shelf-break.

(b) Tidal or shelf-sea fronts

Tidal fronts, as discussed in Section 4.5.1, are boundaries between stratified water and unstratified water, as illustrated in Fig. 6.02(a). They occur over continental shelves where tidal currents generate levels of turbulence at the bottom that are

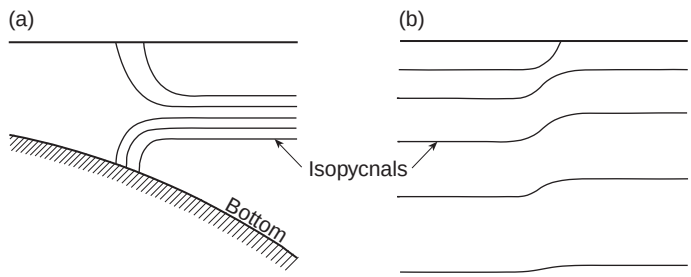

Fig. 6.02 (a) Density section through a tidal front. The region on the left, in the shallower water, is unstratified while the region on the right remains stratified. (b) Density section through a geostrophically balanced current in which the flow is out of the page (in the northern hemisphere) and decreases with depth.

high enough to completely mix the water. Mavor and Bisagni (2001), in a study of fronts on Georges Bank based on satellite-borne radiometer data obtained between 1985 and 1996, demonstrate the seasonal cycle of the tidal front. During winter the upper mixed layer covers the bank and no tidal front is visible. With the warmth of spring, the upper water becomes stratified but over the central part of the bank turbulence is high enough to keep the water column unstratified. As summer progresses the front separating the unstratified water over the bank from the stratified water completely encloses the central region. With the cooling of autumn and winter the stratification on the stratified side of the front is eradicated and the front disappears.

The main reason tidal fronts are of interest is the increased biological activity associated with them. One mechanism to explain this was suggested by Pingree *et al*. (1975). It depends on the variation in the speed of tidal currents between the spring and neap tides (Chapter 7). As the current speed increases during the spring tides, the level of turbulence generated at the bottom increases. This leads to increased mixing in the water column and the area of mixed water increases. The boundary between the mixed and stratified water moves toward deeper water. When the tidal currents decrease during the neap tides, the turbulence declines and the front moves toward shallower water, allowing the area of stratified water to move into the region of unstratified water.

As the front advances, the newly stratified water will contain nutrient levels characteristic of the previously mixed water which according to Simpson and Hunter (1974) are higher than in the upper stratified layers, where presumably they have been depleted by biological activity. Thus, the newly formed part of the front should contain higher concentrations of nutrient than the water that has been stratified for a long time.

Recently a new and perhaps more promising flow of nutrients into tidal fronts has been discovered and explored. Chen and Beardsley (1998), in a computer model of the flow over the steep slopes at the edge of Georges Bank, reveal the existence of a near-bottom flow across the tidal front. The flow is similar to the flow under a shelf-break front mentioned above, in that it is from the deeper side of the front to the shallower side, but the mechanism is different. In the tidal front the strong tidal currents, together with the steep bottom slope and the stratification on one side, combine nonlinearly to produce the near-bottom up-slope flow. The nonlinear effect arises because the velocity of the water varies rapidly in space. Assume, for example, that the average flow speed increases with distance above the bottom and a particle of water moves up-slope on the rising tide further off the bottom than when it returns down-slope on the falling tide. This particle of water moves further up-slope on the rising tide than down-slope on the falling tide. Thus a net flow of particles develops up the slope of the bank under the tidal front. The net flow following the particle is called the Lagrangian current – as opposed to the Eulerian current, which is the current measured at a fixed point. The difference between the Lagrangian and Eulerian currents is the Stokes drift.

Following the modeling work of Chen and Beardsley (1998), Lough and Manning (2001) obtained a detailed set of measurements over Georges Bank, including satellite-tracked drifters and profiles of temperature, salinity, and current velocity. They were able to confirm the existence of the on-bank flow beneath the tidal front as well as other features. These are discussed more fully in Section 6.3.5 and illustrated in Plate 4. Houghton (2002), using dye as a tracer, was able to confirm the existence of the predicted on-bank flow under the tidal front.

(c) Eddies

A perspective drawing of a tidal front with some of the processes associated with it is shown in Fig. 6.03, based on work by Simpson (1981). The front at the surface is shown to be irregular in shape with eddies that twist the cold and warm waters together. It is often suggested that these cause water to be exchanged across the front and thereby contribute a significant flux of nutrients.

In an attempt to examine the potential effects of eddies, Pingree (1979) analyzed a number of eddies in the front found at the Celtic Sea shelf break. His analysis showed that the eddies had a diameter of 20–40 km and may have been created by baroclinic instability. His suggestion, which has been taken up by others, is that the eddies transport nutrients across the front and probably contribute to the enhanced biological productivity in the front. Building on the theoretical work of meteorologists, he derived the equation

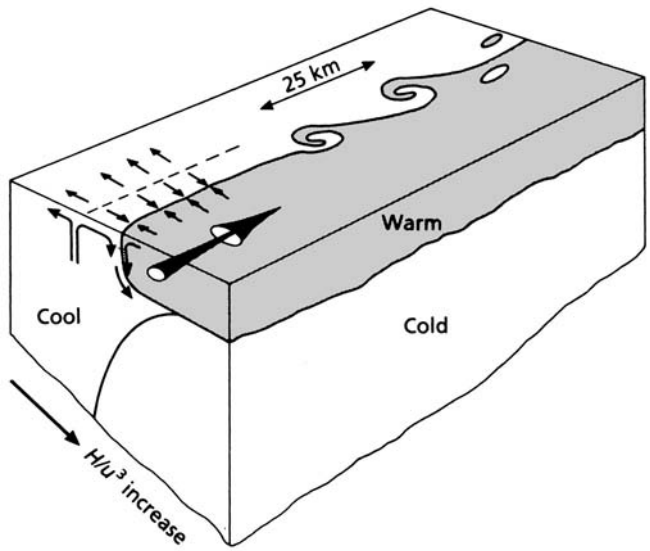

Fig. 6.03 Diagram of the structure and circulation of a tidal front, after Simpson (1981). Note strong along-front mean flow, convergence and downwelling at the front, upwelling on the well-mixed side, and frontal eddies, some of which close on themselves to form isolated patches.

$$F_E = \gamma(gD\Delta\rho/\rho)^{1/2}D\Delta C \tag{6.01}$$

to estimate the flux, by the eddies, of nutrients across the front. F_E is the flux of the nutrient C that exhibits a difference ΔC across the front, ρ is the density, $\Delta\rho$ is the density difference across the front, D is the depth of the upper layer, g is the acceleration due to gravity, and γ is a constant derived from theoretical considerations and equal to 0.0055.

An alternative method of calculating the nutrient flux due to eddies was suggested by Garrett and Loder (1981). In their scheme the nutrient flux is just the number of eddies times the eddy volume times the difference in the nutrient concentration, ΔC. The radius of the eddies is assumed to be four times the Rossby deformation scale, R_i (Section 5.2.3), because this value is the length of the fastest-growing perturbation in baroclinic instability theory. The volume of an eddy of depth D is then $16\pi R_i^2 D$ and the supply of nutrient is $16\pi R_i^2 D \times \Delta C$. If eddies are exchanged across the front every $16R_i$ in time T, the nutrient flux is

$$F_E = \pi R_i \times D \times \Delta C/T \tag{6.02}$$

We shall return to this phenomenon in Section 6.3.3, where the relative magnitudes of the various processes are discussed.

6.2.3 Fronts in the open ocean

(a) Fronts in baroclinic currents

The long crooked finger of yellow lying close to the coast past Cape Hatteras in Plate 2 is the warm water of the Gulf Stream flowing north. The figure, based on a compilation of infrared satellite images, also shows the Gulf Steam turning eastward at the latitude of Chesapeake Bay. On both sides of the flow, and especially to the west or north, the color changes rapidly to green and blue, indicating a rapid drop in temperature. From shipboard measurements, we know that the horizontal temperature change across this 50 km front is roughly 10 °C at the surface. The temperature fronts are intimately tied to similar changes in salinity and density. Thus, a map of one variable is similar to the map of the others.

An idealized section of the density structure across a current such as the Gulf Stream is illustrated in Fig. 6.02(b). The density front associated with the current is the region in the center of the figure where the isopycnals change depth. On either side of the current the isopycnals are flat and no horizontal gradient exists. With depth, the current, along with the horizontal density gradient, decreases. These are characteristics of a baroclinic current as opposed to a barotropic current in which the flow remains constant with depth.

To a first approximation the flow in baroclinic currents is in geostrophic balance. This means (Section 4.2) the flow is horizontal and perpendicular to both the horizontal pressure gradient force arising from the tilted density field and the

Coriolis force which balances it. Under this scenario there are no vertical motions that might bring the nutrient-rich water from the deeper layers up to the euphotic zone to increase biological production.

Olson (2002), among others, points out that vertical currents will be produced within current meanders or loops in the current. When the eastward-flowing Gulf Stream turns to the left, for example, the slope of the density surfaces within the current decrease. This creates a horizontal divergence in the flow on the left side, forcing deeper water to rise toward the surface. When the current turns to the right to complete the loop the opposite happens. Density surfaces become steeper, creating a convergence in the horizontal flow resulting in a downward flow from the surface layer. It is suggested that the upward flow in the first half of the loop probably explains the enhanced biological activity sometimes observed on the north side of the Gulf Stream.

Understanding the details of the situation from shipboard observations is especially difficult because of the high speed of the current (100 km day^{-1}) and relatively long delay between an increase in nutrients and an observable biological response. Anderson and Robinson (2001) avoided this difficulty by studying the problem with a physical–biological model that simulated the details of the flows and biological processes in the Gulf Stream. They found an increase in biological activity associated with meanders, but the activity did not exceed levels found in the slope waters lying north of the current. In another large open-ocean baroclinic flow, the Antarctic Circumpolar Current, Moore and Abbott (2002) studied details of the chlorophyll distribution. They reported that chlorophyll tends to be higher in regions where the current is interacting with large bathymetric features which would disturb the path of the flow, creating meanders. Presumably the enhanced chlorophyll is due to upward nutrient-rich flows in the meanders or eddies.

(b) Mixed-layer fronts

In regions of well-developed mixed layers horizontal temperature and salinity gradients are concentrated into narrow fronts surrounding large areas of very low horizontal gradients. The density difference across the front due to the temperature change is roughly equal and opposite to the density difference due to the salinity change. In this situation there is no horizontal density gradient through the front. These are also called passive fronts or compensating fronts.

Rudnick and Ferrari (1999) demonstrated, in a carefully controlled experiment in the Pacific Ocean, that the temperature and salinity compensation exists down to scales of 10 m. A world survey of such fronts is presented by Rudnick and Martin (2002) based on 15 years of temperature and salinity data from towed, depth-varying instruments. They conclude that compensating fronts 3–4 km wide occur in all the oceans when the mixed layer is deep and where both temperature and salinity vary horizontally.

The horizontal temperature and salinity gradients are probably concentrated by a combination of slumping and vertical mixing (Rudnick and Martin 2002).

The slumping occurs when a horizontal density gradient is created in the mixed layer. The heavy water slumps under the lighter water. The processes that maintain the mixed layer, wind mixing and convection, then homogenize the mixed layer vertically. Thus horizontal density gradients are eradicated. The horizontal scale of the fronts formed this way is less than the internal Rossby radius (Section 5.2.3). When a horizontal density gradient is formed with a scale larger than the Rossby radius horizontal currents will be initiated before slumping is complete. The currents lead to a geostrophic balance which then maintains the current and the horizontal density gradient.

It has been suggested that nutrients and phytoplankton in the upper layer will also be concentrated in the compensating fronts like temperature and salinity. This may lead to temporary regions of enhanced biological activity, although the magnitude of this effect has yet to be demonstrated.

6.3 The biology of tidal fronts

6.3.1 Tidal (or shelf-sea) fronts

A concise description of the mechanism underlying the occurrence of shelf-sea fronts was given by Simpson (1981):

> Over the continental shelf tidal flows exert strong frictional stresses on the seabed. In stress terms, these tidal streams are equivalent to hurricane-force winds in the atmosphere blowing regularly twice a day. As well as playing an important part in the tidal dynamics, these stresses serve to produce turbulent kinetic energy which is responsible for vertical mixing.
>
> Variations in the level of tidal stirring divide the shelf seas, during the summer regime, into well mixed and stratified zones separated by high gradient regions called fronts.

The details of tidal waves and currents will be discussed in Chapter 7, but we may note in passing that most of the dissipation of tidal energy occurs on continental shelves, and the extensive shelf seas of northwest Europe are believed to dissipate one-eighth of the world's tidal energy, about 19×10^{10} J s^{-1} (Miller 1966). One of the earliest systematic studies of a shelf-sea front was Simpson's (1971) study of a persistent front in the Irish Sea. His record of the profile is shown in Fig. 6.04. As the diagram shows, there were tidally mixed waters at 13.6 °C on the eastern side of the front and stratified waters (>15 °C at the surface, <13.2 °C near the bottom) on the western side. As one passed over the front there was a change of surface temperature of 1.4 °C within about 2 km. In a later study of the same front, Simpson and Hunter (1974) reported that in August the nitrate–nitrogen content of the tidally mixed water was about 2 μmol L^{-1} while that of the surface water in the stratified region was less than 1 μmol L^{-1}. On the other hand, the deep water in the stratified region contained 7 μmol L^{-1}. They estimated

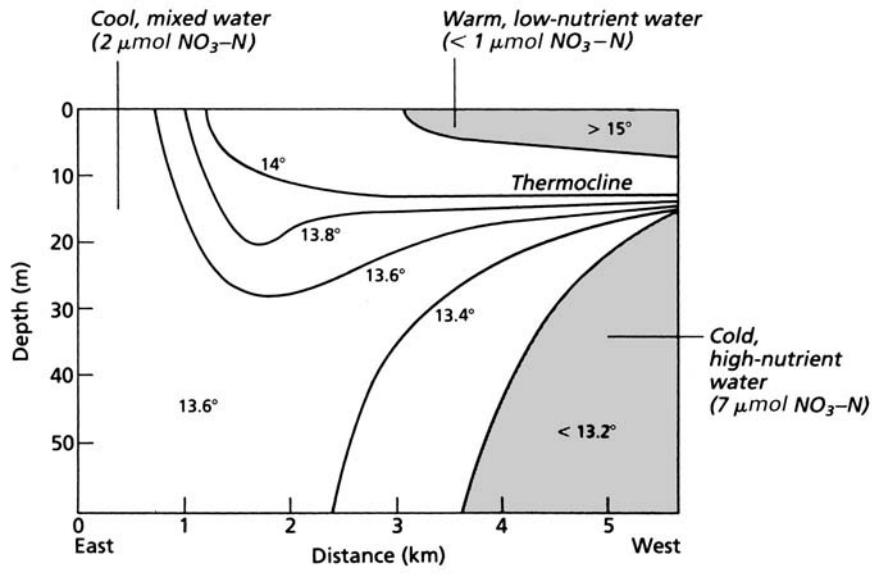

Fig. 6.04 Diagram of the structure of a front in the Irish Sea, based on data in Simpson (1971) and Simpson and Hunter (1974).

that the chlorophyll content of the mixed water was about 1.5 mg m^{-3} (1.5 μg L^{-1}), while that in the surface water of the stratified layer was only 0.5 mg m^{-3}. A moment's reflection on these results (see Fig. 6.04) suggests that if there was a mechanism for mixing the nutrient-rich deep water from the stratified region into the mixed region, or a mechanism for mixing the somewhat nutrient-enriched water from the mixed region into the stratified surface layer, primary production could be expected to increase. As we saw in 6.2.2(b) and will discuss in 6.3.5, such mechanisms do exist.

During the early 1970s biologists had been noticing that shelf-sea fronts were often the sites of persistent high densities of phytoplankton and zooplankton. Le Fèvre and Grall (1970), investigating the distribution of *Noctiluca* (a dinoflagellate that, in high abundance, imparts a blood-red color to the water, known as a "red tide"), noted that red tides occurred in a region off western Brittany characterized by convergence of surface waters with tidally mixed waters on the landward side and stratified waters on the seaward side. It was later shown that this frontal structure extends northward toward the coast of England, across the mouth of the English Channel, and is now known as the Ushant front. Pingree *et al*. (1975) reported that there was high phytoplankton biomass along it, and that the most abundant organism in the phytoplankton was *Gymnodinium aureolum*, a species also noted for red tide formation.

Since the northwest European shelf area was the site of these pioneering studies of shelf-sea fronts, we may make this area the subject of our first case study.

6.3.2 Biological production at northwest European shelf-sea fronts

After the work of Le Fèvre and Grall (1970), the next biological study on the Ushant front was that of Pingree *et al*. (1974). They worked on a section of the front between Jersey and Guernsey and drew particular attention to a strong accumulation of floating seaweed, accompanied by numerous crustaceans, fish, and birds, along a line that was obviously a site of convergence and sinking. The authors drew attention to the possibility that high biomass of phytoplankton at a shelf-sea front might be as much due to convergence as to stimulated growth of phytoplankton at the front. The physics of this situation was discussed in Section 6.2.2(b).

On the next cruise Pingree *et al*. (1975) made a series of observations across the Ushant front in the mouth of the English Channel and to the west of Brittany. On each crossing of the front they encountered a chlorophyll peak. A detailed section (Fig. 6.05) showed that there was a persistent chlorophyll maximum from the surface down to the pycnocline on the stratified side of the front, and a subsurface chlorophyll maximum in the pycnocline some distance behind the front. The suggested explanation was that during the spring-tide period of maximum tidal currents the front is pushed back into the previously stratified area, so that nutrients are brought to the surface. When the tidal currents relax during the neap tides, the waters close to the front that have previously been tidally mixed become stratified and there is a burst of phytoplankton growth. Simpson and Pingree (1978) obtained similar results. They also obtained records of internal wave activity in the stratified region and explained the subsurface chlorophyll maximum in the pycnocline just behind the front as resulting from vertical transport of nutrients across the pycnocline during the passage of internal waves.

In the earlier study (Pingree *et al*. 1975) measurements had been made of the parameters of primary production. In addition to chlorophyll, the researchers measured the light extinction coefficient, the assimilation index (rate of carbon fixed per milligram chlorophyll-*a*), and integrated water-column primary productivity, which they expressed relative to a value of unity for the vertically mixed regime. In the stratified waters away from the frontal region they found that primary production below the thermocline was negligible, but primary production within the thermocline accounted for at least 50% of the total carbon fixed. In the frontal region with a weak thermocline, water-column production was 6.5 times greater than in the tidally mixed area but it was achieved by having more than 40 times the concentration of chlorophyll, which had a relatively low assimilation index.

Subsequently Tett (1981) constructed a one-dimensional model based on Pingree *et al*. (1975). While acknowledging that several mechanisms for the enhancement of primary production might be at work, he singled out vertical mixing as the dominant factor. He modeled the upper layer of the stratified region as nutrient-limited, and the lower layer as light-limited. He considered that in the tidally mixed area the phytoplankton were light-limited because they experienced too low an average level of illumination during their vertical excursions.

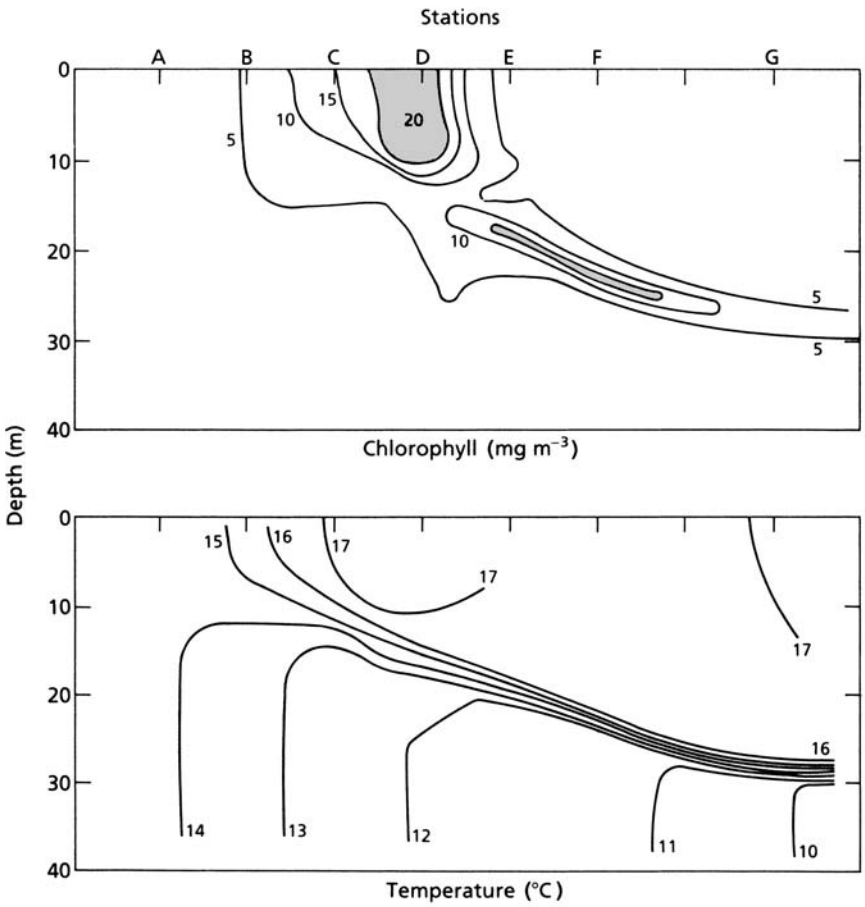

Fig. 6.05 Section through the Ushant front, July 1975, showing a high concentration of chlorophyll near the surface on the stratified side of the front and another high concentration lying just above the thermocline. After Pingree *et al*. (1975).

He considered that in the frontal region, where the pycnocline shallows, the phytoplankton were subject to minimal turbulent transport and were held in a region of moderate illumination from above and moderate rates of nutrient supply by diffusion from below. Model parameters were taken from relevant values in the literature, except that vertical diffusivity was computed from observed vertical temperature gradients and appropriate values for the mean downward heat flux in summer, and physical conditions were set to resemble the situation at a front near the Scilly Isles.

The model was used to simulate changes in stratified, mixed, and frontal stations for 40 days, by which time a steady state had been reached and it was found that the distribution of nutrients and chlorophyll closely resembled the natural situation at the front. In discussion, Tett (1981) emphasized that his aim was only to show that it is *possible* to explain much of the distribution of chlorophyll at a

front as a result solely of vertical mixing of nutrients and chlorophyll. He made no claim that this mechanism was the only process at work.

Recalling the physical mechanisms discussed in Section 6.2.2(b), we see (Fig. 6.03) that it is now understood that a typical shelf-sea front has a strong mean flow parallel with the front, giving rise to baroclinic eddies that often close in on themselves and break free, forming patches of cool water on the warm side, and vice versa. These patches are readily seen in satellite images. If such a water mass, originating from the cool side, eventually mixes with the nutrient-deficient water on the warm side, or vice versa, there will be a net transport of nutrients. This mechanism is one possibility for enhancement of primary production.

In a review of the biological implications of fronts on the northwest European continental shelf, Holligan (1981) pointed out that the distribution of chlorophyll and primary production at the Ushant front varies seasonally (Fig. 6.06). In late April and early May the Ushant front marks the landward limit of the spring bloom taking place in stratified waters offshore. As the season progresses, those diatoms that are not removed by grazing tend to sink and are replaced by flagellates (mostly dinoflagellates) that flourish in the boundary zone between the warm, wind-mixed layer and the cool, tidally mixed water. Finally, by late September, phytoplankton are again most abundant in the surface water on the stratified side of the front. The highest phytoplankton standing crops of the year are found when the flagellates bloom close to the stratified side of the front in July and August.

Holligan (1981) also pointed out that the depth of the mixed water on the Ushant front is 60–100 m. As a consequence, the growth of phytoplankton is light-limited and inorganic nutrients are never fully depleted. Fronts that form in shallow water have a different biological dynamic, for the phytoplankton in the tidally mixed water may not be light-limited, but more probably nutrient-limited. Pingree *et al*. (1978a) identified shallow fronts in the North Sea off Flamborough Head and in the area between the Scottish Island of Islay and the northern tip of Ireland. The tidally mixed areas appeared to have higher nutrient concentrations than the stratified regions, presumably because nutrients were being regenerated by the benthos. The enhanced chlorophyll concentrations associated with these fronts were once again ascribed to the alternation of mixing and stratified regimes present at certain places as a result of the alternation between neap and spring tides.

After presenting this review, Holligan and his colleagues made several intensive studies of the Ushant front (Holligan *et al*. 1984a, 1984b). In late July and early August 1981, a large interdisciplinary team described the vertical distribution of the plankton at three stations representative of stratified, frontal, and vertically mixed regions. The phytoplankton was most dense in the frontal regions (26.5 g C m^{-2}) and was dominated by the dinoflagellate *Gymnodinium aureolum*. At the stratified station there was a relatively small biomass (0.42 g C m^{-2}) of small naked flagellates that were concentrated at a subsurface chlorophyll maximum. The biomass at the tidally mixed station was intermediate in value (7.91 g C m^{-2}) and consisted mainly of diatoms.

Note that these results are explicable in terms of properties discussed in earlier chapters. Diatoms, which tend to be larger than flagellates (although the size

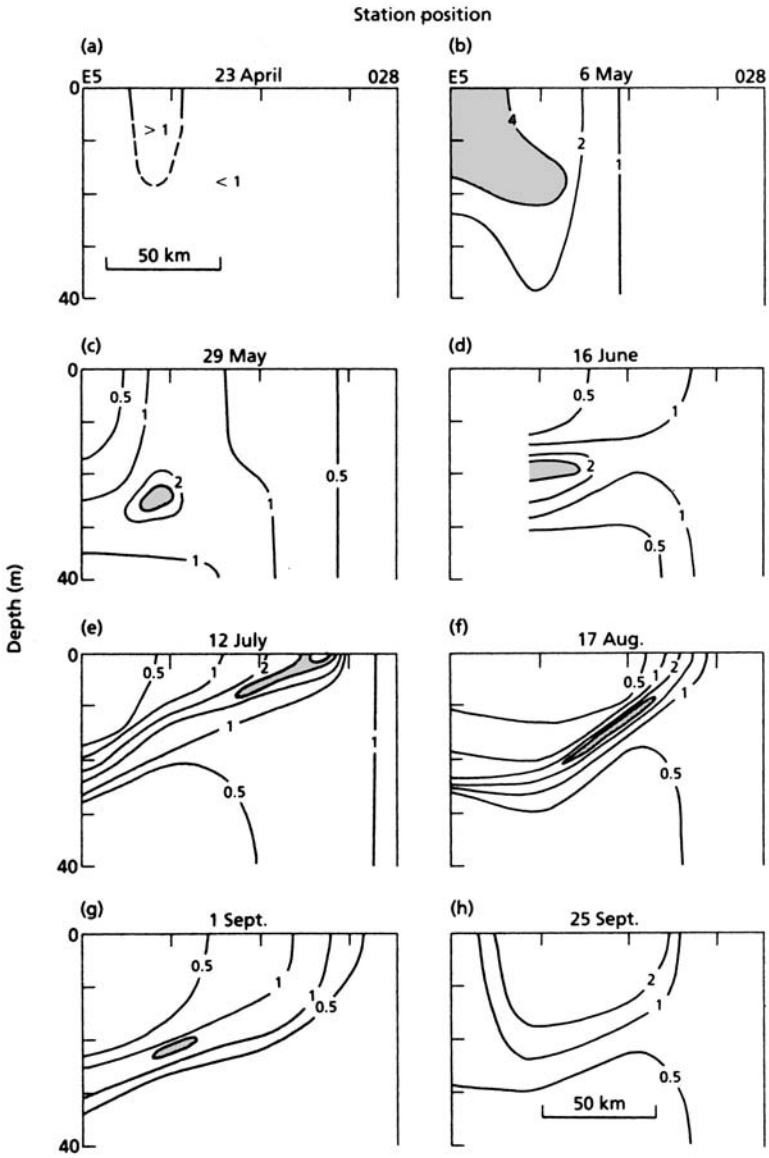

Fig. 6.06 Distribution of chlorophyll-*a* (mg m^{-3}) across the Ushant tidal front on dates given. From Holligan (1981).

ranges overlap), have a marked tendency to sink, and flourish best under turbulent conditions that bring them back to the surface from time to time. The small flagellates in the stratified waters form a subsurface chlorophyll maximum close to the thermocline, where there is a small but significant steady vertical transport of nutrients, possibly supplemented by bursts of increased vertical transport under the influence of internal waves. It is also possible that the flagellates make use

of their locomotory powers to migrate down through the nutricline to take up nutrients and back up again to reach improved illumination (Holligan 1981; see also Kamykowsky *et al*. 1988). Fogg (1985) reported a similar distribution of phytoplankton types in waters adjacent to a front in the western Irish Sea.

When turnover rates were calculated for the phytoplankton (Holligan *et al*. 1984b), it was found that the small flagellates in the stratified, nutrient-limited surface waters were turning over rapidly, estimated at 1.17 doublings per day, the diatoms in the mixed region were achieving only 0.16 doublings per day, and the flagellates in the frontal region were found to have a negative index of population growth. The authors estimated the vertical diffusion coefficient in the stratified region and the frontal area from observations on heat flux, then applied it to the observed nitrate gradient to determine the nitrate flux through the thermocline. Their results suggested that in the stratified region the small flagellates were obtaining about half their nitrogen needs from upwelled nitrate and the other half from recycling of ammonia. Results in the frontal region suggested that the vertical flux of new nitrogen was sufficiently high to have accounted for the accumulation of high biomass of *Gymnodinium* earlier in the season. They stated that the precise mechanisms that permit the accumulation of large biomasses of dinoflagellates in the frontal region are not yet clear, but suggested that one factor is that they appear to be subjected to low grazing mortality compared with other types of phytoplankton.

At each of the three stations studied, the standing stock of microzooplankton and bacteria was between 2.3 and 3.2 g C m^{-2}, with bacteria comprising 10–30%. At the stratified station, though not at the others, the biomass of consumers exceeded that of the phytoplankton. Respiration data indicated that the mesozooplankton were responsible for less than 10% of the oxygen consumption, and microheterotrophs were responsible for the greater part of biological energy dissipation.

6.3.3 What causes dense phytoplankton patches on shallow-sea fronts?

From what we have seen so far, there are two possible mechanisms to account for the high densities of phytoplankton commonly found on shallow-sea fronts: advection as a result of the convergent flows that have been observed at these fronts, or *in situ* growth of phytoplankton populations stimulated by some mechanism for transport of nutrients into the mixed layer of the stratified zone adjacent to the front. As we shall see in Section 6.3.5 and Plate 4, these processes are becoming better understood.

We have seen that the high biomass of phytoplankton is usually found in surface waters on the stratified side of the front in spring and autumn, but in the thermocline in summer. In Chapters 3 and 4 we saw that a spring bloom in surface waters is normally associated with the shallowing of the mixed layer to a critical depth (the Gran effect). This relationship will account for the bloom formation over the whole of the stratified region of the continental shelf but not

for the elevated phytoplankton biomass and productivity adjacent to the front. To achieve this increase by *in situ* growth requires that the supply of nutrients be augmented. There are two possible routes for the nutrients to come, either horizontally across the front from the tidally mixed region or vertically from the nutrient-rich water mass below the thermocline. Let us first examine mechanisms of cross-frontal transport.

(a) Spring–neap tidal cycle

The mechanism most often cited by Pingree and his co-workers is the movement of the front during the spring–neap tidal cycle mentioned in Section 6.2.2(b). During spring tides the tidal currents are at their maximum strength, which means that tidal mixing extends to regions with deeper water – i.e., there is an erosion of the stratified region. During this phase, nutrients from below the thermocline will be brought to the surface in the area covered by the excursion of the front. As the tidal currents relax toward the neaps, the area of tidally mixed water decreases, permitting stratification to return in that same area covered by the excursion of the front. Simpson and Bowers (1981), using satellite images, found that the average spring–neap excursion for eight tidal fronts lying west of Great Britain was 4 km. Loder and Platt (1985) used this figure to calculate that a front advancing and retreating 4 km might cause a supply of 0.12 mmol s^{-1} of nitrate to each meter length of the frontal zone integrated over depth. Similar results were obtained by Morin *et al*. (1993) using satellite-derived temperature data and directly observed correlations between temperature and nitrate content of the water.

(b) Baroclinic eddies

It was shown in Section 6.2.2(c) that the strong net flow parallel with a shelf-sea front gives rise to baroclinic eddies that are known from satellite observations to break free. A cool-water eddy introduced into the stratified side of a front will carry nutrients with it. Loder and Platt (1985) calculated the probable transport of nitrate across a typical shelf-sea front by this mechanism to be about 0.08 mmol m^{-1} s^{-1}.

(c) Residual currents

As we saw in Section 6.2.2, the residual currents in a tidal front are primarily along the front, but a weak cross-frontal circulation induced by internal friction is also expected. Garrett and Loder (1981) provided formulae for this circulation and Loder and Platt (1985) evaluated them for the Ushant front. They arrived at a figure for nitrate transport of less than 0.01 mmol m^{-1} s^{-1}, which is insignificant compared with the transport by the two mechanisms previously described. As we shall see later, work on the tidal front of Georges Bank leads to the view that the role of residual currents in bringing about a cross-frontal flux may have been underestimated.

(d) Vertical transport

Possible mechanisms for vertical transport in the vicinity of a tidal front were described in Section 6.2.2(c). Loder and Platt used the equation

$$F_v = K_v(\Delta C/\Delta z)L_w \tag{6.03}$$

where K_v is the vertical eddy diffusivity and L_w is the cross-frontal distance along which there is significant vertical transfer. Taking the value of $K_v = 10^{-4}$ m^{-2} s^{-1}, which had been obtained by Pingree and Pennycuik (1975) from a stratified station, and $L_w = 10$ km, they calculated the vertical nitrate flux as 0.2 mmol m^{-1} s^{-1}.

Summarizing to this point, the Loder and Platt (1985) calculations suggested that reasonable estimates for the various types of transport of nitrogen into the mixed layer of the stratified water adjacent to the Ushant front were, for every meter length of the front, integrated over depth: spring–neap tidal cycle 0.12 mmol N s^{-1}, baroclinic eddies 0.08 mmol N s^{-1}, residual currents 0.01 mmol N s^{-1}, and vertical transport 0.20 mmol N s^{-1}. From these calculations they concluded that all the mechanisms considered might bring 0.40 mmol N s^{-1} for each meter length of the front. If the frontal area of influence extended for 10 km into the mixed layer, this would equate to a carbon flux of about 0.28 g C m^{-2} d^{-1}.

It is instructive to compare this calculation with those made by Holligan *et al*. (1984b). They concerned themselves with the vertical diffusion of nitrate up through the thermocline at the stratified side of a front. They calculated the vertical diffusion coefficient from observations on downward heat flux over a period of 90 days, and assumed that the coefficient applied equally to the upward flux of nitrate. They then observed the gradients of nitrate at the thermocline on a number of stations and obtained estimates of nitrate flux varying from 32.2 to 399 g nitrate–N d^{-1} for every m^2 of the thermocline surface. These fluxes would be equivalent to "new" carbon production of up to 3 g C m^{-2} d^{-1} and are an order of magnitude higher than those obtained by Loder and Platt (1985). They could have been in error through using a constant value for the vertical diffusion coefficient, based on observations made 90 days apart. Direct measurements (Gargett 1984) indicate that K_v is not a constant because it must vary continuously with the level of turbulence and stratification. The values at the time the nitrate gradients were measured could have been very different from the long-term average.

We shall now return to the question of the role of residual currents in cross-frontal transport. In particular there have been studies at the Georges Bank front, which is the most extensively studied frontal system after the northwest European shallow-sea fronts.

6.3.4 The Georges Bank frontal system

Georges Bank is a major submarine bank lying off the eastern coast of North America between Cape Cod and Nova Scotia. Its characteristics have been extensively

reviewed in Backus and Bourne (1987). Over most of the bank the water depth is 50–60 m and the tidal currents are sufficiently strong to keep the water column vertically mixed throughout the year. Around the bank the combination of freshwater run-off and solar heating causes persistent stratification throughout the spring and summer. As a consequence, a tidal front develops around the central bank, between the mixed and stratified water. (There is, in addition, a clockwise gyre driven primarily by rectification of the strong tidal currents over the sides of the bank, but this phenomenon will be treated in Chapter 7.)

Biological productivity of the waters over the bank is high, and there is intensive fishing of both finfish and shellfish. Since there is a substantial loss of nitrogen associated with removal of commercial catches, it is important to understand the mechanisms for supply of "new" nitrogen to the top of the bank from deeper water. Work on this topic up to 1988 was reviewed by Horne *et al*. (1989).

The position of the front is in rough agreement with the prediction made by Loder and Greenberg (1986) using Simpson and Hunter's (1974) formulation (see Chapter 4).

From observations made in 1985 it is deduced that the front on the northern and northwestern side of the bank makes a twice-daily excursion of 10–15 km as a result of changes in tidal current velocity. Mavor and Bisagni (2001) used 12 years of satellite data to confirm the seasonality and the diurnal excursions of the tidal front. They also showed that through the summer months, as stratification of offshore waters intensifies, the tidal front on the southern and eastern parts of the bank moves about 5 km per month on-bank. Conversely, the front on the northern and western portions moves 5 km per month off-bank, although the cause is not clear.

Records from a fixed station in the frontal zone, where the water depth was 33 m, showed semi-diurnal fluctuations not only in current velocity but also in temperature (approximately 7–15 °C on tides of maximum amplitude). From other data sets it was found that there was a good correlation between nitrate concentration and temperature. It was possible to construct a time series for variations in nitrate concentration with time, indicating semi-diurnal fluctuations between about 1 and 10 mmol m^{-3} on spring tides at the 33 m-deep fixed station.

The current meters at the fixed 33 m station showed the expected gyral current parallel with the front, but also a cross-frontal current averaging 0.05 m s^{-1} at 13 m depth and 0.03 m s^{-1} at 33 m depth, both directed toward the tidally mixed area on the top of the bank. Use of this information in conjunction with the fluctuating nitrate concentrations enabled Horne *et al*. (1989) to calculate a depth-integrated flux of nitrate through the front toward the center of the bank of approximately 12 mmol N m^{-1} s^{-1}. We note that this value is about 30 times the flux calculated for the Ushant front by Loder and Platt (1985). Horne *et al*. (1989) then went on to consider what physical mechanisms might be responsible for this flux.

They first considered shear-flow dispersion. This explanation would work approximately as follows. A parcel of nutrient-rich water moving onto the bank with the tidal flow and returning half a tidal period later might have been subjected to vertical mixing with nutrient-poor surface water and return with its

nutrient concentration reduced. Examination of the data showed that this factor was unlikely to be a major component of the observed flux.

They then compared the estimated cross-frontal transport of nitrogen to the center of the bank (12 mmol N m^{-1} s^{-1}) with the observed biological requirement for nitrogen. During a cruise in August 1985 *in situ* incubations of phytoplankton were carried out in the presence of either ^{14}C (as HCO_3^-) or ^{15}N (as NO_3^- or NH_4^+), and used to calculate rates of photosynthesis and nitrogen uptake. Measurements were made of nutrients, chlorophyll, and physical characteristics of the water column. It was found that, because of the semi-diurnal movement of the front mentioned earlier, some stations on the bank or in the frontal zone were, in fact, stratified. Grouping stations according to their physical characteristics rather than their position led to the conclusion that the frontal stations had the highest carbon fixation rates (265 mg C m^{-2} h^{-1}) and nitrate uptake rates (15.6 mg N m^{-2} h^{-1}), the stratified stations had the lowest (160 mg C m^{-2} h^{-1} and 7.8 mg N m^{-2} h^{-1}), while the mixed stations were intermediate. Nitrate-based "new" production accounted for 60% of the total at frontal stations, 41% at the mixed stations, and only 27% at the stratified stations. The nitrate demand of the phytoplankton populations was 0.36 mmol m^{-2} s^{-1} at the frontal stations, 0.09 mmol m^{-2} s^{-1} at the mixed stations, and 0.018 mmol m^{-2} s^{-1} at the stratified stations. At an oceanic station far from the bank the demand was only 0.02 mmol m^{-2} s^{-1}.

Using reasonable approximations for the area of the mixed zone on the top of the bank, and of those parts of the frontal zone on the bank side of the mooring site, the nitrate requirement of the mixed zone, per meter length of the front, integrated over depth, was estimated at 2.5 mmol N s^{-1} and that of the frontal zone between the bank and the mooring as 2.9 mol N s^{-1}. Hence the calculated supply, 12 mmol N m^{-2} s^{-1}, is roughly twice the total demand by the phytoplankton. Bearing in mind that these calculations are rough approximations, they seem to indicate that at the time of study cross-frontal transport by residual flow was sufficient to meet the observed needs of the phytoplankton, without any requirement for other mechanisms.

A two-dimensional (x, z – horizontal and vertical) coupled physical–biological model of the plankton on Georges Bank during the summer was constructed by Franks and Chen (1996). The output agreed both qualitatively and quantitatively with phytoplankton biomass and nutrient data obtained by Horne *et al*. (1989). The model indicated that a significant proportion of the total phytoplankton production on the bank occurred in the frontal zone, supported largely by nutrients transported from below the euphotic zone off the bank. The largest transport occurred during only a few hours of the tidal cycle, and resulted in the formation of small but dense phytoplankton patches. The authors suggested that temporal transience of the nutrient fluxes and the small scale of the phytoplankton patches would make sampling very difficult and cause the investigators to miss the essential features.

A few years later, Franks and Chen (2001) constructed a three-dimensional biological–physical model of the Gulf of Maine, including Georges Bank. They coupled a simple nutrient–phytoplankton–zooplankton model to a detailed

physical model forced by the M_2 tides and generated patterns of plankton and nutrients that agreed closely with published data. They found that a high proportion of the primary production in summer occurred on the bank side of the tidal fronts, where the waters became alternately stratified and destratified in the progression from neap to spring tides and back. The model suggested primary production around 4 g C m^{-2} d^{-1} in the well-mixed waters on the top of the bank. The authors suggested that the simplicity of the biological model would cause them to view this high figure with some skepticism.

In comparing results from Georges Bank with those from the northwest European area, it must be remembered that the front associated with the gyre on Georges Bank may well show very different physical properties from the shallow-sea fronts off the coast of Europe. Measurements and models to date suggest that the enhanced primary production at the Georges Bank front is made possible by a strong cross-frontal transport of "new" nitrogen. At the European fronts it appears that primary production is enhanced by vertical transport of nitrate and by a variety of mechanisms of cross-frontal transport.

There is a certain amount of information on the distribution and abundance of animals in the Georges Bank tidal front. Tremblay and Sinclair (1992) concluded that larvae of the scallop *Placopecten magellanicus* were retained on the bank by physical processes associated with the front. On the other hand, when sampling a wider variety of planktonic animals, Perry *et al*. (1990) found that some occurred predominantly on the bank (e.g., small copepods), some predominantly off the bank (e.g., most large zooplankton), and some occurred on both sides of the front (e.g., *Calanus finmarchicus*). It was not clear that the front itself had any influence on their distribution. Subsequently, Ashjian *et al*. (2001) conducted surveys across the bank from the continental slope to the Gulf of Maine, using a video plankton recorder. They passed through four main water types, slope water, stratified bank water, well-mixed bank water, and Gulf of Maine water, and found that the distributions of taxa and particles were associated with the water-mass types. Smaller-scale variability in plankton abundance did not appear to be tightly coupled to, or correlated with, physical features.

6.3.5 Heterotrophic activity at shelf-sea fronts

An integrated multidisciplinary study of several kinds of heterotrophic activity at a shallow-sea tidal-mixing front in the Irish Sea was reviewed by Fogg (1985). The investigators recognized three water masses as distinct ecosystems: surface stratified water (SSW), bottom stratified water (BSW), and mixed water (MW).

After thermocline formation the SSW system was occupied by an expanding phytoplankton population that gradually used the available nutrients, then reached a plateau of biomass that was maintained throughout the summer, with the greatest concentration of chlorophyll being on the pycnocline. In parallel was development of heterotrophic populations of bacteria and zooplankton that

expanded until photosynthesis was balanced by heterotrophic activity. At this stage, nitrogen turnover, as measured by urea turnover rates, was rapid and there was a high degree of interdependence between the food-web components that persisted until destabilization of the water column in autumn.

In the bottom stratified water, by contrast, both photosynthesis and heterotrophic activity were at a low level. In the mixed water, where the phytoplankton is light-limited rather than nutrient-limited, bacterial and zooplankton biomasses, heterotrophic activity, and nitrogen turnover rates were lower than in the SSW.

Fogg (1985) reported that, like many others before them, the investigators had found patches of high chlorophyll density in the SSW adjacent to the front and on the pycnocline away from it. However, he said that if chlorophyll concentrations were averaged down to 30 m, the frontal waters were scarcely distinguishable from the rest of the SSW. In other words, the distribution was different, but not the total amount in the water column.

No significant increase in bacterial or zooplankton biomass was found at the front, but a marked increase in physiological activity was observed. In June and July the levels of cellular ATP were about twice those found elsewhere in the SSW, and there were patches of high glucose uptake activity and urea uptake activity adjacent to the front. The tentative explanation put forward by Fogg (1985) is interesting from several points of view. He suggested that eddies formed along the front (see Fig. 6.03) might, by their rotation, induce vertical circulation and bring to the surface concentrations of phytoplankton from the isopycnal region of the SSW. This phytoplankton would be immersed in nutrient-poor water and would be expected to be active photosynthetically but unable to divide. Under these circumstances large quantities of dissolved organic matter (DOM) would be liberated, which might explain the high levels of heterotrophic activity. Fogg (1985) also suggested that this mechanism could account for the appearance of high concentrations of chlorophyll at the surface near the front. It is yet another potential mechanism to add to those discussed in the previous two sections.

When the distributions of zooplankton were examined species by species it was found that the front demarcated distinct communities. *Temora longicornis* and the nauplii of *Acartia clausi* were absent from SSW, whereas *Calanus finmarchicus* and *Membranipora membranacea* were absent from MW. *Oithona similis* was concentrated around the pycnocline, while *Microcalanus pusillus* was found only in the BSW.

On the stratified side of the front most of the zooplankton were found above the thermocline and made limited vertical migrations. When zooplankton found themselves in patches of high concentrations of phytoplankton they ceased vertical migration. Fish eggs, larvae, and post-larvae were more abundant in the frontal zone than elsewhere. Birds, such as Manx shearwaters *Puffinus puffinus*, were more numerous on the stratified side of the front than elsewhere, especially in areas of chlorophyll maxima. The general impression that frontal waters are regions of enhanced primary and secondary productivity is sustained, even though the mechanisms responsible are still a matter of debate.

(a) Benthic productivity

It has been observed (Glémarec 1973, Creutzberg 1985) that in the benthic areas corresponding with a frontal change from tidally mixed waters to summer stratified waters there is a change in benthic community structure. Creutzberg (1985) showed that on a transect across a front off the Dutch coast in the North Sea (Fig. 4.11) the tidally mixed area to the south was marked by sandy sediments, while the stratified area to the north had muddy sediments. The boundary between the two has remained remarkably constant for at least 80 years, and just north of the boundary is a zone about 15 km broad characterized by high organic-matter content and a high biomass of benthic animals.

Two hypotheses have been put forward to explain it. The simplest is that the fast-moving tidal streams of the southern region scour the bottom and carry a heavy load of organic and inorganic sediment. Further north, where tidal streams are slower, a point is reached at which the waters deposit their load of organic and inorganic sediment, creating ideal conditions for the growth and reproduction of benthic organisms. A more complex explanation invokes the presence of a front with its enhanced phytoplankton biomass in the waters above. Sinking of the phytoplankton leads to the accumulation of organic matter in the sediments below.

Creutzberg (1985) made observations on the position of the front and of its chlorophyll distribution on eight occasions between 1982 and 1984. He discovered that there was a chlorophyll maximum that remained stationary over the enriched benthic zone even when the front itself migrated 50–60 km north. His conclusion was that the first of the two explanations was the correct one, namely that the advection of organic matter and its deposition, over a long period, in a position determined by the speed of the tidal currents has led to the development of an enriched benthic community. He suggested that rapid release of nutrients from the enriched benthic community was the cause of the chlorophyll maximum over the top of it. This theory is the converse of the view that holds that deposition of phytoplankton from chlorophyll maxima associated with the front has led to the enrichment of the benthic community. Creutzberg did not go so far as to suggest that release of nutrients from the benthos was the sole cause of chlorophyll maxima at fronts, but it is worth remembering that the bottom stratified water below fronts may be receiving unusually large amounts of nutrients across the benthic boundary layer.

(b) Productivity of zooplankton and fish

In addition to the frequent observation that phytoplankton biomass is enhanced at tidal fronts, conflicting observations have been made on the relative abundance of zooplankton and fish at fronts, compared with the waters on either side. In cases where enhanced biomass of zooplankton has been observed, it has not been clear whether the effect was due to higher rates of population growth in the frontal

zone or to passive advection to the zone of convergence. Uye *et al*. (1992) studied the abundance of copepod nauplii at a tidal front in the Inland Sea of Japan. They found that, in response to the higher productivity of phytoplankton, the egg production rate of individual *Paracalanus* was higher at the front than on either side, but the population density of nauplii was lower. They concluded that the mortality of nauplii was higher at the front because of a higher density of predators that had accumulated there by passive advection.

In Delaware Bay, Epifanio (1987) studied the distribution of larvae of the mud crab *Neopanope* in relation to a tidal front and found that a concentrated patch of larvae was maintained on the stratified side of the front. He proposed a model according to which the larvae in surface waters were first advected toward the front, then carried downward with sinking water at the pycnocline. The larvae responded by migrating up toward the light, so that they found themselves in surface water, and the cycle of transport began again, maintaining the integrity of the patch.

Noting that the abundance of larvae of the sprat *Sprattus* in the North Sea was highest on the non-stratified side of tidal fronts, Munk (1993) found that larval growth rate was highest in the mixed water some distance from the front, was slightly lower in the area of peak larval abundance, and was much lower in the stratified water. He concluded that the enhanced productivity at the front benefited the larvae, and that the slightly reduced growth rate close to the front could be explained by food limitation in the dense larval population found there. Subsequently Valenzuela and Vargas (2002) sampled sprat larvae from a wide range of physical and biological environments in the German Bight area of the North Sea, and off East Anglia, UK. The highest larval densities occurred in a transect across a tidal-mixing front in the German Bight, but growth rates estimated from otoliths were no higher than anywhere else. In fact, there was no variation in average growth rate in relation to food availability or oceanographic conditions in any of the areas studied. They concluded that, on this occasion, food abundance was not a limiting factor for the growth of sprat larvae.

Sampling of larval haddock *Melanogrammus auglefinus* and cod *Gadus morhua* across the southern flank of Georges Bank revealed that the larvae were concentrated across the tidal front in a band 10–20 km wide (Lough and Manning 2001). A 10 km wide tidal-front jet carried water southwest along the 60 m isobath, close to the mixed side of the front, and moved laterally with the diurnal tidal cycle. There was an upwelling flow on the mixed side of the front and a surface convergence with downwelling on the stratified side. Model simulations suggested that the larvae entrained in the convergence zone could be carried deeper in the downwelling and be transported onto the bank under the jet, in the weak cross-isobath residual flow (Plate 4). The authors suggested that the larvae would benefit from the enhanced planktonic productivity associated with the front and be delivered onto the bank, which functions as a larval retention area (see Section 7.3.2).

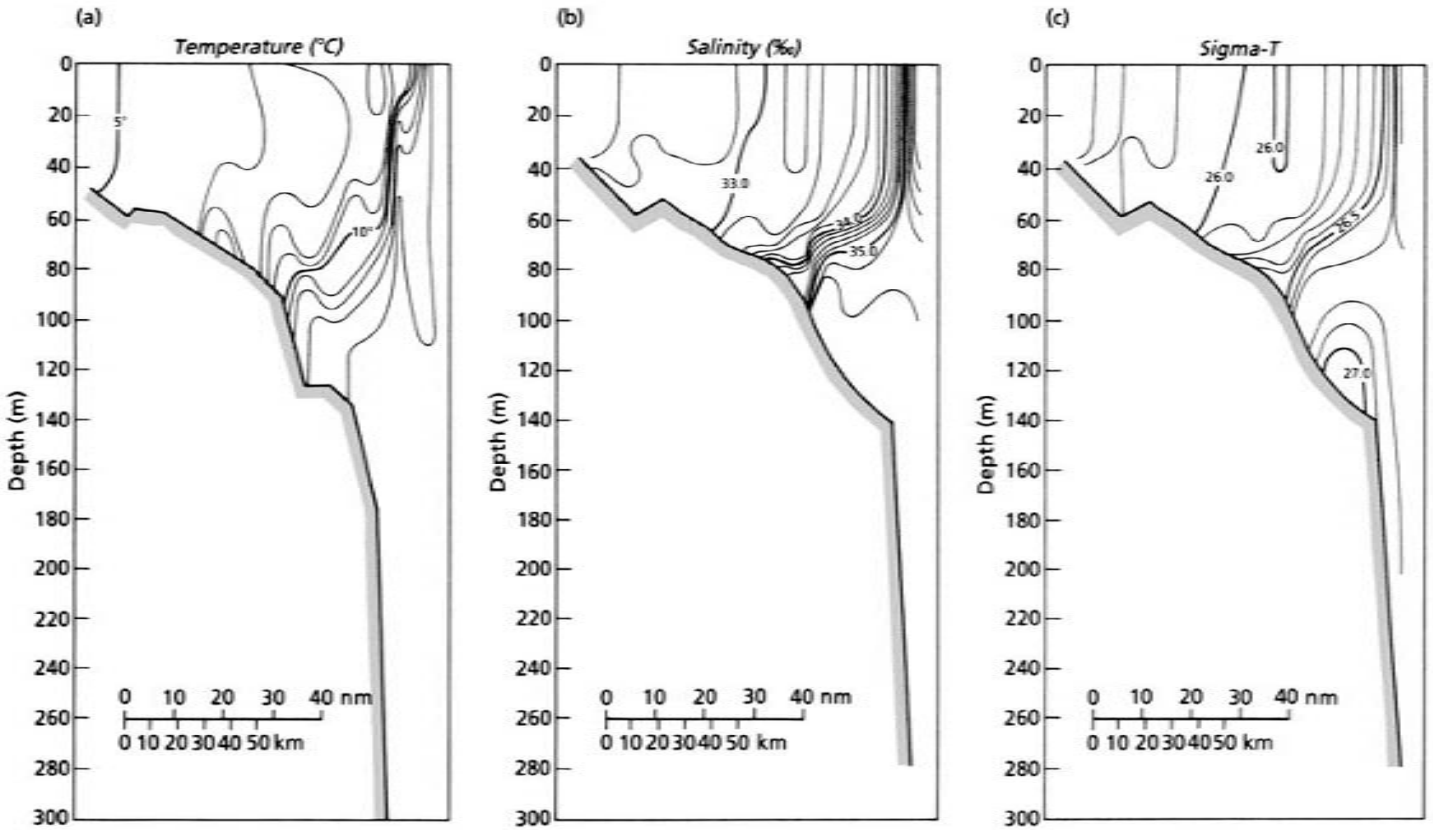

Fig. 6.07 Cross-shelf hydrographic sections south of Rhode Island, United States, April 1974, showing the shelf-break front. From Flagg and Beardsley (1975).

6.4 The biology of shelf-break fronts

Along the outer continental shelf of almost all of eastern North America in winter is to be found a front marking the transition between the colder and fresher shelf water mass and the warmer and more saline slope waters. Data from Flagg and Beardsley (1975) showing the situation south of Rhode Island in early April 1974 (Fig. 6.07) indicate that the shelf water was well mixed at a temperature of 5–10 °C and 32.6–34 salinity, while the offshore waters were mildly stratified (not shown) with a surface temperature of 14–16 °C and about 36 salinity. When the density is considered, these differences tend to compensate for one another so that the σ_t difference across the front was only 0.4 units. In various parts of the eastern seaboard of North America similar changes occur over distances of 7–40 km and a vertical depth ranging from 15 to 60 m (Mooers *et al*. 1978). The front normally straddles the shelf break, intersecting the bottom near the 100 m isobath (60–120 m) and sloping up from the bottom in an offshore direction for about 50 km (0–100 km).

The coming of the spring warming drastically changes the picture. The shelf becomes stratified and below the thermocline, on the deeper part of the shelf, a parcel of water of reduced salinity with a temperature less than about 10 °C becomes isolated from the warmer, shallower waters inshore and the more saline waters offshore. This process was first described in northwest Europe by Vincent and Kurc (1969), who called it the "cold cushion" (*bourrelet froid*) (Fig. 6.08). The effect is to maintain a weak front near the shelf edge below the thermocline, even through the period of summer stratification.

As was mentioned earlier, Mooers *et al*. (1978) have described how the position of the shelf-break front changes under the influence of wind forcing, by the impact of the Gulf Stream rings (see Chapter 8) and in association with the "calving" of lens-shaped parcels ("bubbles") of shelf water of scale 10–20 km, which break through the frontal structure and move offshore. The net result is that the position of the shelf-break front off the east coast of North America may vary in distance from shore by as much as 200 km. The movement is least off the coast of Florida and Georgia to the south, and reaches a maximum at the latitude of Cape Cod. The envelope in which this front moves corresponds with the position of highly productive fisheries, from the Grand Banks off Newfoundland, south to Cape Hatteras.

Ryan *et al*. (1999a, 1999b) observed in satellite data, supplemented by *in situ* observations, that when meanders of the shelf-break front came close to shore and interacted with the shelf break, cold shelf water upwelled from depths in excess of 20 m along frontal isopycnals and gave rise to phytoplankton blooms (Fig. 6.09). The basis for the upwelling was a seaward flow of deep shelf water forced by meander circulation near the shelf break. The meanders progressed along the shelf break at about 9 km d^{-1} causing upwelling events as they moved. The feature may be seen throughout the whole of the Mid-Atlantic Bight and the southern flank of Georges Bank between mid-April and June and it is considered an important aspect of production in this region.

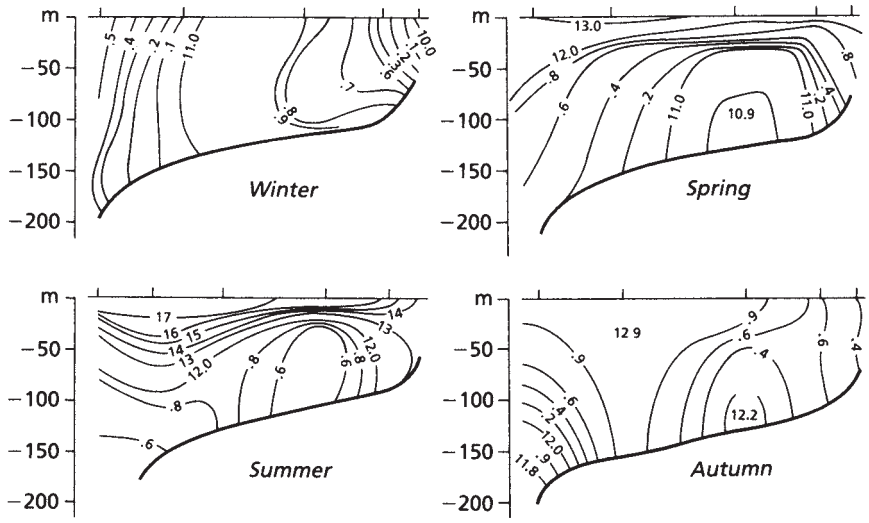

Fig. 6.08 Formation of the "cold cushion" (*bourrelet froid*) on the shelf off Brittany. The structure is visible in spring and becomes warmer and smaller as the seasons advance. Compiled from the data of Le Magueresse and of Vincent and Kurc, by Le Fèvre (1986).

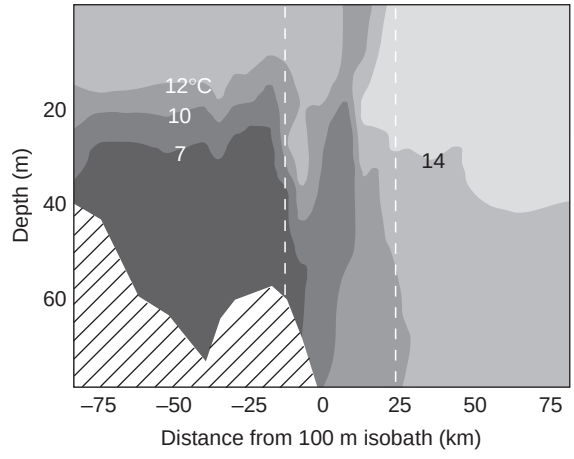

Fig. 6.09 Vertical thermal structure (°C) on a transect through a shelf-break front offshore of New York in June, showing the upwelling of thermocline water to the surface near the 100 m isobath. Vertical dashed lines mark the area of interleaving of shelf and slope waters, with warmer, more saline water inshore of cold fresh water. Hatched area is floor of shelf. From Ryan *et al*. (1999a). Copyright (1999) by the American Society of Limnology and Oceanography, Inc.

6.4.1 Biological production at shelf-break fronts

(a) Plankton biomass and production

There have been various observations of nutrient enrichment and/or enhanced phytoplankton and zooplankton biomass associated with shelf-break fronts. For example, Fournier (1978) reported that the average value for chlorophyll-*a* across the Scotian Shelf (in March 1977) was less than 1 mg m^{-3}, while over the shelf break chlorophyll reached a maximum of 4.2 mg m^{-3}. Herman *et al*. (1981), working on the shelf break south of Nova Scotia, used an undulating "batfish" sampler that measured salinity, temperature, depth, chlorophyll-*a*, and copepods. They found that primary production and copepod abundance were much higher at the front than in surrounding shelf and slope waters, and suggested that convergence of waters at the front was the explanation.

Pingree and Mardell (1981) reported on a series of studies of the Celtic Sea shelf break and pointed out that in summer the edge of the shelf is characterized by a band of water about 1–2 °C cooler than water on either side of it and about 100 km broad. At times the band can be traced for 800 km along the Armorican and Celtic Sea slopes. In it, the levels of inorganic nitrate and chlorophyll are significantly higher than in adjacent water. They noted that there seemed to be an association between the patches of increased chlorophyll and the bottom topography. Although some had invoked upwelling as the mechanism responsible for the presence of cooler, nutrient-rich water at the surface, Pingree and Mardell (1981) were inclined to favor tidally driven internal waves interacting with the bottom topography as the important mechanism.

This idea was developed further by Mazé (1983), Mazé *et al*. (1986), and Pingree *et al*. (1986) to the point where Le Fèvre and Frontier (1988) could write that "a reasonably safe picture of what is taking place has now emerged." Details of the physics of internal waves will be given in Chapter 7, but in summary the story goes approximately as follows. The incoming oceanic barotropic tidal wave is rather small, of the order of 2 m. In stratified water the interaction of the tidal wave with the shelf break gives rise to an internal baroclinic tide with an amplitude that reaches a maximum of about 60 m at the very edge of the shelf. From here it propagates in two directions, toward land and away from it, gradually damping out. Propagation toward the open sea is more or less sinusoidal, but propagation onto the shelf is distorted by the barotropic tidal currents.

There has been much discussion about whether an internal tide would produce the observed reduced temperature and elevated nutrient concentrations in surface waters. It is now thought that there is an interaction between the internal waves and the wind mixing of the layer above the thermocline. Assuming some type of equilibrium between the depth of the thermocline, the temperature of the mixed layer, and the prevailing wind conditions, a forced upward displacement of the thermocline leads to a disruption of that equilibrium. Additional energy is injected into the mixed layer, which leads to an increase in the depth of the mixed layer with upward mixing of cool water from below the thermocline. This water

carries with it additional nutrients, so that the phytoplankton in it can benefit from being in the lighted zone and mixed-layer primary production is enhanced. Another way of looking at it is to consider that the depth of the mixed layer is a function of the buoyancy provided by surface warming and the strength of winds causing mixing. If the thermocline is pushed upward, the mixed layer will tend to return toward its original thickness by mixing upward some of the cooler, nutrient-rich water. The frequency of this occurrence is that of the M_2 tide – i.e., twice daily.

Le Fèvre and Frontier (1988) pointed out that augmentation of the nutrients on a daily basis provides a more-or-less continuous increase in phytoplankton productivity to which the copepod population can respond. This condition is in contrast to the situation at a tidal-mixing front, where the cycle of enhanced production follows the fortnightly cycle of spring and neap tides, leading to a short burst of phytoplankton production every two weeks. It seems unlikely that zooplankton populations could increase and decrease in such a way as to exploit this production to the maximum. Hence shelf-break fronts should show that copepod populations increase in parallel with phytoplankton, while tidal-mixing fronts should not. The limited field data available support this view. Results given by Le Fèvre and Frontier (1988) for the Armorican shelf-break front show increased copepod abundance in the frontal region, suggesting that a classical large-phytoplankton-to-copepod food chain is functioning. On the Ushant tidal-mixing front the dominant zooplankter was the pteropod mollusc *Limacina*, which is known to feed on microzooplankton. They suggested that much of the phytoplankton at this front remains ungrazed by copepods and becomes senescent, giving support to a food web involving bacteria and ciliates, which in turn are taken by *Limacina*. This line of reasoning is supported by the high levels of heterotrophic activity observed by Fogg (1985) and others as characteristic of tidal-mixing fronts.

(b) Fish and birds

Off the northwest coast of Denmark there is a shelf-break front at the interface between the less dense shelf waters and the denser waters of the Norwegian Trench. Munk *et al*. (1999) sampled fish larvae along two transects through this front during May of three successive years, and found that the larvae of cod, whiting *Merluccius bilinearis*, saithe *Pollachius virens*, haddock, and Norway pout *Trisopterus esmarkii* were most abundant at or near the front. The distribution of cod and saithe larvae was centered on the front, haddock and Norway pout larvae tended to be a little offshore of the front, while whiting and saithe tended to be inshore of the front.

On the Norwegian side of the Norwegian Trench, fulmars *Fulmarus glacialis* are present throughout the year and little auks *Alle alle* are winter visitors. The greatest concentrations of fulmars always occur at the shelf break, over the 200 m isobath, and the greatest concentrations of little auks over the 130 m isobath (Skov and Durinck 1998). The hydrography of this area, the Skagerrak, is more complex than in a simple shelf-break front. Baltic water flows seawards

on the northern side and North Sea water flows in to the Baltic on the southern side, creating a frontal zone between them in which there are cyclonic gyres, and upwelling occurs (see Section 6.6.2).

In the southeastern Bering Sea the greatest carbon flux to the pelagic food web is found at the shelf-break front (Iverson *et al*. 1979) and large concentrations of fulmars aggregate near the front in summer and autumn (Schneider 1990).

In summary, the most common view of the mechanism controlling biological productivity at shelf-break fronts is that tidally generated internal waves add energy to the mixed layer, causing a deepening with incorporation of nutrient-rich water from below the nutricline. This process varies in intensity with the M_2 tide so that it produces a twice-daily augmentation of nutrients, a fairly constant elevation of primary production levels, and a corresponding increase in productivity of zooplankton, fish and birds. This mechanism contrasts with that believed to be operative in tidally mixed fronts, where the maximum enrichment of nutrients in primary production coincides with the neap tides at fortnightly intervals. This stimulation of primary productivity is considered to be too infrequent to support an elevated population of macrozooplankton. Instead, there is a burst of phytoplankton production, followed by a period of decline and decomposition, which supports a dense population of bacteria and microzooplankton.

In contrast to this view, the work of physicists using dye-injection experiments and modeling, reviewed in Section 6.2.2(a) and Fig. 6.01, indicates the presence of a frontal circulation capable of bringing deep nutrient-rich water to the surface. The biological implications have yet to be tested.

6.5 The biology of upwelling fronts

As we saw in Chapter 5, there are many places around the world where wind-induced offshore transport of surface waters occurs on a major scale, leading to coastal upwelling. While the forcing winds continue to blow, nutrient-rich waters from below the pycnocline continue to rise to the surface and move offshore, displacing the warmer, less nutrient-rich waters that preceded them. The interface between the upwelled waters and the offshore waters constitutes an upwelling front. A section through such a system (Fig. 6.10) reveals that the front is the place where the pycnocline intersects the surface of the ocean.

During an upwelling event, the front at first forms close to shore, then moves offshore, but at some point an equilibrium is reached at which the front ceases to move offshore and the upwelled waters, as they continue to move offshore, are driven downward beneath the offshore waters (Fig. 6.10). The front lies at a prograde angle. At the surface there is a convergence of waters and a tendency for buoyant biological material to accumulate. When the wind stress decreases and upwelling ceases, the front retreats landward and may disappear.

In spite of the large amount of biological study of upwelling systems (see Chapter 5), there is a surprising lack of detailed information about upwelling fronts. The modeling studies of Thompson (1978) suggested that part of the sinking

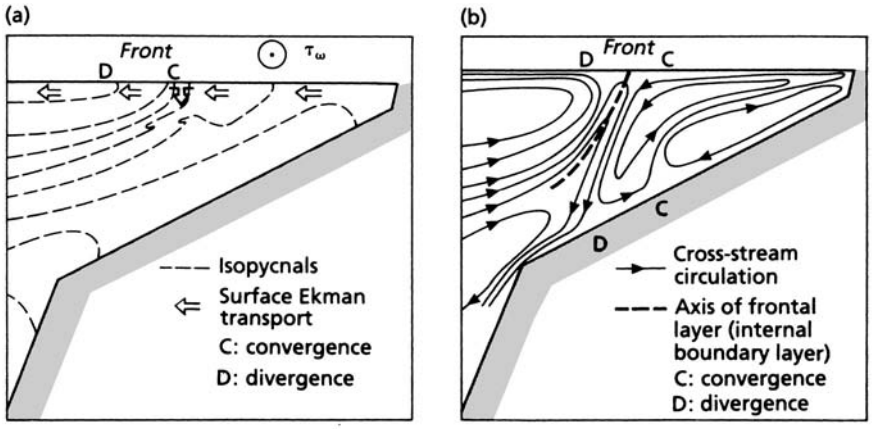

Fig. 6.10 Conceptual model showing (a) density field and (b) cross-shelf circulation in the vicinity of an upwelling front. From Mooers *et al*. (1978).

water is entrained in a shoreward-flowing deeper current, but there may be a one-celled or a two-celled circulation, depending on the wind stress, stratification, current shear, and bottom relief. In any event, the presence of the front is normally marked by a sharp temperature transition from the cold, nutrient-rich upwelled water inshore to the warmer, less nutrient-rich stratified water offshore. Clearly, any mechanism causing a mixing of these waters is likely to stimulate primary productivity.

Pearcy and Keene (1974) studied the upwelling system off Oregon by airborne remote sensing and found abrupt changes in color coincident with changes in temperature that they thought denoted enhanced biological activity at upwelling fronts. Ryther (1967) found large concentrations of a ciliate, *Cyclotrichium meuneri*, which colored the water red, on the inshore edge of an upwelling front off Peru, and Packard *et al*. (1978), after studying the biology of a related ciliate, *Mesodinium rubrum*, in the California upwelling system, showed that large concentrations formed on the inshore edges of upwelling fronts. Peterson *et al*. (1979) studied zooplankton distribution in the Oregon upwelling system and found that very high concentrations were retained shoreward of the front, and were carried below the pycnocline when the upwelling relaxed. Wroblewski (1982) modeled the movement of the various stages of the copepod *Calanus marshallae* in the Oregon upwelling system and showed how vertical migration may interact with the physical oceanography to cause the organisms to move over a spiral path on the continental shelf, moving offshore at the surface but returning in deeper water after sinking at the front. At the highest trophic level, there is evidence that albacore tuna *Thunnus alalunga*, which make trans-Pacific migrations to feed close to the California upwelling systems, tend to concentrate in the vicinity of the upwelling fronts (Laurs *et al*. 1977). On the whole, the biological information that we have

about upwelling fronts is rather fragmentary, and shows that the study of upwelling fronts is much less advanced than that of tidal-mixing fronts.

Armstrong *et al*. (1987) sampled across the southern Benguela system north of Cape Town. They emphasized throughout their account that the frontal zone is dynamic and subject to rapid change, especially since they encountered on the outward boundary of the front a strong north-flowing jet current, with speeds up to almost 1 m s^{-1} and extending to a depth greater than 200 m. However, they found during their cruise that the greatest biomass and productivity of the phytoplankton, when integrated over the euphotic layer, was in the frontal region. Inshore of the front very high concentrations of nutrients and chlorophyll occurred in surface waters, but penetration of light was limited and integrated water-column productivity was correspondingly low. Offshore of the front the nutrient levels in the euphotic zone were extremely low, so that photosynthesis was limited to that level that could be sustained by nutrient recycling. In the frontal region itself, however, relatively high biomasses of phytoplankton were well distributed through the euphotic zone and production rates were high. It was inferred that there was an enhanced supply of new nitrogen into the euphotic zone of the frontal region. The mechanism suggested was the interleaving of differing water masses along isopycnal surfaces as indicated by in-phase variations in the vertical profiles of temperature and salinity. However, as we have seen, mechanisms of cross-frontal transport are not well understood and are under active investigation.

6.6 The biology of plume fronts and estuarine fronts

6.6.1 Plume fronts

At the edges of river or estuarine plumes (see Chapter 4) where water of reduced salinity meets more saline coastal water, fronts are formed that are conspicuously marked by lines of foam and a change in water color. As mentioned in Chapter 4, the less saline, lighter water lens has an elevated surface and is carried by gravity seaward to ride over the top of the more dense coastal water, forming a retrograde front.

An early study of the physics of an estuarine plume front was that carried out by Garvine and Monk (1974) on the Connecticut River plume in Long Island Sound. They showed that adjacent to the front the layer of brackish water was only about 1 m deep, and that the pycnocline sloped up to intersect the surface over a distance of about 50 m. There was a vigorous convergence of surface waters from both sides of the front and locally intense sinking at the front itself.

The available evidence suggests that plume fronts are sites of enhanced biological activity and that fish tend to aggregate there. Pearcy and Keene (1974), who studied the coastal waters of Oregon by airborne remote sensing, found evidence of increased phytoplankton biomass at the Columbia River plume front, and Owen (1968) found that catches of albacore tuna were higher at that front than at other stations nearby. In Japan, Tsujita (1957) found that the spawning and hatching of

Japanese sardine *Sardinops melanostictus* off western Japan was consistently located close to an estuarine plume front.

In the Chesapeake Bay area, there are several places where the rivers emptying into the bay form plume fronts. Tyler and Seliger (1978, 1981) have shown that high concentrations of various phytoplankton species, including the red-tide dinoflagellate *Prorocentrum*, are found in these frontal regions especially in winter and early spring.

In the Mississippi River plume, the densities of larval fishes at the surface were higher in the frontal zone than in the plume itself or the shelf waters (Govoni and Grimes 1992). Attempts to analyze the distribution of assemblages of larvae in relation to physical factors of river plumes did not lead to useful generalizations (see for example Rissik and Suthers 1996). It seems that each species adapts to the physical conditions of a plume front in a different way. On the other hand, a study which focused on the larvae of yellowfin tuna *Thunnus albacares* in the Mississippi River plume (Lang *et al*. 1994), found that chlorophyll-*a* concentrations, macrozooplankton volumes, and larval fish abundance and growth rates all reached their highest values in the plume front.

Gaudy *et al*. (1996) sampled a fixed station off the mouth of the Rhone River, in the Mediterranean Sea, while wind-driven changes caused the plume front to pass through the station. Hydrographic conditions changed from stratified to mixed, and very detailed microbiological data were obtained exactly at the front. In surface waters there was a sharp increase in particle volume in the range 20–25 μm diameter, in ammonia and in dissolved free amino acids. Bacterial biomass and production, flagellate numbers, zooplankton numbers and grazing rates also increased. Within the zooplankton samples there was a marked increase in the numbers of fish eggs and fish larvae. It was clear that the front was a region of greatly enhanced food web activity, much of it attributable to the convergence which is a characteristic feature of such fronts.

An estuarine-plume front separating the fresher, stratified waters of the Baltic Sea from the tidally mixed, more saline waters of the North Sea extends from the northern tip of Denmark in a northeast direction to the coast of Sweden. Josefson and Conley (1997) studied the sediments and the benthic fauna beneath this front. Along benthic transects across the front, the chlorophyll-*a* (chl-*a*) values were much higher under the front than away from it. The ratio chl-*a* / (chl-*a* + phaeopigments) showed a dome-shaped relationship to distances along the transects, indicating that the region under the front was receiving the largest input of fresh phytoplankton. Biomasses of echinoderms (the burrowing ophiuroid *Amphiuma filiformis)*, and various polychaetes, were positively correlated with chl-*a* and with phaeopigments. *Amphiuma* reached densities greater than 3000 m^{-2}.

A benthic study under the plume of the Po River – which is the largest single freshwater input to the Mediterranean – showed that phaeopigments derived from plankton accumulated beneath the front and were associated with increased densities of bacteria and of meiofauna organisms such as copepods, turbellarians, and kinorhynchs (Danovaro *et al*. (2000).

6.6.2 Fronts within estuaries

At least three kinds of fronts occur in estuaries, and they are often grouped together as estuarine fronts (O'Donnell 1993). Most are of relatively small scale, and many form and disperse with every tide. The first kind is the tidal-intrusion front. Such fronts are the result of dense coastal water intruding into an estuary on the flooding tide. A front forms at the interface between the less saline estuarine water and the coastal water, and has much in common with plume fronts. O'Donnell (1993) reviewed theory and observations on such fronts and Brubaker and Simpson (1999) made intensive studies of a tidal-intrusion front in the James River estuary, part of the lower Chesapeake Bay area, using an acoustic Doppler current profiler.

The second kind of front occurs at the interface between tidally mixed and stratified waters and resembles the tidal fronts of the continental shelves. For example, at certain states of the tide the shallow water at the edges of an estuary may be tidally mixed while the deeper water in the middle remains stratified under the influence of the freshwater run-off. O'Donnell (1993) calls this a mixing front.

Shear fronts comprise O'Donnell's (1993) third category. They result from cross-estuary differences in rates of water movement. For example, as water moves up an estuary with the rising tide, the water in the deeper, central part of the estuary may move up faster than the water at the fringes, where the effect of bottom friction slows the flow. This difference results in a horizontal shear, and surface waters converge from each side to form an axial convergence (Nunes and Simpson 1985). In large estuaries where the Coriolis force is significant and outflowing waters tend to keep to one side, while inflowing waters keep to the other, the central region may experience horizontal shear stress, resulting in a frontal zone in which cyclonic gyres form and generate upwelling in their centers (see Section 6.4.1).

The three types of front may appear, disappear, or change from one type to another during a tidal cycle. Each estuary is different, as hydrology interacts with bottom and marginal topography. Several estuaries have now been the subject of physical–biogeochemical modeling (e.g. Shen *et al*. 1999) and attempts have been made to deduce the consequences of frontal circulation for the biota. Eggleston *et al*. (1998) reviewed the literature to date and studied the effect of buoyant plume fronts in an estuary on the distribution of Dungeness crab post-larvae.

6.7 The biology of fronts associated with geomorphic features

When tidal or other currents interact with irregularities in the sea bed, or coastline, it is usual to find consistent patterns of eddies and associated fronts. Pingree *et al*. (1978b) reviewed the formation of fronts at coastal headlands, and Bowman

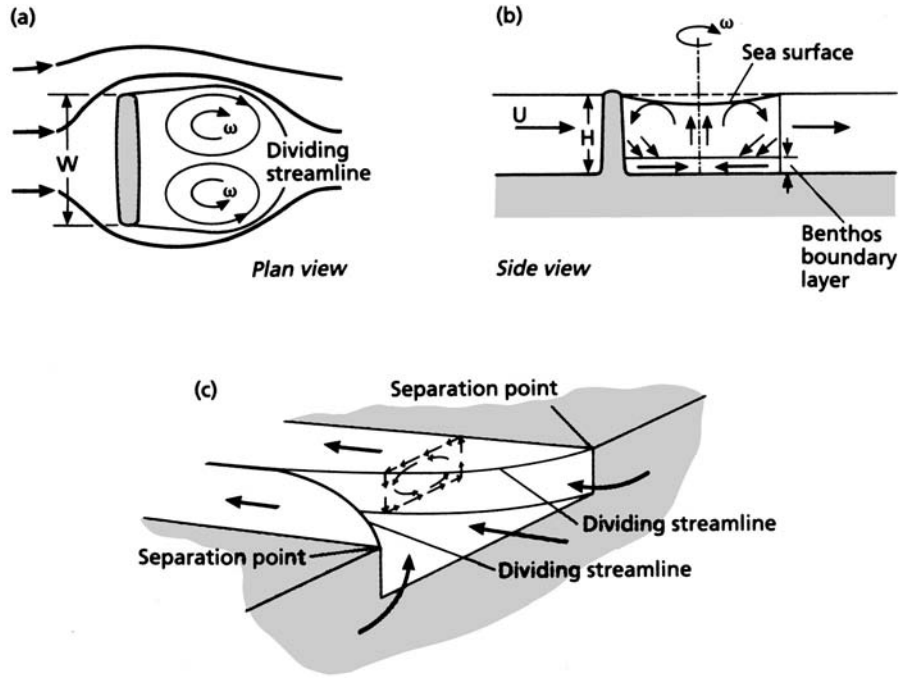

Fig. 6.11 (a) Plan of a commonly occurring flow pattern around a reef in shallow coastal water, showing the front (labeled dividing streamline) separating the area of turbulence in the wake from the less turbulent area beyond. (b) Vertical section showing upwelling produced by the clockwise (southern hemisphere) gyre. (c) Formation of turbulent-mixing region as a tidal stream enters a reef passage. For details see text. From Wolanski and Hamner (1988).

et al. (1986) reviewed the interactions of tidal currents with islands and features of the sea floor. There is scattered evidence of enhanced phytoplankton growth – for example, around islands, off headlands, and above sea mounts – but the mechanisms involved, and the role of fronts in these mechanisms, are as yet not at all clear.

Wolanski and Hamner (1988) reviewed the distribution of zooplankton in relation to topographically controlled fronts formed by headlands, islands, and reefs. When a tidal current streams past one of these structures a front (often called the dividing streamline; Fig. 6.11) may be formed that separates the normal tidal flow from the more turbulent eddies on the downstream side of the object. If the water is fairly shallow the turbulent eddies interact with the bottom, giving rise to convergence and sinking at the front. As a result, surface-dwelling planktonic organisms tend to aggregate there, especially those that are buoyant. In the vicinity of coral reefs, where many species of coral tend to spawn synchronously, very dense aggregations of buoyant coral eggs are formed at these fronts, which can then be readily identified from the air.

Alldredge and Hamner (1980) documented the formation of dense aggregations of zooplankton in the turbulent area downstream of a headland when tidal streaming was at its maximum. Oliver and Willis (1987) reported that high concentrations of coral eggs formed at the topographic fronts at certain stages of the tide remained as coherent linear patches as they drifted away from the places where the fronts had formed. It is clear that calculations of the encounter rates between planktonic organisms around coral reefs, islands, and headlands must not be made on the basis of average density in the water mass, but must take into account the way in which topographically controlled fronts bring about massive aggregations.

It is worth noting in passing that in the situation depicted in Fig. 6.11(c), in which a tidal current streams through a reef passage, nutrient-rich water from depth is upwelled from in front of the reef by Bernoulli suction and stimulates algal production on the reef (Wolanski *et al*. 1988).

6.8 Summary: how fronts enhance biological productivity

More effort has gone into the study of shelf-sea (tidal-mixing) fronts than into any other kind of front. It is now clearly understood that tidally induced currents cause mixing from top to bottom of the water column in many shelf areas. The strength of the tidal currents varies with the diurnal tidal cycle, but also with the fortnightly alternation between spring and neap tides. At places where the depth in relation to the tidal currents is too great for mixing to occur from top to bottom of the water column, thermal stratification occurs in summer. Shelf-sea fronts mark the discontinuity between the tidally mixed region and the stratified region and are frequently found to be the sites of enhanced planktonic biomass and productivity.

Early observations on such fronts emphasized the convergence of surface waters and downwelling that occurs there. Any organisms buoyant enough to resist the downwelling would be expected to aggregate at the front. Thus, it was thought that passive advection was one explanation of the concentrations of planktonic organisms found at fronts.

An alternative explanation invoked the concept of enhanced *in situ* production, made possible by particularly favorable conditions of light and nutrients. In the upper mixed layer of stratified water in summer, phytoplankton growth is usually nutrient-limited because the presence of a pycnocline restricts the upward movement of nutrients from the lower regions, where they are more plentiful. Any mechanism that causes a transfer of nutrients to the surface layer on the stratified side of a front is likely to lead to enhanced biological production. A number of mechanisms have been proposed:

1 The spring–neap tidal cycle. At a fixed position relative to the bottom, the water may be tidally mixed at one stage of the tidal cycle and stratified at another. Nutrients are brought up during the mixing phase and utilized in the upper mixed layer during the stratified phase.

2 Cross-frontal transport. A variety of mechanisms have been proposed for transferring nutrients from the tidally mixed side of the front, where phytoplankton is often light-limited but not nutrient-limited, to the stratified side of the front. Baroclinic eddies, in which parcels of nutrient-rich water break through to the stratified side, have been observed by remote sensing. On Georges Bank a significant cross-frontal transport has been observed, from deep stratified water towards tidally mixed water.
3 Vertical transport. Some evidence suggests that conditions in the frontal zone are favorable for the vertical transport of nutrients through the front to the stratified water above. This movement could result in enhanced phytoplankton in the immediate vicinity of the front.

The relative importance of these three types of mechanism has yet to be evaluated. It is probable that different mechanisms dominate at various times and places. Only a sophisticated multidisciplinary approach using state-of-the-art technology to yield physical and biological data on a range of scales from microns to kilometers will clarify the mechanisms involved.

Shelf-break fronts occur at the interface between cooler, less saline water on a continental shelf and warmer, more saline water offshore. Production of phytoplankton, zooplankton, and fish is particularly high. The mechanism most widely accepted as causing the enhanced production is the generation of tidally driven internal waves at the shelf edge. The consequent rise and fall of the nutricline leads to vertical transport of nutrients into surface water. The process is seen as being of daily occurrence, thus supporting a relatively constant level of enhanced phytoplankton production on which a food web involving zooplankton and fish can be built. This situation has been contrasted with that found at tidal-mixing fronts. At these, the mechanism of enhanced biological production appears to be linked to the neap–spring tidal cycle, so that pulses of high phytoplankton biomass occur at fortnightly intervals. This interval is too long for mesozooplankton populations to be able to exploit the phytoplankton effectively. As a result, there is accumulation, death, and decay of phytoplankton, with the release of dissolved and particulate organic matter, which is exploited by bacteria, ciliates, and specialized macrozooplankton, rather than copepods and fish (see Section 6.4.1).

More recently dye-transport studies and numerical modeling have shown that there are mechanisms for cross-frontal transport and upwelling of nutrient-rich water that could lead to enhanced productivity at shelf-break fronts. The relative importance for biological productivity of these mechanisms, compared with tidally driven internal waves, has not yet been determined.

Upwelling fronts form at the interface between normal shelf water and the cool, nutrient-rich water brought to the surface during wind-driven coastal upwelling. Since upwelling-favorable winds are not constant, but increase and decrease to give recognizable upwelling events, upwelling fronts are also variable in time and space. At the interface, upwelled water is driven down under the warmer shelf water, forming a prograde front. There have been few systematic studies of the

biology of upwelling fronts, but the information that is available suggests that planktonic organisms tend to aggregate on the coastal side of these fronts and that tuna and other pelagic fishes occur there in particularly large numbers.

At places where plumes of fresh or brackish waters run into saline coastal waters it is common to find plume fronts, where the less saline waters ride over the top of the saline waters, forming retrograde fronts and where surface convergence and downwelling occur. Once again we find that there are few systematic studies of the properties of such fronts, but there is fragmentary evidence suggesting that aggregations of plankton form at or near the convergence and that good catches of pelagic fish are often obtained there.

Within estuaries, local changes in depth give rise to small-scale variations in the degree of tidal mixing, and to the formation of fronts between mixed and stratified waters. Such fronts are often formed parallel to the shores of estuaries, separating the tidally mixed shallow waters from the deeper waters stratified under the influence of freshwater run-off. Bathymetric features also give rise to a variety of eddies and fronts in coastal waters. Whenever a tidal current impinges on a geomorphic feature such as a submerged canyon, an island, or a headland, transient fronts are found that form and disperse with the daily or twice-daily tidal cycle. Little is known about the biological significance of these small-scale fronts.

7

Tides, tidal mixing, and internal waves

7.1 Introduction

Tides are created by the gravitational pull of the moon and the sun and are most familiar as a rise and fall in the level of the sea twice a day. This changing water level leads to interesting patterns of zonation of intertidal organisms. They have

been well studied over a long period and we shall not review them here. The tides also generate currents in the water that interact with the bottom to produce turbulence. This bottom-produced turbulence tends to mix the lower layers of the water, and if the currents are sufficiently strong the turbulence may prevent any stratification and a whole area may be permanently tidally mixed. It has been shown that the breeding grounds of a number of stocks of herring *Clupea harengus* are each located in a different, discrete area of strong tidal mixing (Iles and Sinclair 1982), and in this chapter we explore the possible significance of this observation.

In situations where tidal mixing is less strong and the water column becomes stratified, the interaction of the tidal currents with the bottom topography may lead to the formation of internal waves on the thermocline at the tidal period. These waves propagate shoreward and decay causing vertical mixing and the redistribution of nutrients, with important effects on phytoplankton production. Sometimes, as the waves decay, they produce solitary waves and bores which can have a strong influence on the distribution of zooplankton and larval fishes.

As tidal currents move on and off the shallow banks, they interact with bottom topography to generate unidirectional currents that form gyres around those banks. The combination of tidally mixed water over the top of a bank and a gyre around its periphery is thought to provide conditions particularly suitable for the eggs and larvae of fish. In this chapter we shall explore some of these interesting consequences of tidally induced water movement.

7.2 The physics of tides

7.2.1 Tide-generating forces and the equilibrium tide

Tides in the ocean result from a slight imbalance between two forces: the first is the gravitational pull of the moon and sun, and the second is the centripetal force that is required to keep the ocean's water moving along with the rest of the earth in a circular path through space. We examine these forces and motions in this section to show how the main features of the tide are generated.

We first examine the effect of the gravitational force of the moon on the world's ocean in Fig. 7.01. Here the earth and the moon are seen from above the north pole of the earth, and both are assumed to be stationary except for the earth's rotation. Also, the earth in this case has no continents but is covered with a uniform layer of water. If the moon was not present, the oceans would cover the earth to a constant depth. The moon, however, exerts a gravitational attraction on each particle of water in the ocean and causes it to pile up under the moon. An observer at the equator at point O, rotating with the earth through the day, will notice that the depth of the ocean rises and falls once a day. The high tide will always be under the moon and the low tide will be on the side opposite to the moon. This elementary model produces a tide but it is not a very good model because most places on the earth usually have two high and two low tides during the day.

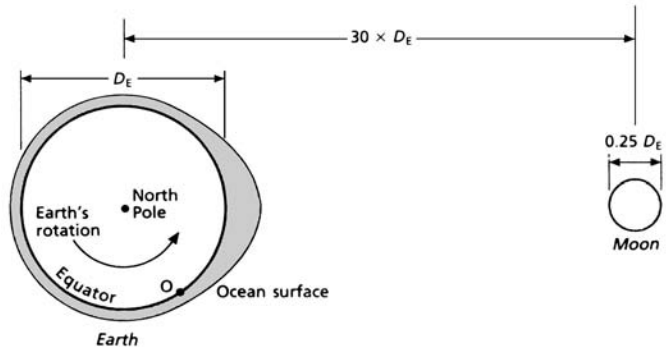

Fig. 7.01 The earth and moon viewed from above the north pole showing the ocean (shaded) pulled by the moon's gravity into a tidal bulge under the moon. An observer is at *O* on the equator.

One needed improvement in the model is found by considering the rotation of the earth–moon pair once every ~29.5 days. To keep a body moving in a circle, a force must be directed toward the center of rotation; otherwise the body would continue in a straight line according to Newton's first law of motion. This phenomenon is, of course, well known to anyone who has swung a ball on the end of a string and let go. The force that maintains the circular motion is called the centripetal force and in the case of the earth–moon system it is supplied by the gravitational force between the two bodies. If the average gravitational pull over the whole earth was not equal to the required centripetal force, the distance between the earth and moon would change until they were equal.

If the earth and the moon each had the same mass, they would rotate about a common center of mass that would lie halfway between the two. But because the earth's mass is roughly 80 times that of the moon the common center of rotation is inside the earth about 1600 km below the surface along a line from the moon to the earth. The rotation of the two bodies about this point is illustrated in Fig. 7.02(a). As the moon moves around this center of mass, the earth also moves around it in a circle with a radius equal to the distance between the center of mass of the earth and the center of mass of the two bodies. The curved lines drawn through the center of the earth and the point *A* illustrate that every point in the earth moves in a circle of similar radius. Because all particles in the earth are moving in circles of identical size, the centripetal force must be the same for every particle. The direction of this force is always toward the moon, which is also toward the center of the circle described by the particle (Fig. 7.02b).

The moon's gravitational pull on the earth decreases with distance from the moon. Particles on the side closest to the moon experience a greater gravitational pull than do particles on the side away from the moon. The average gravitational pull on particles in the earth is found at the center of the earth and must equal the required centripetal force, but the forces are imbalanced for all other

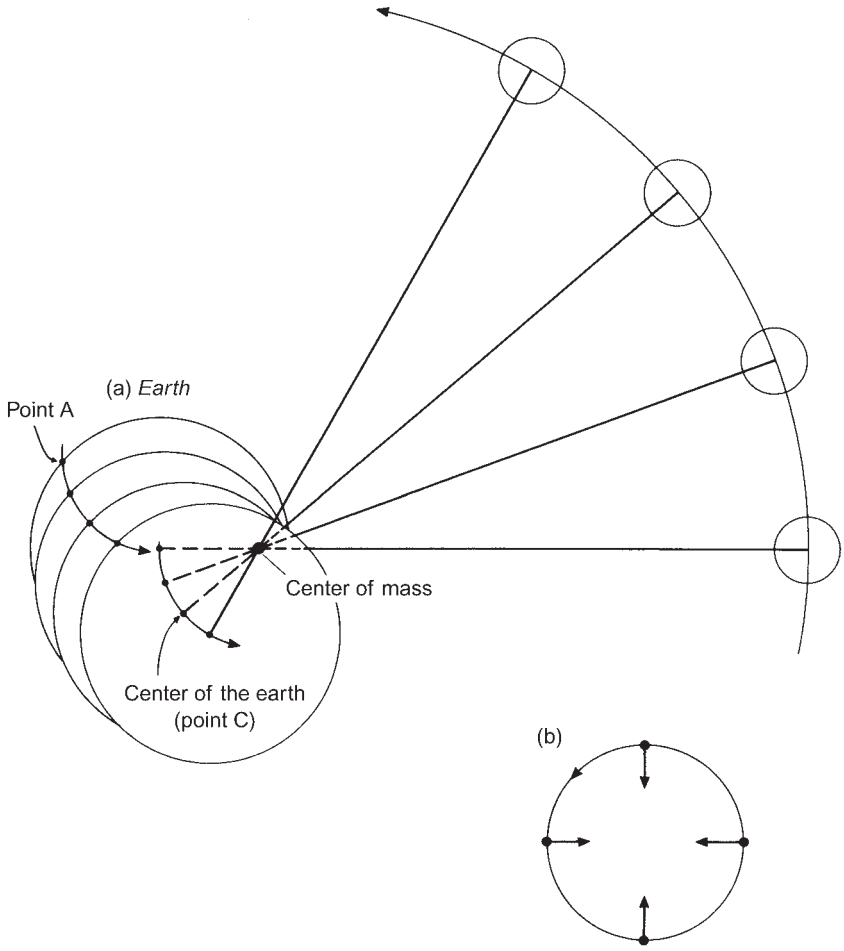

Fig. 7.02 (a) The earth and moon in mutual rotation about the common center of mass. The curves through points *A* and *C* illustrate the curves traced out by typical points on the earth. (b) The circular path of a typical particle on the earth through one cycle of the motion illustrated in (a) and the direction of the centripetal force required to keep the particle traveling in the circle.

points. This imbalance is illustrated in Fig. 7.03, which shows the earth and the moon again from above the north pole. Along the center line perpendicular to the line joining the earth and moon, the gravitational force on each particle supplies the required centripetal force. On the half closest to the moon, the gravitational force is greater than the centripetal force that causes the ocean to pile up under the moon. On the half of the earth away from the moon, the gravitational force is not strong enough to supply all the centripetal force required to keep the particles moving in the required circle, and the particles tend to move farther away. This process creates the tidal bulge on the side of the earth away from the moon.

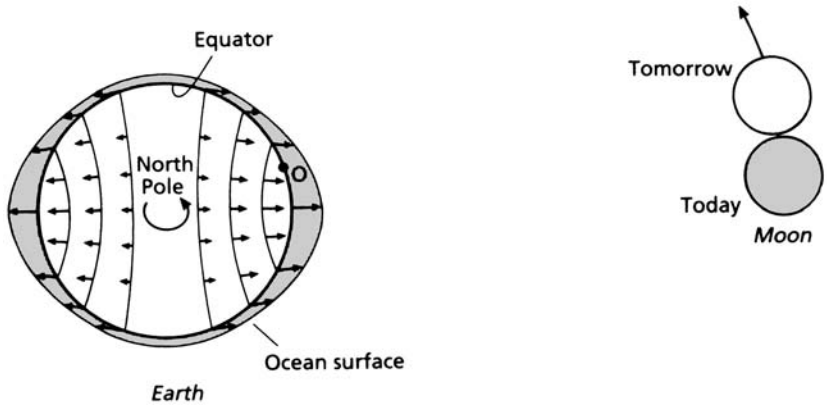

Fig. 7.03 The small arrows on the earth represent the net force due to the imbalance between the gravitational pull of the moon and the centripetal force that leads to "tidal bulges" on two sides of the earth. The moon is shown at two positions one day apart to illustrate the delay of the tides by ~50 minutes each day as seen by the observer at *O*.

The observer at *O* now observes two high tides and two low tides every day as the earth rotates.

So far we see that the centripetal and gravitational forces of the earth–moon system account for the fact that there are two tides every day. Figure 7.03 may also be used to explain why the tides do not occur at the same time every day. The earth and moon rotate around one another in a lunar month that is roughly 29.5 days. As our observer at *O* rotates through exactly one day back to *O* the moon has moved about 12° further around in its orbit to the position marked "tomorrow" in Figure 7.03. The high tide that is under the moon will still be under the moon tomorrow, but it will be observed later in the observer's day. Since the earth spins on its axis at about 4 minutes per degree the tides will appear about 50 minutes later each day.

For the next refinement of these qualitative arguments, consider Fig. 7.04, in which the earth and moon are viewed from the side. Instead of having the moon directly over the equator, as in the previous figures, it is shown about 25° north of the equator. This situation arises because the moon's orbit around the earth is tilted at an angle to the equator. The moon can be found at various angles to the north and south of the equator up to a maximum of 35° depending on the season and the time of the lunar month. The aim of the diagram is to show that the tidal bulges are no longer on the equator, as they were imagined in Figs. 7.01 and 7.03, but now one lies north of the equator under the moon while the other lies on the opposite side of the earth, to the south of the equator. Our observer at *O* now notices that there are two high and two low tides but that the high tides are of unequal height, as are the low tides. This difference is called the diurnal (daily) inequality.

This elementary view of tides on a world with a moon but no sun, without continents, and in an ocean that is always in equilibrium with the forces that are

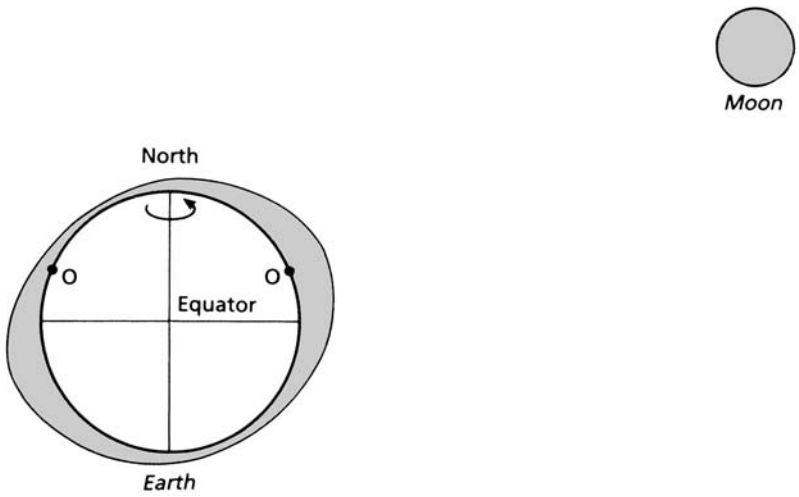

Fig. 7.04 Viewed from the side (north up) and with the moon north of the equator, the tidal bulges are asymmetric about the equator, resulting in the diurnal inequality in the heights of the high and low tides.

acting, is called the equilibrium tide. It cannot predict the tide at any particular location but it does explain some of the main features of the tide such as the diurnal variation, the diurnal inequality in the height of the tide, and the daily delay of ~50 minutes in the time of the highs and lows. The next improvement in the model is introduced by considering the effects of the earth–sun system on top of the effects of the earth–moon system.

The mass of the sun is 27×10^6 times the mass of the moon but its distance from the earth is 400 times that of the moon. Because of this great distance, the gravitational attraction on a particle of water on the earth due to the sun is about one-half that due to the moon. So we can construct diagrams like those shown in Figs. 7.03 and 7.04 for the tide due to the sun, but the height of the tide will be only half that due to the moon. The important effect of the tide due to the sun arises because its tidal bulge moves relative to the moon's tidal bulge throughout the lunar month. When the two tidal bulges coincide they add together to create the extra high tides called the spring tides. When the tidal bulges are opposed their effects tend to cancel one another, creating the neap tides. Thus, the equilibrium tide model can also qualitatively explain the fortnightly inequality in addition to the other effects.

7.2.2 Tides in the real ocean

The equilibrium tide helps us to understand some of the main principles of tides, but when it comes to predicting the tide in the real ocean this theory is of little

help because the water that is raised up as the tidal bulge has to move around a world that is spinning on its axis and that is cluttered with continents. It is possible to formulate a rigorous dynamical theory to predict the tides but the way that the tidal wave moves in an ocean basin is very dependent on the shape of the basin, and is not amenable to simple mathematical description. Such theories can be used in simple situations that have elementary geometries – for example, in bays with flat bottoms and straight vertical sides (Bowden 1983) – but generally the tide must be predicted by extrapolating from existing measurements.

This calculation is normally done by measuring the height of the tide for at least a month, then decomposing the record into sinusoidal constituents. There are three main categories of constituents (Pond and Pickard 1983): (i) semi-diurnal, period about 12 hours; (ii) diurnal, period about 24 hours; and (iii) long period, greater than 24 hours. Although 20 or more constituents may be required to predict the tidal height accurately, the four most important constituents are:

the lunar semi-diurnal	M_2	Period = 12.42 h
the solar semi-diurnal	S_2	Period = 12.00 h
the lunisolar diurnal	K_1	Period = 23.93 h
the principal lunar diurnal	O_1	Period = 25.82 h

The M_2 constituent is roughly twice the amplitude of the other three.

The form of the tide, or the pattern of the water's rise and fall, is not the same at all locations around the oceans but varies according to the relative importance of the different constituents. The four main classifications of the form of the tides are illustrated in Fig. 7.05. The top record, from Immingham, England, illustrates a tide with two high and two low tides every day. Both the highs are about the same height and both the lows are about the same height. Such a tide is called a semi-diurnal in form because there are two per day and both are about the same height. In this case the semi-diurnal constituents dominate the diurnal ones. This fact is often quantified with the ratio $F = (K_1 + O_1)/(M_2 + S_2)$, where each letter stands for the amplitude of the constituent. If F is small (0.11), as in the upper record, the sum of the amplitudes of the diurnal constituents $(K_1 + O_1)$ is small relative to the sum of the semi-diurnal ones $(M_2 + S_2)$.

The four records in Fig. 7.05 show a marked decrease from top to bottom in the amplitude of the semi-diurnal tidal oscillation relative to the diurnal oscillation, which is confirmed by the increase in F from 0.11 to ~19. At San Francisco there are always two tides per day but they are usually of unequal amplitude. At Manila there are two tides per day during the neap tides but only one rise and fall per day during spring tides. At Do-Son there is only one rise and fall of the tide per day throughout the month, which is a purely diurnal form of tidal oscillation. This occurrence is the rarest form of tide. The changing form of the tide between locations is due partly to the shape of the ocean basin in which the tidal wave is contained and partly to the latitude (Hendershott 1981).

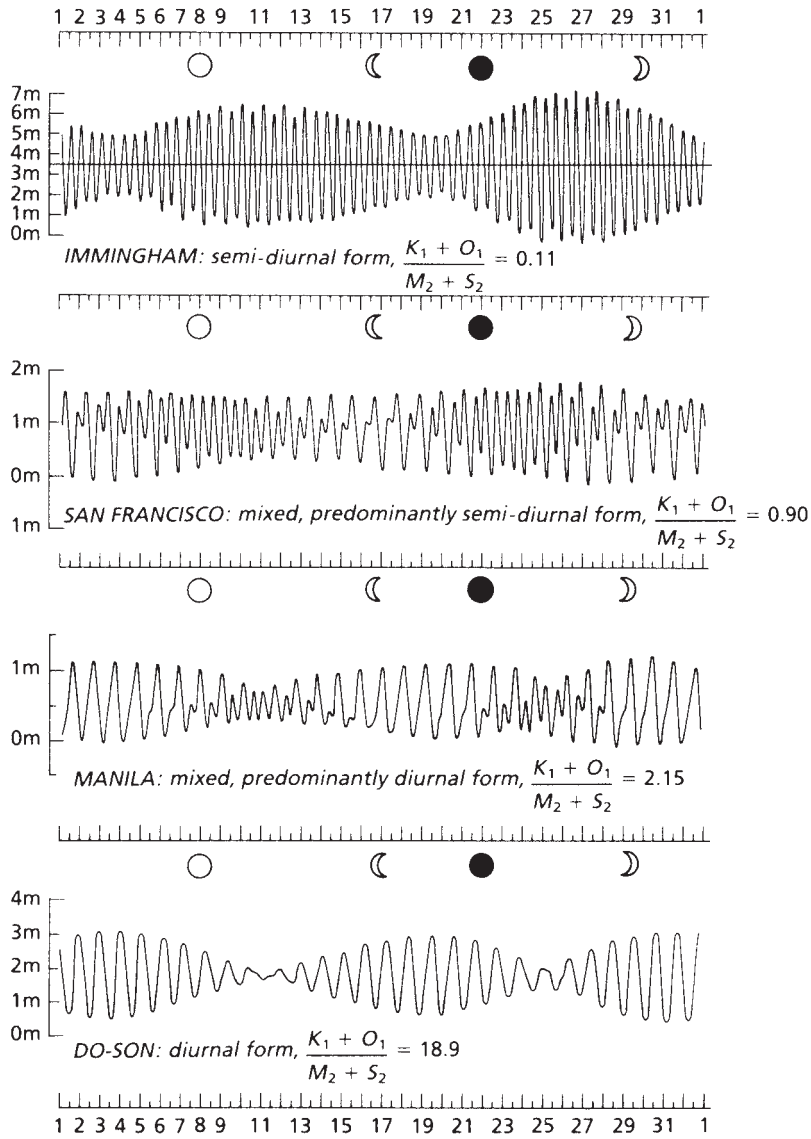

Fig. 7.05 Tidal records through March 1936 at four coastal stations illustrating variations in the amplitudes of the semi-diurnal ($M_2 + S_2$) and diurnal constituents ($K_1 + O_1$). Adapted from Defant (1958).

7.2.3 Moving the tidal bulge over the earth: Kelvin waves

The tidal bulge shown in Fig. 7.04 travels over the surface of the rotating earth as a very long wave. And because the length of the wave is very much greater than the depth of the water it is called a "shallow water" wave, similar to the

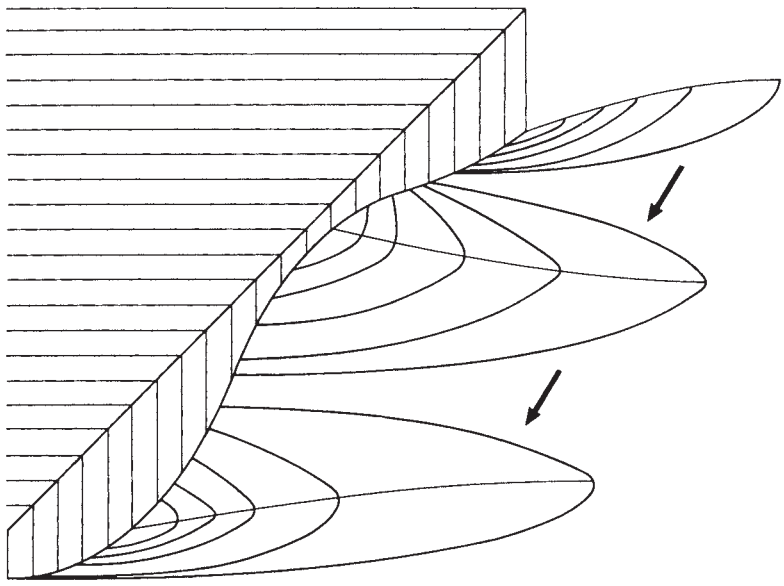

Fig. 7.06 A Kelvin wave traveling from the upper right to the lower left with the coastal wall to the right of its direction of travel. Note that the height of the wave decreases with increasing distance from the coast.

waves that can be set up in a bathtub by making the water rock back and forth. The other kind of wave, the "deep water" wave, is the one normally seen generated by the wind on the ocean's surface. One important feature of shallow-water waves that sets them apart from the deep-water waves is that the velocity of the wave motion is constant throughout the depth of water while the motion in the wind waves dies out a few meters below the surface. Thus the velocity in the tidal wave is approximately constant throughout the depth of the ocean. Such flow is sometimes referred to as a barotropic wave – more specifically a barotropic Kelvin wave.

Because the tidal waves cause the water to move relative to the earth for a long time the Coriolis force is an important feature of the motion. The effect of the Coriolis force is to push the water to the right in the northern hemisphere. Figure 7.06 shows a Kelvin wave traveling south, with the coast to the west of it. The Coriolis effect causes the amplitude of the wave to increase toward the shore and leads to the expression that the wave is "trapped" against the shore. Such a trapped Kelvin wave causes the water particles to move back and forth parallel to the coast as the wave goes by.

The horizontal scale of the wave, or the approximate distance from the coast to where the sea level is undisturbed by the wave, is estimated by the Rossby radius. We used the same scale in estimating the width of the coastal upwelling regions in Section 5.2.3 but in the present case we use the formula

$$R_e = (gh)^{1/2}/f \tag{7.01}$$

where g is the acceleration due to gravity, h is the depth of the water, and f is the Coriolis parameter. In our earlier example we were concerned with two layers of different density and g was replaced with the reduced gravity (g') and h represented the depth of the upper layer. For the Kelvin wave in Fig. 7.06 we put $g = 10$ m s^{-2}, $h = 4000$ m, and $f = 10^{-4}$ s^{-1} to get $R_e = 2000$ km. This value is commonly called the external Rossby radius, or deformation scale, as opposed to the internal Rossby radius derived in Section 5.2.3. The external deformation scale is roughly 100 times the internal one.

7.2.4 Tidal currents

We see from Fig. 7.06 that a coastally trapped Kelvin wave in the northern hemisphere will retain its integrity only if it is moving in a counter-clockwise manner around the coastal margin of a basin. The Coriolis force ensures that it will have a high amplitude close to the coast and a low amplitude far from the coast, typically at a distance of 2000 km. For the North Atlantic basin, therefore, a pattern similar to that shown in Fig. 7.07 develops. In the mid-Atlantic there is an amphidromic point at which there is zero rise and fall with the tides, and the tidal amplitude increases as one moves toward the coast. High tide appears successively at points along the coast, proceeding in a counter-clockwise direction. Similar patterns are found within smaller basins, such as the North Sea.

In the deep ocean the vertical range of the tide, as suggested by the illustration in Fig. 7.07, is only a few centimeters and tidal currents tend to be only a few centimeters per second. Over the continental shelves, however, the currents can be in the meters per second range as they are associated with much higher tidal amplitudes.

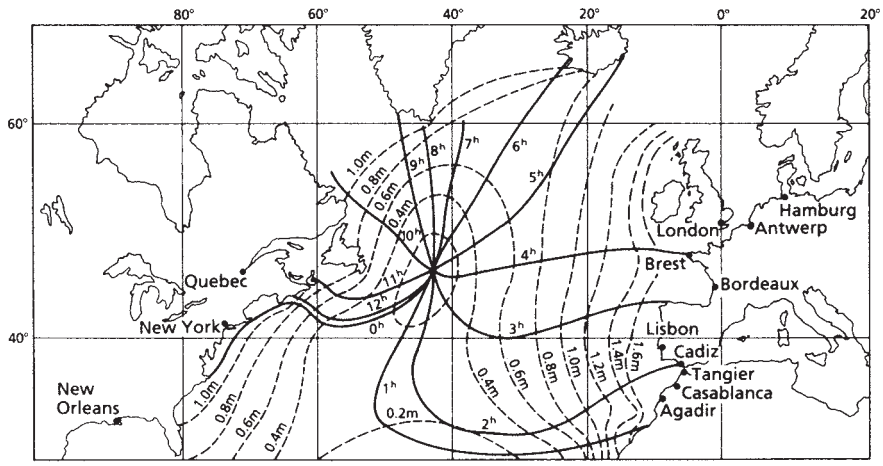

Fig. 7.07 The amplitude (dotted) and phase (solid) of the M_2 tide in the North Atlantic Ocean. The amplitude is in meters and the phase in hours after the passage of the moon over the prime meridian. Adapted from Defant (1958).

The direction of tidal currents varies greatly and depends on the way in which the tidal wave propagates in the local area. Along a straight coast or in a confined channel the currents tend to be parallel to the shore. In open areas the tidal wave is not constrained to be rectilinear, and currents in general will have both north–south (v) and east–west (u) components.

7.2.5 Internal waves

Tidal currents often cause internal waves to be generated on the pycnocline. These waves were mentioned in Section 3.2.3, where it was shown that when the pycnocline is displaced vertically a restoring force is generated that pushes the pycnocline back toward its undisturbed position. This force leads to the possibility of a vertical oscillation and of waves being propagated on the interface. Some features of such a wave on a sharp density interface are illustrated in Fig. 7.08.

The interface in the figure has been placed close enough to the sea surface so that some effects of the internal wave motions are felt at the surface. The lower layer is assumed to be infinitely deep. The wave is propagating from left to right

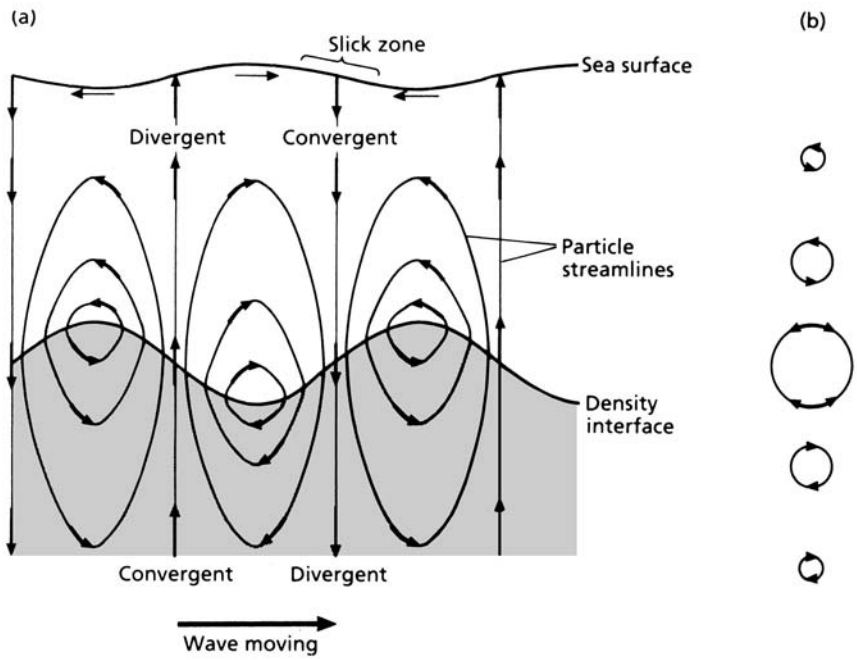

Fig. 7.08 (a) A wave progressing from left to right on the density interface, showing the instantaneous particle streamlines, the resultant surface wave, the zones of convergence and divergence, and the region where slicks are likely to form on the surface. (b) The particle orbits over one cycle due to the passing internal wave. The diameter decreases away from the interface and the direction of the trajectory reverses across the interface as indicated by the double arrows on the central orbit.

and causes the water particles to move along the particle streamlines. These lines indicate the instantaneous paths of the particles while the arrows within the streamlines suggest the magnitudes of the particles' velocities, which diminish with distance away from the interface. As the wave progresses, the pattern of streamlines moves along with it but the individual particles of water remain in their original locations moving in wave-induced circular orbits. The examples of these orbits in Fig. 7.08(b) illustrate that the orbit diameters, like the particle velocities, decrease with distance from the interface.

Interesting biological consequences of the internal wave motion are created by regions of convergent and divergent flow in the upper layer. Above the pycnocline the thickness of the upper layer clearly varies along the length of the wave. As the wave advances, water must flow from the thin regions above the wave crests to the thicker regions above the wave troughs. The water must, therefore, converge behind the wave crests and diverge behind the wave troughs as noted in Fig. 7.08(a). These regions of convergence and divergence exist up through the water column to the sea surface with diminishing intensity but their strength is enough to create a wave in the sea surface. This surface wave has the same length as the interface wave but it is 180° out of phase with the internal wave and has a much smaller amplitude.

On the sea surface the convergent zones cause floating organic matter to accumulate in bands that are ahead of, but parallel to, the wave crests. The organic material increases the surface tension of the surface layer, which reduces the amplitudes of the smaller surface ripples. This change gives the appearance of a band of water that is smoother than the water over the divergent zones where the small waves continue to exist. These smooth patches are often called "slicks." The contrast in the roughness of the sea surface can also be detected by a special instrument called the synthetic aperture radar. When such instruments are carried in aircraft or satellites they allow mapping of the sea surface features over large areas, as demonstrated by New (1988) for an area near the Celtic Sea shelf break.

Below the pycnocline the particle trajectories (Fig. 7.08b) due to the internal wave are opposite in direction to those above the interface. In addition, the regions of divergence and convergence below the interface are displaced by one-half of a wave length from the ones above the interface. These features make sense because the thickness of the lower layer varies along the wave in the opposite sense to the thickness variations above the interface. The reversal in the particle orbits across the interface leads to a shear across the interface that is especially strong at the wave crests and troughs. Halfway between the crests and troughs the motion due to the wave is predominantly vertical, as indicated by the vertical streamlines in Fig. 7.08(a).

The interface waves of Fig. 7.08 are a special form of internal wave. Throughout most of the ocean's depth the density of water increases gently and smoothly rather than rapidly across thin layers. The larger-scale density stratification also supports internal waves but they tend to be oscillations of the whole water column rather than waves confined to the region near an interface. For a description of these large-scale oscillations and a more thorough examination

of the interface waves introduced here, see Roberts (1975), Pond and Pickard (1983), Apel (1987), or New (1988). More information on the biological significance of internal waves is given in Section 7.4.1.

7.2.6 Generating internal interface waves: lee waves and internal bores

One of the more common mechanisms producing internal waves on the pycnocline occurs when the water flows over an obstacle. Long (1954) investigated this process in a long tank filled with two layers of unequal density (Fig. 7.09). The denser layer fills the lower third of the channel. When a small smooth obstacle is placed in the bottom of the channel and the lower layer is forced to flow from left to right, lee waves are formed on the interface between the fluids downstream of the obstacle. These lee waves are moving at the same speed as the water but in the opposite direction. Waves that are shorter than the ones shown travel too slowly for the speed of the water and are swept downstream. The longer and faster waves propagate upstream away from the obstacle. Thus, the observed lee waves are the interface waves that are selected by the speed of the stream. These lee waves are usually associated with steady flows, but often tidal flows generate such waves on the lee side of shallow ridges. When the tidal stream slows down, the waves continue to exist but move away from the obstacle through the more slowly moving water.

Witman *et al*. (1993) noted pulses of warm water containing 2–3 times the normal amount of phytoplankton, close to the bottom, in 29 m of water in the central Gulf of Maine. They found that these pulses were produced by internal waves with a maximum amplitude of 27 m, which periodically carried water from the mixed layer down to the bottom. The internal waves were found to be the lee waves of a rock pinnacle on which were superimposed solitons propagated from Georges Bank (see below). Hence, tidal currents passing over features of the geomorphology probably serve both to mix nutrients up into the surface waters and to carry phytoplankton down to benthic filter-feeding animals.

Another type of lee wave, generated by the same mechanism but over the period of the flood or ebb tide, is sometimes created at the edge of continental shelves.

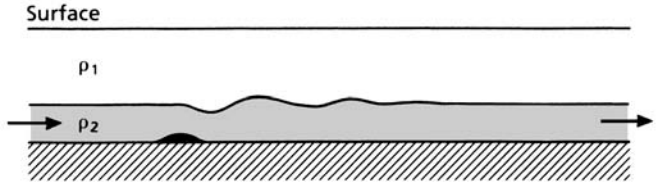

Fig. 7.09 The interface in a two-layer fluid in which the lower layer is moving from left to right over a smooth obstacle whose height is less than the thickness of the lower layer. Adapted from Long (1954).

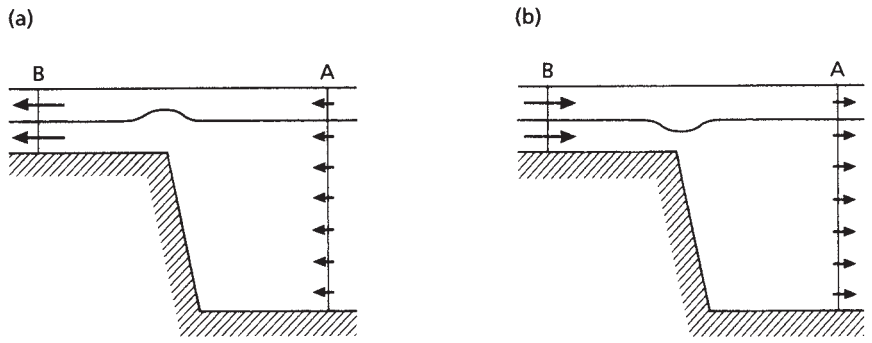

Fig. 7.10 (a) A section through the ocean in the vicinity of a shelf break, illustrating the higher currents of the flood tide over the shallow water at *B* than in the deep ocean at *A* and the resultant rise in the pycnocline at the shelf break. (b) The same situation as in (a) except the tide is ebbing and the pycnocline is depressed at the shelf break.

An elementary illustration of its generation is given in Fig. 7.10. We first assume that the tidal flow through section *A* in the deep water is the same as that through section *B* in the shallow water, and that far away from the shelf edge the currents are the same from top to bottom – that is, the currents are barotropic. On the flood tide, when the water is streaming onto the continental shelf, there must be more water passing through the upper layer in section *B* than through the upper layer in section *A*. This condition occurs because the layer is the same thickness in each location and the water through section *B* is going faster than through *A*. In the lower layer there is more water passing through section *A* than through *B*. The deficiency in the upper layer coupled with the surplus in the lower layer causes the interface between the two to rise in the vicinity of the shelf break. On the ebb flow the opposite occurs and the interface between the layers is forced down, as indicated in Fig. 7.10(b).

The raising and lowering of the pycnocline can be tens of meters and represents a large fraction of the depth of the upper layer. These large undulations propagate as waves both into deep water and over the shelf but because of their large amplitudes nonlinear effects tend to dominate their existence. The fate of the wave, called the internal or baroclinic tide, is outlined in Fig. 7.11. First, the wave is in the form shown in stage 1 and travels toward the left over the shallower water. The front of the wave (to the left) begins to steepen because the troughs of the waves travel slower than the peaks. As the waves get steeper (stage 3) shorter waves begin to form that grow with time until only high-amplitude but short waves remain (stage 5). These short waves, because they are quite far apart relative to their wavelength, are sometimes called solitary waves or solitons. They usually travel in groups, however, and are not really solitary – but they may be treated mathematically as isolated phenomena.

As these packets of solitary waves propagate further onto the shelf their amplitude decreases as the high shears within the waves lead to Kelvin–Helmholtz

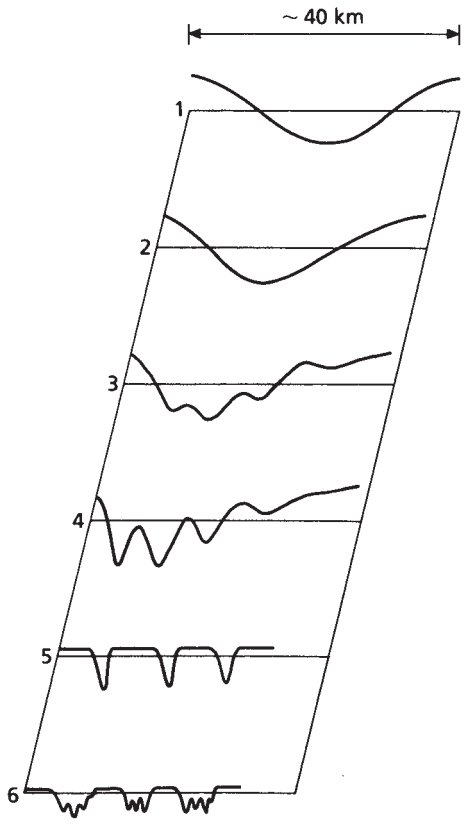

Fig. 7.11 Six stages in the life of the internal tide as it progresses to the left over the shelf, first becoming steeper at the leading edge, then forming shorter waves that become solitary waves that decay into turbulence.

instabilities and turbulence (stage 6). The waves are dissipated within about 30 km of the generation region and it is the conversion to turbulence in this 30 km strip of wave energy that is thought to provide the mixing that increases the nutrient flux up into the euphotic zone and the subsequent biological enhancement (Sandstrom and Elliott 1984, Pingree and Mardell 1985).

An important feature of these waves, beginning at stages 4–5, is that the water in the wave moves along with the wave. Because of this it is sometimes referred to as an internal bore. As suggested by the curves for stages 5 and 6 the bores come in groups. In southern California, according to Pineda (1994), a group will have two to nine bores in spring and summer when the water column is well stratified. The effects of the passage of a bore on the temperature and velocity structure in the water column is well illustrated in Plate 5. The arrival begins with a deep depression in the upper layer that lasts about three minutes. This is followed by series of waves on a thicker upper layer. As indicated by the current vectors the water in the warm upper layer is moving onshore while the cooler

lower layer is moving offshore. In the later stage of the bore the water in the warm upper layer moves offshore, while the water in the cooler lower layer moves toward the shore. The biological importance of the bore is discussed in Section 7.4.4(b).

A slightly different internal-wave phenomenon was observed over the northern edge of Georges Bank in early summer by Loder *et al*. (1992) and Brickman and Loder (1993). They found a depression in the thermocline over the edge of the bank being generated regularly on the ebbing tide. The length of the feature was 2–3 km, rather than the 40 km indicated in stage 1 of Fig. 7.11 for the internal tide. The authors suggested that the depression they observed was an internal hydraulic jump.

Hydraulic jumps are commonly seen on the downstream side of dams where water flowing rapidly down a steep incline reaches a level where the incline is less steep. At this point, the flow slows a little and since more water reaches this point than can be carried away the depth of the water increases sharply. The phenomenon is also often observed in water flowing rapidly over rocks in fast-moving rivers and streams. Brickman and Loder (1993) proposed that the rapid tidal flow off the shallow part of Georges Bank creates a hydraulic jump when the flow reaches the deeper water at the edge of the bank where it slows down. Because the flow occurs in the interior of the water column, they called it an internal hydraulic jump.

The authors also suggested that the observed depression may be partly created by internal waves generated at the edge of the bank as part of the internal tide. On the ebbing tide these waves are unable to propagate away in the direction of the shallow bank against the rapid off-bank tidal flow. They therefore tend to congregate to produce the internal hydraulic jump.

The biological importance of the depressions comes when the tide turns and they are partly carried and partly propagated over the shallow part of the bank where they eventually break as in stage 6 of Fig. 7.11. Brickman and Loder (1993) calculated that the dissipation of these features supplies 0.42 $\mu mol\ m^{-2}\ s^{-1}$ of nitrate into the upper layer. As this amount is roughly equal to the estimated nitrate demand of 0.36 $\mu mol\ m^{-2}\ s^{-1}$, the process may be a major contributor to the increased productivity observed in the region.

7.2.7 Tidal rectification

The bathymetry of continental shelves is often uneven, being marked by shallow banks and basins. Oscillating tidal currents washing back and forth over the banks sometimes generate mean currents at the edge of the bank where the depth is increasing rapidly. This process of extracting energy from an oscillating tidal current to produce a mean unidirectional flow is called tidal rectification. Two places where it is thought to play an important role are around Georges Bank in the Gulf of Maine (Loder 1980) and around large sandbanks in the North Sea (Huthnance 1973).

The rectification of the oscillating flow depends on the fact that the tidal excursion is larger over the bank than in the deep water. This situation is illustrated

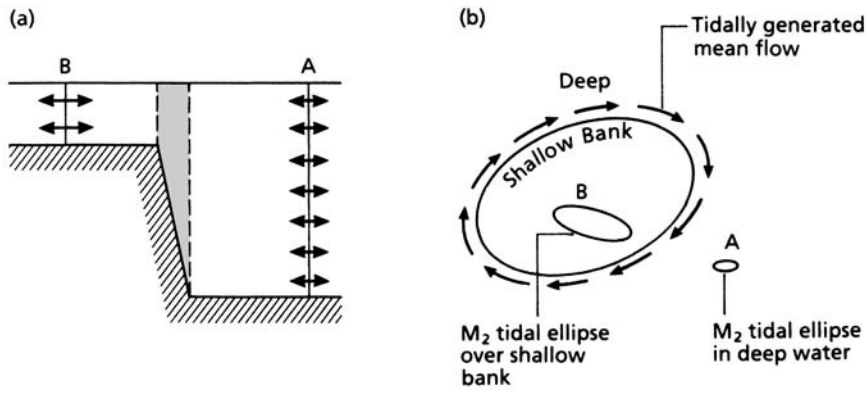

Fig. 7.12 (a) A section through the ocean across the edge of a bank such as Georges Bank in the Gulf of Maine, illustrating that the tidal current is higher in the shallow water than in the deep water. The shaded region over the sloping bottom indicates where the currents are accelerated and decelerated, leading to "tidal rectification" that generates the mean flow around the bank. (b) A view down on the bank shows the large tidal ellipse over the shallow water relative to the ellipse in the deep water, and the tidally generated clockwise flow around the bank.

in Fig. 7.12(a) in a cross-section of the ocean through the edge of the bank, similar to Fig. 7.10 but without density stratification. The tidal flow through the vertical section *A* is the same from top to bottom. If the same amount of water is to pass through section *B* as section *A* the speed of the flow in the shallow water must be larger than in the deep water. The same phenomenon is illustrated in Fig. 7.12(b) by the comparison of the M_2 tidal ellipses over the bank and in the deep water.

The change in speed of the tidal flow between the deep and shallow water occurs in a narrow band over the sloping edges of the bank and creates nonlinear forces associated with the acceleration and deceleration of the water. The rapidly changing speed also affects the magnitude of the forces due to the Coriolis effect and bottom friction, both of which depend on the speed of the flow. It turns out that in this region of rapidly changing forces the balance between them is disturbed in such a way as to produce the clockwise mean flow around the bank as illustrated in Fig. 7.12(b). The details of the mechanisms are not easily described outside the elegant analytic formulations of Loder (1980) and Huthnance (1973) and numerical models of Greenberg (1983).

7.3 Tidal mixing in the water column

We saw in Section 4.5 that tidally driven vertical mixing changes the seasonal pattern of phytoplankton production. There is also evidence that tidally mixed areas are favored as spawning grounds by herring. This section explores the evidence for these ideas.

7.3.1 Tidal mixing and plankton production

If tidal currents are strong enough to mix the water column all year, there is a continuous supply of nutrients from near-bottom waters up to the euphotic zone, which permits phytoplankton production to continue at a good level throughout the summer. This sequence of events is in contrast to the situation in stratified waters, where the supply of nutrients tends to become depleted after the spring bloom. As a result, tidally mixed areas like Georges Bank, near the Gulf of Maine, and the Dogger Bank in the North Sea have levels of primary production considerably higher than adjacent stratified areas of the shelf. It has been found that these sites are often selected as breeding grounds by commercially important fish stocks, and it is of interest to explore the connection between tidal mixing and the early life histories of fish.

7.3.2 Tidally mixed areas and the spawning of fish

Fisheries biologists have long been puzzled by the ability of a single species such as herring to divide into a number of discrete breeding stocks, each with a characteristic place and time of breeding, and often with recognizable small differences in body structure. The feeding adults of the various stocks are often found mixed together in the same place but at breeding time they segregate and return to the place where they were hatched. In this way they maintain genetic differentiation of the stocks. How do they recognize those breeding grounds, and what defines their limits? For some stocks, the breeding ground is readily identified as a group of fjords (e.g., the Norwegian coast) or estuaries (as on the Maine coast), but in other cases there is no clear physical boundary to the spawning ground or the nursery area in which the young fish develop. Iles and Sinclair (1982) noticed that the breeding grounds of a number of herring stocks are located in areas of vigorous tidal mixing, bordered in summer by a tidal front. They proposed that tidally mixed areas act to define and delimit the breeding and nursery areas of a number of stocks of herring, on both sides of the North Atlantic.

The early work on predicting the occurrence of tidally mixed areas was done in waters around the United Kingdom (Section 4.5.1). When tidally driven currents moving across the sea floor are sufficiently strong to generate turbulence that breaks down any stratification in the water column above, that area is said to be tidally mixed. As we showed in earlier chapters, Simpson and Hunter (1974) and Pingree *et al.* (1978a) showed how to predict the occurrence of tidally mixed areas on Georges Bank, Nantucket Shoals, in the mouth of the Bay of Fundy, and off the southwest coast of Nova Scotia.

Iles and Sinclair (1982) showed that there was a remarkable similarity between the distribution of larval herring and the occurrence of tidal mixing, on both east and west coasts of the North Atlantic. In the Gulf of Maine area larval herring are found on Nantucket Shoals, on Georges Bank, and in the tidally mixed

areas off New Brunswick and Nova Scotia. In the North Sea, the spawning grounds of the "Downs," "Banks," and "Buchan–Shetlands" stocks of herring are in tidally mixed areas. Even in the Gulf of St Lawrence, where the occurrence of tidally mixed areas had been predicted by Pingree and Griffiths (1980), five of six major herring spawning grounds are in tidally mixed areas.

The question then arises: what is it about these tidally mixed areas that makes them suitable as herring spawning grounds? Is the food-production process particularly favorable, or could it be that the strong tidal currents remove fine particles and leave behind a gravel particularly suited to herring spawning? Some of these questions were addressed by Lough *et al*. (1989) during a series of dives in a manned submersible on the northeastern edge of Georges Bank. Cod *Gadus morhua* and haddock *Melanogrammus aeglefinus* are pelagic in the water column for the first few weeks after hatching in spring, then become bottom-dwellers about July. They were observed to live and feed primarily on a large pebble-gravel deposit (the gravel pavement), at 70–100 m depth, where their coloration matched that of the substrate. In September the fish began to make night-time forays into the water column to feed on invertebrates. The clockwise gyre (Section 7.2.7) then distributed them more widely over the perimeter of Georges Bank. Parts of the gravel pavement were also found to be the preferred spawning habitat of herring (Valentine and Lough 1991) and a good habitat for scallops *Placopecten magellanicus*. The gravel pavement is produced by the winnowing action of strong currents, which remove fine particles from the material originally deposited by glaciation. This interaction between bottom deposits and tidal currents may prove an important factor in the ecology of fishes, and good management could potentially include a concern that the structure of the gravel pavement community is not destroyed by trawling.

In general (see Chapter 4), tidally mixed areas have a relatively uniform biomass of phytoplankton throughout the growing season, and the zooplankton biomass tends to peak late in the year. Since the herring in these areas may be spring spawners or autumn spawners, there appears to be no critical pattern of food production to which they are adapted. In fact, off southwest Nova Scotia there is an autumn-spawning stock that occupies the tidally mixed area principally in winter, when food production is minimal. There remains the possibility that the young herring make particular use of the high productivity associated with tidal fronts, but this suggestion has not been verified in the field.

Iles and Sinclair (1982) suggested that the important feature of these tidally mixed areas is that the boundaries act as natural barriers to the dispersion of the larvae during early development, thus ensuring the geographical discreteness of the stock. They pointed out that as tidal currents flow over the edges of banks like Georges Bank and the waters surrounding Grand Manan in the Gulf of Maine, the changing topography causes rectification of the currents and anticyclonic gyres are formed (Loder 1980, Loder and Wright 1985, Smith 1989; and see Section 7.2.7). These persist even in winter when the front between stratified and tidally mixed waters disappears, and might well be the physical barrier that reduces dispersal of the young fish. In general, the idea that tidally mixed areas assist in the retention of

fish in young stages of development, thus defining the geographical limits of the breeding grounds of the stock, has come to be known as the larval-retention hypothesis. An important aspect of the hypothesis is the suggestion that the size of the retention area sets an upper limit on the size of the stock that breeds there. Where the breeding ground is in a fjord or an estuary, the land forms a natural boundary of the breeding area. Otherwise, the boundaries of the tidally mixed area serve the same purpose. At one site in the Gulf of St Lawrence that is an important herring breeding ground but is not tidally mixed, there is a geographically fixed gyre that might well serve as a retention area. It should be noted that gyres do not effect 100% retention of fish larvae, but rather are "leaky". For example, a study of haddock larvae hatched on Brown's Bank, off Nova Scotia, found that although most of the larvae were retained, a small proportion escaped and completed their development elsewhere on the shelf (Campana *et al*. 1989).

A modeling study of wind-forced biological–physical interactions on an isolated offshore bank, approximating conditions on Georges Bank, was made by Lewis *et al*. (1994). A semi-spectral primitive equation model was used to study three-dimensional wind- and density-driven circulation. It was coupled to a biological model involving a simple plankton food chain and a single generation of copepods. Typically high winds during winter (13 m s^{-1} for 20 days) caused much of the bank water mass to be replaced with surrounding waters. It caused major reductions in zooplankton populations, which would be expected to cause poor recruitment at higher trophic levels.

Both here and in Section 9.5 it is very noticeable that the argument does not proceed in a rigorous "hard science" manner from one testable hypothesis to another, but consists of fragmented observations on different aspects of a very complex system. Ecologists who choose to investigate the properties of large ecosystems face a dilemma. They may isolate a small part of the system, find a "manageable" problem, and formulate a rigorously testable hypothesis. But the total system, functioning in an integrated manner, is much more than the sum of its parts and at the present stage of development of ecosystem science one often has to resort to the process of collecting evidence that appears to support or not support a particular hypothesis.

7.4 The biological significance of internal waves

7.4.1 Internal waves as nutrient pumps

We may recall what was said about shelf-break fronts in Section 6.2.2(a). It has often been observed that the shelf break is an area of enhanced biological productivity. Fish are particularly abundant there (Fournier 1978) and it is very common to find greater amounts of phytoplankton and zooplankton than in adjacent areas (Herman *et al*. (1981). Often, mesozooplankton in these areas stay above the thermocline during the day, while in adjacent areas they migrate below it.

Pingree and Mardell (1981) reported on a series of studies of the shelf break adjacent to the Celtic Sea in the eastern North Atlantic. In summer this region is characterized by a band of water about 100 km broad that is 1–2 °C cooler than water on either side of it. At times the band can be traced for about 800 km south from the Celtic Sea. The levels of inorganic nitrate and chlorophyll are significantly higher in this band than in adjacent water. Pingree and Mardell suggested that the interaction of tidally driven internal waves with the bottom topography was the cause of the phenomenon. Subsequent studies (Mazé 1983, Pingree *et al*. 1986, Mazé *et al*. 1986) showed that during the off-shelf streaming phase of the barotropic tide the isotherms in the upper shelf region were depressed. When the tide slackened, the depression separated into on-shelf and off-shelf propagating internal tides. At large spring tides the crest-to-trough height of the internal tide was 50–60 m at the point of origin. The off-shelf waves had a wavelength of about 46 km and propagated at about 1.03 m s^{-1} (about 3.7 km h^{-1}) while the on-shelf waves had a wavelength of 31 km and propagated at 0.7 m s^{-1} (about 2.5 km h^{-1}). The latter had a more rapid decay rate, indicating that they caused more vigorous mixing in shelf waters than offshore. As the field data show (Fig. 7.13) the large-amplitude waves had relatively high-frequency internal waves associated with them and concentrated in the troughs. This situation is a clear example of the phenomena described in Section 7.2.5 and Fig. 7.11.

According to New (1988) these short waves produce a roughening of the sea surface that is often visible as a series of "rips," many kilometers long and spaced about 1 km apart. As mentioned earlier, these are detectable from space by synthetic aperture radar imaging, and illustration was given of the occurrence of several groups of these waves over the shelf edge in the Bay of Biscay. Each group of waves indicates the position of a depression of the thermocline in one of the long-period waves. Using a linear numerical model, New (1988) was able to calculate the position and duration of regions of potential instability and the probability that these would cause upward mixing of nutrient-rich water through the thermocline. He found that at spring tides during summer stratification, mixing

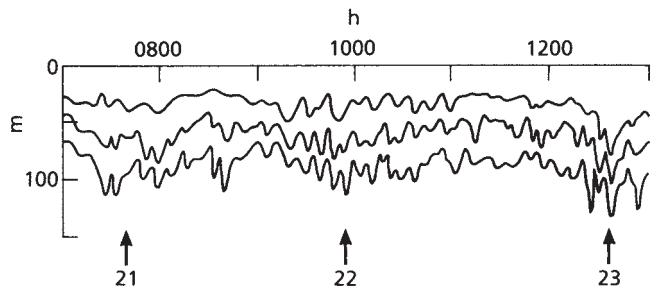

Fig. 7.13 Isopycnals along a line between points 50 and 150 km off the shelf break of the Bay of Biscay. Data were collected between 0700 h and 1300 h. Isopycnals are plotted at densities of 1026, 1026.5, and 1027 kg m^{-3}. Numbers 21–23 indicate tidal troughs with packets of short-period waves. From New (1988).

was highly probable on the shelf and beyond the shelf break. At neap tides the Richardson number was not critical at any location, so no mixing was predicted.

The effect of internal tidal waves when they approach close to shore was investigated at the head of Monterey Canyon in Monterey Bay, California (Shea and Broenkow 1982). They identified a tidal bore that, at the peak of the internal wave, forced a 20 m lens of cold, nutrient-rich water out of the canyon and onto the continental shelf. They considered this tidal bore to be a major contributor to coastal productivity when upwelling was not in progress.

Leichter *et al*. (1996, 1998) studied the effect of tidal bores generated by breaking internal waves, at Conch Reef, Florida Keys (USA). The arrival of bores on the reef slope was linked to a semi-diurnal tide. Arrival was marked by temperature drops of up to 5.4 °C and salinity changes of up to 0.2 parts per thousand in 1–20 minutes. Cool, high-salinity, nutrient-rich water was transported from below the thermocline seaward of the reef and was resident on the reef for up to 4 hours before it mixed with surface waters and receded downslope. The arrival of internal bores was a consistent feature at this site from May to November. In August 1995 the water seaward of the reef was strongly stratified, with a chlorophyll maximum at 45–60 m depth. The frequencies of bore arrival and mean duration of cool-water events increased with depth on the reef slope. Settlement of serpulid worms and growth of corals was greater at 30 m than at 15 m. It was pointed out that internal bores are a predictable, periodic source to the reef of dissolved nutrients, food particles, and invertebrate larvae.

7.4.2 Internal waves and phytoplankton production

We saw in Chapter 3 that a chlorophyll maximum is often close to the pycnocline in stratified waters, and net primary production in this region often constitutes a considerable fraction of the total for the water column. Phytoplankton cells in the upper part of the pycnocline are often nutrient-limited, while those near the base of the pycnocline receive nutrients by turbulent transport from below, but tend to be light-limited. Lande and Yentsch (1988) pointed out that internal waves traveling along the pycnocline are likely both to increase turbulent transport of nutrients and to cause the phytoplankton to oscillate in depth, thereby increasing the average light intensity experienced by them. This condition should be taken into account when making *in situ* measurements of primary production. Vandevelde *et al*. (1987) produced data supporting this view, from the central Gulf of St Lawrence.

7.4.3 Internal waves and kelp production

On Santa Catalina Island, off southern California, the water column is stratified year-round except for brief episodes of vertical mixing. Above the thermocline the temperatures are normally above 15 °C and nitrate values are usually less than

0.5 μmol L^{-1}. Below the thermocline the water is cooler and more nutrient-rich. Average depth of the mixed layer can vary seasonally from 5 m to 30 m, causing strong changes in temperature and nutrient concentration at a depth of, say, 12 m (Zimmerman and Kremer 1984). Superimposed on this seasonal pattern is a twice-daily fluctuation in the position of the thermocline, caused by internal waves that are tidally driven (Cairns and LaFond 1966). At a given depth, the diurnal fluctuations in temperature and nutrients can be as great as the annual fluctuations. Beds of giant kelp straddle the average position of the thermocline, so internal waves cause the incursion of nutrients into the kelp beds twice a day. This input is crucial to the survival of the kelp beds in summer. During the El Niño of 1982–4 (see Section 9.2.1), the 15 °C isotherm was depressed to a depth of 50 m, effectively isolating the kelp beds from the input of nutrients associated with the internal waves.

During the 1957–9 El Niño, a similar depression of the thermocline had caused the kelp beds to be so starved of nutrients that kelp productivity was reduced below the level needed to meet the grazing demands of sea urchins. In other words, nutrient deprivation and sea urchin grazing interacted to cause widespread destruction of kelp beds at that time. By the time of the 1982–4 El Niño, commercial harvesting had reduced sea urchin densities. In spite of deprivation of nutrients, there was less damage to the kelp beds (Tegner and Dayton 1991).

7.4.4 Internal waves concentrate and transport planktonic organisms

There have been two schools of thought about how internal waves might bring about the shoreward transport of planktonic organisms. The first suggestion was that organisms are caught in the slicks that form at the zones of convergence at the surface, above the troughs of internal waves, and travel with the waves. The second was that internal tidal bores, or breaking internal waves, are required before organisms are carried shoreward.

(a) Concentration of organisms without transport

The water movement associated with internal waves, when they are close enough to the surface, is as shown in Fig. 7.08. There are alternating zones of upwelling with divergences and downwelling with convergences. Ewing (1950) drew attention to the fact that convergences associated with internal waves may be visible at the surface as smoother areas, or slicks, on a lightly rippled sea. He pointed out that a surface film of organic matter is naturally present on biologically productive waters and that in the convergence zones this film becomes thicker and is able to damp out small surface ripples. The internal waves are quite long, so that slicks may be hundreds of meters apart, and they move slowly shoreward (~0.2 m s^{-1}) with the internal waves. There is a tendency for buoyant material such as floating seaweed or amorphous organic matter to aggregate at the convergences,

and for planktonic organisms to become associated with the aggregations. This action suggests that the shoreward transport by these slicks may have significance in the adaptations of organisms inhabiting them.

Franks (1997) described, and illustrated with striking photographs, dense algal blooms forming bands at the sea surface and moving towards shore in concert with underlying internal waves. He interpreted the observations by means of a simple mathematical model in which the bands form at the trough of a wave, just behind the zone of maximum convergence. The waves do not carry individual algal cells along with them; the patches are formed and reformed constantly as new algae are drawn in and out of the patches. There is no net advection of plankton. The model failed to reproduce the asymmetric distribution of cells in the bands, with sharp leading edges and diffuse trailing edges. Franks suggested that this feature might be caused by the internal waves breaking as they came into shallow water.

A model published by Lennert-Cody and Franks (1999) included a two-layered water column and both linear and weakly nonlinear waves. Concentrations of cells increased with increasing amplitude of the waves and the ability of the organisms to maintain position in a downwelling. Nevertheless, the model predicted that the maximum concentration of organisms would be less than twice the local background concentration, and would last no longer than the wave period. It appeared that this model would not explain the dense bands of algal blooms seen to move shoreward with the internal waves.

(b) Aggregation and transport of organisms

Shanks (1983) made daily collections of the pelagic megalopa larvae of the crab *Pachygrapsus crassipes* from the end of the 320-m-long pier at the Scripps Institution of Oceanography, California. He found that the daily abundance fluctuated, with fortnightly maxima that occurred about five days before the spring tide. Noting the occurrence of surface slicks, and their relationship to the fortnightly tidal cycles, he used styrofoam cups weighted with sand as small drogues and deployed 50 cups 20 m apart on a line at right angles to the lines of the slicks. On three of the five occasions that he performed this experiment, the cups were not transported by the slicks, but on the other two occasions the cups were caught by the slicks and carried shoreward. At the end of the experiment over 90% were concentrated in two slicks and had been carried 1–2 km shoreward. Associated with these slicks were dense accumulations of flotsam.

In parallel with these physical experiments standard neuston net tows were taken in the slicks and in the rippled water between the slicks to sample the larvae of invertebrates and fishes. On the days when the drogues were concentrated, but not on the other days, the larvae of invertebrates and fishes were concentrated 6–40 times more densely in the slicks than in the water between them. Shanks found that the crab larvae were able to swim vertically fast enough to overcome the effect of a downwelling. Having arrived at the surface, they could maintain their position by clinging to floating detritus. In New Zealand, the crab *Munida*

gregaria has bright red larvae that aggregate near the surface of the sea in daylight. Zeldis and Jillett (1982) documented aggregations of these larvae on what appeared to be mid-shelf internal wave slicks, as well as on plume and headland fronts.

Satellite observations show that tidally generated internal waves are refracted by bottom topography, and that some coastlines are more suitable for the production of internal waves than others (Apel *et al*. 1975). Shanks and Wright (1987) thought that the differential pattern of shoreward transport of slicks might account for some of the patchiness in barnacle distribution on rocky shores. They repeated the experiments of Shanks (1983) using styrofoam cups as drogues and found that barnacle larvae were indeed concentrated in slicks associated with the internal waves, and that settlement of barnacle larvae was more abundant in places where the drogues tended to accumulate. In addition to the barnacle larvae, they found that two kinds of crab larvae and gammarid amphipods were at times concentrated in the slicks. Kingsford and Choat (1986) similarly associated larval and juvenile fish of New Zealand with the slicks above internal waves. None of this work reconciled the observations with the models that showed that surface slicks are constantly forming at the advancing edge and dispersing at the trailing edge, with no net transport of water.

Pineda (1991, 1994, 1999) offered a reconciliation of the dilemma. He proposed that both slicks and organisms were transported shoreward by currents associated with internal bores. As mentioned in Section 7.2.6, the first stage of a bore is recognized by a shoreward transport of warm upper-layer water. During a later stage, the warm water flows offshore while cooler deeper water flows toward the shore. These flows create a temperature variation characteristic of bores that can be identified in temperature records. By analyzing the historical temperature records from the Scripps pier, Pineda showed that bores tended to occur most frequently in summer 6 and 19 days after the new moon, indicating a tidal mechanism. He also found a strong correlation between relatively low water temperatures and settlement of barnacle larvae, so he postulated that internal bores – not surface slicks – were the mechanism transporting the larvae onshore.

Pineda (1994) investigated events that follow the arrival of a parcel of cold water at the shoreline. He found that this water reverses direction and moves offshore close to the bottom, generating a gravity current. This movement has the effect of drawing warm surface water into the shore. In other words, an upwelling of cold water occurs as the internal bore (Section 7.2.6) arrives at the shoreline, and downwelling appears as the cold-water mass retreats along the bottom (Figs. 7.14 and 7.15). The onshore movement of warm water was found to be associated with a distinct warm-water front, in which crab larvae and fish larvae were concentrated.

In a further investigation, Pineda (1999) used an adaptive sampling scheme in a stratified water column 11 m deep. When a large cold bore was detected nearshore, a warm front followed a few hours later. On receiving the advanced warning from the cold bore, he put out strings of temperature loggers in a cross-shaped array, and placed a Doppler current meter in the same area. He also started

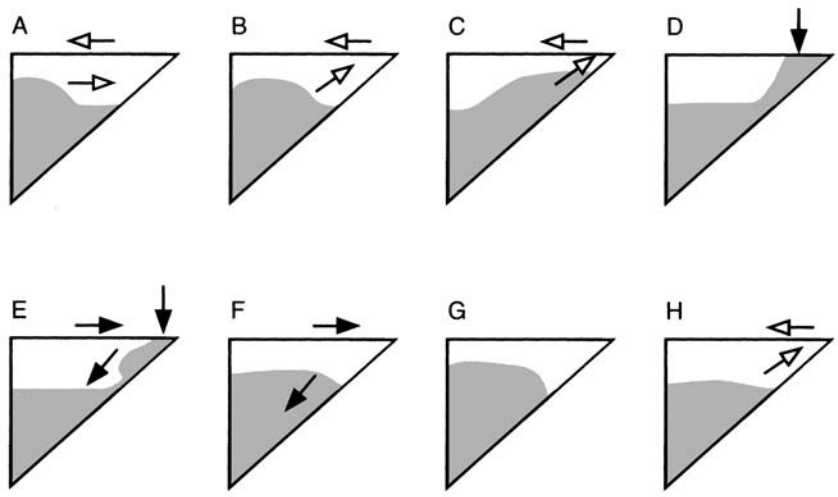

Fig. 7.14 Diagram showing onshore advection of dense water (shaded, A–D), followed by down-slope progression and corresponding onshore advection of warm water (unshaded, E–H). Vertical arrows in D and E mark warm fronts. Other arrows represent currents. From Pineda (1994).

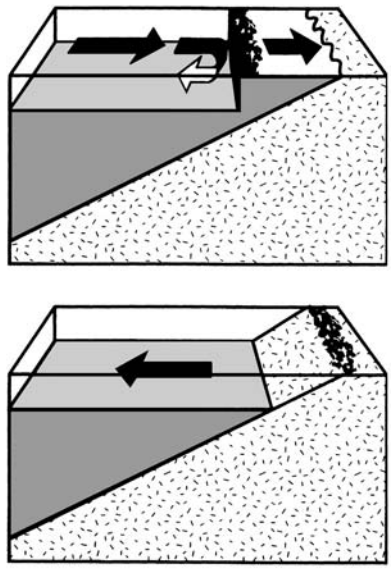

Fig. 7.15 Diagram showing the delivery of debris and larvae to the shoreline by a warm front, and their stranding as the cold water recedes. From Pineda (1994).

plankton sampling. The results (Plate 5) confirmed onshore mass transport above the thermocline and offshore transport below. There were accumulations of larvae of two intertidal barnacles and of crabs behind the warm fronts. While the evidence was not conclusive, it was probable that the larvae were being accumulated by advection from the warm side of the front. Pineda noted that surface slicks were often observed and that these were transported shoreward in the onshore warm flow behind the warm bore front. There is a correlation between the shoreward movement of surface slicks and the movement of larvae, but it is the mean flow generated by the bore that moves both the larvae and the slicks.

The implications of these findings are that quantitative studies of the larval abundances of shallow-water and intertidal organisms must take into account the nonrandom distribution of those larvae in coastal waters, and of the physical mechanisms that may carry them to the coastal shallows from far out on the continental shelf. Since the occurrence of internal waves and slicks is dependent on the tides, it will not be surprising if there is a fortnightly tidal rhythm in inshore transport and settlement. Further studies of the relationship between internal wave packets and bottom topography will be expected to throw light on the patchy distribution of many coastal organisms.

7.5 Tidal currents and topography

7.5.1 Tidal currents and island stirring

Ever since Doty and Oguri (1956) described enhanced phytoplankton biomass and production in the vicinity of Hawaii and coined the phrase "island mass effect," it has been suspected that the disturbance of flow caused by the presence of an island may lead to upwelling of water from below the thermocline and hence nutrient enrichment of surface waters. However, there has been a lack of simultaneous physical and biological measurements to give firm support to the concept. Simpson and Tett (1986) showed that both the Scilly Isles (off the southwest tip of England) and St Kilda (west of the Hebrides, western Scotland) have surface temperatures around the islands about 3 °C lower than the surface layer of the summer stratified region offshore. To the west of the Scilly Isles a plume of chlorophyll exceeding 4 mg chlorophyll-*a* m^{-3} sometimes extends for about 50 km into water that otherwise contains less than 0.5 mg chlorophyll-*a* m^{-3}. At St Kilda, where the tidal currents are less strong, the zone of enhanced chlorophyll-*a* is at a rather lower concentration, 2–3 mg m^{-3}, but it extends over a much larger area, about 5000 km^2. For the Scilly Isles they showed that as tidal currents flow in a curved path around the island mass they are accelerated to a velocity about twice that in the far field, which leads to centrifugal displacement of surface waters and a compensatory upwelling of nutrient-rich deeper water. The biological productivity stimulated by these nutrients gives rise to increased phytoplankton biomass that is advected away from the islands by the residual currents. A numerical model based on the interaction of tidal currents with the Scilly Isles gave results that

were in good agreement with the field observations. Both island groups are nesting grounds for large numbers of seabirds (about one million on the Scilly Isles alone), and the enhancement of primary production by the interaction of the island mass with the tidal currents is thought to be a factor in their success. This mechanism appears to be at work around the Indian Ocean coral atolls of Aldabra and Cosmoledo (Heywood *et al*. 1990). When there were strong and steady flows around the islands, there was doming of isopycnals and enhanced planktonic production; when the flows were weak there were none. Internal waves may also be responsible for upwelling of nutrients around islands. Near Bermuda, Sander (1981) demonstrated the presence of internal waves of up to 30 m amplitude. When he compared the potential for fertilizing surface waters from the internal waves with other potential sources of nutrients, he concluded that the internal wave mechanism was the most important.

Low-frequency internal waves were clearly implicated in the supply of nutrients to the reef system on Tahiti by Wolanski and Delesalle (1995). High-amplitude internal waves with periods of 24 hours or greater raise nutrient-rich water up to 30–40 m depth at the edge of the reef. From that depth large surface waves breaking on the reef force the nutrient-rich water up and onto the reef. The authors suggest the mechanism is linked to the bathymetry of the edge of the reef, which consists of a series of gullies or mini-canyons (grooves) with steep walls (spurs). The surface waves break on the spurs and generate upward flows in the grooves.

7.5.2 Tidal currents and coastal or bottom topography

The flow of tidal currents past coastal headlands often results in vertical transport of nutrients and stimulation of biological production. In a study of these processes around a promontory on an island in British Columbia (St John and Pond 1992, St John *et al*. 1992b), it was found that significant vertical mixing occurred in a plume downstream of the promontory during the ebb tide when the mean velocity through the water column was over 12.7 cm s^{-1}.

At the southwest tip of Nova Scotia, Canada, lies Cape Sable. The waters have long been known to have anomalously low temperatures and high nutrient concentrations and to support high productivity of lobsters *Homarus americanus*, groundfish, shellfish, and herring. Upwelling obviously occurs, and an early explanation (Garrett and Loucks 1976) was that it was driven by centrifugal forces associated with the strong tidal currents along the convex coastline. Tee *et al*. (1993) proposed a new mechanism involving bottom topography, offering field observations and a model in support of their proposal. Residual currents flowing from deep to shallow water across a submarine ridge generate upwelling. These upwelled parcels of water are transported by a longshore current away from the upwelling region and into a region of strong tidal mixing. The combination of topographic upwelling and strong tidal mixing leads to the observed cold-water anomaly and its associated high biological productivity off Cape Sable.

7.6 Tidal currents and vertically migrating organisms

Tidal currents have a minimal velocity on the sea floor and increase velocity with increasing distance from the bottom. An organism rising through a tidal current experiences an increasing rate of displacement. A.E. Hill made a series of investigations into the effect of tidal currents on vertically migrating organisms (references in Hill 1998). We saw in Section 7.2.2 that the M_2 (lunar semi-diurnal) component of the tidal cycle is approximately twice the amplitude of the S_2 (solar semi-diurnal) component. However, the period of the M_2 is 12.42 h, while the period of the S_2 is precisely 12.00 h. Organisms migrating on a 24-hour cycle are therefore in synchrony with the S_2 tides.

(a) Migrations synchronized with the solar day

Hill pointed out that, since many planktonic organisms make diel vertical migrations, these are exact multiples of the S_2 component. Both the vertical migrations and the S_2 tides are sun-synchronized. The migration can therefore interact with the S_2 tidal current to induce long-term horizontal transport (Fig. 7.16). The direction of net transport depends on the phase of the S_2 tidal current relative to local

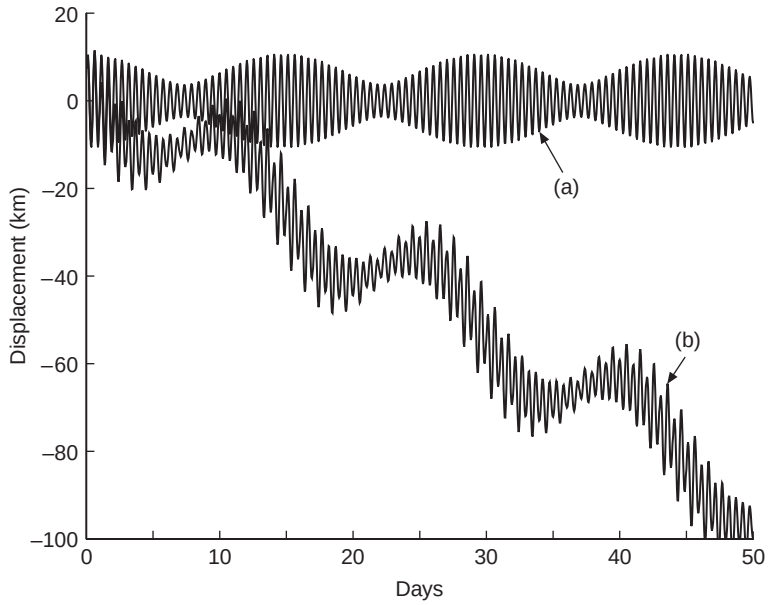

Fig. 7.16 Horizontal displacement versus time for non-migrating and migrating organisms in tidal currents. The currents are a combination of an M_2 oscillation with amplitude of 1 m s^{-1} and an S_2 oscillation with amplitude of 0.5 m s^{-1}. (a) non-migrating organisms which remain at the surface; (b) vertically migrating organisms. Vertical migration interacts with the S_2 constituent to induce unidirectional motion of 2 km d^{-1}. From Hill (1991). Reproduced by permission of Springer-Verlag.

noon. All other tidal components, including the larger M_2, displace migrating organisms in a manner that cancels out over long time periods, because they do not synchronize with the 24-hour cycle of migration.

A vertical profile of velocities through a benthic boundary layer shows that the change in velocity is greatest close to the bottom. Therefore it is organisms that rise from the bottom during their diel migration, as opposed to those that start their vertical migration in mid-water, that experience the greatest horizontal displacement. Using realistic figures for tidal currents, Hill showed that horizontal transport of 4 km d^{-1} is possible for those starting from the bottom.

When a hydrodynamic tidal model of the northwestern European continental shelf was used to construct maps of S_2 currents, and when their effect on vertically migrating plankton was calculated, there emerged regions of convergence, divergence, and retention. For example, the German Bight was predicted to be a zone into which diurnally migrating organisms would tend to converge, and indeed this area is an important nursery ground for young fish. It is probable that tidal currents make a strong contribution to the patchiness of plankton distribution. Another consequence of vertical migration through tidal currents, for organisms that rise to the surface to feed at night, is that they are constantly encountering different patches of (non-migrating) phytoplankton.

(b) Migrations synchronized with the tides

Some organisms make vertical migrations that are synchronized with the tides, rising into the water column when the tide flows in one direction, and staying close to the bottom when the currents flow in the opposite direction. Under these circumstances it is the M_2 component that causes strong horizontal migrations. For example, Arnold and Cook (1984) showed that adult plaice *Pleuronectes platessa* on the Dogger Bank in the North Sea use tidally synchronized vertical migration to get to the feeding ground, then switch to diurnal vertical migration, in which very little net displacement occurs. Vertical migration in synchrony with the M_2 tide is an important life strategy for organisms in estuaries (see Section 4.5.3).

7.7 Summary: the multiple effects of tides

In this chapter we have chosen not to review the enormous body of literature on life between tidemarks. The diurnal or semi-diurnal rise and fall of the tide creates on the shore a vertical pattern of physical zonation in which the lower regions have less exposure to the air, less tendency to dry out, and a more equable temperature, while the upper regions have converse properties. This knowledge creates a delightfully interesting stage on which organisms enact complex biological plays that are only now beginning to be understood. Since this zone is accessible for study by both naturalists and experimental scientists, there is copious literature on the subject that would require a separate volume to do it justice.

Instead, we have concentrated here on the effects of the tides on biological processes remote from shore. We have seen that the vertical mixing in the water column, caused by tidal currents, creates conditions in which nutrients are supplied to the phytoplankton all summer long, creating conditions favorable for the growth of larval and juvenile fishes. It has been noted that a very large proportion of the known herring spawning grounds are in areas that are tidally mixed all year round. Many of these are on offshore banks, where the water shallows enough to permit tidal mixing throughout the water column.

The interaction between tidal currents and offshore banks also tends to create a strong circular flow around the perimeter of a bank, and this feature is thought by some to create a barrier to the dispersal of fish larvae, retaining them in the biologically productive waters over the banks long enough for them to learn to recognize the bank as a site to which they should return for spawning. It has been suggested that this mechanism is important in the evolution of distinct stocks within a single species of fish.

Tidal currents moving over the bottom in stratified water also tend to generate internal waves at the pycnocline. Particularly large waves, 50–70 m in amplitude and of the order of 30 km wavelength, are generated where strong tidal currents flow over the shelf break. These waves are thought to mix nutrient-rich water up into the nutrient-depleted mixed layer, stimulating biological production near the shelf edge. Details of the food webs have not been worked out, but we know that the shelf-break region of the North Atlantic is particularly productive of fish.

On a smaller scale, as internal waves approach shore they create convergences at the surface in which organic films accumulate and produce visible slicks. The slicks are constantly formed and reformed as new phytoplankton cells are drawn into and out of patches. In this model, there is no net advection of cells and no net shoreward movement of water. An additional mechanism has now been proposed. As internal waves approach shore, they break and form internal bores. Associated with these bores is a net transport of water towards shore. It seems likely that internal bores cause a transport of both the slicks and the associated organisms.

Finally, we have seen that as tidal currents interact with islands they cause vertical mixing that brings nutrients to the surface and stimulates biological productivity around the islands. It has been suggested that this mechanism, coupled with some freedom from terrestrial predators, accounts for the large populations of seabirds that find various islands the best places for rearing their young.

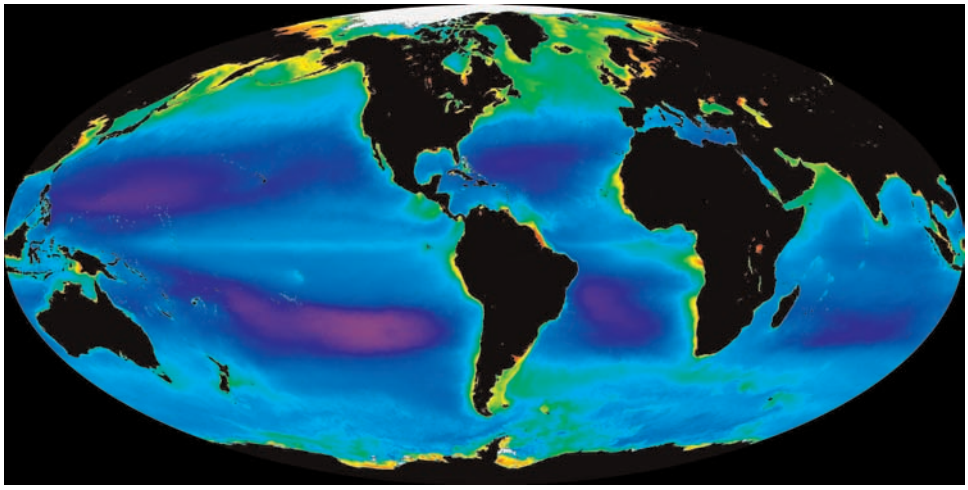

Plate 1 World ocean chlorophyll distribution estimated from the color of the oceans as observed by satellites having color scanners. Regions in the middle of the ocean (dark blue and magenta) have the lowest biomass of phytoplankton and presumably the lowest productivity. Higher phytoplankton biomass (light blue and green) is found along the equator and in bands lying poleward of the mid-ocean gyres. The highest values (yellow and red) are found in the coastal upwelling regions off the west coasts of the Americas and north and south Africa. Some of the high values in coastal and northern regions may be due not to chlorophyll but to suspended organic and inorganic particles, or ice. Image obtained from NASA Goddard Space Flight Center, SeaWiFS Project (seawifs.gsfc.nasa.gov/seawifs.html).

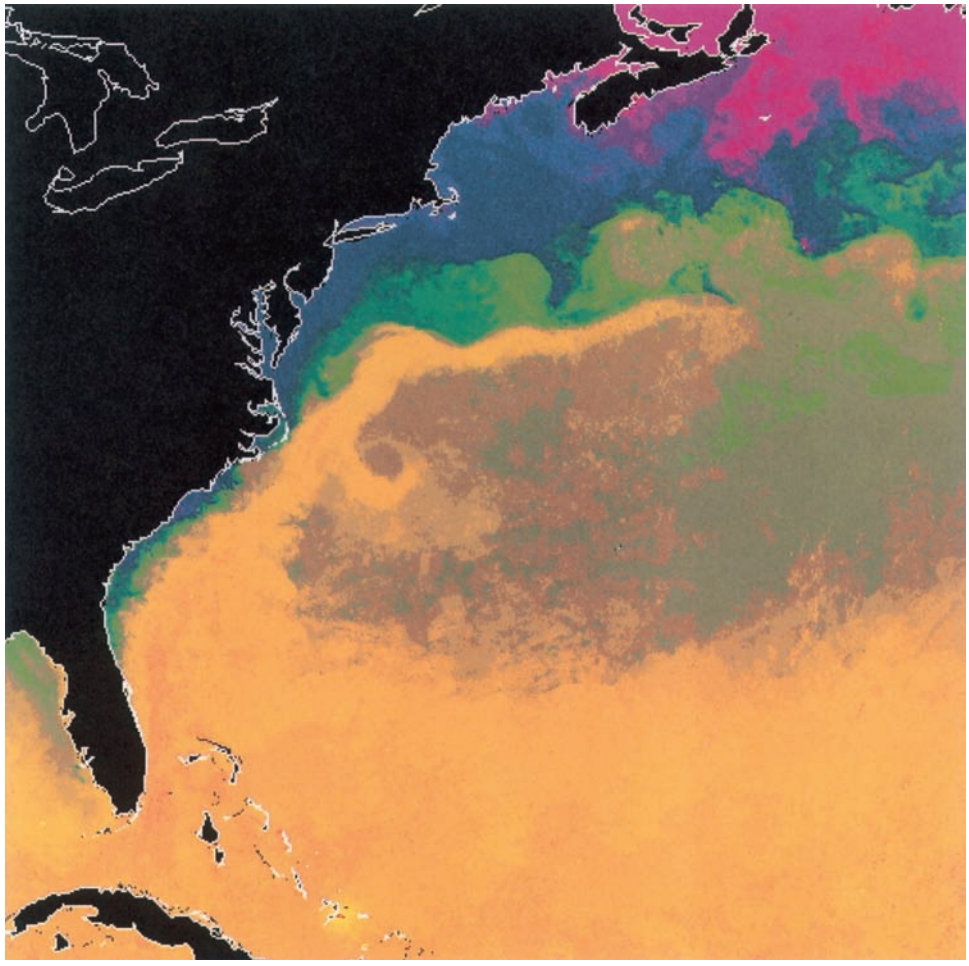

Plate 2 Distribution of surface temperature on the western North Atlantic Ocean on January 19, 1989. Highest temperatures are in the warm (yellow) subtropical waters and in those carried north in the Gulf Stream, where they mix with the colder (green and blue) northern waters. Note the evidence of ring formation on each side of the Gulf Stream. Derived from satellite data, courtesy of NASA and the University of Miami.

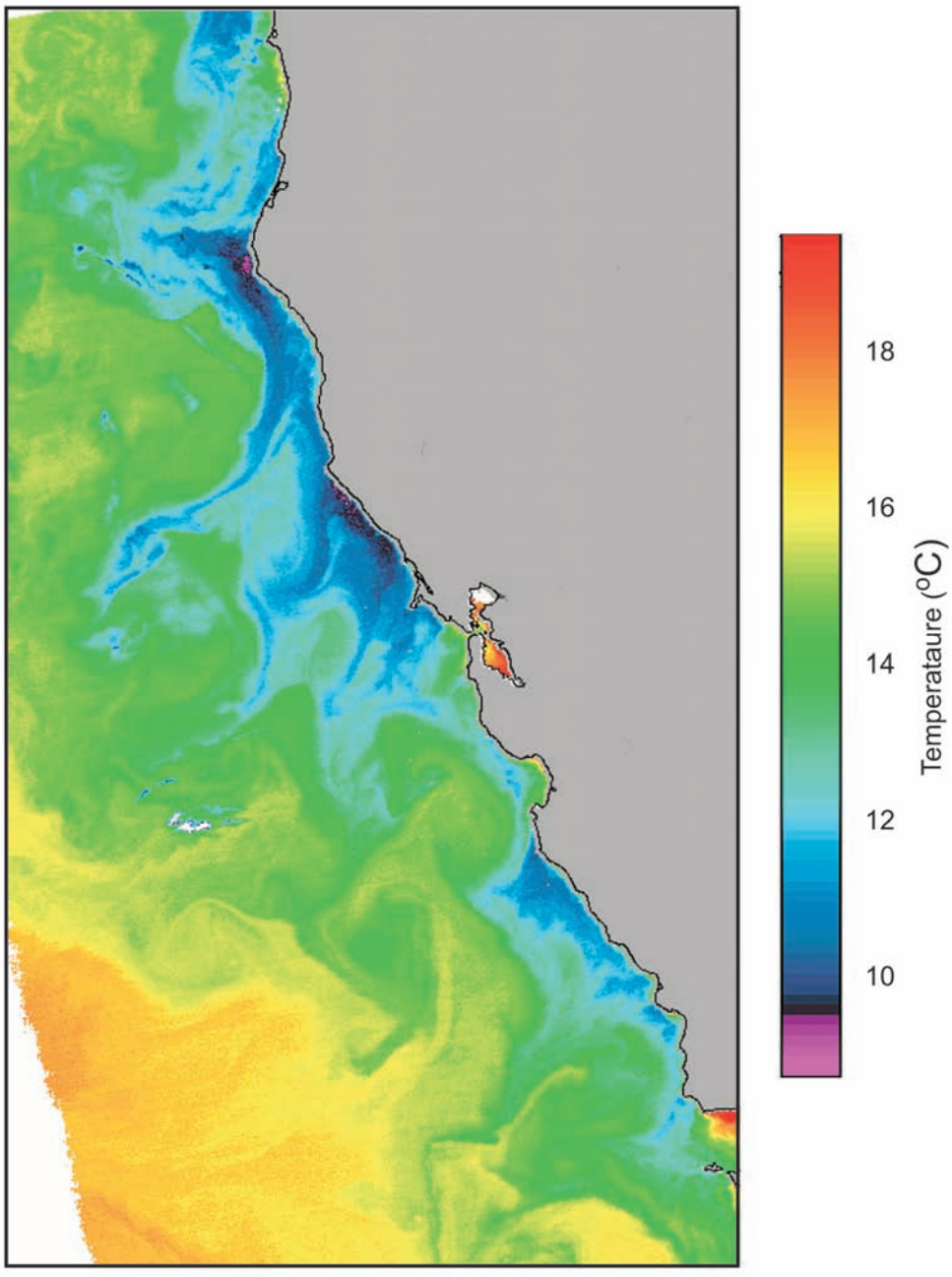

Plate 3 Sea surface temperature off California showing typical upwelling conditions on June 15, 2003. The warmer surface water pushed offshore by the alongshore wind is replaced by cooler water from below. The convoluted distribution of temperature reveals the intricate eddy motion that mixes the warm and cool water. Image from MODIS (Moderate Resolution Imaging Spectroradiometer; modis.gsfc.nasa.gov).

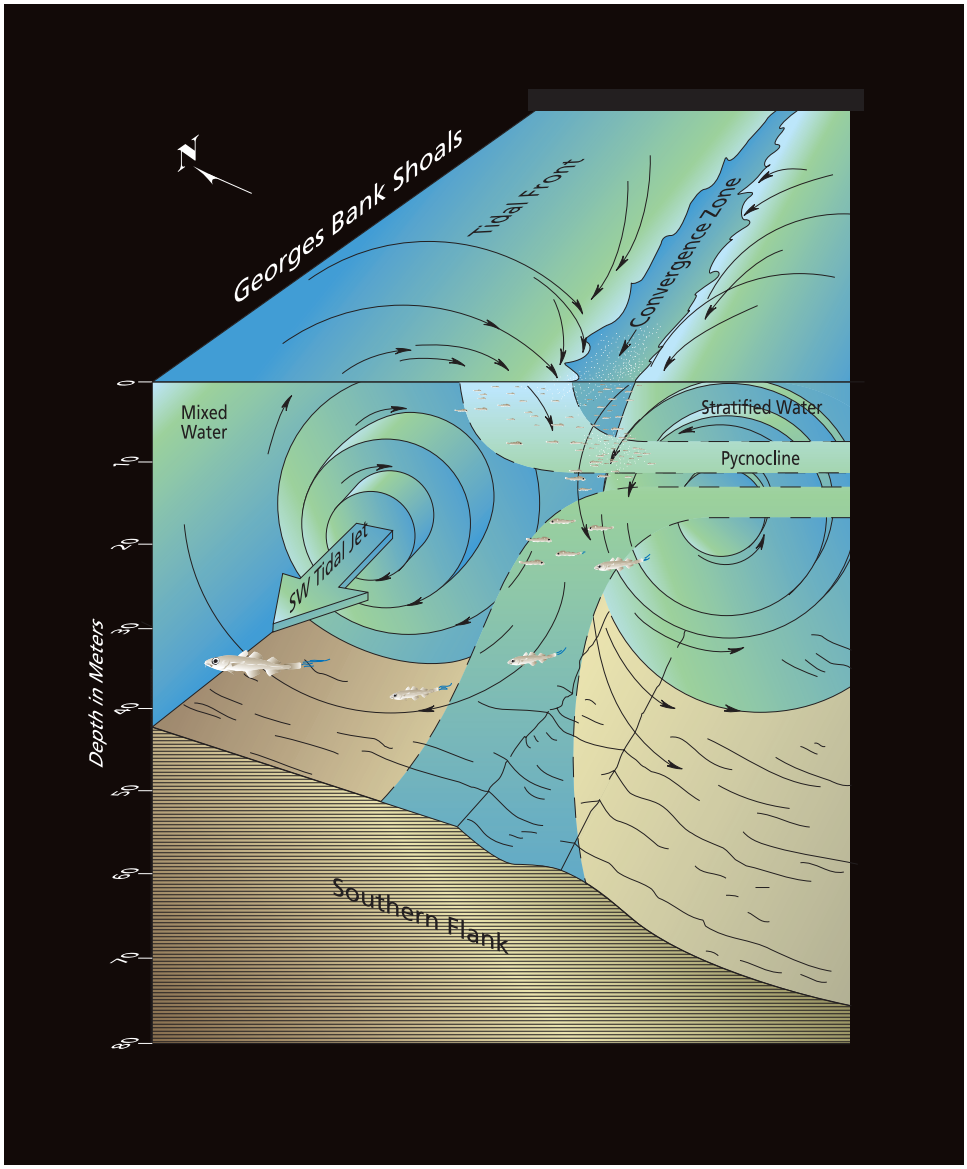

Plate 4 Conceptual model of tidal-front transport of larval haddock and cod, and recruitment to the shoal nursery area on the southern flank of Georges Bank. Secondary circulation shows a two-cell pattern with upwelling on the mixed side of the front and a surface convergence and downwelling on the stratified side. Eggs and larvae caught in the near-surface jet flows of the front near the 60 m isobath could be transported rapidly to the southwest. Eggs and larvae tend to be aggregated in the convergence zone above the surface pycnocline. Larvae downwelled at the convergence zone, or older larvae, which have more developed swimming ability and can be found deeper in the water column, would have the greatest potential for being advected under the jet onto the shoals in the near-bottom (>35 m) cross-isobath flow. After Lough and Manning (2001).

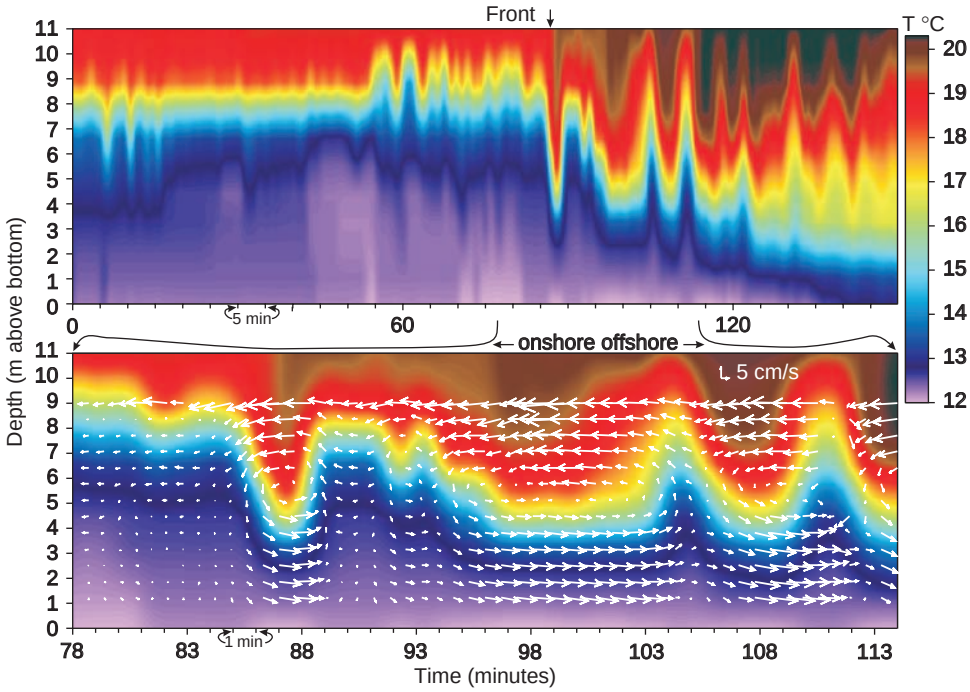

Plate 5 Records of currents and temperature during the passage of a warm front associated with an internal bore moving shoreward (from right to left). The upper record extends for 150 minutes; the lower record is an expansion of minutes 78 to 114. Temperature loggers were at 1, 3, 5, 7, 9, and 11 m above bottom, and were sampled at 8-second intervals. The Doppler current meter was on the bottom and sampled at 10-second intervals. Vectors are shown every 40 seconds and the data were removed because they were contaminated by surface phenomena. See discussion in text pages 268 and 278–80. From Pineda (1999). Copyright (1999) by the American Society of Limnology and Oceanography, Inc.

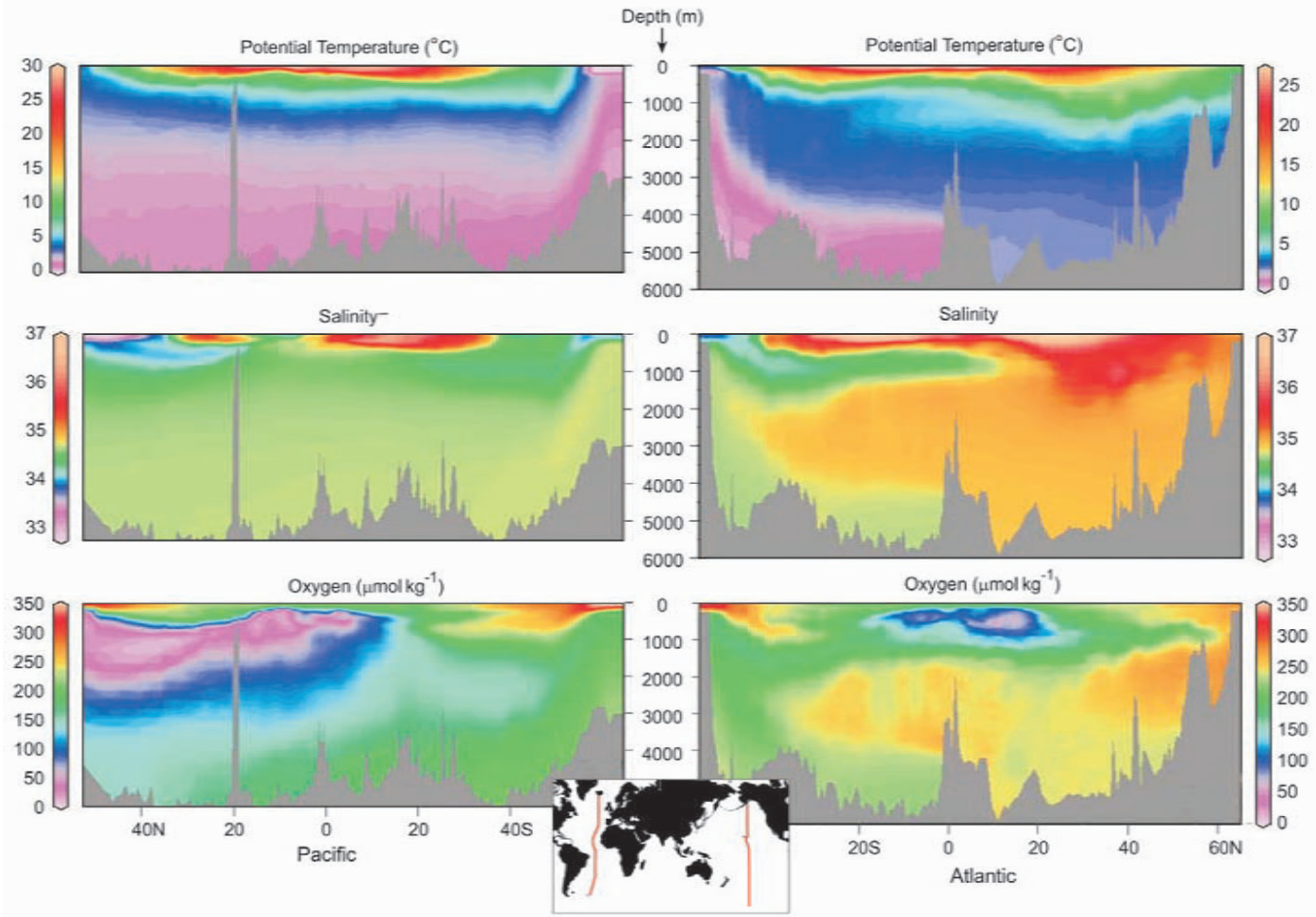

Plate 6 North–south sections of potential temperature, salinity, and dissolved oxygen through the Pacific and Atlantic Oceans. The distributions of these properties through the oceans are due to the sinking of cold dense water at high latitudes, biological consumption of oxygen, heating and evaporation at the surface, and the wind-driven circulation. Figure created from images obtained from the World Ocean Circulation Experiment at www.awi-bremerhaven.de/GEO/eWOCE/gallery/index.html (Schlitzer 2000).

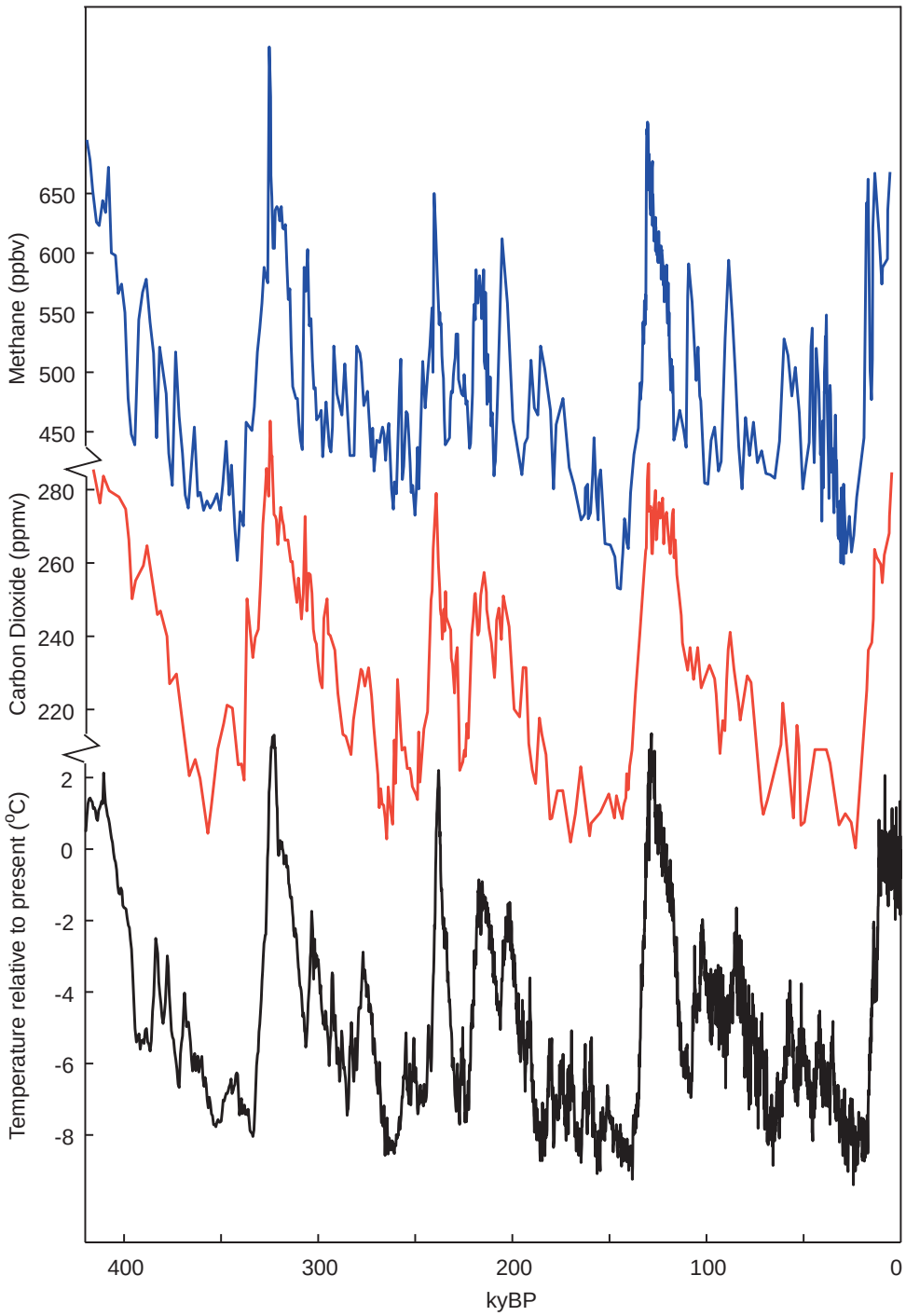

Plate 7 Temperature (red), methane (blue), and atmospheric CO_2 (black) over the past 420,000 years obtained from ice cores in Antarctica. Data published by Petit *et al*. (1999) and obtained from www.nature.com with permission. Figure based on fig. 2.22 in Folland *et al*. (2001).

Part C

Processes on a scale of thousands of kilometers

8

Ocean basin circulation: the biology of major currents, gyres, rings, and eddies

8.1 Introduction

In this chapter we begin to consider the ocean basins in their entirety. We look at the major gyres that circulate anticyclonically in the subtropical regions of the North and South Atlantic and Pacific basins. We note that they are driven by global winds, which in turn are driven by the inequalities in the solar energy flux between the equator and the poles. North of the subtropical gyres in the North Atlantic and North Pacific are subpolar gyres that rotate in the opposite sense (i.e., cyclonically). Some of the most productive waters in the world are in the southern halves of these subpolar gyres, but the seasonal patterns of production are quite different in the two ocean basins.

Along the western margins of all these gyres are particularly intense currents – for example, the Gulf Stream and the Kuroshio Current in the northern subtropical gyres, and the Labrador Current and the Oyashio Current in the subarctic gyres. Organisms within these currents are transported long distances very rapidly, and we find that a variety of commercially important marine organisms, such as salmon, eels, and squid, migrate in these currents in the course of completing their life histories.

There is a tendency among biological oceanographers to take these intense western boundary currents as given natural phenomena, without delving too deeply into the mechanisms that drive them and cause them to be different from eastern boundary currents. However, as we enter an age in which human activity appears to be capable of altering the climate of the planet, and with it the circulation of the ocean, it is appropriate to try to understand the underlying mechanisms in order to try to predict the consequences of climate change. In Section 8.2.1 the theory of what drives boundary currents is explored. The story is not a simple one, and physical oceanographers do not have all the answers, but a study of the theory sheds new light on the functioning of whole ocean basins, and on the way in which they may respond to climate change.

Satellite images of boundary currents show that along some parts of their length they begin to meander. Sometimes the meanders grow so large that the ends are cut off to form isolated rings of water, of the order of 100–300 km in diameter. These rotating water masses, which are particular forms of eddies, retain their distinct identity for several months and have their own special biological characteristics. If they are formed between the boundary currents and the coast, they may impinge on the continental shelf. Their enormous kinetic energy has the effect of drawing large volumes of water off the shelf on one side of the ring, while adding water on the other. The biological consequences for juvenile fish populations inhabiting the shelf water are often quite drastic.

It is now known that eddies are present throughout the ocean, although their energy often appears to decrease with distance from major ocean currents. It seems possible that there is a cascading of energy from the rings associated with the major currents, down to eddies remote from those currents. Since cyclonic eddies have the potential to cause upwelling in their centers, they may well be important in the global primary-production budget.

Finally, in this chapter we note that the centers of the major subtropical gyres are permanently stratified and were once thought to be biologically relatively unproductive. However, more recent work involving long time series and repeated transects has shown that there are several mechanisms producing transient bursts of elevated primary production. They include storm events, mesoscale eddies generated by currents at the periphery of the gyres, and Rossby waves. During the 1990s, discoveries about the properties of ubiquitous picoplankton underlined their ability to maintain production under very low levels of nutrients and light. Finally, it has been shown that the use of trace-metal-clean techniques for measuring primary production leads to much higher measurements than the older techniques, in comparable circumstances. The subtropical gyres occupy a large fraction of the world's ocean, and now that we know that they are more productive than once believed, their fixation of carbon dioxide is an important factor in the budget for carbon dioxide in the atmosphere.

8.2 The winds and the wind-driven circulation

All the major surface currents in the oceans are created by the drag of the wind on the surface of the water. The winds, in turn, are created because the earth's surface is heated unevenly by the sun, making the tropical regions warm and the polar regions cold. If the system were simple, the cold and dense polar air would flow under the warm and light tropical air while the tropical air moved north over the top of the cold polar air. But the fact that it all happens on a spinning sphere complicates the patterns. A very simplified diagram of the two major wind systems, the trades and the westerlies, is given in Fig. 8.01.

The trade winds arise because the warm air in the equatorial regions rises and is replaced by air flowing toward the equator in both the northern and southern hemisphere. The Coriolis force deflects the equatorward flows to the west giving rise to the northeast and southeast trades (winds are named after the direction from which they come, while ocean currents are named after the direction in which they are going). The air in the trade winds comes from the air that rises above the equator and then flows to higher latitudes before descending back to the earth's surface in the subtropical highs. These circular convection cells are known as the Hadley cells and the zone near the equator where the surface winds converge is called the intertropical convergence zone (ITCZ). The ITCZ moves north and south with the seasons, being furthest north in August and furthest south in February, but is always north of the equator (Gill 1982).

The Hadley cells tend to mix the air between the equator and 30° latitude, resulting in low horizontal temperature gradients between 30° S and 30° N throughout the lower 10–20 km of the atmosphere (the troposphere). Poleward of the Hadley cells the temperature at all levels in the troposphere decreases rapidly. This gives rise to a strong horizontal pressure gradient between ~30° latitude and the pole and to strong westerly winds. These winds are perpendicular to the pressure gradient because of the Coriolis effect and are in near geostrophic balance. The

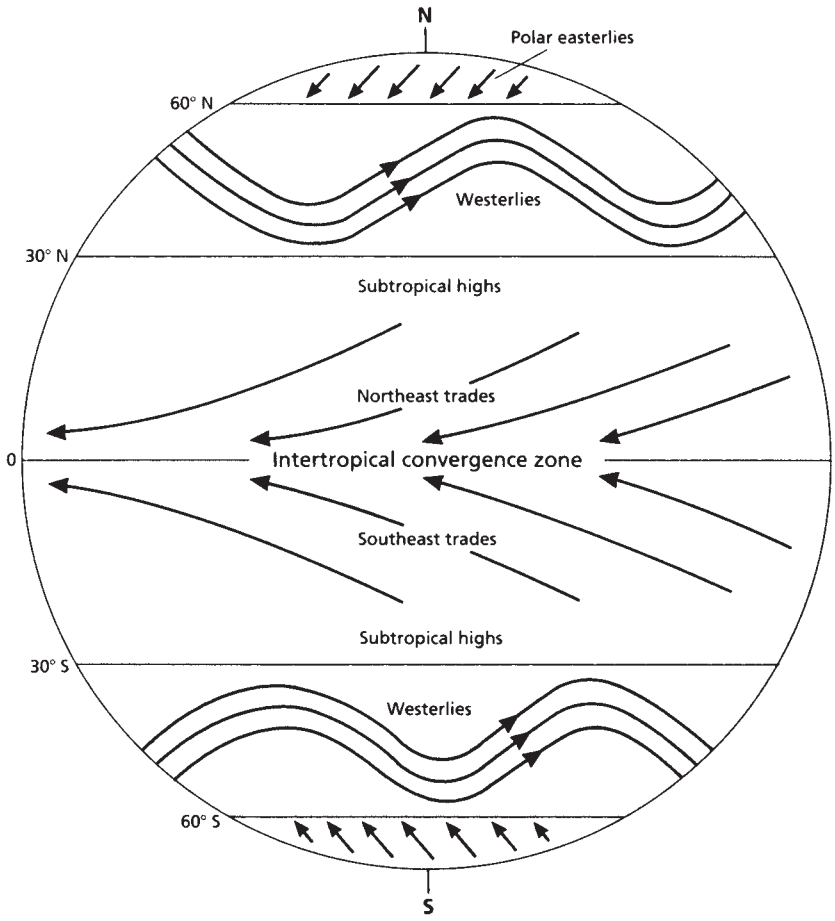

Fig. 8.01 Major wind systems of the world.

westerlies are continuous bands of flow right around the earth and are sometimes called circumpolar vortices. The speed of the flow is not constant at all levels but increases with height and reaches a maximum in the so-called jet stream at ~12 km over ~30° latitude, as illustrated in Fig. 8.02. This figure emphasizes the dominance of the westerly air flow compared with the small easterly flows of the trade winds near the equator and the polar easterlies. In the summer the jet stream is weaker and moves poleward about 10° in latitude.

The westerlies do not stay at a constant latitude right around the globe but meander north and south in waves that are about 10,000 km long. At any one time there are three to five complete waves around the globe but averaged over a month only three are usually visible. These waves are called planetary or Rossby waves and they cause the westerlies at a given longitude to move north and south over periods of a month or so. Since the movement of the weather systems is guided by the westerlies, the shifts in position also alter the paths of the weather systems.

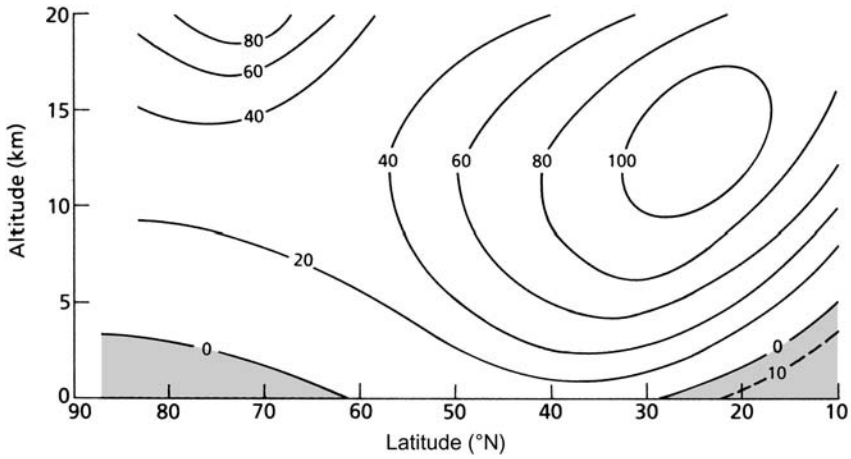

Fig. 8.02 The distribution with altitude and north latitude of the average winter zonal wind speed in km h^{-1}. Winds are toward the east except where shaded. Adapted from Petterssen (1969), with permission of McGraw-Hill, Inc.

This is the process that causes the weather in the mid-latitudes to be different from the average for weeks at a time. As we shall discuss in the next chapter, the position of the westerlies can be shifted in special locations such as the North Atlantic Ocean for much longer periods than Rossby wave fluctuations. The longer-term changes can last for years and are known as oscillations.

The winds shown in Fig. 8.01 drive the ocean currents shown in Fig. 8.03. However, the Coriolis force and its variation with latitude make the link between the wind stress and the water motion less than straightforward. At the equator, where the Coriolis force is zero, the situation is simple and the water moves in the same direction as the wind. The equatorial currents in the Atlantic and Pacific, for example, are mainly parallel to the equator. At other latitudes the Coriolis force is not zero and causes the moving water to be deflected to the right of the wind in the northern hemisphere and to the left in the southern hemisphere. The net direct effect of the wind is a flow perpendicular to the wind in the upper layer of the ocean. This is the Ekman transport, which begins the series of processes that generate the currents seen in the upper layers of subtropical and subpolar oceans.

As is evident in Fig. 8.03, the currents in the subtropics, between latitudes 15 and 45°, form large gyres in which the poleward-flowing currents on the western sides of the oceans are strong and narrow while the currents throughout the remainder of the oceans are broad and slow. In the North Atlantic Ocean, for example, the subtropical gyre is made up of the broad, slow North Atlantic, Canary, and North Equatorial Currents flowing east, south, and west, respectively. The northward-flowing current that completes the gyre is the Gulf Stream, which is narrow and rapid. Similar subtropical gyres of broad, slow currents with strong narrow poleward flows like the Gulf Stream are found in all the other major

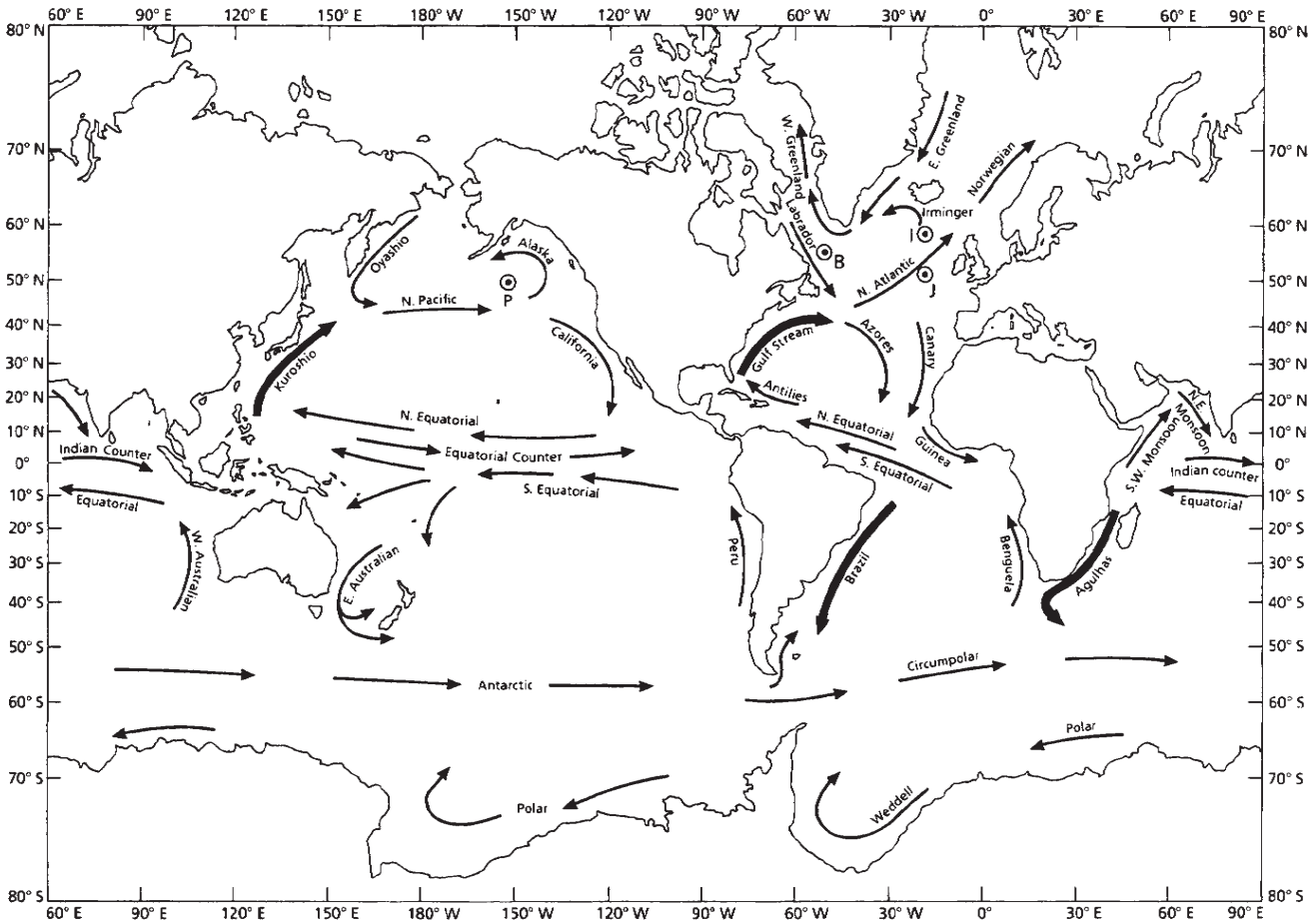

Fig. 8.03 The principal surface currents of the world's oceans. Western boundary currents such as the Gulf Stream are emphasized. Positions of ocean weather ships *B* (*Bravo*), 56.5° N 51.0° W; *I* (*India*), 59.0° N 19° W; *J* (*Juliett*), 52.5° N 20° W, and *P* (*Papa*), 50° N 145° W are indicated by circled dots with letters.

oceans. In the subpolar regions of the North Atlantic and North Pacific, gyres are observed in which the sense of the flow is opposite to that in the subtropical gyres – that is, counter-clockwise. These gyres, like the subtropical ones, contain broad, slow flows throughout most of the ocean with a strong narrow flow on the western side. The strong narrow flows, the Labrador and Oyashio Currents, however, flow toward the equator instead of toward the poles. In the higher latitudes of the southern hemisphere, where there are no obstructing continents to force the formation of gyres, the main current is the Antarctic circumpolar current, which circles the globe at about 50° S.

8.2.1 Theory of the wind-driven circulation

The asymmetry of the currents in the large ocean gyres has been known for centuries but the reason for it remained obscure until Stommel (1948) showed mathematically that the westward intensification of the currents is due to the change in the Coriolis force with latitude. In the following short description we try to outline the main physical processes creating the current, but it is clear from the reviews of Stommel (1965), Fofonoff (1981), Rhines (1986), and Pedlosky (1990) that the subject is vast, complicated, and dynamic, and we can only "scratch the surface." Our account concentrates on the North Atlantic Ocean and begins with the large-scale wind patterns and the Ekman transport.

The important parameter associated with the wind is the force per unit area or stress of the wind drag on the water surface. For the North Atlantic Ocean the yearly average of the strength and direction of the wind stress is shown by Isemer and Hasse (1987) to be similar to the distribution illustrated in Fig. 8.01. There is a maximum eastward stress between 40 and 50° N associated with the westerlies, a region of relative calm at 30° N associated with the subtropical highs, and the maximum westward stress associated with the northeast trade winds at about 15° N. Analyses by Hellerman and Rosenstein (1983) demonstrate that this north–south variation in wind stress is symmetrical across the equator.

To simplify our discussion we reduce the ocean to an idealized rectangle with idealized east–west (zonal) wind stress (Fig. 8.04). Our model ocean extends from 20 to 40° N and from 80 to 20° W with a wind stress that varies sinusoidally from a maximum of 0.1 N m^{-2} toward the east at 40° N to 0.0 N m^{-2} at 30° N, then increases again to 0.1 N m^{-2} to the west at 20° N. This idealized wind ignores any mean winds in the north–south direction (meridional winds), which are small relative to the zonal winds. Mathematically the idealized wind stress can be written

$$\tau_x = 0.1 \sin \frac{\pi}{2L} y \tag{8.01}$$

where τ_x represents the component of the wind stress in the x direction in units of N m^{-2} and y represents the distance north and south of 30° N, which varies between $+L$ and $-L$.

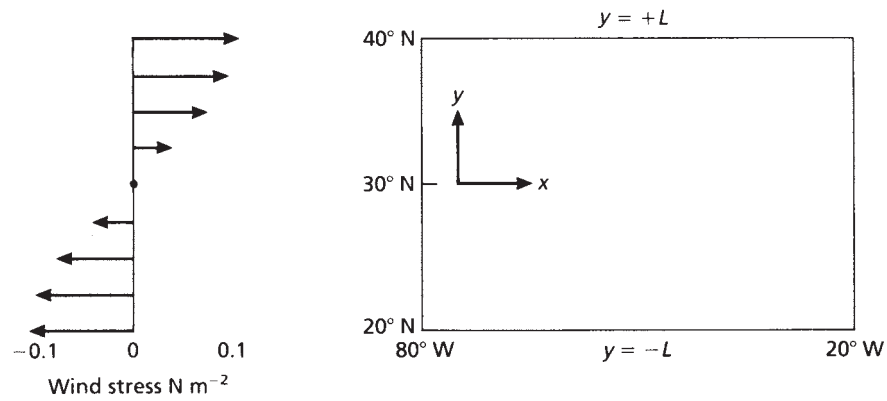

Fig. 8.04 An idealized rectangular ocean (on the right) extending from 20° N to 40° N and from 20° W to 80° W. The coordinate origin is at 30° N 80° W and y is positive to the north; x is positive to the east. The wind stress (on the left) is purely zonal and decreases sinusoidally from 0.1 N m^{-2} at 40° N to −0.1 N m^{-2} at 20° N.

Referring back to Section 5.2.2, we recall that the net effect of a wind stress on the water surface is to produce a transport in the upper layer of the ocean to the right of the wind known as the Ekman drift. The mass transport, M, of this flow is calculated by dividing the wind stress τ by the Coriolis parameter f as in Eqn. 5.02:

$$M = -\tau/f \tag{8.02}$$

If we represent the wind stress with Eqn. 8.01, the Ekman transport is found by substitution of Eqn. 8.01 into Eqn. 8.02 to give

$$M_{yE} = -\frac{0.1}{f}\sin(\pi y/2L) \tag{8.03}$$

where M_{yE} is the meridional Ekman mass transport through a 1-m-wide strip of the ocean in units of kg m^{-1} s^{-1}. This transport is illustrated at the top of Fig. 8.05, which shows a 1-m-wide slice of the ocean between 20 and 40° N from the surface to the main pycnocline at 1000 m. It is a perspective view looking toward the northeast. At the very top, above the surface of the water, is a representation of the wind field with a maximum stress to the east at 40° N and a maximum toward the west at 20° N. The Ekman layer takes up the top 100 m. North of 30° N the westward wind creates the southward Ekman transport shown by the shaded blocks of water with the arrows to indicate movement to the south. South of 30° N the east wind creates a northward transport in the Ekman layer. These oppositely directed transports, therefore, create a convergence in the Ekman layer that increases from zero at the extremities to a maximum in the center of the ocean at 30° N. Because the sea level cannot rise enough to accommodate the convergence it generates a downward velocity in the upper layer, which is indicated in

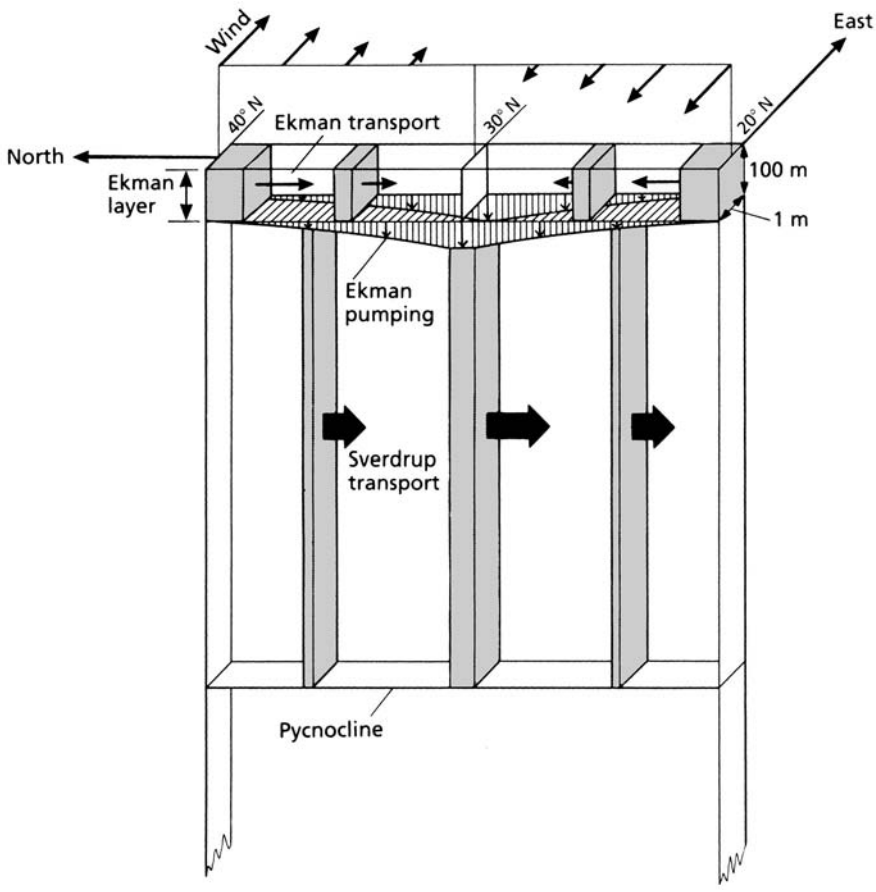

Fig. 8.05 A perspective drawing of a 1-m-wide slice of the ocean between 20° N and 40° N and from the ocean's surface to the pycnocline at 1000 m depth. The wind stress, changing from eastward at the north end to westward at the south end, is shown at the top of the picture. The top 100 m of the ocean is the Ekman layer, which converges toward the center (30° N) under the influence of the wind. Ekman pumping is indicated at the base of the Ekman layer and the southward Sverdrup transport is indicated in the layer above the pycnocline.

the figure by the small arrows at the base of the Ekman layer. The downward flow is referred to as Ekman pumping. (If the velocity at the base of the Ekman layer is upward because of a divergence in the Ekman layer, it is called Ekman suction.)

An expression for the vertical velocity associated with the Ekman pumping can be derived from Eqn. 8.03 by calculating the derivative of the transport with respect to the horizontal coordinate, which in this case is y. The result,

$$dM_{yE}/dy = -\frac{0.1\pi}{2Lf}\cos(\pi y/2L) \tag{8.04}$$

gives the amount of water that is piling up at latitude y. The maximum of this function is found at 30° N, where the cosine is 1.0. At this latitude, with $f = 0.73 \times 10^{-4}\ s^{-1}$, and with $L = 1.1 \times 10^{6}$ m (10° of latitude), the convergence works out to 2.0×10^{-3} kg m^{-2} s^{-1} or 169 kg m^{-2} d^{-1}, which converts to a downward velocity at the base of the Ekman layer of ~0.17 m d^{-1}. This velocity decreases to the north and south along with the cosine function and reaches 0.0 m d^{-1} at 20° N and 40° N.

The ocean beneath the wind-driven layer responds to the downward push of the Ekman pumping with a horizontal flow toward the equator that is many times larger than the Ekman transport. This derived flow, called the Sverdrup transport, is dictated by the fact that the Coriolis force varies with latitude. To understand this response we briefly review the consequences of the law of conservation of angular momentum or vorticity, which we first introduced in Box 5.01.

In oceanography the law is usually expressed by Eqn. 5.05,

$$\frac{f + \zeta}{H} = \text{constant} \tag{8.05}$$

where f is the Coriolis parameter or twice the rate at which the earth rotates about the local vertical relative to the stars, ζ is twice the rate that the water is rotating relative to the earth about the local vertical, and H is the height of the column of water. In discussions of vorticity, f is called the planetary vorticity, meaning that it is the vorticity given to the water by virtue of its being on the rotating planet at the latitude Φ. The term ζ is called the relative vorticity, representing the vorticity of the water relative to the earth.

In the open ocean away from the coasts and intense currents ζ is always close to zero and Eqn. 8.05 becomes

$$f/H = \text{constant} \tag{8.06}$$

Since we wish to know the consequences of a change in the height (dH) of the column of water we calculate the derivative of Eqn. 8.06 with respect to the north–south coordinate y, to get

$$\frac{df}{dy} = \frac{f}{H}\frac{dH}{dy} \tag{8.07}$$

The term df/dy, the rate of change of the Coriolis parameter with latitude, is commonly called β. It exists only because there is a change in the vertical component of the earth's rotation with latitude, and the effects that depend on its existence are referred to as "β effects." If the Coriolis force did not change with latitude there would be no tendency for the water to change latitudes to satisfy Eqn. 8.07 and Sverdrup transport would not exist.

With a little manipulation we can calculate the Sverdrup transport in the model. It turns out to be ~7.2 m^3 s^{-1} through each 1-m-wide meridional strip across

the ocean. If the ocean is 5000 km wide the total Sverdrup transport southward across 30° N is ~36×10^6 m^3 s^{-1} or 36 Sv, where 1 Sv or 1 sverdrup equals 10^6 m^3 s^{-1} in honor of H.U. Sverdrup, the man who contributed so much to understanding the oceans.

The Sverdrup transport is illustrated in Fig. 8.05 by the shaded blocks of water between the Ekman layer and the pycnocline that are moving toward the equator. The volume of the flow varies from a maximum at 30° N to zero at the northern and southern extremes. The diagram also illustrates the fact that the Sverdrup flow in this example is always toward the south even though the winds and the Ekman drifts are in opposite directions in the northern and southern halves of the ocean. The important variable is, of course, the vertical velocity in the Ekman layer, which is downward at all positions across the ocean.

It is a curious fact, evident in Fig. 8.05, that the maximum Sverdrup transport at these latitudes is much larger than the maximum Ekman transport. Intuitively one might expect that the convergence in the Ekman layer would create an equal and opposite compensating divergent flow to keep the sea level and the depth of the Ekman layer constant in time. The Sverdrup flow, however, does nothing to compensate for the Ekman convergence but creates a much larger convergence and divergence in the water columns in the northern and southern halves of the idealized ocean. The Ekman convergence is a maximum at 30° N, while the divergence created by the Sverdrup flow is a maximum along the northern edge of the basin, and the convergence of the Sverdrup flow is a maximum along the southern edge. The Sverdrup flow is clearly not providing a compensation for the converging Ekman layer. If the Sverdrup flow was able to operate alone, the sea level at 40° N would decrease about 1 m per day while the sea level at 20° N would increase by the same amount. Such a change in sea level does not occur because large compensating zonal flows are generated that provide the water for the regions of divergence and remove the water from the regions of convergence.

Because a flow toward the east or west does not involve a change in the Coriolis force and hence a change in the planetary vorticity, it is easier for water to move in these directions than north or south. This explains why the compensating flows are east and west.

This increase is illustrated in Fig. 8.06, where each thin line represents the flow of water crossing 30° N through a 1-m-wide section that comes from the west along latitude $+y$ and returns to the west along latitude $-y$. The broad arrows on the left indicate the zonal flows at latitudes $+y$ and $-y$.

The diagram in Fig. 8.06 represents the flow delivered from one parallel of latitude north of the center line to a symmetric parallel to the south of the center line. A similar picture, from Stommel (1948), is shown on the right in Fig. 8.07 except that the contour lines represent the flow in the whole of the idealized ocean except near the western boundary of the ocean. The contour lines define the paths of the water particles, and between two contours the volume transport stays constant. As the lines get closer together, the speed of the flow increases. The diagram incorporates both the meridional Sverdrup flow, which is constant across each parallel of latitude, and the compensating zonal flows, which

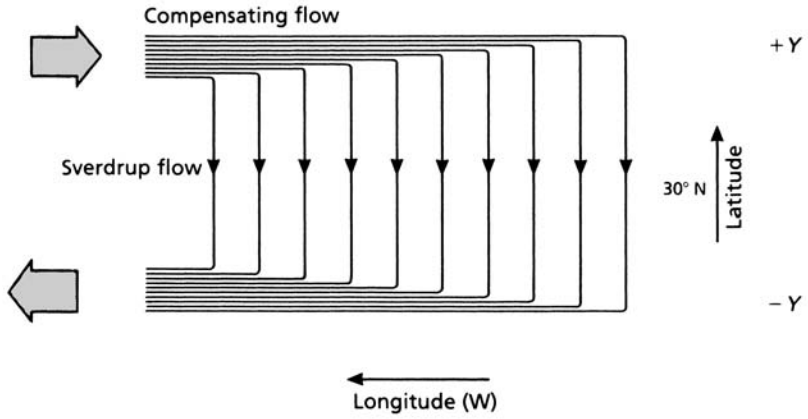

Fig. 8.06 The north–south Sverdrup flow across 30° N is constant at each meridian but the compensating east–west flows at each latitude ($+Y$ and $-Y$) must increase to the west.

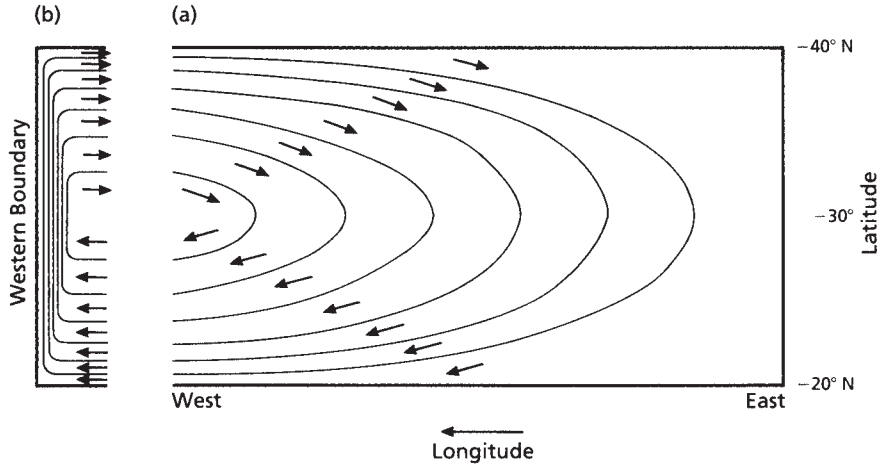

Fig. 8.07 (a) The total wind-driven circulation in the idealized ocean without a western boundary, including the Sverdrup flow and the compensating zonal flows. The transport between contour lines is constant. (b) The presence of the western boundary forces the westward-flowing water of the gyre into a narrow northward current.

increase toward the west. The pattern of currents illustrated in this part of the diagram will continue toward the west for as long as the ocean continues in that direction. There is no mechanism in what we have discussed so far to close the gyre with a flow toward the north. The reason is the fact that water is much easier to move east or west than it is to move north or south.

At the western side of the ocean some force must be generated to overcome the resistance of the water to go north to complete the gyre. The required force was shown by Charney (1955) to derive from the inertia of the westward-flowing

water, which must slow down as it approaches the coast. Any acceleration or deceleration of a mass requires a force. The magnitude of such inertial forces is usually insignificant in the ocean, where normally the only forces of consequence are the Coriolis and pressure-gradient forces involved in the geostrophic balance. The inertial force is dominant in only a narrow region near the coast but its generation causes the deflection of the westward-flowing current toward the north and causes the flow to be squeezed into a narrow rapid flow as shown on the left in Fig. 8.07.

Because both a western boundary and inertial forces are instrumental in creating the Gulf Stream, it has been called a western boundary current or an inertial boundary flow. In our idealized ocean this northward flow completes the gyre of the subtropical wind-driven circulation, but how does the model compare with the observed circulation?

8.2.2 The observed circulation

The near-surface circulation of the North Atlantic subtropical gyre presented in Fig. 8.08 is based on the works of many authors. The general path of the Gulf Stream is similar to the original diagram of Sverdrup *et al*. (1942) but the northern and southern recirculation gyres are shown with greater intensity according to Hogg *et al*. (1986) and Worthington (1976), respectively. The maximum Gulf Stream transport of ~150 Sv occurs at about 65° W. The branching and path of the stream near the southeast Newfoundland ridge are according to Mann (1967) and Clarke *et al*. (1980), while the branches at ~45° N and ~51° N to the east of Newfoundland are discussed by Krauss (1986). The continuation of the stream's branches in the North Atlantic Current to the mid-Atlantic ridge is detailed by Harvey and Arhan (1988) and Sy (1988), and the circulation to the east of the ridge is adapted from Saunders (1982) and Klein and Siedler (1989). The circulation east of the Bahamas is based on Olson *et al*. (1984) and Stommel *et al*. (1978). Some of the flowlines in the eastern basin are not continued south of 35° N to indicate that much of this flow is thought to descend below the surface layers of the southern part of the gyre.

It is clear from Fig. 8.08 that the circulation pattern of our idealized ocean does not reproduce all the features of the real ocean. For example, the location of the maximum flow in the Gulf Stream is not where the model predicts it to be and the maximum flow of the stream is almost four times the Sverdrup transport that we estimated in the previous section to be $\sim 36 \times 10^6$ m^3 s^{-1}. In the model the maximum flow occurs at the latitude where the wind stress is zero and changing from eastward to westward. This point actually occurs at about Cape Hatteras (35° N); however, the Gulf Stream continues to increase in intensity north of this latitude.

Over the past decade the use of analytical models, such as that outlined above, has declined in use as computer simulations have become the most powerful tools for analyzing the ocean's circulation. Bryan *et al*. (1998; available at

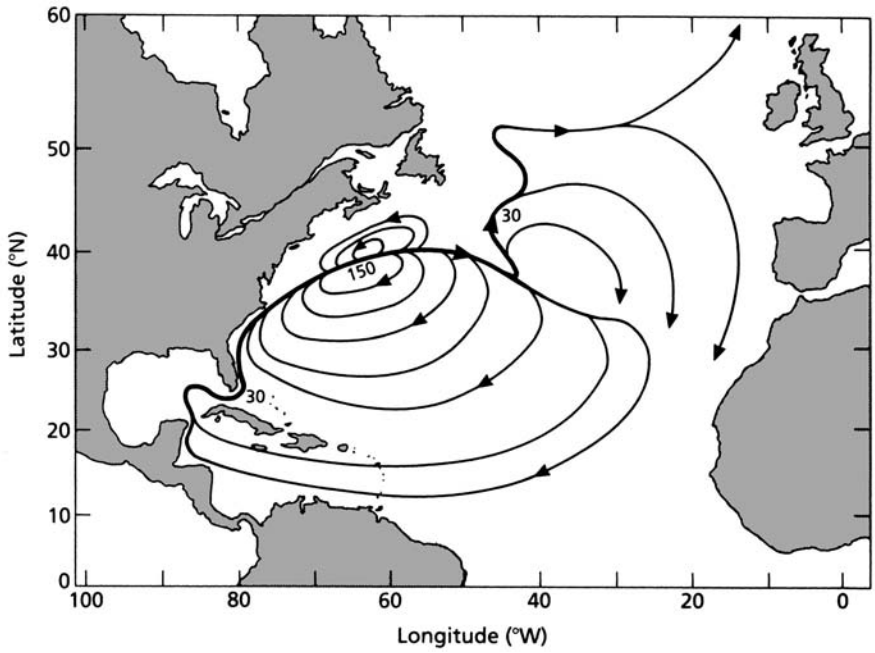

Fig. 8.08 The wind-driven circulation in the North Atlantic subtropical gyre including the Gulf Stream and its branches with some estimates of volume transport in sverdrups. The rapid narrow currents such as the Gulf Stream are indicated by heavy lines. The slow broad flows are shown by light lines.

www.cgd.ucar.edu/oce/bryan/woce-poster.html) demonstrate some of the improvements in a computer simulation of the North Atlantic Circulation. In the earlier simulations, with grid sizes of ~50 km, the Gulf Stream did not separate from the continental shelf at Cape Hatteras but continued northeastward and the strength of the current was less than observed. As the grid sizes decreased to ~10 km the simulations became more realistic with the Gulf Steam separating as observed.

8.2.3 Meanders, rings, eddies, and gyres

(a) Meanders

After the Gulf Stream leaves the coast, it continues eastward as a strong narrow current with relatively barren Sargasso Sea water on the right and more productive slope water on the left. At about 65° W, the current becomes unstable and begins to develop large north–south oscillations, or meanders (Fig. 8.09). In the loops of the meanders enhanced biological activity has been reported, but such activity is not always present. Proper examination of the phenomenon by ship is made nearly

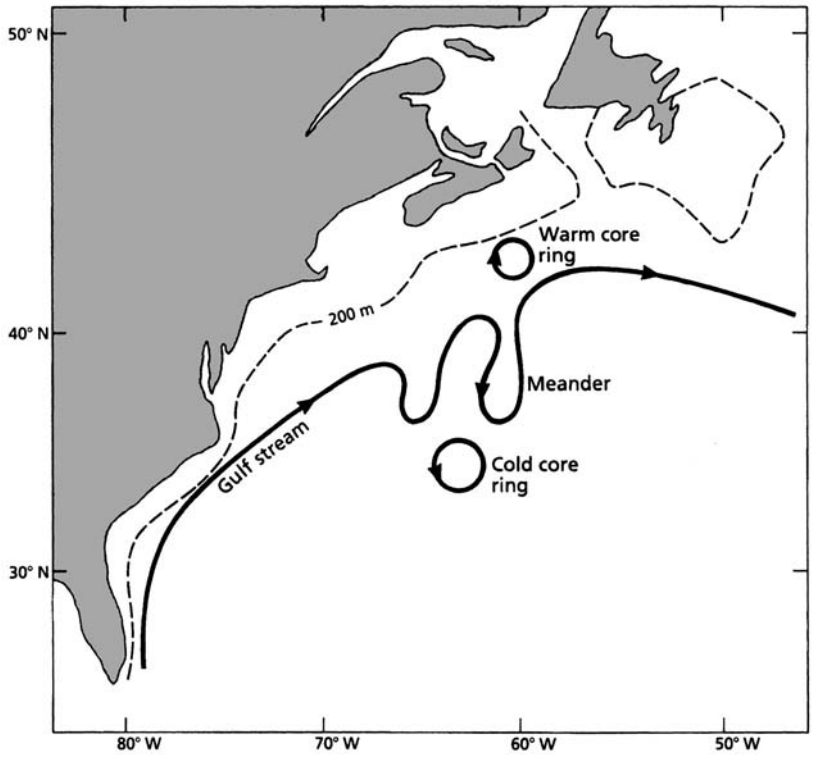

Fig. 8.09 A schematic illustration of meanders in the Gulf Stream and the formation of rings, based on Richardson *et al*. (1978) and Parker (1971).

impossible because of the very high speed of the current (~1 ms^{-1}). It is most effectively studied using computer simulations.

Recently Anderson and Robinson (2001) completed a study using a time-dependent, three-dimensional, physical–biological model with data assimilation. The authors conclude that the meandering process alone does not increase biological activity above that found in the waters to the north of the stream. They do however find that interactions between rings (see below) and the Gulf Stream create significant vertical transports of nutrients and plankton which lead to enhanced levels of biological activity.

(b) Rings

The meanders in the Gulf Stream often grow too large to continue as meanders. The ends then separate into isolated rings of water, as illustrated in Fig. 8.09. The rings to the south of the Gulf Stream rotate counter-clockwise and enclose colder water from the north side of the current; they are known as cold-core rings. The clockwise-rotating rings to the north of the stream are called the warm-core rings because they contain the warmer water from the Sargasso Sea and are surrounded

by the cooler waters found north of the stream. Both kinds of rings are baroclinic phenomena – that is, they are confined to the thermocline or the upper ~1000 m.

Each year there are about 10 cold-core rings formed. Each exists for about a year before it is either reabsorbed into the Gulf Stream or loses its unique properties to diffusion (Ring Group 1981). At any one time the cold-core rings represent about 10% of the surface area of the Sargasso Sea. According to Richardson (1983) the number of warm-core rings formed each year is about half that of cold-core rings. The production rate, however, is quite variable. Sometimes none can be identified in the region north of the Gulf Stream, while at other times the region is almost filled with rings. The warm-core rings also tend to be smaller than the cold-core rings with diameters of ~100 km as opposed to 100–300 km for the cold-core ones.

The rings appear as pools of anomalous conditions because they contain water from the opposite side of the stream having the other side's physical, chemical, and biological properties. As the anomalous conditions change over the approximately one-year life of the ring, through mixing with the ambient water, the biology changes in ways that are unique to the rings, as we discuss in Sections 8.4.3 and 8.4.4.

(c) Eddies

Although rings are a form of eddy, the term eddy is usually reserved for the lower-amplitude current variations that are found throughout the ocean. These oscillations, described by Robinson (1983), tend to be barotropic (constant with depth) as opposed to baroclinic, and because the ocean is full of them they interact in a way that is reminiscent of turbulent eddies. For this reason the properties in the eddies change much more rapidly than the properties within the rings, so the biology of an eddy is less individualistic than that of a ring.

The time scale of one rotation of an eddy is usually 10–30 days, and the horizontal scale between 10 and 100 km, close to the internal Rossby radius (Section 5.2.3). Two terms often used to describe eddies are "synoptic" and "mesoscale." Synoptic is borrowed from meteorology, where it is used to indicate the eddies in mid-latitudes associated with cyclonic storms. It implies a horizontal scale that can be sampled more or less simultaneously. Mesoscale is an ill-defined term indicating an eddy smaller than ocean-basin scale, of the order of 100 km rather than 1000 km.

The energy level of eddies tends to be highest in those close to narrow boundary flows like the Gulf Stream. Currents in these eddies may be about 1 m s^{-1}, while currents in eddies remote from major currents (e.g., in the southeast Pacific) are nearer 0.01 m s^{-1}. It has been suggested (Robinson 1983) that most open-ocean eddies are formed indirectly from strong currents, with a transfer of energy through the eddy field in a way resembling the cascade process described in Section 2.2.6.

As pointed out by Swallow (1976), the variability associated with ocean eddies had been observed for many years before their full importance was discovered,

but they were thought to be transient features associated with the wind or the internal tides. Swallow and Hamon (1960) first observed the currents in the deep open ocean with neutrally buoyant floats and discovered that the currents varied by 0.5 m s^{-1} rather than the expected 0.01 m s^{-1}. Further work revealed that, in total, the eddies in the ocean actually contain more kinetic energy than the mean flows.

(d) Gyres

The word "gyre" is usually used to describe a circular current that is confined by or associated with bathymetric features. The term covers a wide range of spatial scales. Thus, the currents of the Gulf Stream, the North Atlantic Current, the Canary Current, and the North Equatorial Current make up the North Atlantic subtropical gyre at the ocean-basin scale. Over shallow banks such as Georges Bank in the Gulf of Maine there is a continuous current flowing around the bank located over the edge. This circulation is the Georges Bank gyre.

8.2.4 Rossby waves

The 10,000 km long north–south meanders in the westerly winds shown in Fig. 8.01 are, as mentioned in Section 8.2, planetary or Rossby waves. G.C. Rossby (1939) was the man who demonstrated that these meanders propagate westward due to the increase in the vertical component of the earth's rotation with latitude. The waves also occur in the ocean but have, in the past, been difficult to observe. This is because their wavelengths are hundreds of kilometers long and because they create only small variations (0.05–0.1 m) in the sea level as they pass. Since 1992, however, sea level over the whole earth has been measured accurately enough to observe Rossby waves propagating across the ocean (Chelton and Schlax 1996). The sea-level measurements are obtained from a satellite-borne altimeter under the TOPEX/POSEIDON program (topex-www.jpl.nasa.gov).

To see why the waves propagate westward, consider the situation in Fig. 8.10. The two wavy solid lines represent water displaced from lines of constant latitude: north (on the left) and south (on the right). According to Eqn. 8.05 the

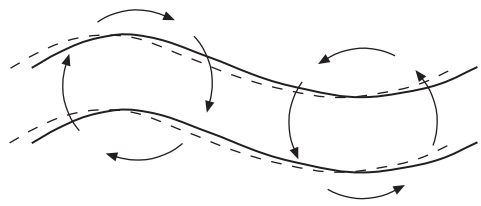

Fig. 8.10 The Rossby wave; displacements to the north/south rotate clockwise/counter-clockwise causing a westward propagation of the disturbance, after Flierl and McGillicuddy (2002).

vorticity of the water is equal to $f + \zeta$ (assuming depth H is a constant) and remains constant as it is displaced. The northward-moving water moves to a region of greater f, i.e., where the surrounding water is rotating faster to the left with the earth. Since f is greater in the north ζ must be decrease to keep $f + \zeta$ constant. The decreased ζ causes the water imported from the south to rotate, relative to the local conditions, to the right as indicated by the circle of arrows.

For the water displaced to the south the opposite occurs. The water moving south encounters a region where the earth's rate of rotation (f) is less. The displaced water then appears to rotate to the left relative to the local vertical. The result of the flows induced by the displacements is to shift the disturbance to the west as suggested by the dashed line.

The initiation of the disturbance that leads to the wave is not yet well understood. It may be from large-scale changes in the wind field over the open ocean or from disturbances in the ocean structure propagated to higher latitudes along the eastern margin of the ocean from tropical latitudes.

Theoretical studies of Rossby waves show they exist in many modes. The first mode is the barotropic mode in which the motion of the water is constant throughout the depth of the ocean. This mode moves quite rapidly across the ocean and creates no known biological response. In the simplest baroclinic mode the motion of the water is not constant with depth but in one direction above the thermocline and in the opposite direction below the thermocline. Because of this the depth of the thermocline may vary by 50 m across the wave. These internal variations may be responsible for the fluctuation in chlorophyll often observed to coincide with the waves, as noted in Section 8.5.1.

8.2.5 The thermohaline circulation

In the discussion of the wind-driven circulation in Sections 8.2.1 and 8.2.2 it was assumed that all oceanic currents are horizontal. This is not however the whole story. There are regions in the ocean where surface waters become denser than the underlying waters and sink, thereby creating a vertical circulation in the ocean. Most of the sinking dense water is formed by cooling in the mid to high latitudes, although some is formed through evaporation, as in the Mediterranean Sea.

The densest waters are formed at high latitudes. Deep convection in the European Arctic (Norwegian, Greenland, and Iceland Seas) produces water masses that are dense enough to descend to the bottom of the North Atlantic after flowing over the sills between Greenland and Scotland. Similarly the dense water formed over the shelves around Antarctica, especially in the Weddell Sea, flow off the shelves and descend to the bottom of the southern extremities of the Atlantic, Indian, and Pacific Oceans. Deep convection also occurs in the Labrador Sea; however, the density of the water produced does not reach that of the bottom waters but of intermediate depths.

The "new" dense waters tend to have properties significantly different from the rest of the ocean. By following these anomalous values the movement of the

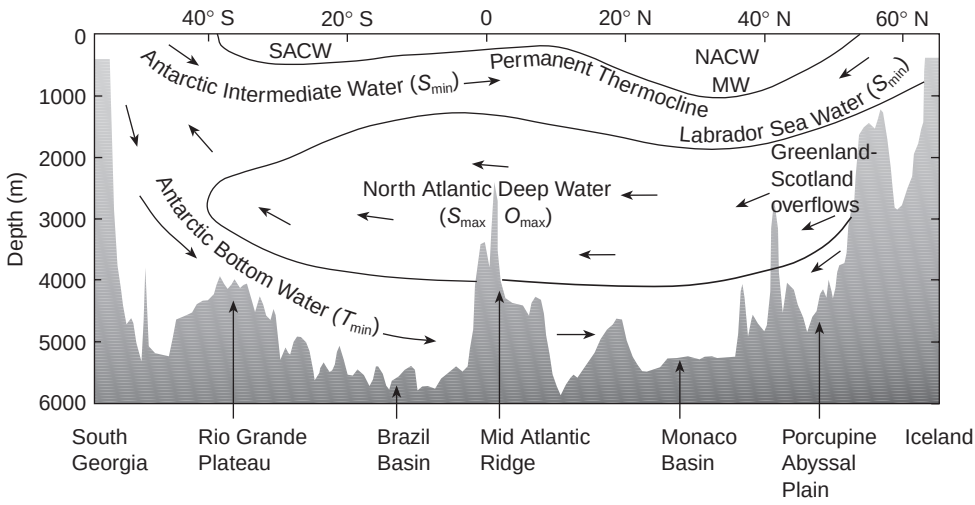

Fig. 8.11 Cross-section through the Atlantic Ocean from Iceland to South Georgia showing the locations of the major water masses and their paths. Above the permanent thermocline are the North and South Atlantic Central Waters (NACW and SACW) and the Mediterranean Water (MW). The bottom profile is the same as for the Atlantic sections in Plate 6. S_{min}, salinity minimum; S_{max}, salinity maximum; O_{max}, oxygen maximum; T_{min}, temperature minimum.

properties of the "new" water can be traced though the ocean. Collectively these flows are known as the thermohaline circulation, as distinct from the wind-driven circulation. An outline of this circulation in the Atlantic Ocean is shown in Fig. 8.11. The surface layers in the subtropical regions are dominated by the subtropical gyres (Fig. 8.08). They contain the North Atlantic Central Water (NACW) and the South Atlantic Central Water (SACW), bounded beneath by a permanent thermocline. These water masses, like all central water masses, are characterized by unique temperature-versus-salinity relationships with depth over large regions of the subtropics.

Beneath these water masses lie waters that are strongly influenced by intermediate depth flows from regions beyond the central gyres. In the North Atlantic, for example, outflow from the Mediterranean Sea (MW) lies below the NACW. And below the MW the influence of the Labrador Sea Water (LSW) can be found, characterized by its low salinity. In the South Atlantic, Antarctic Intermediate Water (AAIW) is formed when cool, low-salinity waters near the surface move north and subduct beneath the SACW.

Mid-depth layers of the Atlantic contain North Atlantic Deep Water (NADW), which originates partly from water that flows into the Atlantic from the Norwegian Sea over the ridge between Iceland and Scotland. It is characterized by higher salinities and higher dissolved oxygen content than the waters above and below. The water at the bottom of the ocean is the coldest. Some originates

in the seas north of Iceland and flows into the Atlantic over the sill in Denmark Strait between Greenland and Iceland. The major contribution to the near-bottom water in the ocean is formed over the continental shelves around Antarctica through cooling and freezing. As the ice grows it incorporates water but not the salt in the water. This left-behind salt increases the salinity (and density) of the water beneath the ice. The resulting dense water flows off the shelves to the bottom of the surrounding oceans as the Antarctic Bottom Water (AABW).

The color images of temperature, salinity and oxygen distributions along sections through the Atlantic and Pacific oceans in Plate 6 vividly illustrate the water-mass distributions. Especially noticeable are the descent, in the south, of cold AABW to the bottom of both oceans; the high-salinity high-oxygen NADW; the intrusion of the low-salinity AAIW and the central water masses in the surface layers. The low-oxygen layer in the North Pacific Ocean is another important feature. Its presence in the North Pacific while the North Atlantic contains water of high oxygen content demonstrates the fact that the water in the North Atlantic is rapidly renewed by the dense high-oxygen water overflows from the Arctic. Water at mid-depths in the North Pacific, by contrast, is renewed very slowly.

The rapid renewal of the water in the northern North Atlantic is a consequence of the formation and sinking of dense waters in the north and their replacement by northward-flowing warm saline water carried by the Gulf Stream and its extension the North Atlantic Current. This exchange of warm surface water for sinking cold water is known as the Meridional Overturning Circulation (MOC).

The warm water carried north by the MOC creates a milder climate in northern Europe than would exist if the MOC stopped. This appears to have happened in the past. Geological records from the deep sea and the continents reveal abrupt climate changes during the last glaciation (Clark *et al*. 2002). Climate shifts are also observed to be related to "deep-water reorganizations" (Adkins *et al*. 1997). These observations suggest that northern Europe is warm when the MOC is active and cold when it is not.

Because of its importance to the European climate there is a new program to monitor the MOC for a number of years with moored instruments across the Atlantic Ocean at 26° N. This experiment began in July 2004, and up-to-date information is available at www.soes.soton.ac.uk/research/groups/ocean_climate/rapidmoc/intro.

The MOC is a special part of the thermohaline circulation discussed above. The MOC is driven by buoyancy forcing but there is not enough energy in the buoyancy forcing to drive the movement of water required to account for the property distributions evident in Plate 6. It is now generally accepted (Wunsch 2002) that the property distributions linked to the thermohaline circulation are not due to buoyancy forcing alone but are mainly a consequence of the wind-driven circulation. It is the only energy source in the ocean large enough to redistribute the water masses.

8.3 Distribution of biological production in ocean basins

We have examined the consequences of differential solar heating at low and high latitudes that, in conjunction with the rotation of the earth, lead to westerly and trade winds. These winds, in turn, drive major anticyclonic subtropical gyres in each of the major ocean basins. Associated with them are powerful western boundary currents that transport large quantities of heat away from equatorial regions. These currents meander and cut off large gyrating bodies of water, the warm- and cold-core rings, that lead independent existences for several months.

We now examine the ways in which organisms have adapted to the various physical regimes. Some use the boundary currents for long-range transport between breeding grounds and feeding areas. Others make several circuits of an ocean gyre while growing to maturity. We shall see that the standard pattern of primary production for open-ocean situations (Chapter 3) is much modified by the presence of rings and gyres, storm events, and lateral transport, with the result that primary and secondary production in the central basins is considerably higher than we thought a decade or two ago.

The biological phenomena associated with the major eastern boundary currents were dealt with in Chapter 5. These are regions of major coastal upwelling that are home for major stocks of sardines and anchovies. When we turn our attention to the western boundary currents and to the whole gyral pattern of circulation we find that well-known species like squid, eels, and salmon make migrations of thousands of kilometers by traveling with these currents. We also find that the larvae of some kinds of coastal invertebrates live long enough in the plankton to make, for example, the crossing of the North Atlantic before settling on the opposite side from where they were hatched. This movement leads to changes in our traditional ideas about gene flow between coastal populations on opposite sides of ocean basins.

8.3.1 Squid and the western boundary currents

Illex illecebrosus, the short-finned squid, is caught in great quantities off the east coast of North America from Georgia to Newfoundland (Coelho 1985). From January to early March larvae occur in slope water along the northern edge of the Gulf Stream, roughly from Cape Hatteras to the latitude of Cape Cod. In May juveniles are found in warm waters along the southern slope of the Grand Banks, and from there they migrate to Canadian inshore waters in late June and July. They grow about 1.5 mm d^{-1} during the summer, and by November many of the males are mature, but the females are less advanced. There appears to be only one year-class and it is thought that the adults return south to spawn on the northern edge of the Gulf Stream, thus completing their life cycle in one year. The recapture of tagged squid confirms that this migration can occur.

Since squid are also caught inshore from Cape Hatteras to Cape Cod, it is inferred that part of the stock leaves the Gulf Stream at the latitude of Cape Cod and moves into the southward-flowing coastal currents. Warm-core rings (see Section 8.4) may play an important part in this shoreward movement. The data supporting the view that the squid use the Gulf Stream to facilitate their migration are reviewed by Rowell and Trites (1985) (see also Trites 1983 and Coelho 1985). The center of the spawning area appears to be the Blake Plateau, off Cape Canaveral, Florida. The larvae and juveniles are thought to enter the Gulf Stream and be transported northward up to 1000 km per week, but many are probably caught up in frontal eddies that delay their northward progress and have the effect of mixing larvae and juveniles of different ages. Dawe and Warren (1992) found that the time series of catches in the United States, on the Scotian Shelf, and off Newfoundland all varied in the same pattern, albeit with more marked fluctuations in the more northern regions. It appeared that when the stocks were abundant in the south they migrated north in greater numbers. Analysis of environmental data showed that Newfoundland catches were inversely correlated with winter iceberg counts on the Grand Banks and positively correlated with high January sea-surface temperatures off the Scotian Shelf. In a review of the history of the fishery, O'Dor and Dawe (1998) showed that catches greatly increased during the 1970s, largely due to the participation of the USSR and Japan, to a peak of about 160,000 tons in 1979. After that, they declined precipitously due to low abundance of squid. Since the species has a one-year life history, it is believed that since 1972 each year's catch has reflected recruitment. It peaked at 4400 tons in 1990 and has been lower than that ever since.

Although details of the causes of recruitment variability are not known, Bakun and Csirke (1998) reviewed the possible physical variables that might influence recruitment, and put forward a number of hypotheses. They suggested that three classes of environmental factors might be involved:

1 enrichment of the food web by physical processes (upwelling, mixing, etc.);
2 opportunity for concentrated patches of food particles to accumulate (stable structure, convergent flow patterns, frontal formations, etc.);
3 flow patterns that enable a population to maintain itself, through adaptive responses, in a continually moving fluid medium.

The authors showed (Fig. 8.12) that the egg masses find a neutrally buoyant level within the pycnocline separating the Gulf Stream from the shelf water. On hatching, the squid paralarvae may rise to the surface layer and be carried by the density-driven flow into the convergent zone at the western edge of the Gulf Stream. South of Cape Hatteras the western edge is enriched by the formation of Gulf Stream frontal eddies (see Section 8.4.1), which cause upwelling of nutrient-rich water from the slope and patches of high phytoplankton biomass, even in winter. North of Cape Hatteras the Gulf Stream meanders cause convergence and downwelling on their leading edges, but divergence and upwelling of nutrient-rich water on their trailing edges (Fig. 8.13). Hence, the frontal processes of the

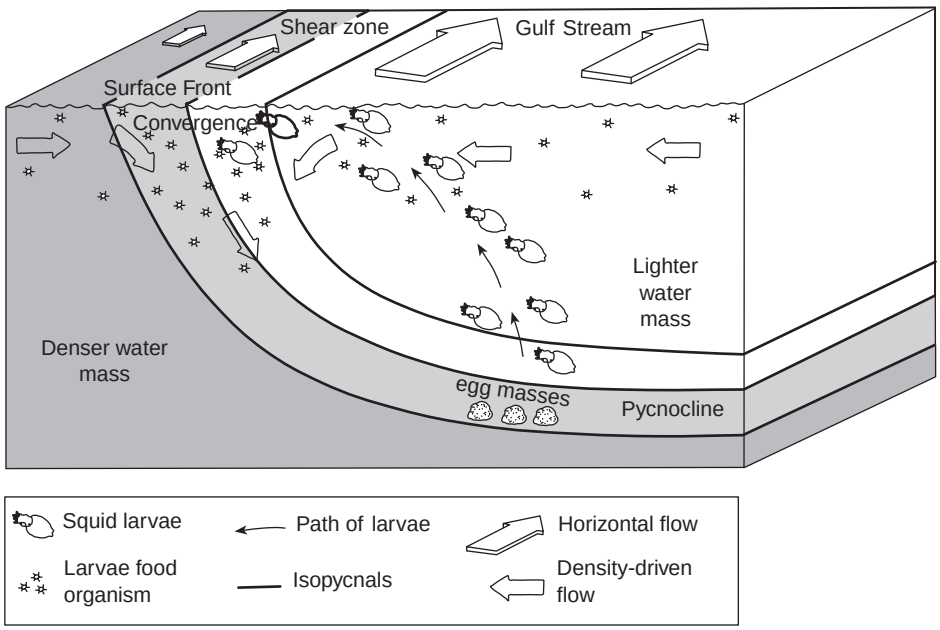

Fig. 8.12 Schematic diagram showing how squid may move during development. Within the pycnocline, squid egg masses find a neutrally buoyant level, where they are suspended at mid-depth under conditions of reduced predation. Upon hatching, squid paralarvae may rise to the surface layer and be carried into the convergent frontal zone by density-driven flow. After Bakun and Csirke (1998). Reproduced by permission of the Food and Agriculture Organization of the United Nations.

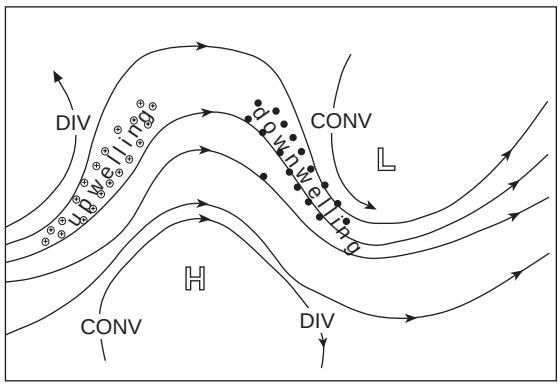

Fig. 8.13 Schematic diagram of the convergent and divergent zones in a Gulf Stream meander pattern. Widening distance between streamlines corresponds to divergence and narrowing distance between streamlines corresponds to convergence. Redrawn from Arnone 1990.

Gulf Stream will tend to support both enrichment of the food web in the areas of divergence and concentrations of food organisms in the areas of convergence. Bakun and Csirke (1998) also reviewed the possible effects of frontal eddies, meanders, and warm-core rings in delaying the northward movement of the squid entrained in them. These effects could explain why, at any given point in the Gulf Stream, the population is found to be of mixed ages.

Dawe *et al*. (1998) showed that low squid abundance off Nova Scotia and Newfoundland was correlated with northward displacement of the Gulf Stream front. This displacement is in turn associated with a slow and meandering Gulf Stream, and more frequent formation of warm-core rings (see Section 8.4.4). The transport of young stages of squid in these rings to coastal waters south of Nova Scotia may result in inefficient northward transport, and poor recruitment in Nova Scotia and Newfoundland.

Perez and O'Dor (1998) reported on the growth rates of short-finned squid from waters of various temperatures, and compared them with the growth rates of squid held in captivity and given unlimited food. They showed that the potential for growth in the warm waters of the Gulf Stream was very high, but in nature the squid were strongly food-limited. After making the transition to cool slope waters their growth potential decreased but they encountered 4–12 times the density of phytoplankton and 3–4 times the density of zooplankton. The authors suggested that the migration from the Gulf Stream to the shelf is driven by food requirements. Individual growth histories depended on their encounters with concentrated patches of food, which in turn were determined by the timing and transport dynamics of the main water masses.

There is an analogous association between the Japanese squid *Todarodes pacificus* and the Kuroshio Current (see map, Fig. 8.03). In this case there are three stocks breeding at different seasons: winter, summer, and autumn. The winter-spawning group is associated with the Kuroshio Current. After spawning in the period January–April in the East China Sea, the larvae and juveniles travel north with the Kuroshio Current, then turn inshore and are caught between the islands of Honshu and Hokkaido in summer. The summer spawning is in another part of the East China Sea, from which the larvae are entrained into the Tsushima Current that flows north between the islands of Japan and the mainland. This current meets a southward-flowing cold coastal current, the Liman Current, and the summer-spawned squid are fished along the boundary between the two. This example clearly illustrates the use of these western boundary jet currents as "rapid transport," enabling the eggs and larvae to develop in winter in warm water while the adults travel north with minimum energy expenditure to exploit the rich feeding grounds further north. Sakurai *et al*. (2000) reported that annual catches in Japan have gradually increased since the late 1980s and proposed that changing environmental conditions have caused the autumn and winter spawning areas in the Tsushima Strait and near the Goto Islands to overlap, and winter spawning sites over the continental shelf and slope in the East China Sea to expand.

8.3.2 Eels and the North Atlantic gyre

The classic work of Schmidt (1922) on the life history and migrations of eels is well known. As a result of extensive collection of the translucent, leaf-like larvae (known as leptocephali) he concluded that there were two species of *Anguilla* in the North Atlantic: the European eel *Anguilla anguilla* and the American eel *Anguilla rostrata*. The smallest larvae of both species were found in the region of the Sargasso Sea, with clear evidence of increasing mean size of European eel larvae as one moved closer to Europe, and increasing size of American eel larvae as one moved north from the Sargasso Sea toward Newfoundland. Schmidt therefore proposed the startling theory that all European eels are derived from a stock that breeds in the Sargasso Sea in winter, and that the leptocephali take over two years to reach the coasts of Europe, where they metamorphose into the adult form and migrate up the rivers and lakes to places far inland. No less startling was the view that this stock is maintained by eels that make the incredibly long breeding migration down the rivers of Europe and thousands of kilometers westward across the Atlantic Ocean to breed in the Sargasso Sea. One wonders whether eels have used the same breeding ground since the two sides of the Atlantic were much closer together, and have continued to colonize all the rivers available in Europe and North America, even though the continents have drifted apart.

In general, the case for the existence of two distinct species has been substantiated. Counts of muscle blocks (myomeres) in the larvae yield a mean of about 114 for European eels and about 106 for American eels. Counts of vertebrae in the adults yield similar differences in the mean values. A study of parasite distribution in the two species supports the view that an ancestral population inhabited both sides of the North Atlantic as well as Greenland, Iceland, and Scandinavia, but that the population split into European and American components when it was forced southward by the Pleistocene glaciation (Marcogliese and Cone 1993). A restriction-enzyme survey of the eels' mtDNA supports the existence of two distinct species (Avise *et al*. 1990). However, the present-day Iceland population appears to contain a small proportion of individuals resulting from hybridization between American and European eels.

Kleckner and McCleave (1985, 1988) made an intensive study of the distribution of Atlantic eels in the Sargasso Sea. They found that the smallest stages were confined to the southern Sargasso Sea, south of a front separating the warm, saline, permanently stratified surface water from more variable subtropical-convergence-zone water to the north.

After examining both historical data and new samples McCleave *et al*. (1987) concluded that the American eel is genetically distinct from the European eel, but that their breeding grounds have a considerable area of overlap. They suggested the existence of some reproductive isolating mechanism, since larval forms with intermediate characteristics have not been found. Small, newly hatched larvae of the American eels were found from mid-February to April and small European

larvae from late February to mid-July. Both species enter the Gulf Stream. American eels grew at a rate of about 0.24 mm d^{-1} from February to October. A large fraction of the population was probably transported northwest in the Antilles Current and entered the Gulf Stream north of the Straits of Florida by April. By May American eel leptocephali were abundant in the Gulf Stream opposite Cape Hatteras and beyond, and during July and August were common between Cape Hatteras and the southeast Newfoundland Rise. From August to November the larvae were common in collections from slope water, inshore of the Gulf Stream, south to Cape Hatteras. It seems likely that the larvae actively migrate westward out of the Gulf Stream, after which they would be carried passively southward in the slope water.

Powles and Warlen (1997) reported that larvae arriving in winter at estuaries in North Carolina (USA) were, on average, about 150 days old and those in New Brunswick (Canada) were about 20 days older. This was consistent with the larvae having been hatched in the Sargasso Sea during the previous summer.

European eels continue eastward in the North Atlantic Current, but the time it takes for them to reach the European estuaries has not been definitively determined. Schmidt (1922) estimated this period to be about 2.5 years, but Boëtius and Harding (1985) concluded that it may be possible for European eel larvae to grow to a size appropriate for metamorphosis in a little more than a year. Schmidt's estimate was influenced by larvae of intermediate size that can be found in the mid-Atlantic at any time of year. It seems probable that a proportion of the larvae traveling in the Gulf Stream and North Atlantic Current find themselves in return flows directed toward the mid-Atlantic (see Fig. 8.08). Here the feeding conditions are poor and their growth is retarded. In fact, they may never reach the shores of Europe. The successful colonists of European rivers may be those eels that traveled in the main stream and completed the journey in a little more than a year.

To complete our mental picture of the way in which eels make use of the major currents of the North Atlantic, we may suppose that the returning adults would travel west by a subtropical route, making maximum use of the Canary and North Equatorial Currents. In this way, their life history would be elegantly adapted to the North Atlantic gyre, with the successful group of larvae riding the western boundary and North Atlantic currents, while the breeding migrations of the adults follow the return flows. This story is a clear indication of how recent improvements of our understanding of the physical oceanography of the North Atlantic have thrown new light on the biology of these remarkable fish. It is now known that in an analogous manner the Japanese eel *Anguilla japonica* breeds at a site in the North Equatorial Current west of the Mariana Islands. From there the eels travel with the Kuroshio Current, which returns them to their juvenile habitats in Japan (Tsukamoto 1992).

Castonguay *et al*. (1994) reported a drastic decline in eel recruitment to the Great Lakes. Between 1985 and 1992 the numbers of juveniles ascending an eel ladder at a hydroelectric dam on the St Lawrence River declined more than 98%. There are no other North American sites with direct counts of migrating juveniles, but in the Bay of Fundy and in Chesapeake Bay catch-per-unit-effort data do not

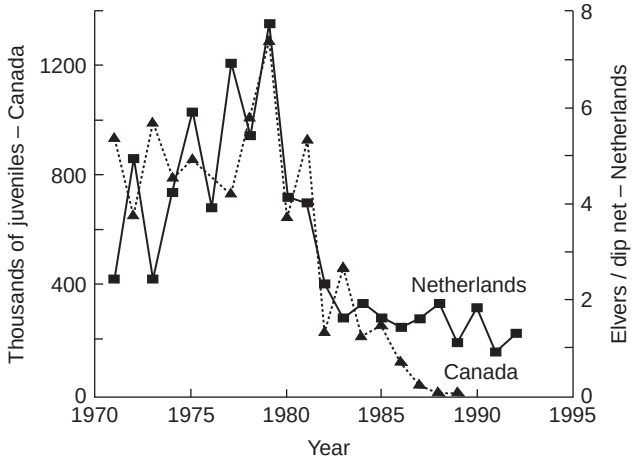

Fig. 8.14 Recruitment of American and European eels as represented by the number of juveniles passing a counting ladder on the St Lawrence River, Canada, and the catch per unit effort of elvers in the Den–Oever estuary of the Netherlands (W. Dekker, unpublished data). From Castonguay *et al*. (1994). Reproduced by permission of Blackwell Publishing Ltd.

indicate a drastic decline in stocks at this time. On the other hand, declines in catch per unit effort were noted in most of Europe, and seem to have occurred at about the same time as the decline in the St Lawrence River. (Fig. 8.14).

While pollution and habitat destruction were probably factors in the decline of both American and European eels, it is unlikely that these factors would produce such a drastic change simultaneously on both sides of the Atlantic. More probably, some ocean-scale change affected both species simultaneously. Of the various possible mechanisms, the authors considered the slowing of the Gulf Stream, for which there is indirect evidence (Drinkwater and Myers 1993), was the most likely to affect the life histories of the two species. Prolongation of the time for transit to Europe might mean that the European eels missed the optimum time for metamorphosis. Eels migrating to the northern rivers of North America might be similarly affected, while those migrating to the more southern rivers were able to metamorphose successfully, in spite of the slower currents. In addition, slowing of the Gulf Stream is associated with more frequent formation of warm core rings (Dawe *et al*. 1998), which may cause more larvae to be advected out of the Gulf Stream and into the southward-flowing coastal waters. We shall return to this topic in Chapter 9.

8.3.3 Salmon and the Alaskan gyre

Whereas eels are catadromous fish, meaning that their spawning migrations are away from the source of fresh water, salmon are anadromous, with their breeding

migrations towards the source of fresh water. They breed in the rivers but migrate out to sea to feed and grow. For many years the whereabouts of Pacific salmon, when they went to sea, were very poorly known, but in the decade of the 1960s an effort was made to obtain the missing information (Royce *et al*. 1968). Yet in 1995 Welch *et al*. (1995) could state

> Despite some 40 years of research, the reasons why salmon undertake their vast ocean migrations are still only poorly understood. The reasons are presumably closely related to their evolutionary biology and production dynamics. Some two-thirds or more of the life history of Pacific salmon (*Oncorhynchus*) is normally spent in the pelagic environment of the open Pacific ocean, a behavioural choice that is under evolutionary control.

Later the authors state "The fish fauna of the Subarctic Domain is dominated by Pacific salmon, despite their need to return to fresh water to reproduce."

The genus *Oncorhynchus* comprises 6 species in the North Pacific: pink salmon *O. gorbusha*, chum salmon *O. keta*, sockeye salmon *O. nerka*, coho salmon *O. kisutch*, chinook salmon *O. tshawytscha*, and steelhead salmon *O. mykiss*. Pink salmon are the most abundant, with chum and sockeye vying for second and third place. The other species are much less abundant. The various species have differing distributions in the north Pacific in spring. For example, the temperatures defining the southern boundaries of distribution are 10.4 °C for pink and chum salmon, 9.4 °C for coho salmon and 8.9 °C for sockeye salmon (Bigler *et al*. 1996).

The migration pattern of pink salmon is the shortest and easiest to understand and may be taken as an example. Spawning takes place in the rivers from mid-July to mid-October. Fry hatch and emerge from the gravel in the following spring and immediately migrate down to the estuaries and coastal waters. They migrate out into the ocean proper between July and September at about one year of age. It is estimated that during the next year they travel between 5500 and 7500 km. They do so by swimming actively downstream with the Alaskan gyre (see map, Fig. 8.03). During the summer they move rapidly north and west, traveling parallel with the coast and feeding voraciously. In winter they move about 10° south into the west-wind drift and in the following spring they swim rapidly toward their parent river, to spawn at two years of age. It is estimated that their average rate of travel is about 18.5 km d^{-1}, but they are substantially helped in this endeavor by the Alaskan gyre. During their travels they feed on squid, euphausiids, copepods, and pteropods, grow to breeding size, and mature large gonads (Kaeriyama *et al*. 2000).

Further to the west, the pink salmon stocks originating on the coast of Asia in East Kamchatka are believed to follow the East Kamchatka Current south until they join the eastward-flowing Kuroshio extension and North Pacific Current, with which they travel through the winter. In the following spring they migrate back to their rivers of origin. In both these cases, the fish travel great distances with the help of the prevailing currents.

Sockeye salmon take longer to complete their life history, spending one or two winters in fresh water before running down to the sea. Those from southern British

Columbia are thought to spend two years at sea, during which they make approximately two circuits of the Alaskan gyre. Sockeye salmon from rivers on the shores of the Bering Sea, on the other hand, stay at sea for three years and appear to make two or three circuits of an extended loop that takes in both the Alaskan gyre and the Bering Sea gyre.

Bigler *et al.* (1996) reported that the numbers of salmon in the North Pacific more than doubled between 1975 and 1995. This is not the place to review in detail the fluctuations of the various species and stocks, but hypotheses about the effects of multi-decadal changes in atmospheric and oceanic circulation will be reviewed in Chapter 9.

8.3.4 Transport of invertebrate larvae across ocean basins

Before we leave the question of the biological importance of the major ocean currents, it is interesting to note that Scheltema (1966) obtained the first good evidence for the transatlantic transport of a larva of a benthic invertebrate. A few years before, the eminent marine benthic ecologist Thorson had concluded that very few invertebrate larvae had even the slightest chance to cross the larger ocean basins. The implication was that invertebrate populations in shallow water on the east and west coasts of the Atlantic were genetically quite distinct.

Scheltema (1966) found veliger larvae, probably of the gastropod *Cymatium parthenopeum*, throughout the Gulf Stream and North Atlantic Current. He calculated from drift-bottle experiments that the average rate of transport of water from the Bahamas to the Azores is 0.4 knots (17.8 km d^{-1}), and he succeeded in keeping the larvae alive in the laboratory for a time longer than that necessary for the transatlantic crossing. He pointed out that *C. parthenopeum* is found on the eastern side of the Atlantic from the Azores to South Africa and on the western side from Bermuda to Brazil. There is no need to postulate an introduction by humans: the survival of larvae throughout a transatlantic crossing may not be so very unusual.

8.4 Biology of eddies and rings associated with major currents

As we have seen, the western boundary currents in both northern and southern hemispheres tend to be fast, deep, and relatively narrow, so that a great deal of energy is concentrated in a relatively small cross-section. These currents have a tendency to meander, and in doing so they form eddies and gyres of various kinds. One kind remains attached to the boundary of the current, and is known as a frontal eddy. Another kind breaks off as a distinct ring with an independent existence. For example, the Gulf Stream rings discussed in Section 8.2.3 may persist as distinct entities for many months, and have been prime targets for investigation of their physical and biological properties. Studies have been made

of rings associated with the Gulf Stream in the western North Atlantic, the Kuroshio Current in the western North Pacific, the Agulhas Current off South Africa and the East Australian Current in the western South Pacific.

8.4.1 Gulf Stream frontal eddies

The Gulf Stream (see Figs. 8.03 and 8.08), as it flows in a northerly direction offshore of Miami, Florida, is about 30 km wide and 300 m deep and has a flow in excess of 25 Sv. It flows close to the edge of the continental shelf until it reaches Cape Hatteras, by which time it has doubled its flow and is approximately 50 km wide and about 1000 m deep. Surface velocity is in the range 2–5 knots and the temperature 25–28 °C. It is bounded on the west side by waters of the continental slope and continental shelf that are much cooler than the Gulf Stream, and on the east side by slightly cooler waters of the Sargasso Sea with a temperature range of 20–24 °C. As discussed in Section 6.2.1 there is a strong front on the westward edge, sometimes known as the "cold wall" of the Gulf Stream.

A consequence of the meandering of the Gulf Stream is that its distance from a particular point on the continental shelf is constantly changing. At a time when this distance is greatest, it is common to find a frontal eddy between the Gulf Stream and the coast (Yoder *et al*. 1981). This eddy often takes the form of a finger-like extension of the Gulf Stream protruding into the shelf water and folding back to enclose a core of cold water (Fig. 8.15). This cold core differs from that contained in cold-core rings formed further north (see Section 8.4.4) in being formed

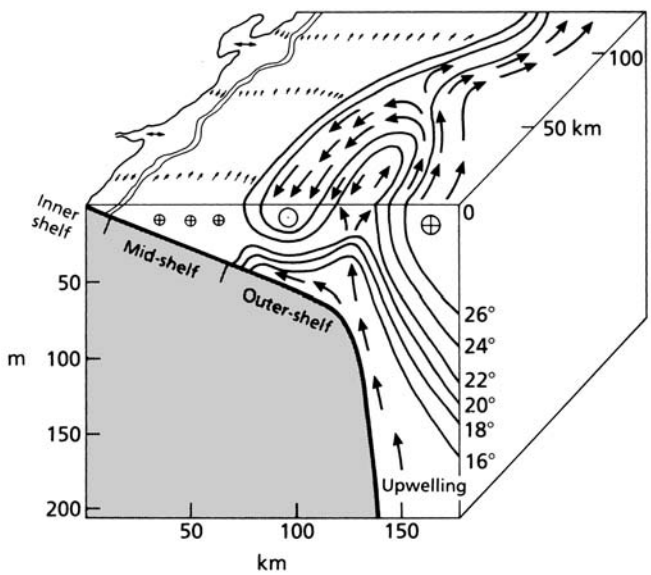

Fig. 8.15 Schematic diagram of a Gulf Stream frontal eddy on the Georgia shelf. Reproduced with permission from Lee *et al*. (1981).

by upwelling of North Atlantic central water from deep in the Gulf Stream. A simplified explanation is that wherever the Gulf Stream in its meandering moves away from the coast, water from deep in the Gulf Stream upwells in the space created. Formation of these structures is a common event south of Cape Hatteras, a new one being formed on average once every two weeks. The upwelled water is rich in nitrate and Lee *et al*. (1981) estimated that this mechanism introduced about 55,000 tons of nitrogen annually to the outer shelf.

In April 1979 a vigorous diatom bloom covering an area of more than 1000 km^2 occupied the cold core of upwelled water, in the region of the 200 m isobath. Primary productivity throughout the year in this region averaged about 2 g C m^{-2} d^{-1} (Yoder *et al*. 1981, 1983). Strong southwesterly winds were found to cause Ekman offshore transport that favored both the formation of an offshore meander of the Gulf Stream and the inshore movement of upwelled water at intermediate depths, to compensate for the offshore transport of the surface layer (Atkinson *et al*. 1984). It is now thought that this upwelling caused by the meandering offshore of the Gulf Stream is the primary mechanism for providing nutrients and stimulating production on the outer continental shelf of the southeastern United States south of Cape Hatteras. Such enrichment may explain why the shelf break south of Cape Hatteras is a breeding center for Atlantic menhaden *Brevoortia tyrannus* and for bluefish *Pomatomus saltatrix* (Atkinson and Targett 1983). Haney (1986) found that the shearwaters *Puffinus gravis* and *Calonectris diomedea* and the storm-petrels *Oceanites oceanicus* and *Oceanodroma castro* were most abundant in the upwelled cold core of frontal eddies, while the black-capped petrel *Pterodroma hasitata* and the bridled tern *Sterna anaethetus* were most abundant in the oligotrophic warm filament inshore of the cold core. North of Cape Hatteras the Gulf Stream moves away from the coast and instead of cold-core frontal eddies we find warm-core ring formation on the shoreward side of the current (see Section 8.4.2).

Tranter *et al*. (1986) showed that slope-water intrusions occurred near Sydney, Australia, and that they seemed to occur when eddies or meanders of the East Australian Current came within 90 km of the shelf break. They made comparisons with the upwelling events associated with the western boundary of the Gulf Stream, but pointed out that the mechanism producing the intrusions must be different, because the continental shelf of that part of Australia is much narrower and does not permit the formation of cold-core frontal eddies of the type found off Florida and Georgia.

8.4.2 Formation of Gulf Stream rings

North of Cape Hatteras the Gulf Stream leaves the edge of the continental shelf and begins to flow in a more or less easterly direction. Every month or two a meander cuts off distinct rings, as in Fig. 8.16. As we saw in Section 8.2.3, cold-core rings form on the south side of the Gulf Stream, and warm-core rings on the north. Once free of the Gulf Stream they tend to move in a southwesterly direction, more or less parallel with the Gulf Stream, at a speed of about 3–5 km d^{-1}.

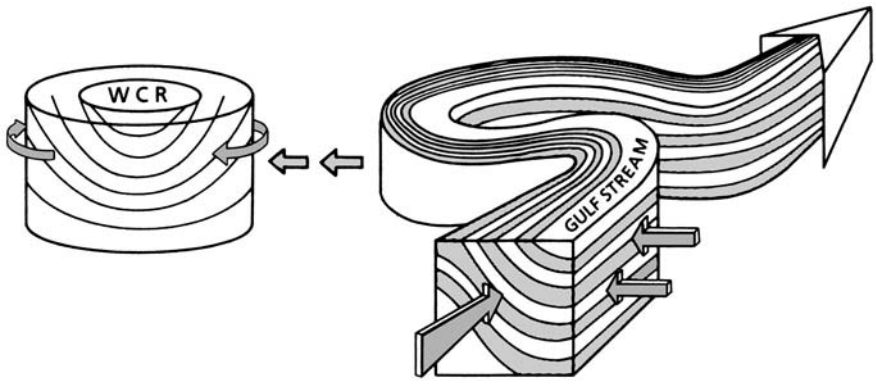

Fig. 8.16 Diagram showing how the Gulf Stream, with its isopycnals sloping upward to the left, gives rise to a warm-core ring with its isopycnals sloping upward toward the perimeter. Arrows show flow of the Gulf Stream, isopycnal flow, and rotation of the warm-core ring. After Yentsch and Phinney (1985).

Eventually, most make contact with the Gulf Stream and are reabsorbed into it, although some lose their identity by diffusion into the surrounding water.

8.4.3 Ecology of cold-core rings

From first principles it would seem that cold-core rings have an interesting potential to stimulate biological production. The water of the core is derived from the slope of the continental shelf and typically has a much larger concentration of plankton, nekton, and nutrients than the Sargasso Sea, into which it is propelled. Their counter-clockwise rotation leads to upwelling in the center. A cross-section of a ring soon after formation (Fig. 8.17) shows bell-shaped isotherms, with 10–16 °C isotherms located about 600 m higher in the water column than their normal Sargasso Sea depth (Ring Group 1981). One important effect is to bring nutrient-enriched water into the euphotic zone.

In a detailed study of ring Bob in 1977, the biological characteristics of the ring changed more rapidly than the physical characteristics. In April the surface concentration of chlorophyll at the center was about 4 mg m^{-3} compared with less than 0.l mg m^{-3} in the Sargasso Sea water, but the concentration declined by a factor of eight between April and August. As the sun heated the surface waters there was a shift to smaller species and greater species diversity, so that the phytoplankton community came to resemble more closely that of the Sargasso Sea. By August the chlorophyll maximum had moved from the upper 20 m to a mean depth of 80 m and its concentration was less than 0.6 mg m^{-3}. Overall, it was estimated that primary production of cold-core rings was about 50% higher than that in the Sargasso Sea and that these rings occupy about 10% of the area of the Sargasso Sea at any one time.

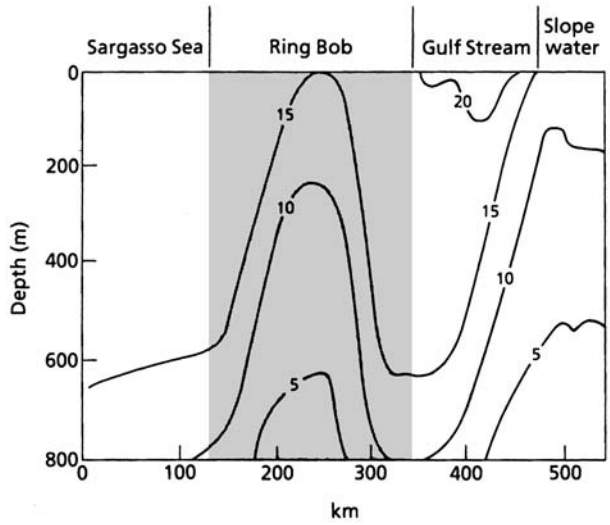

Fig. 8.17 Diagram of a vertical section through cold-core ring Bob to show the elevation of the 5, 10, and 15 °C isotherms. After the Ring Group (1981).

In the ring, zooplankton biomass was typically 1.3 to 1.8 times higher than in the surrounding Sargasso Sea. As might be expected, the species composition (at least in young rings) was characteristic of slope waters. The pteropod *Limacina inflata* and various myctophid fishes became more abundant as the cold-core ring aged. Zooplankters that are carried from the cool water of the slope to the Sargasso Sea in cold-core rings often do not thrive. In a 17-month-old ring, none could be found. Backus and Craddock (1982) studied mesopelagic fishes along a transect from slope water, through a cold-core ring, and into Sargasso Sea water. They found that the slope-water species tended to become more scarce as the ring aged, while several Sargasso Sea species invaded the ring from the top as the water warmed.

In general it seems that cold-core rings have the effect of temporarily boosting the primary production of the Sargasso Sea, to the advantage of a number of Sargasso Sea species that invade the ring from above. Species introduced from the slope water thrive for only a limited period.

8.4.4 Ecology of warm-core rings

The internal structure of a warm-core ring (Fig. 8.18) is in many respects the opposite of that of a cold-core ring. Clockwise circulation causes downwelling at the center, so isotherms and nutriclines are depressed. Yentsch and Phinney (1985) discussed this structure in an interesting way (Fig. 8.16), pointing out that the outer part of the ring, the high-velocity region, is formed from the "cold wall" of the Gulf Stream, which has the usual frontal structure of sloping isopycnals

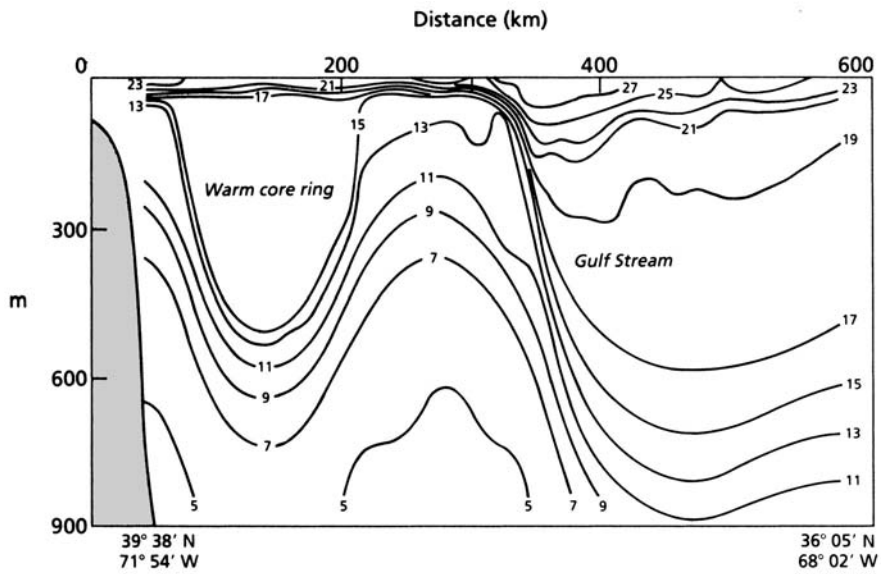

Fig. 8.18 Cross-section of a warm-core ring lying between the Gulf Stream and the continental slope, showing isotherms (°C). After Csanady (1979).

(see Chapter 6). It is to be expected that there will be transport of water along lines of equal density (isopycnal mixing; Woods 1977) and that this process will lead to the upwelling of nutrients in the high-velocity peripheral region.

By analogy with what is known about cold-core rings, it might be supposed that warm-core rings, which have at their center nutrient-depleted Sargasso Sea water, would at first be biologically unproductive and would slowly evolve to take on the character of slope water in which they are immersed. In fact, over the lifespan of a warm-core ring, from its formation from Gulf Stream meander to its eventual rejoining with the Gulf Stream further south and west many months later, its primary productivity seems to be not very different from that of the slope water surrounding it (Hitchcock *et al*. 1985; Chapman and Nof 1988). Productivity is enhanced by two mechanisms. One is the upwelling at the periphery. The other is convective mixing caused by the cooling of surface water as the ring moves north of the Gulf Stream. The deep mixed layer, having discrete boundaries and uniform temperature, is called a thermostad. In it, nutrient-rich water is brought to the surface, generating a burst of primary production. Since the water in the core of a ring has a different temperature regime than the shelf waters, there are times when a warm-core ring is undergoing its "spring bloom" while the surrounding shelf waters are not. However, it is believed that all these complex interactions cause the ring to have a lifetime productivity not very different from the surrounding shelf water.

Studies of the biology of warm-core rings derived from the Kuroshio Current off Japan have tended to give similar results. For example, Waku and Furuya (1998)

found that the primary productivity within a warm-core ring was almost the same as in the cold streamer outside it, with evidence of upwelling of nutrients within the ring. Chiang and Taniguchi (2000) found dense populations of phytoplankton at the nutricline within a ring, presumably supported by upward mixing of nutrients.

(a) Mesozooplankton, fish, and mammals in warm-core rings

Many zooplankton species are advected into warm-core rings from the surrounding slope water (Roman *et al*. 1985), and physical oceanographic studies using salinity as a conservative property confirm that significant lateral exchange of water masses occurs (Olson 1986). In general, a newly formed ring is found to have a low mesozooplankton biomass in the core, consistent with its origin from the Sargasso Sea, but within a few months there is often a biomass as high as or higher than in the slope water.

In contrast to all these changes, mesopelagic fish and siphonophores that characteristically form a nonmigratory acoustic deep scattering layer in the Sargasso Sea were found to be captured in the thermostad of a warm-core ring and could be traced acoustically throughout the life of that ring (Conte *et al*. 1986). There was no evidence of a significant change in abundance and their vertical distribution remained approximately constant for several months in spite of changes in temperature and salinity. On the other hand, acoustic studies in a warm-core ring of the Kuroshio system showed intense sound scattering from zooplankton and fish populations within the ring and very sparse acoustic signals outside it (Aoki and Inagaki 1992).

There have been reports that the eastern boundaries of Gulf Stream warm-core rings are a preferred habitat for sperm whales (Griffin 1999). The whales eat squid and the author proposed that the slope water entrained on the south and east sides of the ring, together with localized upwelling conditions, provides a rich feeding habitat for squid, and hence for the whales.

(b) Interaction of warm-core rings with the continental shelf

Satellite imagery shows that it is not uncommon for warm-core rings to make contact with the continental shelf and for large volumes of cold water to be entrained on their northern side and dragged off the shelf by the rotational movement. Ryan *et al*. (2001) showed for the Georges Bank region that the offshore movement of the shelf water, caused by a Gulf Stream ring, was accompanied by vigorous upwelling and turbulent vertical mixing, which in turn led to enhancement of phytoplankton productivity.

It also seems likely that on the western or southern side of the rings considerable quantities of warm water are injected onto the shelf. It was natural, therefore, that when Markle *et al*. (1980) discovered fish larvae of tropical and subtropical origin on the Scotian Shelf they should attribute their presence to the action of warm-core rings. Similar observations have been made off southern New England.

Friedlander and Smith (1983) identified water advected offshore by a warm-core ring. Contained within the ring were abundant sand lance larvae *Ammodytes* sp. that had been carried off the shelf along with the copepods that form their food. The idea then developed that a strong advection of a shelf-water mass at a time when the larvae of commercially important species of fish are present could have harmful effects on the year-class strength of those species.

Wroblewski and Cheney (1984) explored a warm-core ring off the coast of Nova Scotia and found that larval and juvenile white hake *Urophycis tenuis* were being carried as much as 140 km seaward of the shelf break. They were in much poorer condition than the same species on the continental shelf and the authors thought that they represented a loss from their source populations. The ring being studied also contained many fish larvae of tropical and subtropical origin belonging to the same species reported as immigrants to the Scotian Shelf by Markle *et al*. (1980).

A modeling study (Flierl and Wroblewski 1985) showed that at a time when commercially important fish larvae are being carried by the residual current southwest along the Scotian Shelf, the advection caused by a stationary warm-core ring could cause a 35–50% drop in abundance, depending on the ring size, and a slowly moving ring could, in certain circumstances, remove most of a year-class. Myers and Drinkwater (1989) related remotely sensed data on the presence of warm-core rings on the Scotian Shelf to data on the abundance of larvae from 17 groundfish stocks between 1973 and 1986. For 15 of those stocks, increased warm-core activity was associated with reduced recruitment. A similar analysis for pelagic stocks showed no such relationship.

In the southern hemisphere, a study of an Agulhas Current warm-core ring surrounded by sub-Antarctic water (Dower and Lucas 1993) showed that chlorophyll concentration and primary productivity were lower within the ring than outside it, and a higher proportion of the phytoplankton inside the ring was less than 20 μm in diameter. This finding is similar to the characteristics of a Gulf Stream warm-core ring soon after it has been formed.

Poor year-classes of anchovy *Engraulis capensis* were produced in the Benguela system in 1989 and 1990. By analysis of seabird stomachs it was shown that the most marked decrease in anchovy biomass occurred in June–July 1989. It was postulated that removal of larvae and young anchovy from the shelf by an Agulhas ring was a major factor in the depression of the 1989 year-class (Duncombe Rae *et al*. 1990).

To summarize to this point: cold-core rings are responsible for introducing slope-water species into the central gyres, and warm-core rings introduce tropical and subtropical species not only into slope waters but even onto the continental shelf. Cold-core rings, when newly formed, have a productivity much higher than the central gyres, but as their surface layer warms and their cold-water fauna are driven deeper and deeper, their productivity falls to something close to the productivity of the surrounding gyre. Warm-core rings begin life with a core of low-productivity water, but they also have mechanisms for generating upwelling of nutrient-rich water, especially near the perimeter in the high-velocity zone.

Stratification as a result of spring warming often leads to levels of primary production in the rings greater than that in the surrounding slope water and to subsequent rapid growth of zooplankton populations. Over the life of a warm-core ring its productivity appears to be about the same as that of the slope water.

When a warm-core ring comes in contact with the continental shelf, cold water is advected off the shelf in large amounts, and at times when planktonic fish larvae are present in the water this movement leads to reduced larval survival and subsequently to reduced recruitment in the parent stock. On the other side of the ring, warm water is often injected onto the shelf and is the means of introducing adults and larvae of tropical and subtropical origin into temperate shelf waters.

8.5 Ecology of the central gyres

In Section 8.3 we discussed the major currents associated with the periphery of the huge subtropical gyres. We shall now look at the relatively quiet waters that occupy the central gyral regions. The older view that they are very unproductive "biological deserts" has been changed by a combination of satellite data with long time series of observations at fixed stations, and repeated transects of whole basins.

8.5.1 Primary production in the subtropical gyres

Blackburn (1981) reviewed the evidence indicating that subtropical gyres are the least productive parts of the ocean. Primary production, measured by ^{14}C uptake, was believed to be less than 0.1 g C m^{-2} d^{-1}, with the result that biomass of both phytoplankton and zooplankton is low, the water is very clear with the euphotic zone extending to 75–150 m in depth, and nitrate levels at the surface are in the range of 0–1 μmol L^{-1}. This low productivity was thought to extend to the zooplankton and the fish in the water column. Consideration of these facts led to the description of the subtropical gyres as "biological deserts." However, in 1982, Fitzwater *et al*. produced evidence that primary productivity measurements could be adversely affected by trace-metal contaminants such as iron and other metals in the sampling gear and experimental equipment. The finding was amply confirmed and we should doubt the validity of measurements made before 1982. In what follows we shall see that current estimates of productivity for the gyres are higher than previously thought because higher figures result from improved techniques, including the use of trace-metal-clean techniques, because long time series at fixed stations permit measurements on transient mesoscale events, and because satellite data enable us to assess the frequency and intensity of mesoscale events.

The view of the major gyres as being in a relatively steady state with a low level of primary production and low *f* ratio was first seriously challenged by a

number of different measurements summarized in Eppley (1980). Use of a particle counter to measure changes in particle volume suggested that phytoplankton in oligotrophic subtropical gyres were reproducing at a rate that would lead to an estimated production rate an order of magnitude greater than previous estimates. Measurements by means of particle traps of the rate of sinking of particles out of the euphotic zone were interpreted as reflecting the rate of new production, since in steady state the amount sinking out must be balanced by new production, rather than by production that is being recycled. In the studies reviewed, the traps had collected an average of 68 mg C m^{-2} d^{-1}. If the *f* ratio (see Section 3.2.4) is 0.05, then total production is 1.360 g C m^{-2} d^{-1}, and if $f = 0.10$, total production is 0.680 g C m^{-2} d^{-1}. Comparing these figures with the previously accepted value of <0.1 g C m^{-2} d^{-1}, Eppley (1980) concluded that there is an order-of-magnitude uncertainty about the level of primary production in the large ocean gyres.

Shulenberger and Reid (1981) used a much larger-scale approach than anyone preceding them. They pointed out that, in the open mid-latitude Pacific in summer, a subsurface oxygen maximum is found in which there are values up to 120% of saturation. This maximum lies below or within the pycnocline, and certainly below the warm mixed layer, which they refer to as a density cap. It is usually located above the chlorophyll maximum but below the primary-production maximum (see Fig. 3.01). Values in excess of 100% saturation are found throughout the North Pacific and the area of greatest values is centered on 40° N 160° W.

The authors argued that this oxygen supersaturation accumulates in summer as a result of photosynthesis, and is prevented from equilibrating with the atmosphere by the density cap. Equilibration occurs in winter when the mixed layer deepens and the supersaturated water is circulated in the mixed layer. Allowing 120 days for the build-up of the summer oxygen excess, they calculated that, at a minimum, the rate of photosynthesis must be greater than the rate indicated by ^{14}C incubations by a factor of about four.

After a lively debate about the validity of Shulenberger and Reid's conclusions, Platt *et al*. (1989) conceded that the evidence from oxygen accumulation, sediment trap studies, and direct determinations of the rate of nitrate uptake by phytoplankton in oligotrophic waters shows that the value of new production (see Section 3.2.4) in these waters is much higher than previously believed. This conclusion is very important in relation to the problem of CO_2 accumulation in the atmosphere and the role of the oceans in helping to counteract it. In the long term, organic carbon sinking out of the mixed layer must be balanced by new production, which involves removal of CO_2 from the atmosphere. (This topic will be discussed more fully in Chapter 9.) The explanation of the higher values of new production lies almost certainly in the occurrence of intermittent episodes of upwelling of nutrients and lateral advection of nutrient-rich water. We have to abandon the view that the central gyres are uniform and quiescent and think of them as filled with eddies of varying energy levels (Kerr 1985). Cyclonic eddies will raise the pycnocline and are capable of bringing about upwelling of nutrients.

(a) Data from the Pacific Ocean

Reconciliation of conflicting estimates of productivity of the subtropical gyres has been assisted greatly by the initiation of long-term time series off Hawaii (Hawaii Ocean Time-series, HOT; hahana.soest.hawaii.edu/hot/hot_jgofs.html) and by its Atlantic equivalent, the Bermuda Atlantic Time-series Study (BATS; www.bbsr.edu/cintoo/bats/bats.html – if a URL changes, search the web for Hawaii Ocean Time-series or Bermuda Atlantic Time-series).

Every winter, extratropical cyclones track across the North Pacific from west to east approximately every 5–7 days (Karl and Lukas 1996). A good record of a strong mesoscale event at the HOT station was given by Letelier *et al*. (2000). A combination of a strong wind divergence and the passage of a cyclonic eddy displaced the thermocline upwards by 120 m. Surface chlorophyll-*a* concentrations increased threefold, diatom abundance increased twofold, and there was a change in the light-harvesting efficiency. The authors suggested a strong effort to integrate remotely sensed data with moored and vessel-based time-series records to reach an assessment of the importance of various mechanisms for injecting additional nutrients into the mixed layer. The long-term mean for primary productivity at the station off Hawaii is about 169 g C m^{-2} y^{-1} (Karl *et al*. 1996, Roman *et al*. 2002). This figure is much greater than estimated for the North Pacific gyre prior to 1984, but conforms to data obtained since the advent of trace-metal-clean techniques.

In the South Pacific, it is possible that almost the whole of the South Pacific gyre is under iron limitation. Behrenfeld and Kolber (1999) made frequent measurements of the fluorescence response of the phytoplankton (mostly *Prochlorococcus and Synechococcus*) on a 7000 km transect of the South Pacific Ocean and an even longer transect in the Atlantic Ocean. They discovered diel patterns of fluorescence that were different in the two oceans, and showed experimentally that the features characteristic of the South Pacific phytoplankton were manifestations of iron limitation. Those special features were rapidly lost after *in situ* iron enrichment. They strongly suggested that primary productivity is iron-limited not only throughout the equatorial Pacific (Section 3.2.7) but over much of the vast South Pacific gyre. As was mentioned in Chapter 3, it is probably more accurate to refer to the phenomenon as iron–light co-limitation, as in the model of Flynn and Hipkin (1999).

Cullen and Davis (2003) pointed out that the use of inappropriate blanks (such as deionized water rather than filtered sea water) in the type of fluorescence analysis used by Behrenfeld and Kolber (1999) can lead to wrong interpretation of the results. Behrenfeld and Kolber did not report on their blanks.

(b) Data from the Atlantic Ocean

An overview of the Bermuda BATS data (Michaels and Knap 1996) indicated an average primary production of 161 g C m^{-2} y^{-1}, with a considerable amount of

year-to-year variability. An important cause of the variability was believed to be the variability of depth and duration of winter mixing. After a winter with particularly deep mixing, the concentration of surface nutrients was particularly high, and lasted a long time into the bloom period.

Others factors contributing to interannual variability are mesoscale eddies (both vertical and horizontal components) and Ekman advection from the margins of the gyres. McNeil *et al*. (1999) reported a detailed analysis of a mesoscale eddy that passed across the Bermuda Testbed Mooring site over a 30-day period and demonstrated a significant injection of nutrients into the mixed layer. Many such mesoscale eddies, of the order of 100–300 km in diameter, have been remotely observed. McGillicuddy *et al*. (1998) suggested that, along with some seasonal upwelling generated by winter convective mixing, the vertical flux of nutrients induced by the dynamics of mesoscale eddies is sufficient to balance the nutrient budget of the Sargasso Sea. Using combinations of satellite data and interpretation of shipborne observations of vertical profiles, Sathyendranath *et al*. (1995) suggested that total primary production ranges from a minimum of 60 g C m^{-2} yr^{-1} in the center of the gyre to about 180 g C m^{-2} yr^{-1} at the margins.

Campbell and Aarup (1992) constructed a nitrogen budget for the North Atlantic gyre by assessing the rate of utilization of nitrogen from surface waters and its replacement by seasonal nitracline deepening. Combining this information with satellite data, they calculated that new production is about 18 g C m^{-2} yr^{-1} in the center of the gyre and 24 g C m^{-2} yr^{-1} near the margins. In a comparative study of the Sargasso Sea and various other areas of the world ocean, Platt *et al*. (2003a) modeled the mixed layer in terms of nitrogen input and nitrogen loss. Nitrogen input was determined primarily by episodic deepening of the mixed layer, so that the extent and frequency of mixed-layer deepening determined the rate of supply. The nitrogen supplied was used to drive a photosynthesis model and to calculate the resulting biomass change. Nitrogen loss from the mixed layer was determined by that fraction of the biomass lost by downward export on a daily basis. In the case of the Sargasso Sea, the results indicated an excess of nitrogen loss over input in both spring and summer. In spring, the observed high phytoplankton biomass was reached temporarily as a result of utilizing nitrogen accumulated in the mixed layer during winter. In summer, the data on mixed-layer deepening did not provide enough input of nitrogen to produce the observed phytoplankton biomass. Others have argued that lateral Ekman transport of nitrogen into the North Atlantic gyre from its margins is responsible for enhanced primary production up to 1000 km from the perimeter of the gyre. Williams and Follows (1998) postulated that a westerly wind stress along the southern edge of the subpolar gyre and the northern boundary of the Atlantic subtropical gyre generates equatorward Ekman flow from the nutrient-rich waters of the subpolar gyre (Fig. 8.19). From climatological data they estimated this flux as 0.8–1.7 g N m^{-2} y^{-1}. They suggested that this nitrogen will be distributed towards the center of the gyre by the geostrophic flow, and be responsible for stimulating up to 17% of the total North Atlantic uptake of carbon dioxide. One wonders whether a similar mechanism exists in the Pacific Ocean.

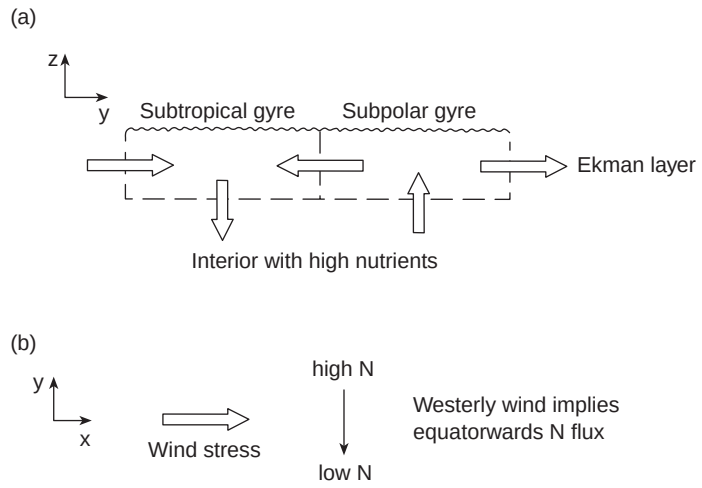

Fig. 8.19 (a) Schematic meridional section showing Ekman transfers through subtropical and subpolar gyres. The wind forcing leads to horizontal divergence over the subpolar gyre, inducing upwelling, and leads to convergence over the subtropical gyre, inducing downwelling. (b) An eastward wind-stress drives an equatorward surface Ekman layer, which leads to high nutrients in the subpolar gyre being swept into the subtropical gyre. Adapted from Williams and Follows (1998).

It is also possible that mesoscale eddies adjacent to the periphery of the North Atlantic subtropical gyre effect horizontal transport of nutrients in to the gyre. Oschlies and Garcon (1998) published a nitrogen-based four-compartment biological model (nitrate, phytoplankton, zooplankton, detritus) coupled with an eddy-resolving circulation model of the North Atlantic into which had been assimilated remotely sensed sea-surface-height data. The results indicated that about one-third of the total flux of nitrate into the euphotic zone in the subtropics and mid-latitudes could be attributed to mesoscale eddies. A close look at the distribution of primary production in various runs of the model showed that enhancement of primary production occurred mainly adjacent to the margins of the subtropical gyre. Garcon *et al*. (2001) suggested that the eddies would be capable of transporting nutrients (both in dissolved and particulate form) horizontally across the mean flow of the currents bounding the gyre, thereby enhancing gyre productivity.

Rossby waves (Section 8.2.4) may also cause changes in productivity in the open ocean. Cipollini *et al*. (2001) observed Rossby waves in ocean color data and suggested two mechanisms to link the waves with productivity. The ~50 m variation in the depth of the thermocline across the wave may alter the supply of nutrients in the euphotic zone. They also suggested that the wave in the thermocline might change the number of phytoplankton cells recorded by the satellite's sensor without changing the total biomass. At about the same time Uz *et al*. (2001), by comparing remotely sensed chlorophyll and sea-surface-height data,

demonstrated that the waves are responsible for 5–20% of the observed variability in the chlorophyll concentration. They suggested that the result is due to variations in productivity due to a Rossby-wave-induced increase followed by a decrease of nutrients in the euphotic zone – in agreement with the first suggestion of Cipollini *et al*. (2001). Another observation of enhanced chlorophyll associated with Rossby waves has been found by Kawamiya and Oschlies (2001) in the Indian Ocean. They believe the signal is due to thermocline depth variations caused by Rossby waves. As the thermocline moves up the deep chlorophyll maximum is brought into contact with the mixed layer, where some of the chlorophyll from the deep layer is mixed into the upper mixed layer. Killworth *et al*. (2004) compared relationships between sea surface height and ocean color to the relationships that were predicted from three possible mechanisms linked to Rossby waves. Their first mechanism, and the one able to account for most of the observed waves in the ocean color, depends on the Rossby wave's north–south currents acting on a north–south chlorophyll gradient in the ocean's surface layer. Westward-propagating anomalies in the chlorophyll distribution are created by bringing water containing more or less chlorophyll than normal to a given latitude. The less successful mechanisms the authors tested depend on the vertical upwelling of nitrate (converted to chlorophyll in the euphotic zone) and the vertical upwelling of chlorophyll itself. The authors suggest that since none of the mechanisms is fully satisfactory in all locations the vertical mechanisms may be responsible for part of the signal in select locations.

Meanwhile, Dandonneau *et al*. (2003) found that in the South Pacific subtropical gyre the Rossby waves were producing alternating divergences and convergences. The chlorophyll maxima were not in the cool water of the divergences, where new nutrients might be brought to the photic layer, but in the convergences, in abnormally warm water. They therefore proposed that the signals interpreted as chlorophyll maxima by the satellite sensors were really aggregates of floating detritus (comparable with the aggregations of floating detritus associated with some forms of fronts). They summarized their position by saying that the Rossby waves are not acting as "rototillers," lifting nutrients to the surface layer as they propagate, but as marine "hay rakes," producing aggregations of detritus that might well provide favorable habitats for a variety of marine organisms.

A larger-scale view of the functioning of the major gyres has been made possible by the initiative to make Atlantic Meridional Transects from 50° N to 50° S, during twice-yearly passages of a research vessel between the UK and the Falkland Islands (Aiken and Bale 2000). Use of the latest instrumentation (such as fast repetition rate fluorometers, optical plankton counters, and acoustic Doppler current profilers applied to the measurement of zooplankton), often mounted on towed undulating oceanographic recorders, has generated much new information. Maranon and Holligan (1999) showed that, as expected, the transition from temperate to subtropical waters is marked by: (i) a sharp drop in total chlorophyll; (ii) a change from predominance of eukaryotic to predominance of prokaryotic pigments, and (iii) a change from absence to presence of divinyl chlorophyll-*a* associated with the prokaryotes. Surprisingly, the variation in

physiological parameters of phytoplankton was as great as the variation in chlorophyll concentration. In two successive crossings of the subtropical gyres, phytoplankton biomass remained constant but the rate of photosynthesis per unit of chlorophyll varied by a factor of three. The authors suggested that the changes were the result of changes in the availability of nutrients from below the thermocline. This finding is a caution against assuming that changes in primary productivity are proportional to changes in chlorophyll-*a* concentration. Knowledge of the physical factors causing vertical transport of nutrient-rich waters is at least as important as remotely sensed data on chlorophyll distribution.

Reporting on 94 vertical profiles of size-fractionated chlorophyll-*a* concentration and primary production rates on Atlantic Meridional Transects, Maranon *et al*. (2001) showed that in oligotrophic regions the total chlorophyll-*a* tended to remain within a relatively narrow range (15–30 mg m^{-2}) but total productivity ranged from 2 to 60 mg C m^{-2} h^{-1}. Moreover, the high productivity areas, including the equatorial divergences, had the same community size structure as the less productive areas, with a predominance of picoplankton. It seems likely that the change in productivity results from physiological changes in the cells stimulated by upward flux of nutrients. This makes it difficult to monitor productivity changes using remotely sensed surface chlorophyll.

The combination of improved measurement techniques, long time series, and a better understanding of the role of winter mixing, Ekman transport of nutrients, mesoscale eddies, and planetary waves has led to a view that the major subtropical gyres are much more productive than once thought. There is also a possibility that inter-decadal changes in ocean circulation have caused productivity to increase over the years (see Chapter 9).

8.5.2 Secondary production in the subtropical gyres

(a) Zooplankton

It is now fairly clear that the largest component of the zooplankton in oligotrophic waters is the microzooplankton that feeds on the very small phytoplankton such as *Prochlorococcus* and *Synechococcus*. When winter mixing or a passing eddy brings fresh nitrate into surface waters, larger cells such as diatoms become more abundant, and after a time mesozooplankton such as copepods also multiply. Shipboard estimates of copepod grazing rates, by means of gut contents and gut evacuation rates, revealed that copepods in the subtropical gyres are responsible for removing less than 3% of the total chlorophyll standing stock and less than 10% of total primary production daily (Huskin *et al*. 2001).

As is well known, copepods are important in the diet of fish. They also play a key role in downward export of biomass. Microzooplankton sink slowly, if at all, and are often mineralized in the mixed layer, but diatoms, mesozooplankton, and zooplankton feces contribute to the downward flux of biomass and the sequestration of carbon. Roman *et al*. (2002) estimated mesozooplankton production rates for the Hawaiian (HOT) and Bermuda (BATS) ocean time-series stations, using

the empirical model of Hirst and Lampitt (1998). This model predicts copepod growth rate from temperature and body size, and is of necessity only a first approximation, since no account is taken of variability of food quality and quantity. The average mesozooplankton biomass at HOT (286 g C m^{-2} y^{-1}) was more than twice that at BATS, even though the annual primary production at the two stations is similar (see Section 8.5.1). The difference is possibly attributable to the more episodic nature of nutrient input at BATS, resulting in mismatches between increases in phytoplankton production and the grazing response by the mesozooplankton. Also, the Bermuda station has periodic blooms of large gelatinous salps, which may compete with the mesozooplankton for food. Estimated mesozooplankton production at HOT (9.48 g C m^{-2} y^{-1}) was also more than twice that at BATS (3.96 g C m^{-2} y^{-1}) and was due to both the higher biomass and the higher estimated growth rates.

The data from the Atlantic Meridional Transect program have changed many of the earlier views about the distribution and role of zooplankton in the subtropical gyres. When near-surface zooplankton were monitored continuously by pumping water through an optical plankton counter, the diurnal pattern of migration caused fluctuations up to two orders of magnitude in the biovolume. Figure 8.20, from Gallienne and Robins (1998), shows the biovolume in May on the meridional transect, plotted on a logarithmic scale and on a linear scale. As expected, the biovolumes in the South Atlantic subtropical gyre and in the Canary Basin of the North Atlantic subtropical gyre were much lower than in the temperate waters to the north and the south. The biomass in the equatorial current systems, between the gyres, was greater than in the South Atlantic subtropical gyre, but about the same as in the Canary basin.

(b) Fish

The structure and dynamics of the fish communities in subtropical gyres were reviewed by Mann (1984). In the euphotic zone (0–100 m) are found fast-swimming predators such as the tunas, bill-fish, and swordfish. Most of them breed in tropical waters but make major excursions into the subtropical gyres. For example, bluefin tuna *Thunnus thynnus* breed in the Caribbean area, and medium-size fish migrate north in summer as far as the latitude of Cape Cod, but large, older fish may migrate as far as Newfoundland or cross the Atlantic and spend the summer in Norwegian waters. These large predators feed on a variety of smaller fishes, on squid, and on larger crustaceans such as euphausiids.

The zone from 200 m to a depth of 1000 m is termed the "mesopelagic zone." From acoustic studies we know that there is a "deep scattering layer" caused by small fish (mostly <10 cm) and larger invertebrates. Many of these animals migrate to the euphotic zone to feed at night. This layer is more or less continuous all the way across the major ocean basins.

Finally, below 1000 m is the bathypelagic zone occupied by fishes with dark coloring, small eyes, weak musculature, and large mouths. Some, like the anglerfishes, have elaborate lures to attract prey. They appear to be adapted

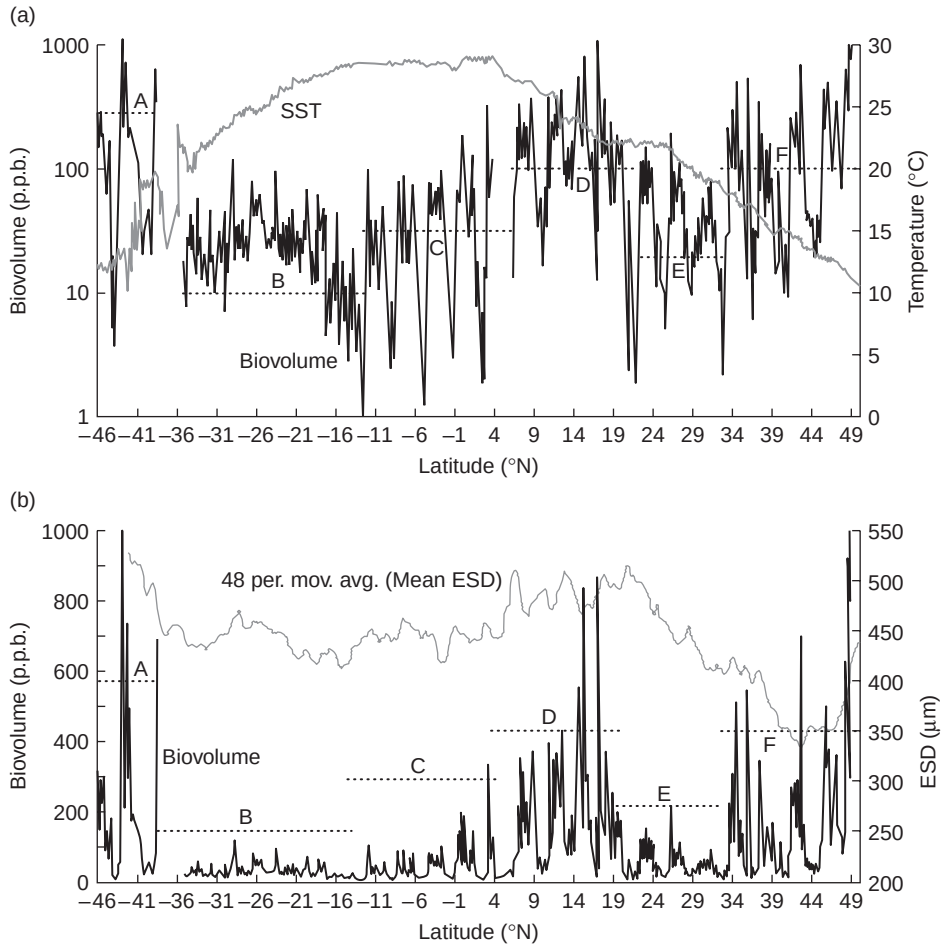

Fig. 8.20 Total biovolume estimated by optical plankton counter (OPC), along an Atlantic Meridional Transect (from 50° N to 50° S, during twice-yearly passages of a research vessel between the UK and the Falkland Islands) plotted (a) on a logarithmic scale along with sea surface temperature (SST), and (b) on a linear scale together with mean equivalent spherical diameter (ESD) of the particles. A, in Falklands current; B, in oligotrophic South Atlantic subtropical gyre; C, in Equatorial Current; D, in West African upwelling; E in oligotrophic Canary Basin; F, in temperate northeast Atlantic. From Gallienne and Robins (1998). Reproduced by permission of Blackwell Publishing Ltd.

to life in a food-poor environment, expending little energy on swimming but taking a large meal whenever something comes within range. Figure 8.21 summarizes the biomass and production data (in kcal m^{-2} and kcal m^{-2} y^{-1}, respectively) for the different depth zones of a subtropical gyre. Using the approximate conversion 1.0 g wet weight = 1.0 kcal, we see that the greatest values are in the mesopelagic fishes. The top carnivores, which are the main commercially

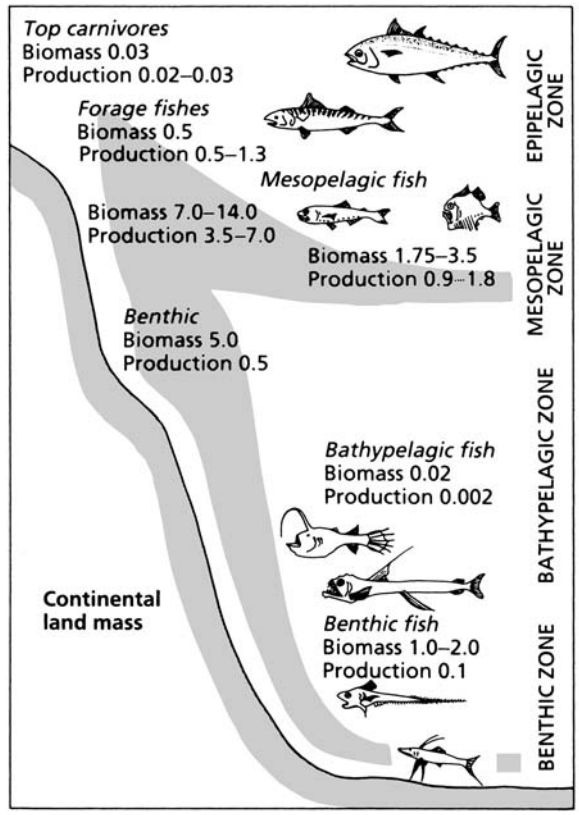

Fig. 8.21 Diagram summarizing mean values of fish biomass (kcal m^{-2}) and production (kcal m^{-2} y^{-1}) in the open ocean. Shading symbolizes decreasing biomass as one moves from the shelf break toward the center of the gyre. From Mann (1984).

important fishes, produce on average only 0.02–0.03 g m^{-2} of new tissue per annum. In turn, the smaller fishes on which they feed are thought to produce 0.5–1.3 g m^{-2} y^{-1}. This growth may be compared with 5–10 g m^{-2} in many continental-shelf areas and 10–20 g m^{-2} in particularly favorable areas such as Georges Bank.

8.6 Subarctic gyres

North of the main anticyclonic subtropical gyres in both the Atlantic and Pacific are smaller, cyclonic subarctic gyres (Fig. 8.03). Parsons and Lalli (1988) analyzed data from ocean weather stations *P* (in the Pacific) and *B*, *I*, and *J* (in the Atlantic) (see Fig. 8.03), together with data from the Continuous Plankton Recorder program (Colebrook 1979) (see Chapter 9), to synthesize a comparative view of plankton ecology in northern parts of the two major ocean basins. This analysis was made before the discovery of iron limitation in this and other parts of the

world ocean (Martin and Fitzwater 1988) but the observations and conclusions are still valid.

The dynamics of the spring bloom in temperate waters was dealt with in Section 3.3.2, using mainly material from the Atlantic Ocean. We shall now see that there seem to be systematic differences in the dynamics of the bloom between Atlantic and Pacific basins. The primary-production data indicate that at ocean weather station *I* (OWSI) in the Atlantic, the arrival of the spring bloom in April is marked by a sharp increase in primary productivity from about 20 to over 300 mg C m^{-2} d^{-1}, while at OWSP in the Pacific there is a slow increase in productivity between January and July, over about the same range of values. Patterns of biomass change are also different in the two basins. In the Atlantic phytoplankton biomass changes by an order of magnitude between winter and summer, while in the Pacific it only doubles during the same period.

Differences between the two basins have their origins in the different winter depths of the mixed layer. In the North Atlantic it is greater than 200 m, while in the North Pacific it is about 100 m. (These differences are, in turn, explicable in terms of the global hydrological cycle; see Chapter 10.) As a result, the phytoplankton in the Pacific are exposed to a more favorable light regime during winter and are able to maintain a moderate level of biomass and production. About 80% of this biomass is in the form of small (<20 μm) cells. These cells are grazed by protozoa, which in turn are preyed upon by two or three common species of copepod – *Neocalanus plumchrus*, *Neocalanus cristatus*, and *Calanus pacificus* – that are relatively large and have only one generation per year. Hence, modest levels of both phytoplankton and zooplankton biomass are maintained through the North Pacific winter. When the surface waters warm in spring and the mixed layer becomes shallower, the zooplankton grazing almost keeps pace with the increase in phytoplankton productivity, so that phytoplankton biomass increases only slowly.

(a) North Atlantic subarctic gyre

In the North Atlantic, by contrast, the mixed layer depth is sufficiently great that phytoplankton production virtually ceases during winter. The dominant copepod, *Calanus finmarchicus*, is adapted to this period of famine by having overwintering copepodites living in cold water over 300 m deep. When the spring bloom of diatoms starts in surface waters there is a lag in the start of zooplankton grazing. Phytoplankton biomass increases to high levels, and much of it may sink without being grazed in the plankton. Then, between April and June, the *Calanus finmarchicus* copepodites rise to the surface layer, complete their development, and begin breeding. In most places these calanoids complete several generations in quick succession. Zooplankton production is much more narrowly pulsed in the Atlantic than it is in the Pacific.

In spite of these ecological differences, the two areas seem to have about the same total levels of phytoplankton and mesozooplankton production, and about the same populations of predators (e.g., euphausiids, jellyfish, chaetognaths, myctophids, squid). It is thought that the more constant biomass of plankton in

the Pacific system supports a greater amount of pelagic fish production (salmon, for instance) while the sinking of the diatom bloom in the Atlantic may support a larger benthic fish production.

In the course of the Atlantic Meridional Transect program, details of the planktonic biomass, size composition, and production in the North Atlantic subarctic gyre were recorded. Maranon *et al*. (2001) noted that in the summer oligotrophic phase picophytoplankton account for about 56% of the carbon fixation and over 70% of the autotrophic biomass. Large cells (>2 μm) predominate during the spring bloom period, but picophytoplankton are always present and contribute to the production in proportion to their biomass. As Fig. 8.20 shows, the North Atlantic subarctic gyre had larger biovolumes of plankton than the subtropical gyre to the south. The increasing proportion of mesozooplankton along the transect is shown by the emergence of a strong diurnal pattern of biomass in the surface waters. The transect, sampled in May, also shows that the mean diameter of the organisms was much lower than in the subtropical gyre. This is a consequence of the North Atlantic transition from a bloom community of diatoms to a summer community of picoplankton and small grazers.

(b) Alaskan gyre

The Alaskan gyre is located in the Gulf of Alaska and extends westward to near the dateline. On the south side is the eastward-flowing Subarctic (or North Pacific) Current, with a velocity around 10 cm s^{-1}. To the north and west is the strong (>30 cm s^{-1}) southwest-flowing Alaska Stream, along the continental slope of Alaska. Both currents are continuous to the ocean bottom. The Subarctic Current bifurcates in the eastern North Pacific, northward to form the Alaska Current and southward to contribute to the California Current. In the center of the Alaskan Gyre there is winter upwelling with a mean velocity of 7×10^{-5} cm s^{-1} (6 cm d^{-1}). The system is strongly influenced, especially in winter, by the atmospheric circulation in the Aleutain Low. When the low is intense, the northward transport in the Alaska Current dominates over the southward transport in the California Current.

We saw in Section 8.3.3 that the Alaskan gyre is the habitat for major stocks of salmon during the ocean-going phase of their lives. Inter-decadal variability in the properties of the gyre is associated with major changes in fish stocks, which will be discussed in Chapter 9. Meantime, Harrison *et al*. (1999) reviewed the physics, chemistry, and biology of this gyre. Their interpretation of the data differs from that of Parsons and Lalli (1988) because, as they point out, the important discovery of iron limitation for large-celled phytoplankton (especially diatoms) by Martin and Fitzwater (1988) dramatically changed our view of the factors controlling primary productivity of Station *P*. It is now clear that the subarctic North Pacific is one of the three major high-nitrate, low-chlorophyll (HNLC) regions of the world (see Section 3.2.7)

The Alaskan gyre has saturating nitrate conditions in surface waters all year, about 16 μM in winter and about 8 μM in summer. The biomass of phytoplankton

is low (chlorophyll usually <0.5 mg m^{-3}) and dominated by small cells (<5 μm). Primary productivity is now believed to lie in the range 140–215 g C m^{-2} y^{-1}. As in other iron-limited areas (Section 3.2.7), it is thought that the small cells are not iron-limited, but their abundance is controlled by the micrograzers. Satellite observation shows episodic occurrences of high phytoplankton biomass, which may result from depositions of iron-rich dust blown from Asia. Utilization of nitrogen by the phytoplankton at Station *P* derives 55% from recycled ammonia, 24% from urea, and 21% from upwelled nitrate.

8.7 Summary: subtropical gyres are not biological deserts

We have seen in this chapter that ocean circulation is closely linked to atmospheric circulation. The difference in solar heating between low and high latitudes, in conjunction with the rotation of the earth, leads to westerly and trade winds, which drive major anticyclonic subtropical gyres in each of the ocean basins. Associated with these gyres are powerful western boundary currents that transport large quantities of heat away from equatorial regions. These currents meander and cut off large gyrating bodies of water, the warm-core and cold-core rings, which lead independent existences for several months. Organisms have adapted to exploit the properties of the currents and the rings. For example, squid breed in warm subtropical waters, then "ride" the western boundary currents to exploit the higher levels of productivity in temperate latitudes. Pacific salmon swim thousands of kilometers with the currents of the subarctic gyres and exploit the abundant food supply during their period of rapid growth. Eel larvae rely on the Gulf Stream to carry them from their subtropical breeding grounds in the Sargasso Sea to the coasts of Europe.

The anticyclonic gyres are permanently stratified (though with seasonal changes in the thickness of the mixed layer) and surface waters have low average levels of nutrients. It was once thought that primary production was uniformly low, relying mostly on the recycling of nutrients between the grazers and the phytoplankton. It is now thought that various mechanisms, such as winter convective mixing, eddies associated with storm events, and horizontal transport from the peripheries of the gyres, lead to transient episodes of upwelling of nutrient-rich water. Even in these gyres the level of "new" production is much higher than previously supposed.

The subarctic gyres have alternating periods of summer stratification and winter mixing, so that there is a seasonal injection of nutrients into surface waters. In the North Atlantic it appears that a bloom of phytoplankton develops when the zooplankton populations in surface waters are at a low level, so that much of the plankton biomass sinks without being grazed. In the Pacific, on the other hand, the depth of the winter mixing is more restricted, and small phytoplankton cells are able to maintain a modest level of primary production throughout the winter, even though the larger phytoplankton are iron-limited. This condition supports a population of zooplankton that, when the spring bloom begins, is able

to keep pace with the growth of phytoplankton and prevent the accumulation of biomass. Hence, biological production in the North Pacific appears to be less strongly pulsed than in the Atlantic.

While the major ocean gyres and their associated ring formations are well recognized and have been extensively studied, it is now believed that eddies permeate all parts of the oceans. Using long time series of observations near Bermuda and Hawaii, in conjunction with satellite observations of the distribution and abundance of cyclonic eddies, it has been shown that these mesoscale features greatly enhance the productivity of the subtropical gyres. Productivity is further enhanced by Ekman transport from the periphery of the gyres.

9

Variability in ocean circulation: its biological consequences

9.1 Introduction

In this chapter we review some of the most exciting developments of the decade 1995–2005. One after another, researchers discovered that major changes in the plankton, the benthos, and the fish stocks were correlated with changes in atmospheric indices such as the North Atlantic Oscillation (NAO), the Aleutian Low

Pressure Index (ALPI), or the Southern Oscillation Index (SOI). It seemed that the changes in atmospheric circulation were driving changes in the circulation of the oceans, which in turn were causing major changes in biological processes. These basin-scale phenomena seem to be linked by a more generalized index, the Atmospheric Circulation Index (ACI). For twenty to thirty years the global air circulation is dominated by westerly winds. Then there is a regime shift, and the westerly winds occur less frequently, while north–south air movements become more prominent. Twenty to thirty years later, the cycle starts over again. The 10–12 major fish stocks which contribute about half of the world's marine fish landings are divisible into those that show increased landings during the westerly wind phase, and those that increase in the other phase.

During the twentieth century, our technological advances in fishing brought us to the point where it is possible to overfish a stock so seriously that it is no longer biologically viable. Fisheries scientists began to try to define the maximum catch that could be taken on a yearly basis while still permitting the stock to remain vigorous; they called it the maximum sustainable yield. At first these calculations were done with the environment of the fish (e.g., physical and chemical conditions, food supply, and predator pressure) held constant. Gradually, fisheries scientists became aware that these assumptions were unrealistic. Large fluctuations in abundance occurred that appeared to be unrelated to pressures of the fishery. In the English Channel between 1925 and 1936, the herring *Clupea harengus* stock went into decline and was replaced by pilchards *Sardina pilchardus*. In various upwelling systems around the world sardines were replaced by anchovies, and vice versa, and cores taken from anaerobic sediment showed that these changes had also occurred before human fishing pressure had become a significant factor.

Perhaps the best-known fluctuations of all are those associated with the El Niño phenomenon off the coast of Peru. Changes in oceanographic conditions (see Chapter 5) led on many occasions to drastic declines in numbers of anchoveta *Engraulis ringens*, with spectacular consequences in terms of deaths of dependent seabirds and mammals.

Not all changes have been negative. During the period 1940–70 the cod *Gadus morhua* stocks greatly expanded their range and abundance on the west coast of Greenland, and in 1960–70 there was a great expansion of the stocks of cod and related species in the North Sea.

Contemporary fisheries management policy, therefore, seeks to control fishing effort against a background of natural fluctuations in stock sizes. For many years the fluctuations seemed totally unpredictable, but as people began to study oceanographic processes on larger and larger scales, it gradually became apparent that many local changes in fish stocks were related to large-scale processes in the ocean. In this chapter, we shall examine several of these processes. In the Pacific Ocean, we shall see that coupling between the ocean and the atmosphere causes an oceanographic oscillation between Peru and Indonesia – the Southern Oscillation – that affects the fish stocks of Peru and many parts of the North Pacific. Over the northeast Pacific, long-term variations in the intensity of the Aleutian low-pressure system drive major changes in biological production and

fish biomass. When the atmospheric low-pressure system is particularly intense the winds around it are strong, causing a speeding up of the associated oceanic gyre, with increased upwelling of nutrient-rich water and enhanced biological production.

In the Atlantic Ocean, we shall see that changes in the pattern of the westerly winds running along the boundary between the subarctic air mass and the subtropical air mass give rise to important shifts in weather patterns. From about 1890 to 1940, conditions in the northeast Atlantic became progressively warmer; southern species of invertebrates and fish extended their range northward, several stocks expanded dramatically, and the balance of species present in the plankton of the English Channel changed radically. Between about 1940 and 1980, there was in the same area an increase in the incidence of cold northerly winds, and the biomass of phytoplankton and zooplankton, though variable, showed a steady downward trend. A number of important fish stocks declined (although at least one showed dramatic improvement) and then toward the end of this period the plankton and fish community of the English Channel reverted to its pre-1930 condition.

To try to understand these changes, it is necessary to study the major features of the dynamics of the earth's atmosphere, and the way in which they interact with the ocean currents.

9.2 Physical variability in the Pacific and Atlantic Oceans

9.2.1 El Niño – Southern Oscillation (ENSO)

The anchovy *Engraulis ringens* fishery off Peru and Ecuador used to yield, in a good year, about 10^7 tons of fish. The fishery exists because equatorward winds along the coast cause nutrients to be upwelled from below the shallow thermocline as described in Section 5.2.2. The catch rate is not constant throughout the year because in November and December warm water from the equatorial region moves south and disrupts the upward flow of nutrients. This change in the oceanographic conditions, because it occurs around Christmas, is called El Niño after the Christ child. In normal years the disruptive phenomenon lasts only a few months and the high-nutrient upwelling returns, but every 3–7 years the high-nutrient flow is confined to a narrow band along the coast or, during severe episodes, completely cut off for up to a year. This condition has a devastating effect on the anchovy fishery, which can decline to one-fifth of the peak catches. The term "El Niño" is now used exclusively for this catastrophic phenomenon.

Until about 40 years ago El Niño was believed to be caused by a decrease in the upwelling-favorable winds and thus an event local to the coasts of Peru and Ecuador. It is now known that El Niño is a small part of an ocean-wide oscillation in the atmosphere called the Southern Oscillation (SO). In this oscillation the pressure gradient between the region of high atmospheric pressure in the eastern equatorial Pacific and the region of low pressure in the area of Indonesia

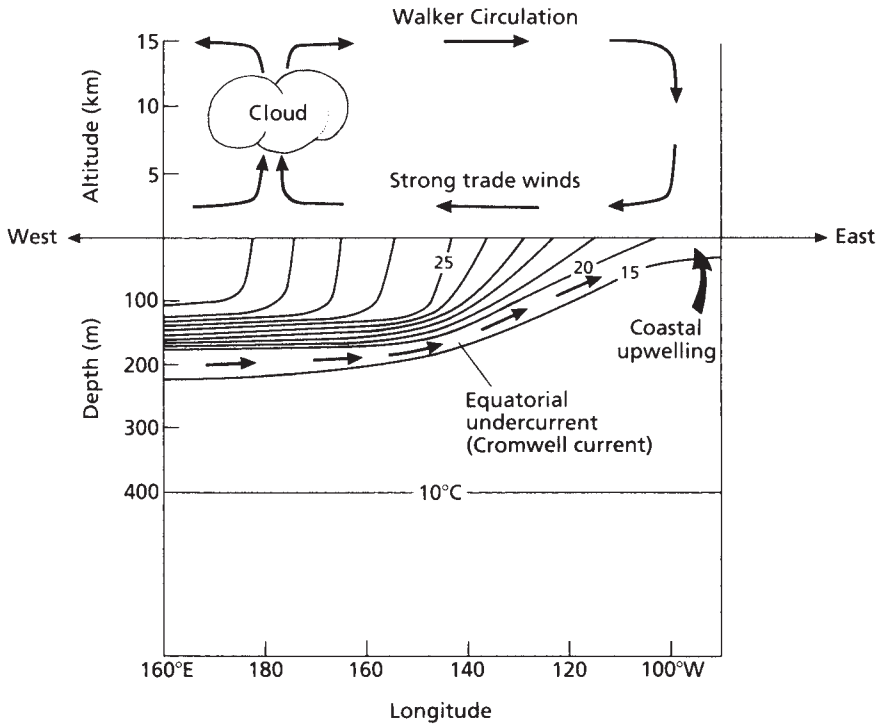

Fig. 9.01 Vertical cross-section of the atmosphere and the ocean along the equatorial Pacific, viewed from the south. Note the zonal Walker circulation in the atmosphere and the thermocline that shallows in the east in response to wind stress at the surface. Also shown are the coastal upwelling off the coast of South America and the equatorial undercurrent flowing east at the base of the thermocline.

becomes higher, then lower, than average. A lower-than-average gradient favors El Niño conditions, while the higher-than-average situation has been called La Niña. The Southern Oscillation is associated with large changes in the climate of the equatorial region and to a lesser extent the subtropical regions. The two phenomena are now often connected as the El Niño – Southern Oscillation, or ENSO. According to Philander (1990), ENSO is the most important source of global climate variability.

Some key features of ENSO along the equatorial Pacific are shown in the vertical section in Fig. 9.01. In the atmosphere the trade winds normally blow westward over the sea surface toward a low-pressure area in the western Pacific located at about 180° W. As the air moves over the warm ocean, it becomes warmer and lighter. In the low-pressure region, the air rises and loses its moisture through rain and eventually circulates back toward the east at upper levels and descends over the eastern Pacific high-pressure cell to complete the circuit. This vertical east–west circulation cell is one of a series that circle the equator known as the Walker circulation.

In the ocean, the trade winds drag the surface water toward the west (Coriolis effect is zero at the equator) in the South Equatorial current. The wind stress along the equator is balanced by a pressure gradient in the opposite direction created by a rise in sea level toward the west of about 40 cm. This pressure gradient is not transmitted into the deep ocean because the density structure in the upper layer of the ocean adjusts to cancel the pressure difference. This change is accomplished by an increase in the thickness of the low-density mixed layer from 30 to 50 m in the east to ~150 m at the middle of the ocean (150° W). In the western half of the ocean the depth of the mixed layer remains roughly constant. The pressure gradient due to the rising sea level is maintained in this region by the westward increase of temperature in the mixed layer.

The large decrease in the sea surface temperature from ~30 °C in the west to ~20 °C in the east is due primarily to upwelling along the equator. The upwelling is created by horizontal Ekman transports away from the equator (Fig. 3.07), which are driven by the trade winds toward the west. In the eastern Pacific, the thermocline lies at ~50 m and upwelling brings cool water from below the thermocline up into the mixed layer. Toward the west, where the thermocline is deeper, the upwelling water increasingly comes from the warm mixed layer.

One of the first signals at the beginning of an El Niño is an increase in sea surface temperature in the east. This leads to a decrease in the east–west sea-surface temperature gradient and then a decrease in the east–west pressure gradient in the atmosphere. The Walker circulation and the trade winds then decrease, leading to a decrease in the Ekman flux away from the equator and a decrease in the westward rise in sea surface height. The thermocline then relaxes from its normal downward slope between 100 and 150° W, resulting in a deeper mixed layer in the east. This, along with the reduced Ekman flux, results in less subthermocline water being brought up into the mixed layer, and the mixed layer warms. The warming in turn causes a further decrease in the east–west sea-surface temperature gradient and a further weakening of the Walker circulation and the trade winds. Thus, the original temperature increase in sea surface temperature leads through positive feedbacks to a further increase in temperature.

As the process continues, the sea surface temperature along the equator becomes considerably higher than normal. This warming is illustrated in Fig. 9.02, which shows the extent and degree of this warming at the "mature phase" of El Niño as calculated by Rasmussen and Carpenter (1982). The figure indicates that a significant change in surface temperature occurred over an area roughly 10,000 km long and 4000 km wide. The maximum of the averaged anomaly lies on the equator at ~130° W longitude and is ~1.6 °C. Today such maps are updated daily and posted at www.pmel.noaa.gov/tao. This is the website of the Tropical Atmosphere Ocean Project, which maintains a network of observing buoys "for improved detection, understanding and prediction of El Niño and La Niña" (McPhaden *et al*. 1998). This site also provides up-to-date ocean temperature sections along the equator similar to that shown in Fig. 9.01. The Climate Prediction Center of the US National Weather Service also provides up-to-date data and forecasts of ENSO at www.cpc.ncep.noaa.gov/products.

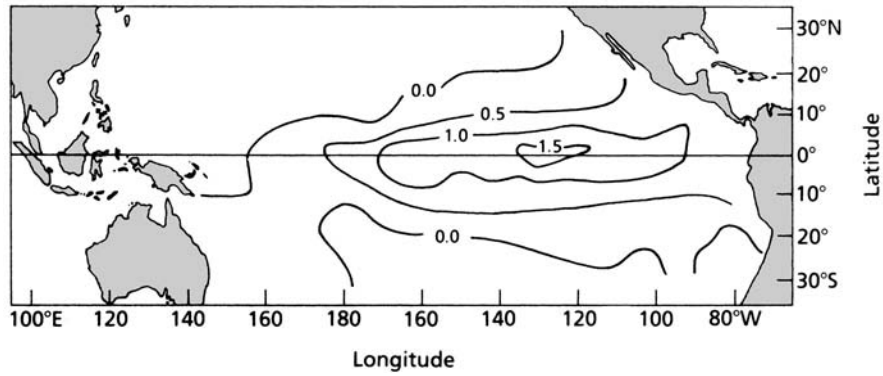

Fig. 9.02 Temperature anomalies in the equatorial Pacific Ocean, averaged from the "mature phase" of six El Niño episodes between 1951 and 1973. Adapted from Rasmusson and Carpenter (1982).

The coastal upwelling off Peru and Ecuador, indicated in Fig. 9.01, continues as the trade winds diminish during El Niño. With the presence of the deeper mixed layer, the upwelling water over the continental shelf tends to be the warmer nutrient-poor water from the mixed layer rather than the cool nutrient-rich water from beneath the thermocline. Thus, the warm water and the disappearance of the anchovy fishery called El Niño are seen to be strongly linked to the ocean-wide changes in both the ocean and the atmosphere, rather than a local phenomenon as originally believed.

La Niña, the opposite of El Niño, begins as El Niño does with an anomaly in the sea surface temperature. In this case, however, the anomaly is a decrease in temperature rather than an increase. The anomaly increases through a positive feedback loop just the reverse of that outlined above for El Niño. Over time, as La Niñas follows El Niños, records of the participating variables such as atmospheric pressure and sea surface temperature accumulate to reveal the cycling between the two phases. One of the common ways of illustrating the phenomenon is an index of the Southern Oscillation, i.e., the Southern Oscillation Index (SOI), which is shown in Fig. 9.03(a). The SOI is based on the monthly anomaly of the sea-level pressure difference between Tahiti and Darwin. Each monthly value is divided by the month's long-term standard deviation and the result, by tradition, multiplied by 10. When the index is negative the pressure difference is less than average and the sea surface temperature along the equator is higher than average as during El Niños. The most intense El Niños are during the years with the greatest decrease in the index, with the largest in 1982–3. The index oscillates back and forth at a 3–7 year period but over the first two-thirds of the record positive values appear to predominate while the opposite is true for the last third. This turns out to be true and is discussed in Section 9.2.2(d) along with long-term changes in other variables.

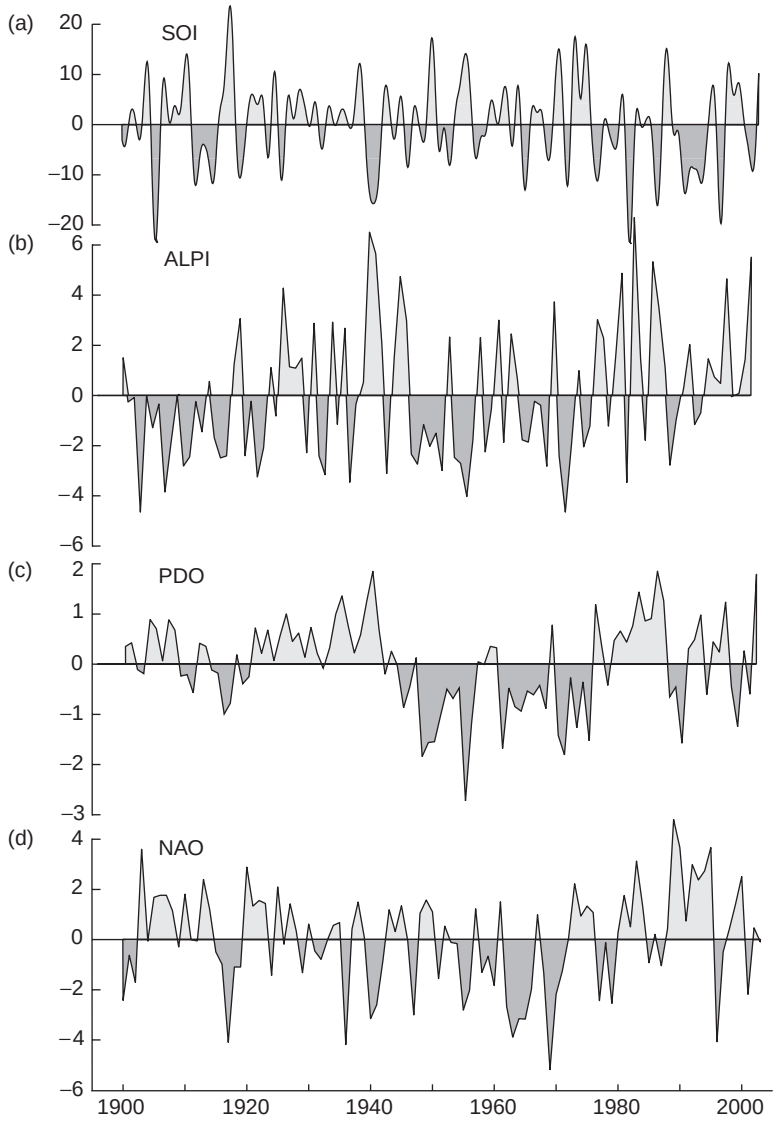

Fig. 9.03 Anomaly time series of (a) the Southern Oscillation Index (SOI), (b) the Aleutian Low Pressure Index (ALPI), (c) the Pacific Decadal Oscillation (PDO), and (d) the North Atlantic Oscillation (NAO) since 1900. Anomalies are relative to the means since 1900. A SOI unit is the anomaly of the monthly pressure difference times 10 and divided by the long-term standard deviation for the month. An NAO unit is similar to an SOI unit except the pressure difference is the seasonal value and it is not multiplied by 10. SOI data obtained from the Commonwealth Bureau of Meteorology (www.bom.gov.au/climate/current/soihtm1.shtml), ALPI from Beamish *et al.* (1997; www.pac.dfo-mpo.gc.ca/sci/sa-mfpd/climate/clm_indx.htm), PDO from N. Mantua (jisao.washington. edu/pdo/PDO.latest), and NAO from J. Hurrell (www.cgd.ucar.edu/~jhurrell/indices.html).

The physical processes involved in the growth of El Niño and La Niña are now quite well understood. However, the processes that carry the oscillation from one phase to the next have been a field of intense study for a number of years. Neelin *et al*. (1998) summarize various theoretical studies and point out that one of the key ingredients is the latitudinal gradient in the rate at which the ocean adjusts to changes in the wind speed. Near the equator, the ocean is roughly in balance with the wind stress and adjusts rapidly to changes in the wind stress. A few degrees away from the equator, as the Coriolis effect increases, the ocean adjusts more slowly to changes in the wind stress. By being slow relative to the wind, the ocean retains properties existing before the change in the wind. Thus, a "memory" of previous conditions resides in the ocean. It is this memory that forms the tendency to damp the present phase and provide the link to the next phase. The oscillation therefore depends on processes in the ocean and the atmosphere as well as the interactions between the two. According to the authors, this is the first atmospheric oscillation to be shown to depend on coupled interactions between the ocean and the atmosphere.

9.2.2 Teleconnections, patterns, and oscillations

(a) Teleconnections

As ENSO proceeds from one phase to the other, the Walker circulation (Fig. 9.01) varies in intensity and position. These variations cause weather changes in a number of locations along the equator. There are, for example, strong correlations between the warm period of ENSO and droughts in Australia, Indonesia, Brazil, and Africa. At the same time, unusually high rainfall occurs along the equator east of 160° E and in Ecuador and Peru, where the deserts bloom and pastures are bountiful (Philander 1990, Wallace *et al*. 1998).

ENSO also has effects on weather at latitudes far north and south of the equator. During El Niño this link begins with sea-surface temperature increases in the eastern equatorial Pacific. The region of ascending moist warm air over the western Pacific (Fig. 9.01) expands toward the east and the volume of rising moist air increases. As the air rises it cools and the moisture condenses to form clouds in the upper atmosphere. As a result, the heat that caused the water to evaporate in the first place (the latent heat) is released. This creates a large additional source of heat energy and the convection grows in intensity, which in turn increases the flow of tropical air in the upper troposphere toward the subtropical regions. This results in changes to the atmospheric circulation and weather in regions distant from the tropical Pacific. These correlations of weather-related phenomena are termed "teleconnections."

The anomalous atmospheric-pressure pattern related to the warm phase of El Niño in the northern hemisphere is shown in Fig. 9.04. During this phase, regions of higher than normal pressure are found in the western Pacific on either side of the equatorial region of high rainfall. Toward higher latitudes, a sequence

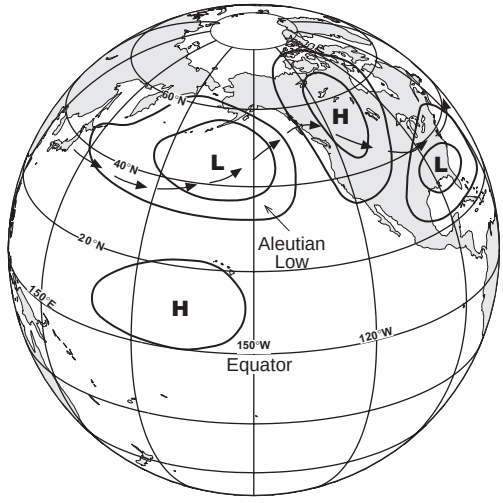

Fig. 9.04 Pattern of anomalous pressure distribution in winter during the warm phase of El Niño. Arrows indicate mean path of westerlies. After Horel and Wallace (1981) and the website of the Joint Institute for the Study of the Atmosphere and Ocean (JISAO), jisao.washington.edu/data_sets/pna.

of alternating high-pressure and low-pressure anomalies forms along a curving eastward path. These anomalies, which are strongest in the winter, cause the path of the mid-latitude westerlies to be distorted as indicated by the line of arrows in Fig. 9.04. The distortion brings westerlies further south in mid-ocean, causing a decrease in the rainfall at Hawaii. At the west coast of North America the westerlies are further north than usual and bring warmer air to Alaska and the Canadian prairies. On the eastern side of North America, the airflow is more northerly than usual and brings more of the cold Arctic air to the eastern United States.

The alternating series of anomalous highs and lows shown in Fig. 9.04 constitutes one of the better-known long-term weather patterns. It is called the Pacific North American pattern and has been used successfully for many years as an aid in long-range forecasting. The pattern is not created by ENSO but is augmented by ENSO.

(b) Pacific Decadal Oscillation

The Aleutian low, noted in Fig. 9.04, dominates the wind field of the North Pacific Ocean. It begins to form during autumn, intensifies and expands during winter, and breaks down in early summer. The extent and depth of the low vary from winter to winter as indicated in Fig. 9.03(b) by the time series of the Aleutian Low Pressure Index (ALPI). This index is the area in km^2 of the low defined by a sea-level pressure of ≤100.5 kPa. As the pressure decreases the area becomes larger so the index is an approximate mirror image of the pressure record within the

low. The oscillations in this record are noticeably longer than those in the SOI. The record also shows long-term variations in which the index tends to stay above or below the long-term average for 15–20 years before changing sign. One of these sign changes occurred in 1976–7, when the index went from being predominantly negative for the previous 30 years to predominantly positive.

During the early 1990s a number of investigations, reviewed by Mantua and Hare (2002), reported significant differences in numerous climatic and biological variables between the years before and after 1977. Differences were also noted before and after the short-lived change from positive to negative values in 1989. The fact that the differences were occurring simultaneously over large areas of the North Pacific Ocean and that they appeared to change sign every 15–20 years led to the concept of the Pacific Decadal Oscillation (PDO). The term "regime shift" was introduced for the differences in the climatic and biological variables that occur when the pressure anomaly changes sign. The PDO is now usually defined by the first principal component of the variations in sea surface temperature north of 20° N in the Pacific Ocean. Its variation over the past century, illustrated in Fig. 9.03(c), shows multiyear variations similar in period to those of the ALPI but more prominent than in the SOI or ALPI series.

The widespread changes in sea surface temperatures that identify the phases of the PDO form the link between the PDO and the changes in biological processes in the ocean which are discussed in Section 9.3.2. The pattern of the sea-surface temperature anomaly during the warm phase of the PDO is indicated in Fig. 9.05. The equatorial waters are warmer than normal and distributed in a pattern similar to the one observed during El Niño (Fig. 9.02).

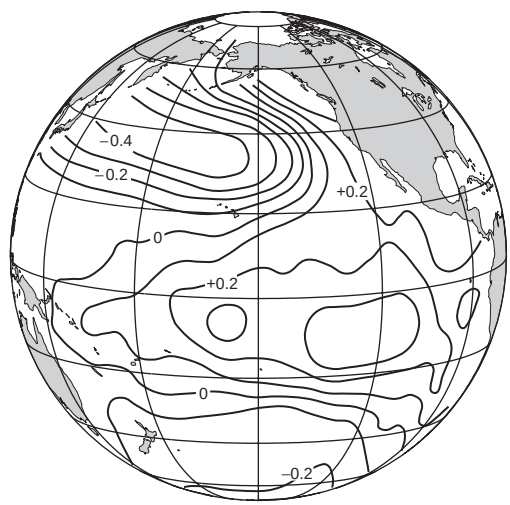

Fig. 9.05 Temperature anomaly (°C) in the Pacific Ocean during the warm phase of the Pacific Decadal Oscillation (PDO), adapted from Mantua and Hare (2002). Reproduced by permission of Terra Scientific Publishing.

In contrast to El Niño, identified by equatorial temperature anomalies, the strongest feature of the PDO is the lower sea surface temperature found throughout most of the northwest Pacific, accompanied by warmer waters off the Americas. The PDO also differs from ENSO in that its period, at 30–40 years, is significantly longer than the 4–7 years for ENSO. While the dynamics of ENSO are rather well known, those of the PDO are not. The phenomenon is being studied in coupled ocean–atmosphere numerical models. A recent example by Schneider *et al*. (2002) suggests the oscillation begins with an anomaly in the Aleutian Low. This creates anomalies in sea surface temperature and Ekman pumping in the central and eastern North Pacific. The temperature anomaly is propagated, over five years, westward via Rossby waves to the region where the Kuroshio and Oyashio Currents meet and flow eastward together. In this region, the temperature anomaly tends to reduce the atmospheric pressure anomaly, thereby returning the atmospheric pressure to the long-term average value.

(c) North Atlantic Oscillation

Another atmospheric pattern, well known since the whaling days in Baffin Bay, is the North Atlantic Oscillation (NAO) described by van Loon and Rogers (1978). The best-known effect of the North Atlantic Oscillation is that warm winters in Europe coincide with cold winters in Labrador and West Greenland, and vice versa. When the NAO is strongly positive, as shown in Fig. 9.06(a), the Icelandic Low, between Iceland and Greenland, is deeper and more persistent than normal. The stronger cyclonic circulation around the low brings colder air over the Labrador Sea, between Greenland and Canada, and warmer than normal air to Europe and the European Arctic, between Norway and Greenland. The colder air over the Labrador Sea tends to produce deeper surface mixed layers in winter – it reached 2300 m after a series of severe winters in the early 1990s (Lazier *et al*. 2002). The warmer air over the Greenland Sea limits the heat loss in winter and the mixed-layer depths are shallower than normal. Across the mid North Atlantic, the westerly winds are stronger than normal, bringing stormy wet weather to Europe. The atmospheric high-pressure system in the subtropical Atlantic (the Azores high) tends to be higher than normal during this phase of the oscillation. It brings stronger winds with increased upwelling in the waters off the northwest African coasts.

In the opposite phase, that is, when the NAO is negative (Fig. 9.06b) the Icelandic low is weaker, less persistent, and located further south, bringing easterly winds to the Labrador Sea which are relatively warm and lead to shallower mixed layers in the winter. At the same time, colder northerly winds are blowing over the Greenland Sea, creating more ice and deeper mixed layers in winter. The westerlies are weaker, leaving northern Europe cooler than normal and Portugal, Spain, and the western Mediterranean Sea wetter. The Azores high is also weaker, with lower wind speeds and decreased upwelling off the northwest African coasts.

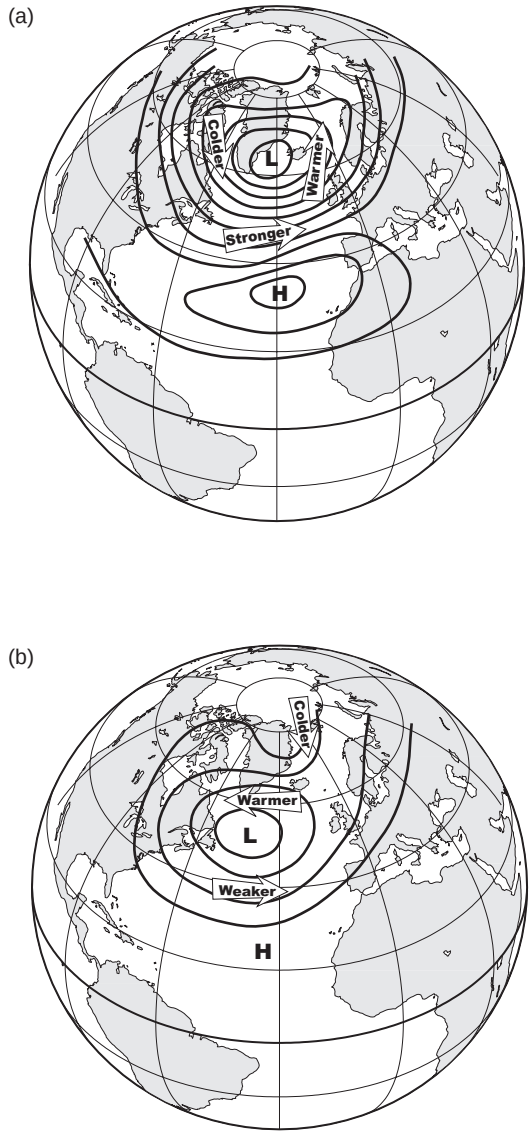

Fig. 9.06 Atmospheric pressure distributions over the northern hemisphere during winter (December, January, and February) for (a) the positive phase of the North Atlantic Oscillation and (b) the negative phase of the North Atlantic Oscillation. Airflow is clockwise around the highs and counter-clockwise around the lows. Adapted from the website of D.B. Stephenson, University of Reading, www.met.reading.ac.uk/cag/NAO.

The state of the North Atlantic Oscillation is often indicated by the average atmospheric pressure difference at sea level between the Azores and Iceland for the winter months of December, January, and February. However, pressure differences between Portugal and Iceland are also used because the records are significantly longer. A time series of these differences (Fig. 9.03d) indicates that either the anomalous high or the low pattern can exist for many years at a time. From the mid-1950s to the early 1970s, for example, the pressure difference was below average, bringing cold air to Europe. Since the early 1970s, on the other hand, the winters with a positive index have dominated, with warm European winters but some of the severest winters on record occurring off Labrador and Greenland.

In recent years the NAO has been found to be an integral part of a larger mode of atmospheric variability in the northern hemisphere. This larger mode was first called the Arctic Oscillation (Thompson and Wallace 1998) but in 2003 the name Northern Annular Mode (NAM) (Thompson *et al*. 2003) was adopted, to match a similar phenomenon in the southern hemisphere. Since the NAO is the most energetic portion of these all-encompassing patterns and has the longest history, we continue to use the old recognizable name. Interest in the NAO has increased greatly over the past decade due to its role in climate change. A recent book by Hurrell *et al*. (2003) reviews many of the recent advances and presents the NAO phenomenon in a "comprehensive manner." The table of contents of the book and the introduction are available at www.agu.org/pubs/book_series.html.

(d) Long-term variations

As noted above, all the time series we have discussed contain multiyear variations. A common way of highlighting such variations is to subtract the mean of the time series to create an anomaly series then to add the anomalies cumulatively from the beginning, that is, integrate the anomaly series. The resulting series of sums is proportional to the area under the anomaly curve from the beginning of the series up to a specified point on the x axis. Since the mean has been removed from the original series the sum of the anomalies is zero and the integrated series begins and ends at zero. During periods when positive anomalies predominate the cumulative sum increases with time and when negative anomalies predominate the cumulative sum decreases.

Examples of cumulative curves are shown in Fig. 9.07 for the four time series discussed in the previous sections: the SOI, ALPI, PDO, and NAO. The three additional series, the Atmospheric Circulation Index (ACI), the Pacific Circulation Index (PCI), and the length of day (LOD) will be introduced below. The first features to note about these curves is that they begin and end at zero (or close to it) and all have periods when they slope up (positive anomalies) and down (negative anomalies). The maxima in the curves occur when an era of positive anomalies changes to an era of negative anomalies and the minima occur when the positive anomalies return.

The curve for the SOI (Fig. 9.07) indicates a period of about 55 years between 1920 and the mid-1970s during which the anomalies tended to be positive,

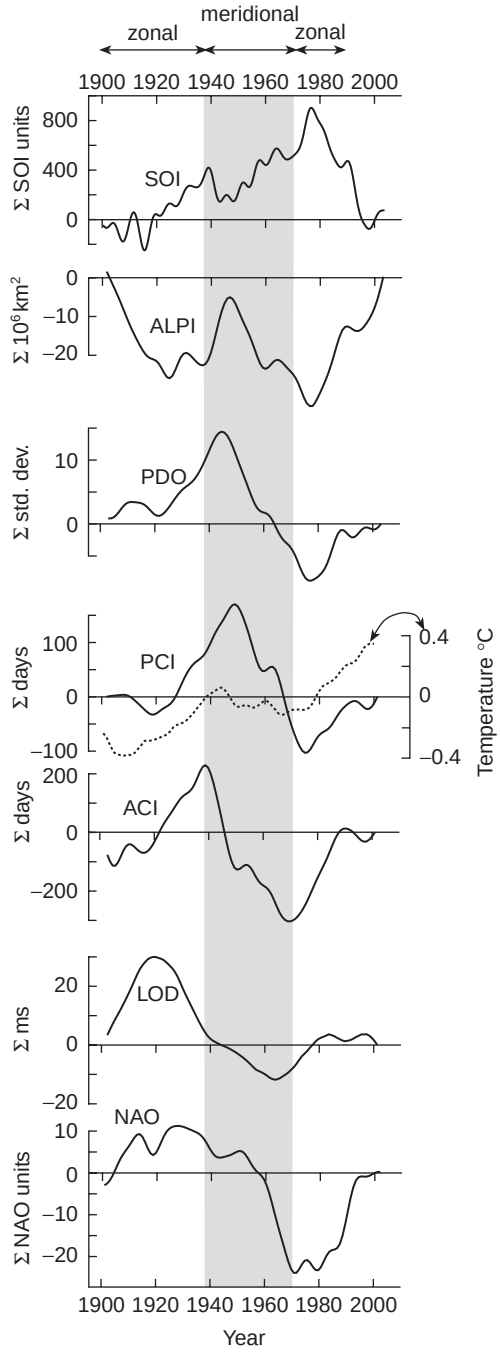

Fig. 9.07 Cumulative sums of the anomaly time series in Fig. 9.03, plus similar curves for the Atmospheric Circulation Index (ACI), Pacific Circulation Index (PCI), and the length of day (LOD) in units of ms. The global temperature relative to the 1961–90 average (adapted from Folland *et al*. 2001 and available at www.IPCC.ch) accompanies the PCI curve. Data obtained from sources outlined for Fig. 9.03, with the addition of LOD data from Beamish *et al*. (1999), PCI and ACI from King *et al*. (1998) (all at www.pac.dfo-mpo.gc.ca/sci/sa-mfpd/climate/clm_indx.htm). The meridional phase of the ACI between 1939 and 1971 is shaded for comparison with Fig. 9.18 (see Section 9.8.1).

suggesting conditions favoring La Niña regimes. Between the mid-1970s and the late 1990s the curve slopes down, indicating a 20-year period when the anomalies tended to be negative, favoring El Niño conditions. Comparing this curve with the anomaly plot in Fig. 9.03(a) demonstrates the clear advantage of the cumulative curve in identifying multiyear variations.

The next two curves in Fig. 9.07, the ALPI and PDO, are very similar to each other. Between the early 1920s and the mid to late 1940s anomalies in both variables tended to be positive. For the PDO this period was characterized by anomalously high sea surface temperatures along the equator and off the west coasts of the Americas. For the ALPI the anomalies were also positive during this period, indicating a deeper Aleutian low than normal with stronger, more persistent Arctic winds over the western Pacific and temperate to tropical air over the eastern Pacific. This phase changed in the 1940s to one when negative anomalies prevailed: a weaker Aleutian low and lower sea surface temperatures along the equator and eastern Pacific but higher in the central and western Pacific. Since this phase ended in the mid-1970s these indices have tended to be positive, indicating a return to conditions prevailing between the early 1920s and mid-1940s.

The PCI and ACI in Fig. 9.07 are indices based on estimates of the direction of the prevailing airflow. The ACI, adapted by Klyashtorin (1998) from the index of Girs (1974), is composed of annual estimates of the airflow over the North Atlantic Ocean, Europe, and Asia. The index is created by first classifying the dominant airflow for each day. Three classes are used: western (W), eastern (E), and meridional (C). The total number of days each class occurs in each year is used to construct time series, for each class, over all the years. The mean of each time series is removed to create three anomaly series. The W and E series are combined to create the WE form of the index, sometimes known as the zonal or latitudinal index. Since the number of days in each year is constant the C or meridional series is the negative of the WE series. To best highlight long-term variations these series are integrated.

The PCI is created using the same technique but includes the atmosphere over the North Pacific Ocean and western North America for the winter period between November and March (King *et al*. 1998). Since the PCI includes the North Pacific its variability is dominated by that of the Aleutian low. This is confirmed visually by comparing the curve for the PCI with that for the ALPI.

An increasing trend in the ACI and PCI indicates predominance of westerlies, while a decreasing trend indicates a decreased occurrence of westerlies and increased occurrence of northerlies. The most interesting fact about the two curves is that their near similarity implies that similar wind changes occur in both east and west hemispheres at the same time. The differences between the curves may arise because one is an annual index and the other a winter index. One notable difference between the two is the timing of the main maximum, which occurs in the late 1930s in the ACI but 10 years later in the PCI.

An interesting comparison is between the ACI and PCI and the global temperature record over the past century included with the PCI curve in Fig. 9.07. Since 1900

the global temperature has risen by ~0.6 ± 0.2 °C. Roughly half this gain occurred between 1910 and 1945 and the other half since 1975. During the years between the warming eras, the temperature remained constant or declined slightly. In the figure, the periods of temperature gain are seen to coincide with the periods of more intense Aleutian and Icelandic lows, while the period of little or no temperature increase between 1945 and 1975 was characterized by less intense lows and weaker westerlies. According to Folland *et al*. (2001) the increase in global air temperature since 1976 did not occur evenly over the whole world. In some regions it decreased; in some it remained the same. The greatest increases occurred in North America, Europe, and Asia, in the winter and spring. Moderate increases occurred in the summer but during the autumn there were no significant changes.

Another curious effect of the waxing and waning of the atmospheric pressure systems and their associated winds is that they cause changes in the length of the day. Klyashtorin (1998) noted this by comparing the ACI with the earth's rate of rotation or its inverse the length of day (LOD). There is a good reason for this correspondence as it is well known that variations in the atmosphere contribute significantly to the observed changes in the length of day, which is now measured routinely to a fraction of a millisecond. Changes that occur tend to be of the order of a few milliseconds. This connection arises because the atmosphere is part of the spinning earth and thus included in the total angular momentum of the earth – a conserved property. To review: the angular momentum of a mass m rotating in a circle a distance r from the axis of rotation at a velocity v is mrv. The angular momentum of the earth is the total of all the products mrv for all the masses making up the solid earth, the oceans and the atmosphere. That total can not change.

If a wind blowing over the earth's surface from west to east increases in speed it tends to increase the angular momentum of the earth because the speed of the air mass increases in the same direction of the earth's rotation. Since the angular momentum can not be increased the speed of rotation slows down (LOD increases) to maintain the total angular momentum of the earth at a constant value. A decreasing east wind has the same effect on the angular momentum as an increasing west wind because the mass of air moving against the direction of earth's rotation is decreasing. An interesting and well-known example of this effect occurs during El Niños. As the easterly wind along the equatorial Pacific decreases during El Niño the angular momentum of the earth tends to increase. In response the earth's rate of rotation decreases and the LOD increases. This is an exceptionally large signal which is now used to help confirm other indications of the onset of an El Niño.

The LOD index is truly a global index, as it reflects changes in the wind and pressure patterns all over the earth as well as changes within the earth and the oceans. Indexes such as the ACI and PCI are based on wind changes, thereby reflecting some of the winds altering the length of day, but not all, since they do not include wind changes in the equatorial regions or in the southern hemisphere. Comparing the cumulative curve of the LOD in Fig. 9.07 with the curves for ACI

and PCI, we find a number of similarities. For example, the period of positive anomalies in the early 1900s, the long period of negative anomalies through the middle of the century, and the return of positive anomalies in the 1960s and 1970s generally agrees with the ACI and PCI. Evidence that the match is not perfect can be seen by comparing the ALPI and LOD curves. At the beginning of the twentieth century a decreasing Aleutian low is coincident with an increasing LOD, but after 1920 the Aleutian low is strengthening and the LOD continues to decrease rather than increase as might be expected if the two were closely linked.

In the future such discrepancies may be removed by comparing the new precise measurements of the LOD with numerical simulations of the atmosphere, which allow twice-daily estimates of its angular momentum. With these tools researchers are now able to examine the relationships between changes in the LOD and changes in the atmosphere. Gross *et al.* (2004), for example, use a numerical atmosphere model to estimate LOD changes between 1980 and 2000 due to wind. The correlation between their estimated LOD and the observed LOD is 0.93. In the future this type of analysis will possibly isolate variations in the LOD caused by wind and pressure changes in the specific area of interest, rather than for the whole earth. When that happens, the LOD will be an indispensable tool for monitoring large-scale wind fields in remote locations.

The final curve in Fig. 9.07 is of the NAO. In the first 20 years of the twentieth century and since the early 1970s the anomalies have been predominantly positive, indicating an intense Icelandic low and stronger-than-normal westerlies. The 1950s and 1960s were marked by negative anomalies, which favor a warmer Labrador Sea and a colder Greenland Sea, as mentioned is Section 9.2.2(c). By comparing the curves for ALPI and NAO it is evident that changes over the latter half of the twentieth century in the Aleutian and Icelandic lows were very similar but in the first half of the century they did not behave as similarly. This dissimilarity suggests the atmospheric patterns over the North Atlantic and North Pacific are not always acting as closely together as suggested by the strong similarity between the PCI and ACI.

Since the ACI is global in scope, and since in a later section we shall discuss fluctuations of fish stocks in relation to fluctuations in the ACI, the records for the twentieth century in Fig. 9.07 have been divided into three regimes based on three phases of the ACI. We see that in almost all the years between 1900 and 1938 the index showed a rising trend. In other words, the anomalies were all positive. This was a period dominated by prevailing west–east or zonal airflow. The next 33 years were dominated by negative anomalies in the WE index and relatively increased north–south or meridional winds. From 1971 to 1990 there was a second period dominated by westerly winds. Thus, there were in the twentieth century three successive regimes in the atmospheric circulation: a zonal regime to 1938, a meridional regime to 1971, and a second zonal regime to 1990. The periods of global temperature increase clearly occur during the zonal regimes, while the period of no temperature increase occurs during the meridional regime.

9.3 Biological variability in the Pacific Ocean

As was mentioned in Section 9.2.2, the Pacific Ocean shows two distinct but interrelated oscillations. El Niño – Southern Oscillation (ENSO) has a period of 4–7 years, is relatively well understood, and is routinely forecast by the US National Weather Service. Then there is an oscillation with a period of 40–50 years, which involves long-term changes in the intensity of the Aleutian low. When that system is abnormally low, cooler-than-average waters are found throughout most of the northwest Pacific, with warmer-than-average waters off the Americas. The two main indices of the oscillation are the Aleutian Low Pressure Index (ALPI), which is proportional to the area of low pressure in winter, and the North Pacific Index (NPI), which is virtually its inverse. In this section we review the evidence that these oscillations produce biological change in the Pacific Ocean.

9.3.1 On the scale of El Niño events

The effects of El Niño – Southern Oscillation (ENSO) events on the upwelling system off Peru were discussed in Chapter 5. At the height of the 1982–3 El Niño event the upwelling waters off Peru were at 29 °C instead of the usual 16–18 °C, had very low nutrient concentrations, and supported a primary productivity that was only about 5% of normal. El Niño years are times of greatly reduced catches of anchoveta, although the exact cause is uncertain. A proportion of the stock migrates south and finds cooler waters less affected by the abnormal surface warming. Others remain in the affected area and die from thermal shock, a lack of suitable food, or perhaps a combination of the two. Since the economy of Peru is tied quite strongly to the anchoveta industry, the social consequences of ENSO events are serious, and there is a great deal of interest in trying to predict their occurrences. This situation is perhaps the clearest example in the world of the influence of physical oceanography on fish productivity.

The effects of ENSO north and south of the equator are documented in Section 9.2.2. At times of El Niño the westerly winds are further south in mid-ocean, but along the shores of North America they extend further north than usual, bringing warmer air and warmer water all the way to Alaska. A thick blanket of abnormally warm water extends northward along the coasts of California and Oregon, and upwelling brings only nutrient-poor water to the surface. Zooplankton biomass is greatly reduced and is characterized by species normally found further south. The boundaries between the waters of the Pacific gyre and the subarctic waters of the Alaska gyre move northward, causing changes in, for example, the migration routes of salmon (Xie and Hsei 1989).

Under these conditions, some species of fish thrive, while others decline. Pacific mackerel *Scomber japonicus*, Pacific herring *Clupea pallasii*, and Pacific hake *Merluccius productus* have better recruitment in El Niño years, probably because there is reduced offshore Ekman transport and reduced loss of larvae by advection

offshore from the productive coastal waters (Bailey 1981, Pearcy 1983, Sinclair *et al*. 1985). The species that decline probably do so because of the reduced productivity of phytoplankton and zooplankton associated with El Niño conditions.

Interesting El Niño effects have been observed on the Asian coast as well (Yamanaka 1985). El Niño is associated with reduced sea surface temperatures, at times as much as 7 °C. Bluefin tuna *Thunnus thynnus* normally spawn southwest of Japan, and a strong fishery is located off the coast of Japan. After spawning, the fish are believed to follow the Kuroshio Current and the North Pacific Current toward the mid-Pacific, where considerable quantities are caught by longlining. During El Niño years, coastal catches decrease and mid-Pacific catches increase, suggesting an eastward shift in the population. At the same time, several cold-water species that normally stay well north of Japan appear further south off the Japanese coast.

If we consider the North Pacific as a whole, there seems to be a counterclockwise shift in species distributions during El Niño years. Off North America, warm-water species extend their ranges northward, while off eastern Asia cold-water species extend their range to the south and east.

9.3.2 On the time scale of the Pacific Decadal Oscillation (PDO)

As we saw in Section 9.2.2, the Aleutian low-pressure system forms in autumn, intensifies and expands during winter, and breaks down in early summer. It dominates the wind field of the North Pacific Ocean, and tends to stay above or below the long-term average for 15–20 years. Times when the long-term trend is changing sign are associated with very far-reaching changes in both the physics and the biology of the North Pacific, and have come to be known as regime shifts. Interpretation of the biological effects is most easily made in terms of the ALPI, which is approximately the same as the PDO.

The changes that occur at the regime shifts have recently been examined by Hare and Mantua (2000), following a study by Ebbesmeyer *et al*. (1991). They examined time series of 100 variables including winter averages of 31 atmospheric and oceanic parameters and annual averages of 69 oceanic species. The data came from the open ocean and the Bering Sea and from locations along the west coast of North America. Among the data included were fish recruitment and catch, zooplankton biomass, air temperatures and pressures, and indexes of atmospheric variations such as the North Pacific Index, the ENSO and the PDO. The authors found strong evidence for changes "throughout the Pacific climate and marine ecosystems." The pressure shift in 1977 led to a deeper Aleutian low, lower sea surface temperatures in the central North Pacific Ocean, and higher temperatures in the coastal regions of the northeast Pacific and Bering Sea. There were higher salmon but lower shrimp populations in Alaskan waters and lower salmon populations off the west coasts of Canada and the United States. At the 1989 regime shift, sea surface temperatures increased in the central North Pacific and declined

in the coastal waters in the Gulf of Alaska. These changes were accompanied by declines in the groundfish in the Bering Sea and salmon in the waters off British Columbia and western Alaska.

According to Hare and Mantua (2000), the regime shifts are clearer in the biological time series than in the climate time series. The authors suggest that by concentrating more on monitoring ecosystems rather than climate variables an earlier identification of the regime shifts would be obtained. They also point out that the differences across the shift in 1989 were not generally the reverse of the differences across the 1976–7 shift, that is, not all parameters returned to states existing prior to 1977. One suggestion is that there are two oscillations, one with anomalies lasting 15–20 years and the other 70 years. When they shift simultaneously the characteristics of the shift will be different than when only one shifts.

A strong low-pressure system (positive ALPI) causes acceleration of the Alaskan current, with increased upwelling of nutrient-rich water and divergence at the center of the Alaskan gyre. This stimulates increased primary and secondary production, and the resulting phytoplankton and zooplankton are advected towards the circumference. Relationships between inter-decadal physical oceanographic changes in the northeast Pacific and changes in the plankton have been reviewed by Francis *et al*. (1998). They focused particularly on the years 1976–7, when sharp changes were observed in the Aleutian Low Pressure Index. Before the change, the index had been declining, and afterwards the trend was positive, towards stronger low-pressure systems. The average summer biomass of zooplankton in the Gulf of Alaska more than doubled between the late 1950s and the 1980s, but the biomass of plankton in the California upwelling system decreased during the same period. Lange *et al*. (1990) reported that in 1976–7 the sedimentation of diatoms in the Santa Barbara Basin decreased 10-fold compared with the average for 1954–72. The biomass of zooplankton decreased up to 70% between the 1950s and the 1980s.

A strong Aleutian low-pressure system decreases the amount of water from the west wind drift that enters the California current (Fig. 9.08). It also causes a warming of coastal waters along the whole of the American seaboard. It is postulated that one or both of these factors contributed to a decrease in productivity in the California Current. Note that similar effects were noted in connection with El Niño. It seems likely that when El Niño coincides with a positive ALPI, the two reinforce one another.

At the time of the 1976–7 regime shift, there was a 30–80% deepening of the winter and spring mixed layer in waters northwest of the Hawaiian islands and over the Emperor Seamounts, while there was a shallowing of the mixed layer in the Gulf of Alaska. Modeling the results of these changes suggests that there would be increased phytoplankton and zooplankton production in the Gulf of Alaska and around Hawaii, but a decrease in the intermediate area over the Emperor Seamounts.

As mentioned, Hare and Mantua (2000) made a very thorough analysis of physical and biological changes associated with the North Pacific regime shifts of the 1970s and 1980s. Using principal component analysis of 100 variables, they

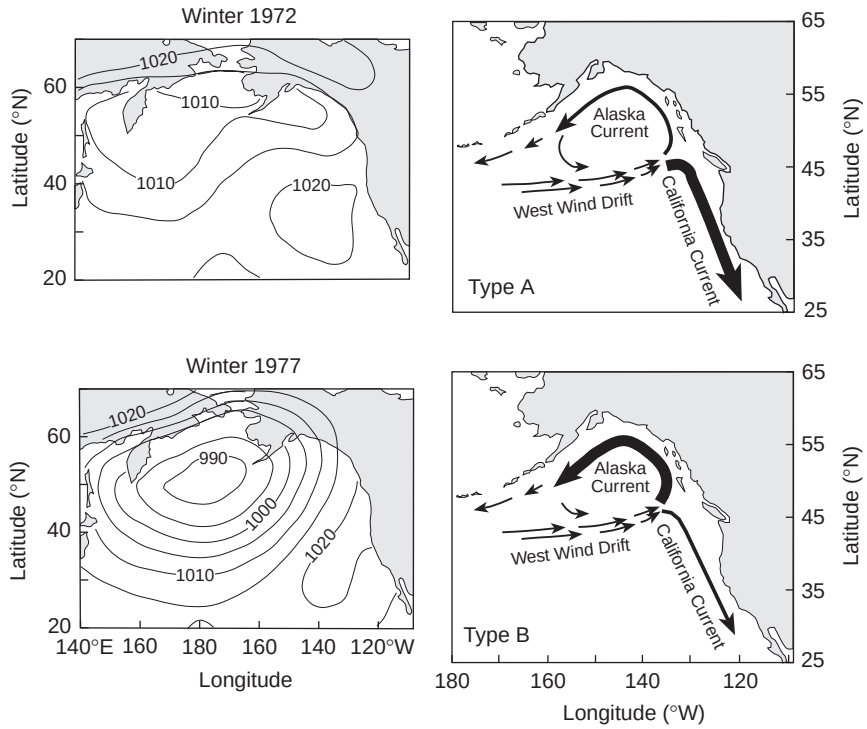

Fig. 9.08 Two alternating patterns of atmospheric circulation postulated by Hollowed and Wooster (1992). On the left are examples of weak and intense Aleutian low-pressure systems, and on the right the suggested changes in balance between the Alaska Current and the California Current. From Francis *et al*. (1998). Reproduced by permission of Blackwell Publishing Ltd.

demonstrated major regime shifts in 1977 and 1989 (Fig. 9.09). During the 1990s, after the second regime shift, the biomass of zooplankton in all areas was much below the long-term average. The Gulf of Alaska shrimp catch and the oyster condition index along the coast of Washington State were also below average during this period. Rudnick and Davis (2003) suggest that the step illustrated in Fig. 9.09 is likely an artifact of the analysis combined with the relatively short lengths of the records used. However, as we shall see, there is much independent evidence for a regime shift in 1977, and some evidence, though less strong, for a regime shift around 1989–90.

Connections between the fish stocks and the ALPI were noted even earlier than connections with the plankton. The Aleutian low and the associated subarctic gyre were particularly vigorous around 1940 and again in the 1980s. Kawasaki (1992) showed that three geographically separated sardine stocks – from the Far East, Chile, and California – followed the same pattern of abundance, being most plentiful in the 1940s and the 1980s (Fig. 9.10). Beamish and Bouillon (1993) showed that total landings of sockeye *Oncorhynchus nerka*, chum *O. keta*, and pink salmon

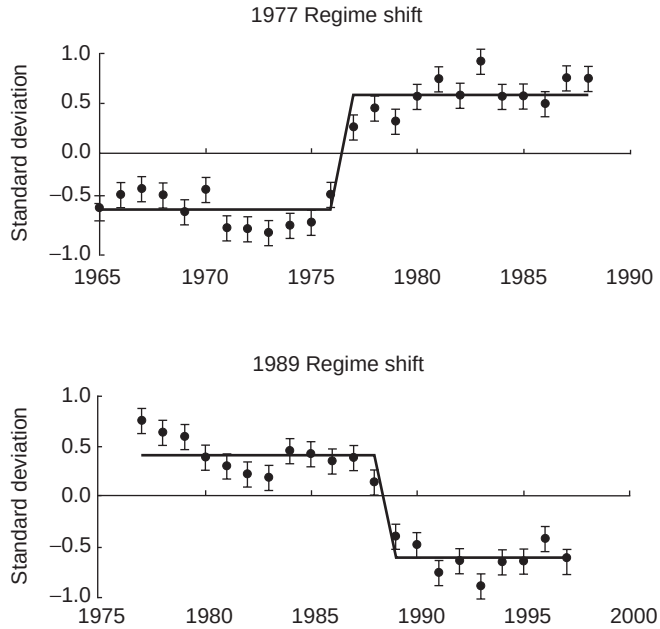

Fig. 9.09 Results from two regime-shift analyses of a composite of 100 environmental time series. The step passes through the mean standard deviation within each regime. The standard error of the 100 time series is indicated for each year. From Hare and Mantua (2000).

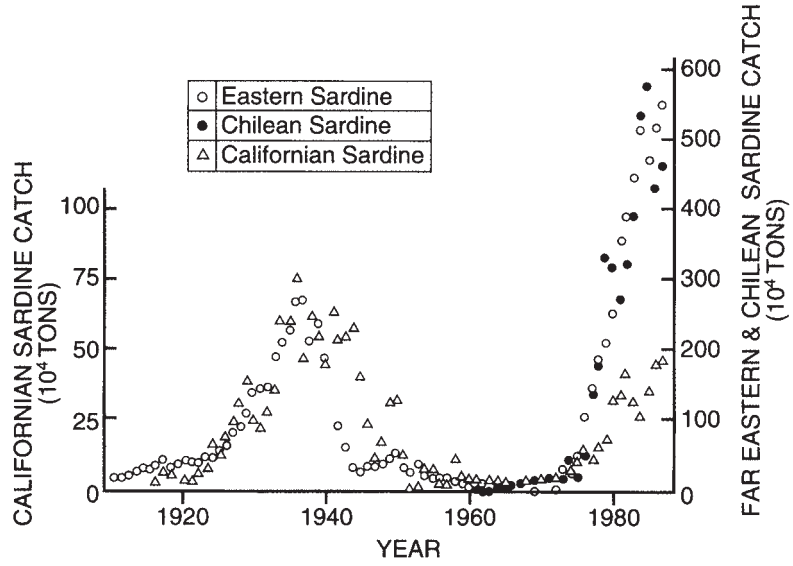

Fig. 9.10 Catches of sardines from three stocks: the Far Eastern, the Chilean, and the Californian, 1910–88. From Kawasaki (1992).

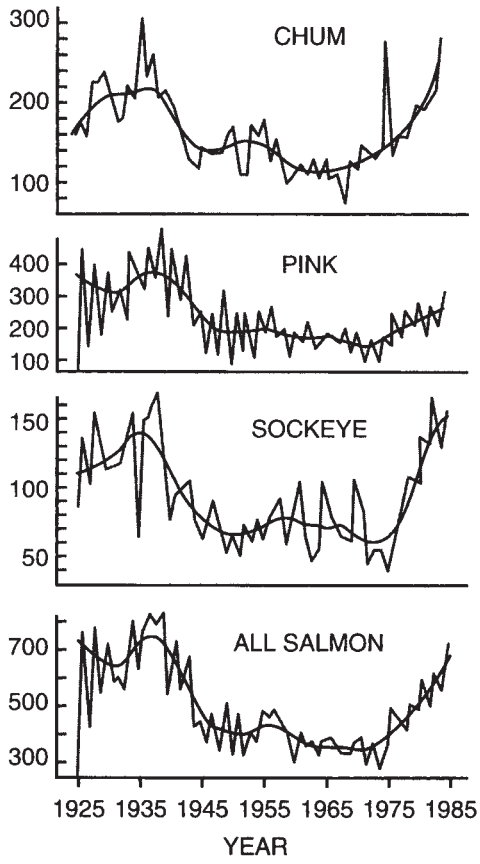

Fig. 9.11 Catch data for sockeye, chum, and pink salmon, and total for all salmon, for the entire North Pacific. Plots show annual catches and a line generated by a LOWESS smoother (bandwidth 0.20) fitted to the data. From Beamish (1993) and Beamish and Bouillon (1993).

O. gorbusha for the North Pacific also showed a similar pattern, with peak landings in the 1940s and the 1980s. More remarkable still was the fact that each species taken separately showed the same pattern (Fig. 9.11). When the landings of Canada, the United States, Japan, and the USSR were examined separately, they also showed the same general trends, albeit with more variability.

Beamish (1993) also made an intensive study of the period 1976–8, when the Aleutian low was changing most rapidly and a marked cooling of waters offshore was accompanied by a warming of coastal waters. He showed that strong year-classes and above-average survival occurred both in salmon stocks and in the majority of non-salmon species spawning from California to the Bering Sea. These fish had a wide range of life-history types. Beamish concluded that the effect was attributable to improved ocean productivity caused by changes in the intensity of the Aleutian low.

In southern California during this same period (1976–9), the southward-flowing California Current was reduced, apparently by the strengthening of the Aleutian low with its attendant northward airflow along the coast, and there was a marked reduction in the amount of upwelling. Chavez *et al*. (2003) reviewed the literature on regime shifts in the Pacific from the point of view of their effects on sardine and anchovy stocks along the eastern side of the North and South Pacific Oceans. Recognizing that anchovies tend to be abundant when sardines are less abundant, they labeled the periods before and after the 1976–7 regime shift as a cool "anchovy regime" followed by a warm "sardine regime." They pointed out that during the anchovy regime the California Current was stronger and broader, leading to a shallower coastal thermocline from California to British Columbia. This resulted in higher primary productivity. During the sardine regime, with intensification of the Aleutian low, the California Current weakened and moved shoreward. Primary and secondary production decreased and seabird populations declined. The physical and biological changes off Peru were similar.

9.3.3 On multi-centennial scales

Finney *et al*. (2002) produced evidence of large-scale synchronous changes in fish stocks over multi-centennial scales. They studied cores of sediments in two Alaskan lakes known to be the spawning grounds of sockeye salmon, and used a third lake, inaccessible to salmon, as their reference lake. They showed that the nitrogen derived from carcasses of fish that have spawned in the lake and died is significant relative to other sources. Changes in the amount of this salmon-derived nitrogen can be indexed by changing sedimentary $\delta^{15}N$ and by changes in the composition of the diatom flora. They found that large changes in abundance of sockeye salmon occurred over the past two millennia and these changes far exceed decadal-scale variability recorded during the past 300 years. A marked multi-centennial decline in Alaskan sockeye salmon occurred between 100 BC and AD 800, but salmon were consistently more abundant from AD 1200 to 1900.

The authors compared these results with published reconstructions of the abundance of Pacific sardines *Sardinops sagax caerula* and northern anchovies *Engraulis mordax* in the Santa Barbara Basin and Gulf of California. From AD 300 to AD 1200 sardines and anchovies were more abundant, at a time when sockeye were less abundant than average. In general, the fluctuations in abundance of California sardines and anchovies were out of phase with Alaskan salmon over low frequencies. In the twentieth century, the fluctuations have been in phase at higher frequencies. Synchronous variability between the various paleographic records suggest that climate-related factors are influencing the abundance of fish over large geographic areas, but that different mechanisms are operating at different time scales.

9.3.4 Effects on coral reefs

The warming of coastal water associated with a strong El Niño has had serious consequences for coral reefs worldwide (Glynn 1985, 1990, Wilkinson 2002). In 1982–3 surface waters of the eastern tropical Pacific were at 30–31 °C for 5–6 months. This warming caused the corals to lose their symbiotic zooxanthellae, giving them a bleached appearance, after which they died within a month. In the most dramatically affected regions, coral mortality was 90–95%. It is thought that the unusually high temperatures experienced from 1976 to 1983 may already have weakened the corals.

The most intense ENSO events of the last 50 years occurred in 1957–8, 1972–3, 1982–3, and 1997–8. By some measures, the 1997–8 event was the strongest of all. On the coast of East Africa, the proportion of corals suffering bleaching varied from <1% in South Africa to >80% on reefs in northern Tanzania and Kenya. Among the islands of French Polynesia there was extensive bleaching, but the severity varied, forming patches on a scale of 100 km. For example, during the summer of 1998 there was extensive cloud cover over Tahiti, and the damage to corals was relatively light. In the lagoons of Belize there was catastrophic mortality following bleaching, and reef cores indicated that this was the first event of this magnitude for at least 3000 years.

The good news was that in the reefs of Costa Rica, Panama, Colombia, and the Galápagos Islands, where extensive bleaching was recorded in 1983, the damage seemed to be less severe in 1998. There were some indications that the corals may now have symbiotic algae that are more resistant to heat damage. Recovery from bleaching events is very variable, depending in part on the amount of collateral stress induced by pollution and manmade disturbance, and in part on the severity of the heat damage. For example, in Kenya the reefs with the strongest impact of ENSO recovered less than 25% in 2–3 years, while in other parts of Kenya the recovery has been 50–100%. For an update on the extent of coral bleaching worldwide, see www.reefbase.org.

9.4 Summary for the Pacific Ocean

Two main patterns of physical oscillation have been seen in the Pacific Ocean. The first is the El Niño – Southern Oscillation (ENSO), with a periodicity of 4–7 years. The second, with periods of 40–50 years, is the Aleutian low, represented by the Aleutian Low Pressure Index (ALPI) or the distribution of sea surface temperature represented by the Pacific Decadal Oscillation (PDO). Some of the physical and biological expressions of these systems are similar, and in the past they have not been clearly distinguished.

The ENSO is best known for its effect on the anchovy stocks of the Peruvian upwelling system. At the height of the warm phase of ENSO, the thermocline

along the coast becomes much deeper and upwelled water is warm and nutrient-poor. Primary production is greatly reduced, and with it zooplankton abundance and anchovy catches. These changes are a manifestation of a basin-wide phenomenon, with teleconnections worldwide, described in Section 9.2.1. One such teleconnection has been called El Niño North. The warm nutrient-poor equatorial Pacific water spreads northward along the coasts of California, Oregon, Washington, and British Columbia to Alaska. Planktonic species and fish extend their range northward, but primary production is greatly reduced. Under these conditions, some species of fish have improved recruitment but many have poor recruitment. On the eastern side of the North Pacific basin species extend their range southward, as if there is a general counter-clockwise shift in the distribution of coastal species in the North Pacific basin during an El Niño year.

In years in which the Aleutian low in winter is particularly intense, similar effects are seen along the North American coast. The Alaskan gyre increases its current speed and extends further south, increasing the upwelling of cold, nutrient-rich water in the center of the gyre, but driving warm subtropical water north along the west coast of North America. The net result is an increase in productivity of the Alaskan gyre and a decrease in productivity in the California Current. The Aleutian low-pressure system and the associated subarctic gyre were particularly vigorous during the 1940s and again in the 1980s, and three geographically distinct sardine stocks showed high landings in the 1940s and 1980s. Similar fluctuations took place in the North Pacific stocks of sockeye, chum, and pink salmon.

The years 1976–7 and 1988–9 were identified as years in which very fundamental and widespread changes in the physical and biological properties of the North Pacific were taking place, and have been labeled regime shifts. In 1976–7, the system shifted to a mode in which the ALPI was strongly positive and productivity of plankton and fish stocks were high. In 1988–9, many of the physical and biological characteristics were reversed, but not all.

Preliminary evidence from a study of salmon migrations into Alaskan lakes indicates that there is another set of mechanisms causing large-scale fluctuations in fish stocks with a periodicity of several hundred years.

9.5 Biological variability in the North Atlantic

As we saw in Section 9.2.2, the physical properties of the North Atlantic climate are dominated by the North Atlantic Oscillation (NAO). When the NAO is strongly positive (Fig. 9.06a), the Icelandic low, centered between Iceland and Greenland, is deeper and more persistent than normal. Cold Arctic air is drawn southeast over Labrador and the westerly winds across the North Atlantic are more to the south than normal. This brings warm, stormy, wet weather to western Europe. During this phase, the Azores high tends to be higher than normal, bringing stronger winds with increased upwelling to the northwest African coast.

When the NAO is strongly negative (Fig. 9.06b), the Icelandic low is weaker, less persistent, and located further south. It brings relatively warm easterly

winds to the Labrador Sea. At the same time, colder northerly winds are blowing over the Greenland Sea. The westerlies in the North Atlantic are weaker, so that northern Europe is colder than normal. The Azores high is also weaker, with lower wind speeds and decreased upwelling off the northwest African coast.

The NAO is indexed by the atmospheric pressure difference between the Azores (or Portugal) and Iceland. A time series of these differences (Fig. 9.03) shows that either an anomalously high or an anomalously low pattern can exist for many years. For example, the pressure difference was well below average from the mid-1950s to the early 1970s. Since the 1970s, winters with a positive index have predominated. There seems to be some correspondence with global mean air temperature (see Chapter 10). The period 1940 to 1970 was a time of cooling, and since 1970 there has been a period of warming.

9.5.1 Variability in the plankton

In the years between the two world wars, Alister Hardy developed a "continuous plankton recorder" (CPR). It consisted of a towed body with a tunnel through it, along which sea water flowed. Across the tunnel was stretched a fine gauze mesh that unrolled continuously from a spool below and wound onto a propeller-driven spool above that was immersed in formalin. In this way, plankton was sampled and preserved continuously so long as the body was in forward motion. After World War II, a mechanism was put in place to have these recorders towed by merchant ships and ocean weather ships on regular routes (Glover 1967). Samples were collected at a standard depth of 10 m and an attempt was made to obtain records at monthly intervals from 12 different geographical areas (Colebrook 1986). For zooplankton, the record extends from 1948 to the present day, and recent analyses are based on 24 species in 247 series. For phytoplankton, a change in the method of enumeration was made in 1958, so analyses start from that time. Nevertheless, records are available for 24 species in 263 series.

(a) 1940s to 1970s: NAO predominantly negative

Colebrook (1986) derived a time series for the abundance of phytoplankton and mesozooplankton in the North Atlantic, using principal components analysis of the data for all species and all areas (Fig. 9.12). There is often a lag between changing oceanographic conditions and changes in the biota. In the case of the North Atlantic plankton, the period of predominantly negative NAO ended in 1972, but a downward trend in the abundance of plankton continued until 1978 (zooplankton) and 1980 (phytoplankton). It seems probable that the declining abundance of phytoplankton influenced the abundance of the zooplankton that feed on them.

Other analyses of the weather patterns in western Europe (Lamb 1969, Dickson *et al*. 1988a) led to the conclusion that in the eastern North Atlantic, during the time of the predominantly negative NAO, there was a progressive increase in

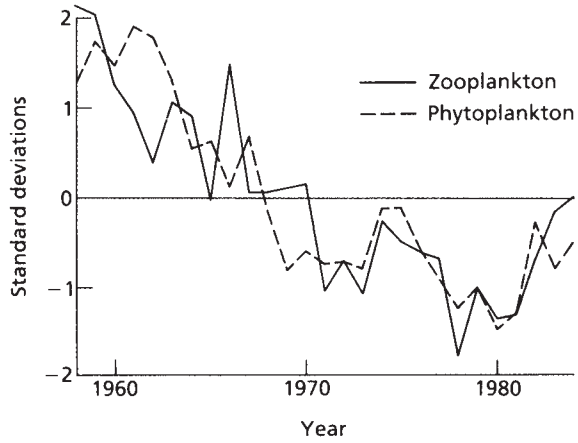

Fig. 9.12 Time series of the abundance of zooplankton and phytoplankton for 1958–84, derived from principal components analyses of the data for all species and all areas. From Colebrook (1986).

the frequency and strength of the northerly winds in winter and spring. This was thought to have caused a delay in onset of stratification, hence a delay in spring blooms of phytoplankton. This in turn was expected to lead to less total primary production and less food available for the zooplankton.

(b) 1980 to 1995: NAO predominantly positive

Open ocean

In seeking to explain the effect of physical changes on the plankton, Reid *et al*. (1998) explored some complicated and poorly understood relations between the NAO and the position of the Gulf Stream. Taylor *et al*. (1998), for instance, reported that the variations in the NAO lagged by two years can account for 60% of the annual variance in the latitude of the Gulf Stream, and a further 9% can be accounted for by including the Southern Oscillation Index. Also, when the NAO is strongly positive and cold Arctic air blows from the northwest across the Labrador Sea, convective intermediate-water formation in the Labrador Sea is vigorous.

The significance of these processes for the plankton is that there are good correlations between the biomass of phytoplankton in the North Atlantic and both the NAO and the position of the Gulf Stream (Taylor 1995). When the NAO is strongly positive the phytoplankton to the west of the UK, in the central northeast Atlantic, shows a positive biomass anomaly and the water a positive temperature anomaly. At the same time, the phytoplankton in the northern northeast Atlantic shows a declining trend and the water has negative temperature anomalies.

Calanus finmarchicus and *C. helgolandicus* are two of the most abundant species in the zooplankton. The former species thrives in colder water. When the NAO

was positive and waters of the central and east Atlantic were showing warm anomalies, *C. finmarchicus* showed a declining trend. *C. helgolandicus*, on the other hand, thrives in warmer water and showed a rising trend when the NAO was positive (Planque and Fromentin 1996, Fromentin and Planque 1996). *C. finmarchicus* is normally more abundant than *C. helgolandicus*, so a positive NAO index was characterized by a declining trend in abundance of *Calanus*. Planque and Reid (1998) showed that in the whole time series of the CPR surveys, the NAO index accounted for 58% of the variation in abundance of *Calanus finmarchicus*.

As with the phytoplankton discussed earlier, this explanation for the effect of the NAO on the zooplankton emphasizes the influence of temperature rather than the influence of wind mixing, although both are involved in the timing of the spring bloom of phytoplankton. Rising temperature could shorten the turnover time of the phytoplankton. Warmer surface water promotes earlier and more intense stratification of the water column, hence an earlier spring bloom. Edwards *et al*. (2001) showed from CPR records that in the area northwest of Scotland the bloom in 1990–95 started about one month later than the average for 1960–95. It is likely that the responses of the two species of *Calanus* are the result of changing food conditions, life-history adaptations to different temperature regimes, and competition between the species.

In the period 1961 to 1991, when the NAO index showed a rising trend, the waters of the Gulf of Maine showed a trend to rising temperatures and the abundance of *Calanus finmarchicus* increased (Conversi *et al*. 2001). The SST was positively correlated with the NAO index with a lag of two years, and the abundance of the copepods was positively correlated with a lag of four years. The positive correlations held at all scales, seasonal, interannual, and inter-decadal. It is not clear why *C. finmarchicus* shows a positive correlation with temperature in the Gulf of Maine but a negative one in the rest of the North Atlantic. It is possible that the abundance of *C. finmarchicus* in this area is more a function of currents transporting developmental stages from deeper water than of the response to temperature *per se* (Greene and Pershing 2000).

Enclosed seas and coastal habitats

In the North Sea, the period 1980 to 1995 was a time of increasing phytoplankton biomass, increasing zooplankton abundance, and explosive growth of populations of some kinds of fish, such as horse mackerel *Trachurus trachurus* (Reid *et al*. 2001; Fig. 9.13). There were also unusual outbreaks of populations of organisms characteristic of the open Atlantic Ocean, such as *Thalassiosira* and *Ceratium* in the phytoplankton and various crustacean larvae and siphonophores in the zooplankton. The suggested explanation is that the positive NAO index was associated with strong southwest winds, which increased the exchange of water between the North Sea and the open Atlantic (Holliday and Reid 2001). It was suggested that 1988 could be regarded as a year of regime shift in the North Sea.

Those same southwest winds led to a transport of high nutrient water from the Kattegat near Denmark to Gullmar Fjord in Sweden. Within Gullmar Fjord, in the years 1985–96, the NAO index accounted for 45% of the variance in spring

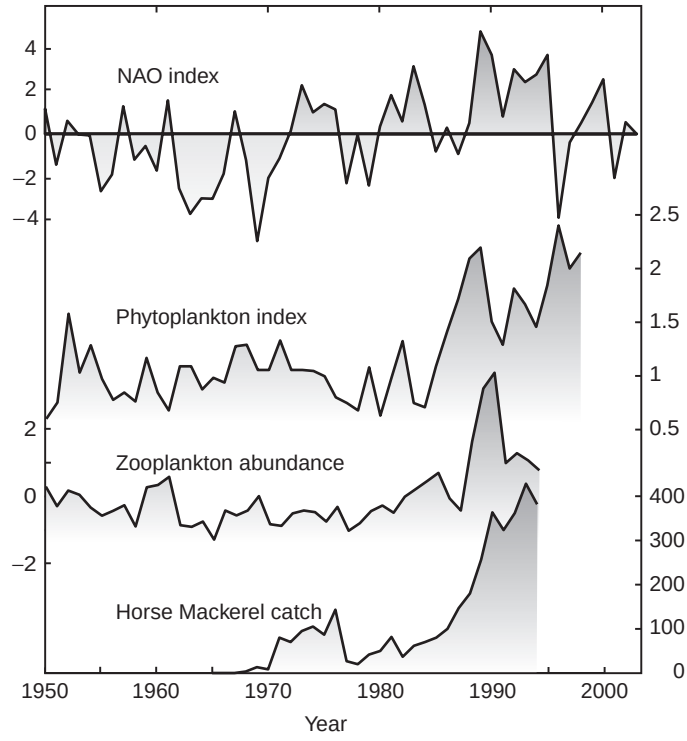

Fig. 9.13 North Sea, 1950–94. Diagram to illustrate the correspondence between the NAO index, the phytoplankton index, the zooplankton index, and horse mackerel catches. The phytoplankton index is the annual mean color from CPR surveys, averaged for the whole North Sea. Zooplankton index is first principal component of fluctuations in the abundance of zooplankton in CPR surveys of the North Sea. Data from Reid *et al*. (2001) and Holliday and Reid (2001). Figure design adapted from fig. 23, *IGBP Science* no. 5 (www.igbp.kva.se).

primary production, 63% of population growth between April and May, and over 90% of the variation in the abundance of the toxic dinoflagellate *Dinophysis* (Lindahl *et al*. 1998, Belgrano *et al*. 1999).

9.5.2 Evidence from the benthos

In a time series of observations on changes in the biomass, abundance, and species number in the subtidal benthos at a site off the German coast of the southern North Sea, Kroncke *et al*. (1998) found clear correlations between the properties of the benthos in the summer and the NAO index of the preceding winter. The authors had previously ruled out changes in sediment composition, coastal morphology,

hot summers, or storm events as important factors in the changes in the benthos. It seemed that mild winters associated with a strongly positive NAO were conducive to increases in the benthos. Particularly large changes in the benthos occurred in 1989 and 1990, reinforcing the idea that this was a period of regime change in the North Sea.

Further north, in western Sweden, Tunberg and Nelson (1998) examined time series of benthic macrofauna biomass and abundance extending 12–20 years, taken from 10 stations at depths of 10 m to 300 m. The data showed cyclical patterns of 7–8 years and the stations down to 100 m were in phase, while the station at 300 m was not. Spectral analysis of the 130-year record of the NAO index indicated that the dominant oscillatory component occurred at a period of 7.9 years. River run-off was well correlated with the NAO index, and the authors suggested that the rivers influenced the abundance of the benthos by changing the nutrient loading and patterns of stratification in coastal waters. Hagberg and Tunberg (2000) similarly found that abundance of macrobenthos in the inner part of Gullmar Fjord correlated with the NAO index, and suggested that the effect was mediated by river run-off.

Cohen and McCartney (reported in Drinkwater *et al*. 2003) used oxygen isotopes and calcification rates to reconstruct the growth history of brain corals near Bermuda. They found that growth was strongly correlated with the NAO index.

9.5.3 Evidence from fish stocks

Fish stocks are noted for their variability. In the face of declining stocks, managers have tended to worry about whether the cause is overfishing, pollution, or destruction of habitat. Until recently, not much attention has been given to natural fluctuations associated with natural changes in the environment. It is now becoming clear that major changes in abundance can be caused by environmental change, quite distinct from human impacts. We have already reviewed evidence for changes in fish stocks correlated with changes in physical aspects of the Pacific Ocean. Similar evidence for a strong influence of environmental factors on the abundance of fish is emerging for the Atlantic Ocean.

The Atlantic cod **Gadus morhua**

Atlantic cod is a major contributor to commercial fisheries in the North Atlantic. Planque and Fredou (1999) conducted a meta-analysis on data from nine major stocks, from Georges Bank in the west to stocks around Newfoundland, Greenland, Iceland, western Europe, and the Barents Sea. They paid particular attention to the relationship of recruitment to temperature near the sea floor. They found that for stocks located in cold water, recruitment was positively related to temperature, while for stocks in warm water the opposite was true. For several stocks in the middle of the temperature range, there was no significant relationship with temperature.

However, the effect of temperature on recruitment is only one of many ways in which physical factors may influence cod stocks. Different aspects have been investigated in the various stocks.

Cod of the Barents Sea

The cod stock of the Barents Sea, north of Norway and western Russia, is one of those for which warm water favors good recruitment. Ottersen and Stenseth (2001) evaluated several statistical models that predicted year-class strength from climate variables during the winter the year-class was spawned. The single most important variable was the NAO index, which alone accounted for 53% of the recruitment variability. The suggested mechanism is that in years when the NAO is positive, the increased inflow of warm water from the southwest transports more *Calanus finmarchicus* into the Barents Sea, providing good feeding conditions for the cod larvae, and the higher temperatures promote higher biological activity at all levels. For example, the consumption of capelin *Mallotus villosus* by cod in the Barents Sea has been shown to increase by 100,000 tons per 1 °C rise in temperature (Bogstad and Gjøsæter 1994). Postulated interactions between the NAO and Barents Sea cod are illustrated in Fig. 9.14.

The west Greenland cod

Between 1917 and 1936, the cod stocks of west Greenland spread progressively further north until they were being caught far above the Arctic circle, near Disko

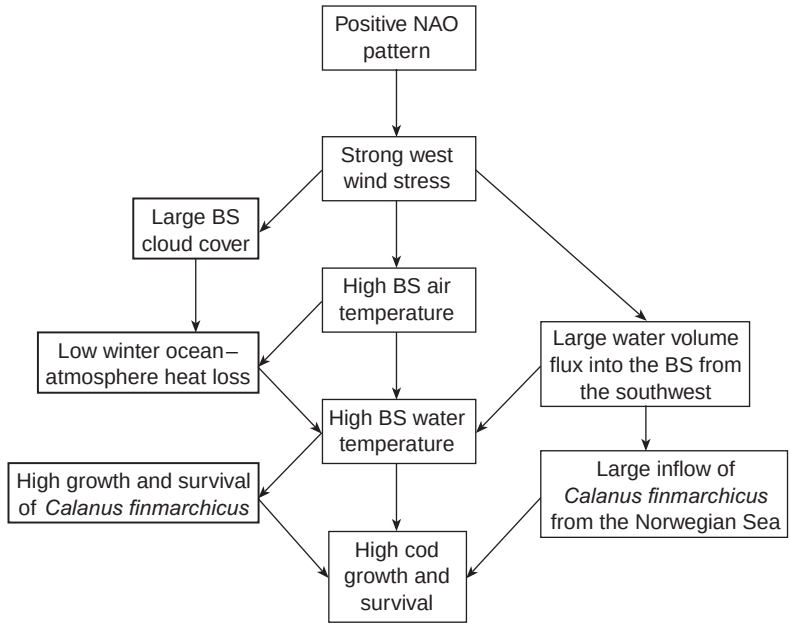

Fig. 9.14 Postulated mechanism linking the NAO to growth and survival of cod in the Barents Sea (BS), from Ottersen and Stenseth (2001). Copyright (2001) by the American Society of Limnology and Oceanography, Inc.

Bay and beyond. This was a time when the NAO index was mostly positive. Although the NAO index began a declining trend about 1948, catches remained high until the early 1960s, then declined and have not recovered.

Tagging experiments showed that when the west Greenland stocks were strong, adults made the 1500 km journey to spawning grounds south of Iceland, and larvae were carried back to Greenland on the Irminger Current. When the weather patterns changed during the 1950s, and the NAO was mostly negative, there were strong northerly winds to the east of Greenland in winter. Cushing (1982) suggested that these conditions might have disrupted the drift of eggs, larvae, and juveniles from Iceland to Greenland. Dickson and Brander (1993) pointed out that before 1950 there were strong easterly winds in the area that would have assisted the movement of larvae in the Irminger current, but after 1950 these winds weakened. It seems that the supply of larvae from Iceland was interrupted about 1950, but the stocks west of Greenland continued to thrive until the early 1960s.

Cod of the northwest Atlantic

The stock of cod on the northern Grand Banks and the Labrador Shelf, once the world's largest cod stock, was heavily exploited in the 1960s, suffered a precipitous decline in the 1970s, rallied briefly during the 1980s, then declined to such low levels that the Canadian government closed the fishery in 1992. A decade later, it showed little sign of recovery. Mann and Drinkwater (1994) suggested that three factors contributed to the collapse of the stock: (i) unfavorable environmental conditions, (ii) reduction in the range of age classes in the stocks, and (iii) overfishing. It was argued that although the stocks had survived equally adverse environmental conditions in earlier decades, reduction in stock biomass and in the range of year-classes had reduced the ability of the stock to survive adverse environmental conditions from about 1970 onward. The synergistic effect of environment and exploitation was deemed important, and a factor to be considered in the future management of this and other stocks.

The connection suggested by Mann and Drinkwater (1994), between the NAO and the growth and survival of cod, was as follows. When the NAO was strongly positive, cold northwest winds over the Labrador Sea caused anomalously cold water on the Labrador Shelf and abnormally large areas of ice coverage. During spring, this water mass moved slowly south. Melting ice led to anomalously low salinity in the surface waters over the Grand Banks and the volume of cold water in the intermediate layer was greater. Hence, conditions on the Grand Banks were unfavorable for the growth and survival of cod larvae.

The relative importance of overfishing and adverse environmental conditions in the collapse of this stock was reviewed in detail by Drinkwater (2002). While there is no doubt that overfishing was a major factor in the decline of the stocks, there is good evidence that environmental conditions were extremely adverse and would have accentuated and accelerated that decline. As we have seen, the NAO index around 1990 had risen sharply and showed the highest and most consistently positive values of the twentieth century. This meant that there were exceptionally cold winters in Labrador, with strong northwesterly winds

bringing Arctic air to the Labrador Sea. This resulted in earlier and more extensive ice formation and anomalously low water temperatures over the Labrador Shelf and the Grand Banks. Along the cod migration routes during the early 1990s, the fish would have experienced temperatures 1 °C colder than was typical during 1930–89, and would have spent three times longer in waters below 0 °C.

Drinkwater (2002) showed that lower temperatures led to slower growth rates and that 30–50% of the decline in cod biomass was due to reduced weight of fish at a given age. It is known that fishermen were systematically dumping underweight cod in the hope of filling their quota with larger fish in better condition. This practice, known as "high grading," contributed to the very high fishing mortalities recorded during the last decade of the fishery.

The cold conditions almost certainly contributed to poor recruitment. There were fewer fish, in poorer condition, producing fewer eggs. Harsh environmental conditions would have led to more larval mortality. At the same time, the stock was suffering from the removal of most of the older, larger fish, which are known to produce larger numbers of eggs, of better quality, than small fish. There was also a southward movement of the stock, into conditions to which they were less well adapted, so that recruitment would probably be reduced.

Hutchings and Myers (1994) had pointed out that equally cold conditions had occurred on the Grand Banks in the 1970s, and the stock had not collapsed. Drinkwater (2002) argued that in the 1970s the cold was of shorter duration and the stocks had a higher proportion of older fish to enable them to maintain recruitment during adverse conditions. It is clear that over-exploitation, in conjunction with adverse environmental conditions, were the two major factors causing the collapse of the stock. Good management requires that stocks be maintained in a condition where they are able to withstand naturally occurring adverse environmental conditions.

At this stage, it is not clear why in the analysis of Planque and Fredou (1999) the relationship of recruitment to temperature seems to be slightly negative in the northern cod stocks. Is it possible that in this heavily exploited stock recruitment has been more affected by removal of the spawning biomass than by environmental factors?

Cod and other gadoids in the North Sea

Between 1960 and 1970, a five-fold increase occurred in the stocks of gadoids (cod, haddock *Melanogrammus aeglefinus*, whiting *Merlangus merlangus*, coalfish *Pollachius carbonarius*, and Norway pout *Trisopterus esmarki*) as a result of good larval survival leading to strong year-classes. It has become known as the gadoid outburst. Cushing (1982) invoked his match/mismatch hypothesis (Cushing 1975) to explain the good year-classes. His hypothesis states that a year-class of fish is strong if the timing of the zooplankton maximum matches the timing of the appearance of the larvae requiring the zooplankton as food, and vice versa. He produced evidence to show that a delay in the zooplankton peak of biomass is favorable to the survival of cod larvae, and suggested that the strong northerly

winds of the 1960s had the effect of delaying the development of plankton in spring, to the advantage of the cod.

The analysis of Planque and Fredou (1999) showed that cod stocks of the North Sea, the Irish Sea, and the Celtic Sea had a trend towards better recruitment at lower temperatures. If Cushing's match/mismatch hypothesis is valid, it is not a question of better survival at lower temperatures, *per se*, but of better survival when the spring zooplankton maximum is delayed by cold weather. Similar considerations could apply to cod on the Grand Banks.

The match/mismatch hypothesis has often been questioned on the grounds that it has only circumstantial evidence to support it. Platt *et al*. (2003b) used remotely sensed color data from the years 1979–2001 to determine the timing of the spring bloom in each of 5604 pixels of an area of the Scotian Shelf where eggs and larvae of haddock occur. They compared these data with information on the abundance of juvenile haddock, normalized to spawning biomass. They found that they could account for 89% of the variance in larval survival by variation in the timing of the spring bloom (Fig. 9.15). There were two exceptionally strong year-classes of haddock, 1981 and 1999, and in each of these years the spring blooms occurred unusually early. Details of the trophic links were not investigated, but this is the first direct evidence for a link between environmental factors and larval survival involving the timing of the spring bloom.

Beaugrand *et al*. (2003) provided convincing evidence for the dependence of cod recruitment on the quality, quantity, and timing of zooplankton blooms in the North Sea, and in doing so provided strong support for the match/mismatch hypothesis. They analyzed nearly 50,000 samples from the Continuous Plankton Recorder surveys of the North Sea and Skagerrak, quantifying six parameters: (i) total calanoid copepod biomass, (ii) mean size of calanoids, (iii) abundance of *Calanus finmarchicus*, (iv) abundance of *C. helgolandicus*, (v) abundance of *Pseudocalanus*, and (vi) abundance of euphausiids. The record was divisible into three periods

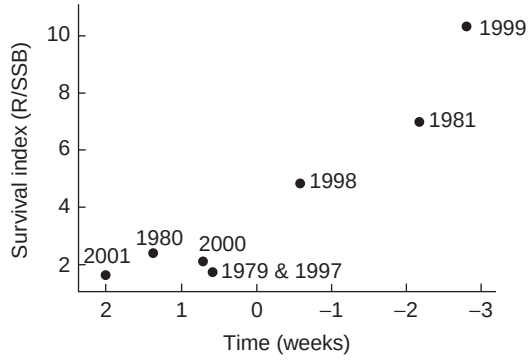

Fig. 9.15 The survival index for haddock on the Scotian Shelf, eastern Canada, plotted against anomalies in the timing of the spring bloom, as determined from remotely sensed color images. R/SSB, Recruitment/Spawning Stock Biomass. From Platt *et al*. (2003b).

with clear differences: 1958–62, 1963–83, and 1984–99. The period 1963–83 was characterized by high abundance of all four classes of food for cod, and by high mean size of calanoid copepods. In twelve of the 21 years during this period, estimated cod recruitment was higher than at any time since 1921, and this was the time of the gadoid outburst. After 1983, the copepods available to cod larvae became progressively smaller and gadoid stocks decreased drastically. These findings support the match/mismatch hypothesis, but the mismatch is in part the result of a switch from a predominance of *C. finmarchicus*, which has its peak biomass early in the year, to a predominance of *C. helgolandicus*, which has two peaks of abundance in the year. Changes in the physical environment of the North Sea, with a regime shift in 1988, were discussed in Section 9.5.1.

Deep-water fish stocks and the Great Salinity Anomaly

The period 1956 to 1969 was one in which the NAO became increasingly negative, culminating in the most negative values of the twentieth century (Figs. 9.03 and 9.07). There was a positive pressure anomaly over Greenland averaging 7 hPa during winter. It was accompanied by abnormally strong and cold northerly winds, especially in winter. Sea ice in the Greenland Sea expanded its range each year and reached a maximum in 1968.

One result of these changes was that abnormal amounts of polar ice and water were brought south to join the East Greenland and East Icelandic Currents so that they became cooler and fresher (Dickson *et al*. 1988b, Cushing 1988). The East Icelandic Current, normally ice-free, began to transport and preserve drift ice, and the East Greenland Current increased greatly in volume. Furthermore, the surface salinities north of Iceland were so low that the water froze before its salinity (and density) could increase through mixing with underlying layers. Below the surface ice, there formed a layer of cold, fresher water about 200–300 m deep that was isolated from underlying layers. Although the effect was first seen in 1962, this water mass reached its minimum temperature in 1967 and minimum salinity in 1968. It retained its identifiable characteristics for nearly two decades, while making an enormous journey around the subarctic gyre (Fig. 9.16). The Great Salinity Anomaly (GSA) traveled around the southern tip of Greenland (1969–70), south along the Labrador coast to the Grand Banks (1971–2), turned eastward along the subarctic front to pass the weather ship *Charlie* in the mid-Atlantic in about 1974, and on to the northwest of the British Isles in 1975 and 1976. Minor portions of the GSA are thought to have penetrated many parts of European coastal waters, but the signal rapidly became confused with local salinity variations. By 1977 the GSA reached the ocean weather ship *Metro* off the Norwegian coast, and in 1978 and 1979 it was off the North Cape and to the west of Spitzbergen. Finally, although the evidence is incomplete, it appears that part of the GSA entered the southward-flowing East Greenland Current in 1981–2. At about the same time, these changes also appear to have found their way into the dense water that flows over Denmark Strait to form the bottom water in the Labrador Sea (Lazier 1988).

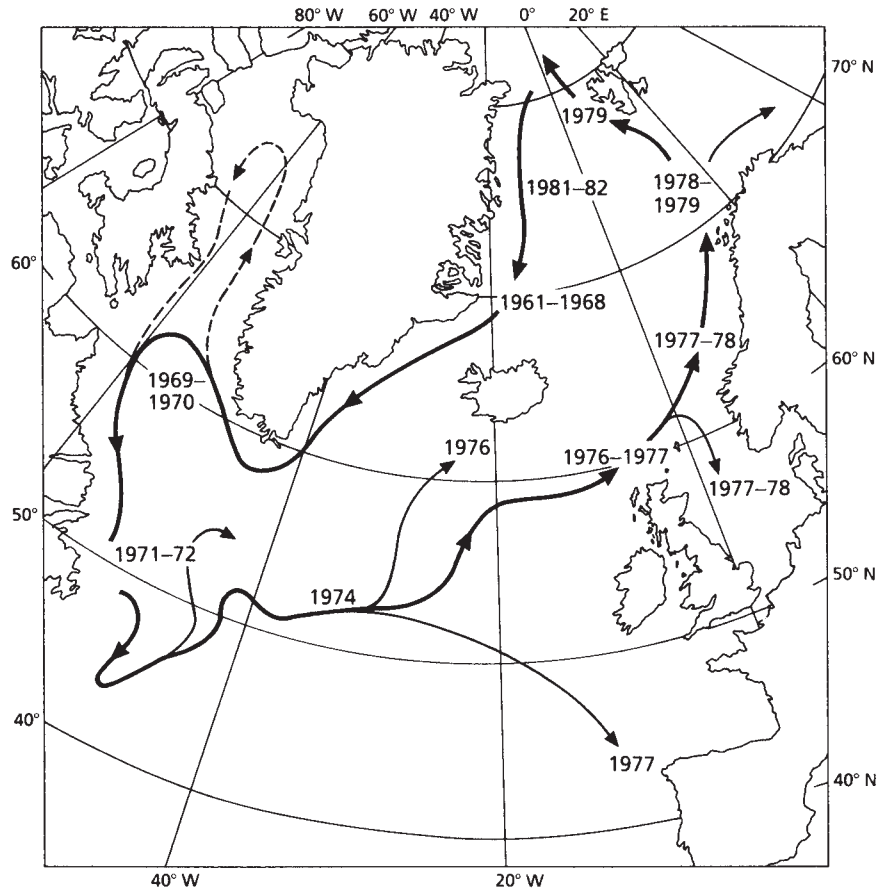

Fig. 9.16 Route followed by the Great Salinity Anomaly, from its formation north of Iceland in 1961–2 to its return to the east coast of Greenland in 1981. Modified from Dickson *et al*. (1988b).

Naturally, the GSA did not retain absolute integrity, for mixing with adjacent waters as it traveled reduced its signal. Nevertheless, from an original water mass just over 2 °C cooler and 0.55 less saline when it left the north of Iceland in 1968, it was still 0.7 °C cooler and 0.11 less saline off the North Cape a decade later. It is possible to calculate that there was a "salt deficit" of approximately 72×10^9 tons as it passed south along the Labrador coast, and a deficit of 47×10^9 tons as it passed through the Faeroe–Shetland channel to the north of Great Britain (Dickson *et al*. 1988b). Since the GSA originally approached Iceland from the Arctic Ocean, it is assumed that high-latitude regions north of the Greenland Sea became correspondingly saltier. The total distance traveled between 1968 and 1979 is of the order of 10,500 km, which indicates a mean speed of about 3 cm s^{-1}, which is consistent with other estimates of the mean circulation speed of the subpolar gyre. What are the biological consequences of this major perturbation of the North Atlantic?

There were marked changes in the plankton community north of Iceland during the formation of the GSA. Astthorsson *et al*. (1983) showed that on various sections off the north coast of Iceland the primary production measured at 10 m depth in spring averaged 2.6 mg C m^{-3} h^{-1} during 1958–64, but between 1965 and 1971 it was only 0.7 mg C m^{-3} h^{-1}. During the same periods, the volume of zooplankton obtained from a standard net haul changed from 10–30 mL per haul to less than 5 mL. They speculated that the presence of the cold, low-salinity water caused a year-round stratification that prevented the renewal of nutrients in the surface layers prior to the spring bloom. This restraint in turn led to greatly reduced primary production and consequently a greatly reduced build-up of zooplankton populations.

On the Grand Banks during the passage of the GSA in 1973, the continuous plankton recorder network indicated that the biomass of phytoplankton was reduced to less than one-third of the average from the previous 13 years, and that similar reductions occurred in the biomasses of copepods and euphausiids.

Cushing (1988) examined the spawning success of 15 stocks of fish whose breeding grounds were thought to lie in the path of the GSA. He performed his analysis by noting the distribution of year-classes in the catches. In 11 of those stocks, the year-classes spawned during the low-salinity years were significantly below normal abundance. Icelandic summer herring had anomalously low abundance from 1965 to 1971. Similarly, Icelandic spring herring had poor year-classes over an even longer period. The effect was visible in cod stocks of east and west Greenland, and the southern Grand Banks, but not in the stocks off Labrador and the northern Grand Banks. Many stocks in the northeast Atlantic and northeast Arctic showed the effect, but some did not, and the reason is not clear.

Low salinity in itself is not thought to cause mortality of young stages, but lowering of temperatures would extend the period of larval development and increase the risk of mortality from predation and other sources. Cushing (1988) looked to reduced food supply as the chief cause of reduced breeding success. In seeking a connection between the physical characteristics of the GSA and the reduced plankton production, he emphasized the possibility that the cooler water would lead to a delay in the onset of summer stratification and hence a delay in the onset of the spring bloom.

It is interesting to note that the formation of the GSA took place in the 1960s, during a period of strongly negative NAO index, but the effect could be traced throughout the decade of the 1970s. It is a clear example of the lags in marine systems, which must be taken into account when looking for correlations between physical and biological phenomena.

Small pelagic fish in coastal waters of western Europe

In the English Channel, herring *Clupea harengus* are near the southern end of their range, while sardines, or pilchards, *Sardina pilchardus* are near the northern end of theirs. Regular oscillation has taken place between herring in cool periods and sardines in warm periods (Southward *et al*. 1988). As we have seen, the cooling

periods correspond to negative values of the NAO, while warm periods correspond to high positive values. Taking the North Sea and the English Channel as a whole, there has been a north–south migration of the boundary between herring and pilchard stocks. In addition, as we saw in Section 9.5.1(b), the productivity of these waters has changed due to changes in the amount of water exchanged between the open Atlantic and these semi-enclosed seas.

Detailed studies that illustrate the changes associated with the changing NAO index were made in the English Channel from early in the twentieth century. For the first 25 years, the NAO was predominantly positive and relatively warm air was brought to the shores of western Europe. It is probable that there was a corresponding warming of coastal waters, or movement of warm water masses to more northerly locations. Cushing (1982) documented the northward movement of animals in the eastern Atlantic during this period. There were three main groups of events. First, an unusually large number of surface-living and pelagic subtropical animals were carried to western France and the British Isles. These included the "Portuguese man-of-war" jellyfish *Physalia physalis*, two species of goose barnacle *Lepas*, and loggerhead turtles *Caretta*. Second, Atlantic, as opposed to Arctic, species of fish and bottom-living animals reached further north than they had previously been recorded. Swordfish *Xiphias gladius*, pollack *Pollachius pollachius*, and ray *Torpedo nobiliana* appeared in Icelandic waters, cod and haddock appeared in the Barents Sea, and the hermit crab *Eupagurus*, together with three species of benthic mollusks, appeared on the Murman coast for the first time. Third, in waters off Nova Scotia there were, during this period, an unusually large number of new records of subtropical species (borne, presumably, by the Gulf Stream) but also of Arctic fish species. We have seen that when the North Atlantic Oscillation pressure index is positive, winds tend to blow from a northerly direction over Labrador, and the weather is colder. The presence of Arctic species off Nova Scotia may reflect a cooling of coastal waters of eastern Canada, with perhaps a strengthening of the Labrador current. All these events reached their peak in the period 1925–35, which Cushing called "the dramatic decade."

The English Channel ecosystem

The end of the dramatic decade marked the beginning of a major change in the biota of the English Channel. Most of the observations on this change were made by staff of the Marine Laboratory at Plymouth, and the most important evidence was collected and summarized by Sir Frederick Russell (1973), so the event is known as the Russell cycle.

The story begins with a decline in recruitment to the herring stock in the western part of the English Channel, beginning in 1925. The last recorded year-class entered the fishery in 1931, and the Plymouth herring stock collapsed in 1936. Throughout this period, macroplankton was being regularly monitored at international station *E-1*, off Plymouth, and samples were taken at the surface and near the seabed for phosphate analysis. It had previously been established that two species of the arrow worm *Sagitta* tended to occur in different water masses and

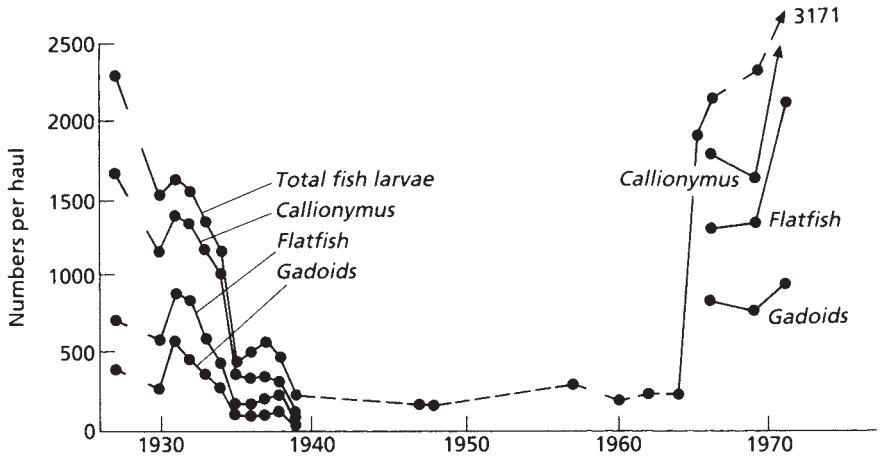

Fig. 9.17 Changes in the abundance of fish larvae in the English Channel 1926–72. These changes are part of the Russell cycle. After Russell (1973).

could be taken as indicators of those water masses. *S. setosa* characterized water that had been found to be resident in the English Channel while *S. elegans* characterized water occurring to the west of the channel, south of Ireland. In the autumn of 1931, the quantity of macroplankton declined by a factor of four, and *S. elegans* was replaced by *S. setosa*. During the next decade, the number of non-clupeid fish larvae (e.g., flatfish, cod family) declined drastically (Fig. 9.17), but the number of pilchard eggs increased. During the same period, the amount of phosphorus present in the water column during winter also declined. The whole ecosystem of the English Channel had changed from one dominated by herring, macroplankton, and bottom-living fishes to one dominated by pilchards and small plankton.

Between 1965 and 1979, the situation reversed itself. In 1965 the total number of fish larvae increased by an order of magnitude. Over the next five years, the winter level of phosphorus rose to pre-1930 levels. In 1970, *S. elegans* came to predominate over *S. setosa* and by 1978 its abundance was back to earlier levels. During the 1970s the number of copepods returned to pre-1930 levels and the number of pilchard eggs decreased. In ecosystem theory, it has long been recognized that multiple stable states may exist for a particular community of organisms, and that relatively small perturbations may cause a flip from one stable state to the other. The point of separation between the two states is referred to as a bifurcation. Discussion of these ideas is to be found in May and Oster (1976), Allen (1985), and Mann (1988). When changes in the North Atlantic Oscillation pressure index caused changes from colder, more northerly weather to warmer, more westerly weather off the coast of western Europe, the biological community of the English Channel was induced to flip from one stable state to another.

The North Sea ecosystem

Between 1965 and 1977, the landings of herring from the North Sea fell from about 1.2 million tons to a very low level, and the fishery was closed from 1977 to 1980. As the stocks fell, so did the recruitment, but from 1980 onward there was greatly improved recruitment from a low biomass of spawning fish, giving reason to suspect that the change was associated with changing environmental factors (Bailey and Steele 1992). The year 1980 was the beginning of a strong positive trend in the NAO.

Aebischer *et al*. (1990) drew attention to parallel changes in climate, plankton, herring, and birds in both the North Atlantic and the North Sea (see also Section 9.5.1). In 1980, all of these factors changed. The climate of western Europe began to warm, the plankton biomass began to increase, and the herring populations showed improved recruitment. Munk and Christiansen (1990) documented improved survival in the herring spawned off southern Scotland and northern England, which would be consistent with these trends. Corten and van de Kamp (1992) reported that during the early 1980s the summer distribution of herring moved from the southeast coast of Scotland, north to the edge of the continental shelf and to the Norwegian Trench. Many juvenile herring from these stocks grew up in the approaches to the Baltic Sea.

Lindeboom *et al*. (1994) documented several changes that occurred in the North Sea at about the same time. In addition to the changes in plankton, herring, and kittiwake *Rissa tridactyla* stocks reported by Aebischer *et al*. (1990), the numbers of dogfish caught declined sharply, starting in 1978 and continuing for a decade. Also in 1978, the velvet swimming crab *Necora puber* disappeared from Dutch coastal waters. In the Wadden Sea, inshore of the chain of islands along the Dutch and German coasts, a sharp increase in phytoplankton and in benthic biomass occurred in the late 1970s; at the same time the number of young eider ducks *Somateria mollissima* increased by two orders of magnitude. The phytoplankton of this area showed a sharp increase in *Phaeocystis* blooms. All of this evidence strongly suggests a major change in the ecosystem of the North Sea and adjacent waters, which Lindeboom and colleagues tentatively characterized as a switch of emphasis from benthic production to predominantly pelagic production.

As we saw in relation to plankton (Section 9.5.1; Fig. 9.13) the late 1980s saw an intensification of the positive NAO winter index, and there were corresponding increases in the biomass of phytoplankton and zooplankton, which in turn were followed by a spectacular increase in the landings of horse mackerel.

Sardine stocks of the eastern Atlantic

Early studies of correlations between landings of sardines *Sardina pilchardus* off Portugal and North Atlantic weather patterns had given conflicting results. Strong northerly winds cause strong upwelling, but the landings of sardines were negatively correlated with some versions of an upwelling index. Guisande *et al*. (2001) made more detailed studies. Using the landings of juvenile sardines in the

port of Vigo, 1980–2000, as an index of recruitment, and calculating the Ekman transport from the wind stress, they found differing relationships of recruitment to Ekman transport in different months. They pointed out that strong offshore Ekman transport implies both strong upwelling of nutrients, which could be a positive factor in larval survival, and strong transport of larvae to offshore waters where there is not enough food to survive. Recruitment was highest in those years with moderate upwelling in February, weak upwelling in March/April, high upwelling during May to August, and low NAO values.

The authors suggested that the moderate wind stress and upwelling in February is associated with a well-stratified surface layer, which gives an early spring bloom, and the weak upwelling in March/April reduces the amount of offshore loss during the spawning season. Strong upwelling in summer stimulates primary and secondary production, hence growth and survival of the juveniles at a time when they are active enough to avoid being carried offshore. Finally, they observed that in years with a low NAO, winter/spring temperatures are warmer and offshore transport is lower.

In contrast, Belveze and Erzini (1983) had previously shown a positive correlation between strength of upwelling and landings of *Sardina pilchardus* off Morocco. There is no convincing explanation for the difference in response to enhanced upwelling by the same species in different areas. The relationship may depend on the range of strength of upwelling that occurs, and on its timing in relation to the life history of the sardines.

The Iberian Peninsula is the northern extreme of the Canary Current upwelling system. Binet (1997) analyzed fisheries and climatic data from the southern end of the same system, off Senegal and Mauritania. He found two periods when southward alongshore wind activity was anomalously high: in the early 1970s and from 1986 onwards. On each occasion, landings of sardines were about three times the long-term average. This increase was accompanied by a southward extension of the range of the stock, for example from a southern limit of 28° N in 1966 to 15° N in 1974. Sardine catches were best correlated with the alongshore wind stress of two years earlier. It was shown that each wind-stress event induced enhanced upwelling, which favored larval survival, except in the few days after hatching, when turbulence and offshore advection reduced survival.

Tuna and other large pelagics

There have been several studies linking the abundance of tuna and other large pelagics to the magnitude of the NAO (reviewed in Drinkwater *et al*. (2003). In the eastern Atlantic the mean recruitment of bluefin tuna *Thunnus thynnus* during periods of high NAO index was nearly double the recruitment in low NAO index years. The opposite is true of northern albacore *Thunnus alalunga*. The eastern bluefin tuna winters and spawns around the Canary Islands and off Morocco, whereas the albacore winters and spawns on the western side of the Atlantic. A positive NAO is associated with warm water in the eastern Atlantic, but cooler water in the western Atlantic, and vice versa. During the early part of the twentieth century, when positive NAO winter indexes predominated, bluefin

tuna and swordfish spread north to Iceland and the Faeroes. During low NAO conditions during the 1960s the bluefin disappeared from these waters, but reappeared during the very high NAO indices of the 1990s.

Atlantic salmon Salmo salar

There is a considerable body of circumstantial evidence that the variability in Atlantic salmon stocks is linked to the NAO (Dickson and Turrell 2000, Drinkwater *et al*. 2003). For example, the trend in the Scottish catch of salmon, which may be used as an index of the general situation in Europe, is negatively correlated with the NAO index. During the positive trend in the NAO in the last 2–3 decades, coastal waters of western Europe have been warming, but those of the central and northwest North Atlantic have been cooling. European salmon spend a large proportion of their lifetime in waters around Iceland and Greenland and show distinct preferences for water above 4 °C. The recent trend in the NAO has caused the area of their preferred thermal habitat to greatly decrease. North American salmon occupy similar habitats during their marine phase and the trend in landings is similar to that in Europe.

Evidence from seabird populations

An ICES working group on seabird ecology (Anonymous 1998) found significant correlations, in the 1950s to 1990s data, between the NAO index and breeding numbers of seabirds on the German Wadden Sea coast. The species involved were fulmar *Fulmarus glacialis*, herring gull *Larus argentatus*, lesser black-backed gull *Larus fuscus*, common gull *Larus canus*, kittiwake *Rissa tridactyla*, black-headed gull *Larus ridibundus*, Sandwich tern *Sterna sandvicensis*, guillemot *Uria aalge*, and razorbill *Alca torda*. In the light of evidence of increases in phytoplankton, zooplankton, benthos, and fish in the North Sea during the positive trend of the NAO, these results may not be surprising. However, the working group drew attention to another possible reason for the changes. During the 1960s there was widespread decline of seabird populations in the Wadden Sea as a result of contamination with organochlorine pesticides and since that time there has been a slow recovery. More information is needed to distinguish effects of the NAO from effects of pollutants.

Breeding numbers of cormorants *Phalacrocorax carbo*, arctic terns *Sterna paradisaea* and common terns *S. hirundo* in the Wadden Sea showed no significant correlations with the NAO. An examination of changes in various UK seabird populations showed no significant correlations with the NAO.

9.6 Summary for the North Atlantic

It is now clear that the changes in atmosphere and ocean indexed by the North Atlantic Oscillation have far-reaching effects on all levels of marine ecosystems: phytoplankton, zooplankton, benthos, fish, and birds. In general, both

the atmospheric events and the biological events are out of phase on the two sides of the Atlantic.

Fluctuations in the NAO (Figs. 9.03 and 9.07) enable us to divide the years of the twentieth century into four main groups. Before 1930 the index was predominantly positive, so that the prevailing winds approaching western Europe were from the south and west, and were warmer than average. Between 1930 and 1950 the index oscillated about the century-long mean. From 1950 to 1971 the index was predominantly negative, creating a period of increasing cold northerly winds over the waters of the northeast Atlantic. Finally, after 1971 there was a return to predominantly positive anomalies similar to those seen in the early part of the twentieth century, with a warming trend off western Europe but a cooling trend off Newfoundland and Labrador. The interactions between changes in the NAO and changes in the various populations of organisms have now been demonstrated by means of statistical correlations.

Based on data from the second half of the century, for which long-term quantitative records are available, it appears that in areas where there is an increase in cold northerly winds in winter and spring, the onset of stratification is delayed and with it the onset of the spring bloom of phytoplankton. The growth and multiplication of zooplankton is temperature-dependent, so the peak of zooplankton biomass is delayed. Conversely, warmer waters advance the blooms of phytoplankton and zooplankton. The larvae of some populations of fish are adversely affected by late blooms, while others benefit. Investigations of benthos on the coast of Germany and Sweden showed that warmer winters favor increased abundance of benthos.

In much of the central and eastern North Atlantic and the North Sea, a warming phase, associated with a positive anomaly in the NAO, leads to the northward spread of southern species. For example, in the English Channel herring stocks move north and are replaced by sardines from further south, while bluefin tuna and swordfish stocks spread north to Iceland and the Faeroes and cod stocks in the Barents Sea show improved recruitment and growth. Conversely, a cooling phase in the eastern North Atlantic, associated with a negative anomaly of the NAO, leads to poor growth and recruitment of cod stocks in the Barents Sea. However, cod stocks in the North Sea, near the southern end of their range, appear to benefit from cooler water and a delayed spring bloom.

In the western North Atlantic, the cold winters in the Labrador Sea, associated with a positive NAO anomaly, create adverse environmental conditions for the cod stocks of the Grand Banks. Systematic overfishing during these conditions led to the collapse of the stocks in the early 1990s. During this same period the warming trend in the waters of western Europe led to record levels of plankton production and rapidly expanding herring and horse mackerel populations.

Beginning about 1917, cod spread north along the coast of western Greenland and subtropical species began to appear off the coast of western Europe. The peak of these incidents was in the period 1925–35, known as "the dramatic decade." In the mouth of the English Channel, pilchard replaced herring, and the numbers of young stages of gadoid fish and flatfish dropped sharply. It is interesting to

note the lag between the onset of the negative trend in the NAO index about 1950, and the downturn in biological events. Cod recruitment in the North Atlantic did not begin to decline until well into the 1950s, the pilchard-dominated community in the English Channel did not begin to decline until about 1965, and the collapse of the west Greenland cod fishery took place between 1968 and 1970.

The northerly winds blowing down the east coast of Greenland created a large mass of cold, low-salinity water that traveled all the way around the subarctic gyre, taking about 15 years. Most fish stocks in its path showed poor recruitment while it was present, possibly because the cold low-salinity water delayed the stratification required to establish the spring bloom of plankton.

Prior to about 1995, our understanding was limited and the patterns of change in fish populations in the North Atlantic were mainly linked to periods of global warming and cooling. It is now apparent that the changing pattern of circulation of the North Atlantic Ocean, as indexed by the NAO, is more directly related to changes in biological processes.

9.7 Variability in the Southern Ocean

As discussed in Section 3.3.9, there is a zone of westerly winds and an associated Antarctic circumpolar current girdling the southern hemisphere around 50° S. Harris *et al*. (1992) showed how Rossby waves in the upper level of the atmosphere cause the zone of westerly winds to shift north and south over Tasmania. This shift is accompanied by alternations of strong winds and calmer periods. The strong winds cause increased mixing along the eastern coast of Tasmania, a condition that favors the growth of larger zooplankton and the jack mackerel *Trachurus declivis* that feed on them. In years with frequent strong-wind events, the jack mackerel populations flourished. In years with fewer wind events and more calm periods, the numbers of krill in the plankton decreased by three or four orders of magnitude and the jack mackerel moved away.

Harris *et al*. (1988) documented a number of other changes in the fishery that are correlated with the oceanographic changes described above. Catches of Tasmanian spiny lobsters *Jasus novaehollandiae* show a clear correlation with high air temperature and pressure, attributable to the intensification of fishing effort that takes place during favorable weather, but also show a significant correlation with the oscillations in the westerly winds, with a time lag of seven years. It appears that recruitment is influenced by the favorable conditions, which leads to enhanced catches seven years later when the lobsters reach catchable size. The importance of the oceanographic conditions is reinforced by the finding of a similar correlation with landings of New Zealand lobsters *Jasus verreauxi* and *J. edwardsii* and a correlation of opposite sign with landings of *J. verreauxi* in New South Wales, Australia. Years of high winds also favor good recruitment of Tasmanian scallops *Pecten fumatus*, bring more southern bluefin tuna *Thunnus maccoyii* into Tasmanian waters, and influence the numbers of leopard seals *Hydrurga leptonyx* migrating northward from Antarctica to Macquarie Island (about 55° S).

Off the western coast of Australia, the southward-flowing Leeuwin Current is a major oceanographic feature. It flows along the shelf break, and is most intense in winter. Close to the coast is a reversing wind-driven coastal current, for which the net flow is northward in the (austral) summer and southward in winter. In non-ENSO years, coastal sea levels are relatively high and the Leeuwin Current is strong. During ENSO years the coastal sea levels fall, and the Leeuwin Current is weaker. The reduced southward transport of tropical water leads to cooler and more saline conditions. The western rock lobster *Panulirus cygnus* releases phyllosoma larvae near the edge of the continental shelf, from where they are carried to the open ocean, and drift for almost a year. They then metamorphose to the puerulus stage and settle in the coastal reefs. In ENSO years, when the Leeuwin Current is weak, the density of settlement of puerulus larvae is below average (Pearce and Phillips 1994). The mechanism affecting the rate of settlement is not known, but there is a strong suggestion that the Leeuwin Current plays a part.

On the other hand, ENSO years are favorable for recruitment of the saucer scallop *Amusium balloti* in Western Australia (Joll and Caputi 1995). Recruitment is negatively correlated ($r = -0.86$) with coastal sea level, and a year of strong ENSO was a year of record high recruitment. It is suggested that a strong Leeuwin Current advects larvae away from suitable settlement grounds. Use of satellite data has made it possible to anticipate some of the changes described above. It seems reasonable to suppose that as the sequence of events connecting atmospheric phenomena with changes in ocean productivity becomes more widely understood in other parts of the world, our ability to forecast trends in stocks of fish and shellfish will show a corresponding improvement.

9.8 A GLOBAL PERSPECTIVE ON INTER-DECADAL CHANGES

We have now reviewed physical and biological processes in the Pacific, Atlantic, and Southern Oceans, showing that for each basin there are coupled atmosphere–ocean processes that have profound effects on food-web processes and on fish production. Since 1998, there have emerged some important ideas that indicate the possibility of a more integrated global view of the links between meteorological processes and food-web processes in the sea.

9.8.1 The Atmospheric Circulation Index (ACI)

Klyashtorin (1998), working with the Atmospheric Circulation Index (ACI; see Section 9.2.2d), explored relationships between this physical index and long-term changes in global landings of the main commercial species of marine fish, using data from 11 stocks yielding almost half the world's total marine catch. Although it is recognized that catch alone is a crude measure of fish abundance, the relationships that Klyashtorin discovered are so striking that we must ask whether they indicate a truly global pattern of linkages between physical phenomena and

the biological processes leading to the production of fish. We have already seen that these linkages occur on the ocean-basin scale. Now let us shift the perspective to global scales. Our analysis differs a little from that of Klyashtorin (1998) in that we have emphasized the various regimes of physical conditions, with their accompanying regime shifts, whereas Klyashtorin chose to discuss "epochs" which corresponded to the rise and fall of fish stocks, and had a regime shift in the middle of each "epoch."

Recalling that on the basis of the ACI the twentieth century is divisible into three main regimes, a zonal with predominantly westerly winds, followed by a meridional with weaker westerlies and a greater predominance of north–south winds, followed by a second zonal regime, with regime changes in 1938 and 1971, we may compare the rise and fall of the landings from various fish stocks with the pattern of regimes. Klyashtorin (1998) showed that in the North and South Pacific there were six major stocks for which the landings rose during zonal regimes and fell during meridional regimes (Fig. 9.18a). For Japanese sardines *Sardinops melanostictus*, California sardines *S. sagax caeruleus*, and Pacific salmon, there is a long history of exploitation and records extend back to the first quarter of the century. There are two periods of growth in landings of each stock, and each period of growth corresponds with a zonal regime. For Peruvian sardines *S. sagax sagax*, Chilean jack mackerel *Trachurus murphyi*, and Alaska pollock *Theragra chalcogramma*, records are confined to the second half of the century, but the main growth in landings is in a zonal regime.

Klyashtorin (1998) also identified two Pacific stocks and three Atlantic stocks (Fig. 9.18b) for which major increases in landings occurred in the meridional regime. The records are of varying length, but in every case the main increase in landings occurred during the period 1938–71.

In almost every instance, we see a substantial lag between the initiation of a trend in the ACI and a corresponding change in the landings of fish. This topic was explored by Jacobson *et al*. (2001). If environmental conditions change and become favorable for a species, one would expect improved growth rates and possibly improved recruitment. Survival and growth are contributors to the rate of secondary production of a stock. Jacobson *et al*. (2001) therefore proposed measurement of the instantaneous or annual production rate of a stock as a sensitive indicator of favorable environmental conditions. For example, in the stock of Japanese sardines, environmental conditions began to improve in 1971, at the beginning of a zonal regime. The instantaneous production rates increased sharply at the beginning of the decade, but estimated biomass of the stock did not increase until the second half of the 1970s and landings did not peak until the mid 1980s (Fig. 9.18a). A sequence of events on this time scale may be fairly typical, and account for the lag between change in conditions and increased landings from the stocks.

Klyashtorin carried the analysis to an even larger scale. He considered the global catch of all the main commercial stocks in the Atlantic and in the Pacific, for the period 1920–94. The smoothed record of catches in the Atlantic and the Pacific, separately and combined, are shown in Fig. 9.19(a). It is seen that the curves

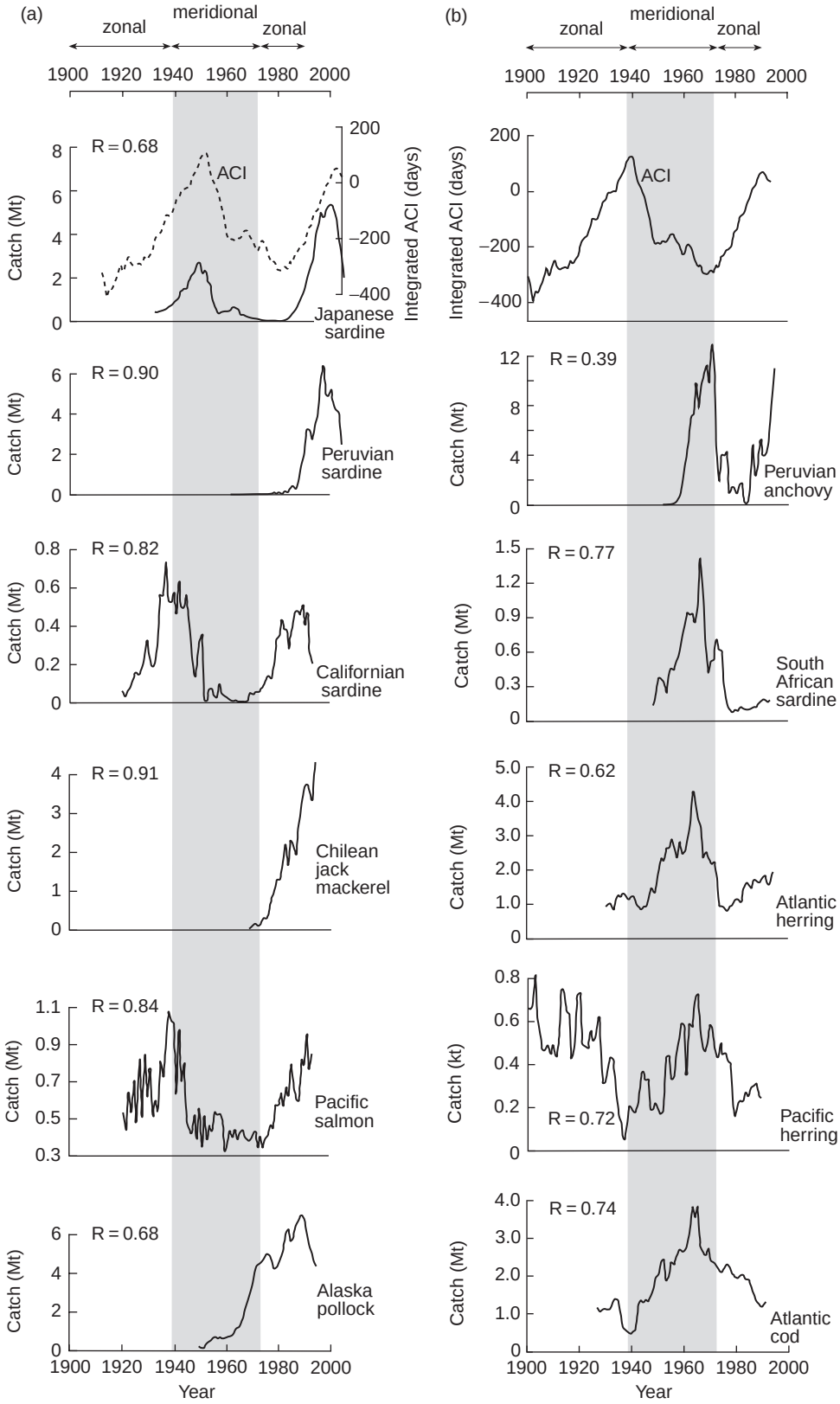
(a)
zonal
meridional
zonal
1900 1920 1940 1960 1980 2000
R = 0.68
ACI
Catch (Mt)
Integrated ACI (days)
Japanese sardine
R = 0.90
Peruvian sardine
R = 0.82
Californian sardine
R = 0.91
Chilean jack mackerel
R = 0.84
Pacific salmon
R = 0.68
Alaska pollock
Year
(b)
zonal
meridional
zonal
1900 1920 1940 1960 1980 2000
ACI
Integrated ACI (days)
R = 0.39
Catch (Mt)
Peruvian anchovy
R = 0.77
South African sardine
R = 0.62
Atlantic herring
R = 0.72
Catch (kt)
Pacific herring
R = 0.74
Atlantic cod
Year

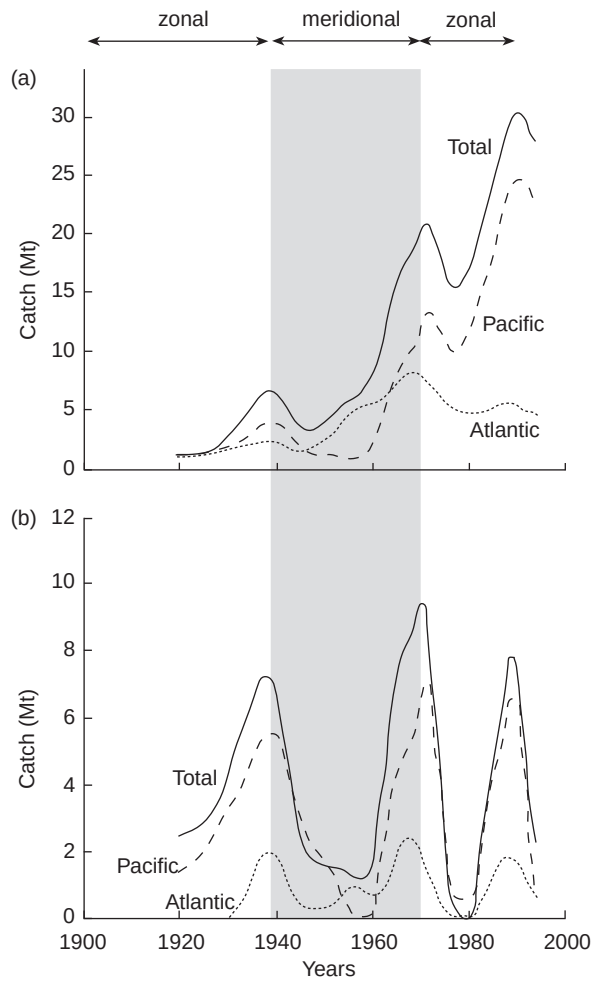

Fig. 9.19 Catch dynamics of 10 main commercial species in the Atlantic and Pacific for 1920–94. (a) Total catches in each ocean and the grand total for both oceans; (b) the same data after long-term trend removal.

display two processes: (i) large-scale oscillations in fish catch and (ii) a general increase in landings, probably resulting from a gradual increase in fisheries extent and fishing-fleet tonnage. When the long-term trend is removed (Fig. 9.19b), we are left with three oscillations in the main commercial catch in both Atlantic and Pacific Oceans. The peaks of the first two catch curves are near the regime

Fig. 9.18 *(opposite)* (a) Time series of landings from six stocks in which the total landings increased during zonal regimes. The ACI and the associated regimes are shown for comparison. (b) Time series of landings from five stocks in which the total landings increased during a meridional regime. The ACI and associated regimes are shown for comparison. Adapted from Klyashtorin (1998).

changes in 1938 and 1971. The suggestion is that during the first zonal regime, species that flourish under these conditions contributed to a rising global catch. After the regime change, these species declined and, after a lag, species that are adapted to the meridional regime increased their biomass. After the regime change in 1971, there was once again a decline in the current stocks and a build-up of those species that flourish in zonal conditions. The third peak in global landings led Klyashtorin to suggest that there was a third regime shift about 1990, but this is not clear from the physical evidence in Fig. 9.07. However, we recall that Hare and Mantua (2000) demonstrated a regime shift in the Pacific in 1989–90 (Section 9.3.2) and Reid *et al*. (2001) proposed that 1988 was a year of regime shift in the North Sea (Section 9.5.1).

We need to remember that many factors in addition to atmospheric forces will have influenced the pattern of landings. For example, the initial rises in landings of Peruvian anchovy and South African sardines were at least partly the result of rapid local expansion of fishing activities. The correlation coefficients in Figs. 9.18(a) and 9.18(b) are impressive, but it is difficult to know how to interpret them in any rigorous manner. The ACI is a cumulative plot of anomalies and the landings are at best rough indices of stock biomass. Nevertheless, when this evidence is considered alongside the mass of evidence that phytoplankton, zooplankton, benthos, fish, and birds are all correlated at the ocean-basin scale with physical indices such as NAO, ALPI, SOI, etc., it looks very much as if the rough outlines of a grand pattern of physical–biological interactions are being sketched in. They offer the exciting possibility of being able to forecast the trends in major stocks on a decadal scale. A first step in clarifying the physical–biological relationships might be to investigate the changes in instantaneous or annual production rates of the stocks, as proposed by Jacobson *et al*. (2001).

Klyashtorin (2001) prepared a report for FAO that was subtitled "The possibility of forecasting." Spectral analysis of 100–150 years of measurements of global temperature anomalies (dT), length of day (LOD), and the ACI showed that all had a 55- to 65-year periodicity. Time series of about 1500 years for air temperature, reconstructed from ice cores and tree rings, suggested a similar 55- to 60-year periodicity. Spectral analysis of a 1600-year time series of estimates of sardine and anchovy biomass in the California upwelling system, based on fish-scale deposits in the sediments, also showed a regular 50- to 70-year fluctuation. Spectral analysis of the catch statistics of Atlantic cod, Pacific salmon, and Pacific herring also showed cyclical fluctuation of 50–55 years, but several other species did not. For some, the record is too short. For others, Klyashtorin suggested that the analysis was inappropriate, because it was developed to analyze sinusoidal processes, whereas the catch dynamics were far from sinusoidal. Using a single cycle trend derived from the time series for each species, Klyashtorin (2001) developed forecasts using the bootstrap method of Efron and Tibshirani (1986). The forecasts were very basic, containing the following assumptions: (i) that catch dynamics corresponded to the smooth model curve; (ii) that the forecast cycle for each species had the same maximum catch as in the previous cycle; and (iii) that there was no change in average fishing intensity and no effects of climate change.

Clearly, this is only the beginning, but it opens the possibility of understanding on a global scale the patterns of variation in fish stocks driven by natural environmental factors. The emergence of predictable patterns allows us to hope that it may be possible to anticipate the times when particular stocks will experience adverse environmental conditions, and to adjust levels of exploitation accordingly.

As we discussed earlier, there may be a lag of a decade or more between the appearance of environmental conditions favorable to the species and an increase in commercial landings. A challenge for the future is to better understand the sequence of events and build the lags into predictive models.

9.8.2 The Atmospheric Circulation Index (ACI) and the basin-specific atmospheric indices

A group of Russian and Canadian scientists met to try to understand the relationship of the ACI to the various pressure-related indices from the northern hemisphere (Beamish *et al*. 1999). Using the technique of accumulating sums of indices (CuSum), they showed that there is indeed a rough correspondence between the ACI and the North Atlantic Oscillation, the Aleutian Low Pressure Index, and the Southern Oscillation Index (Fig. 9.07). In each, there is a major change in the trend between 1976 and 1979.

They then constructed an experimental composite index, which they called the Regime Index (RI). Each of the four pressure-related indices, ALPI, SOI, NAO, and ACI, was normalized by dividing each annual anomaly by the standard deviation of its time series. They reversed the signs of SOI, since it was opposite in trend to the other indices. The four standardized anomalies were summed to give a time series of standardized regime index, and its CuSum was plotted as the Regime Index (Fig. 9.20). It showed an unmistakable regime shift in 1976, the year in which

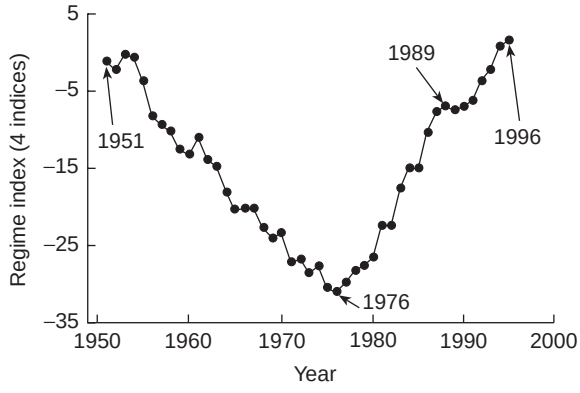

Fig. 9.20 Composite Regime Index for the Pacific Ocean, calculated as the cumulative sum (CuSum) of the standardized anomalies of ALPI, SOI, NAO, and ACI. For further details, see text. From Beamish *et al*. (1999).

biological data point to a major change in the North Pacific marine ecosystem (see Section 9.3.2 and Fig. 9.09). The data in Fig. 9.07 suggest that there was a regime shift in the ACI about 1971, but that the shift in all the indices relating to the Pacific was close to 1976. Future work may explain why Atlantic indices appear to lead Pacific indices by about five years.

9.9 Summary: on the global scale, it all comes together

During the decade leading up to 2005, many workers discovered that there were significant correlations between variations in the landings of commercial species of fish and shellfish and various indices of environmental influence. Correlations do not demonstrate cause and effect but, as a thought experiment, it is instructive to review what is known and to speculate on possible mechanisms of cause and effect. Beginning at the largest scale, the analyses of Klyashtorin (1998) show that the twentieth century can be divided into three or four regimes, two zonal and one meridional, with the possibility that we are now in a second meridional regime.

Zonal regimes

The zonal regimes were times of accelerated global warming, and both the Aleutian low-pressure system and the Iceland–Greenland low-pressure system tended to be abnormally deep in winter. The strong westerly winds associated with them brought warm air and warm water to the coasts of western Europe and to the western seaboard of North America. Corresponding changes in plankton, benthos, fish, and bird populations have been documented.

In the northeast Pacific, during zonal regimes, the deepening of the Aleutian low-pressure system in winter caused the Alaska gyre to be more vigorous, which increased the upwelling of nutrient-rich water at its center. These nutrients stimulated the growth of phytoplankton, and the increases cascaded through the food web, to be reflected in greater fish production. Zonal regimes in the North Pacific are associated with increased landings of salmon, California sardines, and Japanese sardines. In the southern hemisphere, zonal regimes are also associated with increasing landings of Peruvian sardines and Chilean jack mackerel, though the mechanism of teleconnections is less well understood. Landings of Pacific herring declined during zonal regimes.

In the North Atlantic, during zonal regimes, the Iceland–Greenland low-pressure system was deeper than average and the strong westerly winds caused warm water to move northward along the coast of western Europe. There was a northward movement of the range of anchovy and herring, a greater penetration of productive ocean water into the North Sea and the Barents Sea, and a general tendency towards increasing productivity in coastal waters. At the same time, waters off eastern Canada and the USA became cooler, and there were decreases in landings of groundfish.

Meridional regimes

During the meridional regime of 1938–71, the Iceland–Greenland low-pressure system was weaker than average, the waters off eastern Canada and the USA warmed, and catches of groundfish improved. In the central and eastern parts of the North Atlantic there was a cooling trend, leading to delayed blooming of the zooplankton populations, a condition that favored cod and other gadoids. Towards the end of the regime, abnormally large amounts of ice accumulated east of Greenland. On melting, this ice gave rise to a water mass of abnormally low salinity which retained its integrity for a decade. It circulated around the subarctic gyre, causing reduced fish productivity in each region that it passed through. During this meridional regime, the total catch of cod and herring in the North Atlantic increased strongly, as did the catches of sardines off South Africa.

ENSO

The El Niño – Southern Oscillation (ENSO) has a much shorter periodicity, around four years for a cycle compared with 50–55 years for the Atmospheric Circulation Index. However, when its anomalies are plotted cumulatively, it too showed significant change of direction in 1976, the year of a major regime shift. It has a strong effect on coastal fisheries in the Pacific Ocean, and through its teleconnections has strong influences on conditions in the tropical Atlantic, the Indian Ocean, and the shores of Australia and New Zealand. In the North Pacific, and to some extent in the North Atlantic, its effects are seen to complement those of the longer-term oscillations.

The mounting evidence of environmental influences on growth and recruitment in commercial stocks offers exciting possibilities for predicting general large-scale trends in biomass. It would be a wise precaution to take into account the probability that stocks will from time to time experience adverse environmental conditions, and adjust fishing pressure accordingly. Otherwise, many other stocks may follow the fate of the northern cod on the Grand Banks of Newfoundland, where heavy exploitation during a time of environmental adversity led to collapse of the stock.

10

The oceans and global climate change: physical and biological aspects

10.1 Introduction

As we saw in Chapter 8, the oceans have a deep circulation, the thermohaline circulation. Water is heated in equatorial regions, and then moves poleward in major currents, giving off heat to the atmosphere. In subarctic regions cooling and ice formation cause water to become more dense. The water then sinks to form the "deep water." This sinking is the beginning of a long journey close to the ocean floor. Some of the deep water travels south in the Atlantic basin, moves across to the Pacific basin, and there moves slowly northward in a journey that may take a thousand years.

At the regions of deep-water formation large quantities of carbon dioxide dissolved in the water sink to great depth and are removed from contact with the atmosphere. Conversely, at regions of upwelling, especially the large upwellings at the tropical divergence, heating of the cold upwelled water causes it to give off billions of tons of carbon dioxide. These are the major physical mechanisms by which the oceans exchange carbon dioxide with the atmosphere, and there is no particular reason to think that they are not approximately in balance. However, there are in addition important biological processes that remove carbon dioxide from the atmosphere and transfer it to the deep ocean. Over 99% of the carbon dioxide added to the earth's atmosphere throughout its history has been taken up by phytoplankton and sedimented to the sea floor to form the calcareous rocks and the fossil fuels. This biological mechanism is known as the biological pump.

For at least 150 years the carbon dioxide concentration of the atmosphere has been rising as a result of human activities in cutting down the forests and burning fossil fuel. It is now expected that there will be a global rise in atmospheric temperature – the "greenhouse" effect. Before the magnitude of this important change can be predicted, it will be necessary to understand the extent to which the oceans may be a reservoir for excess carbon dioxide. In this chapter we seek first of all to describe the mechanism of global warming and the present-day global carbon cycle. We shall then explore the relative importance of oceanic sources and sinks compared with industrial activities and terrestrial biota. Finally, we shall attempt to peer into the future, and consider what changes might be expected to occur in physical and biological mechanisms for circulating carbon in the ocean if the expected rise in global atmospheric temperature occurs.

10.2 Physical aspects

10.2.1 The greenhouse effect

(a) The process

The average surface temperature of the earth is about 15 °C. If there were no water vapor, carbon dioxide, or methane in the atmosphere, the surface temperature would be below freezing by ~18 °C and all the rivers, lakes, and oceans would be frozen solid. The reason for the higher, more habitable temperature is the fact that these greenhouse gases delay heat from leaving the earth by trapping it in the lower atmosphere.

As pointed out in Chapter 3, all the heat received on the earth comes originally from the sun's surface via electromagnetic radiation with wavelengths between 0.2 and 2.4 μm, often called the short-wave radiation. According to Kiehl and Trenberth (1997), approximately 31% of this incoming radiation is reflected back into space, ~20% is absorbed by the ozone, water vapor, clouds, and dust in the atmosphere, and ~49% is absorbed by the land and water at the earth's surface. All these absorbers in turn radiate heat in the form of electromagnetic radiation.

The wavelength of this "back" radiation is much longer than the incoming radiation, in accordance with Planck's radiation law, which states that cooler bodies radiate at longer wavelengths. The radiation from the surface of the earth and the atmosphere is thus at wavelengths between 5 and 100 μm, the long-wave radiation.

The atmosphere is quite transparent to the short-wave radiation from the sun as indicated above by the fact that only ~20% of the incoming radiation is absorbed by the atmosphere. The long-wave radiation is another story. Roughly 90% of the long-wave radiation leaving the earth's surface is absorbed in the atmosphere by the greenhouse gases. This heat eventually reaches the upper layers of the lower atmosphere and is lost to outer space, but the absorption by the greenhouse gases delays the loss and keeps the lower atmosphere warmer than it would be if the atmosphere were transparent to the long-wave radiation. The amount of heat trapped and the resulting temperature of the atmosphere clearly vary directly with the concentrations of these gases. If the gases are very concentrated, as on the planet Venus, the temperature is very high (+400 °C) and if they are low, as on Mars, the temperature is very low (–50 °C).

On the earth there are seven or so gases that contribute to warming the atmosphere, ranging from the naturally occurring carbon dioxide, water vapor, methane, ozone, and nitrous oxide to the human-produced chlorofluorocarbons. The warming effect of each of these gases is different because their concentrations are different and because they absorb radiation with different efficiencies at different wavelengths. Under clear-sky conditions, Kiehl and Trenberth (1997) estimate that 60% of the warming effect is due to water vapor, 26% to carbon dioxide, 8% to ozone, and 6% to methane and nitrous oxide. The other gases, such as chlorofluorocarbons, contribute ~1% or less to the total warming effect. For life in the oceans, the most important element in these gases is the carbon (C) in the carbon dioxide (CO_2).

(b) The carbon cycle

Estimates of the magnitudes of the carbon reservoirs and fluxes in the global carbon cycle are constantly being updated. A recent summary by Sarmiento and Gruber (2002), illustrated in Fig. 10.01, separates the pre-industrial values from the anthropogenic values. In the atmosphere, for example, there were ~590 Pg of carbon in the pre-industrial era but today the value is ~161 Pg higher for an increase of ~30%. The natural or non-anthropogenic fluxes between the atmosphere and the land and the ocean are approximately in balance in the figure, but the anthropogenic fluxes are out of balance due to the annual input into the atmosphere of 5.4 Pg from the burning of fossil fuels. Of the original 3700 Pg of fossil-fuel carbon, 220 Pg has been put into the atmosphere. Deforestation has added a further 124 Pg for a total of 344 Pg added to the atmosphere over the past 150 years. About 65 Pg of the total is now back in the terrestrial biosphere through such processes as the re-growth of forests, ~161 Pg remains in the atmosphere, and 118 Pg has dissolved in the ocean.

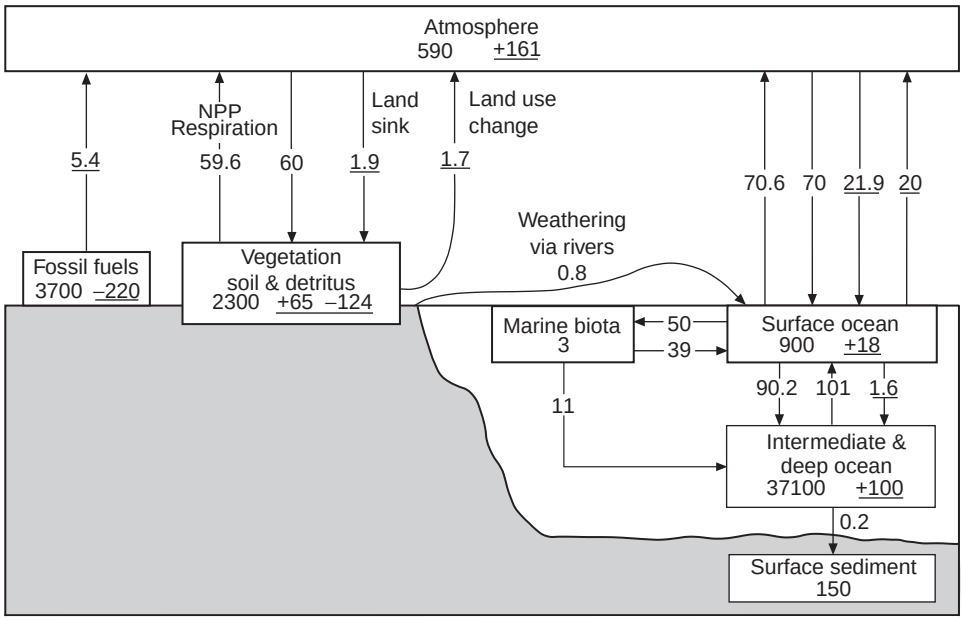

Fig. 10.01 A summary of the global carbon cycle. Reservoir sizes are in Pg C and fluxes (averages over the 1980s) are in Pg C yr^{-1}. Underlined values refer to anthropogenic fluxes and changes in the reservoirs. Values not underlined refer to natural fluxes and pre-industrial values. For the land sink, the +65 is an inferred terrestrial land sink whose origin is speculative and the –124 is the decrease due to deforestation. NPP is net primary production. After Sarmiento and Gruber (2002), and Gruber (2002).

The rate at which carbon dioxide is exchanged between the earth's oceans and the atmosphere depends on the gradient of the partial pressure of the gas across the sea surface. Over the period of a year (Fig. 10.01) ~90.6 Pg of carbon is transferred from the ocean into the atmosphere while ~91.9 Pg enters the ocean from the atmosphere for a net increase in the ocean of roughly 1.3 Pg C y^{-1}. When the CO_2 dissolves in the ocean, 99% dissociates and forms bicarbonate ions (91%) and carbonate ions (8%). Only ~1% retains the CO_2 structure, but it is only this fraction that participates in exchange with the atmosphere (Prentice *et al*. 2001).

Together these forms of carbon make up the dissolved inorganic carbon (DIC) in the ocean. The DIC is usually presented as the "total CO_2" as in the two examples of vertical distributions of total CO_2 in Fig. 10.02. These profiles representing the North Atlantic and North Pacific Oceans exhibit some of the main features common to all the open oceans. For example in the Atlantic the concentration is lowest at the surface and has increased by ~10% at ~1000 m, then stays roughly constant to the bottom. In the surface layer carbon is incorporated into organic compounds, skeletons, and shells, especially during the spring bloom, but when the organisms die the remains sink. Some decompose, releasing the carbon back into the water column, but some are buried in sediments. This flux of

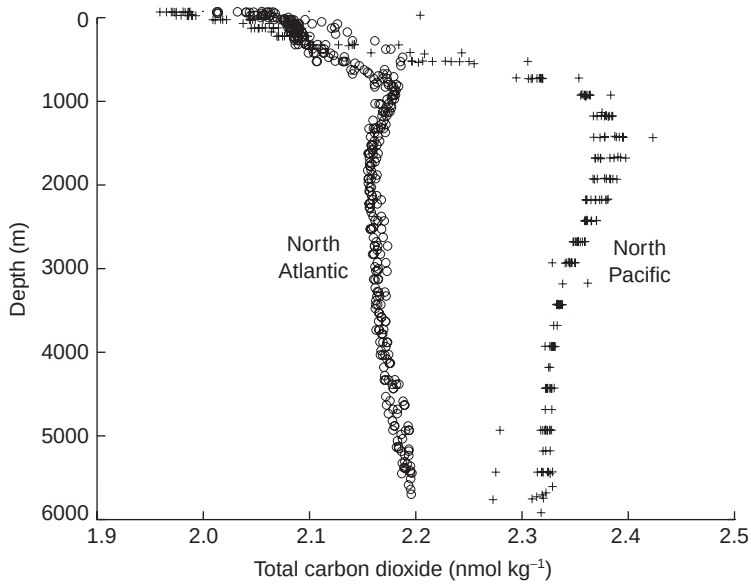

Fig. 10.02 Vertical profiles of total carbon dioxide between 30° and 40° N in the North Atlantic and North Pacific Oceans. Data collected in the Atlantic along 52° W in July 1997 from RV *Knorr* and in the Pacific along 165° W from RV *Tully* in September and October 1994. Values obtained from the Carbon Dioxide Information Analysis Center (cdiac.ornl.gov/oceans/home.html).

carbon out of the euphotic zone into the deeper layers is called the "biological carbon pump" and is explored further in Section 10.3. One result of the downward flux of carbon is the higher concentration in the deeper waters. Also evident in Fig. 10.02 is the greater concentration below 1000 m in the North Pacific than in the North Atlantic. This increase of ~10% is thought to reflect the greater length of time since the deep Pacific has been in contact with the atmosphere and thus the greater length of time it has had to accumulate carbon from sinking plant and animal detritus. The movement of variables such as CO_2 through the deep ocean basins of the world is related to the thermohaline circulation discussed in Section 8.2.5.

10.2.2 Climate change

(a) Carbon dioxide

For the future of life on the earth, the important concern is that the concentrations of the greenhouse gases are increasing, thereby increasing the greenhouse effect. Since 1958 the concentration of CO_2 in the atmosphere has been determined from direct measurements at Mauna Loa, Hawaii and for the centuries before 1958, CO_2

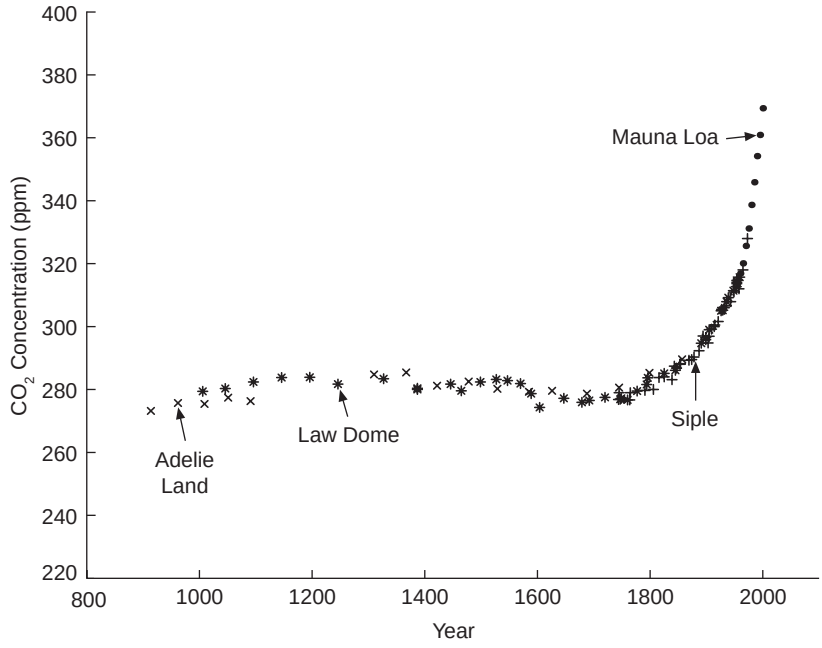

Fig. 10.03 Atmospheric carbon dioxide concentration since the year 900, based on measurements at Mauna Loa since 1958 (Keeling and Whorf 2002) otherwise from ice cores from the Antarctic ice at Adelie Land (Barnola *et al*. 1995), Law Dome (Etheridge *et al*. 1998), and Siple (Neftel *et al*. 1994). Figure design after fig. 3.2(b) in Prentice *et al*. (2001).

concentrations have been determined from analyses of air trapped in glaciers. From the curve in Fig. 10.03 the concentration of CO_2 is shown to have remained relatively constant at 280 ppm from the year 900 to about 1850 when it started to increase to a value of ~370 ppm in 2001 – a 30% increase in 150 years. From the examination of longer records, Prentice *et al*. (2001) conclude that the value observed today has not been exceeded in the past 420,000 years and likely was not exceeded in the past 20 million years. Also the rate at which the CO_2 has increased over the past 150 years appears to be more rapid than any increase observed during the past 20,000 years.

Roughly two-thirds of the increase in anthropogenic CO_2 since 1850 is due to the burning of coal, oil, and gas. The remaining third is due mainly to the release of CO_2 from deforestation. At present, the increase in CO_2 is responsible for 60% of the increase in the greenhouse effect since 1850. Increases in methane and nitrous oxide are responsible for about 20% of the increase and trace gases such as chlorofluoromethanes the remaining 20% (Prentice *et al*. 2001). These well-documented increases raise questions that are of increasing importance throughout the world: What effects are these increases having on the world's temperature, precipitation, sea level, ice cover, and biological processes? And what about the future if the greenhouse effect continues to increase?

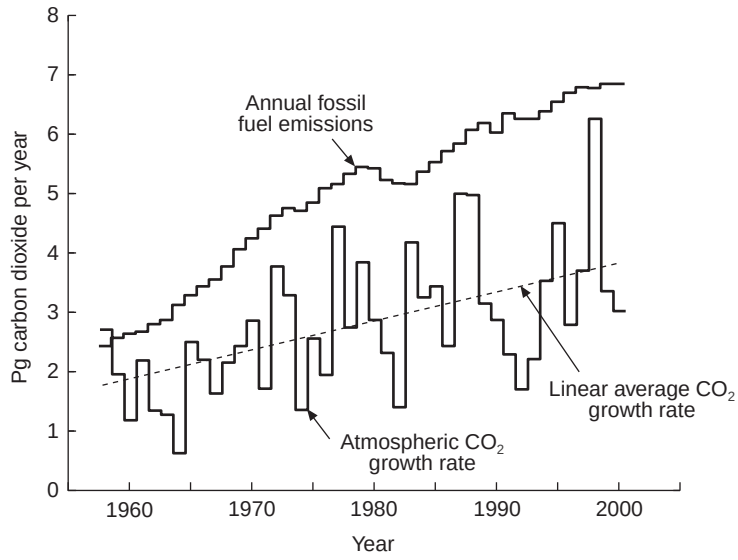

Fig. 10.04 The annual flux of carbon dioxide into the atmosphere from fossil fuel emissions and the annual increase in carbon dioxide observed in the atmosphere, 1958–2000. The difference between the emissions and the accumulation in the atmosphere must be sequestered in the oceans and on land. Adapted from Tans (2001).

One of the interesting features of the recent CO_2 increase in the atmosphere is that the annual growth rate has represented about half the amount of CO_2 estimated to have been put into the atmosphere by human activities. This is illustrated in Fig. 10.04, which shows the annual flux of CO_2 emissions into the atmosphere from fossil fuels compared to the growth rate of the CO_2 observed in the atmosphere between 1958 and 2000. In the late 1950s CO_2 emissions from fossil fuels were ~2.5 Pg y^{-1}, while the increase in the atmosphere was ~1.5 Pg y^{-1}. Recently the CO_2 emissions were ~7 Pg y^{-1} and the increase in the atmosphere ~4 Pg y^{-1}. The whereabouts of the CO_2 represented by the difference, that is, the CO_2 not accumulating in the atmosphere, was until a few years ago unknown. Due to recent advances the "missing CO_2" is now known to be dissolving in the oceans or being incorporated into the terrestrial biomass (Prentice *et al*. 2001).

Because of the recently devised techniques it is now possible to identify anthropogenic carbon dioxide and separate it from that occurring naturally. One method depends on the fact that the $^{13}C/^{12}C$ ratio is lower in fossil-fuel-derived CO_2 than in other CO_2. Recent data from the major oceans (Sarmiento and Gruber 2002) show that anthropogenic carbon tends to be confined to the upper few hundred meters of the ocean. Only in the North Atlantic are measurable concentrations of anthropogenic CO_2 observed in the deep waters. These occur because the deep waters in this ocean are renewed with water that has been in contact with the atmosphere during the period of anthropogenic carbon increase

in the atmosphere. It is expected that anthropogenic carbon will not be detected in the deep Pacific Ocean for ~1000 years.

The annual accumulation of CO_2 in the atmosphere (Fig. 10.04) is far more variable than the annual emissions. Interestingly most of the peaks in the accumulation curve coincide with El Niño events. The peaks in the rate of accumulation in the years 1965–6, 1968–9, 1972–3, 1976–8, 1982–3, 1986–7, and 1997–8 coincide with El Niño episodes. The exception was the strong El Niño in 1992–3, during which a minimum in accumulation rate occurred. This may have been an effect of the cooling of the atmosphere caused by the eruption of Mount Pinatubo in the early 1990s. In their discussion of this phenomenon Prentice *et al*. (2001), however, point out there is no proof of this connection. The reason for the increase in accumulation rate during El Niño episodes also remains controversial. One might think the warmer water in the equatorial Pacific during El Niño events would lead to an increased flux of CO_2 into the atmosphere. Observations however indicate the flux is probably decreased during El Niños in the equatorial region because of the decrease in upwelling along the equator of water with higher CO_2 content. By default the response of the terrestrial biosphere to El Niño events is thought to be responsible for the variations in annual CO_2 accumulation, but the details are not yet understood (Prentice *et al*. 2001). The variations are, however, a small fraction of the total flux. For example the total flux of carbon from the atmosphere in and out of the ocean is ~90 Pg y^{-1} and from the atmosphere in and out of the land-based biomass is ~60 Pg y^{-1}. The variations in the accumulation rate of ~2 Pg C y^{-1} thus represent ~1.5% of the total annual flux.

(b) Temperature

The direct link between the concentration of the greenhouse gases in the atmosphere and the temperature of the atmosphere makes it clear that air temperature is one of the key variables to monitor while the gases increase. Fortunately air temperature has been measured accurately throughout the past 150 years over land and sea. As can be imagined, the temperature records are uneven in quality and coverage, and creating a useful data set for the necessary length of time is prone to some unusual problems. For instance, the air in a city can be ~0.2 °C higher because of the activity in the city and the shape of the buildings. This "heat island" effect must be removed to get a true picture of the long-term temperature trends (Hansen and Lebedeff 1988). At sea, other problems arise. Folland *et al*. (1984) analyzed the available sea-surface temperature data but used only the nighttime values because the sun's warming of the ships during the day produces falsely high values. They also pointed out that the temperatures obtained from ships during World War II appear to be high because the thermometers had to be taken inside the ship to be read, as no lights were allowed on the open deck. These and other spurious signals have to be carefully weeded out of the record as they can create systematic errors that are as large as the signal that is being sought.

Over the past 20 years there have been many efforts to assemble temperature measurements of the air and water from around the globe to arrive at accurate

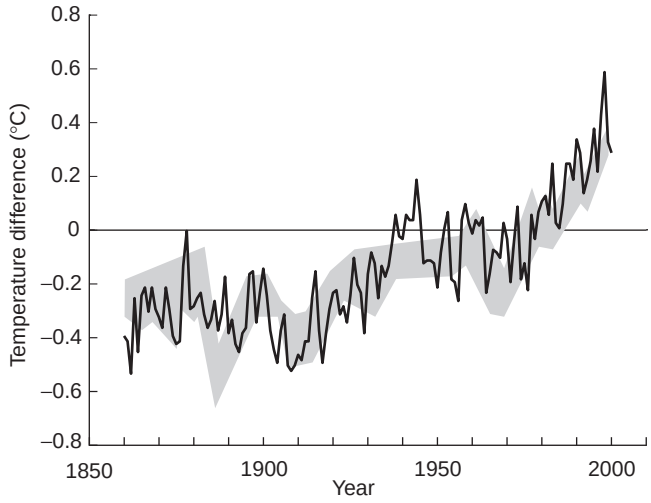

Fig. 10.05 Surface temperature of the earth, including land and marine data, relative to the 1961–90 mean from Jones *et al*. (2001). The grey band approximates the range of temperatures determined by computer simulations of a coupled ocean–atmosphere climate model. Based on fig. 12.7(c) in Mitchell *et al*. (2001).

estimates of the temperature of the surface of the earth. Recent results giving the earth's temperature since 1860 are shown in Fig. 10.05. The temperature is seen to fluctuate about a constant level between 1860 and 1910, and then to rise by about 0.3 °C by the 1940s. This was followed by another period of relatively stable values until the 1970s, when another period of rapid rise began. The total increase in temperature over the past 150 years is estimated to be 0.6 ± 0.2 °C. The small size of the error relative to the total suggests that the observed warming is substantially greater that the observational uncertainties. The eight warmest years of the record occurred in the 1990s, with the warmest being 1998. The geographical distribution of the temperature increase has been examined by Folland *et al*. (2001). They demonstrate that the warming is not the same everywhere and in a few locations surface temperature actually decreased while other regions experienced strong increases.

The gray band in Fig. 10.05 approximates the temperature range, since 1860, estimated with computer simulations of a coupled ocean–atmosphere climate model. The band is based on four separate simulations, which included the natural as well as the anthropogenic forcings. Agreement between the observed and the simulated records is obviously close, suggesting that the models are adequately representing the important processes in the global response to the changing concentrations of the greenhouse gases. When these and other models are used to predict the future temperature on earth (Cubasch *et al*. 2001), the result is a range of values suggesting increases from 1.5 to 5.5 °C over the next 100 years. The average of the model predictions is about 3 °C, or five times the increase observed

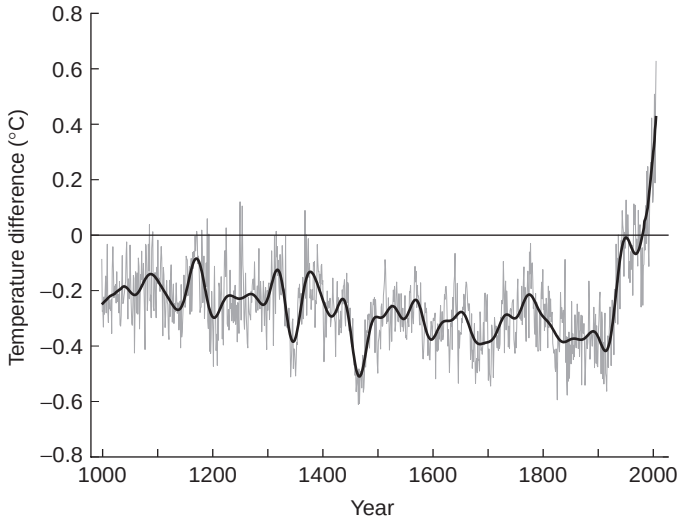

Fig. 10.06 Northern-hemisphere surface air temperature, relative to the 1961–90 mean, based on proxy data between 1000 and 1980 from Mann *et al*. (1999) and the instrumental record between 1860 and 2000 from Jones *et al*. 2001. Based on fig. 2.20 in Folland *et al*. (2001).

over the past 150 years. Models, of course, depend on a number of assumptions that seem reasonable today but which might change greatly in the future. As time passes it will be interesting to observe how the world's declining birthrates and technological improvements affect the predictions.

The 1000-year record of surface temperature in the northern hemisphere shown in Fig. 10.06 was constructed from the instrumental record (Jones *et al*. 2001) and proxy data from variations in tree rings, corals, and ice cores (Mann *et al*. 1999). From the year 1000 to about 1900 temperature decreased at about 0.02 °C per century, consistent with forcing associated with long-period variations in the earth's orbit and rotation (Berger 1988). With this long-term perspective the warming of the twentieth century tracks the increase in CO_2 as expected, and is clearly the anomaly of the millennium.

10.3 The biological pump

Given the existence of a very large, slowly moving deep-ocean circulation that may take a thousand years to traverse the major oceans, we need to look at the mechanisms that will take carbon from the atmosphere and transfer it either to the sea floor or to the deep parts of the ocean, for in either event it will be unable to return to the atmosphere for hundreds of years. We saw earlier that, at the limited areas that are sites of deep-water formation, carbon dioxide dissolved in the water is carried to depth. We will now examine mechanisms operating over

the entire surface of the oceans by which carbon is fixed in photosynthesis and introduced into the deep ocean by the sinking of dead organisms. It is called the biological pump.

10.3.1 The magnitude of carbon fixation in organic matter

The biological fixation of carbon is taking place continuously in the world ocean, but the pattern is extremely complex, as may be seen in the satellite images (Plate 1). At any one place it changes with the alternation of light and dark. In most places this cycle lasts 24 hours, but within the Arctic and Antarctic circles there is a period of continuous darkness in winter and light in summer. It also changes seasonally, especially in temperate waters where there is an alternation of shallow mixed layer in summer and deep mixed layer in winter. Waters of the continental shelves tend to be more productive than the open ocean, and sites of upwelling more productive than sites where upwelling is absent. These phenomena have been reviewed in previous chapters.

Until recently, all estimates of global rates of carbon fixation by phytoplankton have been based on compilations of the world's literature on field measurements made at particular points at particular times. They range from 20 to 55 Pg y^{-1} of carbon. We saw in Section 3.5.2 that by use of satellite data and certain parameters of the water column, Longhurst *et al*. (1995) obtained estimates for global marine primary production in the range 45–50 Pg C y^{-1}, and Behrenfeld and Falkowski (1997), using a simplified set of properties of the water column, arrived at 43.5 Pg C y^{-1}. These figures represent approximately half the primary productivity of the planet. The chief uncertainties in the estimates are in the contribution of nearshore waters. On one hand, the presence of sediment in suspension may cause the color estimates to be too high. On the other hand, satellite sensors tend to saturate when chlorophyll concentrations exceed 5 mg m^{-3}, and may have given underestimates in eutrophic waters. The margin of uncertainty is of the order of 10% of the total. The satellite-derived figures are higher than many early estimates based on radiocarbon incubations. This is partly because the modern trace-metal-clean techniques give higher values for incubations and partly because the satellite observations give high spatial and temporal resolution that could not possibly be captured using shipboard incubations.

In Chapters 3 and 8, we also discussed two categories of primary production: regenerated production, in which the algae use as a nitrogen source the ammonium excreted by the consumers in the system, and new production, in which the algae use nitrate upwelled from below the nutricline. The ratio of new production to total production is called the *f* ratio. In an idealized situation in which the pelagic zone of the ocean is in a biochemical steady state, regenerated production can be considered a closed loop with no net gain or loss of carbon or nitrogen. In this situation the flux of nitrogen leaving the pelagic zone in sedimenting organic particles is balanced by the upward flux of nitrate-N into the zone. Similarly, the downward flux of carbon in organic matter is balanced by uptake from the

atmosphere. (There is also an upward flux of carbon by eddy diffusion, but the vertical gradient in carbon is so slight that this component can be ignored.) This fact brings us to the realization that when considering the magnitude of the biological pumping of carbon from the mixed layer down to the interior of the ocean, it is not the total production that we need to know, but the new production. Hence, even if a routine method is developed for using satellites to determine total net production of phytoplankton over wide areas, it will also be necessary to know the *f* ratio for each area under study.

Fortunately, there is less disagreement among different observers about the levels of new production than about the levels of total production. One of the most difficult problems facing those trying to determine the true magnitude of new production is that much of it is believed to occur as a result of intermittent bursts of upwelling of nitrate, resulting from eddy activity, or internal waves (Section 8.5.1). Any method of observation that is not continuous is likely to miss a proportion of these intermittent events. In a permanently stratified tropical ocean with a deep nutricline, the new production may take place at considerable depth and escape detection by satellites. In places where this production occurs, the lower part of the euphotic zone will have a relatively high proportion of new production (high *f* ratio) while the upper part may function mainly on regenerated nitrogen (low *f* ratio). Hence there is the added difficulty of a non-uniform *f* ratio at a given geographic location. In spite of all these complications, the role of the phytoplankton in pumping carbon down into the interior of the ocean is of such importance in the context of rising atmospheric CO_2 that a great deal of effort is being made to evaluate the magnitude of the new production. For the most part, *f* ratios and hence levels of new production have been determined by studying the dynamics of nitrate and ammonium in incubation experiments, but as we saw in Section 3.5.3, Watts *et al*. (1999) developed a satellite-based method for determining the *f* ratio on ocean-basin scales.

10.3.2 Sinking of organic matter into the interior of the ocean

Primary production may be by organisms of a wide range of sizes, from large diatoms down to picoplankton, and their consumers may be small ciliates, copepods in the mid-size range, larger euphausiids, or large gelatinous zooplankton that nevertheless filter very fine particles. These consumers produce fecal pellets with a great range of sizes and sinking rates.

Interpretation of differing patterns of sinking fluxes is difficult, complex, and far from resolution. One quickly gets into a mass of biological detail. Consider, for example, the timing of the spring bloom of phytoplankton in relation to the ability of zooplankton to consume it. If zooplankton are present in good numbers in surface waters and are able to keep up with the consumption of phytoplankton as fast as it is produced, more phytoplankton carbon will be oxidized in the near-surface waters. On the other hand, common forms of zooplankton such as

copepods produce large quantities of feces that sink rapidly and would have the effect of accelerating downward movement of carbon. We saw in Section 8.6 that the subarctic gyres of the North Atlantic and North Pacific differ in this respect.

Bacteria have the opposite effect. If a dead organism begins to break into smaller particles and release dissolved organic matter, both the particulate and the dissolved organic matter provide food for bacteria, which then multiply rapidly. Bacteria are so small, however, that they have a negligible sinking rate, and large quantities of carbon fixed in surface waters may remain in suspension and be converted back to CO_2 by bacterial respiration. The whole question of the operation of the biological pump is a matter of active debate. See, for example, Fasham (2003). Calculation of the downward transport of carbon by evaluating all the terms in such a complicated food web may be a nearly impossible task. It is not surprising that there have been many attempts to obtain the value of the sinking flux by direct measurement, using particle traps.

Martin *et al*. (1987) reported on the material intercepted in free-floating particle interceptor traps (PITS) placed at depths ranging from 100 to 2000 m in the northeast Pacific off California. They estimated that at 100 m depth a station close to the coast had a downward flux of 7.1 mol C m^{-2} y^{-1} while at the same depth a station far out in the subtropical gyre had a downward flux of only 1.2 mol C m^{-2} y^{-1}.

Using the assumption that the downward flux of carbon is balanced by new production in the euphotic zone, it is possible to compare primary production with downward flux to obtain a carbon-based *f* ratio, *f*(C). These studies yielded *f*(C) ratios estimated at 0.14 for the open ocean and 0.17 for the coastal zone. In an area of active upwelling it was 0.20. Applying these percentages to some of their own primary-production data, Martin *et al*. (1987) tentatively extrapolated to the world ocean, concluding that global total net production was on the order of 50 Pg of carbon, of which 7.4 Pg was new production.

Rather larger estimates of *f*(C) were arrived at by Sambrotto *et al*. (1993). They presented data showing that the ratio of carbon fixed to nitrate taken up by the phytoplankton is often very different from the commonly used value of 6.6 (the Redfield ratio). Older estimates based on nitrate-based production and total nitrogen uptake may be in error. More carbon is fixed per molecule of nitrate taken up than is commonly supposed. Thus, the ratio of new production to total production, the *f* ratio, may be 0.25–0.35 rather than 0.15–0.20, which in turn suggests that the carbon export from surface waters may be on the order of 15 Pg y^{-1}. In this connection, physiological models of phytoplankton have shown that the ratio of carbon fixed to nitrogen used depends on the time frame of measurement and the nutrient status of the algae. For example, in longer experiments, more carbon will be fixed to support dark N assimilation (Flynn *et al*. 2002; Clark *et al*. 2002).

Martin *et al*. (1987) were also able to reconstruct the vertical profiles of sinking organic matter, down to 2000 m. As expected, the deeper a trap was placed, the less material it collected. This study gave a measure of the rate at which organic matter was being decomposed during the journey downward. Flux data from six open-ocean stations were combined and fitted rather well the expression

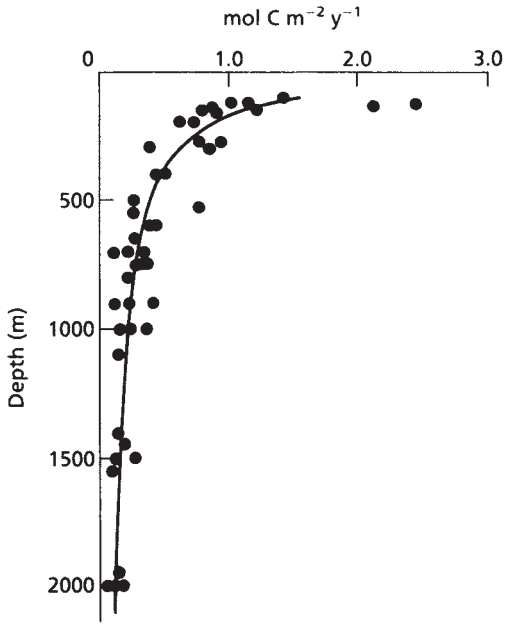

Fig. 10.07 Downward flux of carbon in the northeast Pacific as determined by sediment traps. Composite of six open-ocean stations. From Martin *et al*. (1987).

$$F = 1.53\ (z/100)^{-0.858},\ (r^2 = 0.81) \qquad (10.01)$$

where z is depth in meters.

As Fig. 10.07 shows, the flux at 500 m is only about 0.4 mol C m^{-2} y^{-1} and at 2000 m it is on the order of 0.1 mol C m^{-2} y^{-1}. The difference is accounted for by the oxidation of the organic carbon to CO_2 during its downward journey. It works out that 50% of the carbon removed from the surface is regenerated in less than 300 m, 75% by 500 m, and 90% by 1500 m. The authors conclude that this rapid regeneration in near-surface waters means that the majority of the CO_2 removed from the upper 100 m will be available for exchange with the atmosphere within 10 years. That conclusion may be true for the area studied (between northern California and Hawaii) but in areas where the permanent thermocline is normally less than 100 m from the surface, much of the sinking carbon would be removed to the interior of the ocean and cut off from the atmosphere for at least several decades.

The question then arises, is this situation typical for oligotrophic gyres in the world ocean? Jenkins (1982) and Jenkins and Goldman (1985) studied oxygen utilization rates at a range of depths in the North Atlantic subtropical gyre. Martin *et al*. (1987) converted their carbon oxidation rates to oxygen utilization rates and compared the two sets of results. While the rates at 100 m in the Atlantic were somewhat lower than in the Pacific, the rates measured from 200 to 500 m

were all higher in the Atlantic, indicating that less carbon was oxidized above 200 m and more was oxidized at 200–500 m than in the Pacific.

As part of the Joint Global Ocean Flux Study (JGOFS), a cooperative study was undertaken along a transect in the eastern half of the North Atlantic, known as the North Atlantic Bloom Experiment (NABE). As part of this study, Honjo and Manganini (1993) deployed automated time-series sediment traps for one year at two sites. They found that at a depth of 2 km the annual mass flux was 22 and 27 g m^{-2} at the southern (34° N) and northern (48° N) stations, respectively. At the southern station, material from the spring bloom was identifiable from January to May, constituting 62% of the annual total, and at the northern station from March to May, contributing 50% of the total. When converted to fluxes of particulate organic carbon at 2000 m, the values were 1.03 and 1.38 g C m^{-2} y^{-1} at the southern and northern stations, respectively. These values are close to the 0.1 mol C m^{-2} y^{-1} reported for the northeast Pacific by Martin *et al*. (1987).

Note that these calculations do not take into account any export of dissolved organic matter (DOM). Dissolved molecules do not have a sinking velocity, but if a parcel of water containing significant amounts of DOM is carried to the interior of the ocean, this is a carbon export from the euphotic zone. DOM forms a vast reservoir of global carbon, and one which we know very little about and model in a crude fashion. Vertical migrations of zooplankton are also mechanisms for export. When zooplankton graze in the euphotic zone and respire or defecate in the deep ocean, they are making a carbon transfer that is not measured in traps.

At sites where there has been measurement of the downward flux, the fraction of primary production being exported is called the *e* ratio. To produce data sets for a particular type of ocean habitat, sites with *e* ratios are often combined (mixed) with sites with *f* ratios (on the assumption that new production approximately equals export production). Such mixed data sets are referred to as *ef* ratios. It is found that the *ef* ratio is a positive, non-linear function of total integrated primary production, ranging from less than 0.10 in oligotrophic waters to greater than 0.50 in productive coastal regions (Karl *et al*. 2003).

At any given level of production, the greatest effect on the *ef* ratio is temperature. Laws *et al*. (2000) (Fig. 10.08) generated a model that accounted for 97% of the variance in observed data. A large part of the success of the model is due to the fact that it clearly distinguished between larger plankton, which sink, and microplankton, which do not. At a fixed temperature, the export ratio is low at low rates of primary production, rises steeply at intermediate rates of primary production and plateaus at high rates of primary production. The height of the plateau is greatest at low temperatures, and the region of rapid rise shifts to progressively higher rates of primary production as temperature rises. The model was applied to satellite-based data on global primary production and predicted an annual global export production of 11.1 Pg carbon. Earlier estimates using other methods had been 9.1–10.8 Pg C and 7.2 Pg C.

To understand how important the biological pump is for changing the concentration of carbon dioxide in the atmosphere, it is useful to distinguish three kinds of mechanism for downward export of carbon, i.e., three types of biological pump (Karl *et al*. 2003).

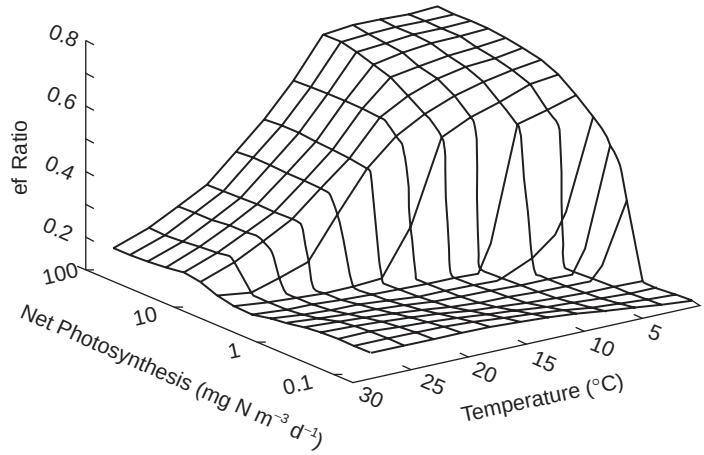

Fig. 10.08 Calculated *ef* ratios as a function of temperature and photosynthetic rate. From Laws *et al*. (2000).

1 The Redfield ratio dissolved/particulate carbon pump

This is the pump about which most is known. The ratio of the elements C, N, and P in the sinking organisms is initially the same as the ratio in the water (i.e. the Redfield ratio; C : P = 106, N : P = 16), although it changes as the organisms decompose during sinking. The production and export of these organisms depends in the long term on an upwelling of nutrient-rich water. Along with the nutrients N and P required for the continued production of the phytoplankton, the upwelled water will contain carbon in the form of CO_2 balancing the amount of carbon originally exported. There is no long-term sequestration of carbon.

2 The N_2-primed prokaryote carbon pump

In an N-limited system in which the biological fixation of N_2 temporarily relieves the system of its limitation, leaving P, Fe, and/or light control of new and export production, there is selection in favor of prokaryote organisms with elevated C : P ratios, (typically 250–300 : 1). Export of this non-Redfield organic matter leads to net removal of C from surface waters, relative to the nutrient-rich upwelled water.

3 The event-driven mass sedimentation carbon pump

Consider a specific physical or biological perturbation that results in a rapid pulse of export to the sea floor. An example would be when an atmospheric deposition of iron-rich dust in an area of iron limitation causes growth and aggregation of diatoms which sink rapidly to the sea floor (see Section 3.2.7). Even if the exported material conforms to the Redfield ratio, it is not in response to upwelled nitrate and carbon dioxide and there is a net removal of carbon from the ocean's surface on a time scale of decades to centuries (Karl *et al*. 2003).

Only type-2 and type-3 events cause a substantial long-term sequestration of carbon in the ocean. If they are found to be of relatively common occurrence, as some suspect, there will be changes in basic understanding of the biogeochemistry of the sea.

10.3.3 Sedimentation on the sea floor

The last stage in this biological pumping is sedimentation on the sea floor. As far as the major ocean gyres are concerned, the rate of carbon fixation by phytoplankton is relatively low. A large proportion of carbon that sinks is regenerated to CO_2 in the water column, so that deep-ocean sediments receive only a 1–2 g m^{-2} of organic carbon annually. Lochte *et al*. (2003) estimated that the global flux to depths greater than 2000 m is 0.34 Pg C yr^{-1}. The whole of the deep-ocean floor accounts for only about 15% of the world's carbon storage.

The situation on the continental shelves is quite different. They have much higher rates of primary production than the open ocean, and budgets show that perhaps half of this production is not grazed by the zooplankton, but sinks to the bottom (Walsh *et al*. 1981, Walsh 1983). One might therefore expect large accumulations of sedimentary carbon on the shelves. Instead, one finds large accumulations on the continental slopes, and the authors postulate that there is cross-shelf transport and export to the continental slopes that worldwide amounts to 2.7 Pg C y^{-1}. Perhaps two-thirds of this carbon is oxidized to CO_2 and returned to shelf and slope waters, but from studies of the organic carbon content of the sediments, their porosity, and ^{210}Pb measurements of sediment accumulation rates, it is concluded that 0.9 Pg of carbon is stored annually on the shelves and slopes, along with another 0.2 Pg in the estuaries and deltas.

10.3.4 The significance of biological fixation of carbon in calcium carbonate skeletons

Many of the uncertainties in marine carbon-cycling models arise from an imperfect understanding of the processes that control the formation and dissolution of calcium carbonate (Iglesias-Rodriguez *et al*. 2002). Reef-building activities by corals and the long-term deposition of tests of such planktonic forms as foraminifera and coccolithophores are mechanisms for the removal of carbon from the mixed layer of the ocean. Worldwide geological deposits of calcium carbonate attest to the long-term and pervasive influence of this activity by marine organisms. The question arises, should this downward flux of inorganic carbon be counted as a term of the biological pump, when considering ocean–atmospheric interactions? Not necessarily. Calcium carbonate precipitation releases CO_2 to solution, while $CaCO_3$ dissolution takes up CO_2 from solution. Both processes obey the reversible reaction

$$CO_2 + CaCO_3 + H_2O \leftrightarrow 2HCO_3^- + Ca^{2+} \qquad (10.02)$$

This reaction is considered to be approximately in equilibrium. Biotic processes that precipitate calcium carbonate drive this equation to the left, while dissolution of the precipitated carbonate drives the equation to the right. It is believed that much of the calcium carbonate precipitated by planktonic organisms is dissolved again in the water column, but it is not clear how much is dissolved in the mixed layer and how much at depth. Moreover, anthropogenic increase in atmospheric CO_2 may lead to increased CO_2 in the water and a decrease in net biological calcification, in reefs as well as in the plankton.

Formation of calcium carbonate removes CO_2 from the mixed layer (and indirectly from the atmosphere) but it also removes calcium. The removal of calcium affects the total alkalinity by the liberation of hydrogen ions. The latter process shifts the equilibrium between bicarbonate and carbon dioxide in the water, leading to the liberation of carbon dioxide to the water and eventually back to the atmosphere.

The addition of CO_2 by this process more than compensates for its removal in the formation of carbonate, so there is no net downward pumping from the atmosphere to the interior of the ocean. One may then ask, "But surely the sinking of calcium carbonate skeletons represents a net downward flux of carbon, a biological pumping?" The answer is, "This flux is compensated for by a change in the alkalinity of the surface waters, but not by a flux of carbon from the atmosphere. In the steady-state situation, the change in alkalinity is compensated by advection of some neutralizing material from other sources, such as the land, and not by a flux of carbon dioxide from the atmosphere." In short, although in geological time most of the carbon dioxide of the atmosphere has ended up as carbon buried in the sediments, it is not clear that the present-day biological calcification mechanisms are contributing significantly to that burial. Houghton *et al.* (2001) (Fig. 10.09) settled for a burial of 0.2 Pg C yr^{-1} on the shelves and 0.2 Pg C yr^{-1} in the deep ocean.

Calcium carbonate precipitation in coccolithophore blooms leads to strong optical signatures that can be detected both *in situ* and remotely. To the satellites, the signature is white scattering, leading to a "bright ocean." When coupled with *in situ* profiles of calcite, it is possible to construct global maps of planktonic calcium-carbonate-precipitating organisms in the ocean. Coccolithophores are found at low abundance in tropical and subtropical seas, but in higher concentrations in temperate seas in summer, following diatom blooms. Export of organic carbon by diatoms in spring can be offset by the efflux of carbon dioxide by coccolithophore blooms later in the year (Falkowski *et al*. 2003).

10.3.5 Summary of the biological pump

Among those attempting to model carbon dioxide fluxes between the atmosphere and the ocean, there is agreement that biological processes lead to a net flux of carbon into the ocean. Part of the primary production in the mixed layer is consumed and respired in that layer so that the carbon dioxide released by

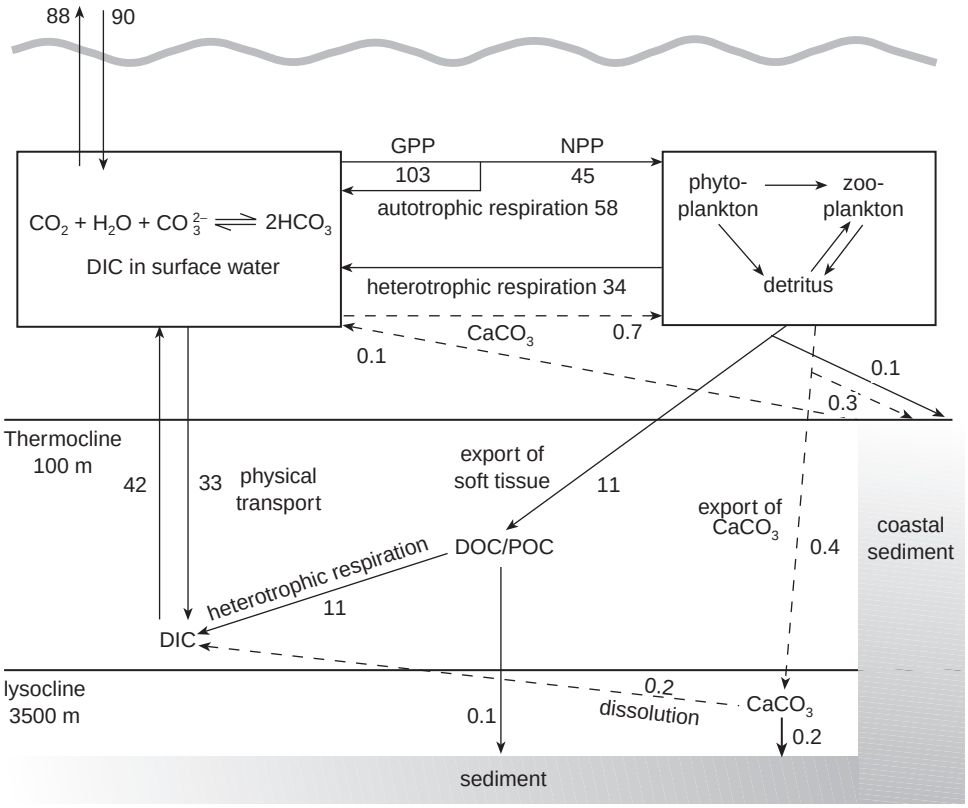

Fig. 10.09 Carbon cycling in the ocean (Pg C yr^{-1}). From Houghton *et al*. (2001). Reproduced by permission of the Intergovernmental Panel on Climate Change.

respiration is returned to the atmosphere, and therefore leads to no net loss to the atmosphere. Another part (equivalent to the "new production") sinks out of the mixed layer, carrying with it fixed carbon that is withdrawn from contact with the atmosphere for some considerable period. Carbon dioxide transfer across the sea surface is dependent on the difference between the partial pressure of carbon dioxide (pCO_2) in surface waters and in the air, multiplied by a gas transfer coefficient. The partial-pressure difference is strongly influenced by biological carbon fixation, since vigorous photosynthesis by algae reduces the carbon dioxide concentration in surface waters (although not enough to limit further carbon fixation). On the other hand, if cold water is upwelled and warmed at the surface, the change in temperature will increase the partial pressure, because warm water saturates at a lower gas concentration than cold water.

The gas transfer coefficient is dependent on such factors as wind strength, degree of surface turbulence, and the shape of the waves. Attempts to quantify these variables in wind-tunnel experiments have led to widely differing results, but some cross-checking against the values used to simulate conditions in the ocean can be

carried out by checking the rate at which radon gas and radioactive carbon have moved between the ocean and the atmosphere.

The following synthesis is derived from Houghton *et al*. (2001). Despite extensive global measurements conducted during the 1990s, measurements of surface water pCO_2 remain sparse, and extensive interpolation in space and time is required to produce global fields. Takahashi *et al*. (1999) interpolated data collected over three decades to derive monthly values of surface water pCO_2 over the globe for a "virtual calendar year" (1995). Using a transfer coefficient dependent on wind speed, monthly net fluxes were calculated and revealed clear regional and seasonal patterns. The greatest flux from the ocean to the atmosphere is believed to result from warming of upwelled water at the equatorial divergences. Although strong biological pumping occurs there, its magnitude is believed to be substantially less than the outgassing resulting from warming of upwelled water. The major sinks for carbon dioxide are found in polar and subpolar regions. Cooling of water as it flows from the equator toward the poles causes it to take up CO_2 from the atmosphere. Deep-water formation, mentioned in Chapter 8, leads to the downward transport of large amounts of the absorbed CO_2. The deep-ocean circulation transports large quantities of CO_2, for example 0.5–1.0 Pg C yr^{-1} southward in the Atlantic basin. Of the various estimates of carbon fluxes in the ocean, those shown in Fig. 10.09 are the ones selected by the Intergovernmental Panel on Climate Change for its report *Climate Change 2001: The Scientific Basis* (Houghton *et al*. 2001). The figures are all in Pg C yr^{-1}. The net flux from the atmosphere into the ocean is estimated at about 2 Pg C yr^{-1}. In the organic carbon cycle, gross global primary production is given as 103, and net primary production as 45. Of this amount, 34 Pg are shown as regenerated above the thermocline and 11 as exported below the thermocline in the form of particulate and dissolved organic matter. Almost all of this exported material is converted to carbon dioxide in the water column, and most of it is carried back above the thermocline by physical processes.

Burial of organic carbon in coastal sediments was discussed in Chapters 4, 5, and 6. The global total is estimated at 0.1 Pg yr^{-1}. Burial in deep-ocean sediments is thought to amount to only 0.01 Pg yr^{-1}. In the inorganic calcium carbonate cycle, total carbon fixation is given as 0.7 Pg C yr^{-1}, with 0.2 buried in coastal sediment and 0.4 exported to the deep ocean. Of this, 0.2 is regenerated into the water column and only 0.2 is buried in deep sediments.

As we saw in Section 10.3.2, most of the downward flux due to the biological pump is approximately in balance with the vertical movement of carbon by physical processes. There are, however, two processes that could cause a significant net sequestration of carbon into the deep ocean. One is blooming of phytoplankton with altered ratios of C : N : P, the other is mass sedimentation of phytoplankton driven by such events as relief of iron limitation. The extent to which they might respond to future increases in carbon dioxide in the atmosphere is unclear. If, however, changes in global temperatures or changes in freshwater run-off lead to changes in the patterns of ocean stratification and/or deep-ocean circulation, the present balance between the biological pump and the upward

physical movement of carbon dioxide might be disrupted. The current understanding is that while the biological pump has clearly made a large difference to atmospheric concentrations of CO_2 over geological time scales, it is not clear what difference, if any, it will make to changes in atmospheric CO_2 concentrations over a time scale of hundreds of years.

10.4 Evidence from paleoclimate studies

The magnitude of the recent rise in atmospheric CO_2 from about 280 ppm in the seventeenth century to over 350 ppm at present should be viewed in the context of long-term changes. From studies of the carbon dioxide content of bubbles formed in the ice caps thousands of years ago, we now know that during the last ice age CO_2 was as low as 180 ppm. Some of the most complete evidence comes from a Vostok ice core (Petit *et al*. 1999). Vostok station is located on the central part of east Antarctica, where the present mean annual temperature is –55.5 °C. The ice core was drilled to a depth of 3623 m and the deepest part is over 400,000 years old (Plate 7). Ambient temperature through the life of the core (expressed as the difference from present surface temperatures) has been estimated from the isotope composition (both deuterium and ^{18}O, which give good agreement). There was a rise of about 10 °C about 15,000 years ago, marking the end of the last ice age. The previous interglacial period was from about 140,000 to 116,000 years BP and its beginning was also signaled by a relatively rapid rise in mean temperature of about 10 °C. The record shows two earlier interglacial periods (Plate 7). The conclusion of Petit *et al*. (1999) is that throughout the 400,000-year record the atmospheric and climate properties oscillated between well-defined and stable boundaries. Present-day atmospheric burdens of carbon dioxide and methane were unprecedented during the past 420,000 years.

Temperatures during the glacial period fluctuated considerably, and this is often attributed to variations in the earth's orbit (Hays *et al*. 1976). As we turn our attention to the record of CO_2 in the bubbles trapped in the ice, there is a remarkable correspondence with the temperature, each rise in temperature being accompanied by a corresponding rise in atmospheric CO_2. At the end of each of the last two glacial periods, when the temperature rose about 10 °C, the carbon dioxide content of the atmosphere rose by about 40%. Interpretation of this result is controversial, analogous to the classic "chicken and egg" situation. Was the temperature change brought about by changing CO_2 levels, or did the changing CO_2 levels result from the climate change?

This text is not the place to debate theories of the causes of ice ages, but it seems to be agreed that a glacial period is brought on by a triggering factor that does not in itself cause the large drop in temperature. The triggering factor leads to a series of climatic feedbacks (such as increasing albedo as a result of the increasing ice cover) that lead to the observed drop in mean temperature, formation of greatly enlarged ice caps, drop in sea level, and so on.

Many regard changes in the earth's orbit ("orbital forcing") as the prime initiating factor (but see Broecker [1992] for a review of arguments against that view). The direction that the earth's axis points, in relation to the stars, cycles every 23,000 years. The obliquity of the earth's axis in relation to its tilted position changes on a cycle of 41,000 years, and its orbital eccentricity has a period of 100,000 years. Evidence that past ice ages have corresponded with these periodicities comes from ocean sediment cores going back 800,000 years (Hays *et al*. 1976; Kerr 1983). Three parameters were measured: (i) oxygen isotopic composition of planktonic foraminifera (a measure of temperature); (ii) a statistical analysis of radiolarian assemblages, previously shown to be correlated with temperature; and (iii) percentages of another radiolarian, not used in the previous data, thought to be an indicator of stratification in the water column. Spectral analysis showed that climatic variation in these records peaked every 23,000, 42,000, and 100,000 years, strongly supporting the theory that orbital forcing is a fundamental cause of quaternary ice ages. Similarly, spectral analysis of the 400,000-year ice-core record (Petit *et al*. 1999) shows that peaks of power occurred at 100, 41, 23, and 19 kyr (Fig. 10.10).

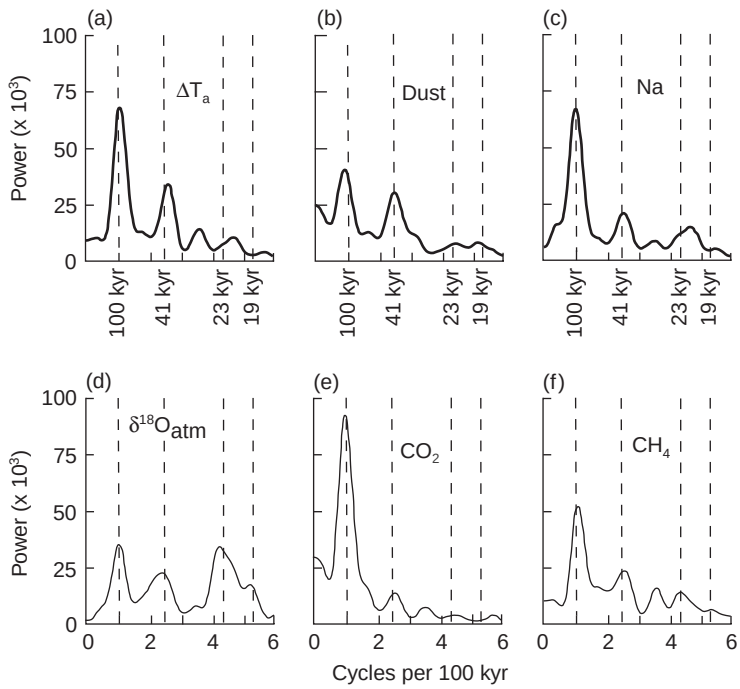

Fig. 10.10 Spectral properties of the Vostok time series. Frequency distribution (in cycles per 100 kyr) of the normalized variance power spectrum (arbitrary units): (a) isotopic temperature; (b) dust; (c) sodium; (d) $\delta^{18}O_{atm}$; (e) CO_2; (f) CH_4. Adapted from Petit *et al*. (1999). Reproduced by permission of Nature Publishing Group.

Glacial periods can be satisfactorily accounted for by various models involving orbital forcing, climatic feedbacks, and atmospheric carbon dioxide (reviewed in Lorius *et al*. 1988), but falling CO_2 levels are responsible for more than half of the effect. This result would not be expected from the direct radiative effect of the CO_2 changes, which require amplification. Petit *et al*. (1999) concluded that in each of the four terminations of a glacial period that they studied there was the same sequence of events. The first was orbital forcing (with a possible contribution of local insolation changes), followed by two strong amplifiers. Greenhouse gases acted first, then deglaciation and ice-albedo feedback. Clearly, the CO_2 changes are essential to the models. This brings us to the question: What caused them?

10.4.1 Theories concerning rapid changes in atmospheric CO_2

Plate 7 shows that each ice age was marked by a long, slow decline in CO_2 levels in the atmosphere and the termination was accompanied by a roughly 40% increase in CO_2. If we could understand the causes and consequences of these changes, we should be in a better position to attempt to forecast the effect of further increases in atmospheric CO_2 as a result of human activities. Obviously, two classes of factors are involved, physical and biological. The ocean is divided into two concentric spheres: the surface mixed layer, whose CO_2 partial pressure is a little above or below atmospheric value, and the deep ocean, which is supersaturated with CO_2 and contains a huge reservoir, 50–60 times that of the atmosphere. Any physical mechanism that increases the transport from the deep ocean to the surface mixed layer will cause a rise in atmospheric CO_2. Alternatively, since the biological pump is responsible for the downward transport of carbon dioxide into the deep ocean, any factor that decreases biological activity while upward transport from the deep ocean continues at its normal rate will lead to increasing atmospheric CO_2.

(a) The Southern Ocean

We saw in Section 3.2.7 that in much of the Southern Ocean primary productivity is iron-limited, and it was hypothesized that inputs of iron by deposition of airborne dust could stimulate primary production and the sequestration of carbon. The Vostock ice core shows that such depositions of dust did occur, and that the power spectra of their occurrences peak at the same frequencies as temperature and greenhouse gases (Fig. 10.10). They occurred during glacial periods and appear to be responsible for holding CO_2 and temperature at low levels. Terminations of glacial periods were preceded by a drop in the level of dust deposition. However, there is a lag between the reduction in dust supply and the rise in CO_2. Broecker and Henderson (1998) suggested that if the deposition of iron caused higher rates of nitrogen fixation during glacial periods, and if this

nitrogen inventory were distributed worldwide by the deep-ocean circulation, there would inevitably be a lag between the decrease in deposition and the increase in atmospheric CO_2. Stephens and Keeling (2000) proposed that extended winter sea ice around the Antarctic continent during glacial times prevented outgassing of CO_2-rich water. A layer of melt-water may also have restricted outgassing during summer.

(b) Tropical waters

Ganeshram *et al*. (1995) pointed out that if water column denitrification, which occurs mainly in the eastern tropical North Pacific, the eastern tropical South Pacific, and the Arabian Sea, were to be markedly reduced, this would increase the amount of nitrate available for stimulating biological pumping. They produced evidence from sediment cores showing greatly reduced water-column denitrification during glacial periods.

Another suite of models has invoked increased nutrient upwelling at the tropical divergence during glacial times, with increased biological pumping and a decrease in atmospheric CO_2 (even though outgassing of CO_2 at the equator would presumably continue). Attempts have been made to calculate changes in ocean productivity between glacial and interglacial times by comparing the organic content and the carbon isotope ratios of the appropriate parts of ocean bottom cores. Sarnthein *et al*. (1988) concluded that there was a massive decrease in new production at low- and mid-latitude upwelling areas at the termination of the last ice age, with a consequent increase in atmospheric CO_2. They attributed it to orbital forcing, leading to an increase in high-latitude insolation, reduction in ice cover, and a reduction in the strength of meridional trade winds.

Mix (1989), while not disagreeing with the conclusions of Sarnthein *et al*. (1988), cited numerous difficulties with interpretation of organic-matter data from cores. He proposed instead to carry out a major reconstruction of ocean productivity in times past, using the community structure of foraminiferan assemblages as his index. Beginning with a global ocean productivity map, he developed for the North and South Atlantic Ocean a relationship between foraminiferan assemblages on the contemporary sea floor ("core tops") and the level of productivity of the waters above. This analysis was done using standard transfer function techniques (Imbrie and Kipp 1971). The result was a regression of measured productivity against estimated productivity with an error envelope of ± 12 g C m^{-2} y^{-1}. Then, turning to the foraminiferan assemblages present at the glacial maximum 18,000 years BP, he constructed surface productivity maps for that time. They were markedly different from contemporary productivity maps. The largest increases were seen at the equator and in subtropical regions, the least in eastern boundary currents. Overall, Mix (1989) estimated an increase of 18% in total primary productivity of the North Atlantic. Using the arguments of Eppley and Peterson (1979) that show that higher rates of production tend to have a higher proportion of new production, Mix (1989) estimated that new production would have been 38% higher overall, and 87% higher in equatorial regions, during the coldest period of the last ice age.

The consequences of this increased biological pumping would have been a reduction in atmospheric CO_2. The earlier suggestion that this CO_2 reduction was caused by an increase in dissolved nutrients in the deep ocean is rejected. Instead, modifications of the present-day atmosphere–ocean interactions are invoked. During the ice ages, it is suggested, a stronger thermal gradient between the poles and the equator resulted in stronger trade winds and stronger upwelling of nutrient-rich water, particularly at the equator.

Sundquist (1993) reviewed these arguments and added a further important consideration. Because the amount of CO_2 in the deep ocean is 50–60 times that of the atmosphere, and a delicate balance exists between carbonate, bicarbonate, and dissolved CO_2, any mechanism that changes this balance in the deep ocean can liberate large quantities of CO_2, a portion of which will find its way into the atmosphere at sites of upwelling. Hence, the mechanism delivering biologically fixed carbonate to the deep ocean ("the carbonate pump") is intimately related to events during deglaciation. This scenario for the life of an ice age now appears to have the following components:

1 Changes in the earth's orbit led to reduced solar radiation at high latitudes, lower temperatures, and spread of the polar ice caps.
2 Increase in the thermal gradient between the poles and the equator led to strengthening of trade winds and to complex changes in the patterns of primary production in the oceans including increased upwelling of nutrient-rich water at the equator.
3 Increased upwelling caused enhanced biological pumping, and a decrease in atmospheric CO_2, which in turn led to further cooling.
4 Pulses of iron-rich dust falling in the Southern Ocean stimulated biological production and sequestration of carbon. Part of the effect was to stimulate nitrogen-fixing organisms, which added to the inventory of nitrogen in the world's oceans.

After an appropriate period the orbital position of the earth changed enough to begin a reversal of the process.

Note that this model predates the idea of three types of biological pump (Karl *et al*. 2003; see Section 10.3.2) and would now require some modification. It would not work if the carbon in upwelled, nutrient-rich water balanced the biological carbon export.

10.4.2 Postulated changes in the rate of deep-water formation

We saw in Section 8.2.5 that the world's major source of deep-water formation is in the North Atlantic. Broecker *et al*. (1985) pointed out that as polar water sinks, water from the south moves north to take its place. While doing so, it cools and about 5×10^{21} calories of heat are released into the atmosphere each year. This

energy modifies the climate of the North Atlantic basin and adjacent land areas. The water that sinks in the Norwegian and Greenland Seas is relatively deficient in nitrogen and phosphorus. Foraminifera in surface sediments taken from the floor of the North Atlantic have a low cadmium-to-calcium ratio, indicative of this low nutrient status.

Broecker *et al*. (1985) reviewed the evidence that the formation of deep water in the North Atlantic was severely reduced in glacial times. It has been found that the cadmium-to-calcium ratio in benthic foraminifera was higher in glacial times than today, indicating a more nutrient-rich water. It has also been shown that their stable carbon isotope signature in glacial times was indicative of deep water much more like that found in the Pacific during the same period. All this evidence suggests that the organisms living deep in the North Atlantic were in water that had a different origin than today, and this finding opens the possibility that in glacial times the thermohaline circulation of the world was radically different than it is today. Even the possibility of reversal, with deep-water formation in the Pacific and upwelling in the Atlantic, should not be ruled out. Just how this would relate to the scenario reviewed above in Section 10.4.1 remains unclear.

Evidence that radical changes have occurred in the operation of the deep circulation of the North Atlantic has been reviewed by Bond (1995). From interpretations of foraminiferan communities and stable isotopes of carbon and oxygen in cores, it has been shown that major shifts in the operation of the "Atlantic Conveyor" arose during the last glaciation. Confirmation of major changes in bottom current speed were obtained by studying grain size distribution in cores. Details of the various findings are not in agreement, but it now seems certain that major changes in deep-ocean circulation accompanied the climate fluctuations during the last ice age.

There have been many attempts to model the effect of rising atmospheric CO_2 and temperature on the thermohaline circulation. As temperature rises, rainfall and run-off in North America increase, and the warming and freshening of the North Atlantic Current makes it more resistant to sinking for intermediate and deep-water formation. For example, Stocker and Schmitner (1997) made a model that showed that with atmospheric CO_2 concentrations rising to 750 ppm in 100 years (approximately the present rate of increase), the thermohaline circulation shut down. If the atmospheric concentration of 750 ppm is attained more slowly, the circulation simply slows down. Other models make different predictions and there is no consensus about the risk that global warming will radically change the thermohaline circulation. However, considering the enormous effect that the "Atlantic Conveyor" has on the climate of Western Europe, control of the rate of increase of atmospheric CO_2 appears to be crucial.

10.5 Phytoplankton and dimethylsulfide

In addition to their role in fixation of carbon dioxide, phytoplankton are thought by some workers to influence the earth's climate through the production of dimethylsulfide, or DMS (Charlson *et al*. 1987). The idea has come to be known

as the CLAW hypothesis, from the names of the authors. Most species of phytoplankton excrete DMS, and some of it escapes to the atmosphere, where it reacts to form a sulfate and a methane sulfonate aerosol (MSA). The latter substance stimulates the formation of clouds over the oceans, thus increasing albedo and reducing temperature at the earth's surface.

Dimethylsulfide is the only volatile sulfur compound excreted by phytoplankton and its biological function is unclear. It is a breakdown product of dimethylsulfoxide (DMSO), which may have an osmotic function in some species. The concentration of DMS in surface waters is only weakly correlated with the biomass or productivity of the phytoplankton. Once released into the water, DMS may be broken down photochemically, removed by bacteria, or released into the atmosphere. Rates of emission from the sea to the atmosphere are in the range of 2.2–5.7 mmol m^{-2} y^{-1}, with the highest values being found in warm, highly productive coastal regions. Coccolithophorids, which are most abundant in tropical, oligotrophic waters, have a high rate of DMS production per unit biomass, while diatoms have a low rate of production.

Cloud condensation nuclei (CCN) are essential to the formation of clouds of liquid water droplets. It is thought that at the present time the air over continents has an abundance of particles that could act as CCN, but that air over the oceans remote from land has a relative shortage of suitable particles. Water-soluble sulfates are believed to be the natural CCN in the marine air. Sea-salt particles are possible candidates, but concentrations at cloud height are much too low for them to be important. Attention therefore focused on "non-sea-salt sulfate," and DMS was identified as the most likely precursor of such sulfate particles.

Charlson *et al*. (1987) developed at considerable length the technical arguments that led them to believe that an increase in DMS in the atmosphere (with water content held constant) would lead to a larger number of smaller droplets, and that this development would increase the earth's albedo, which, in turn, would have a cooling effect. Since DMS is released into the atmosphere at the highest rate in tropical waters, the authors argued that it serves a useful function in moderating the extremes of temperature over the tropical oceans. They saw this condition as part of the global feedback control to which Lovelock (1979) drew attention in his book *Gaia*.

The importance of DMS as a climatic influence was challenged by Schwartz (1988). He argued that if DMS emissions have a strong influence on global albedo, an even stronger effect should be detectable from manmade sulfur dioxide emissions, for these are thought to release twice as much sulfur into the atmosphere as the phytoplankton. Moreover, the release is mostly in the northern hemisphere, and has increased to its present level during the past 100 years. Schwartz searched the records for any evidence of higher albedo in areas most under the influence of industrial sulfur emissions, and found none. He also found no evidence of reduced temperatures in the northern hemisphere compared with the southern. His conclusion was that anthropogenic sulfates do not have an important effect on the cloud component of albedo. By extension, he suggested that neither do the products of DMS emission. On the other hand, Legrand *et al*. (1991) showed

that in the Vostok ice core (Plate 7) the levels of DMS and non-sea-salt sulfate (NSSS) in the atmosphere were much greater during the later stages of the last glacial period than they are today, suggesting that this condition was a factor in global cooling.

An important body of data pertinent to this subject was published by Prospero and Savoie (1989). They reported on analyses of methane sulfonate aerosol (MSA) and NSSS on eight Pacific islands. They took Fanning and American Samoa as sites totally remote from industrial activity and found that the ratio MSA/NSSS was 0.065. They then used this ratio to calculate the proportion of non-sea-salt sulfates derived from DMS at other Pacific sites. They concluded that about 80% of all cloud condensation nuclei over the North Pacific were attributable to DMS from phytoplankton. They claimed that most of the industrial sulfur emissions emphasized by Schwartz are deposited on land, locally or regionally, so that, for example, only 20–25% of those produced in North America are exported from the continent. In light of these conclusions, the original hypothesis of Charlson *et al*. (1987) may still be valid. The possibility that, in the context of global warming, DMS production by phytoplankton could be a negative feedback, moderating some of the effects of increasing atmospheric CO_2, cannot be ruled out.

Reviewing the role of natural and manmade aerosols, Charlson and Wigley (1994) concluded that anthropogenic sulfur emissions far exceed those from phytoplankton, and that it is highly probable that global warming would have been greater, especially in the northern hemisphere, if there had not been an increase in albedo associated with the sulfur aerosols. In the elaborate coupled ocean–atmosphere model of Mitchell *et al*. (1995), the addition of a term for sulfate aerosols considerably improved the agreement with global means and large-scale patterns of temperature in recent decades.

Boyd and Doney (2003) reported that DMS-mediated increases in cloud albedo are thought capable of cooling the planet by about 1 °K, but that the CLAW hypothesis remains untested. Meantime, Kettle *et al*. (1999) produced maps containing 15,000 observations of DMS levels in the surface ocean. In mid-summer in both the northern and the southern hemispheres there are high DMS concentrations in Southern Ocean polar waters, and in the subarctic northeast Atlantic and northeast Pacific Oceans. Anderson *et al*. (2001) expanded the database of Kettle *et al*. (1999), and succeeded in predicting the global fields of DMS, using a combination of chlorophyll, irradiance, and nutrients. The main producers of DMS precursors are the haptophyte algae such as coccolithophores, *Phaeocystis*, and the assorted group that develops under iron enrichment, collectively known as the "HNLC haptophores." More work is needed to predict how these haptophore stocks would respond to climate change.

10.6 Summary: our new world of climate change

Almost every topic discussed in this chapter is marked by large areas of uncertainty. Yet we are confronted with urgent global problems, and to meet these

challenges we need all the insight we can muster about the interactions of the atmosphere, the terrestrial biota, and the oceans.

Changes in global temperature

It is clear from the information reviewed in earlier parts of this chapter that the anthropogenic greenhouse gases (principally carbon dioxide, methane, nitrous oxide, halocarbons and ozone) have been responsible for significant global warming, while natural and anthropogenic aerosols have tended to reduce global temperature. The net effect has been an increase of 0.6 ± 0.2 °C in the temperature of the earth's surface over the past 150 years. Simulation models that include the known natural and anthropogenic forcing factors provide good agreement with the temperature record (Houghton *et al*. 2001). Using such a model and a variety of scenarios for energy use in the future (IPCC 2000), the global temperature is predicted to rise between 1.5 °C and 5.8 °C, with an average about 3 °C, by the year 2100. This is about five times the rate of increase observed over the past 150 years and without precedent during the last 10,000 years, based on paleoclimate data. It is expected that there will be more frequent extremely high maximum temperatures. How will this warming be distributed over the globe? The various models agree that the maximum warming will be in the high latitudes of the northern hemisphere (mainly because of melting ice and changing albedo) and the minimum will be in the Southern Ocean (due to ocean heat uptake). Beyond those predictions, further details depend on what scenario for anthropogenic emissions is used and to what extent poorly understood phenomena such as aerosol effects or deep-water formation are included in the model. For example, models that allow for deep-water formation and thermohaline circulation show a warming minimum in the North Atlantic, while other models do not.

Changes in sea level

Since the last glacial maximum about 20,000 years ago, the global sea level has risen by over 120 m as a result of melting ice and thermal expansion of the water column. The most rapid rise was between 15,000 and 6000 years ago, with an average rate of 10 mm yr^{-1}. In the last 3000 years the average rate has been 0.1–0.2 mm yr^{-1}, but during the twentieth century it was 10 times greater, 1.0–2.0 mm yr^{-1}, or 0.1–0.2 m per century. The largest component has been caused by thermal expansion, as the oceans become warmer.

Projecting into the future, thermal expansion is likely to be the major cause of change, followed by the melting of mountain glaciers and ice caps. The ice sheets in Greenland and Antarctica, which are in cold climates with low precipitation, are expected to make a smaller contribution than the mountains and glaciers in temperate climates. The range of predictions based on various scenarios is for a sea level rise of 0.13–0.94 m by 2100, with a central value of 0.48 m, which is about 2–4 times the rate during the twentieth century.

How will natural systems respond to changes in sea level? If sea-level rise is too rapid, natural succession of coastal ecosystems cannot occur because the rate of change is faster than anything that has occurred since the last glaciation. The effect will be exacerbated where developed areas behind the coastal systems are physically protected. For example, under a scenario of a half-meter rise by the year 2100, it is estimated that more than 10,000 km^2 of coastal wetland could be lost in the contiguous United States. In the short term, as marshes flood, die, and decompose, the release of nutrients would stimulate productivity, but the loss of detritus-based food webs and of habitat for seabirds, spawning fish, shrimp, and shellfish would likely lead to reduced fisheries yields. If coastal protection is absent, it may be possible for some coastal communities, such as salt marshes and mangrove stands, to migrate inland with the rising waters.

Looking beyond North America, it seems possible that a large proportion of the surface area of countries like Bangladesh and various Pacific islands will be completely inundated, with severe consequences for the human populations and the natural environments.

Changes in precipitation

The models predict that globally averaged water vapor, evaporation, and precipitation will increase, but there will be strong regional variability. Mean precipitation will increase in most tropical areas, decrease in most subtropical areas, and increase in high latitudes. The intensity of rainfall events will increase. As discussed in Section 10.4.2, the lower density of the mixed layer, caused by the increase in temperature and freshwater run-off, is expected to weaken the northern hemisphere thermohaline circulation. This in turn would reduce but not eliminate the warming of western Europe.

Consequences for oceanographic processes

In the 1980s, in the days of less sophisticated models of climate change, predictions were made about the combined effect of the various element of climate change (e.g. Wright *et al*. 1986, Frank *et al*. 1988). Some of these predictions still stand as reasonable, others need modification. A modified list might look like this:

- Rising temperatures and increased evaporation will lead to a more vigorous hydrological cycle.
- In the tropics and in temperate and polar latitudes, the increase in precipitation will lead to more river run-off and increased stability of stratification on the shelves. Nutrients in river run-off will stimulate primary productivity, and earlier stratification in temperate waters will lead to earlier spring blooms. Buoyancy-driven currents, such as the Labrador Current, might be less strong.
- The thickness, areal extent, and duration of ice cover will decrease.

- Enhanced warming at high latitudes will lead to a reduced meridional gradient in atmospheric temperatures and a general reduction in wind stress. This in turn will lead to reduced flow in the wind-driven gyres, so that, for example, the Gulf Stream and the Kuroshio Current will be less strong.
- If there is a general reduction in wind stress and increased precipitation in tropical and temperate areas, it might be expected that there would be less upwelling of nitrogen both in the tropical upwelling areas and in temperate areas during summer stratification. This would tend towards decreased primary production.
- Since the land is expected to warm faster than the ocean, there will be an intensification of the temperature gradient between land and sea, and perhaps enhanced upwelling and primary production in coastal upwelling systems (Bakun 1990).

Consequences for populations of marine organisms

In Monterey Bay, California, the annual mean shoreline water temperatures have increased by 0.75 °C during the past 60 years, while decadal mean summer maximum temperatures have increased by 2.2 °C. In the intertidal fauna, the abundance of southern species has increased while the abundance of northern species has decreased, indicating a northward shift in species ranges (Barry *et al*. 1995). As one might expect, global warming would lead to a poleward shift in the range of some species. This has already been reported for anchovy *Engraulis encrasicholus* and herring *Clupea harengus* stocks off western Europe during a warming episode associated with the North Atlantic Oscillation (Section 9.5.3). Warming trends in coastal waters of California, accompanied by decreasing biomass of zooplankton, have been reported by Roemmich and McGowan (1995), but it is not clear whether this was a long-term trend resulting from climate forcing or was part of an interdecadal fluctuation (Hill 1995).

On the eastern seaboard of North America, during the warming trend of the 1940s, there was a northward shift in the abundance and distribution of mackerel *Scomber scombrus*, lobster *Homarus americanus*, and menhaden *Brevoortia tyrannus*. Green crab *Carcinus maenas* established a resident population north of any previously recorded location. During the cooling trend of the 1960s, American plaice *Hippoglossoides platessoides* and butterfish *Poronotus triacanthus* retracted their range southward, and capelin *Mallotus villosus* and spiny dogfish *Squalus acanthias* extended their migrations southward. Other species, such as haddock *Melanogrammus aeglefinus*, yellowtail flounder *Limanda ferruginea*, winter flounder *Pseudopleuronectes americanus*, and winter skate *Raja ocellata*, appeared not to change their range in response to temperature changes, and it is suggested that their distribution is determined more by the presence of an appropriate bottom type. From all of this evidence it is concluded that in the Gulf of Maine, for example, many species might be displaced northward by global warming, and their place taken by an assemblage of fishes more characteristic of the Mid-Atlantic Bight. This population would include menhaden, butterfish, red hake *Urophycis chuss*,

silver hake *Merluccius bilinearis*, and herring. From Chapter 9 we may recall that the warming event of the 1940s was associated with a strong northward extension of the range of cod *Gadus morhua* in West Greenland, and we may speculate that a similar event might be precipitated by global warming in the twenty-first century.

On the other hand, indirect food-chain effects can produce results contrary to expectation. Species such as cod and haddock might be adversely affected by warming. It was found in the Gulf of Maine area that the ctenophore *Pleurobrachia* (a jellyfish-like animal), when present in its peak abundance (>1 m^{-3}), can graze down the zooplankton on which larval cod and haddock rely. Normally, the larval fish occur in spring and the ctenophores in mid-summer so competition for food is minimal. However, in 1983 the sea surface was unusually warm between January and April and the time of peak ctenophore abundance advanced from summer to spring. As a result, the ctenophores and larval haddock coincided, and the 1983 haddock year-class was the lowest on record (Frank 1986). Hence, there is a possibility that freshening and warming of the coastal waters off Nova Scotia and in the Gulf of Maine might lead to reduced success of cod and haddock recruitment.

In Section 8.4.4 it was shown that when a warm-core ring interacts with the continental shelf, there could be adverse effects on year-classes of fish because the larvae are swept off the shelf and dispersed into the open ocean. One prediction that could be made is that this situation will occur less frequently because reduction in strength of the Gulf Stream as a result of global warming will lead to the formation of fewer warm-core rings.

In the discussion of tidal currents (Section 7.3.2) it was shown that the distribution of herring spawning grounds in the North Atlantic often coincides with tidally mixed areas, and that the young stages often seem to be retained in those areas for a considerable period. It was further suggested that the upper limit of the size of a spawning stock might be determined by the limits of the tidally mixed area. Under the conditions of global warming, with a freshening of coastal waters, a small decrease in the extent of tidally mixed areas might be expected, which might have some consequence for the herring stocks.

To turn from species of commercial importance to more broad ecological principles, the freshening of coastal waters might be expected to lead to earlier onset of stratification in areas that are not tidally mixed, and hence a lengthening of the period of stratification. This change will shift the growth advantage from larger to smaller cells in the phytoplankton. In general, it should lead to a lengthening of the food chain between the primary producer and the larger consumer species. In longer food chains the loss of energy in respiration and of nutrients in excretion leads to a lower secondary productivity at the higher trophic levels subject to human exploitation. On the other hand, lobsters and scallops might be expected to thrive under these conditions. Lobster landings have shown interesting positive correlations with river run-off in the first year of the lobster's life (Section 4.7.2) and scallop year-class success has been positively correlated with the water temperature in the year in which they were recruited.

One might have hoped that it would be possible to offer an opinion as to whether ocean productivity would be higher or lower as a consequence of global warming. Certainly many features, such as the reduced wind stress and greater water-column stability in north temperate coastal waters, suggest less upwelling of nutrient-rich water and hence reduced productivity. On the other hand, waters that are now ice-covered for a substantial part of the year will become ice-free and have increased productivity. We can say for certain that things will be different, and that those who exploit the ocean resources in a particular place will need to pass through a painful period of adjustment, but it is not possible to say what the overall effect will be on global ocean productivity.

Part D

Discussion and conclusions

11

Questions for the future

Introduction

We have reviewed the dynamics of marine ecosystems from three perspectives. In Chapter 2 we concentrated on the turbulent flow of the water surrounding the organisms to understand better how algae obtain inorganic nutrients and microscopic animals obtain their food. Chapters 3 to 8 reviewed the biological and physical processes associated with the formation of phytoplankton concentrations in spring blooms, at fronts, in coastal upwelling areas, at shelf edges, in rings, and in estuaries. The final perspective, in Chapters 9 and 10, was of long-term variations in biological productivity due to decadal-scale variations in weather patterns.

In all of these discussions we reviewed information on consumer dynamics where it was available, but by far the greater part of the text concerns phytoplankton. There are two reasons for this bias. One is that phytoplankton production is a prerequisite for almost all other kinds of biological production, and is in its turn almost totally dependent on the transport of nutrients from deep water by physical processes. The other is that for many years we have been able to measure chlorophyll continuously by means of a fluorometer, and this has served as a useful index of phytoplankton biomass, albeit a rough one. The ratio of chlorophyll to carbon varies five-fold, so our estimates of phytoplankton biomass are at best approximate. Instruments for the continuous measurement of zooplankton biomass were devised more recently and are still under development.

As marine ecology emerges as an integrated discipline concerned with the physics, chemistry, and biology of the oceans, there is a search for generalities around which to organize the multiplicity of observations. We see this search revolving around four questions:

1 Is there a common mechanism to account for the occurrence of high biological productivity in a variety of physical environments?

2 To what extent are events in marine ecosystems determined by physical processes, and to what extent are the outcomes modified by interactions within the biological community?

3 How can we develop concepts and models that span the enormous range of scales in marine ecology, from the microscopic to the global and from seconds to geological ages?
4 How do we explain an apparent synchrony in the variations in the biomasses of fish stocks worldwide?

Is there a common mechanism to account for the occurrence of high biological productivity in a variety of physical environments?

A widely accepted generalization is that phytoplankton production is limited primarily by the supply of nitrate and that global primary production is a function of the various physical mechanisms making nitrate available in the photic zone. Evidence in support of this hypothesis is summarized below. However, the discovery that large elements of the phytoplankton are limited by the availability of trace elements such as iron and silicon means that work is needed to generate more complex models of global primary production. Furthermore, the discovery of the widespread abundance of extremely small photosynthetic cells, many of which are unable to use nitrate, requires a radical reshaping of concepts about the control of primary production in the sea.

It was pointed out by Legendre (1981), and is amply confirmed by our review, that there is one sequence of events that occurs in a variety of physical settings and on time scales ranging from a few hours to a year, and that normally leads to an increase in phytoplankton production. The essence of it is strong vertical mixing followed by stratification of the water column. As first described by Gran (1931) and presented as a quantitative model by Sverdrup (1953), it was offered as the explanation of the spring bloom in temperate waters. The vertical mixing brings nutrients from depth to surface waters, and the formation of stratification confines the phytoplankton to a well-lit zone in which daily photosynthesis exceeds daily respiration. The driving forces for vertical mixing are convective cooling and wind stress at the surface. The chief agent of stratification is solar heating.

In estuaries and parts of the continental shelf vertical mixing may be driven by tidal currents interacting with the bottom, and stratification may be mainly a function of freshwater run-off, but the effect on the phytoplankton is the same. The major difference is the time scale. The strength of tidal currents varies with a diurnal rhythm and with the fortnightly cycle of spring and neap tides. When tidal currents are strong, vertical mixing is also strong, and when tidal currents are weak stratification is more marked. We have reviewed examples of high phytoplankton productivity corresponding with each period of stratification.

At tidally mixed fronts, the area of tidal mixing increases with the spring tides and decreases on the neap tides, causing the front to move back and forth horizontally. At some geographical locations there is an alternation of tidal mixing and stratification that leads to enhanced phytoplankton production and biomass.

Similarly, in areas noted for their coastal upwelling, the prevailing wind brings cool nutrient-rich water to the surface and a relaxation of that wind permits surface warming and stratification. The high productivity is associated with the relaxation of the winds, as the phytoplankton utilizes the upwelled nutrients. Even in areas of more or less continuous winds, a horizontal succession of events can be detected. Close to the coast, nutrients are abundant in the freshly upwelled water, but as it streams away from the area of upwelling stratification sets in and phytoplankton biomass increases. Still further from the coast is a zone in which the zooplankton become more abundant as they feed on the phytoplankton. A similar zonation is found in relation to equatorial upwelling.

Here, then, is a mechanism of biological productivity that is found in situations as diverse as a temperate estuary and a mid-ocean band of upwelling running parallel with the equator. The alternation of vertical mixing and stratification is surely one of the most important sequences in marine ecology. In Chapter 3, we referred to examples that appeared to contradict the Gran/Sverdrup model – namely, instances where a phytoplankton bloom was initiated in the apparent absence of stratification. A bloom (i.e., an accumulation of phytoplankton biomass) is the result of the growth term for a phytoplankton population being significantly larger than the loss term. Platt *et al*. (1994) pointed out that the loss term is usually either grazing or sinking, so if these processes were unusually low, biomass could accumulate and a bloom could form. If light increased rapidly due to increasing day length, or if the actual depth of the mixed layer was less than that indicated by profiles of conductivity or temperature, the growth term could increase while the loss terms remained unchanged. The last situation is thought to occur when a body of water is subject to an unusually low level of wind mixing for a protracted period. The phytoplankton are moved vertically at such a slow rate that they are able to grow and multiply in the absence of a clearly defined shallow thermocline. Because in the examples on record of blooms forming before the onset of stratification, the critical parameters for the test of these mechanisms were not measured, no conclusive evidence has been gathered for violation of the Gran/Sverdrup model.

Making a clear distinction between changes in phytoplankton productivity and the accumulation of biomass (i.e., bloom formation) has enabled oceanographers to begin the development of a global classification of pelagic ecosystems (Banse and English 1944; Longhurst 1995, 1998) that embodies the Gran/Sverdrup model in conjunction with other physical and biological mechanisms. For example, Longhurst calls the areas exhibiting the classical pattern of spring bloom and subsidiary autumn bloom the Westerlies Biome. A variant of this pattern is found in the North Pacific, where the formation of a deep mixed layer in winter is limited by the low salinity of the surface waters (see Section 3.3.8). Poleward of this area, where spring comes very late but the days of summer are very long, the main bloom takes place in summer. A subsidiary fall bloom in that locale may be mediated by reduced grazing pressure as the zooplankton sink to overwintering depths. Areas exhibiting this pattern are called the Polar Biome. The Trades Biome is the area that is permanently stratified and in which the biomass of phytoplankton

fluctuates with small amplitude in response to seasonal variations in trade winds. Finally, Longhurst (1998) recognizes a Coastal Boundary Zone Biome in which a wide range of mechanisms, including tidal mixing, internal waves, wind stress, river run-off, or topography, cause periodic upwelling that is interspersed with stratification caused by either surface warming or reduced salinity. These mechanisms are analyzed in Chapters 4–7 of this textbook. All are consistent with the Gran/Sverdrup model.

Just as oceanographers were beginning to think that they had a grasp on seasonal cycles of phytoplankton production worldwide, two new observations suddenly made the whole picture much more complex. One was the finding that large areas of the ocean appear to have their primary production limited by the availability of micronutrients such as iron and silicon. The second was that perhaps more than half of the biomass of primary producers in the oligotrophic gyres is made up of cyanobacteria, *Prochlorococcus*, etc. These organisms may be unable to utilize nitrate. Both findings require that current production models based on the vertical transport of nitrate-rich water will need to be supplemented by totally different kinds of models. This is an important area for future research.

To what extent are events in marine ecosystems determined by the physical processes? To what extent are the outcomes modified by interactions within the biological community?

Most of the text of this book deals with situations in which physical factors strongly influence biological events in predictable ways. However, there are some situations in which the course of events is strongly influenced by the biology, and the consequences of physical events are not predictable without taking the biology into account. Examples are given below, but much remains to be done to understand how interactions such as competition, predation, or adaptation within the biological communities modify the expected consequences of a physical process.

Does the concept of auxiliary energy help clarify physical–biological relations?

In our review we have seen that physically the ocean is controlled by heating and cooling, freshwater run-off, wind-driven currents, eddies, turbulence, and vertical stratification. The solar energy that provides the heating is also captured by phytoplankton, passed from one organism to the other through the feeding process, and finally dissipated in the heat of respiration. Physical oceanography deals with the first of these pathways and biological oceanography with the second. In marine ecology we become concerned with both, and we then notice that the two pathways are interrelated. Water movement breaks down the boundary layers around organisms, transports nutrients and waste products, and influences the rate of encounter between planktonic predators and their prey.

Organisms use currents to assist their migrations and sessile organisms occupy sites with a range of current speeds appropriate to their way of life. These physical energies assist the transfer of energy in the biological food web without themselves taking part in the process. From a biological point of view they have been labeled auxiliary energy.

The concept was first elucidated by Odum (1967a, 1967b), who drew attention to the way in which the ebb and flow of the tide assists the productivity of a salt marsh, and the way in which agricultural productivity (as measured by energy flow) is enhanced by the use of auxiliary energy to prepare the ground, remove weeds, spread fertilizers, and so on. In the history of agriculture the auxiliary energy has changed from being human labor (the farmer and his family) through the use of domestic animals to the present-day use of fossil fuels. Odum drew attention to the fact that the auxiliary energy for a salt marsh is provided free by nature, while the auxiliary energy of a farm is costly.

Margalef (1974, 1978b) pointed out that the physical energy that upwells nutrient-rich water in the ocean is an energy subsidy to the phytoplankton. He showed that a model relating photosynthesis to energy of upwelling is, in many situations, a better predictor of phytoplankton production than the more complex contemporary models involving light, nutrients, and temperature. He also developed detailed explanations of the morphology and physiology of various phytoplankton species in terms of their adaptations to high or low levels of auxiliary energy. For example, diatoms tend to be characteristic of turbulent water in which nutrients are being upwelled vigorously, while flagellates are better suited to low-turbulence, low-nutrient waters.

The topic was further explored by Legendre (1981; Legendre and Demers 1984, 1985; Legendre *et al*. 1986). He and his colleagues pointed out that high biological productivity often occurs at places where there is a sudden change of auxiliary energy, such as fronts, thermoclines, sediment–water interfaces, and the underside of ice. They also pointed out that for there to be an effective physical–biological interaction there must be a matching of scales in time and space. For example, since the doubling time for phytoplankton cells is in the range of hours to days, favorable physical conditions must persist for at least a few days for there to be a marked increase in phytoplankton populations. A good example of the importance of matching time scales was reviewed in Chapter 6. High phytoplankton productivity on tidally mixed fronts is stimulated by changes in the strength of tidal mixing and has a periodicity of 14 days, whereas high productivity at the shelf break is stimulated by internal waves that form on the ebbing tides with a semi-diurnal rhythm. Since the generation time of mesozooplankton is of the order of weeks, they cannot reproduce fast enough to use the pulses of primary production occurring at fortnightly intervals on the tidally mixed fronts, but they are able to build their populations by using the more continuous supply of phytoplankton generated in association with the internal lee waves at the shelf break.

One of the problems inherent in trying to build the concept of auxiliary energy into numerical models is that it is difficult to determine what proportion of the

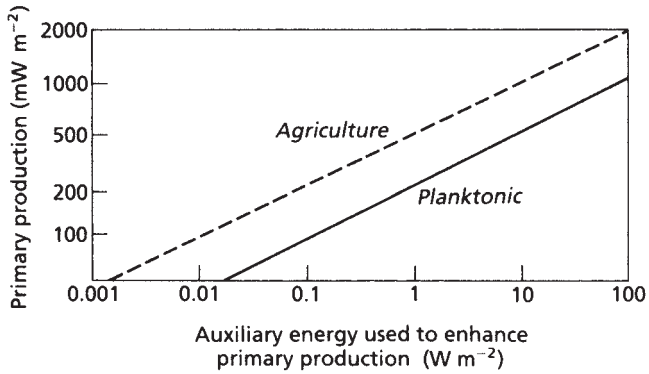

Fig. 11.01 Auxiliary energy (W m^{-2}) used to enhance primary production in agricultural systems and in the phytoplankton. From Margalef (1978a).

energy of physical processes impinges on biological processes. Margalef (1978a) made some rough estimates and developed comparative plots of the regressions of primary production in the plankton and in agriculture on auxiliary energy (Fig. 11.01). The diagram shows that a given amount of primary production in the plankton requires about 10 times more auxiliary energy than the same production on land. This finding is not surprising when we recall that in the ocean nutrient regeneration often occurs at great depth, far removed from the euphotic zone, whereas on land nutrients are regenerated in the soil, close to the roots of the plants.

It will be interesting to see whether the concept of auxiliary energy leads to better models of primary production. Now that it is possible to obtain vertical profiles of turbulence (see Section 3.3.3), data on primary production as a function of turbulent energy may begin to accumulate. Lande *et al*. (1989) used data on the vertical distribution of cell concentrations and turbulence to calculate the population growth rates at different depths of those phytoplankton cells that could be regarded as nonmotile and neutrally buoyant. These cells were all in the size range known as ultraphytoplankton, and consisted of prochlorophytes (<1 μm), cyanobacteria (~1 μm), small eukaryotes (<2 μm), and larger eukaryotes (2–4 μm). Taking the dispersal due to turbulent diffusion as the loss term, they calculated the population growth rate necessary to compensate for this loss, at various depths. For all groups, the highest population growth rates occurred near the bottom of the euphotic zone, near the top of the nutracline. Cyanobacteria grew most rapidly at 85–95 m and eukaryotes at 100–115 m depth. Below 150 m growth rates were all negative and cell numbers decreased exponentially with depth.

More recently, Bahamon and Cruzado (2003) used a vertically resolved turbulence-driven ecological model to simulate the intra-annual variability of ecological processes in the upper 300 m of water of the Catalan Sea, in the northwest Mediterranean, and in the subtropical northeast Atlantic. The results were

generally in agreement with observations. Alcaraz *et al*. (2002) measured the balance between production and respiration in planktonic communities, using laboratory microcosms with different levels of turbulence. Net primary production was highest under conditions of alternating turbulence and calm periods. Respiration was higher under turbulent conditions, but the change was less marked than in the case of primary production. The ratio of primary production to respiration (an index of community production) was higher under turbulent conditions. The results indicate a need to study the selection of planktonic food webs in the presence of turbulence.

Do biological processes significantly modify the effects of physical processes?

In the majority of situations we have reviewed, biological processes appear to be strongly influenced by the physics, while the physical processes are largely independent of the biology. This perception led Hartline (1980) to write an article entitled "Coastal upwelling: physical factors feed fish." In estuaries, on continental shelves, and in the open ocean, the physical processes appear to set the stage (albeit a constantly changing stage) on which the biological play is enacted. The organisms are adapted to the physical conditions that occur in a given place, but, in the short term, the physical conditions are very little affected by the biology.

There are some exceptions. Lewis *et al*. (1983) documented an example of short-term feedback from biological to physical processes. They showed that at an oligotrophic ocean station the chlorophyll maximum was sufficiently strong that the heat absorbed from the downwelling radiation caused local heating of the water, which caused increased vertical mixing and deepening of the mixed layer. The chlorophyll maximum also decreased the rate of heating of the water immediately below it, thereby increasing the stability of that part of the thermocline. The phenomenon is probably widespread in the ocean.

Stramska and Dickey (1993) summarized several examples of local heating caused by absorption of light in phytoplankton cells and provided new data from the North Atlantic. They modeled the situation and found that such local heating was a factor in the stabilization of the water column and formation of a bloom that preceded the seasonal thermocline.

When we turn to a time scale of thousands of years, the feedback from biology to physics is far from trivial. The present composition of the earth's atmosphere and the present average temperature at the surface of the earth have been profoundly influenced by living organisms. Volcanoes have been constantly adding to the carbon dioxide content of the atmosphere, but 99.5% of that carbon dioxide has been transported to the ocean sediments by marine organisms. They fixed carbon dioxide in their calcareous skeletons and incorporated carbon dioxide in their organic matter. As they sank to the bottom of the ocean, they

gave rise to the carbonaceous rocks and to the deposits of fossil fuel. Without these processes it is likely that the carbon dioxide content of the atmosphere would be very high and the temperature of the surface of the earth would be about 400 °C. Life as we know it would be impossible.

Biological processes are also thought to have played a major part in starting and ending the ice ages. It has been found that the rise in mean temperature (about 10 °C) associated with the end of the last glaciation was accompanied by a rise in atmospheric carbon dioxide. There is not yet agreement about the mechanisms involved. Changes in the earth's orbit are believed to have had a triggering effect, but it seems that there was also a sharp decrease in the fixation of atmospheric carbon dioxide by the phytoplankton. If this hypothesis turns out to be correct, biological processes are responsible for profoundly influencing the composition of the atmosphere, the temperature of the earth's surface, and as a consequence, the temperature and circulation of the whole global ocean.

This fact should not blind us to the limitations of the biological pump as a factor for offsetting anthropogenic increases in atmospheric carbon dioxide (Section 10.3.5). For about 1000 years before the Industrial Revolution, atmospheric CO_2 was relatively stable, so that the biological pump must have been in equilibrium with processes returning CO_2 from the ocean to the atmosphere. No evidence exists to suggest that the biological pump responds to changing atmospheric CO_2 directly, so it would not be a factor in sequestering anthropogenic carbon (Iglesias-Rodriguez *et al*. 2002). On the other hand, any global change that modified ocean circulation and materially altered the upwelling of nutrients would be likely to change the operation of the biological pump and the exchange of CO_2 between ocean and atmosphere.

In seeking clarification of the consequences of adding anthropogenic carbon dioxide to the atmosphere, the suite of models current in 2005 must be adjusted to take into account the realities of present understanding of the functioning of the phytoplankton. A large proportion of the biomass of the phytoplankton consists of minute cells, the cyanobacteria, which may not be able to use nitrate and may therefore be relatively unresponsive to the vertical transport of nitrate from deep water. In many regions there is an unused supply of nitrate in the mixed layer, because the diatoms are inhibited by shortages of micronutrients such as iron or silicon. In this situation, inputs of these trace elements from atmospheric dust particles can have more effect than an upwelling of nitrate-rich water. Furthermore, the biological pump, which is thought to play a key role in transporting carbon from the atmosphere to the deep ocean, appears to have several modes, not all of which result in sequestration of carbon.

Poor matching of time scales leads to inefficient use of phytoplankton production in the pelagic food webs, but places where phytoplankton sinks to the bottom because of lack of planktonic consumers are often the places that are important for the burial of carbon and its removal from the global carbon cycle for perhaps hundreds of years.

Each of these aspects of biological–physical relationship presents a complex suite of questions for the future.

How can we develop concepts and models that span the enormous range of scales in marine ecology, from the microscopic to the global and from seconds to geological ages?

The recognition that organisms must respond to physical phenomena at a wide range of scales is generating a need for many more studies that take into account more than one scale. For example, the sediments of the deep sea were once considered constant and spatially uniform. We now know that they constitute rich mosaics of environmental conditions, influenced by the productivity of the overlying water column, sediment structure, oxygen availability, water movement, and physical disturbance by such events as earthquakes. Each of these factors operates at a different scale. What is the net effect on the biota? At this stage it is possible to produce only conceptual models of the physical–biological interactions. Much remains to be discovered.

The drawing in Fig. 11.02 helps to illustrate some problems of scale that confront us in the future. The figure represents the 1000 km domain of a fictitious fish that is shown moving from place to place on its annual migration. From their spawning grounds in the early spring the fish swim to the upper layer of the open ocean to feed on the zooplankton that are feeding on the early phytoplankton blooms. Later they move to a tidal front over the shelf before swimming on to feed on a small spawning fish. They next move on to the outer region of the continental shelf where internal tidal waves have enhanced the productivity, and finally they end up back at their own spawning grounds.

The fish swim thousands of kilometers over the year to feed at a series of areas of enhanced productivity that are each about 50 km wide. From the size of territory associated with each species it is clear that complete studies of fish will need to cover a much larger area than studies of phytoplankton. The time scales associated with the two organisms are also much different. Individual phytoplankton live for a few days and the population of a patch can change significantly over the same length of time. Fish live for 5–10 years and measurable changes in their population occur over a year or so. Thus, besides covering a large area, the study of fish will also have to take a long time to understand the causes of any variations in time. The length and time scales associated with the populations are sometimes plotted jointly on a chart such as the one shown in Fig. 11.03 (Steele 1981).

The fish's domain, in the upper right of the figure, is thousands of kilometers across and the population takes years to change significantly. Phytoplankton, at the other extreme, change their numbers quickly and are concentrated over small scales. The length and time scales of the zooplankton lie in between those of the phytoplankton and the fish. They also lie in between the other two as prey to the fish and predators to the phytoplankton. The health of the fish population is obviously dependent on the health and availability of the zooplankton, which in turn is dependent on the phytoplankton, but these links between the groups

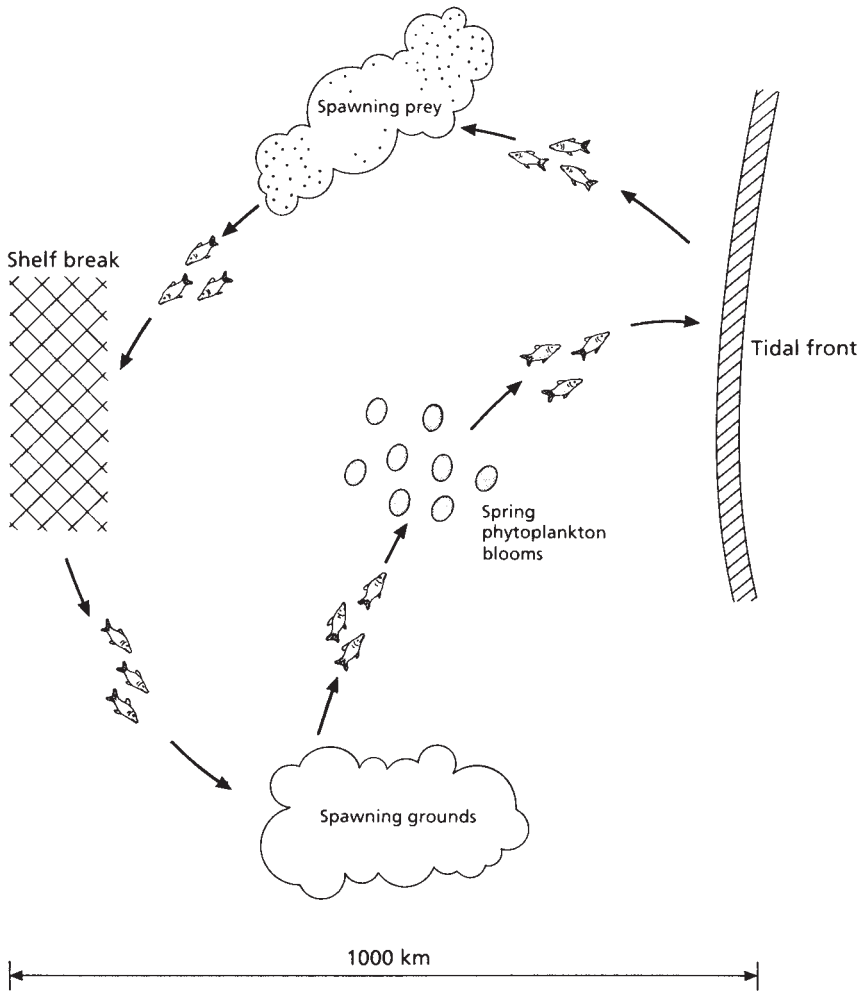

Fig. 11.02 A schematic diagram to illustrate the contrast between the 1000 km scale of the fish's domain and the 50 km scale of the various features, such as fronts and plankton blooms, upon which the fish depend.

can be rather "elastic." That is, the zooplankton population covers a sufficiently larger area and is sufficiently mobile to survive short-term fluctuations in the phytoplankton population at any one location. The fish in turn are mobile enough not to be strongly affected by a decline of zooplankton in one area. The larger organisms, therefore, because of their mobility are able to smooth out the effects of fluctuations in the population of the prey. The population of the smaller organisms, however, will tend to fluctuate inversely with the population of the predator. Thus a large fish population may reduce the zooplankton population and lead to a higher phytoplankton population.

Changes in the environment will also cause large variations in the populations of the smaller organisms. Violent storms can disrupt and disperse spawning

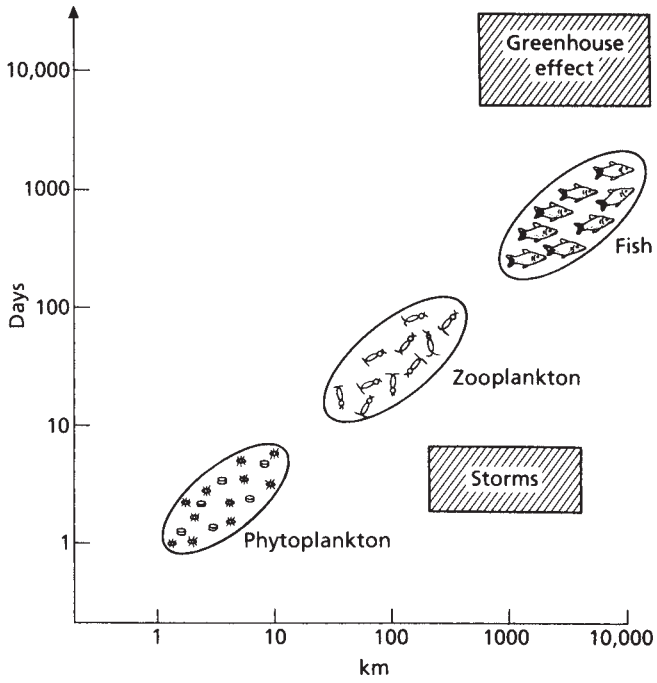

Fig. 11.03 The horizontal scale of phytoplankton, zooplankton, and fish populations plotted against the time required for a significant change in the population. The time and length scales of storms and climatic effects such as a change in the greenhouse effect are also plotted for comparison.

fish and increase the turbulence in the upper layer to disperse plankton patches. Longer-term changes in temperature such as those expected from the greenhouse effect will change the phytoplankton species of a given region, and possibly the locations of phytoplankton concentrations will change. A plankton population is said to absorb the variations due to storms and adapt to the multiyear variations (Steele 1988).

Not shown in Figs. 11.02 and 11.03 are important relationships between the fish and its predators, and between the fish and its prey. It is also necessary to understand fluctuations in the other fish populations inhabiting the same space as the one illustrated because they may strongly interact. The diagram in Fig. 11.03 may then sprout other axes to depict these other relationships such as the different trophic levels and the different levels of hierarchy of each particular species. Four axes are too many to show on one diagram, so for simplicity the time/length-scale plane is sometimes collapsed to a line with the assumption that time scales increase directly in proportion to the length scales. Such a figure is given in Fig. 11.04. It must be remembered that the simplification comes at the cost of ignoring some important effects such as short- and long-term meteorological forcing.

Diagrams like those in Figs. 11.03 and 11.04 help to organize marine ecology and aid in separating the important and tractable relationships that have to be

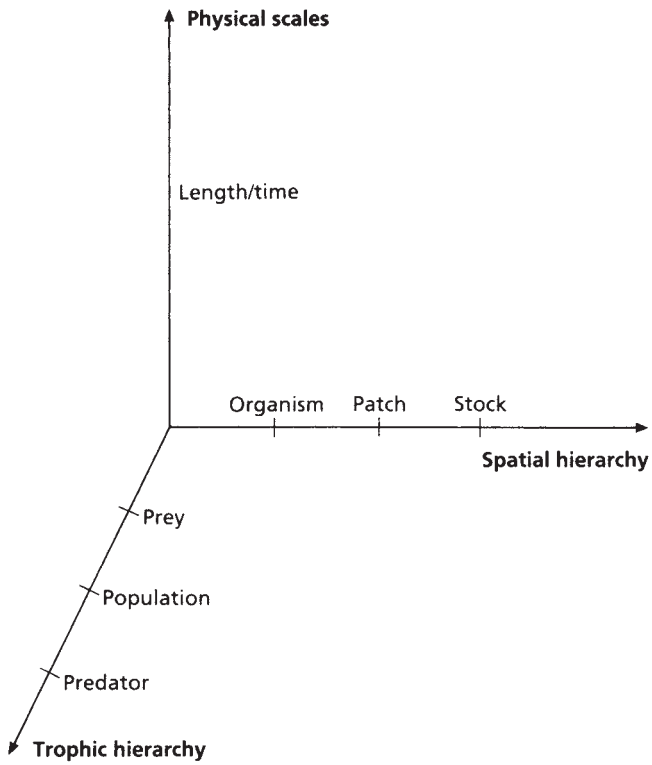

Fig. 11.04 The three main ecological variables plotted on a three-dimensional grid as suggested by Steele (1988).

understood. One initiative aimed at understanding the interactions between the passively floating phytoplankton, the actively swimming zooplankton, and the turbulence in the water was discussed at a workshop entitled "Small-scale biophysical coupling" (Bucklin *et al.* 1989). The participants in this workshop were experts in acoustics, numerical modeling, physical oceanography, and biological oceanography. They agreed that progress in the field is most likely to be made through study of small-scale physical and biological processes with the object of understanding how the small organisms, both passive and active, interact with one another and with the small-scale physical processes.

To achieve this understanding they proposed to obtain observations over a series of length and time scales. At the 1 m scale, optical and acoustic instruments should obtain high-resolution time-series observations of currents and the movements of particles and organisms from 5 μm to 5 mm in size. Results from these fine-scale observations should lead to the development of accurate parameterizations of the fine-scale physical and biological processes that can then be used in the models connecting the fine-scale observations to the large-scale ones.

The observations over the larger scales should include the use of submersibles to observe zooplankton, moored instruments to record temperature, velocity, and light intensity, temperature and velocity microstructure profilers, drifters, and an acoustic imaging array – in short, a high-resolution multidiscipline experiment using the most advanced instrumentation.

As we mentioned in Chapter 10, any process that affects the upwelling of nutrients in the ocean will affect the activity of the biological pump and, in turn, the carbon dioxide content of the atmosphere. This upwelling can be affected by storms (time scale 1 week), by annual cycles of stratification and mixing, by ENSO-type events with a time scale of 5–10 years, by thermocline ventilation with a time scale of about 30 years, and by thermohaline circulation with a characteristic time scale of about 500 years (Denman 1993, 1994; Denman and Abbott 1994). If we wish to understand how the biological pump might respond to climate change, we must study processes on all of these scales and find ways of integrating them. Denman and Abbott (1994), in the course of a detailed study of satellite images of the California Current upwelling system, showed that the phytoplankton cells (identified by pigment color patterns) act as passive markers of water movement. Their biological dynamics of growth, death, and sinking are slow compared with the physical dynamics. Thus, pigment color as detected by satellite can be used as a marker for the study of physical processes in active upwelling areas. This system is likely to be a useful tool for future studies.

Meantime, investigators are learning to study various types of organisms at several scales simultaneously. For example, Bucklin *et al*. (2000) reported progress on the use of molecular biology to characterize distinct varieties of the copepod *Calanus finmarchicus* in the major circulation units of the North Atlantic, namely the Norwegian Sea, the northern North Atlantic, and the western North Atlantic. They found that the selected genetic traits were useful for differentiating populations of the copepod from the major gyres, but also enabled them to characterize populations from small-scale patches, to units the size of the North Sea and the Norwegian Sea, through to the major subtropical and subarctic gyres.

Other researchers are finding that benthic communities lend themselves to analysis on a range of scales in time and space. For example, Dayton *et al*. (1999) investigated inter- and intraspecific competition among the most conspicuous kelps in a California kelp forest. The study extended over nine years through a cold-water, nutrient-enriched La Niña period and a warm-water, nutrient-stressed El Niño period. While there were many seasonal and interannual phenomena, the authors were able to show that the intensity of canopy competition with the giant kelp *Macrocystis* was very much a function of the inter-decadal-scale oceanographic regime shifts.

Sala *et al*. (1998) reviewed the destruction of kelp beds in the Mediterranean Sea by sea urchin overgrazing, which is a powerful influence on the structure of benthic algal assemblies. They found that large-scale oceanographic events were important in regulating urchin abundance. Similarly, Scheibling and Hennigar (1997) showed that the mass mortalities of sea urchins in Nova Scotia, Canada, were functions of large-scale oceanographic processes. When sea urchin populations

were decimated, rocky substrates were colonized by kelps and other macroalgae, with important implications for the coastal fishery.

Working in quite a different habitat, Levin *et al*. (2001) studied environmental influences in species diversity in deep-sea sediments. Most existing information comes from regional-scale sampling. Local species diversity shows clear geographic variation on scales of 100–1000 km. They found that many species exist as metapopulations whose regional distribution depends on a balance among global-scale, landscape-scale, and small-scale dynamics. Deep-sea sediments, constituting the most extensive habitat on earth, were once considered constant, spatially uniform, and isolated. They are now recognized as a dynamic, richly textured environment that is inextricably linked to the global biosphere through gradients of mixed-layer productivity, sediment heterogeneity, oxygen availability, hydrodynamic regimes, and catastrophic physical disturbance. At this stage it is possible to produce only conceptual models of the interrelations between different communities.

In the English Channel, Sanvicente-Anorve *et al*. (1996) found that the mechanisms affecting large-scale distribution of benthic species diversity are different from those acting on a smaller scale. They suggested aspects of the hydrosedimentary process that could determine the patterns at various scales.

For a review of progress in studying fish populations on a range of scales, see the symposium "Space, time and scale: new perspectives in fish ecology and management" with an introductory article by Mason and Brandt (1999). Both fresh and saltwater habitats are reviewed. Sometimes methods developed in lake habitats can be applied in the ocean. For example, Brandt and Jech (1995) used underwater acoustics to measure fish population density, size, and spatial distribution, and coupled this information with bioenergetic and foraging models. They showed that the spatial patterning of fish distribution could have profound and nonlinear effects on predator–prey interactions and other ecological processes.

These studies represent only the beginning of a process designed to understand ecosystem processes at all scales up to the global.

How do we explain an apparent synchrony in the variations in the biomasses of fish stocks worldwide?

There are interesting and potentially enormously useful correlations between interdecadal, global-scale changes in atmospheric patterns and the aggregated landings of many of the major exploited fish stocks. Establishing credible linkages between these large-scale atmospheric phenomena and the biomasses of fish stocks will require studies at the whole range of length scales from the microscopic through to basin-wide and global, and from seconds to centuries.

Prior to 1998 there had been many isolated observations about the tendency of major fish stocks to fluctuate in synchrony. For example, landings from three sardine stocks from Chile, California, and eastern Asia rose and fell in synchrony between 1920 and 1990, as did salmon landings in Canada, the United States, Japan,

and the USSR during the same period. Control of stocks by large-scale physical oceanographic processes seemed the most likely explanation. In 1998 Klyashtorin examined atmospheric circulation on a global scale and showed correlations with the landings from 11 major fish stocks yielding almost half the world's total marine catch.

The pattern of atmospheric events demonstrated by Klyashtorin (1998) involved classifying the global atmospheric circulation into (i) zonal regimes, with predominantly westerly winds, and (ii) meridional regimes with weaker westerly winds and a greater predominance of north–south winds. The twentieth century showed a zonal regime followed by a meridional regime, followed by another zonal regime, with regime shifts in 1938 and 1971. It is possible that there was another regime shift in 1990, but in 2005 it was still not clear whether another meridional regime was in progress.

Klyashtorin's analysis of fish landings showed that in the North and South Pacific there were six major stocks for which the landings rose during zonal regimes and fell during meridional regimes, and that for three Pacific stocks – for which the records exist only for the second half of the century – the main growth in landings was in a zonal regime. There are also two Pacific stocks and three Atlantic stocks for which major increases in landings occurred in the meridional regime. Based on these correlations, the case is persuasive that the changes in atmospheric circulation led to changes in ocean circulation, which in turn led to changes in the productivity of the fish stocks.

The practical implications for better management of fish stocks are enormous, but to test Klyashtorin's interesting hypothesis a great deal of work is needed. First, it will be necessary to rule out the counter-hypothesis that the changes in fish landings are primarily the result of changes in fishing effort. For stocks for which we have a century of records, it may rapidly become clear that the counter-hypothesis is untenable. However, there are stocks such as the Peruvian anchovy *Engraulis ringens* and Alaska pollock *Theragra chalcogramma* in which intensive fishing began at about the same time as a regime shift, and it will be necessary to partition the change in landings between change in fishing effort and change in environmental conditions.

Based on the material reviewed in this text, there are plausible physical mechanisms to explain the connection between physical oceanographic changes and changes in fish biomass. However, one feature of the correlations is that there are often time lags of several years between the physical changes and the shifts in population biomass. For each stock, it will be necessary to trace the changes in food webs induced by the physical environment, and test the plausibility of the observed time lags.

The work on this topic must also take into account the question raised earlier in this chapter in response to the second question. We must not go too far in treating the fish production system as a mechanism responding solely to physical factors. Different organisms in the food web respond differently to a given physical change, and interactions between organisms will modify the response of the total community.

In hindsight it appears that heavy exploitation of a stock at a time when it faces adverse environmental conditions is a sure recipe for disaster. If Klyashtorin's hypothesis proves robust, it seems likely that in the future it will be possible to forecast the times when environmental conditions are adverse for particular stocks and adjust fishing pressure accordingly. Much work is now required both to carry forward the science of physical–biological interactions as they concern the fish stocks, and to devise management schemes that allow flexibility in levels of exploitation.

These are only a few of the challenges facing the next generation of marine ecologists.

Appendix

Table A.01 Variables, constants, and nondimensional numbers.

Symbol	*Quantity or variable*	*Typical value and/or units*
A	Area of cross-section	m^2
α	Thermal expansion coefficient (water)	10^{-4} °C^{-1}
α, α_λ	Absorption coefficient	~0.1 m^{-1} for red light ~0.001 m^{-1} for blue light
β	Variation of Coriolis parameter with latitude	2×10^{-11} m^{-1} s^{-1} ($\varphi = 45°$)
C	Concentration of a substance	kg m^{-3}
C_D	Drag coefficient	varies with shape and flow
c	Specific heat of water	4.2 kJ kg^{-1} °C^{-1}
D	Molecular diffusivity	1.5×10^{-7} m^2 s^{-1} (heat) 1.5×10^{-9} m^2 s^{-1} (salt)
D_c	Compensation depth	m
D_E	Ekman depth	~80 m
D_t	Tidal energy dissipation	W m^{-2}
d	Typical diameter	m
δ	Boundary layer thickness	m
ε	Turbulent energy dissipation	W kg^{-1}
F	Flux	kg m^{-2} s^{-1}
F_D	Drag force	N
f	Coriolis parameter ($2\Omega \sin \varphi$)	10^{-4} s^{-1} ($\varphi = 45°$)
ϕ	Latitude	degrees
g	Gravitational acceleration	9.98 m s^{-2}
g'	Reduced gravity ($g\Delta\rho/\rho$)	0.01 m s^{-2}
h	Height of water column	m
I	Intensity of light	W m^{-2}
J	Energy, in joules	N m
K	Half-saturation constant	kg m^{-3}
K_h	Horizontal eddy diffusivity	500 m^2 s^{-1}
K_v	Vertical eddy diffusivity	10^{-4} m^2 s^{-1}

Table A.01 *(cont'd)*

Symbol	*Quantity or variable*	*Typical value and/or units*
l	Typical length	m
L_b	Buoyancy length scale $(\varepsilon/N^3)^{1/2}$	1–60 m
L_d	Diffusive length scale $2\pi(vD^2/\varepsilon)^{1/4}$ (Batchelor scale)	0.2–1.0 mm
L_v	Viscous length scale $2\pi(v^3/\varepsilon)^{1/4}$ (Kolmogoroff scale)	6–35 mm
M	Molar concentration	1 mol = 1 g-at L^{-1}
μM	Micromolar concentration	1 μmol = 1 μg-at L^{-1}
M_E	Ekman transport	kg m s^{-1}
N	Force, in newtons	kg m s^{-2}
N	Brunt–Väisälä frequency $(g/\rho \times d\rho/dz)^{1/2}$	10^{-3}–10^{-2} s^{-1}
Pa	Pressure, in pascals	N m^{-2}
R_e	External Rossby radius $(gh)^{1/2}/f$	1000 km
R_i	Internal Rossby radius $(g'h)^{1/2}/f$	30 km
Re	Reynolds number ud/v	
Ri	Richardson number $\frac{g}{\rho}\frac{d\rho}{dz}/\left(\frac{du}{dz}\right)^2$	0.1–1.0
ρ	Density	1000 kg m^{-3} (fresh water) 1026 kg m^{-3} (salt water)
σ_t	Sigma-t (density anomaly)	$(\rho - 1000)$ kg m^{-3}
τ	Stress	N m^{-2}
t	mass	1000 kg (metric ton)
u, v, w	Components of velocity along x, y, z	m s^{-1}
$\bar{u}$, $\bar{v}$, $\bar{w}$	Average velocity	m s^{-1}
u', v', w'	Fluctuating component of velocity	m s^{-1}
u_*	Friction velocity $(\tau/\rho)^{1/2}$	m s^{-1}
v	Kinematic viscosity	10^{-6} m^2 s^{-1} (water)
W	Power, in watts	J s^{-1}
Ω	Angular velocity	rad s^{-1}
x, y, z	Position coordinates	m
ζ	Relative vorticity	s^{-1}

Table A.02 Basic units.

Quantity	*Name*	*Symbol*
mass	gram	g
length	meter	m
time	second	s
amount of substance	mole	mol
temperature	degree Celsius	deg C, °C

Table A.03 Prefixes.

Prefix	*Factor*	*Symbol*
pico	10^{-12}	p
nano	10^{-9}	n
micro	10^{-6}	μ
milli	10^{-3}	m
centi	10^{-2}	c
deci	10^{-1}	d
deca	10	da
hecto	10^{2}	h
kilo	10^{3}	k
mega	10^{6}	M
giga	10^{9}	G
Tera	10^{12}	T
Peta	10^{15}	P

References

Abelson, A., Miloh, T., and Loya, Y. (1993) Flow patterns induced by substrata and body morphologies of benthic organisms, and their roles in determining availability of food particles. *Limnol. Oceanogr.* **38**, 1116–1124.

Adkins, J.F., Boyle, E.A., Keigwin, L., and Cortijo, E. (1997) Variability of the North Atlantic thermohaline circulation during the last interglacial period. *Nature* **390**, 154–156.

Aebischer, N.J., Coulson, J.C., and Colebrook, J.M. (1990) Parallel long-term trends across four marine trophic levels and weather. *Nature* **347**, 753–755.

Aguilera, J., Jimenez, C., Rodriguez-Maroto, J.M., and Niell, F.X. (1994) Influence of subsidiary energy on growth of *Dunaliella viridis* Teodoresco: the role of extra energy in algal growth. *J. Appl. Phycol.* **6**, 323–330.

Aiken, J. and Bale, A.J. (2000) An introduction to the Atlantic Meridional Transect (AMT) Programme. *Prog. Oceanogr.* **45**, 251–256.

Alber, M. and Valiela, I. (1995) Organic aggregates in detrital food webs: incorporation in bay scallops (*Argopecten irradians*). *Mar. Ecol. Prog. Ser.* **121**, 117–124.

Alcaraz, M., Marrase, C., Peters, F., Arin, L., and Malits, A. (2002) Effects of turbulence conditions on the balance between production and respiration in marine planktonic communities. *Mar. Ecol. Prog. Ser.* **242**, 63–71.

Alheit, J. and Bernal P.A. (1993) Effects of physical and biological changes in the biomass yield of the Humboldt Current system. In *Large Marine Ecosystems* (ed. K. Sherman, L.M. Alexander, and B.D. Gold), pp. 53–68. American Association for the Advancement of Science Press, Washington DC.

Alheit, J. and Niquen, M. (2004) Regime shifts in the Humboldt Current ecosystem. *Progress in Oceanography* **60**, 201–222.

Alldredge, A.L. and Cohen, Y. (1987) Can microscale chemical patches persist in the sea? Microelectrode study of marine snow, fecal pellets. *Science* **235**, 689–691.

Alldredge, A.L. and Hamner, W.M. (1980) Recurring aggregations of zooplankton by a tidal current. *Estuar. Coast. Mar. Sci.* **10**, 31–37.

Allen, P.M. (1985) Ecology, thermodynamics and self-organization: towards a new understanding of complexity. In *Ecosystem Theory for Biological Oceanography* (ed. R.E. Ulanowicz and T. Platt). *Can. Bull. Fish. Aquat. Sci.* **213**, 3–26.

Anderson, L.A. and Robinson, A.R. (2001) Physical and biological modeling in the Gulf Stream region II. Physical and biological processes. *Deep-Sea Res. I* **48**, 1139–1168.

Anderson, S.M. and Charters, A.C. (1982) A fluid dynamic study of water flow through *Gelidium nudifrons*. *Limnol. Oceanogr.* **27**, 399–412.

Anderson, T.R., Spall, S.A., Yool, A., Cipollini, P., Challenor, P.G., and Fasham, M.J.R. (2001) Global fields of sea surface dimethylsulfide predicted from chlorophyll, nutrients and light. *J. Mar. Syst.* **30**, 1–20.

Anonymous (1998) Evidence for decadal scale variations in seabird population ecology and links with the North Atlantic Oscillation. In *Oceanography Committee. Report of the Working Group on Seabird Ecology*, pp. 29–32. ICES CM 1998/C:5.

Ansa-Emmin, M. (1982) Fisheries in the CINECA region. *Rapp. P.-v. Réun. Cons. Int. Explor. Mer.* **180**, 405–422.

Aoki, I. and Inagaki, T. (1992) Acoustic observations of fish schools and scattering layers in a Kuroshio warm core ring and its environs. *Fish. Oceanogr.* **1**, 137–142.

Apel, J.R. (1987) *Principles of Ocean Physics*. Academic Press, New York. 634 pp.

Apel, J.R., Byrne, H.M., Proni, J.R., and Charnell, R.L. (1975) Observations of oceanic internal and surface waves from the Earth Resources Technology Satellite. *J. Geophys. Res.* **80**, 865–881.

Armstrong, D.A., Mitchell-Innes, B.A., Verhaye-Dua, F., Waldron, H., and Hutchings, L. (1987) Physical and biological features across the upwelling front in the southern Benguela. In *The Benguela and Comparable Ecosystems* (ed. A.I.L. Payne, J.A. Gulland, and K.H. Brink). *S. Afr. J. Mar. Sci.* **5**, 171–190.

Arnold, G.P. and Cook, P.H. (1984) Fish migration by selective tidal stream transport: first results of a computer simulation for the European continental shelf. In *Mechanisms of Migration in Fishes* (ed. J.D. McCleave *et al.*), pp. 227–261. Plenum Press, New York.

Arnone, R.A. (1990) Acoustic imaging of biological and physical processes within Gulf Stream meanders. *Naval Oceanographic and Atmospheric Research Lab. Report* NOARL-JA-352-050-9. 4 pp.

Ashjian, C.J., Davis, C.S., Gallager, S.M., and Alatalo, P. (2001) Distribution of plankton, particles, and hydrographic features across Georges Bank described using the Video Plankton Recorder. *Deep-Sea Res. II* **48**, 245–282.

Astthorsson, O.S., Hallgrimsson, I., and Jonsson, G.S. (1983) Variations in zooplankton densities in Icelandic waters in spring during the years 1961–1982. *Rit. Fiskideildar* (*J. Mar. Res. Inst. Reykjavik*) **7**, 73–113.

Atkins, W.R.G. (1928) Seasonal variation in the phosphate and silicate content of sea water during 1926 and 1927 in relation to the phytoplankton crop. *J. Mar. Biol. Assoc.* **15**, 191–205.

Atkinson, L.P. and Targett, T.E. (1983) Upwelling along the 60-m isobath from Cape Canaveral to Cape Hatteras and its relationship to fish distribution. *Deep-Sea Res. II* **30**, 221–226.

Atkinson, L.P., O'Malley, P.G., Yoder, J.A., and Paffenhöfer, G.A. (1984) The effect of summertime shelf break upwelling on nutrient flux in southeastern United States continental shelf waters. *J. Mar. Res.* **42**, 969–993.

Austin, J.A. (2002) Estimating the mean ocean–bay exchange rate of the Chesapeake Bay. *J. Geophys. Res.* **107** (C11), 3192–3199.

Avise, J.C., Nelson, W.S., Arnold, J., Koehn, R.K., Williams, G.C., and Thorsteinsson, V. (1990) The evolutionary genetic status of Icelandic eels. *Evolution* **44**, 1254–1262.

Backus, R.H. and Bourne, D.W. (eds.) (1987) *Georges Bank*. MIT Press, Cambridge, MA. 593 pp.

Backus, R.H. and Craddock, J.E. (1982) Mesopelagic fishes in Gulf Stream cold core rings. *J. Mar. Res.* **40** (suppl.), 1–20.

Bahamon, N. and Cruzado, A. (2003) Modelling nitrogen fluxes in oligotrophic environments: NW Mediterranean and NE Atlantic. *Ecol. Model.* **163**, 223–244.

Bailey, K.M. (1981) Larval transport and recruitment of Pacific hake *Merluccius productus*. *Mar. Ecol. Prog. Ser.* **6**, 1–9.

Bailey, R.A. and Steele, J.H. (1992) North Sea herring fluctuations. In *Climate Variability, Climate Change and Fisheries* (ed. M.H. Glantz), pp. 213–230. Cambridge University Press, Cambridge.

Baird, M.E. and Emsley, S.M. (1999) Towards a mechanistic model of plankton population dynamics. *J. Plankton Res.* **21**, 85–126.

Bakun, A. (1973) Coastal upwelling indices, west coast of North America 1946–71. *NOAA Tech. Rep.* NMFS SSRF-671. US Dept. Commerce, Seattle, WA.

Bakun, A. (1990) Global climate change and intensification of coastal ocean upwelling. *Science* **247**, 198–201.

Bakun, A. and Csirke, J. (1998) Environmental processes and recruitment variability. In *Squid recruitment dynamics: the genus* Illex *as a model, the commercial* Illex *species and influences on variability* (ed. P.G. Rodhouse, E.G. Dawe, and R.K. O'Dor), pp. 103–124. *FAO Fish. Tech. Pap.* 376. FAO, Rome.

Bakun, A. and Parrish, R.H. (1982) Turbulence, transport and pelagic fish in the California and Peru current systems. *CalCOFI Rep.* **23**, 99–112.

Banse, K. and English, D.C. (1994) Seasonality of coastal zone color scanner phytoplankton pigment in the offshore oceans. *J. Geophys. Res.* **99** (C4), 7323–7345.

Barber, R.T. and Smith, R.L. (1981) Coastal upwelling ecosystems. In *Analysis of Marine Ecosystems* (ed. A.R. Longhurst), pp. 31–68. Academic Press, New York.

Barber, R.T., Chavez, F.P., and Kogelschatz, J.E. (1985) Biological effects of El Niño. In *Seminario Regional Ciencas Tecnologia y Agression Ambiental: El Fenomeno "El Niño"* (ed. M. Vegas), pp. 399–438. Contec Press, Lima, Peru.

Barnola, J.M., Anklin, M., Porcheron, J., Rayaud, D., Schwander, J., and Stauffer, B. (1995) CO_2 evolution during the last millennium as recorded by Antarctic and Greenland ice. *Tellus* **47B**, 264–272.

Barry, J.P., Baxter, C.H., Sagarin, R.D., and Gilman, S.E. (1995) Climate-related, long-term faunal changes in a California rocky intertidal community. *Science* **267**, 672–675.

Barth, J.A., Pierce, S.D., and Smith, R.L. (2000) A separating coastal upwelling jet at Cape Blanco, Oregon and its connection to the California current system. *Deep-Sea Res. II* **47**, 783–810.

Barton, E.D., Huyer, A., and Smith, R.L. (1977) Temporal variation observed in the hydrographic regime near Cabo Corbeiro in the northwest African upwelling region, February to April 1974. *Deep-Sea Res.* **24**, 7–24.

Batteen, M.L. (1997) Wind-forced modeling studies of currents, meanders, and eddies in the California Current System. *J. Geophys. Res.* **102C**, 985–1010.

Batteen, M.L., Martinez, J.R., Bryan, D.W., and Buch, E.J. (2000) A modeling study of the coastal eastern boundary current system of Iberia and Morocco. *J. Geophys. Res.* **105C**, 14173–14195.

Beamish, R.J. (1993) Climate and exceptional fish production off the west coast of North America. *Can. J. Fish. Aquat. Sci.* **50**, 2270–2291.

Beamish, R.J. and Bouillon, D.R. (1993) Pacific salmon production trends in relation to climate. *Can. J. Fish. Aquat. Sci.* **50**, 1002–1016.

Beamish, R.J., Neville, C.M., Thomson, B.L., Harrison, P.J., and St John, M. (1994) The effect of Fraser River discharge on interannual production of Pacific salmon and herring in the Strait of Georgia. *Can. J. Fish. Aquat. Sci.* **51**, 2843–2855.

Beamish, R.J., Neville, C.E., and Cass, A.J. (1997) Production of Fraser River sockeye salmon (*Oncorhynchus nerka*) in relation to decadal-scale changes in the climate and the ocean. *Can. J. Fish. Aquat. Sci.* **54**, 543–554.

Beamish, R.J., Noakes, D.J., McFarlane, G.A., Klyashtorin, L., Ivanov, V.V., and Kurashov, V. (1999) The regime concept and natural trends in the production of Pacific salmon. *Can. J. Fish. Aquat. Sci.* **56**, 516–526.

Beaugrand, G., Brander, K.M., Lindley, J.A., Souissi, S., and Reid, P.C. (2003) Plankton effect on cod recruitment in the North Sea. *Nature* **426**, 661–664.

Behrenfeld, M.J. and Falkowski, P.G. (1997) Photosynthetic rates derived from satellite-based chlorophyll concentration. *Limnol. Oceanogr.* **42**, 1–20.

Behrenfeld, M.J. and Kolber, Z.S. (1999) Widespread iron limitation of phytoplankton in the South Pacific Ocean. *Science* **283**, 840–843.

Behrenfeld, M.J., Esaias, W.E., and Turpie, K. (2002) Assessment of primary production at the global scale. In *Phytoplankton Productivity: Carbon Assimilation in Marine and Freshwater Ecosystems* (ed. P.J.Le B. Williams, D.N. Thomas, and C.S. Reynolds), pp.156–186. Blackwell Science, Oxford.

Belgrano, A., Lindahl, O., and Hernroth, B. (1999) North Atlantic Oscillation, primary productivity and toxic phytopankton in the Gullmar Fjord, Sweden (1985–1996) *Proc. Roy. Soc. Lond. B* **266**, 425–430.

Belveze, H. and Erzini, K. (1983) The influence of hydroclimatic factors on the availability of sardine (*Sardinus pilchardus*) in the Moroccan Atlantic fishery. *FAO Fish Rep.* **291**, 285–327.

Berg, H.C. and Purcell, E.M. (1977) Physics of chemoreception. *Biophys. J.* **20**, 193–215.

Berger, A. (1988) Milankovitch theory and climate. *Rev. Geophys.* **26**, 624–657.

Bienfang, P.K., Syper, J., and Laws, E. (1983) Sinking rate and pigment responses to light-limitation of a marine diatom: implications to dynamics of chlorophyll maximum layers. *Oceanol. Acta* **6**, 55–62.

Bigelow, H.B. (1927) Physical oceanography of the Gulf of Maine. *Bull. US Bureau Fisheries* **40**, 511–1027.

Bigler, B.S., Welch, D.W., and Helle, J.H. (1996) A review of size trends among north Pacific salmon (*Oncorhynchus* spp.). *Can. J. Fish. Aquat. Sci.* **53**, 455–465.

Binet, D. (1997) Climate and pelagic fisheries in the Canary and Guinea currents 1964–1993: the role of trade winds and the southern oscillation. *Oceanologica Acta* **20**, 177–190.

Binet, D., Samb, B., Taleb Sidi, M., Levenez, J.J., and Servain, J. (1998) Sardine and other pelagic fisheries changes associated with multi-year trade wind increases in the southern canary current. In *Global Versus Local Changes in Upwelling Systems*, pp. 211–233. Colloq. Semin. Inst. Fr. Rech. Sci. Dev. Coop. ORSTOM. Editions de l'ORSTOM, Paris.

Bissett, W.P. and 6 other authors (2001) Resolving the impacts and feedback of ocean optics on upper ocean ecology. *Oceanography* **14**, 30–53.

Blackburn, M. (1981) Low latitude gyral regions. In *Analysis of Marine Ecosystems* (ed. A.R. Longhurst), pp. 3–30. Academic Press, New York.

Blanton, J.O., Atkinson, L.P., de Castillejo, F.F., and Montero, A.L. (1984) Coastal upwelling off the Rias Bajas, Galicia, Northwest Spain, I. Hydrographic studies. *Rapp. P.-v. Réun. Cons. Int. Explor. Mer.* **183**, 79–90.

Blanton, J.O., Tenore, K.R., Castillejo, R., Atkinson, L.P., Schwing, F.B., and Lavin, A. (1987) The relationship of upwelling to mussel production in the rias on the western coast of Spain. *J. Mar. Res.* **45**, 497–511.

Boëtius, J. and Harding, E.F. (1985) A re-examination of Johannes Schmidt's Atlantic eel investigations. *Dana* **4**, 129–162.

Bogstad, B. and Gjøsæter, H. (1994) A method for estimating the consumption of capelin by cod in the Barents Sea. *ICES J. Mar. Sci.* **51**, 273–280.

Boje, R. and Tomczak, M. (eds.) (1978) *Upwelling Ecosystems*. Springer-Verlag, Berlin. 303 pp.

Bond, G.C. (1995) Climate and the conveyor. *Nature* **377**, 383–385.

Botsford, L.W. (2001) Physical influences on recruitment to California Current invertebrate populations on multiple scales. *ICES J. Mar. Sci.* **58**, 1081–1091.

Boudreau, B., Simard, Y., and Bourget, E. (1991) Behavioural response of the planktonic stages of the American lobster *Homarus americanus* to thermal gradients, and ecological implications. *Mar. Ecol. Prog. Ser.* **76**, 13–23.

Boudreau, B., Simard, Y., and Bourget, E. (1992) Influence of a thermocline on vertical distribution and settlement of post-larvae of the American lobster *Homarus americanus* Milne-Edwards. *J. Exp. Mar. Biol. Ecol.* **162**, 35–49.

Bouman, H.A., Platt, T., Sathyendranath, S., Irwin, B.D., Wernand, M.R., and Kraay, G.W. (2000). Bio-optical properties of the subtropical North Atlantic. II. Relevance to models of primary production. *Mar. Ecol. Prog. Ser.* **200**, 19–34.

Bousfield, E.L. (1955) Ecological control of the occurrence of barnacles in the Miramichi Estuary. *Bull. Nat. Mus. Can.* **137**, 1–69.

Bowden, K.F. (1983) *Physical Oceanography of Coastal Waters*. Ellis Horwood, New York. 302 pp.

Bowen, J.D., Stolzenbach, K.D., and Chisholm, S.W. (1993) Simulating bacterial clustering around phytoplankton cells in a turbulent ocean. *Limnol. Oceanogr.* **38**, 36–51.

Bowers, D.G. and Simpson, J.H. (1987) Mean position of tidal fronts in European-shelf seas. *Continental Shelf Res.* **7**, 35–44.

Bowman, M.J. and Iverson, R.L. (1978) Estuarine and plume fronts. In *Oceanic Fronts in Coastal Processes* (ed. M.J. Bowman and W.E. Esaias), pp. 87–104. Springer-Verlag, New York.

Bowman, M.J., Yentsch, C.M., and Peterson, W.J. (eds.) (1986) *Tidal Mixing and Plankton Dynamics*. Springer-Verlag, Berlin.

Boyd, P.W. and Doney, S.C. (2003) The impact of climate change and feedback processes on the ocean carbon cycle. In *Ocean Biogeochemistry: the Role of the Ocean Carbon Cycle in Global Change* (ed. M.J.R. Fasham), pp. 157–193. Springer-Verlag, Berlin.

Boyd, P.W. and 7 other authors (1995a) The N.E. subarctic Pacific in winter: 1. Biological standing stocks. *Mar. Ecol. Prog. Ser.* **128**, 11–24.

Boyd, P.W., Whitney, F.A., Harrison, P.J., and Wong, C.S. (1995b) The N.E. subarctic Pacific in winter: 2. Biological rate processes. *Mar. Ecol. Prog. Ser.* **128**, 25–34.

Boyd, P.W. and 34 other authors (2000) A mesoscale phytoplankton bloom in the polar Southern Ocean stimulated by iron fertilization. *Nature* **407**, 695–702.

Brandt, A., Sarabun, C.C., Seliger, H.H., and Tyler, M.A. (1986) The effects of a broad spectrum of physical activity on the biological processes in the Chesapeake Bay. In *Marine Interfaces Ecohydrodynamics* (ed. J.C.J. Nihoul), pp. 361–384. Elsevier, Amsterdam.

Brandt, S.B. and Jech, J.M. (1995) Integrating acoustics with ecological modelling: making the most of the spatial information in acoustic data. In *ICES International symposium on fisheries and plankton acoustics held in Aberdeen 12–16 June 1995*, pp. 1–5. ICES, Copenhagen.

Breaker, L.C., Kelley, J.G.W., Burroughs, L.D., Miller, J.L., Balasubramaniyan, B., and Zaitzeff, J.B. (1999) The impact of a high discharge event on the structure and evolution of the Chesapeake Bay plume, based on model results. *J. Mar. Environ. Eng.* **5**, 311–349.

Brezinski, M.A., Phillips, D.R., Chavez, F.P., Friederich, G.E., and Dugdale, R.C. (1997) Silica production in the Monterey, California, upwelling system. *Limnol. Oceanogr.* **42**, 1694–1705.

Brickman, D. and Loder, J.W. (1993) Energetics of the internal tide on northern Georges Bank. *J. Phys. Oceanogr.* **23**, 409–424.

Brink, K.H., Halpern, D., and Smith, R.L. (1980) Circulation in the Peru upwelling system near 15 deg. S. *J. Geophys. Res.* **85**, 4036–4048.

Brock, J.C. and McClain, C.R. (1992) Interannual variability of phytoplankton blooms observed in the northwestern Arabian Sea during the Southwest Monsoon of 1979. *J. Geophys. Res.* **97**, 733–750.

Brock, J.C., Sathyendranath, S., and Platt, T. (1993) Modelling the seasonality of subsurface light and primary production in the Arabian Sea. *Mar. Ecol. Prog. Ser.* **101**, 209–221.

Broecker, W.S. (1992) Upset for Milankovitch theory. *Nature* **359**, 779–780.

Broecker, W.S. and Henderson, G.M. (1998) The sequence of events surrounding Termination II and their implications for the cause of glacial–interglacial CO_2 changes. *Paleoceanography* **13**, 352–364.

Broecker, W.S., Peteet, D.M., and Rind, D. (1985) Does the ocean–atmosphere system have more than one stable mode of operation? *Nature* **315**, 21–26.

Brubaker, J.M. and Simpson, J.H. (1999) Flow convergence and stability at a tidal estuarine front: acoustic Doppler observations. *J. Geophys. Res.* **104** (C8), 18257–18268.

Bryan, F.O., Smith, R.D., Maltrud, M.E., and Hecht, M.W. (1998) *Modeling the North Atlantic Circulation: From Eddy Permitting to Eddy Resolving*. www.cgd.ucar.edu/oce/bryan/woce-poster.html

Bucklin, A., Brandt, A., and Orr, M. (1989) *Small-scale Bio-physical Coupling*. Preliminary report of workshop sponsored by the Office of Naval Research, Washington, DC.

Bucklin, A., Astthorsson, O.S., Gislason, A., Allen, L.D., Smolenack, S.B., and Wiebe, P.H. (2000) Population genetic variation of *Calanus finmarchicus* in Icelandic waters: preliminary evidence of genetic differences between Atlantic and Arctic populations. *ICES J. Mar. Sci.* **57**, 1592–1604.

Budyko, M.I. (1974) *Climate and Life*. Academic Press, New York. 508 pp.

Bugden, G.L., Hargrave, B.T., Sinclair, M.M., Tang, C.L., Therriault, J.-C., and Yeats, P.A. (1982) Fresh water runoff effects in the marine environment: the Gulf of St. Lawrence example. *Can. Tech. Rep. Fish. Aquat. Sci.* No. 1078, 89 pp.

Bumpus, D.F. (1976) Review of the physical oceanography of George's Bank. *ICNAF Res. Bull.* **12**, 119–134.

Bundy, M.H., Gross, T.F., Vanderploeg, H.A., and Strickler, J.R. (1988) Perception of inert particles by calanoid copepods: behavioural observations and a numerical model. *J. Plankton. Res.* **20**, 2129–2152.

Butman, C.A. (1986) Larval settlement of soft-sediment invertebrates: some predictions based on an analysis of near-bottom profiles. In *Marine Interfaces Ecohydrodynamics* (ed. J.C.J. Nihoul), pp. 487–513. Elsevier, Amsterdam.

Butman, C.A., Grant, W.D., and Stolzenbach, K.D. (1986) Predictions of sediment trap biases in turbulent flows: a theoretical analysis based on observations from the literature. *J. Mar. Res.* **44**, 601–644.

Cairns, J.L. and LaFond, E.C. (1966) Periodic motion of the seasonal thermocline along the southern California coast. *J. Geophys. Res.* **71**, 3905–3915.

Campana, S.E., Smith, S.J., and Hurley, P.C.F. (1989) A drift-retention dichotomy for larval haddock (*Melanogrammus aeglefinus*) spawned on Brown's bank. *Can. J. Fish. Aquat. Sci.* **46** (Suppl. 1), 93–102.

Campbell, J.W. and Aarup, T. (1992) New production in the North Atlantic derived from seasonal patterns of surface chlorophyll. *Deep-Sea Res.* **39A**, 1669–1694.

Caparroy, P. and Carlotti, F. (1996) A model for *Acartia tonsa*: effect of turbulence and consequence for the related physiological processes. *J. Plankton. Res.* **18**, 2139–2177.

Carpenter, R.C. and Williams, S.L. (1993) Effects of algal turf canopy height and microscale topography on profiles of flow speed in a coral forereef environment. *Limnol. Oceanogr.* **38**, 687–694.

Carpenter, R.C., Hackney, J.M., and Adey, W.H. (1991) Measurements of primary productivity and nitrogenase activity of coral reef algae in a chamber incorporating oscillatory flow. *Limnol. Oceanogr.* **36**, 40–49.

Carr, M.-E. (2002) Estimation of potential productivity in eastern boundary currents using remote sensing. *Deep-Sea Res. II* **49**, 59–80.

Castonguay, M., Hodson, P.V., Moriarty, C., Drinkwater, K.F., and Jessop, B.M. (1994) Is there a role of ocean environment in American and European eel decline? *Fish. Oceanogr.* **3**, 197–203.

Chapman, D.C. and Lentz, S.J. (1994) Trapping of a coastal density front by the bottom boundary layer. *J. Phys. Oceanog.* **24**, 1464–1479.

Chapman, R. and Nof, D. (1988) The sinking of warm-core rings. *J. Phys. Oceanogr.* **18**, 565–583.

Charlson, R.J. and Wigley, T.M.L. (1994) Sulfate aerosols and climate change. *Sci. Am.* February 1994, 48–57.

Charlson, R.J., Lovelock, J.E., Andreae, M.O., and Warren, S.G. (1987) Oceanic phytoplankton, atmospheric sulphur, cloud albedo and climate. *Nature* **326**, 655–661.

Charney, J.G. (1955) The Gulf Stream as an inertial boundary layer. *Proc. Natl. Acad. Sci. USA* **41**, 731–740.

Chavez, F.P. and Barber, R.T. (1987) An estimate of new production in the equatorial Pacific. *Deep-Sea Res.* **34A**, 1229–1243.

Chavez, F.P. and Smith, S.L. (1995) Biological and chemical consequences of open ocean upwelling. In *Upwelling in the oceans: Modern processes and ancient records* (ed. C.P. Summerhayes, K.-C. Emeis, M.V. Angel, R.L. Smith, and B. Zeitschel), pp 149–170. Wiley, New York.

Chavez, F.P., Ryan, J., Lluch-Cota, S.E., and Niquen, C.M. (2003) From anchovies to sardines and back: multidecadal changes in the Pacific Ocean. *Science* **299**, 217–221.

Chelton, D.B. and Schlax, M.G. (1996) Global observations of oceanic Rossby waves. *Science* **272**, 234–238.

Chen, C. and Beardsley, R.C. (1998) Tidal mixing and cross-frontal particle exchange over a finite amplitude asymmetric bank: a model study with application to Georges Bank. *J. Mar. Res.* **56**, 1163–1201.

Chiang, K.-P. and Taniguchi, A. (2000) Distribution and modification of diatom assemblages in and around a warm-core ring in the western North Pacific frontal zone, east of Hokkaido. *J. Plankton Res.* **22**, 2061–2074.

Chisholm, S.W. (2000) Stirring times in the Southern Ocean. *Nature* **407**, 685–687.

Chisholm, S.W., Olson, R.J., Zettler, E.R., Goericke, R., Waterbury, J.B., and Welschmeyer, N.A. (1988) A novel free-living prochlorophyte abundant in the oceanic euphotic zone. *Nature* **334**, 340–343.

Chisholm, S.W. and 7 other authors (1992). *Prochlorococcus marinus* nov. gen. nov. sp.: an oxyphototropic marine prokaryote containing divinyl chlorophyll *a* and *b*. *Arch. Microbiol.* **157**, 297–300.

Chriss, T.M. and Caldwell, D.R. (1984) Universal similarity and thickness of the viscous sublayer at the ocean floor. *J. Geophys. Res.* **89**, 6403–6414.

Cipollini, P., Cromwell, D., Challenor, P.G., and Raffaglio, S. (2001) Rossby waves detected in global ocean colour data. *Geophys. Res. Lett.* **28**, 323–326.

Clark, D.R., Flynn K.J., and Owens, N.J.P. (2002) The large capacity for dark-nitrate assimilation in diatoms may overcome nitrate-limitations of growth. *New Phytol.* **155**, 101–108.

Clark, P.U., Pisias, N.G., Stocker, T.F., and Weaver, A. (2002) The role of the thermohaline circulation in abrupt climate change. *Nature* **415**, 863–869.

Clarke, R.A., Hill, H.W., Reiniger, R.F., and Warren, B.A. (1980) Current system south and east of the Grand Banks of Newfoundland. *J. Phys. Oceanogr.* **10**, 25–65.

Cloern, J.E. (1991) Tidal stirring and phytoplankton bloom dynamics in an estuary. *J. Mar. Res.* **49**, 203–221.

Cloern, J.E., Alpine, A.E., Cole, B.E., Wong, R.L.J., Arthur, J.F., and Ball, M.D. (1983) River discharge controls phytoplankton dynamics in the north San Francisco Bay estuary. *Estuar. Coast. Shelf Sci.* **16**, 415–429.

Codispoti, L.A. and Friederich, G.E. (1978) Local and mesoscale influences on nutrient variability in the northwest African upwelling region near Cabo Corbeiro. *Deep-Sea Res.* **25**, 751–770.

Codispoti, L.A., Dugdale, R.C., and Minas, H.J. (1982) A comparison of the nutrient regimes off northwest Africa, Peru and Baja California. *Rapp. P.-v. Réun. Cons. Int. Explor. Mer.* **180**, 184–201.

Coelho, M.L. (1985) Review of the influence of oceanographic factors on cephalopod distribution and life history. *NAFO Sci. Coun. Studies* **9**, 47–57.

Colebrook, J.M. (1979) Continuous plankton records: seasonal cycles of phytoplankton and copepods in the North Atlantic Ocean and the North Sea. *Mar. Biol.* **51**, 23–32.

Colebrook, J.M. (1986) Environmental influences on long-term variability in marine plankton. *Hydrobiologia* **142**, 309–325.

Conte, M.H., Bishop, J.K.B., and Backus, R.H. (1986) Nonmigratory, 12 kHz, deep scattering layers of Sargasso Sea origin in warm-core rings. *Deep-Sea Res.* **33A**, 1869–1884.

Conversi, A., Piontkovski, S., and Hameed, S. (2001) Seasonal and interannual dynamics of *Calanus finmarchicus* in the Gulf of Maine (Northeastern US shelf) with reference to the North Atlantic Oscillation. *Deep-Sea Res. II* **48**, 519–530.

Corner, E.D.S., Head, R.N., and Kilvington, C.C. (1972) On the nutrition and metabolism of zooplankton. VIII. The grazing of *Biddulphia* cells by *Calanus helgolandicus*. *J. Mar. Biol. Ass. UK* **52**, 847–861.

Corten, A. and van de Kamp, G. (1992) Natural changes in pelagic fish stocks of the North Sea in the 1980s. *ICES Mar. Sci. Symp.* **195**, 402–417.

Creutzberg, F. (1985) A persistent chlorophyll-*a* maximum coinciding with an enriched benthic zone. In *Proceedings of the Nineteenth European Marine Biology Symposium* (ed. P.E. Gibbs), pp. 97–108. Cambridge University Press, Cambridge.

Csanady, G.T. (1979) The life and death of a warm-core ring. *J. Geophys. Res.* **84** (C2), 777–780.

Csanady, G.T. (1981) Circulation in the coastal ocean. *Adv. Geophys.* **23**, 101–183.

Cubasch, U. and 8 other authors (2001) Projections of future climate change. In *Climate Change 2001: the Scientific Basis. Contribution of Working Group I to the Third Assessment Report of the Intergovernmental Panel on Climate Change* (ed. J.T. Houghton *et al.*). Cambridge University Press, Cambridge. [www.ipcc.ch]

Cullen, J.J. (1991) Hypotheses to explain high-nutrient conditions in the open sea. *Limnol. Oceanogr.* **36**, 1578–1599.

Cullen, J.J. and Davis, R.F. (2003) The blank can make a big difference in oceanographic measurements. *Limnol. Oceanogr. Bull.* **12**, 29–35.

Cunha, M.E. (2002) Physical control of biological processes in a coastal upwelling system: comparison of the effects of coastal topography, river runoff and physical oceanography in the northern and southern parts of Portuguese coastal waters. Unpublished Ph.D. thesis, University of Lisbon, Portugal.

Currie, J.T. (1984) Microscale nutrient patches: do they matter to the plankton? *Limnol. Oceanogr.* **29**, 211–214.

Cury, P. and Roy, C. (1989) Optimal environmental window and pelagic fish recruitment success in upwelling areas. *Can. J. Fish. Aquat. Sci.* **46**, 670–680.

Cury, P., Roy, C., and Faure, V. (1998) Environmental constraints and pelagic fisheries in upwelling areas: the Peruvian puzzle. *S. Afr. J. Mar. Sci.* **19**, 159–167.

Cushing, D.H. (1968) Grazing by herbivorous copepods in the sea. *J. Cons. Int. Explor. Mer.* **32**, 70–82.

Cushing, D.H. (1969) Upwelling and fish production. *FAO Fish. Tech. Paper* No. 84, 38 pp.

Cushing, D.H. (1971) Upwelling and the production of fish. *Adv. Mar. Biol.* **9**, 255–334.

Cushing, D.H. (1975) *Marine Ecology and Fisheries*. Cambridge University Press, Cambridge. 278 pp.

Cushing, D.H. (1982) *Climate and Fisheries*. Academic Press, London. 373 pp.

Cushing, D.H. (1988) The northerly wind. In *Towards a Theory on Biological–Physical Interactions in the World Ocean* (ed. B.J. Rothschild), pp. 235–244. Kluwer, Dordrecht.

Cushing, D.H. (1989) A difference in structure between ecosystems in strongly stratified waters and those that are only weakly stratified. *J. Plankt. Res.* **11**, 1–14.

Dade, W.B. (1993) Near-bed turbulence and hydrodynamic control of diffusional mass transfer at the sea floor. *Limnol. Oceanogr.* **38**, 52–69.

Dalton, R. (2002) Ocean tests raise doubts over use of algae as carbon sink. *Nature* **420**, 722.

Dandonneau, Y. (1988) Seasonal or aperiodic cessation of oligotrophy in the tropical Pacific Ocean. In *Towards a Theory on Biological–Physical Interactions in the World Ocean* (ed. B.J. Rothschild), pp. 137–156. Kluwer, Dordrecht.

Dandonneau, Y., Vega, A., Loisel, H., DuPenhoat, Y., and Menkes, C. (2003) Oceanic Rossby waves acting as a "hay rake" for ecosystem floating by-products. *Science (Wash.)* **302**, 1548–1551.

Danovaro, R., Gambi, C., Manini E., and Fabiano, M. (2000) Meifauna response to a dynamic river plume front. *Mar. Biol.* **137**, 359–370.

da Silva, A.J. (1986) River run-off and shrimp abundance in a tropical coastal ecosystem: the example of the Sofala Bank (Central Mozambique). In *The Role of Freshwater Outflow in Coastal Marine Ecosystems* (ed. S. Skreslet), pp. 329–344. Springer-Verlag, Berlin.

Davis, C.S., Flierl, G.R., Wiebe, P.H., and Franks, P.J.S. (1991) Micropatchiness, turbulence and recruitment in plankton. *J. Mar. Res.* **49**, 109–151.

Dawe, E.G. and Warren, W.G. (1992) Recruitment of short-finned squid in the Northwest Atlantic Ocean and some environmental relationships. *J. Cephal. Biol.* **2**, 1–21.

Dawe, E.G., Colbourne, E.B., and Drinkwater, K.F. (1998) Environmental effects on short-finned squid recruitment to Canadian waters. *Northwest Atlantic Fisheries Organization (NAFO).* NAFO SCR Doc. 98/54.

Dayton, P.K., Tegner, M.J., Edwards, P.B., and Riser, K.L. (1999) Temporal and spatial scales of kelp demography: the role of oceanographic climate. *Ecol. Monogr.* **69**, 219–250.

Defant, A. (1958) *Ebb and Flow*. University of Michigan Press, Ann Arbor, MI. 121 pp.

De Madariaga, I., Gonzalez-Azpiri, L., Villate, F., and Orive, E. (1992) Plankton responses to hydrological changes induced by freshets in a shallow mesotidal estuary. *Estuar. Coast. Shelf Sci.* **35**, 425–434.

Demaster, D.J. and Pope, R.H. (1996) Nutrient dynamics on the Amazon shelf: results from AMASSEDS. *Cont. Shelf Res.* **16**, 263–289.

Denman, K.L. (1993) The ocean carbon cycle and climate change: an analysis of interconnected scales. In *Patch Dynamics* (ed. S.A. Levin, T.M. Powell, and J.H. Steele), pp. 213–223. Springer-Verlag, Berlin.

Denman, K.L. (1994) Scale-determining biological–physical interactions in oceanic food webs. In *Aquatic Ecology: Scale, Pattern and Process* (ed. P.S. Giller, A.G. Hildrew, and D.G. Rafaelli), pp. 377–402. Blackwell Science, Oxford.

Denman, K.L. and Abbott, M.R. (1994) Time scales of pattern evolution from cross-spectrum analysis of advanced very high resolution radiometer and coastal zone color scanner imagery. *J. Geophys. Res*. **99**, 7433–7442.

Denny, M. (1999) Are there mechanical limits to size in wave-swept organisms? *J. Exp. Biol*. **202**, 3463–3467.

Denny, M.W., Gaylord, B.P., and Cowen, E.A. (1997) Flow and flexibility, II. The roles of size and shape in determining wave forces on the bull kelp *Nereocystis leutkeana*. *J. Exp. Biol*. **200**, 3165–3183.

Denny, M., Gaylord, B., Helmuth, B., and Daniel, T. (1998) The menace of momentum: dynamic forces on flexible organisms. *Limnol. Oceanogr*. **43**, 955–968.

Dickson, R.R. and Brander, K.M. (1993) The effects of a changing windfield on cod stocks of the North Atlantic. *Fish. Oceanogr.* **2**, 124–153.

Dickson, R.R. and Turrell, W.R. (2000) The NAO: the dominant atmospheric process affecting oceanic variability in home, middle and distant waters of European Atlantic Salmon. In *The Ocean Life of Atlantic Salmon: Environmental and Biological Factors Influencing Survival* (ed. D. Mills), pp. 92–115. Fishing News Books, Oxford.

Dickson, R.R., Kelly, P.M., Colebrook, J.M., Wooster, W.S., and Cushing, D.H. (1988a) North winds and production in the eastern North Atlantic. *J. Plankton Res.* **10**, 151–169.

Dickson, R.R., Meincke, J., Malmberg, S.-A., and Lee, A.J. (1988b) The "great salinity anomaly" in the northern North Atlantic 1968–1982. *Prog. Oceanogr.* **20**, 103–151.

Dietrich, G. (1950) Die anomale Jahresschwankung des Wärmeinhalts im englischen Kanal, ihre Ursachen und Auswirkungen. *Deutsche Hydrograph. Zeit.* **3**, 184–201.

Digiacomo, P.M. (2000) Satellite observations of phytoplankton variability in the California Current system: El Niño to eddies. *Diss. Abst. Int. Pt B: Sci. and Eng*. **60**, 3784.

Digiacomo, P.M. and Holt, B. (2001) Satellite observations of small coastal ocean eddies in the Southern California Bight. *J. Geophys. Res.* **106** (C10), 22521–22522.

Doty, M.S. and Oguri, M. (1956) The island mass effect. *J. Cons. Int. Explor. Mer.* **22**, 33–37.

Dower, J.F., Miller, T.J., and Leggett W.C. (1997) The role of microscale turbulence in the feeding ecology of larval fish. *Adv. Mar. Biol.* **31**, 169–220.

Dower, K.M. and Lucas, M.I. (1993) Photosynthesis–irradiance relationships and production associated with a warm-core ring shed from the Agulhas retroflection south of Africa. *Mar. Ecol. Prog. Ser.* **95**, 141–154.

Drinkwater, K.F. (1986) On the role of freshwater outflow on coastal ecosystems – A workshop summary. In *The Role of Freshwater Outflow in Coastal Marine Ecosystems* (ed. S. Skreslet), pp. 429–438. Springer-Verlag, Berlin.

Drinkwater, K.F. (1987) "Sutcliffe revisited": previously published correlations between fish stocks and environmental indices and their recent performance. In *Environmental Effects on Recruitment to Canadian Atlantic Fish Stocks* (ed. R.I. Perry and K.T. Frank), pp. 41–61. Can. Tech. Rep. Fish. Aquat. Sci. 1556.

Drinkwater, K.F. (1988) The effect of freshwater discharge on the marine environment. In *Proceedings of a Symposium on the Interbasin Transfer of Water: Impact and Research Needs for Canada* (ed. W. Nicholaichuk and F. Quinn), pp. 415–430. Department of the Environment, National Hydrology Research Centre, Saskatoon, Canada.

Drinkwater, K.F. (2002) A review of the role of climate variability in the decline of northern cod. In *Fisheries in a Changing Climate* (ed. N.A. McGinn), pp. 113–130. American Fisheries Society, Bethesda, MD.

Drinkwater, K.F. and Frank, K.T. (1994) Effects of river regulation and diversion on marine fish and invertebrates. *Aquatic Conservation: Freshwater and Marine Ecosystems* **4**, 135–151.

Drinkwater, K.F. and Myers, R.A. (1993) Investigations of the mean, seasonal and interannual variability in the position of the north wall of the Gulf Stream between 45° W and 75° W. *NAFO SCR Doc.* 93/49. 6pp.

Drinkwater, K.F. and 8 other authors (2003) The response of marine ecosystems to climate variability associated with the North Atlantic Oscillation. In *The North Atlantic Oscillation: Climatic Significance and Environmental Impact* (ed. J.W. Hurrell, Y. Kushnir, G. Ottersen, and M. Visbeck), pp. 211–234. Geophysical Monograph 134. American Geophysical Union, Washington DC.

Dugdale, R.C. and Goering, J.J. (1967) Uptake of new and regenerated forms of nitrogen in primary productivity. *Limnol. Oceanogr.* **12**, 196–206.

Dugdale, R.C., Wilkerson, F.P., and Minas, H.J. (1995) The role of a silicate pump in driving new production. *Deep-Sea Res. I* **42**, 697–719.

Duncombe Rae, C.M., Boyd, A.J., and Crawford, R.J.M. (1992) "Predation" of anchovy by an Agulhas ring: a possible contributory cause of a very poor year class of 1989. *S. Afr. J. Mar. Sci.* **12**, 167–173.

Dyer, K. (1973) *Estuaries: a Physical Introduction*. Wiley, London.

Ebbesmeyer, C.C., Cayan, D.R., McLain, D.R., Nichols, F.H., Peterson, D.H., and Redmond, K.T. (1991) 1976 step in the Pacific climate: forty environmental changes between 1968–1975 and 1977–1984. In *Proceedings of the Seventh Annual Climate (PACLIM) Workshop, April 1990* (ed. J.L. Betancourt and V.L. Tharp), pp. 115–126. California Department of Water Resources. Interagency Ecological Studies Program Technical Report 26.

Eckman, J.E. and Duggins, D.O. (1991) Life and death beneath macrophytic canopies: effects of understory growth rates and survival of marine benthic suspension feeders. *Oecologia* **87**, 473–487.

Edwards, M., Rid, P., and Planque, B. (2001) Long-term regional variability of phytoplankton biomass in the Northeast Atlantic, 1960–1995. *ICES J. Mar. Sci.* **58**, 39–49.

Efron, B. and Tibshirani, R. (1986) Bootstrap methods for standard errors, confidence intervals and other measures of statistical accuracy. *Stat. Sci.* **1**, 54–77.

Eggleston, D.B., Armstrong, D.A., Elis, W.E., and Patton, W.S. (1998) Estuarine fronts as conduits for larval transport: hydrodynamics and spatial distribution of Dungeness crab postlarvae. *Mar. Ecol. Prog. Ser.* **164**, 73–82.

Eilertsen, H.C. (1993) Spring blooms and stratification. *Nature* **363**, 24.

Eldridge, P.M. and Sieracki, M.E. (1993) Biological and hydrodynamic regulation of the microbial food web in a periodically mixed estuary. *Limnol. Oceanogr.* **38**, 1666–1679.

Epifanio, C.E. (1987) The role of tidal fronts in maintaining patches of brachyuran zoeae in estuarine waters. *J. Crustacean Biol.* **7**, 513–517.

Eppley, R.W. (1980) Estimating phytoplankton growth rates in the central oligotrophic oceans. In *Primary Productivity in the Sea* (ed. P.G. Falkowski), pp. 231–242. Plenum, New York.

Eppley, R.W. and Peterson, B.J. (1979) Particulate organic matter flux and planktonic new production in the deep ocean. *Nature* **282**, 677–680.

Eppley, R.W., Renger, E.H., and Harrison, W.G. (1979) Nitrate and phytoplankton production in southern California waters. *Limnol. Oceanogr.* **24**, 483–494.

Etheridge, D.M., Steele, L.P., Langenfelds, R.L., Francey, R.J., Barnola, J.-M., and Morgan, V.I. (1998) Historical CO_2 records from the Law Dome DE08, DE08-2 and DSS ice cores. In *Trends: a Compendium of Data on Global Change*. Carbon Dioxide Information Analysis

Center, Oak Ridge National Laboratory, US Department of Energy, Oak Ridge, TN. [cdiac.ornl.gov/trends/co2/lawdome.html]

Evans, G.T. and Parslow, J.S. (1985) A model of annual plankton cycles. *Biol. Oceanogr.* **3**, 327–347.

Ewing, G. (1950) Slicks, surface films and internal waves. *J. Mar. Res.* **9**, 161–187.

Falkowski, P.G. (1995) Ironing out what controls primary production in the nutrient rich waters of the open ocean. *Global Change Biol.* **1**, 161–163.

Falkowski, P.G. and Wirick, C.D. (1981) A simulation model of the effects of vertical mixing on primary productivity. *Mar. Biol.* **65**, 69–75.

Falkowski, P.G., Laws, E.A., Barber, R.T., and Murray, J.W. (2003) Phytoplankton and their role in primary, new, and export production. In *Ocean Biogeochemistry: the Role of the Ocean Carbon Cycle in Global Change* (ed. M.J.R. Fasham), pp. 99–121. Springer-Verlag, Berlin.

Fasham, M.J.R. (ed.) (2003) *Ocean Biogeochemistry: the Role of the Ocean Carbon Cycle in Global Change.* Springer-Verlag, Berlin. 297 pp.

Fasham, M.J.R. and Pugh, P.R. (1976) Observations on the horizontal coherence of chlorophyll-*a* and temperature. *Deep-Sea Res.* **23**, 527–538.

Finney, B.P., Gregory-Eves, I., Douglas, M.S.V., and Smol, J.P. (2002) Fisheries productivity in the northeastern Pacific Ocean over the past 2200 years. *Nature* **416**, 929–933.

Fitzwater, S.E., Knauer, A., and Martin, J.H. (1982) Metal contamination and its effect on primary production measurements. *Limnol. Oceanogr.* **27**, 544–551.

Flagg, C.N. and Beardsley, R.C. (1975) The 1974 M.I.T. New England shelf dynamics experiment (March 1974) Part 1, Hydrography. *MIT Report* **75-1**.

Flierl, G. and McGillicuddy, D.J. (2002) Mesoscale and submesoscale physical–biological interactions. In *The Sea, Vol 12: Biological–Physical Interactions in the Sea* (ed. A.R. Robinson, J.J. McCarthy, and B.J. Rothschild), pp. 113–186. Wiley, New York.

Flierl, G.R. and Wroblewski, J.S. (1985) The possible influence of warm core Gulf Stream rings upon shelf water larval fish distribution. *Fish. Bull.* **83**, 313–330.

Flynn, K.J. (2003a) Do we need complex mechanistic phytoacclimation models for phytoplankton? *Limnol. Oceanogr.* **48**, 2243–2249.

Flynn, K.J. (2003b) Modelling multi-nutrient interactions in phytoplankton; balancing simplicity and realism. *Prog. Oceanogr.* **56**, 249–279.

Flynn, K.J. and Hipkin, C.R. (1999) Interactions between iron, light, ammonium and nitrate: Insights from the construction of a dynamic model of algal physiology. *J. Phycol.* **35**, 1171–1190.

Flynn, K.J., Clark, D.R., and Owens, N.J.P. (2002) The dark assimilation of nitrogen by phytoplankton, II: a modelling study of different strategies. *New Phytol.* **155**, 109–119.

Fofonoff, N.P. (1981) The Gulf Stream system. In *Evolution of Physical Oceanography* (ed. B.A. Warren and C. Wunsch), pp. 112–139. MIT Press, Cambridge, MA.

Fogg, G.E. (1985) Biological activities at a front in the western Irish Sea. In *Proceedings of the Nineteenth European Marine Biology Symposium* (ed. P.E. Gibbs), pp. 87–96. Cambridge University Press, Cambridge.

Folland, C.K., Parker, D.E., and Kates, F.E. (1984) Worldwide marine temperature fluctuations 1856–1981. *Nature* **310**, 670–673.

Folland, C.K. and 8 other authors (2001) Observed climate variability and change. In *Climate Change 2001: the Scientific Basis. Contribution of Working Group I to the Third Assessment Report of the Intergovernmental Panel on Climate Change* (ed. J.T. Houghton *et al.*). Cambridge University Press, Cambridge. [www.ipcc.ch]

Fortier, L. and Leggett, W.C. (1982) Fickian transport and the dispersal of fish larvae in estuaries. *Can. J. Fish. Aquat. Sci.* **39**, 1150–1163.

Fortier, L. and Leggett, W.C. (1983) Vertical migrations and transport of larval fish in a partially mixed estuary. *Can. J. Fish. Aquat. Sci.* **40**, 1543–1555.

Fournier, J.M., Marra, J., Bohrer, R., and Van Det, M. (1977) Plankton dynamics and nutrient enrichment of the Scotian Shelf. *J. Fish. Res. Board Can.* **34**, 1004–1018.

Fournier, R.O. (1978) Biological aspects of the Nova Scotian shelf break fronts. In *Oceanic Fronts in Coastal Processes* (ed. M.J. Bowman and W.E. Esaias), pp. 69–77. Springer-Verlag, New York.

Francis, R.C., Hare, S.R., Hollowed, A.B., and Wooster, W.S. (1998) Effects of interdecadal climate variability on the oceanic systems of the NE Pacific. *Fish. Oceanogr.* **7**, 1–21.

Frank, K.T. (1986) Ecological significance of the ctenophore *Pleurobrachia pileus* off southwestern Nova Scotia. *Can. J. Fish. Aquat. Sci.* **43**, 211–222.

Frank, K.T., Perry, R.I., Drinkwater, K.F., and Lear, W.H. (1988) *Changes in the Fisheries of Atlantic Canada Associated with Global Increases in Atmospheric Carbon Dioxide: a Preliminary Report*. Can. Tech. Rep. Fish. Aquat. Sci. No. 1652, 52 pp.

Franks, P.J.S. (1997) Spatial patterns in dense algal blooms. *Limnol. Oceanogr.* **42**, 1297–1305.

Franks, P.J.S. and Chen, C. (1996) Plankton production in tidal fronts: a model of Georges Bank in summer. *J. Mar. Res.* **54**, 631–651.

Franks, P.J.S. and Chen, C. (2001) A 3-D prognostic numerical model study of the Georges Bank ecosystem. Part II: biological–physical model. *Deep-Sea Res. II* **48**, 457–482.

Fransz, H.G. and Gieskes, W.W.C. (1984) The unbalance of phytoplankton and copepods in the North Sea. *Rapp. P.-v Réun. Cons. Int. Explor. Mer.* **183**, 218–225.

Frechette, M. and Bourget, E. (1985a) Food-limited growth of *Mytilus edulis* L. in relation to the benthic boundary layer. *Can. J. Fish. Aquat. Sci.* **42**, 1166–1170.

Frechette, M. and Bourget, E. (1985b) Energy flow between the pelagic and benthic zones: factors controlling particulate organic matter available to an intertidal mussel bed. *Can. J. Fish. Aquat. Sci.* **42**, 1158–1165.

Frechette, M., Butman, C.A., and Geyer, W.R. (1989) The importance of boundary-layer flows in supplying phytoplankton to the benthic suspension feeder *Mytilus edulis* L. *Limnol. Oceanogr.* **34**, 19–36.

Friedlander, A. and Smith, D. (1983) Sand lance larvae found in entrainment feature associated with a warm core ring off Hudson Canyon. *Coast. Oceanogr. Climatol. News* **2**, 3–4. (Obtainable from Center for Ocean Management Studies, University of Rhode Island, Kingston, RI 02881.)

Fromentin, J.-M. and Planque, B. (1996) *Calanus* and environment in the eastern North Atlantic, II. Influence of the North Atlantic Oscillation on *C. finmarchicus* and *C. helgolandicus*. *Mar. Ecol. Prog. Ser.* **134**, 111–118.

Gallegos, C.L. and Platt, T. (1982) Phytoplankton production and water motion in surface mixed layers. *Deep-Sea Res.* **29A**, 65–76.

Gallienne, C.P. and Robins, D.B. (1998) Trans-oceanic characterization of zooplankton community size structure using an optical plankton counter. *Fish. Oceanogr.* **7**, 147–158.

Gammelsrod, T. (1992) Variation in shrimp abundance on the Sofala Bank, Mozambique, and its relation to the Zambesi River runoff. *Estuar. Coast. and Shelf. Sci.* **35**, 91–103.

Ganeshram, R.S., Pedersen, T.F., Calvert, S.E., and Murray, J.W. (1995) Large changes in oceanic nutrient inventories from glacial to interglacial periods. *Nature* **376**, 755–758.

Garcon, V.C., Oschlies, A., Doney, S.C., McGillicuddy, D., and Waniek, J. (2001) The role of mesoscale variability on plankton dynamics in the North Atlantic. *Deep-Sea Res. II* **48**, 2199–2226.

Gargett, A.E. (1984) Vertical eddy diffusivity in the ocean interior. *J. Mar. Res.* **42**, 359–393.
Garrett, C.J.R. and Loder, J.W. (1981) Dynamical aspects of shallow-sea fronts. *Phil. Trans. Roy. Soc. Lond. A* **302**, 562–581.
Garrett, C.J.R. and Loucks, R.H. (1976) Upwelling along the Yarmouth Shore of Nova Scotia. *J. Fish. Res. Bd. Can.* **33**, 116–117.
Garvine, R.W. (1986) The role of brackish plumes in open shelf waters. In *The Role of Freshwater Outflow in Coastal Marine Ecosystems* (ed. S. Skreslet), pp. 47–65. Springer-Verlag, Berlin.
Garvine, R.W. and Monk, J.D. (1974) Frontal structure of a river plume. *J. Geophys. Res.* **79**, 2251–2259.
Gaudy, R., Bianchi, M., Pagano, M., and Soto, Y. (1996) Cross frontal variation in hydrological and biological structures in a river plume area (Rhone mouth, N.W. Mediterranean Sea) *Hydrobiologia* **324**, 131–140.
Gavis, J. (1976) Munk and Riley revisited: nutrient diffusion transport and rates of phytoplankton growth. *J. Mar. Res.* **34**, 161–179.
Gaylord, B. (1999) Detailing agents of physical disturbance: wave-induced velocities and accelerations on a rocky shore. *J. Exp. Mar. Biol. Ecol*. **239**, 85–124.
Gaylord, B. and Denny, M.W. (1997) Flow and flexibility, I. Effects of size, shape and stiffness in determining wave forces on the stipitate kelps *Eisenia arborea* and *Pterygophora californica. J. Exp. Biol*. **200**, 3165–3183.
Gaylord, B., Blanchette, C.A., and Denny, M.W. (1994) Mechanical consequences of size in wave-swept algae. *Ecol. Monogr*. **64**, 287–313.
Gerard, V.A. and Mann, K.H. (1979) Growth and production of *Laminaria longicruris* (Phaeophyta) populations exposed to different intensities of water movement. *J. Phycol.* **15**, 33–41.
Gerritsen, J. and Strickler, J.R. (1977) Encounter probabilities and community structure in zooplankton: a mathematical model. *J. Fish. Res. Board Can.* **34**, 73–82.
Gill, A.E. (1982) *Atmosphere–Ocean Dynamics*. International Geophysics Series 30. Academic Press, New York.
Girs, A.A. (1974) *Macrocirculation method for long-term meteorological prognosis.* Hydromedisdat Publ., St. Petersburg (Leningrad). 480 pp. (in Russian)
Glantz, M.H. (1985) Climate and fisheries: a Peruvian case study. *CPPS Boletin ERFEN* **15**, 13–31.
Glémarec, M. (1973) The benthic community of the European North Atlantic continental shelf. *Oceanogr. Mar. Biol. Ann. Rev.* **11**, 263–289.
Glover, R.S. (1967) The continuous plankton recorder survey of the North Atlantic. *Symp. Zool. Soc. Lond.* **19**, 189–210.
Glynn, P.W. (1985) El Niño-associated disturbance to coral reefs and post-disturbance mortality by *Acanthaster planci*. *Mar. Ecol. Prog. Ser.* **26**, 295–300.
Glynn, P.W. (1990) Coral mortality and disturbances to coral reefs in the tropical eastern Pacific. In *Global Ecological Consequences of the 1982–83 El Niño–Southern Oscillation* (ed. P.W. Glynn), pp. 55–126. Elsevier, Amsterdam.
Goldman, J.C. (1984a) Oceanic nutrient cycles. In *Flows of Energy and Materials in Marine Ecosystems: Theory and Practice* (ed. M.J.R. Fasham), pp. 137–170. Plenum Press, New York.
Goldman, J.C. (1984b) Conceptual role for microaggregates in pelagic waters. *Bull. Mar. Sci.* **35**, 462–476.
Govoni, J.J. and Grimes, C.B. (1992) The surface accumulation of larval fishes by hydrodynamic convergence within the Mississippi River plume front. *Continental Shelf Res.* **12**, 1265–1276.

Gowen, R.J., Stewart, B.M., Mills, D.K., and Elliott, P. (1995) Regional differences in stratification and its effect on phytoplankton production and biomass is the northwestern Irish Sea. *J. Plankton Res.* **17**, 753–769.

Gower, J.F.R., Denman, K.L., and Holyer, R.J. (1980) Phytoplankton patchiness indicates the fluctuations spectrum of mesoscale oceanic structure. *Nature* **288**, 157–159.

Graham, J.J. (1972) Retention of larval herring within the Sheepscot estuary of Maine. *Fish. Bull.* **70**, 299–305.

Graham, W.M. and Largier, J.L. (1997) Upwelling shadows as nearshore retention sites: the example of northern Monterey Bay. *Cont. Shelf Res.* **17**, 509–532.

Gran, H.H. (1931) On the conditions for the production of plankton in the sea. *Rapp. P.-v. Réun. Cons. Int. Explor. Mer.* **75**, 37–46.

Gran, H.H. and Braarud, T. (1935) A quantitative study of the phytoplankton in the Bay of Fundy and the Gulf of Maine (including observations on hydrography, chemistry and turbidity). *J. Biol. Bd. Canada* **1**, 279–433.

Greenberg, D.A. (1983) Modeling the mean barotropic circulation in the Bay of Fundy and Gulf of Maine. *J. Phys. Oceanogr.* **13**, 886–904.

Greene, C.H. and Pershing, A.J. (2000) The response of *Calanus finmarchicus* populations to climate variability in the Northwest Atlantic: basin-scale forcing associated with the North Atlantic Oscillation. *ICES J. Mar. Sci.* **57**, 1536–1544.

Gries, T., John, K., Fields, D., and Strickler, J.R. (1999) Size and structure of "footprints" produced by *Daphnia*: impact of animal size and density gradients. *J. Plankt. Res.* **21**, 509–523.

Griffin, R.B. (1999) Sperm whale distribution and community ecology associated with a warm-core ring off Georges Bank. *Mar. Mamm. Sci.* **15**, 33–51.

Grindley, J.R. (1964) On the effect of low-salinity water on the vertical migration of estuarine zooplankton. *Nature* **203**, 781–782.

Gross, R.S., Fukumori, I., Menemenlis, D., and Gegout, P. (2004) Atmospheric and oceanic excitation of length-of-day variations during 1980–2000. *J. Geophys. Res.* **109**, B01406. doi:10.1029/2003JB002432

Gruber, N. (2002) WOCE and beyond. *World Ocean Circulation Experiment* (WOCE) conference, San Antonio, TX, November 18–22, 2002. [www.nodc.noaa.gov/WOCE/woce_conf2002]

Guisande, C., Cabanas, J.M., Vergara, A.B., and Riviero, I. (2001) Effect of climate on recruitment success of Atlantic Iberian sardine *Sardina pilchardus*. *Mar. Ecol. Prog. Ser.* **223**, 243–250.

Gundersen, J.K. and Jørgensen, B.B. (1990) Microstructure of diffusive boundary layers and the oxygen uptake of the sea floor. *Nature* **345**, 604–607.

Hachey, H.B. (1935) The effect of a storm on an inshore area with markedly stratified waters. *J. Biol. Board Can.* **1**, 227–237.

Hagberg, J. and Tunberg, B.G. (2000) Studies in the covariation between physical factors and the long-term variation of the marine soft-bottom fauna in Western Sweden. *Estuar. Coast. Shelf Sci.* **50**, 373–385.

Halim, Y., Morcos, S.A., Rizkalla, S., and El-Sayed, M.K. (1995) The impact of the Nile and of the Suez Canal on the living marine resources of the Egyptian Mediterranean waters (1958–1986). In *Effects of Riverine Inputs on Coastal Ecosystems and Fisheries Resources*, pp. 19–57. FAO Fish. Tech. Pap. 349. FAO, Rome.

Haney, J.C. (1986) Seabird segregation at Gulf Stream frontal eddies. *Mar. Ecol. Prog. Ser.* **28**, 279–285.

Hansen, J. and Lebedeff, S. (1988) Global surface air temperature: update through 1987. *Geophys. Res. Lett.* **15**, 323–326.

Hare, S.R. and Mantua, N.J. (2000) Empirical evidence for North Pacific regime shifts in 1977 and 1989. *Prog. Oceanogr.* **47**, 103–145.

Harris, G.P., Davies, P., Nunez, M., and Meyers, G. (1988) Interannual variability in climate and fisheries in Tasmania. *Nature* **333**, 754–757.

Harris, G.P., Griffiths, F.B., and Clementson, L.A. (1992) Climate and fisheries off Tasmania: interactions of physics, food chains, and fish. In *Benguela Trophic Functioning* (ed. A.I.L. Payne, K.H. Brink, K.H. Mann, and R. Hillborn). *S. Afr. J. Mar. Sci.* **12**, 585–597.

Harrison, P.J., Boyd, P.W., Varela, D.E., Takeda, S., Shiomoto, A., and Odate, T. (1999) Comparison of factors controlling phytoplankton productivity in the NE and NW subarctic Pacific gyres. *Prog. Oceanogr.* **43**, 205–234.

Hartline, B.K. (1980) Coastal upwelling: physical factors feed fish. *Science* **208**, 38–40.

Harvey, J. and Arhan, M. (1988) The water masses of the central North Atlantic in 1983–84. *J. Phys. Oceanogr.* **18**, 1855–1875.

Hays, J.D., Imbrie, J., and Shackleton, N.J. (1976) Variations in the earth's orbit: pacemaker of the ice ages. *Science* **194**, 1121–1131.

Hayward, T.L. and Venrick, E.L. (1982) Relation between surface chlorophyll, integrated chlorophyll and integrated primary production. *Marine Biology* **69**, 247–252.

Hellerman, S. and Rosenstein, M. (1983) Normal monthly wind stress over the world ocean with error estimates. *J. Phys. Oceanogr.* **13**, 1093–1104.

Hempel, G. (1982) The Canary current: studies of an upwelling system. *Rapp. P.-v Réun. Cons. Int. Explor. Mer.* **180**, 1–455.

Hendershott, M.C. (1981) Long waves and ocean tides. In *Evolution of Physical Oceanography* (ed. B.A. Warren and C. Wunsch), pp. 292–341. MIT Press, Cambridge, MA.

Herbland, A. and Voituriez, B. (1979) Hydrological structure analysis for estimating the primary production in the tropical Atlantic Ocean. *J. Mar. Res.* **37**, 87–101.

Herman, A.W., Sameoto, D.D., and Longhurst, A.R. (1981) Vertical and horizontal distribution patterns of copepods near the shelf-break south of Nova Scotia. *Can. J. Fish. Aquat. Sci.* **38**, 1065–1076.

Heywood, K.J., Barton, E.D., and Simpson, J.H. (1990) The effect of flow disturbance by an oceanic island. *J. Mar. Res.* **48**, 55–73.

Hill, A.E. (1991) A mechanism for horizontal zooplankton transport by vertical migration in tidal currents. *Mar. Biol.* **111**, 485–492.

Hill, A.E. (1998) Diel vertical migration in stratified tidal flows: Implications for plankton dispersal. *J. Mar. Res.* **56**, 1069–1096.

Hill, D.K. (1995) Pacific warming unsettles ecosystems. *Science* **267**, 1911–1912.

Hill, L. and Coelho, M.L. (2001) Portuguese fisheries in Portugal for the period 1950–1999: comparison with ICES data. In *Fisheries Impacts on North American Ecosystems: Catch, Effort and National/Regional Data Sets* (ed. D. Zeller, R. Watson, and D. Pauly), pp. 187–190. Fisheries Centre Research Reports 9 (3).

Hirst, A.G. and Lampitt, R.S. (1998) Towards a global model of in situ weight-specific growth in marine planktonic copepods. *Mar. Biol.* **132**, 247–257.

Hitchcock, G.L., Langdon, C., and Smayda, T.J. (1985) Seasonal variations in the phytoplankton biomass and productivity of a warm-core Gulf Stream ring. *Deep-Sea Res.* **32A**, 1287–1300.

Hogg, N.G., Pickart, R.S., Hendry, R.M., and Smethie, W.J. (1986) The northern recirculation gyre of the Gulf Stream. *Deep-Sea Res.* **33A**, 1139–1165.

Holbrook, N.M., Denny, M.W., and Koehl, M.A.R. (1991) Intertidal "trees": consequences of aggregation on the mechanical and photosynthetic properties of sea-palms, *Postelia palmaeformis* Ruprecht. *J. Exp. Mar. Biol. Ecol.* **146**, 39–67.

Holliday, N.P. and Reid, P.C. (2001) Is there a connection between high transport of water through the Rockall Trough and ecological changes in the North Sea? *ICES J. Mar. Sci.* **58**, 270–274.

Holligan, P.M. (1981) Biological implications of fronts on the northwest European continental shelf. *Phil. Trans. Roy. Soc. A* **302**, 547–562.

Holligan, P.M. and 8 other authors (1984a) Vertical distribution and partitioning of organic carbon in mixed, frontal and stratified waters of the English Channel. *Mar. Ecol. Prog. Ser.* **14**, 111–127.

Holligan, P.M., Williams, P.J.Le B., Purdie, D., and Harris, R.P. (1984b) Photosynthesis, respiration and nitrogen supply of plankton populations in stratified, frontal and tidally mixed shelf waters. *Mar. Ecol. Prog. Ser.* **17**, 201–213.

Holligan, P.M., Pingree, R.D., and Mardell, G.T. (1985) Oceanic solitons, nutrient pulses and phytoplankton growth. *Nature* **314**, 348–350.

Hollowed, A.B. and Wooster, W.S. (1992) Variability of winter ocean conditions and strong year classes of Northeast Pacific groundfish. In *Hydrobiological Variability in the ICES Area, 1980–1989*, pp. 433–444. ICES Marine Science Symposia 195. ICES, Copenhagen.

Holm-Hansen, O. (1985) Nutrient cycles in Antarctic marine ecosystems. In *Antarctic Nutrient Cycles and Food Webs* (ed. W.R. Siegfried, P.R. Condy, and R.M. Laws), pp. 6–10. Springer-Verlag, Berlin.

Honjo, S. and Manganini, S.J. (1993) Annual biogenic particle fluxes to the interior of the North Atlantic Ocean; studied at 34° N 21° W and 48° N 21° W. *Deep-Sea Res. II* **40**, 587–607.

Horel, J.D. and Wallace, J.M. (1981) Planetary-scale atmospheric phenomena associated with the southern oscillation. *Monthly Weather Rev.* **109**, 813–829.

Horne, E.P.W. and 6 other authors (1989) Nitrate supply and demand at the Georges Bank tidal front. *Scientia Marina* **53** (2–3), 145–158.

Houghton, J.T., Jenkins, G.J., and Ephraums, J.J. (eds.) (1990) *Climate Change: the IPCC Assessment*. Cambridge University Press. Cambridge. 365 pp.

Houghton, J.T. and 7 other authors (2001) *Climate Change 2001: the Scientific Basis.* University Press, Cambridge. 881 pp.

Houghton, R.W. (1997) Lagrangian flow at the foot of a shelfbreak front using a dye tracer injected into the bottom boundary layer. *Geophys. Res. Lett.* **24**, 2035–2038.

Houghton, R.W. (2002) Diapycnal flow through a tidal front: a dye tracer study on Georges Bank. *J. Mar. Systems* **37**, 31–46.

Houghton, R.W. and Visbeck, M. (1998) Upwelling and convergence in the Middle Atlantic Bight shelfbreak front. *Geophys. Res. Lett.* **25**, 2765–2768.

Howard, K.L. and Yoder, J.A. (1997) Contribution of the subtropical oceans to global primary production. In *Space Remote Sensing of Subtropical Oceans* (ed. C.-T. Liu), pp. 157–168. COSPAR Colloquia Series **8**. Pergamon Press, Oxford.

Howarth, R.W. (1996) Nitrogen cycling in the North Atlantic and its watersheds. *Biogeochemistry* **35** (special issue). (Also published separately by Kluwer, Dordrecht.)

Howarth, R.W., Butler, T., Lunde, K., Swaney, D., and Chu, C.R. (1993) Turbulence and planktonic nitrogen fixation: a mesocosm experiment. *Limnol. Oceanogr.* **38**, 1696–1711.

Huisman, J., van Oostveen, P., and Weissing, F.J. (1999) Critical depth and critical turbulence: two different mechanisms for the development of phytoplankton blooms. *Limnol. Oceanogr.* **44**, 1781–1787.

Hunter, J.R. (1972) Swimming and feeding behaviour of larval anchovy, *Engraulis mordax*. *Fish. Bull. US* **73**, 453–462.

Huntsman, S.A. and Barber, R.T. (1977) Primary production off northwest Africa: the relationship to wind and nutrient conditions. *Deep-Sea Res.* **24**, 25–33.

Hurd, C.L. (2000) Water motion, marine macroalgal physiology, and production. *J. Phycol.* **36**, 453–472.

Hurd, C.L. and Stevens, C.L. (1997) Flow visualization around single and multiple-bladed seaweeds with various morphologies. *J. Phycol*. **33**, 360–367.

Hurd, C.L., Harrison, P.J., and Druehl, L. (1996). Effect of seawater velocity on inorganic nitrogen uptake by morphologically distinct forms of *Macrocystis integrifolia* from wave-sheltered and exposed sites. *Mar. Biol.* **126**, 205–214.

Hurd, C.L., Stevens, C.L., Laval, B.E., Lawrence, G.A., and Harrison, P.J. (1997) Visualization of seawater flow around morphologically distinct forms of the giant kelp *Macrocystis integrifolia* from wave-sheltered and exposed sites. *Limnol. Oceanogr.* **42**, 156–163.

Hurrell, J.W., Kushnir, Y., Ottersen, G., and Visbeck, M. (eds.) (2003) *The North Atlantic Oscillation: Climatic Significance and Environmental Impact*. Geophysical Monograph **134**. American Geophysical Union, Washington, DC. 279 pp.

Huskin, I., Anadon, R., Woodd-Walker, R.S., and Harris, R.P. (2001) Basin-scale latitudinal patterns of copepod grazing in the Atlantic Ocean. *J. Plankton Res.* **23**, 1361–1371.

Hutchings, J.A. and Myers, R.A. (1994) What can be learned from the collapse of a renewable resource? Atlantic cod, *Gadus morhua*, of Newfoundland and Labrador. *Can. J. Fish. Aquat. Sci.* **51**, 2126–2146.

Hutchinson, G.E. (1967) *A Treatise on Limnology*, Vol. 2. Wiley, New York. 1116 pp.

Huthnance, J.M. (1973) Tidal current asymmetries over the Norfolk sandbanks. *Estuar Coast. Mar. Sci.* **1**, 89–99.

Huyer, A. (1976) A comparison of upwelling events in two locations: Oregon and northwest Africa. *J. Mar. Res.* **34**, 531–546.

Iglesias-Rodriguez, M.D., Armstrong, R., Feely, R., Hood, R., and Kleypas, J. (2002) Progress made in study of ocean's calcium carbonate budget. *Eos* **83**, 365–375.

Iles, T.D. and Sinclair, M. (1982) Atlantic herring: stock discreteness and abundance. *Science* **215**, 627–633.

Imbrie, J. and Kipp, N.G. (1971) A new micropalaeontological method for quantitative palaeoclimatology: application to a late Pleistocene Caribbean core. In *The Late Cenozoic Glacial Ages* (ed. K. K. Turekian), pp. 77–181. Yale University Press, New Haven, CT.

Incze, L.S., Hebert, D., Wolff, N., Oakey N., and Dye, D. (2001) Changes in copepod distribution associated with increased turbulence from wind stress. *Mar. Ecol. Prog. Ser.* **213**, 229–241.

IPCC (2000) *Special Report on Emissions Scenarios: a Special Report of Working Group III of the Intergovernmental Panel on Climate Change.* Cambridge University Press, Cambridge.

Isemer, H.J. and Hasse, L. (1987) *The Bunker Climate Atlas of the North Atlantic Ocean, Vol. 2: Air–Sea Interactions*. Springer-Verlag, Berlin.

Iverson, R.L. and 9 other authors (1979) Ecological significance of fronts in the southeastern Bering Sea. In *Ecological Processes in Coastal and Marine Systems* (ed. R.L. Livingstone), pp. 437–465. Plenum Press, New York.

Jackson, G.A. (1980) Phytoplankton growth and zooplankton grazing in oligotrophic oceans. *Nature* **284**, 439–441.

Jackson, G.A. (1989) Simulation of bacterial attraction and adhesion to falling particles in an aquatic environment. *Limnol. Oceanogr.* **34**, 514–530.

Jackson, G.A. (1990) A model of the formation of marine algal flocs by physical coagulation processes. *Deep-Sea Res.* **37A**, 1197–1211.

Jackson, G.A. (1995) Comparing observed changes in particle size spectra with those predicted using coagulation theory. *Deep-Sea Res. II* **42**, 159–184.

Jacobson, L.D. and 14 other authors (2001) Surplus production, variability, and climate change in the great sardine and anchovy fisheries. *Can. J. Fish. Aquat. Sci.* **58**, 1891–1903.

Jai Shin, Y., Roy, C., and Cury, P. (1998) Clupeoids' reproductive strategies in upwelling areas: a tentative generalization. In *Global Versus Local Changes in Upwelling Systems*, pp. 409–422. Colloq. Semin. Inst. Fr. Rech. Sci. Dev. Coop. ORSTOM. Editions de l'ORSTOM. Paris.

Jamart, B.M., Winter, D.F., Banse, K., Anderson, G.C., and Lam, R.K. (1977) A theoretical study of phytoplankton growth and nutrient distribution in the Pacific Ocean of the northwest U.S. coast. *Deep-Sea Res.* **24**, 753–773.

Jamart, B.M., Winter, D.F., and Banse, K. (1979) Sensitivity analysis of a mathematical model of phytoplankton growth and nutrient distribution in the Pacific Ocean off the northwest US coast. *J. Plankton Res.* **1**, 267–290.

Jarre-Teichmann, A. and Christensen, V. (1998) Comparative modelling of trophic flows in four large upwelling ecosystems: global versus local effects. In *Global Versus Local Changes in Upwelling Systems*, pp. 423–446. Colloq. Semin. Inst. Fr. Rech. Sci. Dev. Coop. ORSTOM. Editions de l'ORSTOM. Paris.

Jenkins, W.J. (1982) Oxygen utilization rates in a North Atlantic subtropical gyre and primary production in oligotrophic systems. *Nature* **300**, 246–248.

Jenkins, W.J. and Goldman, J.C. (1985) Seasonal oxygen cycling and primary production in the Sargasso Sea. *J. Mar. Res.* **43**, 465–491.

Jerlov, N.J. (1976) *Marine Optics*. Elsevier Oceanography Series 14. Elsevier, Amsterdam.

Johnson, D.R., Weidemann, A., Arnone, R., and Davis, C.O. (2001) Chesapeake Bay outflow plume and coastal upwelling events, physical and optical properties. *J. Geophys. Res.* **106** (C6), 11613–11622.

Joint, I. and Groom, S.B. (2000) Estimation of phytoplankton production from space: current status and future potential of satellite remote sensing. *J. Exp. Mar. Biol. Ecol.* **250**, 233–255.

Joll, L.M. and Caputi, N. (1995) Geographic variation in the reproductive cycle of the saucer scallop (*Amusium balloti*) along the Western Australian coast. *Mar. Freshwat. Res.* **46**, 779–792.

Jones, B.H. and Halpern, D. (1981) Biological and physical aspects of a coastal upwelling event observed during March–April 1974 off northwest Africa. *Deep-Sea Res.* **28A**, 71–81.

Jones, P.D., Parker, D.E., Osborn, T.J., and Briffa, K.R. (2001) Global and hemispheric temperature anomalies: land and marine instrumental records. In *Trends: a Compendium of Data on Global Change*. Carbon Dioxide Information Analysis Center, Oak Ridge National Laboratory, US Department of Energy, Oak Ridge, TN. [cdiac.esd.ornl.gov/trends/temp/jonescru/jones.html]

Jones, R., Flynn, K.J., and Anderson, T. (2002) The effect of food quality on carbon and nitrogen growth efficiency in *Acartia tonsa*. *Mar. Ecol. Prog. Ser.* **235**, 147–156.

Jørgensen, B.B. and Boudreau, B.P. (2001) Diagenesis and sediment–water exchange. In *The Benthic Boundary Layer: Transport Processes and Biochemistry* (ed. B.P. Boudreau and B.B. Jorgensen), pp. 211–244. University Press, Oxford.

Jørgensen, B.B. and Revsbech, N.P. (1985) Diffusive boundary layers and the oxygen uptake of sediments and detritus. *Limnol. Oceanogr.* **30**, 111–122.

Josefson, A.B. and Conley, D.J. (1997) Benthic response to a pelagic front. *Mar. Ecol. Prog. Ser.* **147**, 49–62.

Jumars, P.A., Deming, J.W., Hill, P.S., Karp-Boss, L., Yager, P.L., and Dade, W.B. (1993) Physical constraints on marine osmotrophy in an optimal foraging context. *Mar. Microb. Food Webs* **7**, 121–159.

Jury, M.R. and Brundrit, G.B. (1992) Temporal organization of upwelling in the Southern Benguela ecosystem by resonant coastal trapped waves in the ocean and atmosphere. *S. Afr. J. Mar. Sci.* **12**, 219–224.

Justic, D., Rabalais, N.N., Turner, E., and Wiseman, W.J. (1993) Seasonal coupling between riverborne nutrients, net productivity and hypoxia. *Mar. Poll. Bull*. **26**, 184–189.

Kaartvedt, S. and Svendsen, H. (1990) Impact of freshwater runoff on physical oceanography and plankton distribution in a western Norwegian fjord: an experiment with a controlled discharge from a hydroelectric power plant. *Estuar. Coast. Shelf Sci.* **31**, 381–395.

Kaeriyama, M. and 8 other authors (2000) Feeding ecology of sockeye and pink salmon in the Gulf of Alaska. *NPAFC Bull.* **2**, 55–63.

Kamykowsky, D., McCollum, S.A., and Kirkpatrick, G.J. (1988) Observations and a model concerning the translational velocity of a photosynthetic marine dinoflagellate under variable environmental conditions. *Limnol. Oceanogr.* **33**, 57–65.

Karl, D.M. and Lukas, R. (1996) The Hawaii Ocean Time-series (HOT) program: background, rationale and field implementation. *Deep-Sea Res. II* **43**, 129–156.

Karl, D.M. and 6 other authors (1996) Seasonal and interannual variability in primary production and particle flux at Station ALOHA. *Deep-Sea Res. II* **43**, 539–568.

Karl, D.M. and 12 other authors (2003) Temporal studies of biogeochemical processes determined from ocean time-series observations during the JGOFS era. In *Ocean Biogeochemistry: the Role of the Ocean Carbon Cycle in Global Change* (ed. M.J.R. Fasham), pp. 239–267. Springer-Verlag, Berlin.

Karp-Boss, L., Boss, E., and Jumars, P.A. (1996) Nutrient fluxes to planktonic osmotrophs in the presence of fluid motion. *Ocean. Mar. Biol. Ann. Rev.* **34**, 71–107.

Kawamiya, M. and Oschlies, A. (2001) Formation of a basin-scale surface chlorophyll pattern by Rossby waves. *Geophys. Res. Lett.* **28**, 4139–4142.

Kawasaki, T. (1992) Mechanisms governing fluctuations in pelagic fish populations. In *Benguela Trophic Functioning* (ed. A.I.L. Payne, K.H. Brink, K.H. Mann, and R. Hilborn). *S. Afr. J. Mar. Sci.* **12**, 873–879.

Keeling, C.D. and Whorf, T.P. (2002) Atmospheric CO_2 concentrations derived from in situ air samples collected at Mauna Loa Observatory, Hawaii. In *Trends: a Compendium of Data on Global Change*. Carbon Dioxide Information Analysis Center, Oak Ridge National Laboratory, US Department of Energy, Oak Ridge, TN. [cdiac.ornl.gov/trends/co2/sio-keel-flask/sio-keel-flaskmlo.html]

Kepkay, P.E. (1994) Particle aggregation and the biological reactivity of colloids. *Mar. Ecol. Prog. Ser.* **109**, 293–304.

Kerr, R.A. (1983) Orbital variation–ice age link strengthened. *Science* **219**, 272–274.

Kerr, R.A. (1985) Long-lived small eddies are criss-crossing the oceans carrying the effects of local mixing hundreds and even thousands of kilometres. *Science* **230**, 793.

Kettle, A.J. and 31 other authors (1999) A global database of sea surface dimethylsulfide (DMS) measurements and a procedure to predict sea surface DMS as function of latitude, longitude and month. *Global Biogeochem. Cycles* **13**, 399–444.

Kiehl, J.T. and Trenberth, K.E. (1997) Earth's annual global mean energy budget. *Bull. Am. Met. Soc.* **78**, 197–208.

Kifani, S. (1998) Climate dependent fluctuations of the Moroccan sardine and their impact on fisheries. In *Global Versus Local Changes in Upwelling Systems*, pp. 235–247. Colloq. Semin. Inst. Fr. Rech. Sci. Dev. Coop. ORSTOM. Editions de l'ORSTOM. Paris.

Killworth, P.D., Cipollini, P., Uz, B.M., and Blundell, J.R. (2004) Physical and biological mechanisms for planetary waves observed in satellite-derived chlorophyll. *J. Geophys. Res*. **109** (C7), C07002; doi: 10.1029/2003JC001768.

Kimmerer, W.J. (2002) Physical, biological and management responses to variable freshwater flow into the San Francisco estuary. *Estuaries* **25**, 1275–1290.

King, F.D. and Devol, A.H. (1979) Estimates of vertical eddy diffusion through the thermocline from phytoplankton nitrate uptake rates in the mixed layer of the eastern tropical Pacific. *Limnol. Oceanogr.* **24**, 645–651.

King, F.D., Cucci, T.L., and Townsend, D.W. (1987) Microzooplankton and macrozooplankton glutamate dehydrogenase as indices of the relative contribution of these fractions to ammonium regeneration in the Gulf of Maine. *J. Plankton Res.* **9**, 277–289.

King, J.R., Ivanov, V.V., Kurashov, V., Beamish, R.J., and McFarlane, G.A. (1998) *General Circulation of the Atmosphere over the North Pacific and its Relationship to the Aleutian Low North Pacific*. North Pacific Anadromous Fish Commission Doc. No. 318, 18 pp.

Kingsford, M.J. and Choat, J.H. (1986) Influence of surface slicks on the distribution and inshore movement of small fish. *Mar. Biol.* **91**, 161–171.

Kiørboe, T. (1993) Turbulence, phytoplankton cell size, and the structure of pelagic food webs. *Adv. Mar. Biol.* **29**, 1–72.

Kjelson, M.A., Raquel, P.F., and Fisher, F.W. (1982) Life history of fall-run juvenile Chinook salmon, *Oncorhynchus tshawytscha*, in the Sacramento–San Joaquin estuary, California. In *Estuarine Comparisons* (ed. V.S. Kennedy), pp. 393–411. Academic Press, New York.

Kleckner, R.C. and McCleave, J.D. (1985) Spatial and temporal distribution of American eel larvae in relation to North Atlantic Ocean current systems. *Dana* **4**, 67–92.

Kleckner, R.C. and McCleave, J.D. (1988) The northern limit of spawning by Atlantic eels (*Anguilla* spp.) in the Sargasso Sea in relation to thermal fronts and surface water masses. *J. Mar. Res.* **46**, 647–667.

Klein, B. and Siedler, G. (1989) On the origin of the Azores current. *J. Geophys. Res.* **94**, 6159–6168.

Klyashtorin, L.B. (1998) Long-term climatic change and main commercial fish production in the Atlantic and Pacific. *Fish. Res.* **37**, 115–125.

Klyashtorin, L.B. (2001) *Climate Change and Long-term Fluctuations of Commercial Catches*. FAO Fisheries Technical Paper 410. FAO, Rome. 86 pp.

Koehl, M.A.R. (1984) Mechanisms of particle capture by copepods at low Reynolds numbers: possible modes of selective feeding. In *Trophic Interaction within Aquatic Ecosystems* (ed. D.G. Meyers and J.R. Strickler), pp. 135–166. American Association for the Advancement of Science, Washington, DC.

Koehl, M.A.R. (1986) Seaweeds in moving water: form and mechanical function. In *On the Economy of Plant Form and Function* (ed. T.J. Givnish), pp. 603–634. Cambridge University Press, Cambridge.

Koehl, M.A.R. (1999) Ecological biomechanics of benthic organisms: life history, mechanical design and temporal patterns of mechanical stress. *J. Exp. Biol.* **202**, 3469–3476.

Koehl, M.A.R. and Alberte, R.S. (1988) Flow, flapping and photosynthesis of *Nereocystis leutkeana*: a functional comparison of undulate and flat blade morphologies. *Mar. Biol.* **99**, 435–444.

Koehl, M.A.R. and Strickler, J.R. (1981) Copepod feeding currents: food capture at low Reynolds number. *Limnol. Oceanogr.* **26**, 1062–1073.

Koseff, J.R., Holen, J.K., Monismith, S.G., and Cloern, J.E. (1993) Coupled effect of vertical mixing and benthic grazing on phytoplankton populations in shallow, turbid estuaries. *J. Mar. Res.* **51**, 843–868.

Kroncke, I., Dippner, J.W., Heyen, H., and Zeiss, B. (1998) Long-term changes in macrofaunal communities off Norderney (East Frisia, Germany) in relation to climate variability. *Mar. Ecol. Prog. Ser.* **167**, 25–36.

Krauss, W. (1986) The North Atlantic current. *J. Geophys. Res.* **91**, 5061–5074.

Krauss, W. (1993) Ekman drift in homogeneous water. *J. Geophys. Res.* **98**, 20187–20209.

Kremer, J.N. and Nixon, S.W. (1978) *A Coastal Marine Ecosystem: Simulation and Analysis*. Springer-Verlag, New York. 217 pp.

Kumar, N. and 6 other authors (1995) Increased biological productivity and export production in the glacial southern ocean. *Nature* **378**, 675–680.

Lamb, H.H. (1969) The new look of climatology. *Nature* **223**, 1209–1215.

Lancelot, C., Hannon, E., Becquevort, S., Veth, C., and De Baar, H.J.W. (2000) Modeling phytoplankton blooms and carbon export production in the Southern Ocean: dominant controls by light and iron in the Atlantic sector in Austral spring 1992. *Deep-Sea Res. I* **47**, 1621–1662.

Lande, R. and Lewis, M.R. (1989) Models of photoadaptation and photosynthesis by algal cells in the turbulent mixed layer. *Deep-Sea Res.* **36A**, 1161–1175.

Lande, R. and Yentsch, C.S. (1988) Internal waves, primary production and the compensation depth of marine phytoplankton. *J. Plankton Res.* **10**, 565–571.

Lande, R., Li, W.K., Horne, E.P.W., and Wood, A.M. (1989) Phytoplankton growth rates estimated from depth profiles of cell concentration and turbulent diffusion. *Deep-Sea Res.* **36**, 1141–1159.

Landry, F.P., Miller, T.J., and Leggett, W.C. (1995) The effects of small-scale turbulence on the ingestion rate of fathead minnow (*Pimephales promelas*) larvae. *Can. J. Fish. Aquat. Sci.* **52**, 1714–1719.

Lang, K.L., Grimes, C.B., and Shaw, R.F. (1994) Variations in the age and growth of yellowfin tuna larvae, *Thunnus albacares. Environ. Bio. Fish.* **39**, 259–270.

Lange, C.B., Burke, S.K., and Berger, W.H. (1990) Biological production off southern California is linked to climate change. *Clim. Change* **16**, 319–329.

Lasker, R. (1975) Field criteria for the survival of anchovy larvae: the relation between inshore chlorophyll maximum layers and successful first feeding. *Fish. Bull. US* **73**, 847–855.

Lasker, R. (1978) The relation between oceanographic conditions and larval anchovy food in the California current: identification of factors leading to recruitment failure. *Rapp. P.-v. Réun. Cons. Int. Explor. Mer.* **173**, 212–230.

Lasker, R. (1988) Food chains and fisheries: an assessment after 20 years. In *Towards a Theory on Biological–Physical Interactions in the World Ocean* (ed. B.J. Rothschild), pp. 173–182. Kluwer, Dordrecht.

Lauria, M.L., Purdie, D.A., and Sharples, J. (1999) Contrasting phytoplankton distributions controlled by tidal turbulence in an estuary. *J. Mar. Syst.* **21**, 189–197.

Laurs, R.M., Yuen, H.S.H., and Johnson, J.H. (1977) Small-scale movements of albacore, *Thunnus alalunga*, in relation to ocean features as indicated by ultrasonic tracking and oceanographic sampling. *Fish. Bull. US* **75**, 347–355.

Lawler, J.P., Weinstein, M.P., Chen, H.Y., and Englert, T.L. (1988) Modeling of physical and behavioral mechanisms influencing recruitment of spot and Atlantic croaker to the Cape Fear estuary. *Am. Fish. Soc. Symp.* **3**, 115–131.

Laws, E.A., Falkowski, P.G., Smith, W.O., Ducklow, H., and McCarthy, J.J. (2000) Temperature effects on export production in the open ocean. *Global Biogeochem. Cycles* **14**, 1231–1246.

Lazier, J., Hendry, R., Clarke, A., Yashayaev, I., and Rhines, P. (2002) Convection and restratification in the Labrador Sea, 1990–2000. *Deep-Sea Res. I* **49**, 1819–1835.

Lazier, J.R.N. (1988) Temperature and salinity changes in the deep Labrador Sea, 1962–1986. *Deep-Sea Res.* **35A**, 1247–1253.

Lazier, J.R.N. and Mann, K.H. (1989) Turbulence and diffusive layers around small organisms. *Deep-Sea Res.* **36A**, 1721–1733.

LeBlond, P.H., Hickey, B.M., and Thompson, R.E. (1986) Runoff-driven coastal flow off British Columbia. In *The Role of Freshwater Outflow in Coastal Marine Ecosystems* (ed. S. Skreslet), pp. 309–318. Springer-Verlag, Berlin.

Lee, T.N., Atkinson, L.P., and Legeckis, R. (1981) Observations on a Gulf Stream frontal eddy on the Georgia continental shelf, April 1977. *Deep-Sea Res.* **28A**, 347–378.

Leetmaa, A., McCreary, J.P., and Moore, D.W. (1981) Equatorial currents: observations and theory. In *Evolution of Physical Oceanography* (ed. B.A. Warren and C. Wunsch), pp. 186–196. MIT Press, Cambridge, MA.

Le Fèvre, J. (1986) Aspects of the biology of frontal systems. *Adv. Mar. Biol.* **23**, 164–299.

Le Fèvre, J. and Frontier, S. (1988) Influence of temporal characteristics of physical phenomena on plankton dynamics, as shown by northwest European marine ecosystems. In *Towards a Theory on Biological–Physical Interactions in the World Ocean* (ed. B.J. Rothschild), pp. 245–272. Kluwer, Dordrecht.

Le Fèvre, J. and Grall, J.R. (1970) On the relationships of *Noctiluca* swarming off the western coast of Brittany with hydrological features and plankton characteristics of the environment. *J. Exp. Mar. Biol. Ecol.* **4**, 287–306.

Legendre, L. (1981) Hydrodynamic control of marine phytoplankton production: the paradox of stability. In *Ecohydrodynamics: Proceedings of the 12th International Liège Colloquium on Ocean Hydrodynamics* (ed. J.C.J. Nihoul), pp. 191–207. Elsevier, Amsterdam.

Legendre, L. and Demers, S. (1984) Towards dynamic biological oceanography and limnology. *Can. J. Fish. Aquat. Sci.* **41**, 2–19.

Legendre, L. and Demers, S. (1985) Auxiliary energy, ergoclines and aquatic biological production. *Naturaliste Can. (Rev. écol. syst.)* **112**, 5–14.

Legendre, L., Demers, S., and LeFaivre, D. (1986) Biological production at marine ergoclines. In *Marine Interfaces Ecohydrodynamics* (ed. J.C.J. Nihoul), pp. 1–54. Elsevier, Amsterdam.

Legrand, M., Feniet-Saigne, C., Saltzman, E.S., Germain, C., Barkov, N.I., and Petrov, V.N. (1991) Ice-core record of oceanic emissions of dimethylsulphide during the last climate cycle. *Nature* **350**, 144–146.

Lehman, J.T. and Scavia, D. (1982a) Microscale patchiness of nutrients in plankton communities. *Science* **216**, 729–730.

Lehman, J.T. and Scavia, D. (1982b) Microscale nutrient patches produced by zooplankton. *Proc. Natl. Acad. Sci. USA* **79**, 5001–5005.

Leichter, J.J., Wing, S.R., Miller, S.L., and Denny, M.W. (1996) Pulsed delivery of subthermal water to Conch Reef (Florida Keys) by internal tidal bores. *Limnol. Oceanogr.* **41**, 1490–1501.

Leichter, J.J., Shellenbarger, G., Genovese, S.J., and Wing, S.R. (1998) Breaking waves on a Florida (USA) coral reef: a plankton pump at work? *Mar. Ecol. Prog. Ser.* **166**, 83–97.

Lennert-Cody, C.E. and Franks, P.J.S. (1999) Plankton patchiness in high-frequency internal waves. *Mar. Ecol. Prog. Ser.* **186**, 59–66.

Lepage, S. and Ingram, R.G. (1986) Salinity intrusion in the Eastmain River estuary following a major reduction in freshwater input. *J. Geophys. Res.* **91** (C1), 909–915.

Letelier, R.M. and 6 other authors (2000) Role of late winter mesoscale events in the biogeochemical variability of the upper water column of the North Pacific subtropical gyre. *J. Geophys. Res.* **105** (C12), 28723–28739.

Levin, L.A. and 11 other authors (2001) The function of marine critical transition zones and the importance of sediment biodiversity. *Ecosystems* **4**, 430–451.

Lewis, C.V.W., Davis, C.S., and Gawarkiewicz, G. (1994) Wind forced biological–physical interactions on an isolated offshore bank. *Deep-Sea Res. II* **41**, 51–73.

Lewis, M.R., Cullen, J.J., and Platt, T. (1983) Phytoplankton and the thermal structure in the upper ocean: consequences of non-uniformity in chlorophyll profile. *J. Geophys. Res.* **88** (C4), 2565–2570.

Lewis, M.R., Cullen, J.J., and Platt, T. (1984a) Relationships between vertical mixing and photoadaptation of phytoplankton: similarity criteria. *Mar. Ecol. Prog. Ser.* **15**, 141–149.

Lewis, M.R., Horne, E.P.W., Cullen, J.J., Oakey, N.S., and Platt, T. (1984b) Turbulent motions may control phytoplankton photosynthesis in the upper ocean. *Nature* **311**, 49–50.

Lewis, M.R., Harrison, W.G., Oakey, N.S., Hebert, D., and Platt, T. (1986) Vertical nitrate fluxes in the oligotrophic ocean. *Science* **234**, 870–873.

Li, W.K.W. (2002) Macroecological patterns of phytoplankton in the northwestern North Atlantic Ocean. *Nature* **419**, 154–157.

Lindahl, O., Belgrano, A., Davidsson, L., and Hernroth, B. (1998) Primary production, climatic oscillations, and physico-chemical processes: the Gullmar Fjord time-series data set (1985–1996). *ICES J. Mar. Sci.* **55**, 72–729.

Lindeboom, H., Van Raaphorst, W., Beukema, J., Cadée, G., and Swennen, C. (1994) Sudden changes in the North Sea and Wadden Sea: oceanic influences underestimated? ICES CM. 16 pp.

Lochte, K. Anderson, R., Francois, R., Johnke, R.A., Shimmield, G., and Vetrov, A. (2003) Benthic processes and the burial of carbon. In *Ocean Biogeochemistry: the Role of the Ocean Carbon Cycle in Global Change* (ed. M.J.R. Fasham), pp. 195–216. Springer-Verlag, Berlin.

Loder, J.W. (1980) Topographic rectification of tidal currents on the sides of Georges Bank. *J. Phys. Oceanogr.* **10**, 1399–1416.

Loder, J.W. and Greenberg, D.A. (1986) Predicted positions of tidal fronts in the Gulf of Maine region. *Cont. Shelf Res.* **6**, 397–414.

Loder, J.W. and Platt, T. (1985) Physical controls on phytoplankton production at tidal fronts. In *Proceedings of the 19th European Marine Biology Symposium* (ed. P.E. Gibbs), pp. 3–21. Cambridge University Press, Cambridge.

Loder, J.W. and Wright, D.G. (1985) Tidal rectification and frontal circulation on the sides of George's Bank. *J. Mar. Res.* **43**, 581–604.

Loder, J.W., Brickman, D., and Home, E.P.W. (1992) Detailed structure of currents and hydrography on the northern side of Georges Bank. *J. Geophys. Res.* **97**, 14331–14342.

Lohrenz, S.E. and 6 other authors (1999) Nutrients, irradiance and mixing as factors regulating primary production in coastal waters impacted by the Mississippi River plume. *Cont. Shelf Res.* **19**, 1113–1141.

Long, R.R. (1954) Some aspects of the flow of stratified fluids II. Experiments with a two-fluid system. *Tellus* **6**, 97–115.

Longhurst, A.R. (1976) Interactions between zooplankton and phytoplankton profiles in the eastern tropical Pacific Ocean. *Deep-Sea Res.* **23**, 729–754.

Longhurst, A.R. (1981) Significance of spatial variability. In *Analysis of Marine Ecosystems* (ed. A.R. Longhurst), pp. 415–441. Academic Press, London.

Longhurst, A.R. (1995) Seasonal cycles of pelagic production and consumption. *Progress in Oceanography* **36**, 77–167.

Longhurst, A.R. (1998) *Ecological Geography of the Sea*. Academic Press, San Diego. 398 pp.

Longhurst, A.R. and Harrison, W.C. (1989) The biological pump: profiles of plankton production and consumption in the upper ocean. *Prog. Oceanogr.* **22**, 47–123.

Longhurst, A.R. and Herman, A.W. (1981) Do oceanic zooplankton aggregate at, or near, the deep chlorophyll maximum? *J. Mar. Res.* **39**, 353–356.

Longhurst, A.R. and Williams, R. (1979) Materials for plankton modelling: vertical distribution of Atlantic zooplankton in summer. *J. Plankton Res.* **1**, 1–28.

Longhurst, A., Sathyendranath, S., Platt, T., and Caverhill, C. (1995) An estimate of global primary production in the ocean from satellite radiometer data. *J. Plankton Res.* **17**, 1245–1271.

Lorius, C., Barkov, N.I., Jouzel, J., Korotkevich, Y.S., Kolyakov, V.M., and Raynaud, D. (1988) Antarctic ice core: CO_2 and climatic change over the last climatic cycle. *Eos* (*Trans. Am. Geophys. Union*) **69**, 681–684.

Lough, R.G. and Manning, J.P. (2001) Tidal-front entrainment and retention of fish larvae on the southern flank of Georges Bank. *Deep-Sea Res. II* **48**, 631–644.

Lough, R.G. and Mountain, D.G. (1996) Effect of small-scale turbulence on feeding rates of larval cod and haddock in stratified water on Georges Bank. *Deep-Sea Res. II* **43**, 1745–1772.

Lough, R.G. and 6 other authors (1989) Ecology and distribution of juvenile cod and haddock in relation to sediment type and bottom currents on eastern Georges Bank. *Mar. Ecol. Prog. Ser.* **56**, 1–12.

Lovelock, J.E. (1979) *Gaia*. Oxford University Press, Oxford.

Lucas, L.V., Cloern, J.E., Koseff, J.R., Monismith, S.G., and Thompson, J.K. (1998) Does the Sverdrup critical depth model explain bloom dynamics in estuaries? *J. Mar. Res.* **56**, 375–415.

Lucas, L.V., Koseff, J.R., Cloern, J.E., Monismith, G., and Thompson, J.K. (1999) Processes governing phytoplankton blooms in estuaries. 1: The local production–loss balance. *Mar. Ecol. Prog. Ser.* **187**, 1–15.

Lynch, D.R., Lewis, C.V.W., and Werner, F.E. (2001) Can Georges Bank larval cod survive on a calanoid diet? *Deep-Sea Res.* II **48**, 609–630.

MacIntyre, S., Alldredge, A.L., and Gotschalk, C.C. (1995) Accumulation of marine snow at density discontinuities in the water column. *Limnol. Oceanogr.* **40**, 449–468.

MacIsaac, J.J., Dugdale, R.C., Barber, R.T., Blasco, D., and Packard, T.T. (1985) Primary production cycle in an upwelling center. *Deep-Sea Res.* **32**, 503–529.

MacKenzie, B.R. and Leggett, W.C. (1991) Quantifying the contribution of small-scale turbulence to the encounter rates between larval fish and their zooplankton prey: effect of wind and tide. *Mar. Ecol. Prog. Ser.* **73**, 149–160.

MacKenzie, B.R., Miller, T.J., Cry, S., and Leggett, W.C. (1994) Evidence for a dome-shaped relationship between turbulence and larval fish ingestion rates. *Limnol. Oceanogr.* **39**, 1790–1799.

Malakoff, D. (1998) Death by suffocation in the Gulf of Mexico. *Science* **281**, 190–192.

Malone, T.C. (1982) Factors influencing the fate of sewage-derived nutrients in the lower Hudson estuary and New York Bight. In *Ecological Stress in the New York Bight: Science and Management* (ed. G.F. Mayer), pp. 301–320. Estuarine Research Foundation, Columbia, SC.

Malone, T.C. (1984) Anthropogenic nitrogen loading and assimilation capacity of the Hudson River estuarine system, USA. In *The Estuary as a Filter* (ed. V.S. Kennedy), pp. 291–311. Academic Press, Orlando, FL.

Mann, C.R. (1967) The termination of the Gulf Stream and the beginning of the North Atlantic current. *J. Geophys. Res.* **14**, 337–359.

Mann, K.H. (1984) Fish production in open ocean ecosystems. In *Flows of Energy and Materials in Marine Ecosystems: Theory and Practice* (ed. M.J.R. Fasham), pp. 435–458. Plenum Press, New York.

Mann, K.H. (1988) Towards predictive models for coastal marine ecosystems. In *Concepts of Ecosystem Ecology* (ed. L.R. Pomeroy and J.J. Alberts), pp. 291–316. Springer-Verlag, New York.

Mann, K.H. and Drinkwater, K.F. (1994) Environmental influences on fish and shellfish production in the Northwest Atlantic. *Environ. Rev.* **2**, 16–32.

Mann, M.E., Bradley, R.S., and Hughes, M.K. (1999) Northern hemisphere temperatures during the past millennium: inferences, uncertainties, and limitations. *Geophys. Res. Lett.* **26**, 759–762. [www.ngdc.noaa.gov/paleo/recons.html]

Mantua, N.J. and Hare, S.R. (2002) The Pacific Decadal Oscillation. *J. Oceanogr.* **58**, 35–44.

Maranon, E. and Holligan, P.M. (1999) Photosynthetic parameters of phytoplankton from 50° N to 50° S in the Atlantic Ocean. *Mar. Ecol. Prog. Ser.* **176**, 191–203.

Maranon, E. and 6 other authors (2001) Patterns of phytoplankton size structure and productivity in contrasting open-ocean environments. *Mar. Ecol. Prog. Ser.* **216**, 43–56.

Marcogliese, D.J. and Cone, D.K. (1993) What metazoan parasites tell us about the evolution of American and European eels. *Evolution* **47**, 1632–1635.

Margalef, R. (1974) Associacon o exclusionen le distribucion des especies del mimo genero en algas unicelulares. *Mem. R. Acad. Cienc. Artes Barcelona* **42**, 353–372.

Margalef, R. (1978a) Life-forms of phytoplankton as survival alternatives in an unstable environment. *Oceanologica Acta* **1**, 493–509.

Margalef, R. (1978b) What is an upwelling system? In *Upwelling Ecosystems* (ed. R. Boje and M. Tomczak), pp. 12–14. Springer-Verlag, Berlin.

Markle, D.F., Scott, W.B., and Kohler, A.C. (1980) New and rare records of Canadian fishes and the influence of hydrography on resident and nonresident Scotian Shelf ichthyofauna. *Can. J. Fish. Aquat. Sci.* **37**, 49–65.

Marra, J. (1978) Effect of short-term variations in light intensity on photosynthesis of a marine phytoplankter: a laboratory simulation study. *Mar. Biol.* **46**, 191–202.

Marra, J., Houghton, R.W., and Garside, C. (1990) Phytoplankton growth at the shelf-break front in the Middle Atlantic Bight. *J. Mar. Res.* **48**, 851–868.

Marshall, S.M. and Orr, A.P. (1928) The photosynthesis of diatom cultures in the sea. *J. Mar. Biol. Assoc.* **15**, 321–364.

Martin, J.H. (1990) Glacial–interglacial CO_2 exchange: the iron hypothesis. *Paleoceanogr.* **5**, 1–13.

Martin, J.H. and Fitzwater, S.E. (1988) Iron deficiency limits phytoplankton growth in the north-east Pacific subarctic. *Nature* **331**, 341–343.

Martin, J.H., Knauer, G.A., Karl, D.M., and Broenkow, W.W. (1987) VERTEX: carbon cycling in the northeast Pacific. *Deep-Sea Res.* **34A**, 267–285.

Martin, J.H. and 43 other authors (1994) Testing the iron hypothesis in ecosystems of the equatorial Pacific ocean. *Nature* **371**, 123–129.

Mason, D.M. and Brandt, S.B. (1999) Space, time, and scale: new perspectives in fish ecology and management. *Can. J. Fish. Aquat. Sci.* **56** (Suppl. 1), 1–3.

Mathisen, O.A., Thorne, R.E., Trumble, R.J., and Blackburn, M. (1978) Food consumption of pelagic fish in an upwelling area. In *Upwelling Ecosystems* (ed. R. Boje and M. Tomczak), pp. 111–123. Springer-Verlag, Berlin.

Mavor, T.P. and Bisagni, J.J. (2001) Seasonal variability of sea-surface temperature fronts on Georges Bank. *Deep-Sea Res. II* **48**, 215–243.

May, R.M. and Oster, G.F. (1976) Bifurcations and dynamic complexity in simple ecological models. *Am. Nat.* **110**, 573–599.

Mazé, R. (1983) Formation d'ondes internes induits dans un golfe par le passage d'une dépression et par la marée. Application en Golfe de Gascogne. *Ann. Hydrograph.* **8**, 45–58.

Mazé, R., Camus, Y., and Le Tareau, J.Y. (1986) Formation de gradients thermiques à la surface de l'ocean, au-dessus d'un talus, par interaction entre les ondes internes et le mélange du au vent. *J. Cons. Perm. Int. Explor. Mer.* **42**, 221–240.

McCarthy, J.J. (2002) Biological responses to nutrients. In *The Sea, Vol. 12: Biological–Physical Interactions in the Sea* (ed. A.R. Robinson, J.J. McCarthy, and B.J. Rothschild), pp. 219–244. Wiley, New York.

McCarthy, J.J. and Goldman, J.C. (1979) Nitrogenous nutrition of marine phytoplankton in nutrient-depleted waters. *Science* **203**, 670–672.

McCave, I.N. (1984) Size spectra and aggregation of suspended particles in the deep ocean. *Deep-Sea Res.* **31A**, 329–352.

McCleave, J.D., Kleckner, R.C., and Castonguay, M. (1987) Reproductive sympatry of American and European eels and the implications for migration and taxonomy. In *Common Strategies of Anadromous and Catadromous Fish* (ed. M.J. Dadswell, R.J. Klauda, C.M. Moffitt, R.L. Saunders, R.A. Rulifson, and J.E. Cooper), pp. 286–297. Am. Fish. Soc., Bethesda, MD.

McClimans, T.A. (1986) Laboratory modelling of dynamic processes in fjords and shelf waters. In *The Role of Freshwater Outflow in Coastal Marine Ecosystems* (ed. S. Skreslet), pp. 67–84. Springer-Verlag, Berlin.

McCreary, J.P., Kohler, K.E., Hood, R.R., and Olson, D.B. (1996) A four-compartment ecosystem model of biological activity in the Arabian Sea. *Prog. Oceanogr.* **37**, 193–240.

McGillicuddy, D.J. (1995) One-dimensional numerical simulation of primary production: Lagrangian and Eulerian formulations. *J. Plankton Res.* **17**, 405–412.

McGillicuddy, D.J. and 8 other authors (1998) Influence of mesoscale eddies on new production in the Sargasso Sea. *Nature* **394**, 263–266.

McNeil, J.D., Jannasch, H.W., Dickey, T., McGillicuddy, D., Brzezinski, M., and Sakamoto, C.M. (1999) New chemical, bio-optical and physical observations of upper ocean response to the passage of a mesoscale eddy off Bermuda. *J. Geophys. Res.* **104** (C7), 15537–15548.

McPhaden, M.J. and 14 other authors (1998) The tropical ocean–global atmosphere observing system: a decade of progress. *J. Geophys. Res.* **103** (C7), 14169–14240.

Mead, K.S. and Denny, M.W. (1995) The effect of hydrodynamic shear stress on fertilization and early development of the purple sea urchin *Strongylocentrotus purpuratus. Biol. Bull. Mar. Lab. Woods Hole* **188**, 46–56.

Michaels, A.F. and Knap, A.H. (1996) Overview of the US JGOFS Bermuda Atlantic Time-series study and the hydrostation S program. *Deep-Sea Res. II* **43**, 157–198.

Miller, G.R. (1966) The flux of tidal energy out of the deep oceans. *J. Geophys. Res.* **71**, 2485–2489.

Mills, E.L. (1989) *Biological Oceanography: an Early History, 1870–1960*. Cornell University Press, Ithaca, NY. 378 pp.

Mitchell, J.F.B., Johns, T.C., Gregory, J.M., and Tett, S.F.B. (1995) Climate response to increasing levels of greenhouse gases and sulphate aerosols. *Nature* **376**, 501–504.

Mitchell, J.F.B., Karoly, D.J., Hegerl, G.C., Zwiers, F.W., Allen, M.R., and Marengo, J. (2001) Detection of climate change and attribution of causes. In *Climate Change 2001: the Scientific Basis. Contribution of Working Group I to the Third Assessment Report of the Intergovernmental Panel on Climate Change* (ed. J.T. Houghton *et al.*). Cambridge University Press, Cambridge. [www.ipcc.ch]

Mix, A.C. (1989) Influence of productivity variations on long-term atmospheric CO_2. *Nature* **337**, 541–544.

Moisan, J.R. and Hofmann, E.E. (1996) Modeling nutrient and plankton processes in the California coastal transition zone. *J. Geophys. Res.* **101** (C10), 22693–22704.

Mommaerts, J.P., Pichot, G., Ozer, J., Adam, Y., and Baeyens, W. (1984) Nitrogen cycling and budget in Belgian coastal waters: North Sea areas with and without river inputs. *Rapp. P.-v. Réun. Cons. Int. Explor. Mer.* **183**, 57–69.

Mooers, C.N.K., Flagg, C.N., and Boicourt, W.C. (1978) Prograde and retrograde fronts. In *Oceanic Fronts in Coastal Processes* (ed. M.J. Bowman and W.E. Esaias), pp. 43–58. Springer-Verlag, New York.

Moore, J.K. and Abbott, M.R. (2002) Surface chlorophyll concentrations in relation to the Antarctic Polar Front: seasonal and spatial patterns from satellite observations. *J. Mar. Systems* **37**, 69–86.

Moore, J.K., Doney, S.C., Kleypas, J.A., Glover, D.M., and Fung, I.Y. (2002a) An intermediate complexity marine ecosystem model for the global domain. *Deep-Sea Res. II* **49**, 403–462.

Moore, J.K., Doney, S.C., Glover, D.M., and Fung, I.Y. (2002b) Iron cycling and nutrient-limitation patterns in surface waters of the world ocean. *Deep-Sea Res. II* **49**, 463–507.

Morel, F.M.M., Rueter, J.G., and Price, N.M. (1991) Iron nutrition of phytoplankton and its possible importance in the ecology of ocean regions with high nutrients and low biomass. *Oceanography* **4**, 56–61.

Morin, P., Wafar, M.V.M., and Le Corre, P. (1993) Estimation of nitrate flux in a tidal front from satellite-derived temperature data. *J. Geophys. Res.* **98** (C3), 4689–4695.

Muck, P. and Sanchez, G. (1987) The importance of mackerel and horse mackerel predation for the Peruvian anchoveta stock (a population and feeding model). In *The Peruvian Upwelling Ecosystem: Dynamics and Interactions* (ed. D. Pauly, P. Muck, J. Mendo, and I. Tsukayama), pp. 279–293. International Center for Living Resources, Manila, Philippines.

Muck, P., Rojas de Mendiola, B., and Antonietti, E. (1989) Comparative studies on feeding in the larval anchoveta (*Engraulis ringens*) and sardine (*Sardinops sagax*). In *The Peruvian Upwelling Ecosystem: Dynamics and Interactions* (ed. D. Pauly, P. Muck, J. Mendo, and I. Tsukayama), pp. 86–96. International Center for Living Resources, Manila, Philippines.

Muelbert, J.H., Luis, M.R., and Kelley, D.E. (1994) The importance of small-scale turbulence in the feeding of herring larvae. *J. Plankton Res.* **16**, 927–944.

Müller-Navara, S. and Mittelstaedt, E. (1985) *Schadstoffbereitung and Schadstoffbelastung in der Nordsee. Eine Medellstudie*. Deutsches Hydrographisches Institut, Hamburg. 50 pp.

Mullon, C., Cury, P., and Penven, P. (2002) Evolutionary individual-based model for the recruitment of anchovy (*Engraulis capensis*) in the southern Benguela. *Can. J. Fish. Aquat. Sci.* **59**, 910–922.

Munk, P. (1993) Differential growth of larval sprat *Sprattus sprattus* across a tidal front in the North Sea. *Mar. Ecol. Prog. Ser.* **99**, 17–27.

Munk, P. and Christiansen, V. (1990) Larval growth and drift pattern and the separation of spawning groups in the North Sea. *J. Fish. Biol.* **37**, 135–148.

Munk, P., Larsson, P.O., Danielssen. D.S., and Moksness, E. (1999) Variability in frontal zone formation and distribution of gadoid fish larvae at the shelf break in the north-eastern North Sea. *Mar. Ecol. Prog. Ser.* **177**, 221–233.

Munk, W. and Riley, G.A. (1952) Absorption of nutrients by aquatic plants. *J. Mar. Res.* **11**, 215–240.

Muschenheim, D.K. (1987a) The dynamics of near-bed seston flux and suspension-feeding benthos. *J. Mar. Res.* **45**, 473–496.

Muschenheim, D.K. (1987b) The role of hydrodynamic sorting of seston in the nutrition of a benthic suspension feeder, *Spio setosa* (Polychaeta: Spionidae). *Biol. Oceanogr.* **4**, 265–288.

Myers, R.A. and Drinkwater, K. (1989) The influence of Gulf Stream warm core rings on recruitment of fish in the northwest Atlantic. *J. Mar. Res.* **47**, 635–656.

Nair, R.R. and 7 other authors (1989) Increased particle flux to the deep ocean related to monsoons. *Nature* **338**, 749–751.

Namias, J. and Cayan, D.R. (1984) El Niño: implications for forecasting. *Oceanus* **27**, 41–47.

Narimousa, S. and Maxworthy, T. (1985) Two-layer model of shear-driven coastal upwelling in the presence of bottom topography. *J. Fluid. Mech.* **159**, 503–531.

Narimousa, S. and Maxworthy, T. (1987) Coastal upwelling on a sloping bottom: the formation of plumes, jets and pinched-off cyclones. *J. Fluid. Mech.* **176**, 169–190.

Neelin, J.D. and 6 other authors (1998) ENSO theory. *J. Geophys. Res.* **103** (C7), 14261–14290.

Neftel, A. and 6 other authors (1994) Historical CO_2 record from the Siple Station ice core. In *Trends: a Compendium of Data on Global Change*. Carbon Dioxide Information Analysis Center, Oak Ridge National Laboratory, US Department of Energy, Oak Ridge, TN. [cdiac.ornl.gov/trends/co2/siple.htm]

Nelson, G. (1992) Equatorward wind and atmospheric pressure spectra as metrics for primary productivity in the Benguela system. *S. Afr J. Mar. Sci.* **12**, 19–28.

New, A.L. (1988) Internal tidal mixing in the Bay of Biscay. *Deep-Sea Res.* **35A**, 691–697.

Nichols, F.H. (1985) Increased benthic grazing: an alternative explanation for low phytoplankton biomass in northern San Francisco Bay during the 1976–77 drought. *Estuar. Coast. Shelf Sci.* **21**, 379–388.

Nichols, F.H., Cloern, J.E., Luoma, S.N., and Peterson, D.H. (1986) The modification of an estuary. *Science* **231**, 567–573.

Nixon, S.W. (2003) Replacing the Nile: are anthropogenic nutrients providing the fertility once brought to the Mediterranean by a great river? *Ambio* **32**, 30–39.

Norcross, B.L. (1991) Estuarine recruitment mechanisms of larval Atlantic croakers. *Trans. Am. Fish. Soc.* **120**, 673–683.

Norcross, J.J. and Stanley, E.M. (1967) Inferred surface and bottom drift, June 1963 through October 1964: circulation of shelf waters off the Chesapeake Bight. *Prof. Pap. Environ. Sci. Serv. Admin.* **3**, 11–42.

Nunes, R.A. and Simpson, J.H. (1985) Axial convergence in a well-mixed estuary. *Estuar. Coast. Shelf Sci.* **20**, 637–649.

Nunes Vas, R.A. (1994) Turbulence closure model of estuarine stratification. *J. Geophys. Res.* **99**, 16143–16160.

Oakey, N.S. and Elliott, J.A. (1980) Dissipation in the mixed layer near Emerald Basin. In *Marine Turbulence* (ed. J.C.J. Nihoul), pp. 123–133. Elsevier, Amsterdam.

Obata, A., Ishizaka, J., and Endoh, M. (1996) Global verification of critical depth theory for phytoplankton bloom with climatological in situ temperature and satellite ocean color data. *J. Geophys. Res.* **101** (C9), 20657–20667.

O'Donnell, J. (1993) Surface fronts in estuaries. *Estuaries* **16**, 12–39.

O'Dor, R.K. and Dawe, E.G. (1998) *Illex illecebrosus*. In *Squid recruitment dynamics: the genus* Illex *as a model, the commercial* Illex *species and influences on variability* (ed. P.G. Rodhouse, E.G. Dawe, and R.K. O'Dor), pp. 77–104. FAO Fish. Tech. Pap. 376. FAO, Rome.

Odum, H.T. (1967a) Biological circuits and marine systems of Texas. In *Pollution and Marine Ecology* (ed. T.A. Olsen and F.J. Burgess), pp. 99–157. Wiley, New York.

Odum, H.T. (1967b) Energetics of world food production. In *The World Food Problem: a Report of the President's Science Advisory Committee* (I.L. Bennett, Chairman), vol. 3, pp. 55–94. The White House, Washington, DC.

Okubo, A. (1987) Fantastic voyage into the deep: marine biofluid mechanics. In *Mathematical Topics in Population Biology, Morphogenesis and Neurosciences* (ed. E. Teromoto and M. Yamaguti), pp. 32–47. Springer-Verlag, New York.

Oliver, J.K. and Willis, B.L. (1987) Coral-spawn slicks in the Great Barrier Reef: preliminary observations. *Mar. Biol.* **94**, 521–529.

Olson, D.B. (1986) Lateral exchange with Gulf Stream warm-core ring surface layers. *Deep-Sea Res.* **33A**, 1691–1704.

Olson, D.B. (2002) Biophysical dynamics of ocean fronts. In *The Sea, Volume 12: Biological–Physical Interactions in the Sea* (ed. A.R. Robinson, J.J. McCarthy, and B.J. Rothschild), pp. 187–218. Wiley, New York.

Olson, D.B., Schott, F.A., Zantopp, R.J., and Leaman, K.D. (1984) The mean circulation east of the Bahamas as determined from a recent measurement program and historical XBT data. *J. Phys. Oceanogr.* **14**, 1470–1487.

O'Reilly, J.E. and Busch, D.A. (1984) Phytoplankton primary production on the northwest Atlantic shelf. *Rapp. P.-v. Réun. Cons. Int. Explor. Mer*. **183**, 255–268.

O'Reilly, J.E., Evans-Zetlin, C., and Thomas, J.P. (1981) The relationship between surface and average water column concentrations of chlorophyll-a in northwestern Atlantic shelf water. ICES CM 1981/L17. 19 pp.

Ortner, P.B., Wiebe, P.H., and Cox, J.L. (1980) Relationships between oceanic epizooplankton distributions and the seasonal deep chlorophyll maximum in the northwest Atlantic Ocean. *J. Mar. Res.* **38**, 507–531.

Ortner, P.B., Wiebe, P.H., and Cox, J.L. (1981) Reply to "Do oceanic zooplankton aggregate at, or near, the deep chlorophyll maximum?" *J. Mar. Res.* **39**, 357–359.

Osborn, T.R. (1978) Measurements of energy dissipation adjacent to an island. *J. Geophys. Res.* **83**, 2939–2957.

Osborn, T.R. (1980) Estimates of the local rate of vertical diffusion from dissipation measurements. *J. Phys. Oceanogr.* **10**, 83–89.

Osborn, T.R. (1996) The role of turbulent diffusion for copepods with feeding currents. *J. Plankton Res.* **18**, 185–195.

Oschlies, A. and Garcon, V. (1998) Eddy-induced enhancement of primary production in a model of the North Atlantic Ocean. *Nature* **394**, 266–269.

Ottersen, G. and Stenseth, N.C. (2001) Atlantic climate governs oceanographic and ecological variability in the Barents Sea. *Limnol. Oceanogr.* **46**, 1774–1780.

Owen, R.W. (1968) Oceanographic conditions in the northeast Pacific and their relation to the albacore fishery. *Fish. Bull.* US **66**, 503–526.

Packard, T.T., Blasco, D., and Barber, R.T. (1978) *Mesodinium rubrum* in the Baja California upwelling system. In *Upwelling Ecosystems* (ed. R. Boje and M. Tomczak), pp. 73–89. Springer-Verlag, Berlin.

Palomera, I. and Rubies, P. (1982) Kinds and distribution of fish eggs and larvae off northwest Africa in April/May 1973. *Rapp. P.-v. Réun. Cons. Int. Explor. Mer*. **180**, 356–358.

Pape, E.H. and Garvine, R.W. (1982) The subtidal circulation in Delaware Bay and adjacent shelf waters. *J. Geophys. Res.* **87**, 7955–7970.

Parker, C.E. (1971) Gulf Stream rings in the Sargasso Sea. *Deep-Sea Res.* **18**, 981–993.

Parrish, R.H., Bakun, A., Husby, D.M., and Nelson, C.S. (1983) Comparative climatology of selected environmental processes in relation to eastern boundary current pelagic fish production. In *Proceedings of the Expert Consultation to Examine Changes in Abundance and*

Species Composition of Neritic Fish Resources (ed. G.D. Sharp and C.J. Csirke), pp. 731–737. FAO Fisheries Report 291(3). FAO, Rome.

Parsons, T.R. and Lalli, C.M. (1988) Comparative oceanic ecology of the plankton communities of the subarctic Atlantic and Pacific Oceans. *Oceanogr. Mar. Biol. Ann. Rev.* **26**, 317–359.

Partensky, F., Hess, W.R., and Vaulot, D. (1999) *Prochlorococcus*, a marine photosynthetic prokaryote of global significance. *Microbiol. Mol. Biol. Rev.* **63**, 106–127.

Pasciak, W.J. and Gavis, J. (1974) Transport limitation of nutrient uptake in phytoplankton. *Limnol. Oceanogr.* **19**, 881–888.

Pasciak, W.J. and Gavis, J. (1975) Transport limited nutrient uptake rates in *Dytilum brightwellii*. *Limnol. Oceanogr.* **20**, 604–617.

Patterson, M.R., Sebens, K.P., and Olson, R.R. (1991) In situ measurements of flow effects on primary production and dark respiration in reef corals. *Limnol. Oceanogr.* **36**, 936–948.

Pawlik, J.R. and Butman, C.A. (1993) Settlement of a marine tube worm as a function of current velocity: interacting effects of hydrodynamics and behavior. *Limnol. Oceanogr.* **38**, 1730–1740.

Pawlik, J.R., Butman, C.A., and Starzak, V.R. (1991) Hydrodynamic facilitation of gregarious settlement of a reefbuilding worm. *Science* **251**, 421–424.

Payne, A.I.L., Gulland, J.A., and Brink, K.H. (eds.) (1987) The Benguela and comparable ecosystems. *S. Afr. J. Mar. Sci.* **5**, 1–956.

Payne, A.I.L., Brink, K.H., Mann, K.H., and Hilborn, R. (eds.) (1992) Benguela trophic functioning. *S. Afr. J. Mar. Sci.* **12**.

Pearce, A.F. and Phillips, B.F. (1994) Oceanic processes, puerulus settlement and recruitment of the Western Rock Lobster *Panulirus cygnus*. In *The Biophysics of Marine Larval Dispersal* (ed. P.W. Sammarco and M.L. Heron), pp. 279–303. American Geophysical Union. Washington, DC.

Pearcy, W. (1983) Abiotic variations in regional environments. In *From Year to Year* (ed. W.S. Wooster), pp. 30–34. Washington Sea Grant Publication, University of Washington, Seattle, WA.

Pearcy, W.G. and Keene, D.F. (1974) Remote sensing of water colour and sea surface temperatures off the Oregon coast. *Limnol. Oceanogr.* **19**, 573–583.

Pedlosky, J. (1990) The dynamics of the oceanic subtropical gyres. *Science* **248**, 316–322.

Peffley, M.B. and O'Brien, J.J. (1976) A three-dimensional simulation of coastal upwelling off Oregon. *J. Phys. Oceanogr.* **6**, 164–180.

Peinert, R. (1986) Production, grazing and sedimentation in the Norwegian coastal current. In *The Role of Freshwater Outflow in Coastal Marine Ecosystems* (ed. S. Skreslet), pp. 361–374. Springer-Verlag, Berlin.

Perez, J.A.A. and O'Dor, R.K. (1998) The impact of environmental gradients on the early life inshore migration of the short-finned squid *Illex illecebrosus. S. Afr. J. Mar. Sci.* **20**, 293–303.

Perry, R.I. and 6 other authors (1990) The Georges Bank frontal system: mechanisms of plankton retention or dispersal. ICES CM, L8.

Peters, F. and Marrasé, C. (2000) Effects of turbulence on plankton: an overview of experimental evidence and some theoretical considerations. *Mar. Ecol. Prog. Ser.* **205**, 291–306.

Peters, F., Marrasé, C., Gasol, J.M., Sala, M.M., and Arin, L. (1998) Effects of turbulence on bacterial growth mediated through food web interactions. *Mar. Ecol. Prog. Ser.* **172**, 293–303.

Petersen, J.E., Sanford, L.P., and Kemp, W.M. (1998) Coastal plankton responses to turbulent mixing in experimental ecosystems. *Mar. Ecol. Prog. Ser.* **171**, 23–41.

Peterson, W.T., Miller, C.B., and Hutchinson, A. (1979) Zonation and maintenance of copepod populations in the Oregon upwelling zone. *Deep-Sea Res.* **26A**, 467–494.

Petit, J.R. and 18 other authors (1999) Climate and atmospheric history of the past 420,000 years from the Vostok ice core, Antarctica. *Nature* **399**, 429–436.

Petrie, B., Topliss, B.J., and Wright, D.W. (1987) Coastal upwelling and eddy development off Nova Scotia. *J. Geophys. Res.* **29** (C12), 12979–12991.

Petterssen, S. (1969) *Introduction to Meteorology*. McGraw-Hill, New York.

Philander, S.G. (1990) *El Niño, La Niña and the Southern Oscillation*. Academic Press, New York.

Pile, A.J. and Young, C.M. (1999) Plankton availability and retention efficiencies of cold-seep symbiotic mussels. *Limnol. Oceanogr.* **44**, 1833–1839.

Pineda, J. (1991) Predictable upwelling and shoreward transport of planktonic larvae by internal tidal bores. *Science* **253**, 548–550.

Pineda, J. (1994) Internal tidal bores in the nearshore: warm-water fronts, seaward gravity currents and the onshore transport of neustonic larvae. *J. Mar. Res.* **52**, 427–458.

Pineda, J. (1999) Circulation and larval distribution in internal tidal bore warm fronts. *Limnol. Oceanogr.* **44**, 1400–1414.

Pingree, R.D. (1979) Baroclinic eddies bordering the Celtic Sea in late summer. *J. Mar. Biol. Ass. UK* **59**, 689–698.

Pingree, R.D. and Griffiths, D.K. (1980) A numerical model of the M2 tide in the Gulf of St. Lawrence. *Oceanologica Acta* **3**, 221–225.

Pingree, R.D. and Mardell, G.T. (1981) Slope turbulence, internal waves and phytoplankton growth at the Celtic Sea shelf-break. *Phil. Trans. Roy. Soc. Lond. A* **302**, 663–682.

Pingree, R.D. and Mardell, G.T. (1985) Solitary internal waves in the Celtic Sea. *Prog. Oceanogr.* **14**, 431–444.

Pingree, R.D. and Pennycuik, L. (1975) Transfer of heat, fresh water and nutrients through the seasonal thermocline. *J. Mar. Biol. Ass. UK* **55**, 261–274.

Pingree, R.D., Forster, G.R., and Morrison, G.K. (1974) Turbulent convergent tidal fronts. *J. Mar. Biol. Ass. UK* **54**, 469–479.

Pingree, R.D., Pugh, P.R., Holligan, P.M., and Forster, G.R. (1975) Summer phytoplankton blooms and red tides along tidal fronts in the approaches to the English Channel. *Nature* **258**, 672–677.

Pingree, R.D., Holligan, P.M., Mardell, G.T., and Head, R.N. (1976) The influence of physical stability on spring, summer and autumn phytoplankton blooms in the Celtic Sea. *J. Mar. Biol. Ass. UK* **56**, 845–873.

Pingree, R.D., Bowman, M.J., and Esaias, W.E. (1978a) Headland fronts. In *Oceanic Fronts in Coastal Processes* (ed. M.J. Bowman and W.E. Esaias), pp. 78–86. Springer-Verlag, Berlin.

Pingree, R.D., Holligan, P.M., and Mardell, G.T. (1978b) The effects of vertical stability on phytoplankton distributions in the summer on the northwest European shelf. *Deep-Sea Res.* **25**, 1011–1028.

Pingree, R.D., Mardell, G.T., and New, A.L. (1986) Propagation of the internal tides from the upper slopes of the Bay of Biscay. *Nature* **321**, 154–158.

Planque, B. and Fredou, T. (1999) Temperature and the recruitment of Atlantic cod. *Can. J. Fish. Aquat. Sci.* **56**, 2069–2077.

Planque, B. and Fromentin, J.-M. (1996) *Calanus* and environment in the eastern North Atlantic. 1: Spatial and temporal patterns of *C. finmarchicus* and *C. helgolandicus*. *Mar. Ecol. Prog. Ser.* **134**, 101–109.

Planque, B. and Reid, P.C. (1998) Predicting *Calanus finmarchicus* abundance from a climate signal. *J. Mar. Biol. Ass. UK* **78**, 1015–1018.

Platt, T. and Sathyendranath, S. (1988) Oceanic primary production: estimation by remote sensing at local and regional scales. *Science* **241**, 1613–1620.

Platt, T. and Subba Rao, D.V. (1975) Primary production of marine microphytes. In *Photosynthesis and Productivity in Different Environments* (ed. J.P. Cooper), pp. 249–280. Cambridge University Press, Cambridge.

Platt, T. and 6 other authors (1989) Biological production of the oceans: the case for consensus. *Mar. Ecol. Prog. Ser.* **52**, 77–88.

Platt, T., Woods, J.D., Sathyendranath, S., and Barkmann, W. (1994) Net primary production and stratification in the ocean. In *The Polar Oceans and Their Role in Shaping the Global Environment* (ed. D.M. Johannesen, R.D. Muench, and D.E. Overland), pp. 247–254. Geophysical Monograph 85. American Geophysical Union. Washington, DC.

Platt, T., Sathyendranath, S., Edwards, A.M., Broomhead, D.S., and Ulloa, O. (2003a) Nitrate supply and demand in the mixed layer of the ocean. *Mar. Ecol. Prog. Ser.* **254**, 3–9.

Platt, T., Fuentes-Yaco, C., and Frank, K.T. (2003b) Spring algal bloom and larval fish survival. *Nature* **423**, 398–399.

Pond, S. and Pickard, G.L. (1983) *Introductory Dynamical Oceanography*, 2nd edn. Pergamon Press, Oxford.

Powles, P.M. and Warlen, S.M. (1997) Migration rates of *Anguilla rostrata* larvae arriving at North Carolina and New Brunswick from the Sargasso Sea, estimated from daily growth increments. Annual Int. Symp. Fish. Soc. British Isles. *Ichthyoplankton Ecol*. **39**.

Prandtl, L. (1969) *The Essentials of Fluid Dynamics*. Blackie, London. 451 pp.

Prentice, I.C. and 9 other authors (2001) The carbon cycle and atmospheric carbon dioxide. In *Climate Change 2001: the Scientific Basis. Contribution of Working Group I to the Third Assessment Report of the Intergovernmental Panel on Climate Change* (ed. J.T. Houghton *et al*.). Cambridge University Press, Cambridge. [www.ipcc.ch]

Price, J.F., Weller, R.A., and Schudlich, R.R. (1987) Wind-driven ocean currents and Ekman transport. *Science* **238**, 1534–1538.

Pritchard, D.W. (1967) What is an estuary: physical viewpoint. In *Estuaries* (ed. G.H. Lauff), pp. 52–63. American Association for the Advancement of Science, Washington, DC.

Pritchard, D.W. (1989) Estuarine classification: a help or hindrance? In *Estuarine Circulation* (ed. B.J. Neilson, A. Kuo, and J. Brubaker), pp. 1–38. Humana Press, Clifton, NJ.

Prospero, J.M. and Savoie, D.L. (1989) Comparison of oceanic and continental sources of non-sea-salt sulphate over the Pacific Ocean. *Nature* **339**, 685–687.

Provenzano, A.J., McConaugh, J.R., Philips, K.B., Johnson, D.F., and Clark, J. (1983) Vertical distribution of first stage larvae of the blue crab *Callinectes sapidus* at the mouth of Chesapeake Bay. *Estuar. Coast. Shelf Sci.* **16**, 489–499.

Purcell, E.M. (1977) Life at low Reynolds number. *Am. J. Physics* **45**, 3–11.

Purcell, E.M. (1978) The effect of fluid motions on the absorption of molecules by suspended particles. *J. Fluid Mech.* **84**, 551–559.

Rabalais, N.N., Turner, R.E., Justic, D., Dortch, Q., Wiseman, W.J., and Sen Gupta, B.K. (1996) Nutrient changes in the Mississippi River and system responses on the adjacent continental shelf. *Estuaries* **19**, 386–407.

Rasmusson, E.M. and Carpenter, T.H. (1982) Variations in tropical sea surface temperature and surface wind fields associated with the southern oscillation/El Niño. *Monthly Weather Rev.* **110**, 354–384.

Rasmusson, E.M. and Wallace, J.M. (1983) Meteorological aspects of the El Niño/southern oscillation. *Science* **222**, 1195–1202.

Rattray, M. and Hansen, D.V. (1962) A similarity solution for circulation in an estuary. *J. Mar. Res.* **20**, 121–133.

Reid, P.C., Planque, B., and Edwards, M. (1998) Is observed variability in the long-term result of the Continuous Plankton Recorder Survey a response to climate change? *Fish. Oceanogr.* **7**, 282–288.

Reid, P.C., Borges, M.de F., and Svendsen, E. (2001) A regime shift in the North Sea circa 1988 linked to changes in the North Sea horse mackerel fishery. *Fisheries Res.* **50**, 163–171.

Rendell, A.R., Horrobin T.M., Jickells, T.D., Edmunds, H.M., Brown, J., and Malcolm, S.J. (1997) Nutrient cycling in the Great Ouse Estuary and its impact on nutrient fluxes to the Wash, England. *Estuar. Coast. Shelf Sci.* **45**, 653–668.

Revelante, N. and Gilmartin, M. (1976) The effects of Po River discharge on phytoplankton dynamics in the northern Adriatic Sea. *Mar. Biol.* **34**, 259–271.

Rhines, P. (1986) Vorticity dynamics of the oceanic general circulation. *Ann. Rev. Fluid Mech.* **18**, 433–497.

Richards, F.A. (ed.) (1981) *Coastal Upwelling*. American Geophysical Union. Washington, DC. 529 pp.

Richardson, P.L. (1983) Gulf Stream rings. In *Eddies in Marine Science* (ed. A.R. Robinson), pp. 19–45. Springer-Verlag, New York.

Richardson, P.L., Cheney, R.E., and Worthington, L.V. (1978) A census of Gulf Stream rings, spring 1985. *J. Geophys. Res.* **83**, 6136–6145.

Richman, J.G., de Szoeke, R.A., and Davis, R.E. (1987) Measurements of near-surface shear in the ocean. *J. Geophys. Res.* **92** (C3), 2851–2858.

Ridgwell, A.J. and Watson, A.J. (2002) Feedback between aeolian dust, climate and atmospheric CO_2 in glacial times. *Paleoceanography* **17**, 4, 1059; doi: 10.1029/2001PA000729.

Riebesell, V. (1991) Particle aggregation during a diatom bloom. I: Physical aspects. *Mar. Ecol. Prog. Ser.* **69**, 273–280.

Riebesell, V. (1992) The formation of large marine snow and its sustained residence in surface waters. *Limnol. Oceanogr.* **37**, 63–76.

Riisgård, H.A., Poulsen, L., and Larsen, P.S. (1996) Phytoplankton reduction in near-bottom water caused by filter-feeding *Nereis diversicolor* – implications for worm growth and population grazing impact. *Mar. Ecol. Prog. Ser.* **141**, 47–54.

Riley, G.A. (1937) The significance of the Mississippi River drainage for biological conditions in the northern Gulf of Mexico. *J. Mar. Res.* **1**, 60–74.

Riley, G.A. (1941) Plankton studies. IV: Georges Bank. *Bull. Bingham Oceanogr. Coll.* **7**, 1–73.

Riley, G.A. (1942) The relationship of vertical turbulence and spring diatom flowering. *J. Mar. Res.* **5**, 67–87.

Riley, G.A. (1970) Particulate organic matter in sea water. *Adv. Mar. Biol.* **8**, 1–118.

Riley, G.A., Stommel, H., and Bumpus, D.F. (1949) Quantitative ecology of the plankton of the western North Atlantic. *Bull. Bingham Oceanogr. Coll.* **12**, 1–169.

The Ring Group (1981) Gulf Stream cold-core rings: their physics, chemistry and biology. *Science* **212**, 1091–1100.

Rissik, D. and Suthers, I.M. (1996). Feeding in a larval assemblage: the nutritional significance of an estuarine plume front. *Mar. Biol.* **125**, 233–240.

Ritzrau, W. (1996) Microbial activity in the benthic boundary layer: small-scale distribution and its relationship to the hydrodynamic regime. *J. Sea Res.* **36**, 171–180.

Roberts, J. (1975) *Internal Gravity Waves in the Ocean.* Marcel Dekker, New York.

Robinson, A.R. (1983) Overview and summary of eddy science. In *Eddies in Marine Science* (ed. A.R. Robinson), pp. 3–15. Springer-Verlag, New York.

Rodriguez, J. and 9 other authors (2001) Mesoscale vertical motion and the size structure of phytoplankton in the ocean. *Nature* **410**, 360–363.

Roemmich, D. and McGowan, J. (1995) Climatic warming and the decline of zooplankton in the California current. *Science* **267**, 1324–1326.

Roman, M.R. and Boicourt, W.C. (1999) Dispersion and recruitment of crab larvae in the Chesapeake Bay plume: physical and biological controls. *Estuaries* **22**, 563–574.

Roman, M.R., Gauzens, A.L., and Cowles, T.J. (1985) Temporal and spatial changes in epipelagic microplankton and mesoplankton biomass in warm-core Gulf Stream Ring 82-B. *Deep-Sea Res.* **32A**, 1007–1022.

Roman, M.R., Adolf, H.A., Landry, M.R., Madin, L.P., Steinberg, D.K., and Zhang, X. (2002) Estimates of oceanic mesozooplankton production: a comparison using the Bermuda and Hawaii time-series data. *Deep-Sea Res. II* **49**, 175–192.

Rossby, C.G., Willett, H.C., Holmboe, J., Namias, J., Page, L., and Allen, R. (1939) Relation between variations in the intensity of the zonal circulation of the atmosphere and the displacements of the semi-permanent centers of action. *J. Mar. Res.* **2**, 38–54.

Rothschild, B.J. (1988) Biodynamics of the sea: the ecology of high dimensionality systems. In *Towards a Theory on Biological–Physical Interactions in the World Ocean* (ed. B.J. Rothschild), pp. 527–548. Kluwer, Dordrecht.

Rothschild, B.J. and Osborn, T.R. (1988) Small-scale turbulence and plankton contact rates. *J. Plankton Res.* **10**, 465–474.

Rowe, G.T., Clifford, C.H., and Smith, K.L. Jr. (1977) Nitrogen regeneration in sediments off Cap Blanc, Spanish Sahara. *Deep-Sea Res.* **24**, 57–63.

Rowe, P.M. and Epifanio, C.E. (1994) Flux and transport of larval weakfish in Delaware Bay, USA. *Mar. Ecol. Prog. Ser.* **110**, 115–120.

Rowell, T.W. and Trites, R.W. (1985) Distribution of larval and juvenile *Illex* (Mollusca: Cephalopoda) in the Blake Plateau region (Northwest Atlantic). *Vie Milieu Ser. C* **35**, 149–161.

Royce, W.F., Smith, L.S., and Hartt, A.C. (1968) Models of oceanic migrations of Pacific salmon and comments on guidance mechanisms. *Fish. Bull.* **66**, 441–462.

Rozengurt, M.A. and Haydock, I. (1991) Effects of freshwater development and water pollution policies on the world's river–delta–estuary–coastal zone ecosystems. In *Coastal Wetlands* (ed. H.S. Bolton), pp. 85–99. American Society of Civil Engineers, New York.

Rozengurt, M.A., Josselyn, M., and Hertz, M. (1985) The impact of water diversions on the river–delta–estuary–sea ecosystems of San Francisco Bay and the Sea of Azov. In *San Francisco Bay: Issues, Resources, Status and Management* (ed. D.M. Goodrich), pp. 35–62. *NOAA Estuary-of-the-month Seminar Series* **6**. US Dept. Commerce, NOAA Estuarine Programs Office, Washington, DC.

Rudnick, D.L. and Davis, R.E. (2003) Red noise and regime shifts. *Deep-Sea Res. I* **50**, 691–699.

Rudnick, D.L. and Ferrari, R. (1999) Compensation of horizontal temperature and salinity gradients in the ocean mixed layer. *Science* **283**, 526–529.

Rudnick, D.L. and Martin, J.P. (2002) On the horizontal density ratio in the upper ocean. *Dynamics Atm. Oceans* **36**, 3–21.

Ruiz, J. and Izquierdo, A. (1997) A simple model for the break-up of marine aggregates by turbulent shear. *Acta* **20**, 597–605.

Russell, F.S. (1973) A summary of the observations of the occurrence of planktonic stages of fish off Plymouth 1924–72. *J. Mar. Biol. Ass. UK* **53**, 347–355.

Ryan, J.P., Yoder, J.A., and Cornillon, P.C. (1999a) Enhanced chlorophyll at the shelf-break of the Mid-Atlantic Bight and Georges Bank during the spring transition. *Limnol. Oceanogr.* **44**, 1–11.

Ryan, J.P., Yoder, J.A., Barth, J.A., and Cornillon, P.C. (1999b) Chlorophyll enhancement and mixing associated with meanders of the shelf-break front in the Mid-Atlantic Bight. *J. Geophys. Res.* **104C**, 23479–23493.

Ryan, J.P., Yoder, J.A., and Townsend, D.W. (2001) Influence of Gulf Stream warm-core ring on water mass and chlorophyll distributions along the southern flank of Georges Bank. *Deep-Sea Res. II* **48**, 159–178.

Ryther, J.H. (1967) Occurrence of red water off Peru. *Nature* **214**, 1318–1319.

Ryther, J.H. (1969) Photosynthesis and fish production in the sea. *Science* **166**, 72–80.

Saiz, E. and Alcaraz, M. (1991) Effects of small-scale turbulence on development time and growth of *Acartia grani* (Copepoda: Calanoida). *J. Plankton Res.* **13**, 873–883.

Saiz, E. and Alcaraz, M. (1992) Free-swimming behaviour of *Acartia clausi* under turbulent water movement. *Mar. Ecol. Prog. Ser.* **80**, 229–236.

Saiz, E. and Kiørboe, T. (1995) Predatory and suspension feeding in the copepod *Acartia tonsa* in turbulent environments. *Mar. Ecol. Prog. Ser*. **122**, 147–158.

Saiz, E., Alcaraz, M., and Paffenhofer, G.-A. (1992) Effect of small-scale turbulence on feeding rate and gross growth efficiency of three Acartia species. *J. Plankton Res.* **14**, 1085–1097.

Sakshaug, E. and Slagstad, D. (1992) Sea ice and wind: effects on primary productivity in the Barents Sea. *Atmosphere–Ocean* **30**, 579–591.

Sakurai, Y., Kiyofuji, H., Saitoh, S., Goto, T., and Hiyama, Y. (2000) Changes in the inferred spawning area of *Todarodes pacificus* due to changing environmental conditions. *ICES J. Mar. Sci*. **57**, 24–30.

Sala, E., Boudouresque, C.F., and Harmelin-Vivien, M. (1998) Fishing, trophic cascades, and the structure of algal assemblages: evaluation of an old but untested paradigm. *Oikos* **82**, 425–439.

Sambrotto, R.N. and 9 other authors (1993) Elevated consumption of carbon relative to nitrogen in the surface ocean. *Nature* **363**, 248–250.

Sander, F. (1981) A preliminary assessment of the main causative mechanisms of the "Island Mass" effect of Barbados. *Mar. Biol.* **64**, 199–205.

Sandstrom, H. and Elliott, J.A. (1984) Internal tides and solitons on the Scotian Shelf: a nutrient pump at work. *J. Geophys. Res.* **89**, 6415–6426.

Sanford, E., Bermudez, D., Bertness, M.D., and Gaines, S.D. (1994) Flow, food supply, and acorn barnacle population dynamics. *Mar. Ecol. Prog. Ser*. **104**, 49–62.

Santos, A.M.P. and Peliz, Á. (2003) Dynamics of marine ecosystems off the Western Iberian Peninsula: local contributions to Globec. *Global Change Newsletter* **54**, 15–17.

Santos, A.M.P., Borges, M.de F., and Groom, S. (2001) Sardine and horse mackerel recruitment and upwelling off Portugal. *ICES J. Mar. Sci.* **58**, 589–596.

Santos, A.M.P., Peliz, Á, Dubert, J., Oliviera, P.B., Angėlico, M.M., and Ré, P. (2004) Impact of a winter upwelling event on the distribution and transport of sardine eggs and larvae off western Iberia: a retention mechanism. *Cont. Shelf Res.* **24**, 149–165.

Sanvicente-Anorve, L., Lepretre, A., and Davoult, D. (1996) Large-scale spatial pattern of the macrobenthic diversity in the eastern English Channel. *J. Mar. Biol. Assoc. UK* **71**, 153–160.

Sarmiento, J.L. and Gruber, N. (2002) Sinks for Anthropogenic Carbon. *Physics Today*, August 2002, 30–36. [www.physicstoday.org]

Sarnthein, M., Winn, K., Duplessy, J.-C., and Fontugne, M.R. (1988) Global variations of surface ocean productivity in low and mid-latitudes: influence on CO_2 reservoirs of the deep ocean and the atmosphere during the last 21,000 years. *Paleoceanography* **3**, 361–399.

Sathyendranath, S, Longhurst, A., Caverhill, C.M., and Platt, T. (1995) Regionally and seasonally differentiated primary production in the North Atlantic. *Deep-Sea Res. I* **42**, 1773–1802.

Saunders, P.M. (1982) Circulation in the eastern North Atlantic. *J. Mar. Res.* **40** (suppl.), 641–657.

Savidge, G. (1981) Studies of the effects of small-scale turbulence on phytoplankton. *J. Mar. Biol. Ass. UK* **61**, 477–488.

Scheibling, R.E. and Hennigar, A.W. (1997) Recurrent outbreaks of disease in sea urchins *Strongylocentrotus droebachiensis* in Nova Scotia: Evidence for a link with large-scale meteorologic and oceanographic events. *Mar. Ecol. Prog. Ser.* **152**, 155–165.

Scheltema, R.S. (1966) Evidence for transatlantic transport of gastropod larvae belonging to the genus *Cymatium*. *Deep-Sea Res.* **13**, 83–95.

Schlitzer, R. (2000) Electronic Atlas of WOCE hydrographic and tracer data now available. *Eos* (*Trans. Am. Geophys. Union*) **81**(5), 45.

Schmidt, J. (1922) The breeding places of the eel. *Phil. Trans. Roy. Soc. B* **211**, 178–208.

Schneider, D.C. (1990) Seabirds and fronts: a brief overview. *Polar. Res.* **8**, 17–23.

Schneider, N., Miller, A.J., and Pierce, D. (2002) Anatomy of North Pacific Decadal Variability. *J. Climate* **15**, 586–605

Schwartz, S.E. (1988) Are global cloud albedo and climate controlled by marine phytoplankton? *Nature* **336**, 441–445.

Schwartzlose, R.A. and 13 other authors (1999) Worldwide large-scale fluctuations of sardine and anchovy populations. *S. Afr. J. Mar. Sci.* **21**, 289–347.

Schwing, F.B. and Mendelssohn, R. (1997) Increased coastal upwelling in the California Current. *J. Geophys. Res.* **102**, 3421–3438.

Serra, R., Cury, P., and Roy, C. (1998) The recruitment of the Chilean sardine (*Sardinops sagax*) and the "optimal environmental window". In *Global Versus Local Changes in Upwelling Systems*, pp. 267–274. Colloq. Semin. Inst. Fr. Rech. Sci. Dev. Coop. ORSTOM. Editions de l'ORSTOM. Paris.

Shanks, A.L. (1983) Surface slicks associated with tidally forced internal waves may transport pelagic larvae of benthic invertebrates and fishes shoreward. *Mar. Ecol. Prog. Ser.* **13**, 311–315.

Shanks, A.L. and Trent, J.D. (1979) Marine snow: microscale nutrient patches. *Limnol. Oceanogr.* **24**, 850–854.

Shanks, A.L. and Wright, W.G. (1987) Internal-wave-mediated shoreward transport of cyprids, megalopae, and gammarids and correlated longshore differences in the settling rate of intertidal barnacles. *J. Exp. Mar. Biol. Ecol.* **114**, 1–13.

Shea, R.E. and Broenkow, W.W. (1982) The role of internal tides in the nutrient enrichment of Monterey Bay, California. *Estuar. Coast. Shelf Sci.* **15**, 57–66.

Sheldon, R.A., Prakash, A., and Sutcliffe, W. (1972) The size distribution of particles in the ocean. *Limnol. Oceanogr.* **17**, 327–340.

Shelton, P.A. and Hutchings, L. (1982) Transport of anchovy, *Engraulis capensis* Gilchrist, eggs and early larvae by a frontal jet current. *J. Cons. Int. Explor. Mer.* **40**, 185–198.

Shen, J., Boon, J.D., and Kuo, A.Y. (1999) A modeling study of a tidal intrusion front and its impact on larval dispersion in the James River Estuary, Virginia. *Estuaries* **22**, 681–692.

Shulenberger, E. and Reid, J.L. (1981) The Pacific shallow oxygen maximum, deep chlorophyll maximum and primary productivity reconsidered. *Deep-Sea Res.* **28A**, 901–919.

Shushkina, E.A. (1985) Production of principal ecological groups of plankton in the epipelagic zone of the ocean. *Oceanology* **25**, 653–658.

Siegel, H., Gerth, M., and Muztke, A. (1999) Dynamics of the Oder river plume in the southern Baltic Sea: satellite data and numerical modeling. *Cont. Shelf Res*. **19**, 1143–1159.

Silver, M.W. and Alldredge, A.L. (1981) Bathypelagic marine snow: deep-sea algal and detrital community. *J. Mar. Res.* **39**, 501–530.

Silver, M.W., Shanks, A.L., and Trent, J.D.F. (1978) Marine snow: microplankton habitat and source of small-scale patchiness in pelagic populations. *Science* **201**, 371–373.

Simpson, J.H. (1971) Density stratification and microstructure in the western Irish Sea. *Deep-Sea Res.* **18**, 309–319.

Simpson, J.H. (1981) The shelf-sea fronts: implications of their existence and behaviour. *Phil. Trans. R. Soc. Lond. A* **302**, 531–546.

Simpson, J.H. and Bowers, D. (1981) Models of stratification and frontal movement in shelf seas. *Deep-Sea Res.* **28A**, 727–738.

Simpson, J.H. and Hunter, J.R. (1974) Fronts in the Irish Sea. *Nature* **250**, 404–406.

Simpson, J.H. and Pingree, R.D. (1978) Shallow sea fronts produced by tidal stirring. In *Oceanic Fronts and Coastal Processes* (ed. M.J. Bowman and W.E. Esaias), pp. 29–42. Springer-Verlag, New York.

Simpson, J.H. and Tett, P.B. (1986) Island stirring effects on phytoplankton growth. In *Tidal Mixing and Plankton Dynamics* (ed. M.J. Bowman, C.M. Yentsch, and W.T. Peterson), pp. 41–76. Springer-Verlag, New York.

Sinclair, M., Tremblay, M.J., and Bernal, P. (1985) El Niño events and variability in a Pacific Mackerel (*Scomber japonicus*) survival index: support for Hjort's second hypothesis. *Can. J. Fish. Aquat. Sci.* **42**, 602–608.

Sinclair, M., Bugden, G.L., Tang, C.L., Therriault, J.-C., and Yeats, P.A. (1986) Assessment of effects of freshwater runoff variability on fisheries production in coastal waters. In *The Role of Freshwater Outflow in Coastal Marine Ecosystems* (ed. S. Skreslet), pp. 139–160. Springer-Verlag, Berlin.

Sissenwine, M.P., Cohen, E.B., and Grosslein, M.D. (1984) Structure of the Georges Bank ecosystem. *Rapp. P.-v. Réun. Cons. Int. Explor. Mer*. **183**, 243–254.

Sjøtun, K., Fredriksen, S., and Rueness, J. (1998). Effect of canopy biomass and wave exposure on growth in *Laminaria hypoborea. Eur. J. Phycol.* **33**, 337–343.

Skov, H. and Durinck, J. (1998) Constancy of frontal aggregations of seabirds at the shelf break in the Skagerrak. *J. Sea Res.* **39**, 305–311.

Skreslet, S. (1986) *The Role of Freshwater Outflow in Coastal Marine Ecosystems*. Springer-Verlag, Berlin. 453 pp.

Smayda, T.J. (1970) The suspension and sinking of phytoplankton in the sea. *Oceanogr. Mar. Biol. Ann. Rev.* **8**, 353–414.

Smith, P.C. (1989) Circulation and dispersal on Brown's Bank. *Can. J. Fish. Aquat. Sci.* **46**, 539–559.

Smith, P.E. and Eppley, R.W. (1982) Primary production and the anchovy population in the southern California bight: comparison of time series. *Limnol. Oceanogr.* **27**, 1–17.

Smith, P.E. and Lasker, R. (1978) Position of larval fish in an ecosystem. *Rapp. P.-v. Réun. Cons. Int. Explor. Mer*. **173**, 77–84.

Smith, W.O. and Demaster, D.J. (1996) Phytoplankton biomass and productivity in the Amazon River plume: correlation with seasonal river discharge. *Cont. Shelf Res*. **16**, 292–319.

Sommer, U. (1988) Some size relationships in phytoplankton motility. *Hydrobiologia* **161**, 125–131.

Sorokin, Y.I., Sukhanova, I.N., Konolova, G.V., and Pavelyeva, E.B. (1975) Primary production and phytoplankton in the area of equatorial divergence in the equatorial *Pacific. Trans. Inst. Oceanol*. **102**, 108–122.

Soutar, A. and Isaacs, J.D. (1969) History of fish populations inferred from fish scales in anaerobic sediments off California. *Calif. Coop. Ocean. Fish. Invest. Rep*. **13**, 63–70.

Southward, A.J., Boalch, G.T., and Maddock, L. (1988) Fluctuations in the herring and pilchard fisheries of Devon and Cornwall linked to changes in climate since the 16th century. *J. Mar. Biol. Ass. UK* **68**, 423–445.

Stacey, M.W., Pond, S., and LeBlond, P.H. (1986) A wind-forced Ekman spiral as a good statistical fit to low frequency currents in a coastal strait. *Science* **233**, 470–472.

Steele, J.H. (1981) Some varieties of biological oceanography. In *Evolution of Physical Oceanography* (ed. B.A. Warren and C. Wunsch), pp. 376–383. MIT Press, Cambridge, MA.

Steele, J.H. (1988) Scale selection for biodynamic theories. In *Towards a Theory on Biological–Physical Interactions in the World Ocean* (ed. B.J. Rothschild), pp. 513–526. Kluwer, Dordrecht.

Steele, J.H. (1998) From carbon flux to regime shift. *Fish. Oceanogr.* **7**, 176–181.

Steele, J.H. and Yentsch, C.S. (1960) The vertical distribution of chlorophyll. *J. Mar. Biol. Ass. UK* **39**, 217–226.

Stephens, B.B. and Keeling, R.F. (2000) The influences of Antarctic sea ice on glacial–interglacial CO_2 variations. *Nature* **404**, 171–174.

Stevens, D.E., Kohlhorst, D.W., Miller, L.W., and Kelly, D.W. (1985) The decline of striped bass in the Sacramento–San Joaquin Estuary, California. *Trans. Am. Fish Soc*. **114**, 12–30.

St John, M.A. and Pond, S. (1992) Tidal plume generation around a promontory: effects on nutrient concentrations and primary productivity. *Continental Shelf Res.* **12**, 339–354.

St John, M.A., Harrison, P.J., and Parsons, T.R. (1992a) Tidal wake mixing: localized effects on primary production and zooplankton distribution in the Strait of Georgia, British Columbia. *J. Exp. Mar. Biol. Ecol.* **164**, 261–274.

St John, M.A., MacDonald, J.S., Beamish, R.J., and Choromanski, E. (1992b) The Fraser River plume: some preliminary observations on the distribution of juvenile salmon, herring and their prey. *Fish. Oceanogr.* **1**, 153–162.

Stocker, T.F. and Schmittner, A. (1997) Influence of CO_2 emission rates on the stability of the thermohaline circulation. *Nature* **388**, 862–865.

Stommel, H. (1948) The westward intensification of wind-driven ocean currents. *Trans. Am. Geophys. Union* **29**, 202–206.

Stommel, H. (1965) *The Gulf Stream: a Physical Description*, 2nd edn. Cambridge University Press, Cambridge.

Stommel, H., Niiler, P., and Anati, D. (1978) Dynamic topography and recirculation of the North Atlantic. *J. Mar. Res.* **36**, 449–468.

Stramska, M. and Dickey, T.D. (1993) Phytoplankton blooms and the vertical structure of the upper ocean. *J. Mar. Res.* **51**, 819–842.

Strass, V. and Woods, J.D. (1988) Horizontal and seasonal variation of density and chlorophyll profiles between the Azores and Greenland. In *Towards a Theory on Biological–Physical Interactions in the World Ocean* (ed. B.J. Rothschild), pp. 113–136. Kluwer, Dordrecht.

Strickler, J.R. (1984) Sticky water: a selective force in copepod evolution. In *Trophic Interactions within Aquatic Ecosystems* (ed. D.G. Meyers and J.R. Strickler), pp. 187–242. American Association for the Advancement of Science. Washington, DC.

Strickler, J.R., Squires, K.D., Yamazaki, H., and Abib, A.H. (1997) Combining analogue turbulence with digital turbulence. *Sci. Mar.* **61** (Suppl. 1), 197–204.

Sundby, S. (1995) Wind climate and foraging of larval and juvenile Arcto-Norwegian cod. In *Climate Change and Northern Fish Populations* (ed. R.J. Beamish). *Can. Spec. Publ. Fish. Aquat. Sci.* **121**, 405–415.

Sundby, S. and Fossum, P. (1990) Feeding conditions of Arcto-Norwegian cod larvae compared with the Rothschild–Osborne theory on small-scale turbulence and plankton contact rates. *J. Plankton Res.* **12**, 1153–1162.

Sundby, S., Ellertsen, B., and Fossum, P. (1994) Wind effects on the vertical distribution of first-feeding cod larvae and their prey, and on the encounter rates between them. In *ICES Symposium on Cod and Climate Change* (ed. J. Jacobsson *et al.*), paper no. 26. ICES, Copenhagen.

Sundquist, E.T. (1993) The global carbon dioxide budget. *Science* **259**, 934–941.

Sutcliffe, W.H. (1973) Correlations between seasonal river discharge and local landings of the American lobster (*Homarus americanus*) and Atlantic halibut (*Hippoglossus hippoglossus*) in the Gulf of St. Lawrence. *J. Fish. Res. Bd. Can.* **30**, 856–859.

Sverdrup, H.U. (1953) On conditions for the vernal blooming of phytoplankton. *J. Cons. Perm. Int. Exp. Mer*. **18**, 287–295.

Sverdrup, H.U., Johnson, M.W., and Fleming, R.H. (1942) *The Oceans: Their Physics, Chemistry and General Biology*. Prentice-Hall, Englewood Cliffs, NJ. 1060 pp.

Swallow, J.C. (1976) Variable currents in mid-ocean. *Oceanus* **19**, 18–25.

Swallow, J.C. (1984) Some aspects of the physical oceanography of the Indian Ocean. *Deep-Sea Res.* **31A**, 639–650.

Swallow, J.C. and Hamon, B.V. (1960) Some measurements of deep-sea currents in the eastern North Atlantic. *Deep-Sea Res.* **6**, 155–168.

Sy, A. (1988) Investigation of large-scale circulation patterns in the central North Atlantic: the North Atlantic current, the Azores current and the Mediterranean water plume in the area of the mid-Atlantic ridge. *Deep-Sea Res.* **35A**, 383–413.

Takahashi, T.H.R. and 8 other authors (1999) Net sea-air CO_2 flux over the global oceans: an improved estimate based on the sea–air pCO_2 difference. In *Proceedings of the 2nd International Symposium on CO_2 in the Oceans*, pp. 9–15. Center for Global Environmental Research, National Institute for Environmental Studies. Tsukuba, Japan.

Tans, P.P. (ed.) (2001) *CMDL Summary Report 26*. Climate Monitoring and Diagnostics Laboratory, Boulder, CO. [www.cmdl.noaa.gov/publications/annrpt26]

Taylor, A.H. (1995) North–south shifts of the Gulf Stream and their climatic connection with the abundance of zooplankton in the UK and its surrounding seas. *ICES J. Mar. Sci.* **52**, 711–721.

Taylor, A.H., Jordan, M.B., and Stephens, A. (1998) Gulf Stream shifts following ENSO events. *Nature* **393**, 638.

Tee, K.T., Smith, P.C., and LeFaivre, D. (1993) Topographic upwelling off Southwest Nova Scotia. *J. Phys. Oceanogr.* **23**, 1703–1726.

Tegner, M.J. and Dayton, P.K. (1991) Sea urchins, El Niños, and the long-term stability of Southern California kelp forest communities. *Mar. Ecol. Prog. Ser.* **77**, 49–63.

Tenore, K.R. and 9 other authors (1982) Coastal upwelling in the Rias Bajas, N.W. Spain, contrasting the benthic regimes of the Rias de Arosa and de Duras. *J. Mar. Res.* **40**, 701–772.

Tett, P. (1981) Modelling phytoplankton production at shelf-sea fronts. *Phil. Trans. Roy. Soc. Lond. A* **302**, 605–615.

Thomas, W.H. and Gibson, C.H. (1990) Quantified small-scale turbulence inhibits a red-tide dinoflagellate, *Gonyaulax polyedra* Stein. *Deep-Sea Res.* **37A**, 1583–1593.

Thomas, W.H. and Gibson, C.H. (1992) Effects of small-scale turbulence on the dinoflagellate *Gymnodinium sanguineum* (*splendens*): contrasts with *Gonyaulax* (*Lingulodinium*) *polyedra*, and the fishery implication. *Deep-Sea Res.* **39A**, 1429–1437.

Thomas, W.H., Vernet, M., and Gibson, C.H. (1995) Effects of small-scale turbulence on photosynthesis, pigmentation, cell division and cell size in the marine dinoflagellate *Gonyaulax polyedra. J. Phycol.* **31**, 50–59.

Thompson, D.W.J. and Wallace, J.M. (1998) The Arctic Oscillation signature in the wintertime geopotential height and temperature fields, *Geophys. Res. Lett.* **25**, 1297–1300.

Thompson, D.W.J., Lee, S., and Baldwin, M.P. (2003) Atmospheric processes governing the Northern Hemisphere Annular Mode/North Atlantic Oscillation. In *The North Atlantic Oscillation: Climatic Significance and Environmental Impact* (ed. J.W. Hurrell, Y. Kushnir, G. Ottersen, and M. Visbeck). Geophysical Monograph 134. American Geophysical Union, Washington, DC.

Thompson, J.D. (1978) Role of mixing in the dynamics of upwelling systems. In *Upwelling Ecosystems* (ed. R. Boje and M. Tomczak), pp. 203–222. Springer-Verlag, Berlin.

Thordardottir, T. (1986) Timing and duration of spring blooming south and southwest of Iceland. In *The Role of Freshwater Outflow in Coastal Marine Ecosystems* (ed. S. Skreslet), pp. 345–360. Springer-Verlag, Berlin.

Tolmazin, D. (1985) Changing coastal oceanography of the Black Sea. 1: Northwest shelf. *Prog. Oceanogr.* **15**, 217–276.

Traganza, E.D., Conrad, J.C., and Breaker, L.C. (1981) Satellite observations of a cyclonic upwelling system and a giant plume in the California current. In *Coastal Upwelling* (ed. F.A. Richards), pp. 228–241. American Geophysical Union, Washington, DC.

Traganza, E.D., Silva, V.M., Austin, D.M., Hanson, W.L., and Bronsink, S.H. (1983) Nutrient mapping and recurrence of coastal upwelling centers by satellite remote sensing: its implication to primary production and the sediment record. In *Coastal Upwelling: its Sediment Record* (ed. E. Suess and J. Thiede), part A, pp. 61–83. Plenum Press, New York.

Traganza, E.D., Redalje, D.G., and Garwood, R.W. (1987) Chemical flux, mixed layer entrainment and phytoplankton blooms at upwelling fronts in the California coastal zone. *Cont. Shelf Res.* **7**, 89–105.

Trager, G.C., Hwang, J.S., and Strickler, J.R. (1990) Barnacle suspension feeding in variable flow. *Mar. Biol.* **105**, 117–127.

Tranter, D.J., Carpenter, D.J., and Leech, G.S. (1986) The coastal enrichment effect of the east Australian current eddy field. *Deep-Sea Res.* **33A**, 1705–1728.

Tremblay, M.J. and Sinclair, M. (1992) Planktonic sea scallop larvae (*Placopecten magellanicus*) in the Georges Bank region: broadscale distribution in relation to physical oceanography. *Can. J. Fish. Aquat. Sci.* **49**, 1597–1615.

Trites, R.W. (1983) Physical oceanographic features and processes relevant to *Illex illecebrosus* spawning in the western North Atlantic and subsequent larval distribution. *NAFO Sci. Coun. Studies* **6**, 39–55.

Trull, T., Rintoul, S.R., Hadfield, M., and Abraham, E.R. (2001) Circulation and seasonal evolution of polar waters south of Australia: implications for iron fertilization of the Southern Ocean. *Deep-Sea Res. II.* **48**, 2439–2466.

Trumble, R.J., Mathisen, O.A., and Stuart, D.W. (1981) Seasonal food production and consumption by nekton in the northwest African upwelling system. In *Coastal Upwelling* (ed. F.A. Richards), pp. 458–463. Am. Geophys. Union, Washington, DC.

Tsuda, A. and 25 other authors (2003) A mesoscale iron enrichment experiment in the western subarctic Pacific induces a large scale centric diatom bloom. *Science* **300**, 958–961.

Tsujita, T. (1957) The fisheries oceanography of the east China Sea and Tsuchima Strait. 1: The structure and ecological character of the fishing grounds. *Bull. Seikai Reg. Fish. Lab.* **13**, 1–47.

Tsukamoto, K. (1992) Discovery of the spawning area for the Japanese eel. *Nature* **356**, 789–791.
Tunberg, B.G. and Nelson, W.G. (1998) Do climatic oscillations influence cyclical patterns of soft-bottom macrobenthic communities on the Swedish west coast? *Mar. Ecol. Prog. Ser.* **170**, 85–94.
Turner, J.S. (1973) *Buoyancy Effects in Fluids*. Cambridge University Press, Cambridge.
Tyler, M.A. and Seliger, H.H. (1978) Annual subsurface transport of a red tide dinoflagellate to its bloom area: water circulation patterns and organism distributions in the Chesapeake Bay. *Limnol. Oceanogr.* **23**, 227–246.
Tyler, M.A. and Seliger, H.H. (1981) Selection for a red tide organism: physiological responses to the physical environment. *Limnol. Oceanogr.* **26**, 310–324.
Utter, B.D. and Denny, M.W. (1996) Wave-induced forces on the giant kelp *Macrocystis pyrifera* (Agardh.): field test of a computational model. *J. Exp. Biol.* **199**, 2645–2654.
Uye, S.-I., Yamaoka, T., and Fujisawa, T. (1992) Are tidal fronts good recruitment areas for herbivorous copepods? *Fish. Oceanogr.* **1**, 216–232.
Uz, B.M., Yoder, J.A., and Osynchny, V. (2001) Pumping of nutrients to ocean surface waters by the action of propagating planetary waves. *Nature* **409**, 587–600.
Valdivia, J.E. (1978) The anchoveta and El Niño. *Rapp. P.-v. Réun. Cons. Int. Explor. Mer.* **173**, 196–202.
Valentine, P.C. and Lough, R.G. (1991) The sea-floor environment and the fishery of eastern Georges Bank. Open File Report 91-439. US Geol. Survey, NMFS Woods Hole, MA. 25 pp.
Valenzuela, G.S. and Vargas, C.A. (2002) Comparative larval growth rate of *Sprattus sprattus* in relation to physical and biological oceanographic features in the North Sea. *Arch. Fish. Mar. Res.* **49**, 213–230.
van der Lingen, C.D., Hutchings, L., Merckle, D., van der Westhuizen, J.J., and Nelson, J. (2001) Comparative spawning habits of anchovy (*Engraulis capensis*) and sardine (*Sardinops sagax*) in the southern Benguela upwelling ecosystem. In *Spatial Processes and Management of Marine Populations* (ed. G.H. Kruse *et al.*), pp. 185–209. University of Alaska Sea Grant, AK-SG-01-02.
van der Maarel, M.J.E.C., Sprenger, W., Haanstra, R.J., Forney, L.J. (1999) Detection of methanogenic archaea in seawater particles and the digestive tract of a marine fish species. *FEMS Microbiol. Lett.* **173**, 189–194.
Vandevelde, T., Legendre, L., Theriault, J.-C., Demers, S., and Bah, A. (1987) Surface chlorophyll maximum and hydrodynamics of the water column. *J. Mar. Res.* **4–5**, 377–396.
van Loon, H. and Rogers, J.C. (1978) The seesaw in winter temperatures between Greenland and northern Europe. Part I. General description. *Monthly Weather Rev.* **106**, 296–310.
Vedel, A. (1998) Phytoplankton depletion in the benthic boundary layer caused by suspension-feeding *Nereis diversicolor* (Polychaeta): grazing impact and the effect of temperature. *Mar. Ecol. Prog. Ser.* **163**, 125–132.
Vincent, A. and Kurc, G. (1969) Hydrologie: variations saisonnierres de la situation thermique du Golfe de Gascogne en 1967. *Rev. Trav. Inst. Peches Maritimes* **33**, 203–212.
Vinogradov, M.E. (1981) Ecosystems of equatorial upwellings. In *Analysis of Marine Ecosystems* (ed. A.R. Longhurst), pp. 69–93. Academic Press, New York.
Vogel, S. (1996) *Life in Moving Fluids: the Physical Biology of Flow*. 2nd edn. Princeton University Press, Princeton, NJ. 467 pp.
Waku, M. and Furuya, K. (1998) Primary production and community respiration in a warm streamer associated with the Kuroshio warm core ring in spring. *J. Oceanogr.* **54**, 565–572.

Waldron, H.N. and Probyn, T.A. (1992) Nitrate supply and potential new production in the Benguela system. *S. Afr. J. Mar. Sci.* **12**, 29–39.

Wallace, J.M., Rasmusson, E.M., Mitchell, T.P., Kousky, V.E., Sarachik, E.S., and von Storch, H. (1998) On the structure and evolution of ENSO-related climate variability in the tropical Pacific: lessons from TOGA. *J. Geophys. Res.* **103** (C7), 14241–14259.

Walsh, J.J. (1983) Death in the sea: enigmatic phytoplankton losses. *Prog. Oceanogr.* **12**, 1–86.

Walsh, J.J. and 6 other authors (1980) The spawning habitat of the Peruvian anchovy, *Engraulis ringens. Deep-Sea Res.* **27A**, 1–27.

Walsh, J.J., Rowe, G.T., Iverson, R.L., and McRoy, C.P. (1981) Biological export of shelf carbon is a sink of the global CO_2 cycle. *Nature* **291**, 196–201.

Ware, D.M. and Thomson, R.E. (1991) Link between long-term variability in upwelling and fish production in the northeast Pacific Ocean. *Can. J. Fish. Aquat. Sci.* **48**, 2296–2306.

Warren, B. (1983) Why is no deep water formed in the North Pacific? *J. Mar. Res.* **41**, 327–347.

Watson, A.J., Bakker, D.C.E., Ridgwell, A.J., Boyd, P.W., and Law, C.S. (2000) Effect of iron supply on Southern Ocean CO_2 uptake and implications for glacial atmospheric CO_2. *Nature* **407**, 730–733.

Watts, L.J., Sathyendranath, S., Caverhill, C., Maass, H., Platt, T., and Owens, N.J.P. (1999) Modelling new production in the northwest Indian Ocean region. *Mar. Ecol. Prog. Ser.* **183**, 1–12.

Webb, K.L. and D'Elia, C.F. (1980) Nutrient and oxygen redistribution during a spring neap tidal cycle in a temperate estuary. *Science* **207**, 983–985.

Weinstein, M.P., Weiss, S.L., Hodson, R.G., and Gerry, L.R. (1980) Retention of three taxa of postlarval fishes in an intensely flushed tidal estuary, Cape Fear River, North Carolina. *Fish. Bull.* **78**, 419–435.

Weiss, G.M., Harding, L.W. Jr., Itsweire, E.C., and Campbell, J.W. (1997) Characterizing lateral variability of phytoplankton chlorophyll in Chesapeake Bay, with aircraft ocean color data. *Mar. Ecol. Prog. Ser.* **149**, 183–199.

Welch, D.W., Chigrinsky, A.I., and Ishida, Y. (1995) Upper thermal limits on the oceanic distribution of Pacific salmon (*Oncorhynchus* spp.) in the spring. *Can. J. Fish. Aquat. Sci.* **52**, 489–503.

Wheeler, W.N. (1980) Effect of boundary layer transport on the fixation of carbon by the giant kelp *Macrocystis pyrifera. Mar. Biol.* **56**, 103–110.

White, F.M. (1988) *Heat and Mass Transfer.* Addison-Wesley, New York.

Wiggert, J.D. and 6 other authors (2000) The Northeast Monsoon's impact on mixing, phytoplankton biomass and nutrient cycling in the Arabian Sea. *Deep-Sea Res. II* **47**, 1353–1385.

Wildish, D.J. and Kristmanson, D.D. (1979) Tidal energy and sublittoral macrobenthic animals in estuaries. *J. Fish. Res. Bd. Can.* **36**, 1197–1206.

Wildish, D.J. and Kristmanson, D.D. (1984) Importance to mussels of the benthic boundary layer. *Can. J. Fish. Aquat. Sci.* **41**, 1618–1625.

Wilkinson, C. (ed.) (2002) *Status of Coral Reefs of the World*. AIMS, Townsville, Australia. 378 pp.

Williams, P.J.Le B. and Muir, L.R. (1981) Diffusion as a constraint on the biological importance of microzones in the sea. In *Ecohydrodynamics* (ed. J.C.J. Nihoul), pp. 209–218. Elsevier, Amsterdam.

Williams, R., Conway, D.V.P., and Hunt, H.G. (1994) The role of copepods in the planktonic ecosystems of mixed and stratified waters of the European shelf seas. *Hydrobiologia* **292**, 521–530.

Williams, R.G. and Follows, M.J. (1998) The Ekman transfer of nutrients and maintenance of new production over the North Atlantic. *Deep-Sea Res. I* **45**, 461–489.

Wing, S.R., Botsford, L.W., Largier, J.L., and Morgan, L.E. (1995) Spatial structure of relaxation events and crab settlement in the northern California upwelling system. *Mar. Ecol. Prog. Ser.* **128**, 199–211.

Wing, S.R., Largier J.L., and Botsford, L.W. (1998) Coastal retention and longshore meroplankton near capes in eastern boundary currents: examples from the California Current. In *Benguela Dynamics* (ed. S.C. Pillar, C.L. Moloney, A.I.L. Payne, and F.A. Shillington). *S. Afr. J. Mar. Sci* **19**, 119–127.

Witman, J.D., Leichter, J J., Genovese, S.J., and Brooks, D.A. (1993) Pulsed phytoplankton supply to the rocky subtidal zone: Influence of internal waves. *Proc. Natl. Acad. Sci. USA* **90**, 1686–1690.

Wolanski, E. and Delesalle, B. (1995) Upwelling by internal waves, Tahiti, French Polynesia. *Cont. Shelf Res.* **15**, 357–368.

Wolanski, E. and Hamner, W.M. (1988) Topographically controlled fronts in the ocean and their biological influence. *Science* **241**, 177–181.

Wolanski, E., Drew, E., Abel, K.M., and O'Brien, J. (1988) Tidal jets, nutrient upwelling and their influence on the productivity of the alga *Halimeda* in the Ribbon Reefs, Great Barrier Reef. *Estuar. Coast. Shelf Sci.* **26**, 169–201.

Wolf, K.U. and Woods, J.D. (1988) Lagrangian simulation of primary production in the physical environment the deep chlorophyll maximum and nutricline. In *Towards a Theory on Biological–Physical Interactions in the World Ocean* (ed. B.J. Rothschild), pp. 51–70. Kluwer, Dordrecht.

Wood, L. and Hargis, W.J. (1971) Transport of bivalve larvae in a tidal estuary. In *4th European Marine Biology Symposium* (ed. D.J. Crisp), pp. 21–44. Cambridge University Press, Cambridge.

Woods, J.D. (1977) Parameterization of unresolved motions. In *Modelling and Prediction of the Upper Layers of the Ocean* (ed. E.B. Kraus), pp. 118–140. Pergamon Press, New York.

Woods, J.D. (1988) Scale upwelling and primary production. In *Towards a Theory on Biological–Physical Interactions in the World Ocean* (ed. B.J. Rothschild), pp. 7–38. Kluwer, Dordrecht.

Woods, J.D. and Barkmann, W. (1986) The response of the upper ocean to solar heating. I: The mixed layer. *Quart. J.R. Met. Soc.* **112**, 1–27.

Woods, J. and Barkmann, W. (1993) Diatom demography in winter: simulated by the Lagrangian Ensemble method. *Fish. Oceanogr.* **2**, 202–222.

Woods, J.D. and Onken, R. (1982) Diurnal variation and primary production in the ocean: preliminary results of a Lagrangian ensemble model. *J. Plankton Res.* **4**, 735–756.

Wooldridge, T.H. and Callahan, R. (2000) The effects of a single freshwater release into the Kromme estuary. 3: Estuarine zooplankton response. *Water S.A.* **26**, 311–318.

Wooster, W.S., Bakun, A., and McLain, D.R. (1976) The seasonal upwelling cycle along the eastern boundary of the North Atlantic. *J. Mar. Res.* **34**, 131–141.

Worthington, L.V. (1976) *On the North Atlantic Circulation*. Johns Hopkins Oceanographic Studies **6**, Johns Hopkins University Press, Baltimore. 110 pp.

Wright, D.G., Hendry, R.M., Loder, J.W., and Dobson, F.W. (1986) Oceanic changes associated with global increase in atmospheric carbon dioxide: a preliminary report for the Atlantic coast of Canada. *Can. Tech. Rep. Fish. Aquat. Sci.* **1426**. 78 pp.

Wright, L.D., Friedrichs, C.T., and Hepworth, D.A. (1997a) Effects of benthic biology on bottom boundary layer processes, Dry Tortugas bank, Florida Keys. *Geo-Mar. Lett.* **17**, 291–298.

Wright, L.D., Schaffner, L.C., and Maa, J.P.-Y. (1997b) Biological mediation of bottom boundary layer processes and sediment suspension in the lower Chesapeake Bay. *Mar. Geol.* **141**, 27–50.

Wroblewski, J.S. (1982) Interaction of currents and vertical migration in maintaining *Calanus marshallae* in the Oregon upwelling zone: a simulation. *Deep-Sea Res.* **29A**, 665–686.

Wroblewski, J.S. and Cheney, J. (1984) Ichthyoplankton associated with a warm-core ring off the Scotian Shelf. *Can. J. Fish. Aquat. Sci.* **41**, 294–303.

Wunsch, C. (2002) What is the thermohaline circulation? *Science* **298**, 1179–1181.

Wyatt, T. and Jenkinson, I.R. (1993) The North Atlantic turbine: views of production processes from a mainly North Atlantic perspective. *Fish. Oceanogr.* **2**, 231–243.

Wyrtki, K. (1962) The upwelling in the region between Java and Australia during the south-east monsoon. *Aust. J. Mar. Freshwater Res.* **13**, 217–225.

Wyrtki, K. (1964) Upwelling in the Costa Rica dome. *Fish. Bull. US* **63**, 335–372.

Xie, L. and Hsieh, W.W. (1989) Predicting the return migration routes of the Fraser River sockeye salmon (*Oncorhynchus nerka*). *Can. J. Fish. Aquat. Sci.* **46**, 1287–1292.

Yamanaka, H. (1985) Effect of El Niño on fish migration and yield in the western Pacific Ocean. In *International Conference on the TOGA Scientific Programme*, pp. VI-16 to VI-22. WMO/TD No. 65. World Climate Research Programme Publication Series No. 4.

Yamazaki, H., Osborn, T.R., and Squires, K.D. (1991) Direct numerical simulation of planktonic contact in turbulent flow. *J. Plankton Res.* **13**, 629–644.

Yamazaki, H., Mackas, D.L., and Denman, K.L. (2002) Coupling small-scale physical processes with biology. In *The Sea, Vol. 12: Biological–Physical Interactions in the Sea* (ed. A.R. Robinson, J.J. McCarthy, and B.J. Rothschild). Wiley, New York.

Yen, J., and Strickler, J.R. (1996) Advertisement and concealment in the plankton: what makes a copepod hydrodynamic conspicuous? *Invertebr. Biol*. **115**, 191–205.

Yen, J., Sanderson, B., Strickler, J.R., and Okubo, A. (1991) Feeding currents and energy dissipation by *Eucheta rimana*, a subtropical pelagic copepod. *Limnnol. Oceanogr*. **36**, 362–369.

Yentsch, C.S. and Phinney, D.A. (1985) Rotary motions and convection as a means of regulating primary production in warm core rings. *J. Geophys. Res.* **90** (C2), 3237–3248.

Yin, K., Goldblatt, R.H., Harrison, P.J., St John, M.A., Clifford, P.J., and Beamish, R.J. (1997a) Importance of wind and river discharge in influencing nutrient dynamics and phytoplankton production in summer in the central Strait of Georgia. *Mar. Ecol. Prog. Ser.* **161**, 173–183.

Yin, K., Harrison, P.J., and Beamish, R.J. (1997b) Effects of a fluctuation in Fraser River discharge on primary production in the central Strait of Georgia, British Columbia, Canada. *Can. J. Fish. Aquat. Sci*. **54**, 1015–1024.

Yoder, J.A., Atkinson, L.P., Lee, T.N., Kim, H.H., and McLain, C.R. (1981) Role of Gulf Stream frontal eddies in forming phytoplankton patches on the outer southeast shelf. *Limnol. Oceanogr.* **26**, 1103–1110.

Yoder, J.A., Atkinson, L.P., Bishop, S.S., Hofmann, E.E., and Lee, T.N. (1983) Effect of upwelling on phytoplankton productivity of the outer southeastern United States continental shelf. *Cont. Shelf Res.* **4**, 385–404.

Zeldis, J.R. and Jillett, J.B. (1982) Aggregation of pelagic *Munida gregaria* (Fabricius) (Decapoda, Anomura) by coastal fronts and internal waves. *J. Plankton Res.* **4**, 839–857.

Zimmerman, R.C. and Kremer, J.N. (1984) Episodic nutrient supply to a kelp forest ecosystem in Southern California. *J. Mar. Res.* **42**, 591–604.

Index

Note: Page numbers in *italics* refer to figures; those in **bold** to tables.